ABSTRACT

Title of Dissertation: A LARGE SURVEY FOR VERY LOW SURFACE BRIGHTNESS GALAXIES

James J. Marshall, Doctor of Philosophy, 2004

Dissertation directed by: Professor Stacy S. McGaugh
Department of Astronomy

This dissertation presents the results of a survey for very low surface brightness galaxies in the field population. These galaxies have such low brightness per unit area on the night sky that they are difficult to detect and have been overlooked by many previous surveys. By covering a large area, approximately 91 $\deg^2$, and reaching a low limiting surface brightness, approximately 25.4 R mag arcsec^{-2}, we are able to detect these galaxies down to a surface brightness level that has not been well explored, allowing us to check and extend previous results.

We describe the observations, data reduction procedure, astrometric and photometric calibrations which are performed using IRAF. The data analysis procedure involves detecting objects using the SExtractor program, performing a star/galaxy separation, and fitting the detected objects with a galaxy model using the GIM2D package for IRAF in order to measure their parameters. We

perform a series of cuts on the objects to eliminate detections with potential problems, using the results of the data analysis steps to remove objects that are stellar-like, saturated, unresolved, have poor χ^2 values for the model fit, have very large disk scale lengths, or reached model fitting limits of 85° inclination and a bulge/total ratio of 0 or 1. We then selected objects that were brighter than 18.25 mag in R, had a bulge/total ratio $B/T < 0.3$ (disk dominated), and inclination $i < 35°$ (relatively face-on) as our sample to study, a total of 757 objects. The results of our study indicate that the observed surface brightness distribution is peaked at a disk central surface brightness of 20.5 R mag arcsec^{-2} and the intrinsic surface brightness distribution, obtained by applying a volume correction to the observed distribution, is consistent with a flat distribution out to approximately 24.25 R mag arcsec^{-2}. We also examine the number–magnitude relation for our detections, the assumption that galaxy disks are transparent by using the inclination as a measure of the transparency, and the relation between the disk and bulge scale lengths. The results are summarized and some possibilities for future study are presented.

A LARGE SURVEY FOR VERY LOW SURFACE BRIGHTNESS GALAXIES

by

James J. Marshall

Dissertation submitted to the Faculty of the Graduate School of the
University of Maryland, College Park in partial fulfillment
of the requirements for the degree of
Doctor of Philosophy
2004

Advisory Committee:

Professor Stacy S. McGaugh, Chair
Dr. Greg Aldering
Professor Rabindra N. Mohapatra
Professor Christopher S. Reynolds
Professor Sylvain Veilleux

DEDICATION

To my parents, for their love and support.

ACKNOWLEDGEMENTS

This work would not have been possible without the guidance and instruction of Stacy McGaugh and the assistance of Greg Aldering who provided a number of very helpful scripts and programs. Special thanks also goes to the following people for making their software pacakges freely available: Emmanuel Bertin (SExtractor), Luc Simard (GIM2D for IRAF), and Austin B. Tomaney (DIFIMPHOT for IRAF). We acknowledge the use of NASA's *SkyView* facility (http://skyview.gsfc.nasa.gov) located at NASA Goddard Space Flight Center. This research has made use of the USNOFS Image and Catalogue Archive operated by the United States Naval Observatory, Flagstaff Station
(http://www.nofs.navy.mil/data/fchpix/).

On a personal note, I would like to thank all of my family, friends, and teachers for the love, friendship, education, and support they have given me over the years. You have all played important roles in my life

and for all you have done, I am grateful. For their support during the very trying last few months of completing this dissertation, I would like to give a special thank you to the following people: Donna Pierce, Mia Bovill, Joe Martino, Fred Berendse, Jamison Maley, and most of all, my mother. You helped make a very difficult and stressful time for me more bearable. Thank you.

TABLE OF CONTENTS

LIST OF TABLES

LIST OF FIGURES

Chapter 1

Introduction

The study of low surface brightness (LSB) galaxies, ones with peak surface brightnesses at or below that of the background sky, is a relatively young and rapidly growing field. As recently as approximately 30 years ago, the existence of these objects was still under question. The primary problem was, and still is, one of observational bias and selection effects — the night sky is bright enough to mask very diffuse, faint galaxies and therefore detecting such objects is an extremely difficult task. However, once they were detected and mounting observations and data confirmed their existence, their importance became apparent. This new population of galaxies held the potential to have a dramatic influence on our understanding of galaxies and cosmology. Therefore it is vital that we seek them out in order to get a clearer picture of the true population of galaxies that remained hidden for so long.

1.1 Visibility of Low Surface Brightness Galaxies

As Impey & Bothun (1997) note, no galaxies can be detected below a certain percentage of the night sky brightness while above that limiting isophote, a galaxy must have a large enough apparent size for it to be distinguished from a star. This problem was initially touched upon by Zwicky (1957) and later by Arp (1965), but the first quantitative study of it was made by Disney (1976). His work was motivated by that of Freeman (1970) who used a sample of 36 disk galaxies, the only ones with surface photometry available then, and showed that 28 of them appeared to have B band central surface brightnesses $\mu_0(B) \approx 21.65 \pm 0.3$ mag arcsec^{-2}, an observation which has since come to be known as "Freeman's law". While this is only applicable for disk galaxies, prior work by Fish (1964) demonstrated a similar law for elliptical galaxies. Freeman himself says that his conclusions are often overstated (Freeman 1999), noting that the sample he used was inhomogeneous, the data were mostly photographic, and this work was done before the idea of dark matter in galaxies was well established. Nevertheless, it was an important step in motivating further work.

Disney (1976) demonstrated that Freeman's law could be explained by selection effects. Describing the radial surface brightness profile $\sigma(r)$ of galaxies with the equation

$$\log(\sigma(r)/\sigma(0)) = -(r/\alpha)^{1/\beta} \tag{1.1}$$

(his Equation 1) where α is a scale length and $\beta = 1$ for spirals and 4 for ellipticals, he derived an equation for the apparent radius of the galaxy in terms of the limiting and central surface brightnesses. Plotting this equation, apparent radius

vs. limiting minus central surface brightness, shows that the distribution of spiral galaxies is strongly peaked around the Freeman value and ellipticals show a similar, but broader peak around the Fish value. This indicates that galaxies with surface brightness away from the Freeman or Fish values will be under-represented in diameter limited surveys. Allen & Shu (1979) later demonstrated that the lack of observed high surface brightness (HSB) systems must be real, but selection effects could explain the low surface brightness end of the observed distribution. A more accurate determination of this visibility function was performed by Disney & Phillipps (1983), again illustrating that the observed distribution will be rather sharply peaked almost regardless of the intrinsic distribution. A derivation of the visibility function for two component, bulge/disk galaxies was performed by Davies (1990), and McGaugh et al. (1995) later demonstrated just how powerful these selection effects can be, deriving the visibility function for both diameter limited and flux limited surveys. They also emphasized that a correction for these volume sampling effects must be applied to any survey. While it was possible that this peaked distribution was an intrinsic property of the galaxy population, studies such as these showed that it was a selection effect and LSB galaxies do exist.

1.2 Potential Impact of Low Surface Brightness Galaxies

As the evidence for the existence of LSB galaxies mounted through events such as the discovery of many of them in the Fornax cluster (Phillipps et al. 1987) and the accidental discovery of the giant LSB galaxy called Malin 1 (Bothun

et al. 1987), the realization of their impact on cosmology became apparent. They will provide a contribution to the luminosity density of the universe and since they were overlooked in early surveys, their contribution can be significant. For example, McGaugh (1996) notes that while most of the luminosity density comes from HSB objects and almost none comes from the extremely LSB objects that are essentially invisible ($\mu_0 > 27$ B mag arcsec^{-2}), the truly LSB systems could produce a small, but significant amount of the light (10–30%). Likewise, they can be an important contributor to the mass density of the universe; McGaugh (1996) notes that their contribution here is a greater proportion of the total than their proportion of the total luminosity density because the mass-to-light ratio is observed to increase with decreasing surface brightness. Examination of their rotation curves suggest that LSB galaxies are dark matter dominated at almost all radii (see, for example, de Blok & McGaugh (1997)) and therefore they provide important information regarding dark matter and galaxy formation. de Blok et al. (2001) performed a study of the mass density profiles of LSB galaxies and found that for a power law profile $\rho(r) \sim r^{\alpha}$, the inner slopes are best fit with $\alpha = -0.2$, implying that their halos are dominated by cores. As they note, this is inconsistent with cold dark matter simulations which typically find $\alpha \leq -1$, implying that the halos are dominated by cusps. LSB galaxies can also offer insight into galaxy evolution by providing information on a different class of galaxies, stretching old ideas into new regimes. One example is the study by Zwaan et al. (1995) which found that LSB galaxies follow the same Tully–Fisher relation (Tully & Fisher 1977) as HSB galaxies, indicating that their mass-to-light ratios must be a factor of 2 larger. This suggests that the mass surface density may be an important parameter in determining the luminosity evolution

of galaxies. They could also play an important role in the interpretation of quasar absorption lines which serve as a probe of gas along the line of sight. Simulations by Linder (1998) have shown that a large fraction of Lyman α absorbers can arise in LSB galaxies and that the contribution from HSB galaxies may be relatively unimportant. The identification of a known LSB galaxy as the source of Lyman α absorption in the spectrum of one quasar by Bowen et al. (2001) provides support for this idea. LSB galaxies are a powerful tool in the study of cosmology and galaxies in general and Impey & Bothun (1997) provide a good review of their applications in various fields.

1.3 Comparison of Surveys

This survey was designed to discover new very LSB galaxies, specifically to help quantify the population of galaxies with B band central surface brightnesses of $24 < \mu_0(B) < 26$ which has not be covered in depth by other surveys. For example, the survey by O'Neil & Bothun (2000) finds only 11 galaxies with $23.75 < \mu_0(B) < 25.0$. Our survey covers a wide area ($\sim$100 deg^2) and is expected to allow for the detection of galaxies with $\mu_0(R) \approx 25$ mag arcsec^{-2} ($\mu_0(B) \approx 26$), about 2 mag arcsec^{-2} fainter in central surface brightness than previous surveys. Therefore it provides a very good connection between the very deep, small area surveys and the very wide area, shallow surveys.

To demonstrate the advantage of our survey, we compare it with other similar surveys for LSB galaxies. The survey by Schwartzenberg et al. (1995) detected over 500 galaxies with $\mu_0 > 22.5$ V mag arcsec^{-2} in 1.2 deg^2. They have found objects with $\mu_0 = 26.5$ in V and thus reach a very faint level, but the area surveyed is roughly equivalent to one of our fields; we cover a much larger area and

can reach a similarly faint limiting surface brightness of $\mu_\ell \approx 27$ in R. Impey et al. (1996) detect 693 galaxies in 786 deg^2 at a limiting isophote of 26 B mag arcsec^{-2}; this provides extremely good sensitivity to higher surface brightness LSB galaxies, but our survey should be approximately 1 mag deeper since we collect over five times as many galaxy photons at a given surface brightness. A survey of the Cancer and Pegasus clusters as well as an area in the direction of the Great Wall was performed by O'Neil et al. (1997). In the 27 deg^2 surveyed, they detected 127 galaxies with $\mu_0 > 22$ B mag arcsec^{-2} for a detection threshold of $\mu_\ell \sim 27$ in B and diameter limit of $14''$. Our survey covers approximately four times the area and can reach a limit roughly 0.5–1 mag deeper. In addition, they have surveyed mainly dense regions like clusters. Our field survey covers a much wider range of environments and in this sense serves as a good complement to their survey. Dalcanton et al. (1997) surveyed 17.5 deg^2 at Palomar Observatory and discovered 7 pure disk LSB galaxies with $23 < \mu_0 < 25$ in V. Our survey covers approximately six times this area and collects about 2–3 times as many galaxy photons at a given surface brightness. Along with the fact that the skies at Cerro Tololo Inter-American Observatory are darker than at the Palomar Observatory, our survey is about 0.5–1 mag deeper. Morshidi-Esslinger et al. (1999) detected 2435 LSB galaxies in the range $\mu_0 = 22.5$–24.5 B mag arcsec^{-2} over 2187 deg^2, but use automated plate measuring (APM) scan data of UK Schmidt photographic plates as Impey et al. (1996) did. Then as before, our survey should be approximately 1 mag deeper. The Millennium Galaxy Catalog described by Liske et al. (2003) covers 37.5 deg^2 to an isophotal detection limit of 26 B mag arcsec^{-2}. Our survey can reach a limit approximately 2 mag fainter and covers an area over 2.5 times as large.

Chapter 2

Observations and Data Reduction

2.1 Description of the Data

The data for this survey were obtained by Stacy McGaugh and his colleagues Greg Aldering (Lawrence Berkeley National Laboratory) and Mario Mateo (University of Michigan) at the Cerro Tololo Inter-American Observatory (CTIO) in Chile over six observing runs between 1995 and 1997: September 1995 (Aldering), April 1996 (McGaugh), May 1996 (Aldering), August 1996 (McGaugh), April 1997 (McGaugh), and October 1997 (Mateo). Each run lasted between ten and fourteen days. The observations were made with the 0.61m (24″) Curtis Schmidt telescope, a Schmidt telescope with a f/3.5 beam and a 96.66″/mm plate scale. Two of the primary advantages of using the Schmidt telescope for surveys are its large area and large etendue, the product of collecting area and field of view, giving a high survey efficiency. The telescope is fitted with a 2048×2408 STIS CCD, a thick, front-illuminated CCD with 21 micron pixels giving a pixel scale of 2.028″/pixel thus providing a field of view of about 1.15 deg^2; later observations used a thinned and backside illuminated CCD. The fold mirror does not fill the field of view, so the edges of the field are vignetted by ∼10% compared

to the center while the extreme corners are down by ∼20% — this pattern is well corrected using sky flat fields. Image quality over the entire field is good in that the chip is in focus across the field of view so abberation is not a problem. However, we did find that scattered light is an issue; this creates a sort of halo around the stars which is brighter and more noticeable for brighter stars. The CCD has a Metachrome coating in order to provide blue and ultraviolet sensitivity below the standard 4700Å cutoff due to polysilicon gates on the CCD. As our observations were taken in the red, the coating has no real beneficial effect. However, we should note that a crack in this coating is visible in the twilight flat field images (and also appeared to grow slightly from night to night) and therefore this and any other similar defects in the coating that would be visible in the object images are removed in the flat fielding stage of the data reduction. These and other details about the Curtis Schmidt telescope can be found in the user's manual (Smith 1998).

The observations were made through a wide square-bandpass filter covering the region 5600–7300Å. This particular filter (Harvard R) was chosen because it provides the highest throughput while avoiding night sky emission lines. There were actually two very similar, but not identical filters used: one of two $4'' \times 4''$Harvard R filters was used for the first four observing runs (September 1995, April 1996, May 1996, August 1996), but a custom made "VLSBG R" mimicking the original Harvard R was used for the remaining runs (April 1997, October 1997); see Figure 2.1 for a transmission plot of this filter. The reason for this change was that before our survey was completed, the original Harvard R filter was removed from CTIO's set of filters. It was Harvard's private filter, custom made for supernova searches, and we were unable to gain access to it in later

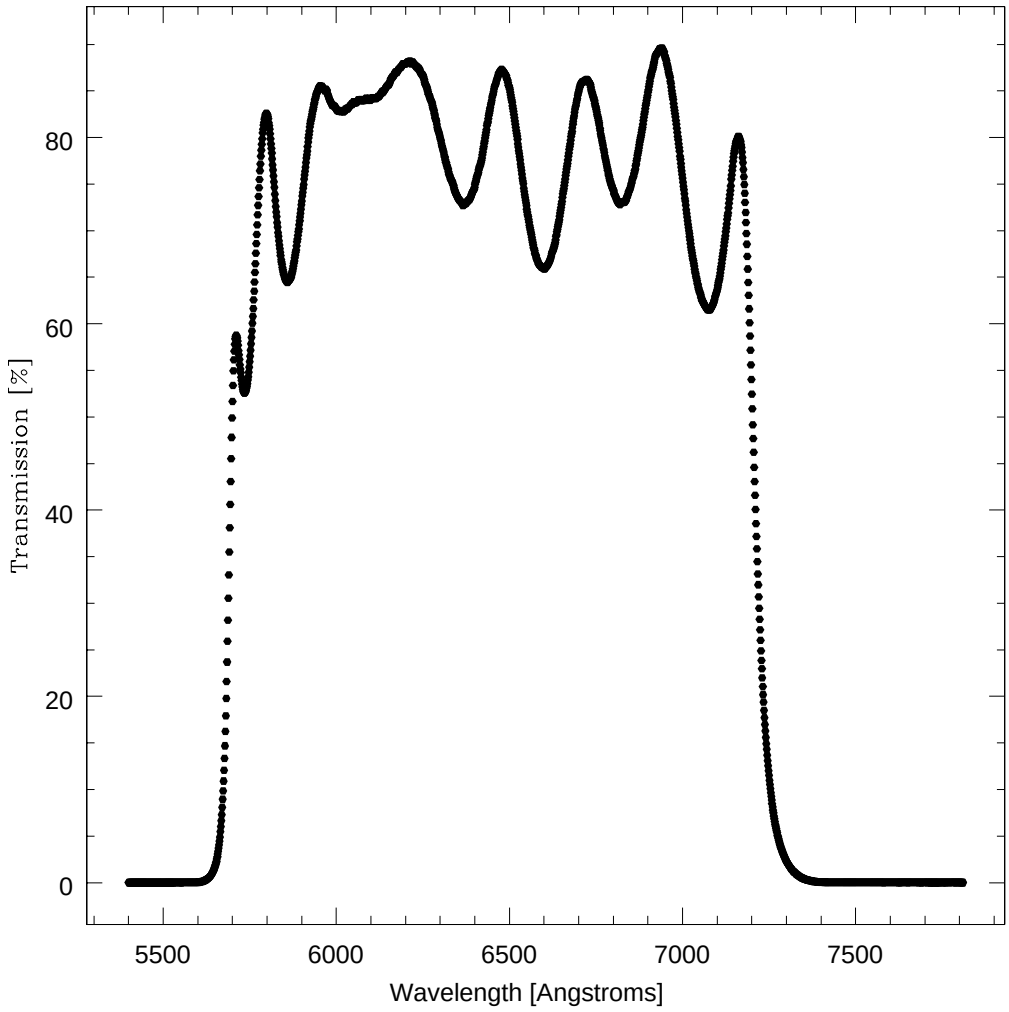

Figure 2.1: Transmission plot for the VLSBG R filter.

observing runs so we had to have our own filter made. Both filters were well calibrated in that the transmission profile was carefully measured.

The observations were taken near the zenith, typically within about 2 hours of the meridian. A shift-and-stare mode was used with a shift size of 1–2′ and each field was observed over at least two nights. In this method of observing, the first

image is taken centered on one position then each following image is taken at a position slightly shifted from the previous one. A typical sequence of ten images had the center position shifted in a 3×3 square with the tenth image being shifted in the direction of the center of that square. This shifting between exposures is also called dithering the images. Each individual exposure was 500 seconds and the shifting was performed in order to assist in the data reduction, especially as it relates to the detection of large LSB galaxies. Because the images must be shifted in order to combine them into a final image, any potential problems with the CCD will similarly be shifted around and thus easily eliminated with a clipping algorithm during the combination procedure. The actual sky brightness for each field was monitored during the observations and the cumulative exposure time was varied in order to reach a signal-to-noise ratio of 5 per pixel at $\mu_\ell = 27$ R mag arcsec^{-2} uniformly throughout the survey; this resulted in approximately 20 observations per field for a total time of $\sim$ 10000 seconds or roughly 2.8 hours per field. Because the signal-to-noise ratio per pixel is essentially

$$S/N = \frac{C_{obj}t}{\sqrt{C_{obj}t + C_{sky}t}} \tag{2.1}$$

where S/N is the signal-to-noise ratio, C_{obj} is the object flux in photoelectrons/s/pixel, t is the exposure time in s, and C_{sky} is the sky flux in counts/s/pixel, excluding noise from the detector (e.g., readout noise and dark current) which is negligible compared to the sky noise for these observations. In order to maintain a fixed signal-to-noise ratio for a specified object flux, if the flux of the background sky changes, the exposure time must also change to compensate. Surface brightness is simply flux/area and since each pixel has the same area, the equation provides a quick way to determine at the telescope how many observations of a given field will be required to obtain the desired signal-to-noise ratio based on

how the sky level is changing. As each image was taken, the intensity of the sky in the frame was noted and used in this equation to track the S/N at $C_{obj} = 27$ R mag arcsec^{-2}. The observed standard star fields were used to make a crude estimate of the calibration to allow conversion between counts and magnitudes.

The fields for this survey were selected from pre-existing surveys, primarily the Las Campanas Redshift Survey (LCRS) (Shectman et al. 1996), but also the ESO Slice Project (ESP) (Vettolani et al. 1997) so that redshifts would already be available for the high surface brightness (HSB) galaxies in this survey. Great care was taken to select the darkest fields for this survey. They were chosen at a high galactic latitude to avoid bright stars, the ecliptic, and Galactic dust as indicated by IRAS 100μm emission and sky glow was generally weak because the period of observations spanned a minimum between solar cycles. Fields were also selected so that no stars brighter than seventh magnitude were within three degrees of the field. Using only the darkest fields is very important for the detection of very LSB objects because the brighter the background the more difficult it becomes to detect such objects. In addition, during the observations great precautions were taken to avoid any possible light leaks to the CCD from within the dome — all lights were either covered, turned off, or dimmed as much as possible, using a lot of electrical tape to cover LEDs on the instrument, an opaque curtain was placed in the stairwell leading up to the dome floor, and flashlights were not used in the dome during an exposure. The entire survey covers approximately 100 deg^2 which is an extremely large area for a survey of this depth; most surveys that reach a comparable depth cover an area less than 1 deg^2. However, the final observing run has not been included in this work for a number of reasons, but primarily because it was taken with a different CCD than the rest of the survey

thus requiring additional work to reduce properly. Five of the six observing runs made are included so we have approximately 80% of the full survey reduced and analyzed here, plenty for our purposes. The final run can always be reduced and analyzed later as part of future work on this project. A summary of the available observing runs is available in Table 2.1.

2.2 Image Reduction

As previously noted, observations of survey fields were dithered, slightly shifting the position of the telescope in between consecutive exposures. A primary reason for doing this is that any artifacts or flaws in the CCD will be at different locations in each exposure because the image is centered on a different portion of the CCD in each exposure. When the frames are shifted and combined, a simple sigma clipping algorithm can easily remove such artifacts and flaws which will clearly stand out as outlying points. Additional discussion about dithering can be found in, e.g., Hook & Fruchter (2000). While this has no real effect on the actual reduction of the individual images, it does affect the creation of the final image as all the individual exposures have to be shifted to line up properly before combining them. So the shift-and-stare method of observing used here allows for easier removal of CCD flaws or artifacts in the image at the cost of complicating the image combination procedure.

The data reduction was performed using the Image Reduction and Analysis Facility (IRAF) software package. Most of the initial steps follow the standard CCD data reduction procedure; see e.g., Massey (1997). First an overscan correction is made that subtracts the electronic pedestal level from the images. Several hundred analog to digital units (ADUs) were added to the images taken at the

telescope; this "bias" must be subtracted off and a small non-exposed section of the image is used for this. This is done for every image taken because the bias level is not stabilized and can vary by a few ADU due to any number of factors such as the telescope position or temperature. It is also a slight function of position on the CCD chip and primarily varies along the columns. Therefore within the non-exposed overscan region the data are averaged in the x direction then fit as a function of y and that fit is subtracted from each column in the image. the image. This removes the bias to first order. The images are then trimmed to remove the overscan region which is no longer necessary and the first few columns which contain no data, leaving only good data on the frames. The regions to be cut out in this manner are defined in the image headers.

Our data are in what IRAF calls quadformat because we used a non-standard readout method for our observations. The Array Controller (Arcon) hardware and software system that controls the CCDs at CTIO allows the observer to reduce the readout time by reading out the CCD chip from four amplifiers, one at each corner of the CCD, instead of a single amplifier. Our data have the same readout noise for all four quadrants, 3.8 e^-, but the gain was slightly variable: 1.9, 2.1, 2.1, and 2.3 e^-/ADU. Since IRAF tasks require a single gain value, we use 2.1 as the value for the entire field. The September 1995 run did not have image headers with the readout noise or gain values so we added them since these values are needed. Originally data taken in this format had to be reduced using the CTIO submitted ARED package, specifically the QUADRED task in the QUAD package within ARED, but only the overscan and trim corrections would have required special treatment. Once those two steps have been completed the quadformat has been accounted for and the image can be reduced in exactly the

same way as a standard, single readout image. However, with the update of IRAF to version 2.12 this is no longer necessary. The standard CCDRED package of tasks has been updated to handle quadformat images and the ARED package is no longer necessary. Thus we ran the updated version of CCDRED's CCDPROC task initially to perform just the overscan and trim corrections. Additional details regarding the reduction of multi-readout images can be found in Smith (1993). As an example of quadformat data, we provide the first observation of the survey in Figure 2.2. This is the raw data; the trim and overscan steps have not yet been applied to it. Notice that the overscan region has been placed at the center of the image. This makes it easier to remove in the trimming step because all four overscan sections can be removed at once. The left and right edges of the frame have some columns with no data and need to be removed. The image headers include this information so that the trimming step can automatically remove these columns along with the overscan regions.

Next a zero or bias correction is made using frames with zero second integration times. Since the overscan correction was performed after averaging in the x direction, we have not yet removed any column-to-column structure that may have been present in the bias level. By subtracting zero second integration frames that have already been overscan corrected from the other images, we can remove the structure in the bias level. The zero frames were averaged together using the CCDRED task ZEROCOMBINE without any rejection algorithm or scaling. A second pass through CCDPROC was then performed to apply this zero correction on all the other images. An exception was the May 1996 observing run where no zero frames were taken, Greg Aldering having determined that the overscan correction was sufficient. The second pass through CCDPROC is

essentially skipped for this run by setting the zerocor parameter to "no" for this and all future executions of CCDPROC for this observing run.

Dark frames, long exposures with the shutter closed, are then used to subtract off any dark current (background added on long exposures) and light leaks should any be present; this is a first order correction. These images were only taken at night when conditions prevented observing. Our examination of the dark frames shows little real structure so we use a mean value for the dark frame instead of the full image. However, there is a noticeable difference between the number of counts obtained in each of the four quadrants so each quadrant was averaged separately and a new image created where each quadrant's value was the calculated mean. It is this image that is used to perform the correction. The dark level varies between observing runs, but the highest average value used was 3.1 ADU on a 4024 s exposure, the longest dark frame. All dark frames were initially average combined together using the CCDRED task DARKCOMBINE with an average sigma clipping algorithm, 3σ high and low, scaled by exposure time. The image was then copied to a new image, an average value for each quadrant determined using IMSTATISTICS, and an IMREPLACE run to replace all values within each quadrant with the determined mean value. In order to simplify this step somewhat, an IRAF script called mystats.cl written by Greg Aldering which calls IMSTATISTICS was actually used, the primary advantage of it being that it performs iterative rejection of outliers and writes values such as the mean to package variables so that they can be easily accessed by other programs. This makes automating and scripting this procedure simpler than it would have been using IMSTATISTICS (which does not have an easy way for another program to reference the mean value it obtains). Another run through CCDPROC was then

made to perform the dark correction. An exception was the April 1997 run for which no dark frames were taken. We decided that making this correction using images taken on other observing runs would not necessarily be any better than just not doing this correction for this run. Thus, as with the no zero correction in the May 1996 run, we essentially skip this step in the reduction of this run by setting the darkcor parameter in CCDPROC to "no" for this and all later executions of CCDPROC for this observing run.

The last main step is to flat field the images in order to divide out any pixel to pixel gain variations as well as any larger scale spatial variations. While the previous effects were all additive, the flat field variations are multiplicative. Since this is all part of a standard reduction procedure, the IRAF tasks are designed to perform these corrections in the proper manner without extra user input (i.e., we don't have to tell it the flat fields get divided while the other corrections get subtracted). However, since the flat fielding step is very important for this project designed to find galaxies with surface brightnesses near and well below that of the background sky, it is worth noting the difference as there will be a second flat fielding step performed in a somewhat different manner from the standard reduction procedure.

We initially use twilight flats rather than dome flats since the sky will most likely look somewhat different to the CCD than a simple illuminated white spot (dome flat). These images were average combined using the FLATCOMBINE task with an average sigma clipping rejection algorithm, 3σ high and low, with mode scaling. An exception was the May 1996 run where a median combine was performed — with only eight twilight flat fields available, this was a better choice. Scaling by the inverse of the mode is performed in order to correct for any

possible variations in the illumination of the flat fields over the series of exposures; given that we are using twilight flats and the sky brightness is definitely changing during twilight, it is necessary to scale the flat fields in this manner. Another pass through CCDPROC was then made in order to apply the twilight flat fields to the images. The fields are automatically normalized, a mean being calculated which is used to scale the flat field before dividing it into the input image.

Since the night sky will likely look different from the twilight sky, we created sky flat fields to correct the twilight flat fields already applied to the images. The unshifted object images from each night are average combined with IMCOMBINE using a ccdclip rejection algorithm, 3σ high and low, in order to remove objects from the field. The fields are not shifted so that we can easily eliminate objects from them; the objects will be scattered all over the field, but should only appear in a very small number of the frames at a given pixel and are easily removed by applying this rejection during the combination. We also scale and weight by the mode in order to account for differences between individual observations — scaling by the mode normalizes out any variations in sky level over time and weighting by the mode gives higher weight to the pixels with more sky photons. Once we have these sky flat field images, we normalized them with the NORMALIZE task because we want to retain the actual number of counts in the background. At this point, we checked each of these nightly sky flats to make sure they were acceptable. In a few cases there were not enough observations on a given night to create a good sky flat this way. In the April 1996 run, night 1 only had eight images and these did not create a good sky flat; stars were not completely clipped away, leaving bright patches in the field. We applied the sky flat from night 2 to the night 1 data. The flat fields were visually examined

and while there is some variation from night to night, it is typically low between neighboring nights making this substitution a reasonable one. Also, nights 12 and 13 of this run separately didn't have enough fields to be usable so they were combined together and used on both nights. Night 13 of the August 1996 run was similar, only having a few observations of one field, but it was in a different filter from the rest of the run, so we omitted this night from consideration. After visually verifying that the normalized sky flats are acceptable, we divide them into the object images to apply them. We also write a new line to the image headers, in the style of the CCDRED task, to indicate that this sky flat fielding step has been performed.

After these steps have been completed, the images have been overscan corrected, trimmed, zero/bias corrected, dark corrected, and flat fielded using twilight flats that were corrected with sky flats created from the object images. An IRAF script we called reduce.cl was written to perform these steps, up to the creation of the sky flat fields. Since we needed to check the sky flats before applying them, the script creates them, but does not apply them. An example of a fully reduced image is provided in Figure 2.3. This completes the primary part of the data reduction, but frame masks still remain to be made and the individual object images have to be shifted and combined together.

The next step is to account for bad columns and pixels within the frames. This is done by creating a frame mask, an image where the locations of bad and good pixels are given values of zero and one, respectively. Bad columns and pixels are located on both the dark frames and the twilight flats creating two separate masks which are then combined to create the final frame mask. All bad pixels in the dark frame were accounted for in its mask while the flat field's mask only

takes into account bad pixels that appeared to remain in the object images even after the flat field correction had been done. These two masks were multiplied together to create the frame mask which is then used when combining the object images together. In the case of the April 1997 run when no dark frames were taken, we used the dark mask from the April 1996 run (the only run reduced to this stage at that time) to construct the frame mask. In order to leave the object images unchanged, we chose not to apply the mask directly. Instead, we add a BPM (bad pixel mask) keyword to the header of the object images that contains the file name of the frame mask we wish to apply. When we use IMCOMBINE to combine the object images, it will use the mask named in the BPM keyword along with task parameters that identify what type of mask it is (i.e., that bad pixels have a value of zero here) to apply the mask in the combination process.

Each field was observed many times, normally around 20, and the observations were dithered around so that the CCD was centered on a slightly different place within the field on each observation. In order to combine the many images into a single image, we must determine the shifts required to align all of the images together. Greg Aldering provided us with some scripts and programs designed for this purpose which permits us to automate this procedure. The primary inputs are a list of images and the full width at half-maximum (FWHM) of the point spread function (PSF) and standard deviation of the background for each. In order to measure FWHM values, we made use of the IRAF contributed package DIFIMPHOT (Tomaney & Crotts 1996) and its GETPSFS task. This task combines calls to the standard IRAF task DAOFIND and the DIFIMPHOT tasks IMFWHM and ISOPSF to detect objects to some maximum data value and use a user specified number of the brightest stars to calculate the FWHM. Some initial

checks using IMEXAMINE showed that the FWHM was approximately 2 pixels, so this value was used as the initial estimate for GETPSFS. We manually iterated, running GETPSFS with the last output FWHM value as a new initial estimate, until the same value was returned twice in a row. For some images, instead of converging to a single value, two alternating values were obtained. The difference being very small, we simply used the average of the two values in these cases. The average value of the FWHM determined using GETPSFS was approximately 1.7 pixels with the vast majority of the results being in the range of 1.3–2.0 pixels. The standard deviation of the background was determined simply by running IMSTATISTICS on each field with a 3σ high and low clipping factor for a maximum of 15 iterations. The lists of image names, FWHM values, and standard deviation of the background values were placed into separate files for use as input to Aldering's IRAF script newcoadd_prep.cl which also calls two other C programs, quickmatch (originally written by Robert Quimby and modified by Greg Aldering) and match_w_geomap (by Aldering). The basic operation of newcoadd_prep is to call DAOFIND to detect objects, use the quickmatch program to match them from one frame to a reference frame, use IRAF's GEOMAP task to get a linear transformation between frames, match fainter stars with match_w_geomap and the GEOMAP transformation, run IRAF's WPHOT task to do photometry and measure accurate center coordinates, then calculate the (x,y) pixel offset of the frame from the reference frame. This is done for all frames in the input list (the first one is considered the reference frame) and then a new IRAF script is created that contains the commands and sets the parameters for combining the images. Running this new script performs the combination and gives us a single, combined image from all of the individual input images. The fields were average

combined and bad pixels were rejected by applying the frame masks named in the image header's BPM keyword. A sigma clipping algorithm, 3σ high and low, was also applied and the images were scaled and weighted by the exposure time. Once this last step is done for all of the observed fields, we have our final fully reduced and combined images. An example of a fully combined field is shown in Figure 2.4. Figure 2.4. The effects of dithering the images is apparent in the edges and corners where not all fields overlap, leaving less or no data in these areas. Bad columns were very well removed by the frame masks. Typically the only bad columns left are associated with bright, saturated stars, something that the frame mask, created from dark and twilight flat field exposures, could not be expected to handle. The scattered light halos around stars that are ghost images from internal reflections are also clearly visible in this image. The flatness of these final combined images was checked using the mystats.cl script to measure the statistics for twenty five 100 pixel square boxes arranged in an even grid over the field. Any obviously deviant measurements were removed before calculating the median variation in the results for each field. The results vary between fields and typically range from about 0.1% to about 0.9%; the average value is approximately 0.4%.

Table 2.1: Summary of Observing Runs

Dates	Length	Observer	Filter
Fields Observed			
1995 Sep 9–22	14 days	Greg Aldering	Harvard R
LCRS 0020-39a, 0020-45a, 0100-39a, 0100-39b, 0220-39a, 0300-39a, 2140-45a, 2140-45b, 2220-39a, 2220-39b, 2300-39a, 2320-42a, 2340-39a			
1996 Apr 11–25	14 days	Stacy McGaugh	Harvard R
LCRS 1003-03:E, 1003-06:E, 1027-03:E, 1051-12:W, 1139-03:E, 1139-12:W, 1151-12:E, 1215-12:E, 1239-12:E, 1351-03:E (unusable), 1403-03:W, 1439-12:W (unusable)			
1996 May 9–18	10 days	Greg Aldering	Harvard R
LCRS 1015-12:E, 1039-03:W, 1051-12:E, 1127-03:E, 1203-12:E, 1227-12:E, 1303-12:W, 1339-03:E, 1351-03:W, 1415-03:W, 1439-12:W, 1516-03:H, 2155-45:W			
1996 Aug 9–21	12 days	Stacy McGaugh	Harvard R
LCRS 0035-45:W, 0100-45:W, 0154-39:M, 0154-39:W, 0155-45:E, 0234-39:W, 0235-45:E, 2100-45:E, 2114-39:E, 2115-45:E, 2154-39:E, 2154-39:M, 2154-39:W, 2155-45:E, 2155-45:W, 2234-39E, 2234-39:W, 2314-39:E, 2314-39:M, 2315-45:E, 2315-45:W, 2354-39:M, 2354-39:W, 2355-45:E, 2355-45:M			
1997 Mar 31 – Apr 11	11 days	Stacy McGaugh	VLSBG R
LCRS 1032-06:S, 1036-06:S, 1040-06:S, 1044-06:S, 1048-06:S, 1052-06:S, 1056-06:S, 1100-06:S, 1104-06:S, 1108-06:S, 1112-06:S, 1203-12:E, 1427-06:W, 1439-03:E, 1439-03:M, 1439-06:H, 1451-06:H, 1503-03:M, 1503-03:W, 1515-03:W			

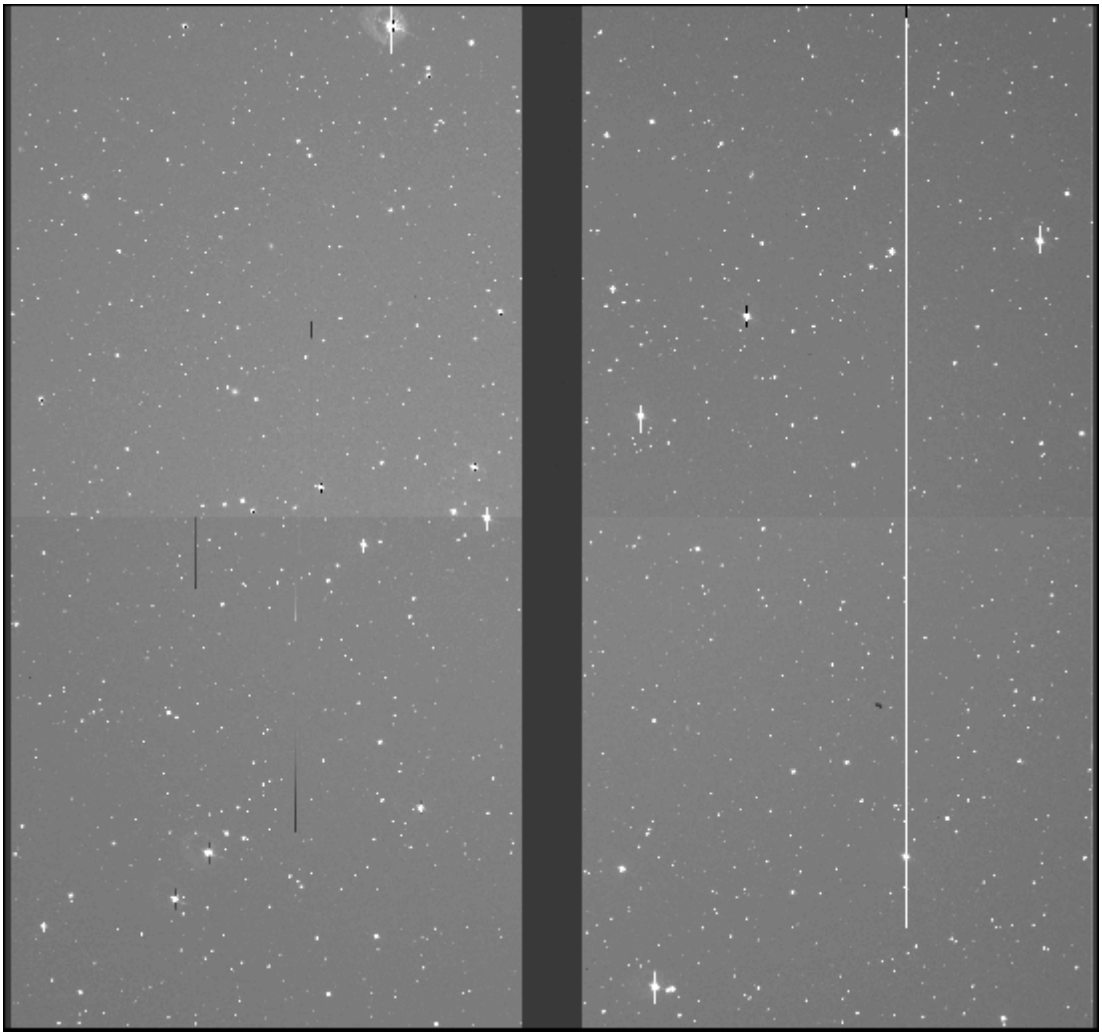

Figure 2.2: Example of the raw data. This is field F2140-45a, the first observation of the survey. Notice that the quadproc format places the overscan region in the center of the image to facilitate trimming. The few columns with no data on the left and right edges of the frame are removed in the trimming step.

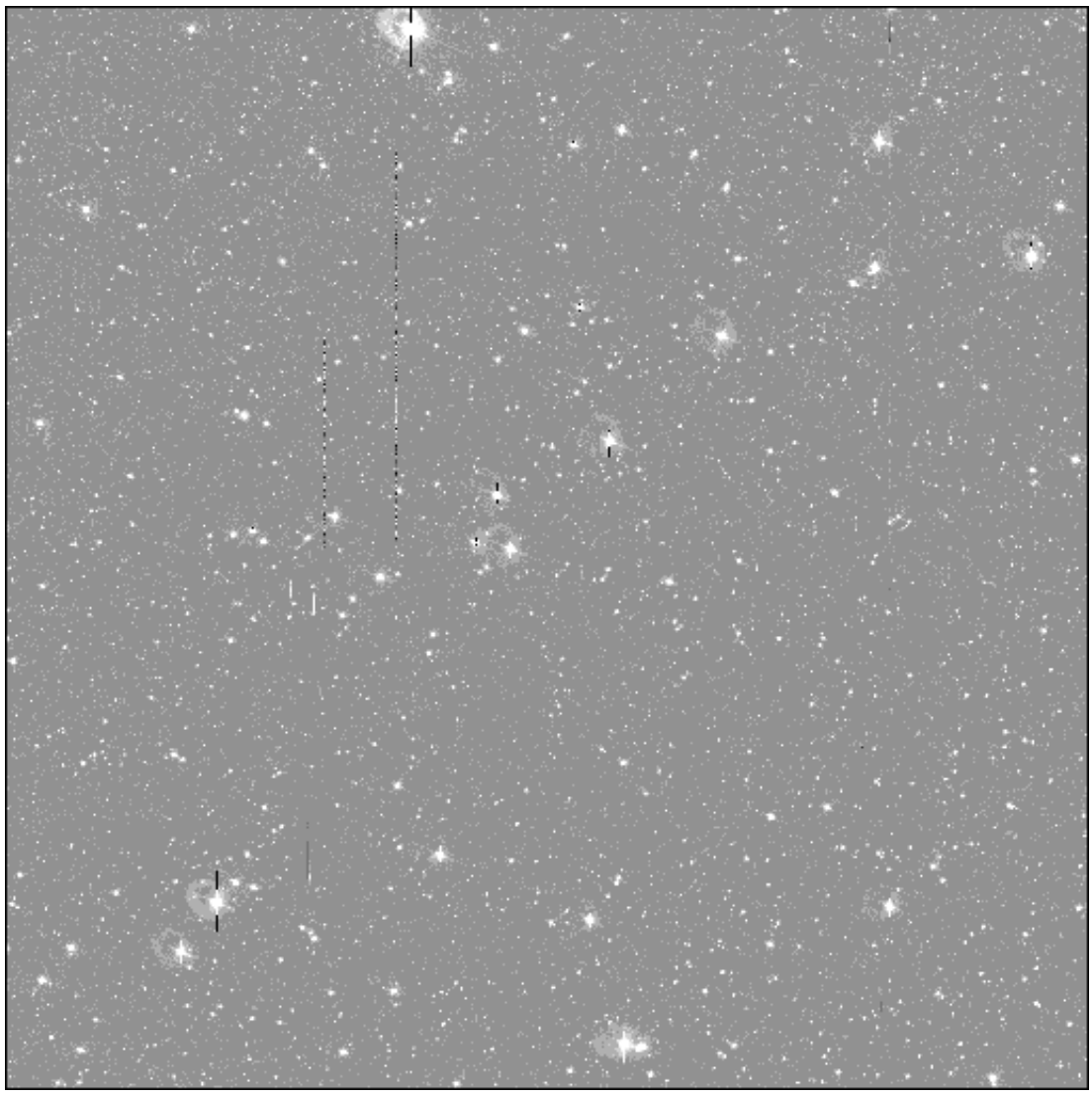

Figure 2.3: Example of a fully reduced frame. This is field F2140-45a, the first observation of the survey, and one of the images that goes into the combination to produce the final image. Bad columns are still visible because the frame mask is applied during combination.

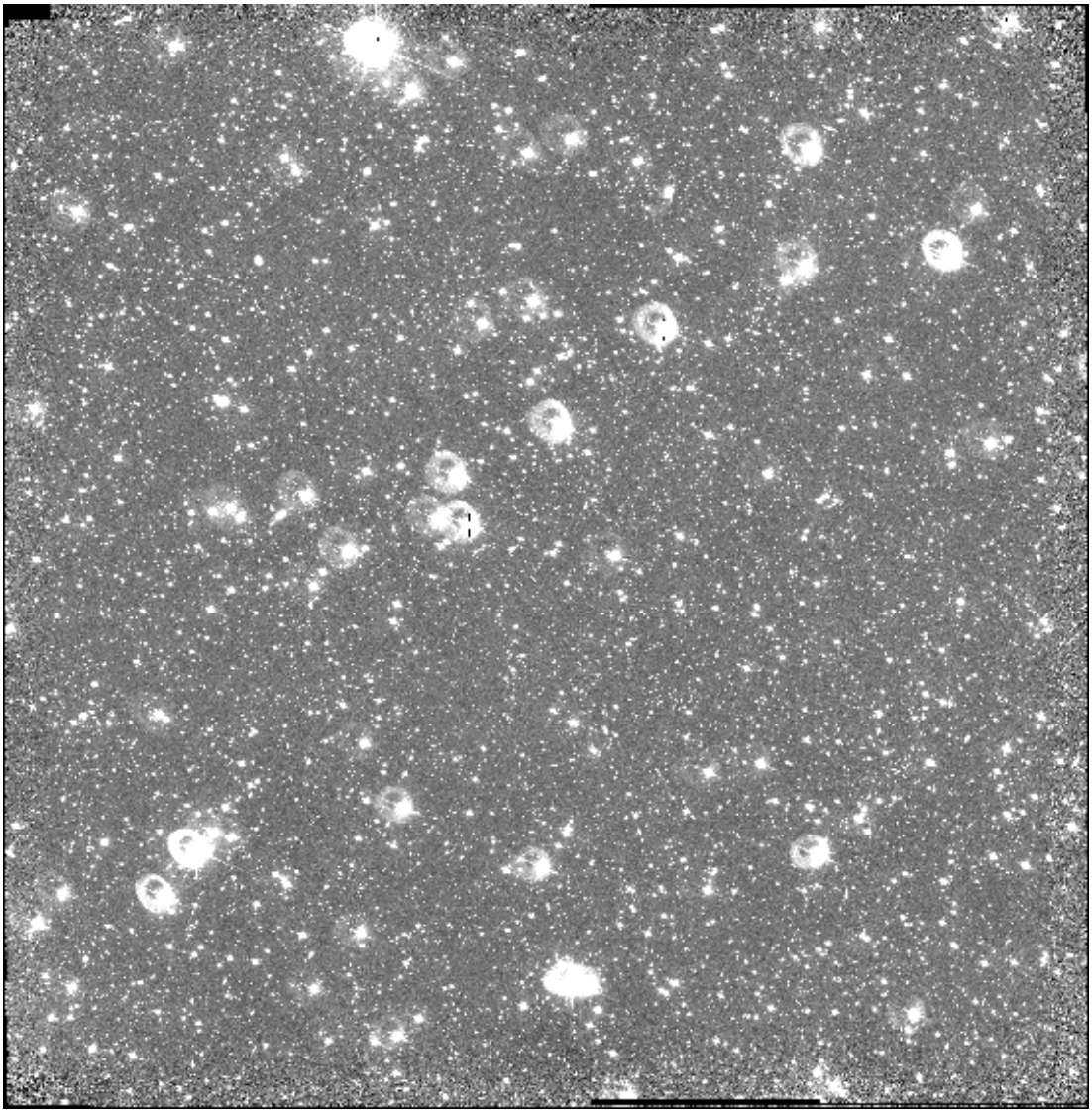

Figure 2.4: Example of a fully reduced, combined frame. This is field F2140-45a, the first observation of the survey and was created by combining 20 separate observations.

Chapter 3

Data Calibration

Calibrating the data required two steps: performing an astrometric calibration on each field in order to allow conversion between pixel coordinates (x,y) and sky coordinates (right ascension α, declination δ) and performing a photometric calibration for each night of each run to convert instrumental magnitudes into actual R band magnitudes.

3.1 Astrometric Calibration

Before we began the actual calibration process, we first checked that the image header coordinates for the centers of the fields were approximately correct. We used *SkyView* (McGlynn et al. 1997, 1998), available on the world wide web at http://skyview.gsfc.nasa.gov/cgi-bin/titlepage.pl, and the advanced interface to have the most options available. Using the coordinates from the image headers of each of our fields, we retrieved images from the Digitized Sky Survey. We then visually matched the results to our fields and adjusted the coordinates if necessary, re-centering the image for a better match. Once we obtained a fairly good match, the coordinates were written down for future reference. In most cases

the values in the image headers were fairly accurate, but some fields benefited from having those values adjusted. All coordinates were obtained in the J2000.0 system although the coordinates in the image headers were for different epochs (1950 or the time of the observation, e.g., 1995.7). The J2000.0 system is used consistently in all remaining steps.

Essentially, the astrometric calibration process is simply one of coordinate transformation: given a set of points with known positions in one system that can be located in a second system, calculate how to transform between the two systems. This is often referred to as finding the plate solution. Obviously this must be done separately for each field we observed (each "plate" we have). For details about the process, see works on spherical astronomy such as Smart (1931) or Green (1985). IRAF's IMCOORDS package has tasks for making the all of the required calculations, greatly simplifying the amount of work required to determine the plate solutions. One important thing to note, however, is that a reference point is required for each field. Because our two dimensional images are projections of the three dimensional celestial sphere, this projection must be accounted for. Typically this is done by projecting the celestial sphere onto a tangent plane where the tangential point is the center of the image. However, we do not know the exact sky coordinates of the center of our field. So instead, we chose to use a star that is very close to the center of the field. We accessed the United States Naval Observatory (USNO) Flagstaff Station's Image and Catalog archive via the world wide web at http://www.nofs.navy.mil/data/fchpix/ to retrieve information from the USNO-B1.0 catalog. We started with a $30' \times 30'$ box and a magnitude range of $7 < m < 17$ in the R band centered on the coordinates determined above, then adjusted the size and/or magnitude range until the star

names were automatically printed on the output finder chart; the star IDs are only printed if 50 or less B1.0 catalog stars are in the chart. We then visually matched this with our field, selected a star that was very close to the center to act as the reference point, then wrote down its (α,δ) coordinates. Then we extracted a $30'$ radius and $7 < m < 17$ magnitude range in the R band list of stars from the catalog, saving their (α,δ) coordinates to a file for use with the IMCOORDS tasks.

We began the determination of the plate solution by running the task CCFIND on the lists of USNO-B1.0 stars in order to locate them in the fields. Required input parameters include the coordinate system used (J2000.0 here), x and y rotation of the field, the pixel scale, and the reference point's coordinates in both (α,δ) and (x,y). This produced a match file with the input (α,δ) coordinates and the located (x,y) pixel coordinates listed together. The output list of pixel coordinates can be marked on the images of the fields to check that the detections were made properly. We did this in the beginning in order to select the size and magnitude range parameters to use when extracting the star lists. The values we used do not cover the entire field, but it turns out that the detections are less accurate near the corners of the images anyway. By taking a $30'$ radius and omitting the corners we get a better calculated transformation. The chosen magnitude range is sufficiently faint to return a large number of stars, approximately 850 stars per field on average. Next, the CCMAP task was run to calculate the plate solution from the match file. Required parameters include the coordinate system used, the (α,δ) coordinates of the reference point, the type of projection ("tnx", briefly described below), the fitting geometry ("general" which allows a distortion term), the fitting function (polynomial), the orders (cubic in

all parameters), and type of cross terms ("half", the IRAF recommended type for higher order plate solutions). The calculated solution is placed in a database file. Finally, the CCSETWCS task was run to update the image header with a world coordinate system (WCS) determined from the plate solution stored in the database file and the match file. All the required parameters here are set using information in the input files and do not need to be set separately in the task parameters; the values from the input files would override them.

The WCS and plate solution can be tested using the STARFIND and CCTRAN tasks. We tested some solutions, but opted to skip the STARFIND step, instead using the pixel coordinate lists found by the CCMAP task. If the solutions we placed in the image headers were accurate and being used correctly, we should get the same (α,δ) coordinates that we started with. That was the case, but the results were not exactly identical which assured us that the computed solution was in fact being used properly and we didn't just get some simple reversal of the initial process that located the (x,y) coordinates using the (α,δ) coordinates. Once we have used the solution to set a WCS in the image headers, it is simple to calculate (α,δ) coordinates from the (x,y) coordinates of any galaxies and objects we detect by simply running lists of (x,y) through the CCTRAN task.

An additional note about the projection is necessary. IRAF allows for a variety of projections to be used with these tasks. We realized that given the large size of our fields ($\sim$1 deg^2) and their location (some as low as $\delta \sim -45°$) we would expect some distortion that a simple, linear tangent plane would not fit well. Therefore we decided to use what IRAF calls a "tnx" projection: a standard tangent plane projection plus a polynomial fit to the residuals. By accounting for the residuals in this manner, we are able to get a more accurate calibration than

the usual tangent plane projection alone would provide. This is a non-standard projection that may not be recognized outside of IRAF and certain specific tasks. This is not a problem because the coordinate transformations we need will all be performed in IRAF with tasks that do recognize and handle this projection.

3.2 Photometric Calibration

In order to be able to convert between the instrumental magnitudes that we measure on our images and real, R band magnitudes, we need to perform a photometric calibration. This involves measuring the instrumental magnitudes for a set of known, standard stars and using their known, real magnitudes to calculate the transformation between the two. We observed a number of different standard star fields throughout the course of each observing run for this purpose. The vast majority of our standard star fields came from Landolt (1992), primarily the Selected Area fields which contained many stars, but a few other fields containing fewer standard stars were also observed. A few fields from the E-regions of Graham (1982) were also observed. This process is done on a nightly basis in order to preserve any small changes in the calibration from night to night. Also, since our survey fields were observed over multiple nights and then combined together, it is important to know what the calibration is for each night.

The first step was to locate the standard stars in the fields. Lists of the stars' coordinates are easy to obtain. Since we had just completed the astrometric calibration, it was a simple matter to convert those (α,δ) coordinates to (x,y) pixel coordinates via the CCFIND task as before, using one of the standard stars near the center of the distribution as the tangential point for the projection. This is not necessarily near the center of the field. However, the standard star fields

are generally much smaller than our field of view and it is important to make sure the transformation is accurate near the stars. This might not happen if we chose the tangential point to be near the center of the field when most of the standard stars were off near one side of the image, for example. To make later steps simpler, the coordinate lists we passed to CCFIND here also included the star names and the R band magnitudes; these columns simply get passed along unchanged into the output. After CCFIND has created its match file as output, we copied the columns with the (x,y) coordinates into a separate file and then used the IRAF task TVMARK to mark them on a display of the standard star field. This was done to ensure that only standard stars that were detected properly go into the following steps. We removed from the list cases where the transformation got the wrong star (sometimes when two standard stars were very close, they would both get detected as one of the two stars), the detection didn't get a star (probably due to stellar proper motions), it was in between two stars and we couldn't tell which was the that should have been detected, or if it was on or very near a noticeably bad column in the frame. Some stars that were near bad columns, but appeared to be far enough away that we could measure their magnitudes well were left in.

The next step was to obtain instrumental magnitudes for the standard stars. We decided to use the IRAF task QPHOT for this. While there are other, more detailed tasks to do photometry, some initial trials with them determined that QPHOT works sufficiently well for our needs so we chose to use this simpler task rather than dealing with a more complex one that involved many more parameters and settings. The task also uses the exposure time from the image headers to normalize the computed magnitudes to 1 second. Since the standard

star fields were observed with different exposure times, this makes sure that the results have been normalized before we calculate the zeropoint. We ran QPHOT in non-interactive mode on all of the standard star fields using the files containing the (x,y) pixel coordinates created in the previous step as input telling the task where to make its measurements. We set the zmag parameter to zero to make sure we get instrumental magnitudes; this parameter identifies the zeropoint of the magnitude scale, but this is what we are trying to determine. Task parameters for defining where aperture photometry is performed include the radius of the aperture, determined by viewing radial profile plots of standard stars and selecting a value that should collect all of the stellar light (4 pixels), the inner radius of the sky annulus (5 pixels, to leave a small gap between sky and star), and the width of the sky annulus (also 5 pixels, giving about 4.7 times as many sky pixels as star pixels). The results of the photometry measurements are output to a file.

We are now in a position to calculate the zeropoint for each night. We chose to do this in a graphical manner, using the gplot plotting program (a driver for the PGPLOT package) which has some useful features including the ability to calculate statistics on a subset of the data read in. But first, all of the data we require must be placed into a single file to be read by gplot. Instrumental magnitudes and airmasses were extracted from the QPHOT output file, R band magnitudes were extracted from the match file created in the first step (locating standard stars with CCFIND), and these values were pasted into a new file. The calibration was obtained via the equation

$$m_{std} = m_{instr} - \xi - kX \tag{3.1}$$

where m_{std} is the known R band magnitude of the standard star, m_{instr} is the

measured instrumental magnitude of the standard star, ξ is the zeropoint of the magnitude scale, k is the atmospheric extinction coefficient, and X is the airmass. The value of k is variable with wavelength, but it is approximately constant (within a few hundredths) over the range of wavelengths our filters cover, about 5600–7300Å. Since we are using nearly square bandpass filters, a simple average of the highest and lowest wavelengths with at least 1% transmission locates the center at 6484Å. Within the IRAF distribution there is a file containing values of the atmospheric extinction coefficient that were taken from Stone & Baldwin (1983) and Baldwin & Stone (1984); by performing a linear interpolation between the two values around the point we found for the center of our filter, we find $k = 0.1047$. If we instead use a weighted average, weighting the wavelengths by the transmission percentage, we find the center to be at 6454Å resulting in an interpolated value for k of 0.1080. During the May 1996 observing run, Greg Aldering determined $k = 0.0867$. In a few cases we had enough observations of standard star fields at a large enough range in airmass to calculate a slope and thus a value for k. Because the standard star fields were observed over a range of airmasses, the plots generally show small clumps of points when we plot the uncorrected zeropoint $m_{std} - m_{instr}$ of the standard stars vs. airmass X. We then selected a range in airmass for each clump and used gplot's statistics output option to determine the median zeropoint at the median airmass of the clump; these values are all stored in a separate file. Using these median values, we found that k typically ranged from 0.12–0.16. As this will be a relatively small correction compared to the difference between the R band and instrumental magnitudes, we adopt $k = 0.1$.

As an example of this procedure, one of the nights where we could calculate a

slope from the data is shown in Figure 3.1. This is night 3 from the August 1996 observing run where the standard stars spanned a range in airmass of $1.04 < X < 1.51$. Performing a simple linear regression fit to all points results in a slope of -0.10, the value we adopted above. As k in Equation 3.1 is defined to be negative, this is $k = 0.1$. We also calculated the median zeropoint for each clump of points and have included these on the plot as filled diamonds; the slight offset in X from the individual points is from rounding the value of the airmass. When we fit these median values we obtain a slope of -0.13 for the points with $X < 1.3$ and a slope of -0.15 for all points. In addition we plot the nightly zeropoints in Figure 3.2 to check how consistent the zeropoint is throughout each run. Here we have simply assigned a running index to each night in each observing run. Observing run 1 is points 1–7, run 2 is 8–19, run 3 is 20–27, run 4 is 28–38, and run 5 is 39–49. All of the zeropoints have been calculated for an airmass $X = 1.0$ and the value is quite consistent from night to night. In fact, over the first four observing runs which spanned almost one year (September 1995 to August 1996), the value is nearly constant — the median value is 20.40 with a standard deviation of only 0.014. The maximum and minimum values for this period spanned only 0.05 mag. The fifth observing run also has an essentially constant zeropoint, but its value is noticeably different from the previous runs. While a variety of factors could affect the zeropoint calibration, air transparency or dust for example, this change is more likely due to a slightly different filter being used in this run. As described in Chapter 2, this is the first run where we used the "VLSBG R" filter that was designed to mimic the original Harvard R filter used earlier in the survey.

In order to apply the calibration to our fields, we first need the zeropoint at the airmass of each field. This was obtained by simply taking the point calculated

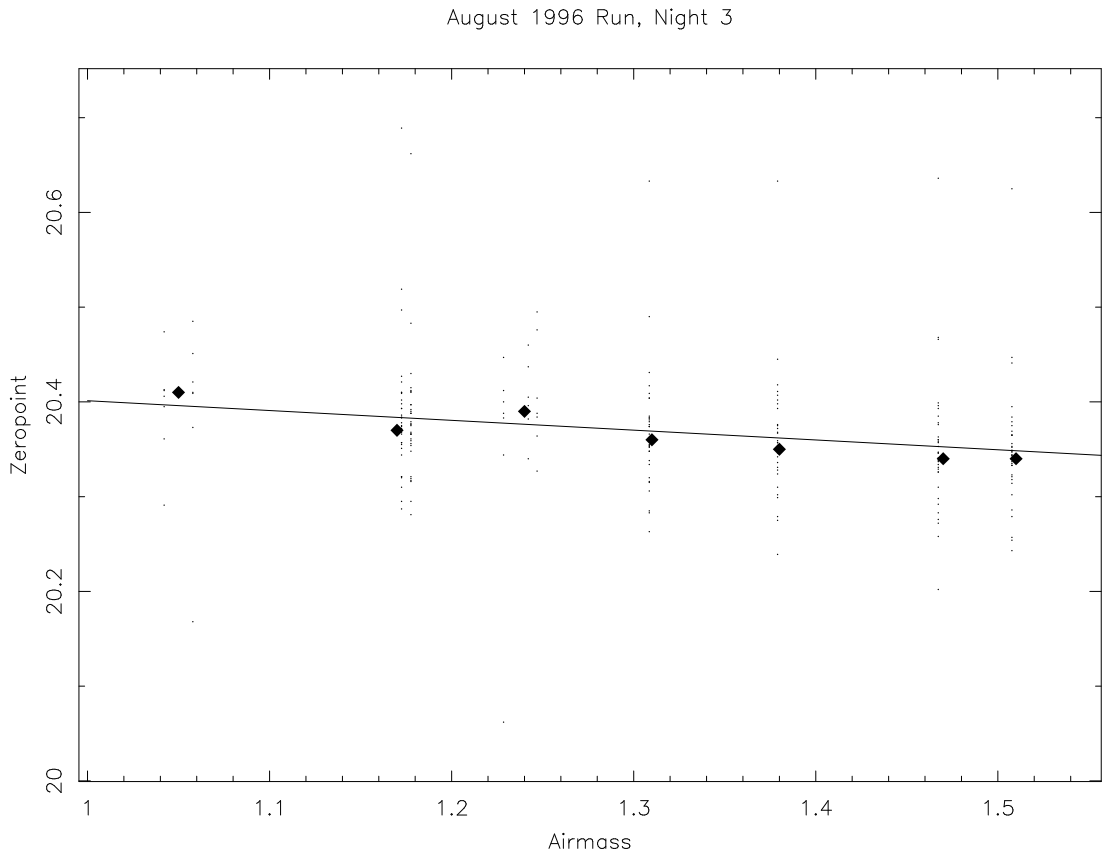

Figure 3.1: Plot of zeropoint vs. airmass for night 3 of the August 1996 observing run. Solid diamonds are rounded, median values for each clump of points. A linear regression fit to all points gives a slope of -0.10, our adopted value, and this line is drawn on the plot. Fitting the median values for clumps of points with airmass $X < 1.3$ gives a slope of -0.13 while using the median values for all seven clumps of points gives -0.15.

above with the airmass closest to that of the survey field (an airmass value for each field is present in the image headers) and the known slope of the line through that point (the coefficient k) to calculate the zeropoint for another airmass. These extrapolations are small, typically involving differences in airmass of only about

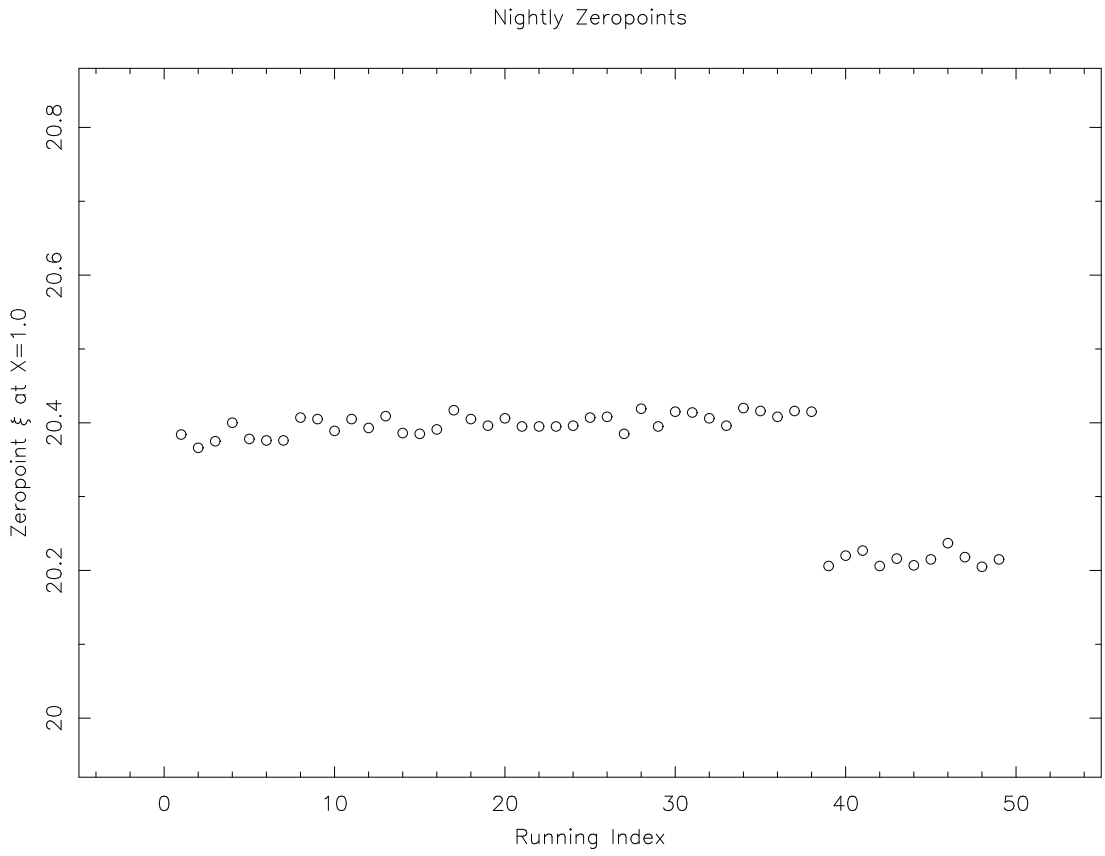

Figure 3.2: Plot of nightly zeropoints at airmass $X = 1.0$ against running index number. Observing run 1 is points 1–7, run 2 is 8–19, run 3 is 20–27, run 4 is 28–38, and run 5 is 39–49. The change of filter for run 5 is the likely explanation for the change in zeropoint.

0.1, producing small (± 0.01) changes in the zeropoint values. Now having values applicable to each survey field, we checked the values for the nights that were combined together to produce each final survey image. The values do vary from night to night, but the differences are typically no more than 0.03. Since they are so close together, we chose to take a simple weighted mean to determine the zeropoint for each field, weighting the zeropoint from each night included by

the number of observations of the field made on that night. Once these final, combined zeropoints are calculated, the photometric calibration is done and we can convert between instrumental magnitudes and R band magnitudes. The zeropoint values are written into the image headers for future reference and are given in Table 3.1 where the fields are ordered numerically by observing run the same as in Table 2.1; the two unusable fields are omitted as are two fields that were observed more times on other observing runs since we will not be using these duplicate observations.

However, there were a few concerns that needed to be addressed during the photometric calibration. The final nights of the September 1995 (night 14) and May 1996 (night 10) observing runs had no standard star field observations, but good images of survey fields were obtained on these nights. In both cases the measured zeropoint is quite constant over the last few nights of the run (see Figure 3.2 above). Therefore, we adopted the zeropoint value from the previous nights for use on the final nights of these two runs. Night 6 of the September 1995 observing run originally had a calculated zeropoint of ~ 19.9, very different from the ~ 20.4 of the other nights. Checking the observing log, we found a note that indicated cirrus clouds were present on that night and decided that this must be the cause of the problem. As this entire night was affected by cirrus, no images from this night were used in calculating a zeropoint or creating combined survey fields.

Table 3.1: Photometric Zeropoint of Each Field

LCRS Field	Zeropoint	LCRS Field	Zeropoint	LCRS Field	Zeropoint
0020-39a	20.36	0020-45a	20.37	0100-39a	20.38
0100-39b	20.37	0220-39a	20.37	0300-39a	20.37
2140-45a	20.36	2140-45b	20.37	2220-39a	20.35
2220-39b	20.38	2300-39a	20.36	2320-42a	20.34
2340-39a	20.38				
1003-03:E	20.38	1003-06:E	20.38	1027-03:E	20.38
1051-12:W	20.40	1139-03:E	20.38	1139-12:W	20.40
1151-12:E	20.39	1215-12:E	20.39	1239-12:E	20.39
1403-03:W	20.38				
1015-12:E	20.39	1039-03:W	20.37	1051-12:E	20.39
1127-03:E	20.38	1227-12:E	20.40	1303-12:W	20.38
1339-03:E	20.38	1351-03:W	20.37	1415-03:W	20.38
1439-12:W	20.37	1516-03:H	20.38	2155-45:W	20.37
0035-45:W	20.41	0100-45:W	20.42	0154-39:M	20.41
0154-39:W	20.41	0155-45:E	20.40	0234-39:W	20.41
0235-45:E	20.40	2100-45:E	20.40	2114-39:E	20.35
2115-45:E	20.41	2154-39:E	20.38	2154-39:M	20.39
2154-39:W	20.37	2155-45:E	20.40	2234-39:E	20.41
2234-39:W	20.41	2314-39:E	20.41	2314-39:M	20.41
2315-45:E	20.41	2315-45:W	20.40	2354-39:M	20.41
2354-39:W	20.41	2355-45:E	20.40	2355-45:M	20.39
1032-06:S	20.19	1036-06:S	20.20	1040-06:S	20.20
1044-06:S	20.19	1048-06:S	20.20	1052-06:S	20.22
1056-06:S	20.19	1100-06:S	20.21	1104-06:S	20.21
1108-06:S	20.20	1112-06:S	20.21	1203-12:E	20.22
1427-06:W	20.19	1439-03:E	20.20	1439-03:M	20.20
1439-06:H	20.20	1451-06:H	20.20	1503-03:M	20.19
1503-03:W	20.20	1515-03:W	20.21		

Chapter 4

Data Analysis

The data analysis requires two primary steps: detecting objects in the images and then fitting them with a galaxy model. These steps were performed using the SExtractor (Source Extractor) program by Bertin & Arnouts (1996) and the GIM2D package for IRAF by Simard et al. (2002). In order to fit only objects that were more likely to be galaxies than stars, a star/galaxy separation step was performed in between the detection and fitting steps.

4.1 Detection of Objects

There are a variety of methods available for automatically detecting objects on astronomical images. After examining some of the options, we decided to use the SExtractor program for this step. Some of the advantages of this program are that it was designed to process large images in batch mode, specifically large amounts of survey data, and it was designed to be both quick and robust in its detection of objects of all shapes and sizes. It is therefore well suited to our needs for this survey. We downloaded, compiled, and locally installed version 2.3 released on 20 May 2003.

As Bertin & Arnouts (1996) describe in detail, SExtractor operates in the following manner: it estimates the sky background, detects objects via thresholding, deblends merged detections, filters the detections, performs photometry, and performs a star/galaxy separation. The user's manual by Bertin (2003) and the handbook by Holwerda (2003) are other useful references that describe how the program operates. The sky background is estimated for each mesh in a grid covering the entire image by a method that combines sigma clipping and estimating the mode of the distribution. Detection is done via thresholding, selecting objects with some minimum number of connected pixels above some minimum threshold; a filter can be applied here to smooth the image and help detect lower surface brightness objects. Deblending uses a multiple isophotal analysis technique to model the light distribution in the form of a tree structure after which the algorithm traces down the tree (towards the trunk) deciding if each branch should be considered a separate component. There is also an option to turn on cleaning, a step that checks to see if a detection would be made if there were no neighboring objects. Photometry can be performed according to a number of algorithms including isophotal, corrected isophotal (assuming a symmetric Gaussian profile to correct for flux contained in the wings of the profile), adaptive aperture using ellipses as described by Kron (1980), and fixed aperture sizes. The star/galaxy separation is performed according to the program's neural network classification scheme.

To run the program, a number of files are required — one each for the configuration, parameters, filter, and neural network. A variety of example files are included in the software package. The configuration file contains all of the required input parameters for the program, the parameters file contains a list of

the desired output parameters, the filter file contains a convolution mask used for filtering detections, and the neural network file contains neural network weights used in star/galaxy classification. As the star/galaxy separation scheme becomes less accurate at fainter magnitudes, it is unreliable and we do not use these automatic classifications for our separation. For filtering, we examined the provided sample filters, the small pyramidal function which is the default, Gaussian, Mexican hat, and top hat, as well as a more galaxy-like filter with a shallower profile than the default suggested by Greg Aldering. While the choice of filter does have some effect on the results, we saw no obvious difference in the list of detections that would make one choice clearly better than another. Therefore we decided to use the galaxy-like filter since it should more closely match the profiles of the objects we are interested in finding unlike, for example, the default filter which is designed to detect point sources.

The parameters file was set to output the five values that we would require in the following step — the detected object's x and y positions, the background value at the centroid position, the standard deviation of the background, and the isophotal area of the detected object. Also output for use in star/galaxy separation are MAG_AUTO, the magnitudes measured with adaptive ellipses as in Kron (1980), the half light radius (FLUX_RADIUS with a value of 0.5 for PHOT_FLUXFRAC in the input configuration file), an aperture magnitude using a 2 pixel diameter, and the internal flags calculated by SExtractor which note any possible problems with the detections. The parameter MU_THRESHOLD, the surface brightness corresponding to the threshold, was also output so that we could examine these values. The standard deviation of the background that we require is not a standard output option in SExtractor. The GIM2D package

is able to automatically recalculate the value of the background and its standard deviation though so as long as the values here are non-negative, we will not have trouble. We thus chose to output SExtractor's stellarity index, the result of the neural network's star/galaxy separation, in place of the standard deviation of the background. A segmentation image, one that identifies each pixel as belonging to a certain object or the background sky, is also required, but this option is set as part of the configuration file and input parameters. As the configuration file has the most parameters that need to be set, our choices there will be outlined in some detail.

The configuration file requires information in a few different categories. For image information, it needs the gain of the CCD, the zeropoint of the magnitude scale, and the saturation level of the CCD. The gain is the effective gain which for our average combined images is $2.1N$ where 2.1 is the gain of a single image and N is the number of images combined (Davis 1994). The zeropoint of the magnitude scale is also an effective value meaning the exposure time must be accounted for. Since we calculated zeropoints that were uncorrected for exposure time, we must add $2.5 \log t$ to those values before giving them to SExtractor. For our $t = 500$ s average combined images, this requires adding 6.75 to the previously calculated zeropoints. The saturation level is the maximum good data value and was set to 38000 ADU, the value being determined by examining some of the images. The CCD does not actually saturate until approximately 65000 ADU, but the linearity starts to roll off severely at approximately 40000 ADU (Walker 1995). When we plotted the radial profiles of some of the brighter stars in the images with the IRAF IMEXAMINE task, we saw that the brightest points that were not saturated had values of approximately 38000 ADU, therefore we used

this value for the saturation level. However, for the case of LSB galaxies, this is not particularly important. Under the background category, we set the size of the background mesh to a 128×128 pixel square, the maximum suggested value, which resulted in a fairly smoothed map that still picks up smaller scale variations. The background filter size was set to 3, the default value. We also allow the background to be recalculated locally in later steps using an annulus 8 pixels thick to match the DAOPHOT package's suggested value of approximately 4*FWHM. The detection and analysis thresholds were set to 3σ and the minimum number of pixels required was 10. We also examined the results using a minimum size of 5 pixels. This detects more objects, but they typically appeared to be small stars so we chose to use the larger value. The galaxy-like filter we selected is applied before detecting objects and spurious detections are cleaned with an efficiency of 1.0; suggested values are 0.1–10 with lower meaning the object has brighter wings and more aggressive cleaning is required; 1.0 performed well for us. Choosing the deblending parameters was difficult because it was essentially impossible to get it to perform perfectly so we had to decide upon what appeared to be working the best, correctly deblending most multiple objects while not incorrectly separating single objects into multiple ones. After testing various values of the parameters, we eventually choose to set the number of deblending thresholds to 32, the default value and the user manual's suggested value, and the minimum contrast parameter to 0.001, the minimum value suggested in the user's manual. There are parameters for the photometry and star/galaxy classification as well. While we do not use these as final values, it is important to set them to appropriate values since we will use the magnitudes when performing star/galaxy separation. The method of masking neighbors for photometry was set to "CORRECT" which

replaces affected pixels by values of pixels symmetric with respect to the source center; this is the default option. Aperture magnitudes were set to be measured with a 2 pixel diameter, parameters affecting the measurement of MAG_AUTO were left at their default values which the handbook by Holwerda (2003) says are probably the best, and PHOT_FLUXFRAC was set to 0.5 in order to get the half light radius with the output parameter FLUX_RADIUS. For the automatic star/galaxy separation, we set the pixel scale to 2.028″/pixel.

Once all of the parameters and files are set, we are ready to run SExtractor on our fields. In order to simplify this, a simple UNIX shell script was created to run SExtractor on all of the survey fields. Parameters that changed for each field were put on the command line. These included the name of the output catalog, the effective gain of the image, the effective zeropoint of the magnitude scale, the seeing FWHM, and the name of the segmentation image. When complete, we have the information we need to fit the detections with GIM2D, but first a star/galaxy separation must be performed in order to shorten the lists of detections. We also have a measure of the limiting surface brightness for our detections. While the value of MU_THRESHOLD does vary between fields and even for individual objects within each field, it is relatively constant (see Figure 4.1). We therefore take the median of the median values for each field and determine that $\mu_\ell = 25.43$ R mag arcsec^{-2} with a standard deviation of 0.13 for the 3σ threshold we set. A quick check shows that the limit for a 1σ detection threshold is $\mu_\ell \approx 26.6$ R mag arcsec^{-2} which is roughly the limit the survey was designed to reach (27 R mag arcsec^{-2}). Therefore in order to detect galaxies with the lowest surface brightness possible, future work will need to run with a detection threshold of approximately 1σ. We compared the background measure-

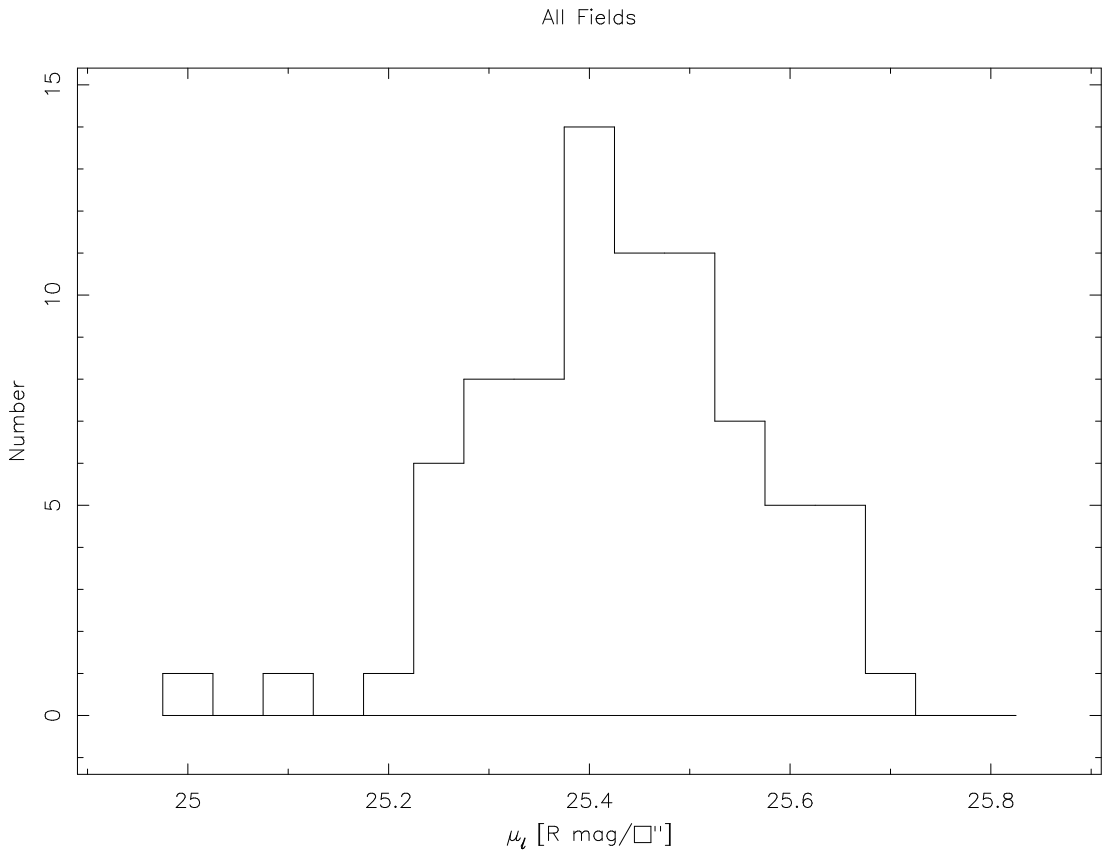

Figure 4.1: Histogram plot showing the distribution of the limiting surface brightness for all fields in the survey.

ments made by the SExtractor program for a few fields with the results of the IRAF IMSTATISTICS task run on the full field and in a small, relatively clean region of the image using 3σ clipping and iterated, if necessary, a maximum of 10 times. The results for the background values are quite consistent, varying by about 1–2 counts or roughly 0.3% for values around 800 counts. The errors in these measurements showed a bit more variation. The full field measurement with IMSTATISTICS had the highest standard deviation, roughly 1.5 counts higher than the SExtractor RMS error which in turn was roughly 1.5 counts higher than

the IMSTATISTICS standard deviation measured in a relatively clean area of the image. For example, a randomly chosen field, LCRS 1339-03:E, had values of 7.74, 6.24, and 4.60, respectively. This suggests that the presence of objects in the images may be affecting the threshold value measured by SExtractor, raising it above the true value. It is also possible that the intended limit was not reached at the 3σ level due to the variation in the sky across the field. The goal was to reach a 0.1% level of flatness, but as described in Chapter 2 the average value for the median variation in the fields was measured to be approximately 0.4%, about 4 times higher than the expected level. We expect that this is at least partially due to scattered light from the stars in the images because we see noticeable halos around the brighter stars.

4.2 Star/Galaxy Separation and Catalog Trimming

Star/Galaxy separation is a difficult task — at fainter magnitudes, it becomes increasingly more difficult to make an accurate distinction. Since we have performed a large survey, it is not possible for us to inspect every detection by eye to decide which ones to fit. We need some diagnostic on which to base our cuts.

However, before we begin, we note that the detections will cover the entire survey field, but because we dithered our images, the edges and corners of the combined field will not have information from all of the input fields. The data here will not be as reliable as that near the center of the field which includes information from all input images. Therefore we want to exclude detections near the edges of the combined frames from the following analysis. Since we started

with images that were 2048×2048 pixels, we decided to trim the detection list to only include objects within a 2048×2048 pixel square centered on the image center. It is possible that this also removes some good data, but we chose to be conservative. The image centers are determined by displaying the images in IRAF and using the display program's control panel to read off the coordinates of the center and then the x and y coordinates 1024 pixels greater than and less than that were calculated. To be included, objects must be within this range in both x and y. Then a simple UNIX script called trimedge was written that calls the UNIX program awk to check the (x,y) position columns in the catalog, printing out only the lines that meet our requirements. The output from this script is then placed into a new file and it is this trimmed catalog that is used in future steps. Combining all of the individual fields' catalogs into a single file for use in star/galaxy separation, this results in approximately 462000 objects.

For the star/galaxy separation, we examined a number of possible options and decided to use two plots as the basis of our separation: magnitude vs. isophotal area and a 2 pixel diameter aperture magnitude vs. magnitude. We obtain all of these values from SExtractor, "magnitude" refers to the MAG_AUTO values, and the 2 pixel diameter aperture magnitude will be referred to as the core magnitude. As extended objects, we expect that galaxies will be larger than stars at a given magnitude, allowing us to separate them in the mag–area plot. The ratio of the core magnitude to the (total) magnitude is a representation of the concentration of the object and this particular plot will be referred to as the concentration plot. As such, we expect the stars to be much more highly concentrated than the galaxies, also allowing us to separate them in this space.

Our first plots show that the stars and galaxies do separate into different

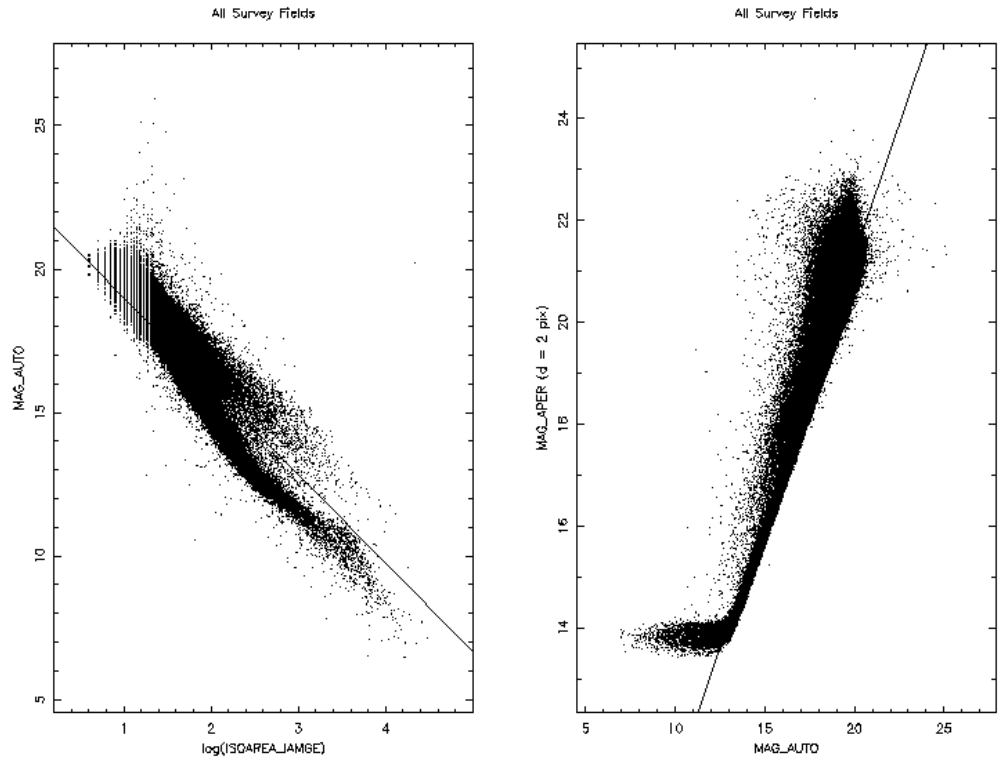

Figure 4.2: Mag–area and concentration plots used for star/galaxy separation with initial lines for cuts.

populations on these two plots as we expect as illustrated in Figure 4.2. In the mag–area plot, the stars tend to lie in the lower branch while the galaxies tend to lie in the upper branch where they are larger for a given magnitude than the objects in the lower branch. In the concentration plot, the stars tend to lie along the diagonal line (and smaller horizontal line at the bottom) while the galaxies which are less concentrated tend to fill up a larger space. The lines drawn on each plot were estimated by eye as a separation between the two populations. In the mag–area plot it was drawn to remove all of the stellar branch in the region

Table 4.1: SExtractor Internal Flags

Value	Meaning
1	Object has close neighbors that significantly bias MAG_AUTO or more than 10% of the integrated area is affected by bad pixels.
2	Object was originally blended with another.
4	At least one pixel is (close to) saturated.
8	Object is truncated (too close to image boundary).
16	Aperture data are incomplete/corrupted.
32	Isophotal data are incomplete/corrupted.
64	Memory overflow occurred during deblending.
128	Memory overflow occurred during extraction.

where the separation is visible. In the concentration plot it was drawn to lie along the left edge of the lower part of the diagonal stellar band since very few objects fall away from that band in this region of the plot. It was also drawn to approximately parallel the right edge of the band which is very clear. The fact that both plots separate out as we expected serves as confirmation that these are suitable for performing star/galaxy separation.

We examined the internal flags calculated by SExtractor for every detection since these are always computed and indicate any possible problems SExtractor encountered. These values and a summary of their meanings as given in the manual (Bertin 2003) are presented in Table 4.1. If multiple problems exist, the individual flag numbers are added together to obtain the final flag value. We first tried taking only objects that had no problems and were unflagged (a flag value of zero) and making the same plots as before, but this removed far too many detections, many of which were clearly located in the galaxy branch of the

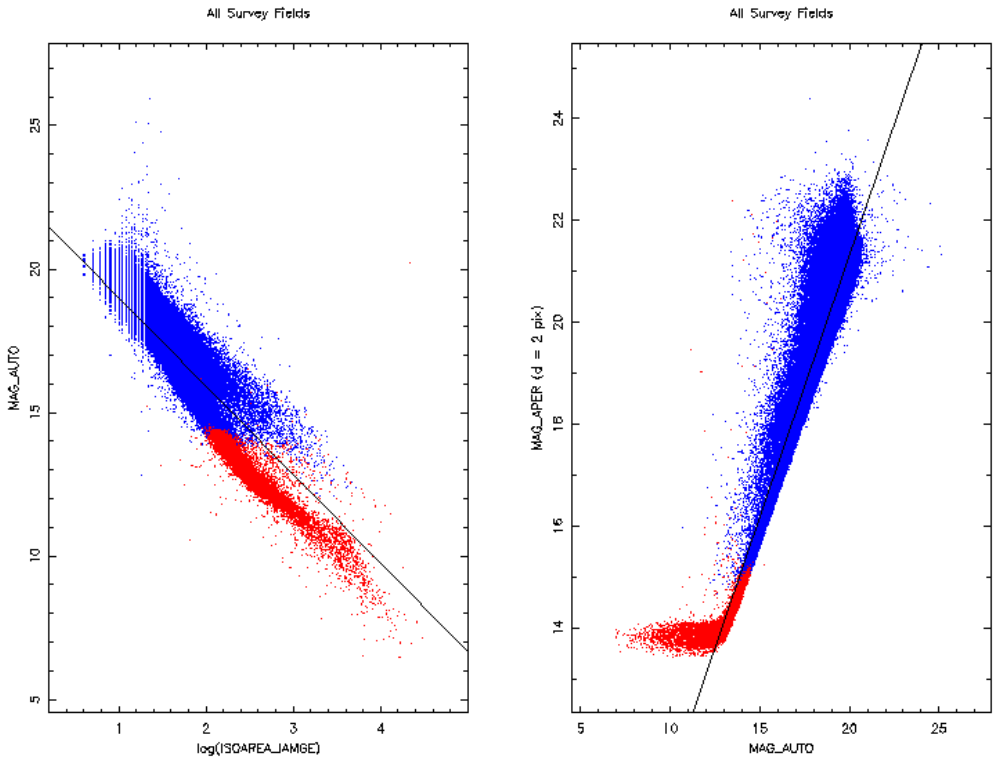

Figure 4.3: Mag–area and concentration plots for star/galaxy separation where blue points have FLAGS < 4 and red points have FLAGS ≥ 4.

plots. We then tried making the cut at FLAGS < 4. A value of 4 or above means the object is saturated or worse. This cut performs well, covering the lowest end of the star branch in both plots as shown in Figure 4.3 where the blue points have FLAGS < 4 and the red points have FLAGS ≥ 4. The lines are the same as those in Figure 4.2. This removes many of the objects that are clearly stars, e.g., because they are saturated, and this becomes our first cut on the catalogs.

Next we examined the half light radius of the objects. We expect that any object with a small half light radius, 1 pixel or less, is unresolved and most likely

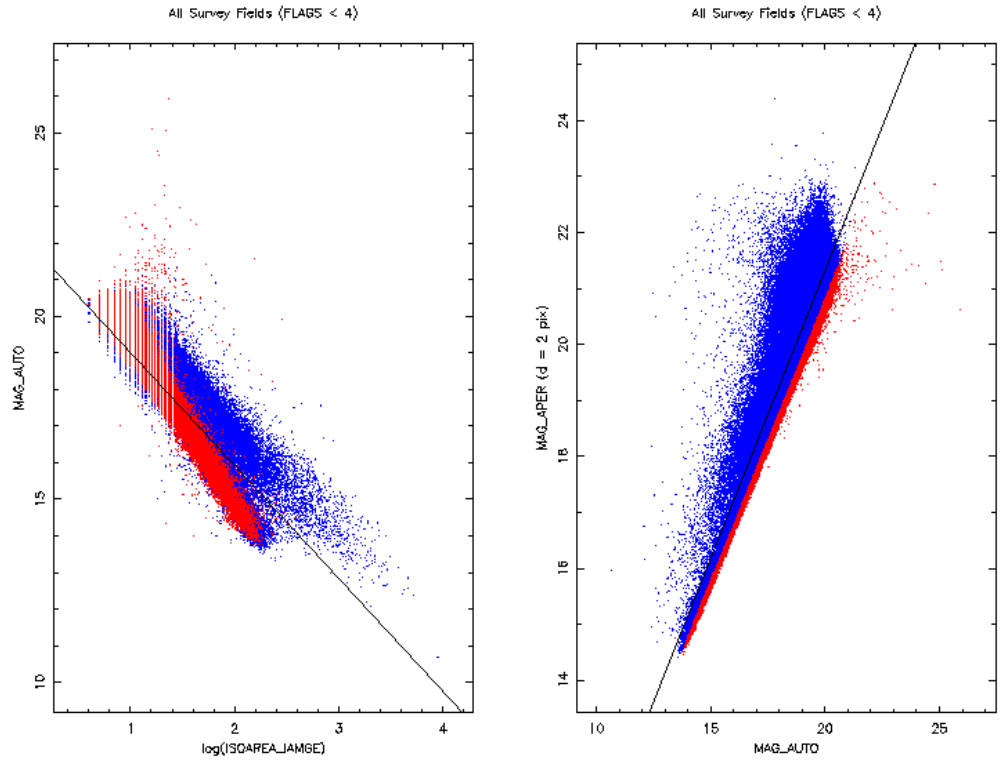

Figure 4.4: Mag–area and concentration plots for star/galaxy separation where blue points have $r_{half} > 1$ and red points have $r_{half} \leq 1$. Points with FLAGS $\geq$ 4 have been removed.

a star. We created the same plots as before, but this time colored points with $r_{half} > 1$ in blue and points with $r_{half} \leq 1$ in red. These plots are shown in Figure 4.4 and the objects with FLAGS ≥ 4 have already been removed from these plots. It is clear that the vast majority of the red points lie along the stellar branch in each of these plots, and in a different region of the branch than the first cut on the SExtractor flags, so we conclude that it is safe to cut these objects from our catalogs. Different values of r_{half} were examined for this cut,

but using a fraction of a pixel only would have removed fewer objects while using a larger value, for example 2 pixels, would have included objects in the galaxy branch of the plots. Therefore we use $r_{half} = 1$ as the dividing line for the cut.

Now we check the dividing lines we estimated on the original plots. The stellar branch in the concentration plot has not been affected very much and so our line there is still a good estimate of where the cut should be made. We use this line which has the equation

$$\text{MAG\_APER (d = 2 pix)} = 1.03\text{MAG\_AUTO} + 0.77 \tag{4.1}$$

for the cut in this plane. In the mag–area plot though, the lower portion of the stellar branch, at bright magnitudes and large sizes, is now gone. Our original line was estimated to remove all of these points, but our first cuts, primarily the one on the SExtractor FLAGS parameter, has done this already. Therefore we can now adjust our line in the mag–area plot to more closely fit the separation in the fainter magnitude, smaller size area of the plot. Using the red points where $r_{half} \leq 1$ and the region where the stellar and galaxy branches are still noticeably separated as a guide, we estimate a new line for the cut in this plane. This is illustrated in Figure 4.5 which is the same as the left hand plot of Figure 4.4, but with the new line in place of the old one. The equation for this line is

$$\text{MAG\_AUTO} = -4.375 \log \text{ISOAREA\_IMAGE} + 24.625 \tag{4.2}$$

and this is the line that we use to perform the cut in this plane.

When we make one of these two cuts and plot the remaining objects in the other plane (e.g., cut on the concentration plot line, plot the results in the mag–area plane) we see that many objects are left below the cut line in this plane. Therefore we apply both cuts to the catalogs in order to remove as many star-

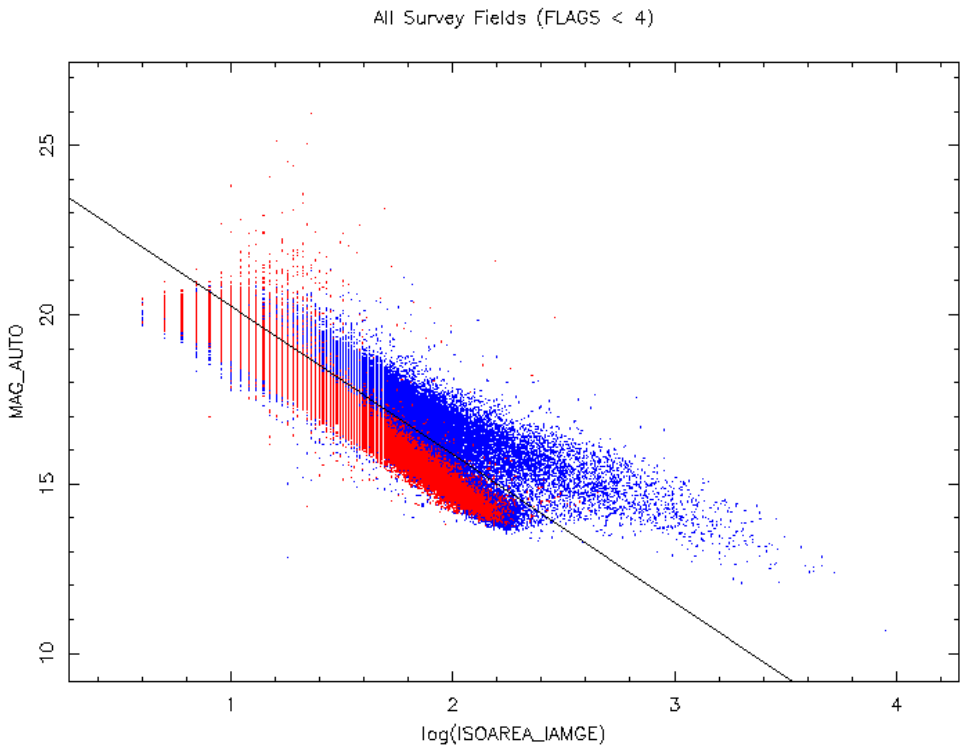

Figure 4.5: Mag–area plot for star/galaxy separation where blue points have $r_{half} > 1$ and red points have $r_{half} \leq 1$. This line has been revised from the initial line to perform a better cut in the fainter magnitude, smaller area region of the plot once the FLAGS ≥ 4 cut has removed most of the brighter magnitude, larger area region of the stellar branch.

like objects as possible. By performing all of these cuts on the edge trimmed catalogs — removing objects with FLAGS ≥ 4 which have at least one pixel (nearly) saturated or worse, $r_{half} \leq 1$ which are effectively unresolved, or fall below the two cut lines we drew in the mag–area and concentration plots — we bring the list of detections down to approximately 64000 objects and have

increased the chance that these are galaxies rather than stars. As no cut will be perfect, particularly at faint magnitudes, it is possible that we have cut out some galaxies and included some stars, but this is unavoidable. However, any galaxies that are lost in this process are small and probably lie at high redshifts. Such galaxies are not relevant for our study which is designed to detect very LSB galaxies in the local universe.

4.3 Fitting the Detections

As with the detection of objects, there are various methods available for fitting the detections. After examining some of them, we chose to use the GIM2D package for IRAF. This package was designed to perform bulge/disk decompositions on low signal-to-noise images of distant galaxies. We do not know how distant the objects we detect are, but we are searching for LSB galaxies which are generally low signal-to-noise objects making this package suitable for our needs. It was also a natural choice to use since it takes as input the output from SExtractor, the program we chose to use for detecting objects. We downloaded, compiled, and locally installed the latest version, 2.2.1 released in March 2001.

4.3.1 Determining Point Spread Functions

While SExtractor provides the majority of the information we need to run GIM2D on our detections, an important piece is not automatically provided — the point spread function (PSF) at the location of each detection. Therefore, we use IRAF's DAOPHOT package to create PSFs for the image. While we could create separate PSFs at the location of each detection using the (x,y) coordinates output from

SExtractor, it is somewhat easier to do this after setting up the fitting with GIM2D so this will be described at the appropriate point later.

Before running any tasks however, we must set the parameters for them. They are located in the parameter set tasks DAOPARS, DATAPARS, FINDPARS, FITSKYPARS, CENTERPARS, and PHOTPARS. Most values will be able to remain constant, but some important ones that vary are: the minimum good data value in DATAPARS which was set to 7σ below the background sky following the suggestion of Davis (1994); the FWHM of the PSF in DATAPARS which was set to the values previously determined using DIFIMPHOT's GETPSFS task (since this is normally around 1.5–2.0 any other FWHM dependent parameters can remain constant to simplify things and this will not cause problems); the standard deviation of the background in DATAPARS which was determined by running IMSTATISTICS with 3σ clipping iteratively (15 times is more than enough for it to converge); the zeropoint of the magnitude scale in PHOTPARS which is set to the previously determined zeropoints uncorrected for exposure time (the tasks will do this correction). The psfrad parameter in DAOPARS need not be variable and we choose to make it a constant. But it is important to choose an appropriate value because this sets the size of the resulting PSFs. We set this to a radius of 7 pixels following a DAOPHOT guide that says, "this radius should equal the radius at which the radial profile of the brightest star of interest disappears into the noise" (Davis 1994, §6.10.7). We performed tests on a few fields and found that this radius typically varied from about 4–6 pixels for most stars that do not appear to be saturated or partially so, brighter stars tending to have a larger radius than fainter stars. We decided that a 5 pixel radius may not be sufficiently large in all cases while using a 9 pixel radius was probably too large

given that the LSB galaxies we are interested in should not be bright enough to require PSFs that fit the brighter stars that well. Since user guides recommend making this value an odd integer, 7 pixels was the most suitable value here.

Other relevant parameters in these parameter sets include the following. In DAOPARS: the form of the analytic component of the PSF model was set to be Gaussian, the order of the empirical component of the PSF model was set to 2 (quadratic) because the PSF does vary across the field, the fitting radius was set to 3 pixels following a DAOPHOT guide's recommendation. In DATAPARS: the image scale was set to 1 so that we work in pixels, the maximum good data value was set to 38000 ADU as before, the noise model was set to be Poisson, and the image header keywords for the effective readout noise, effective gain, exposure time, airmass, filter, and observation time were set to the appropriate values. The FINDTHRESH task in the NPROTO package was used to calculate the effective readout noise and effective gain given the number of images combined (N), the readout noise and gain for a single image, and the type of combination. As described in Davis (1994), for our average combined images, the equations are:

$$\text{effective gain} = N * \text{gain} \tag{4.3}$$

and

$$\text{effective readout noise} = \sqrt{N} * \text{readout noise} \tag{4.4}$$

As the default values of gain and readout noise in the image headers are for a single image, the effective values were added under the keywords EFFGAIN and EFFRON. In FINDPARS: the threshold for feature detection was 3σ. In FITSKYPARS: the sky was fit using the mode of the distribution, the sky annulus had an inner radius of 8 pixels (1 more than the PSF size to leave a gap) and

width of 8 pixels, with 3σ clipping high and low and 10 iterations maximum. In CENTERPARS: no centering was applied since DAOFIND was already run to determine center positions. In PHOTPARS: weighting was constant.

With all the relevant parameters set, we can run the usual sequence of DAOPHOT tasks — DAOFIND to locate stars in the images, PHOT to do photometry on them, PSTSELECT to choose which stars to use for determining the PSF, and PSF to create the PSF. A number of files are created during this process and most of it is performed automatically, using default file names and parameter values, the relevant ones being set in the parameter sets already. An important step here that required manual checking was the selection of which stars to use in the calculation of the PSF. The PSTSELECT task chose a maximum of 200 stars to use for calculating the PSF, but the PSF task was run in interactive mode to check these automatic choices. Stars that had nearby faint neighbors, looked to be galaxies instead of stars, or were located on or near a bad column were removed. The rejection was done primarily based on radial profile plots, but mesh and/or contour plots were also used as checks. Typically this resulted in removing approximately 30 objects. After the PSF was created, we tested it by using the NSTAR task to fit the model to the PSF stars and neighbors then subtracting them from the image using the SUBSTAR task. While not perfect, residuals were present, many initial trials indicated that the stars were subtracted out fairly well, at least when they were not saturated or very large. We chose not to remove stars using this procedure because the residuals that were left behind could still be found if we were to rerun SExtractor which would not improve the detection process. In addition, the very bright, saturated stars have such strong residuals that SExtractor could end up detecting multiple objects in place

of one. This would cause problems in the star/galaxy separation stage because these multiple objects would have inaccurate parameters making it very difficult to know if we had separated them out properly. After performing these steps on each survey field, we have the required PSF models.

4.3.2 Fitting Models to the Detections

A detailed description of the GIM2D package can be found in Simard et al. (2002), but to summarize, using the output of SExtractor objects are detected in the image, deblended using the segmentation image, and each one is extracted to a thumbnail or "postage stamp" image. With the PSF at the location of each detection, the objects are fit with a 12 parameter bulge/disk galaxy model that the user can select using a Metropolis fitting algorithm (Metropolis et al. 1953). The parameters are total flux in ADU (L_{tot}), bulge fraction (B/T), bulge effective radius in pixels (r_e), bulge ellipticity ($e \equiv 1 - b/a$ where a and b are the semi-major and semi-minor axes, respectively), bulge position angle in degrees (ϕ_b), exponential disk scale length in pixels (r_d), disk inclination in degrees (i), disk position angle in degrees (ϕ_d), sub-pixel x offset of the galaxy center in pixels (dx), sub-pixel y offset of the galaxy center in pixels (dy), background residual level in ADU (db), and exponential power index (n as in $r^{1/n}$). As noted in Simard et al. (2002), this 12 dimensional parameter space can be very complicated with local minima and so it is important that the fitting algorithm used not be fooled by such local minima. The Metropolis algorithm was designed for use in complicated parameter spaces and why the author chose it for this package. However, not being fooled by local minima comes at the expense of computing time; it is not a fast algorithm.

Following the cookbook by Tran (2000) we have already completed many of the initial steps since SExtractor has already been run on all fields and the required output obtained. The catalog file output by SExtractor needs to be renamed to have a .gfxt extension for GIM2D and must contain in the first five columns the x and y positions of the detected objects, the background value at the centroid positions, the standard deviation of the background, and the isophotal area of the detected object. As noted in the SExtractor section, since GIM2D will recalculate the background, any non-negative values can be used for the standard deviation of the background and we passed the star/galaxy classifier's stellarity index through in this column. Additional columns may be included if the user desires; they will not affect the operation of GIM2D tasks.

Parameters for the GIMFIT2D task must then be edited. The ones that must be set are the name of the parameter value file, if parameters are determined from input image moments (yes), if the input image should be symmetrized (no), if the background parameters should be recomputed (yes), the PSF type ("user" since we have DAOPHOT output), a file name for the PSF image, the number of parameter space samples to use (200), the effective gain of the CCD, and the core oversampling factor (1 since we did not oversample). The higher the number of samples, the more rigorous GIMFIT2D is about testing a model, this number of iterations must be accepted by the algorithm after achieveing convergence before it can stop, and the longer it takes to run. Hence we set it to the minimum suggested value of 200 to keep the run times reasonable. We also note that there is a parameter for the disk internal absorption coefficient which we leave at the default value of zero — the disks are assumed to be optically thin. The parameter file is simple and just contains the initial number of models to sample

the parameter space, also set to 200, on the first line and then one line for each of the 12 parameters in the model, in the order listed above, with five numbers: the initial guess, the best value, the minimum value, the maximum value, and the initial perturbation. The first two values are always the same in the file.

The guide by Tran (2000) describes how to modify this parameter file for different types of galaxy models including de Vaucouleurs (bulge) plus exponential disk, Sersic only, Sersic bulge plus exponential disk, and exponential bulge plus exponential disk. As found by de Vaucouleurs (1948), elliptical galaxies have a relation between their surface brightness and radius that is now typically written as

$$\Sigma(r) = \Sigma_e 10^{\{-3.33[(r/r_e)^{1/4}-1]\}} = \Sigma_e \exp\{-7.67[(r/r_e)^{1/4}-1]\} \tag{4.5}$$

where Σ_e is the surface brightness at the effective radius r_e and the constant is chosen so that if the galaxy were circularly symmetric and this relation held true for all radii, half of the total light would be enclosed within r_e and is known as the de Vaucouleurs $R^{1/4}$ law. The bulge components of disk galaxies are also often well fit by this relation. The Sersic (1968) profile is a generalization of this relationship where the power law dependence on radius is not required to be $1/4$, but allowed to be $1/n$:

$$\Sigma(r) = \Sigma_e \exp\{-k[(r/r_e)^{1/n}-1]\} \tag{4.6}$$

where the parameters have the same meanings as for the $R^{1/4}$ law. As noted in Simard et al. (2002), here the constant $k = 1.9992n - 0.3271$ so that r_e remains the radius enclosing half the total light. The exponential profile used to model the disk component is simply

$$\Sigma(r) = \Sigma_0 \exp(-r/r_d) \tag{4.7}$$

where Σ_0 is the central surface brightness and r_d is the exponential scale length. We tested each of these models and examined the results. The χ^2 values of the fits were very similar from model to model on each given detection, but looking at them by eye it seemed that the Sersic fits were just slightly worse. We therefore decided to use a de Vaucouleurs profile for the bulge component with an exponential profile for the disk component since these are the traditional models for these two components.

Next, parameters for the GSCRIPTER task must be checked. This task operates on the SExtractor output in order to create a file for use in extracting thumbnail images of detections from the input images and to create an IRAF script for running the GIMFIT2D task on each thumbnail to fit the detections. Important parameters in GSCRIPTER are the file names for these files, the path to output the thumbnails to (we use a subdirectory with the same name as the survey field), minimum extraction radius (25 pixels), the extraction area (20), and if we are using different PSFs for each object (yes). The extraction radius and area were chosen with some testing and using the suggestions in the guide. A 25 pixel radius is sufficiently large to contain the detections and an area of 20, the highest recommended value, ensures that there are enough sky pixels in the thumbnail image. Once this is done, GSCRIPTER is run and then the task XGAL is run to extract thumbnails from the survey images and segmentation mask images.

At this point, PSFs at the location of each detection are created. The GIM2D tasks require actual images of the PSF, not simply the model created with DAOPHOT earlier. The extracted thumbnails are named using the (x,y) pixel coordinates of the detections so with a simple IRAF script we can copy

these names into files then manipulate them via text substitutions and pasting columns together to create a new IRAF script with a series of commands for the DAOPHOT SEEPSF task to create a PSF image at the given location from the previously determined PSF. Given the naming conventions used by GIM2D, it was simpler to do this at this point when we already had some images named this way.

The fitting is then performed by running the GIMFIT2D task on all of the detections via the script created by GSCRIPTER. The script can be run on multiple computers simultaneously without major problems so we did this in order to help speed up the process. The scripts would stop running, often because one computer tried to open files another computer already opened, and when this happened they were restarted. During initial runs with GIM2D, we noticed that fits were performed at roughly one every few minutes for the majority of the detections, but there were of course exceptions, most notably for the brighter objects. The full catalogs from SExtractor contained about 7000–8000 objects per field and we estimated that GIM2D would take a week or more to finish processing each field. In order to shorten the time, we performed the cuts described in the last section and performed a star/galaxy separation before fitting. This allowed us to drop the lists by roughly a factor of ten, to about 800 objects per field on average, meaning each field could be processed in about one day. By running each field on two computers simultaneously and processing a number of fields at once on many different computers, we were able to process all of the fields in about 1.5 weeks.

4.4 Calculating Additional Parameters and Tabulating the Results

While GIM2D provides a good automated way of fitting our detections, some values we are interested in, namely surface brightnesses, are not provided. The log files output by GIM2D consist of best fit values for all 12 parameters of the model and 99% confidence interval values for each, the reduced χ^2 of the fit, the half light radius of the model, values for four different asymmetry indices, two as described in Schade et al. (1995) and two new ones introduced in Simard et al. (2002), and two parameters from the automated classification system of Abraham et al. (1994, 1996), a concentration index and an asymmetry index. These are described in detail in Simard et al. (2002) and the GIM2D package help files, but briefly, Schade's asymmetry parameters are approximately the total residual flux (R_T) and the asymmetric residual flux (R_A) expressed as a fraction of the total galaxy flux. GIM2D introduces A_z, the sum of fluxes in pixels in the object or background considered part of an asymmetric component normalized by the total object flux, and D_z, the sum of fluxes in the object with symmetrical counterparts about the object center that do not belong to the object normalized by the total object flux and is calculated outside the half light radius. The log files also contain information about every model tested during the fitting, making them very large. All of the values just noted are at the end of the log file, however, making it a simple matter to extract them for use in calculations. A short IRAF script is used to copy the final 28 lines of each detection's log file to new files after which the original log files are deleted. In this way we retain all of the final results while saving storage space.

The calculation of additional values is handled with a combination of IRAF and awk scripts. An IRAF script we called getres2.cl is the main driving program. It first uses the UNIX grep command to copy all the output GIM2D results into a single file. Grep is used rather than something simpler such as the UNIX cat command because by using grep we can force the file name to be included in the output. This is important because the integer (x,y) coordinates of the detections are in the file names; the output results only have the fractional pixel offsets of the object centers from these values. Everything after the root of the file name is deleted through a series of global replacement commands and then the single file is split back into individual files via the UNIX split command. We then call two awk scripts called extract-par.awk and extract-asym.awk to create two files of output, one containing just the primary fit parameters, the other containing only the asymmetry parameters. After doing this, we delete the split files. We then run an awk script to compute the additional values we desire and 99% confidence limits for them as well as convert radii from pixels to arcseconds. As the script involves trigonometric functions, it was actually run with gawk, the GNU Project's version of awk since standard awk cannot correctly handle these functions. The final stage of the IRAF script is to take the integer values of (x,y) from the image file names and use the dx, dy values in the GIM2D output to calculate the actual (x,y) position of the objects. A few global replacements to modify the file names and a simple awk script performs this task. As the gawk script that performs the calculation of new values is the heart of this script, it will be described in some detail here.

At the top of the gawk script some values are set including the zeropoint of the magnitude scale ξ, the image scale (2.028 $''$/pixel), the exposure time (t = 500

s), and the constant π. First the bulge effective radius and confidence limits, disk scale length and confidence limits, and half light radius (no confidence limits available) are converted from pixels to arcseconds. Next, confidence limits of some GIM2D output parameters are converted to standard deviations for use in determining errors in the values we calculate. Assuming a Gaussian distribution, the GIM2D output 99% confidence limits limits correspond to $\sim 2.58\sigma$ so 1σ values are calculated by simply subtracting the error from the best fit value and then dividing by 2.58. When we did this however, we made all results positive and accounted for the sign in the equations when calculating errors. Errors were then calculated in terms of standard deviations and converted back to 99% confidence limits by adding or subtracting 2.58σ to the calculated values to match the errors as output by GIM2D. All error propagation equations were obtained using the standard procedure that errors sum in quadrature and propagate by partial derivatives. So for example, a function $f(x, y, z)$ would have $\sigma_f^2 = (\sigma_x \partial f/\partial x)^2 + (\sigma_y \partial f/\partial y)^2 + (\sigma_z \partial f/\partial z)^2$. Any terms that did not contribute significantly to the errors, typically the zeropoint and exposure time terms, were dropped from the equations for simplicity.

We calculate magnitudes from the output fluxes (L_{tot}) by

$$m = \xi - 2.5 \log(L_{tot}/t) \tag{4.8}$$

and the errors by

$$\sigma_m = 1.086 \frac{\sigma_{L_{tot}}}{L_{tot}} \tag{4.9}$$

Having the bulge to total ratio (B/T) we get the disk to total ratio ($D/T = 1 - B/T$) to slightly simplify the equations for the disk central surface brightness, μ_0. However, we cannot calculate this value if $D/T = 0$ or $r_d = 0$ so we check

these conditions first and flag μ_0 and all related values if either is true. If both are false, we then calculate

$$\mu_0 = \xi - 2.5 \log \left(\frac{L_{tot}(D/T)}{2\pi r_d^2 t} \right) \tag{4.10}$$

and use

$$\sigma_{\mu_0}^2 = 1.18 \frac{\sigma_{L_{tot}}^2}{L_{tot}^2} + 1.18 \frac{\sigma_{B/T}^2}{(D/T)^2} + 4.72 \frac{\sigma_{r_d}^2}{r_d^2} \tag{4.11}$$

In order to account for the measured inclination, we also calculate

$$\mu_{0,i} = \xi - 2.5 \log \left(\frac{L_{tot}(D/T)}{2\pi r_d^2 t \cos(i)} \right) \tag{4.12}$$

and its errors with

$$\sigma_{\mu_{0,i}}^2 = 1.18 \frac{\sigma_{L_{tot}}^2}{L_{tot}^2} + 1.18 \frac{\sigma_{B/T}^2}{(D/T)^2} + 4.72 \frac{\sigma_{r_d}^2}{r_d^2} + 1.18 \sigma_i^2 \tan^2 i = \sigma_{mu_0}^2 + 1.18 \sigma_i^2 \tan^2 i \tag{4.13}$$

where i and σ_i have been converted from degrees to radians. As we are only interested in the amount of light in the disk component here, we use $L_{tot}(D/T)$ for the flux. Similarly, we calculate the effective surface brightness of the bulge component, μ_e, and its errors after checking to make sure that neither $B/T = 0$ nor $r_e = 0$ using

$$\mu_e = \xi - 2.5 \log \left(\frac{L_{tot}(B/T)}{22.6645 r_d^2 t} \right) \tag{4.14}$$

and

$$\sigma_{\mu_0}^2 = 1.18 \frac{\sigma_{L_{tot}}^2}{L_{tot}^2} + 1.18 \frac{\sigma_{B/T}^2}{(B/T)^2} + 4.72 \frac{\sigma_{r_e}^2}{r_e^2} \tag{4.15}$$

Here we take the amount of light in the bulge component to be $L_{tot}(B/T)$. These equations for surface brightnesses were obtained from the previously described equations for the de Vaucouleurs profile (Equation 4.5) and the exponential disk profile (Equation 4.7). These equations were integrated over radius, from zero to infinity, and angle, which simply averages out to 2π since the equations have no

dependence on angle. The results were then converted to the magnitude scale by taking $-2.5\log$ and the zeropoint term added in to scale them properly. When including the inclination, we noted that r_d is the value along the semi-major axis (a) and so the value along the semi-minor axis (b) is given by $r_d(b/a)$ where $\cos(i) = b/a$.

In addition to calculating the surface brightnesses of the components separately, we also want a measure of the surface brightness of each object as a whole. The output half light radii, when they are non-zero, are used for this purpose. The simplest way is to calculate the surface brightness inside the half light radius using

$$\mu_{r<r_{half}} = \xi - 2.5\log\left(\frac{L_{tot}}{2\pi r_{half}^2}\right) \tag{4.16}$$

whose errors are computed via

$$\sigma_{\mu_{r<r_{half}}} = 1.086\frac{\sigma_{L_{tot}}}{L_{tot}} \tag{4.17}$$

A better measure, in that it retains more dynamic range, is the surface brightness at the half light radius. This is harder to calculate, but we have all the information necessary to do so. The profile of both components combined is given by the sum of Equations 4.5 and 4.7:

$$\Sigma(r) = \Sigma_e \exp\{-7.67[(r/r_e)^{1/4} - 1]\} + \Sigma_0 \exp(-r/r_d) \tag{4.18}$$

Since $\mu_e = -2.5\log\Sigma_e$ and $\mu_0 = -2.5\log\Sigma_0$ we find that $\Sigma_e = 10^{-0.4\mu_e}$ and $\Sigma_0 = 10^{-0.4\mu_0}$. By substituting these into the equation above and then converting the whole thing into the magnitude scale by taking $-2.5\log$ of it and setting $r = r_{half}$ we obtain:

$$\mu_{r_{half}} = -2.5\log\left(10^{-0.4\mu_e}\exp\left\{-7.67\left[\left(\frac{r_{half}}{r_e}\right)^{1/4} - 1\right]\right\} + 10^{-0.4\mu_0}\exp\left(-\frac{r_{half}}{r_d}\right)\right) \tag{4.19}$$

The error equation is determined as before, but the more complicated starting equation results in a more complicated error equation. Some of the original terms appear repeatedly so for simplicity we define

$$D \equiv 10^{-0.4\mu_0} \exp(-r_{half}/r_d) \tag{4.20}$$

and

$$B \equiv 10^{-0.4\mu_e} \exp\{-7.67[(r_{half}/r_e)^{1/4} - 1]\} \tag{4.21}$$

Note that these are not the same B and D of the B/T and D/T ratios. With these definitions, the error equation can be written as

$$\begin{aligned}\sigma^2_{\mu_{r_{half}}} = \sigma^2_{\mu_e} \left(\frac{B}{B+D}\right)^2 + \sigma^2_{r_e} \left(\frac{-2.08B}{B+D} \left(\frac{r_{half}}{r_e}\right)^{1/4}\right)^2 \\ +\sigma^2_{\mu_0} \left(\frac{D}{B+D}\right)^2 + \sigma^2_{r_d} \left(\frac{-1.09 D r_{half}}{(B+D) r_d^2}\right)^2\end{aligned} \tag{4.22}$$

The disk surface brightnesses used here are the ones that do not include the inclination. Cases involving radii with zero values had to be accounted for since gawk does not automatically correctly take limits (e.g., it does not recognize that $\exp(-r_{half}/r_d) \to 0$ if $r_d = 0$; the division by zero error causes problems). Therefore in this section of the program file, having already checked for $r_{half} = 0$, we check to see if B/T is zero, one, or neither. If only one component exists and its radius is zero, we flag the values for $\mu_{r_{half}}$, otherwise we calculate it using only the relevant terms in the equations. If both components exist, we have to check both radii. If both r_e and r_d are zero, we flag the values as before. If only one is zero, we make the calculation as if this component did not exist; only the component with a non-zero radius will contribute to the surface brightness at the half light radius. If both are non-zero, the calculation is done using both components and all terms in the equations. Inspection of some results shows

that with only one exception the cases we are flagging here do not occur; that is, if $r_{half} \neq 0$ we do not find $B/T = 1$ and $r_e = 0$, $B/T = 0$ and $r_d = 0$, or $0 < B/T < 1$ and $r_e = r_d = 0$ (one radius or the other may still be zero, but both are not). If the half light radius is non-zero, a value for the surface brightness at that radius is calculable.

After this is complete, we have to run one final series of commands to turn the (x,y) pixel coordinates into (α,δ) coordinates. These could be written into a script, but as the file names involved have to be changed for each run, it is as easy to copy and paste the commands into the IRAF command line as it is to make a script, change them there, then run it. Essentially, we cut the first two columns from the results files, the (x,y) coordinates, into one file and place the remaining columns into another file. The IRAF task CCTRAN is then run to convert the coordinates and place them into a new file which is then pasted with the rest of the original table files into new table files.

Chapter 5

Examining the Results

Now that we have generated catalog files containing all of the objects we detected according to specified limits that met the selection criteria described in the previous chapter, we want to get an overall sense of what we have found. A brief visual examination of the detections reveals some problem cases that passed the star/galaxy separation stage. Thus our first step here is to determine additional cuts on parameters from the model fitting that will allow us to exclude as many of these bad detections as possible. We then use a plot of number counts vs. magnitude to estimate the magnitude to which we are complete. Finally, we select a sample of relatively face-on, disk dominated systems to study in the following chapter.

5.1 Removing Bad Detections

A preliminary visual examination of the detected objects can be done easily within IRAF using the TVMARK task to mark their locations on a displayed image. Doing this reveals that a number of objects are actually two or more objects that were fit as a single one, stars, or objects too small to visually classify

as either star or galaxy. While these are easily seen by the human eye, with over 64000 detections in our catalog, it is not feasible to visually check every one of them to remove such bad detections. We need to decide upon an automated way to remove them so we examine the model fit parameters output by GIM2D to choose additional cuts. Since no cut is perfect we will probably remove some galaxies and leave some stars. However, we attempted to be conservative with our selections in order to minimize the loss of good data.

Our first cut is almost identical to one made during the star/galaxy separation stage — any objects with a model fit half light radius $r_{half} = 0$ is considered unresolved and removed from the catalogs. As noted by Simard et al. (2002), these are likely to be stars and looking at some of them shows that this is that case; they do not appear to be galaxies. A small sample of these objects taken from our deepest field is shown in Figure 5.1. Our survey was designed to be very uniform, but one field was observed almost three times as often as the other fields. This is F2100-45:E and it has 59 individual observations combined into it instead of the usual 20. This improves the signal to noise ratio of this field making it easier to detect objects, providing more examples to look at when considering what cuts to make. Therefore most of our examples are taken from this field. This first cut removes only 416 objects from our list of 64462 detections. At very low values of r_{half} this is not a very strong cut; there are only 597 objects with $r_{half} \leq 0.1''$ and 940 objects with $r_{half} \leq 0.2''$. At larger values it becomes a more serious cut which would remove 2496 objects with $r_{half} \leq 0.5''$ (about 0.25 pixel) and 6279 objects with $r_{half} \leq 1''$ (about 0.5 pixel). Therefore we keep the cut conservative and only remove objects that have half light radii of exactly zero. The reason such objects exist even after we made a cut on r_{half} already is because

of the different fitting algorithms of the two programs — GIM2D has a model PSF to use, SExtractor does not. We also note that having so few unresolved, stellar-like objects at this point is an indication that our initial star/galaxy separation performed well.

The next parameter we checked was the reduced χ^2 of the model fit. Initial examination and testing of results indicated that some very obvious galaxies ended up with χ^2 values around 6–7, limiting the effectiveness of this as a cut. When we looked at objects with even higher χ^2 values we saw that many of these appeared to be stars or they had neighboring objects that probably affected the model fit. We can therefore use a loose cut on χ^2 to remove some of the worst fit detections from the catalog, none of which we expect to be galaxies. We tested a number of cuts and chose to reject objects with $\chi^2 \geq 10$ which removes 1462 detections. A small sample of these objects taken from our deepest field is shown in Figure 5.2. This is not a particularly strong cut towards higher values; increasing the cut to 20 removes 855 objects and at 30, 649 objects are removed. It becomes stronger at lower values though. Cutting at $\chi^2 = 5$ removes 2704 objects and cutting at 2 removes 8746 objects. However, having already seen that galaxies can have $\chi^2 \approx 6$, leaving the cut at 10 is a reasonable and fairly conservative cut.

We also expect that objects with very large scale lengths, we consider the disk scale length specifically, are not likely to be real galaxies. We checked cuts at a few different values and saw that this is not a particularly strong cut at larger values. For $r_d \geq 100, 50, 30, 20, 10$ arcsec, We detect 102, 482, 1238, 2571, and 7742 objects respectively. Initial examination of results showed that some detections with r_d in the range of 20–30″ could be galaxies, though it is difficult

to be sure for the fainter objects. Therefore we choose to accept only objects with $r_d < 30''$. A small sample of objects from our deepest field that do not pass this cut are shown in Figure 5.3.

In addition, we observe that when pairs of objects incorrectly get fit together as a single object, they are very often fit with a highly inclined model. The GIMFIT2D fitting program is making a reasonable attempt in these cases, using an elongated profile for the model to encompass the two separate light profiles in the image. Therefore we expect objects with the fitting program's maximum inclination of 85° to be bad detections. This is a fairly strong cut. There are 10139 objects with $i = 85°$ and 13861 with $i \geq 84°$; roughly 1/6 of our detections will be removed by taking out objects with $i = 85°$ and a small sample of these objects from our deepest field are shown in Figure 5.4. However, looking at these by eye shows that the vast majority of such fits are clearly bad detections, mostly pairs of objects, and not very highly inclined galaxies. Not all of them were pairs of objects and some of them may in fact be LSB galaxies. This is to be expected since no cut will be perfect. But our inspection shows that this will remove a large number of bad detections and so it is worth sacrificing a very small number of potentially real LSB galaxies to make this cut. We also checked the detections at the other extreme and found that there were only 88 objects with $i = 0$ and 337 with $i \leq 1°$. We do not deem it necessary to remove these objects because there are so few of them, the more face-on objects are the ones we are most interested in, and we expect the fitting to be more accurate for the face-on objects than the highly inclined ones.

We also examine the B/T ratio which when plotted against other parameters such as magnitude (see Figure 5.5) shows lines at $B/T = 0$ and $B/T = 1$

suggesting that these are artifacts of the fitting process reaching the minimum and maximum allowed values for this parameter. This is a stronger cut on the disk dominated end than the bulge dominated end: there are 15907 objects with $B/T = 0$ and 20607 with $B/T \leq 0.05$ while there are only 814 objects with $B/T = 1$ and 1679 with $B/T \geq 0.95$. Since we are primarily interested in disk galaxies, the high B/T cut is not as important as the low B/T cut, but it is still necessary to remove bad detections. Also, we expect that any stellar-like objects that passed the star/galaxy separation stage will likely be fit by galaxy models with very high bulge fractions. A visual inspection of some $B/T = 1$ objects indicates that this is the case; many of them do appear to be stars as Figure 5.6 demonstrates with detections on our deepest field. A visual inspection of some of the $B/T = 0$ objects indicates that most are bad detections, primarily cases where two or more objects were fit as one. Some objects that are too small to distinguish visually whether they are stars or galaxies are also part of this population. Some examples of these types of objects from our deepest field are shown in Figure 5.7.

The combination of these cuts allows us to remove many of the obviously bad (non-galaxy) detections as possible in an automatic way which is necessary given the large number of detections. Since these cuts cannot be perfect, we have attempted to keep them on the conservative side in order to minimize the number of galaxies removed and non-galaxies retained. Once we apply them to our catalog, we are left with 43167 objects from the original 64405. Since it is possible for individual detections to fail more than one cut, we have counted such objects multiple times in our descriptions above. This is why the total number of objects actually removed from the catalog is smaller than the descriptions above,

taking each cut in isolation, would imply.

After all of these additional cuts have been applied, we have our main galaxy catalog. In order to provide a visual sense of the kind of objects in the catalog, we provide examples of detections in two fields for varying levels of the face-on (inclination corrected) disk central surface brightness, $\mu_{0,i}$. Three examples within 0.5 mag surface brightness bins from 20.0 to 24.5 are shown in Figures 5.8, 5.9, and 5.10 for field F2100-45:E, the deepest field, and in Figures 5.11, 5.12, and 5.13 for field F0154-39:M. We have used negative images here to help make the lower surface brightness features easier to see. We anticipate that at least some galaxies may have very LSB disks because they are bulge dominated. In this case, very little light is left for the disk component and it will therefore naturally have a low surface brightness. We also note that for $\mu_{0,i} \gtrsim 24$ R mag arcsec^{-2} the results appear to be less reliable, but this point will be examined further in the following chapter.

To put the scale of these thumbnail images in perspective, Figure 5.14 shows field F2100-45:E with a thumbnail sized box included towards the lower right. The full field shown here is 2048×2048 pixels making it about 1.15° on a side. The thumbnail sized box, in green, is 52×52 pixels making it about 1.76′ on a side. It has been centered on one of the detections, the lower right image in Figure 5.9.

5.2 Estimating Completeness

In order to get a measure of how complete this catalog is, we can use a number–magnitude plot. In Figure 5.15 we plot the differential number counts, log(N/0.5mag/deg^2), vs. m for our data and that of Yasuda et al. (2001) from the Sloan Digital Sky

Survey (SDSS). We obtained the number of objects per square degree by dividing the total number counts in each magnitude bin by the area included in our catalog. As noted in Chapter 2, the pixel scale of 2.028″/pixel gives an area of approximately 1.15 deg for a 2048×2048 pixel area. Our images are larger than this due to the shifting and combining process used, but we selected only objects within this area for fitting, so for our purposes here, each field has an area of about 1.15 deg^2. With 79 fields available for study, our total area is about 91.14 deg^2. In order to properly align the two data sets, we have converted the Gunn r magnitudes of Yasuda et al. to our R band magnitudes using:

$$R = r - 0.51 - 0.15 * (g - r) \tag{5.1}$$

This is taken from Windhorst et al. (1991) and the approximate (g-r) color is taken to be 0.8 using Yasuda et al. (2001) where their Figure 2 shows (r-i) vs. (g-r) plots with the peak density near that value. We note that there is a relatively steady increase in the number of objects detected at fainter magnitudes for both our data (the circle points) and the Yasuda et al. data (the square points). It is not exactly linear and the shape of the curve depends on cosmology and how the geometry deviates from a Euclidean geometry. But the clear turn over by R $\approx$ 18.75 mag in our data indicates that we have reached our limit of completeness. This is not an effect of cosmology since the SDSS data continue to rise. Other work such as that of Shanks et al. (1984), Tyson (1988), Yoshii & Takahara (1988), and Metcalfe et al. (1991) present similar plots which show the curve continuing to rise to fainter magnitudes, further confirming that we are seeing the effects of incompleteness here. We want our sample to be as complete as possible while also retaining as many objects as possible. The brighter the cut, the more complete we will be, but the fewer objects we will have to study later,

so the choice is something of a compromise between these two factors. To get a more detailed curve, we also plot our data with a smaller bin size, using 0.25 mag instead of 0.5 mag, in Figure 5.16. Here, the point for the 18.0–18.25 bin seems to be the beginning of the roll over. The counts appear to begin to decrease at this point and beyond this the curve rolls over and drops off. In Figure 5.15, the point for the 18.0–18.5 bin is clearly low compared to the SDSS data, but the larger bin size on this plot makes it somewhat harder to see where the roll over actually begins. Using these two plots as guides, we decide to place our cut at m = 18.25. This allows us to retain as many objects as possible while maintaining a high level of completeness.

5.3 Sample Selection

If we now plot the distribution of objects with observed disk central surface brightness after all of the above cuts have been made to remove as many bad detections as possible, excluding the magnitude cut, we find that it has a large, broad peak around $\mu_0 = 21.25$ R mag arcsec^{-2} as shown in Figure 5.17. If we include the magnitude cut as in Figure 5.18, we see a similar structure, a large broad peak around $\mu_0 = 20.25$, but there is also a long tail with a high number of objects at low surface brightness. In order to perform a meaningful analysis of the detections, we will restrict the sample further by selecting disk dominated systems that are relatively face on. By using low inclination objects, we help minimize the correction of the observed surface brightness to a face-on value which is what we are interested in knowing. This also reduces the effects of internal extinction and thus the dependence of the results on this factor. The selection of disk dominated systems is used because we are interested in the properties of disks

and also for simplicity; studying the properties of these objects is easier with fewer parameters. Together these two selections give us a clean sample that will be simple to analyze. For reference, we note that a study of bulge dominated LSB galaxies has been performed by Beijersbergen et al. (1999).

As previously noted, the cuts on B/T and inclination can be strong and we want to retain as many objects as possible so we examine the results of various cuts on the B/T ratio and the inclination. We expect that the shape of the distribution will not change significantly with more restrictive cuts once we have obtained a good sample of objects; the only major change should be that the total number of objects decreases. We begin by looking at the effects of cutting on each of these parameters separately. In Figure 5.19 we show how the distribution changes with different cuts on B/T and in Figure 5.20 we show the effects for cuts on i. We plot the counts against the face-on (inclination corrected) disk central surface brightness here since this is the quantity we are interested in studying. In the series of cuts on B/T we see that the shape of the distribution appears to remain about the same in the area of $B/T \approx 0.3$; this happens around $i \approx 30$–45 degrees for the cuts on i. We also note that excluding objects with high B/T basically removes the high tail at low surface brightnesses seen in Figure 5.18. Since we separated the total flux into the bulge and disk components according to the B/T ratio, this is expected. A high B/T object will have less light in the disk component which will naturally tend to result in a lower surface brightness disk. Examining the effect of the cuts in this area, we decide to accept only objects with $B/T \leq 0.30$ and $i < 35^{\circ}$. We have chosen these cuts because as demonstrated in Figure 5.21, the general shape of the distribution, particularly on the low surface brightness end, shows only small changes when the cuts are

altered by small amounts.

At this point we recall that during the calculation of parameters described in the previous chapter we flagged surface brightnesses that could not be calculated due to problems such as a zero radius or the component not existing (e.g., there is no disk component and thus no disk surface brightness if $B/T = 1$, a pure bulge system). While our cuts on B/T have taken care of part of this problem, it is possible for objects with $r_d = 0$ to have passed all the previous cuts. Not very many did though; there are only 353 such objects in the catalog of 43167. They would not be studied anyway, but it will be simpler to remove them from the catalog now. To make sure that we do remove all such objects, we will simply cut out objects with negative disk central surface brightnesses (the flag was -999) along with these selection cuts. When we apply these cuts and the magnitude cut to the catalog, we are left with 757 objects. These objects along with their their results from the GIM2D fitting package and parameters we calculated from those results are listed in the Appendix as Tables C.1 through C.4. In the next chapter we perform a more detailed analysis of this surface brightness distribution. As a check of the disk central surface brightnesses that we will be using ($\mu_{0,i}$), we compare these values to the surface brightness at the half light radius ($\mu_{r_{half}}$), as calculated by Equation 4.19. As noted in Chapter 4, this value serves as a measure of the surface brightness of the object as a whole, rather than a value for just one of its components. We find that $\mu_{r_{half}}$ is consistently fainter than $\mu_{0,i}$, by about 1.67 mag arcsec^{-2} on average. Since we have selected a disk dominated sample here, we expect the half light radius to fall outside any bulge component and inside the disk component. The surface brightness measured at that point should be fainter than the central surface brightness of the disk and these are

reasonable values for the difference, confirming that we have reasonable values for the disk central surface brightnesses.

We have performed three levels of cuts to reach this point so it is worth reviewing them briefly. The objects that are removed in these steps have the following properties:

- Performing star/galaxy separation using SExtractor results
    1. FLAGS ≥ 4, saturated or worse
    2. $r_{half} < 1$ pixel, unresolved and most likely stars
    3. Lie in the stellar regions of the magnitude–area and concentration plots; Equations 4.1 and 4.2 define the cut lines shown in Figures 4.4 and 4.5
- Finding bad detections using GIM2D results
    1. $r_{half} = 0$, unresolved and most likely stars
    2. $\chi^2 \geq 10$, model has poor goodness-of-fit
    3. $r_d \geq 30''$, unrealistic, primarily stars
    4. $i = 85°$, possible, but primarily pairs of objects fit as one
    5. $B/T = 1$, fitting artifact, primarily stars
    6. $B/T = 0$, fitting artifact, primarily two or more objects fit as one
- Selecting the sample to study
    1. $m \geq 18.25$, rejecting objects beyond the approximate level of completeness
    2. $B/T > 0.3$, leaving disk dominated systems

3. $i \geq 35^{\circ}$, leaving relatively face-on systems

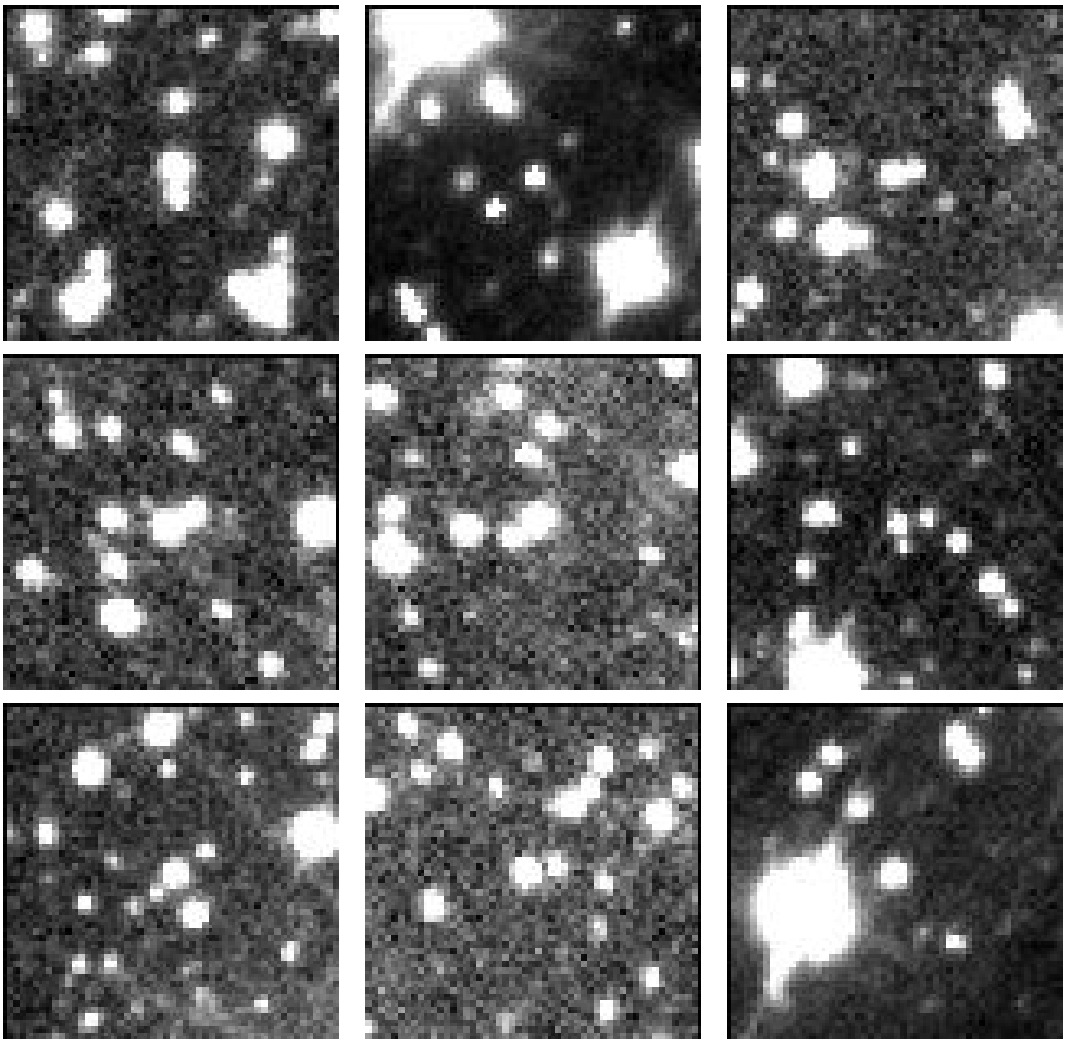

Figure 5.1: Examples of detections with $r_{half} = 0$ in field F2100-45:E. These are considered unresolved objects and none look like galaxies, they all appear to be stars. In this and all other similar figures in this chapter, the specified objects are at the centers of the thumbnails and each thumbnail is $1.76'$ on a side.

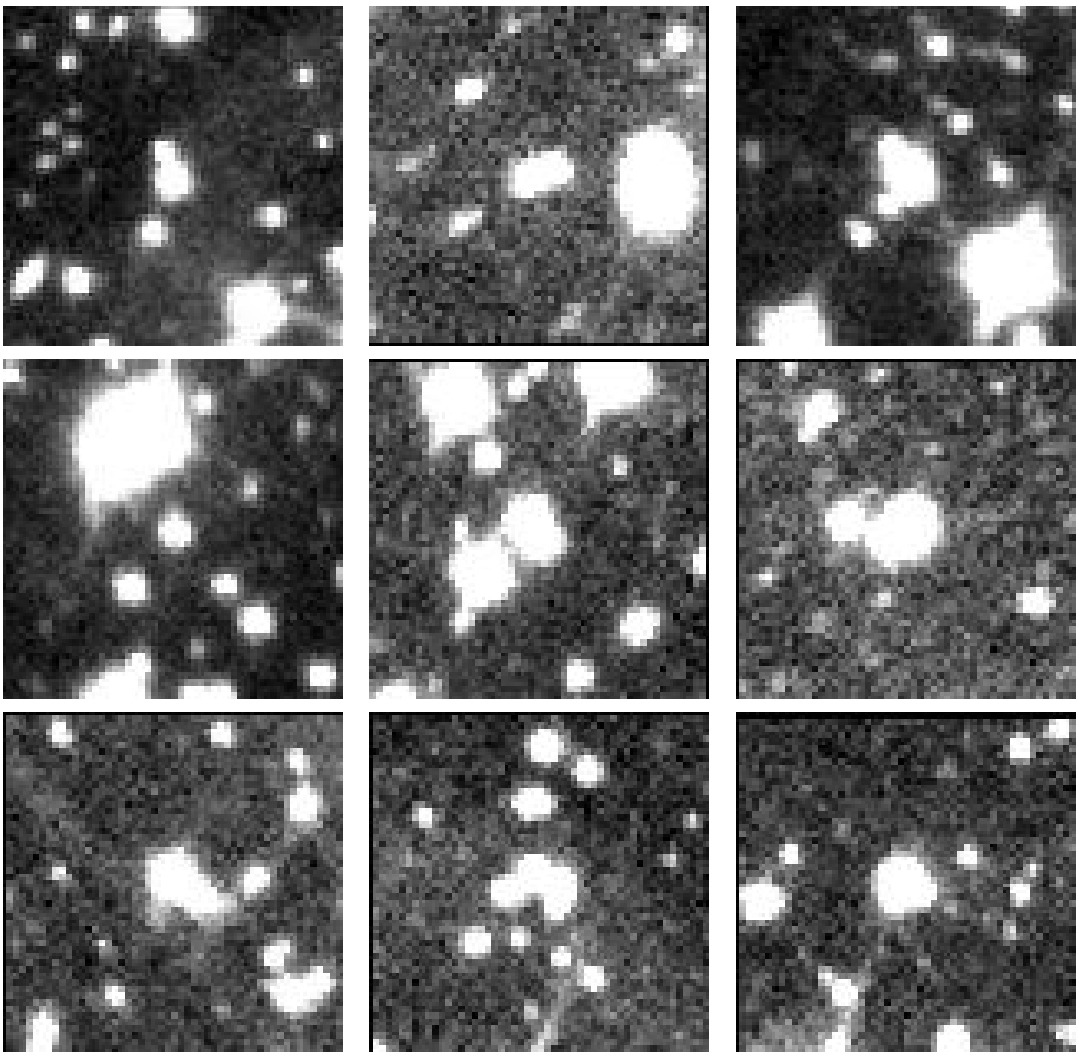

Figure 5.2: Examples of detections with $\chi^2 \geq 10$ in field F2100-45:E. Most appear to be stars or lie near one or more objects that affected the fit.

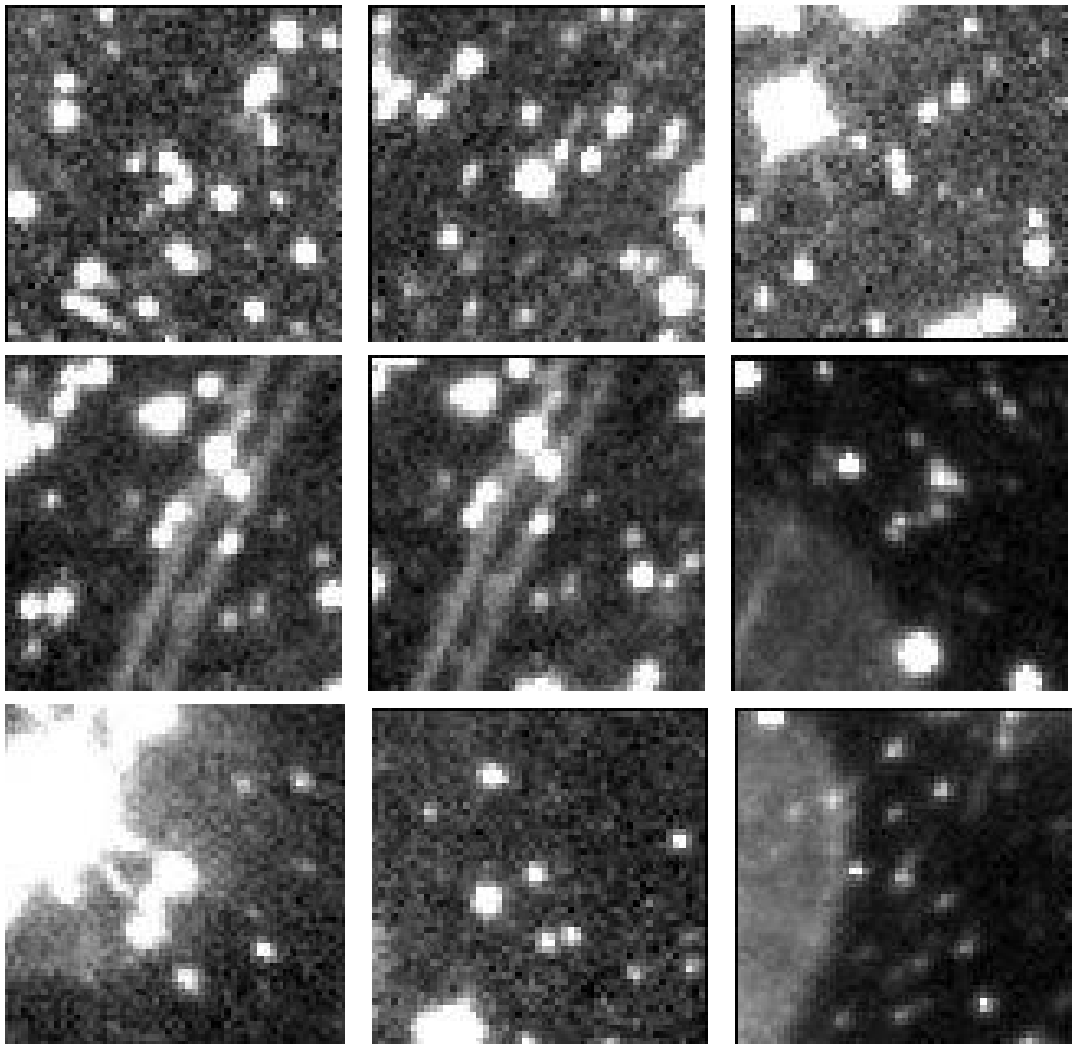

Figure 5.3: Examples of detections with $r_d \geq 30''$ in field F2100-45:E. Most are pairs or single objects that appear to be stars, not galaxies.

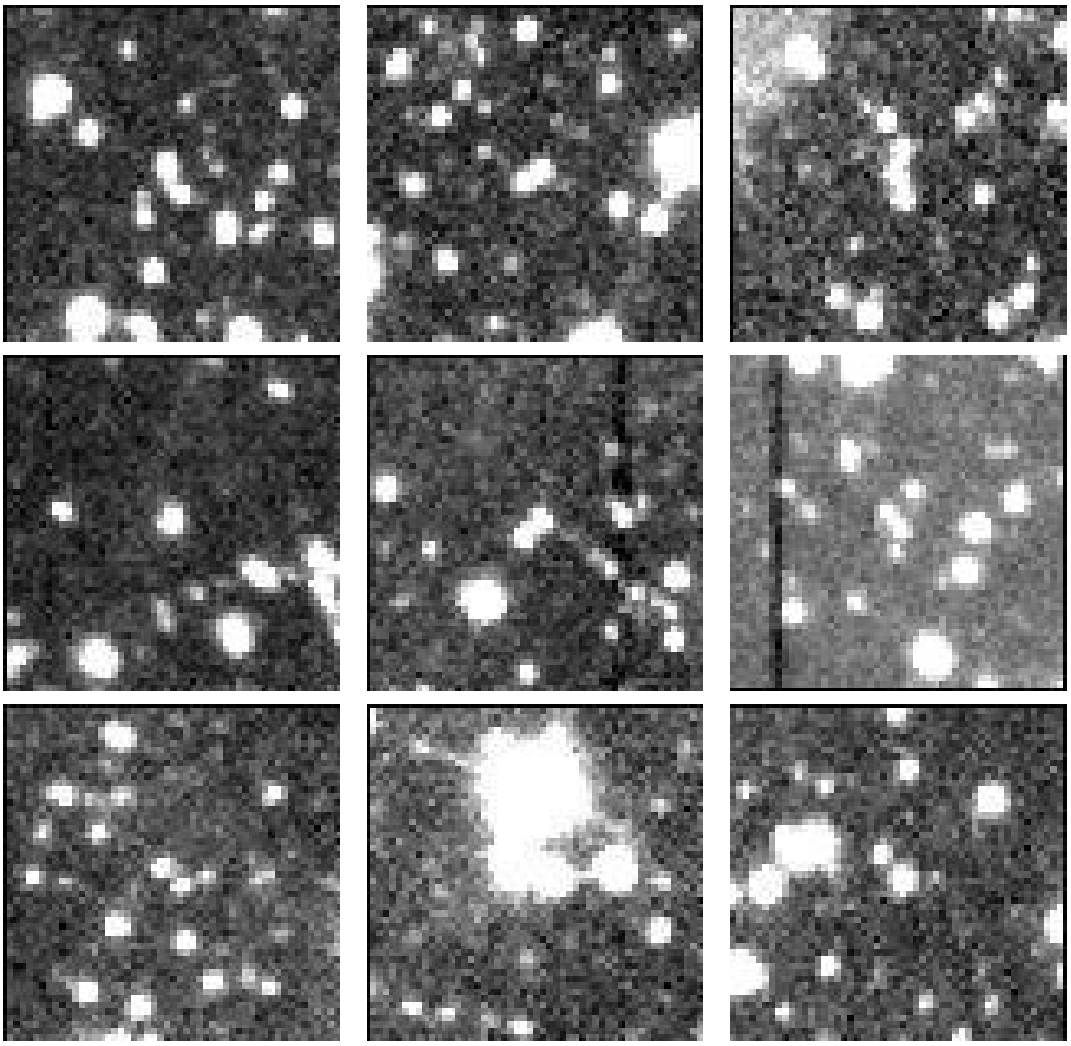

Figure 5.4: Examples of detections with $i = 85°$ in field F2100-45:E. Most are two or more objects that were fit as a single object.

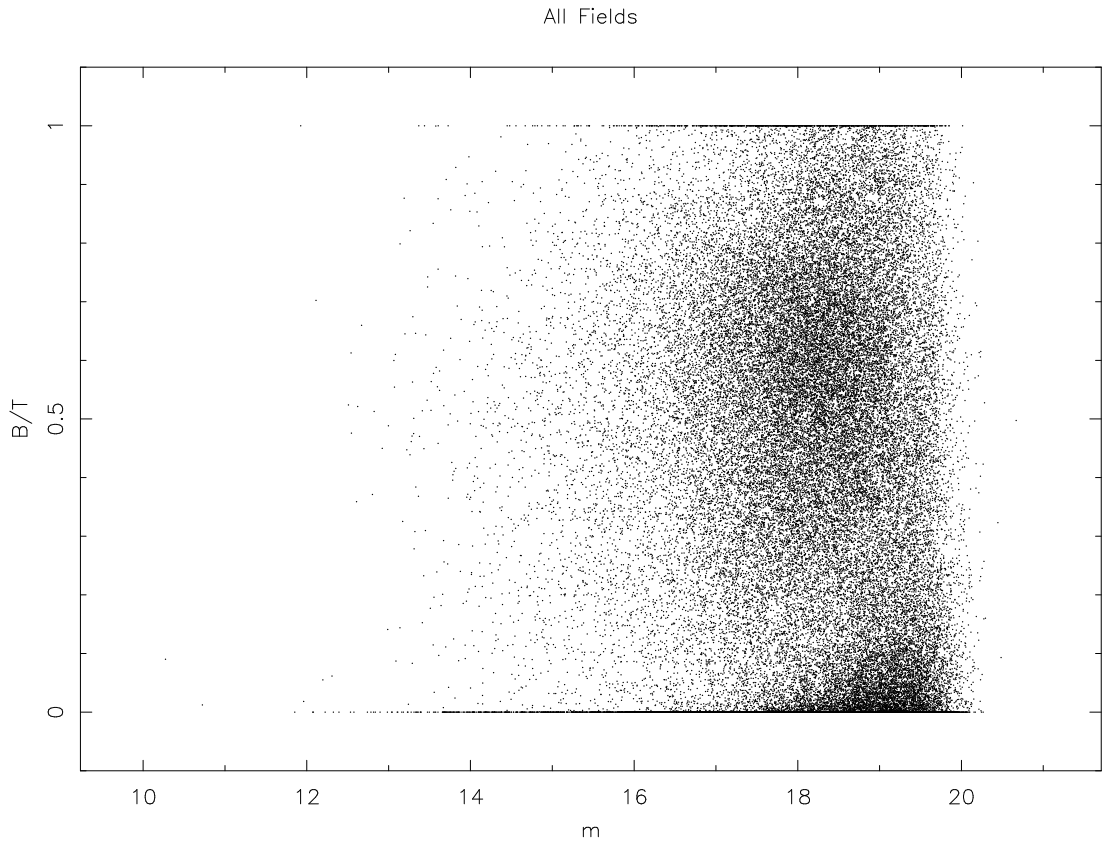

Figure 5.5: Plot of B/T vs. magnitude which shows lines at the minimum and maximum values of B/T. We expect these are artifacts of the fitting process and these objects can safely be cut from the catalogs as unreliable for further study.

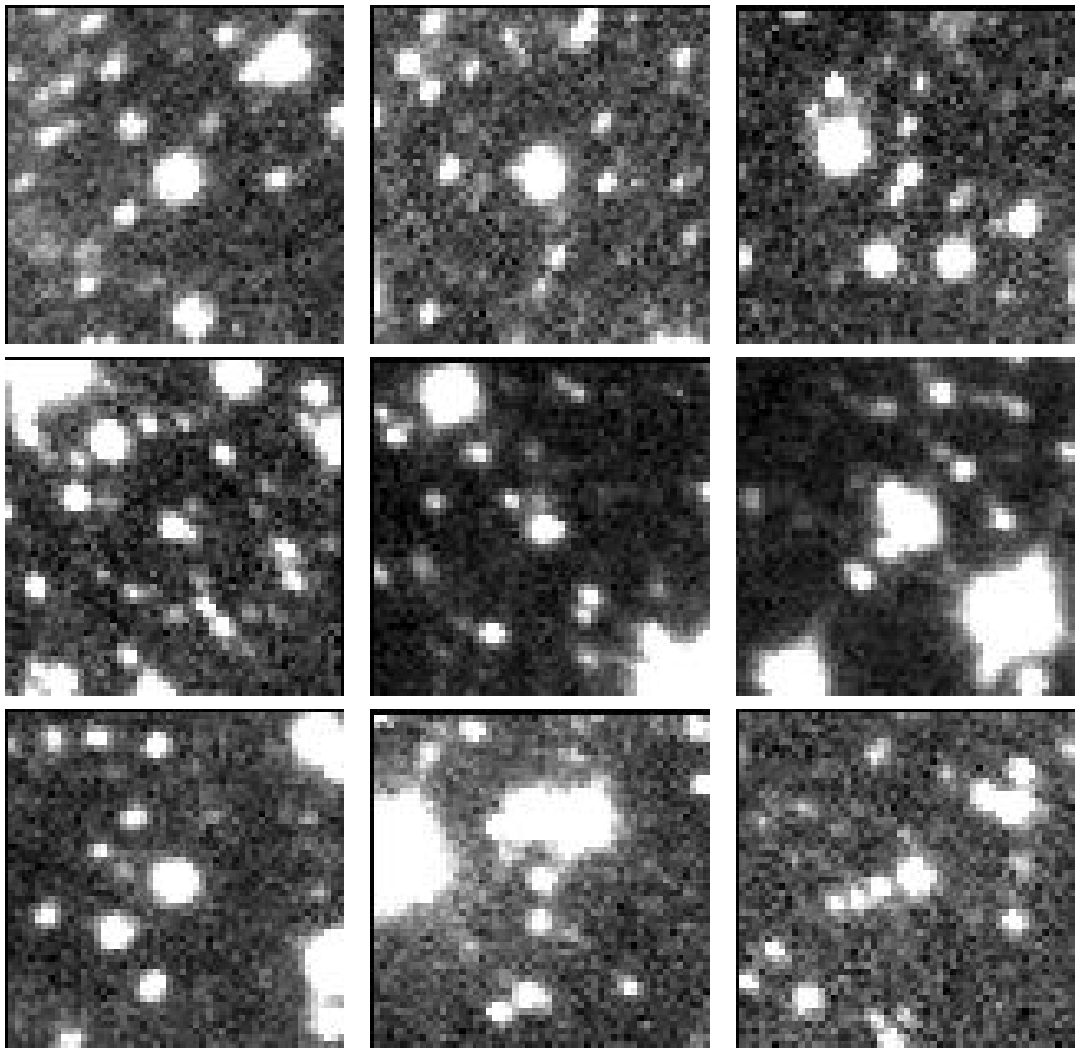

Figure 5.6: Examples of detections with $B/T = 1$ in field F2100-45:E. Most appear to be stars, not galaxies.

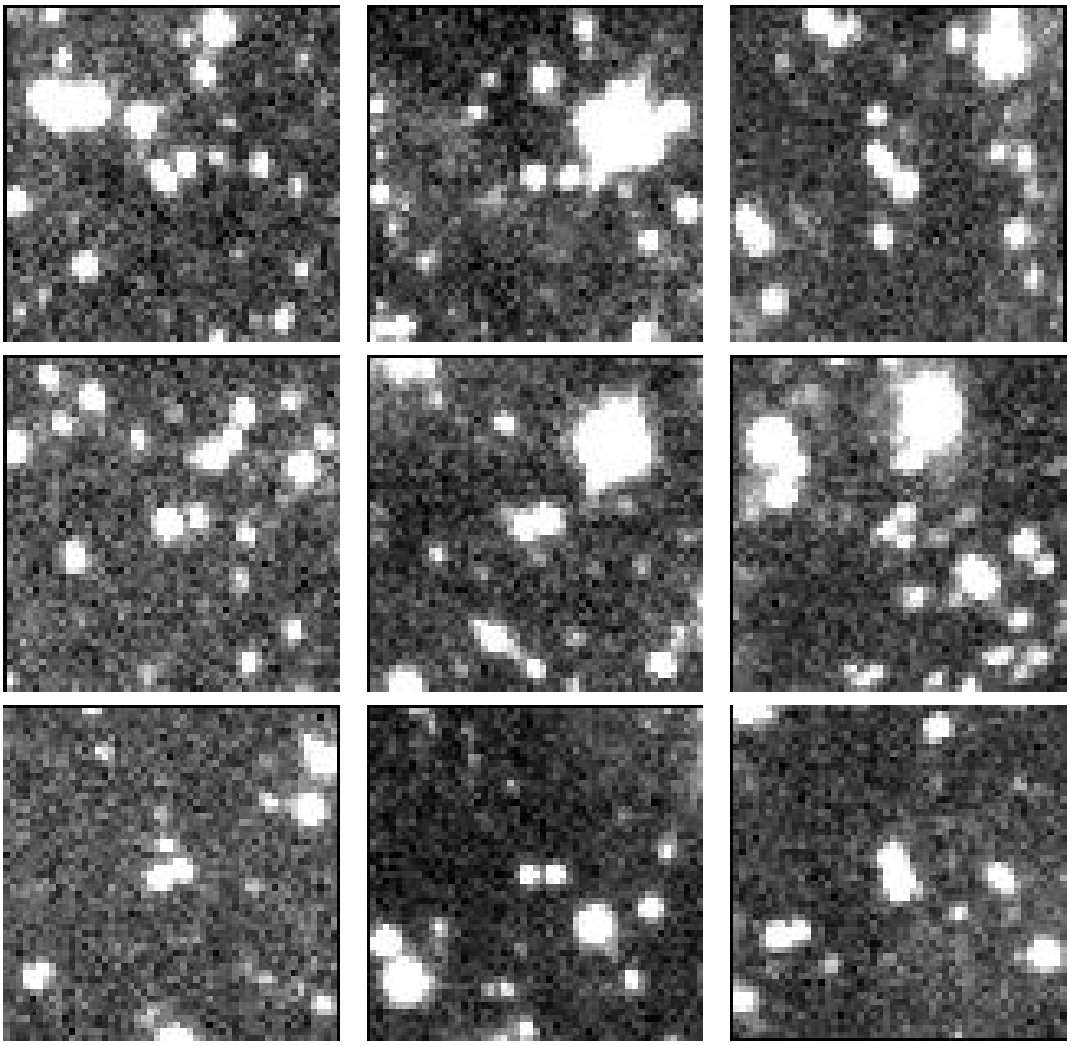

Figure 5.7: Examples of detections with $B/T = 0$ in field F2100-45:E. Most are two or more objects that were fit as a single object.

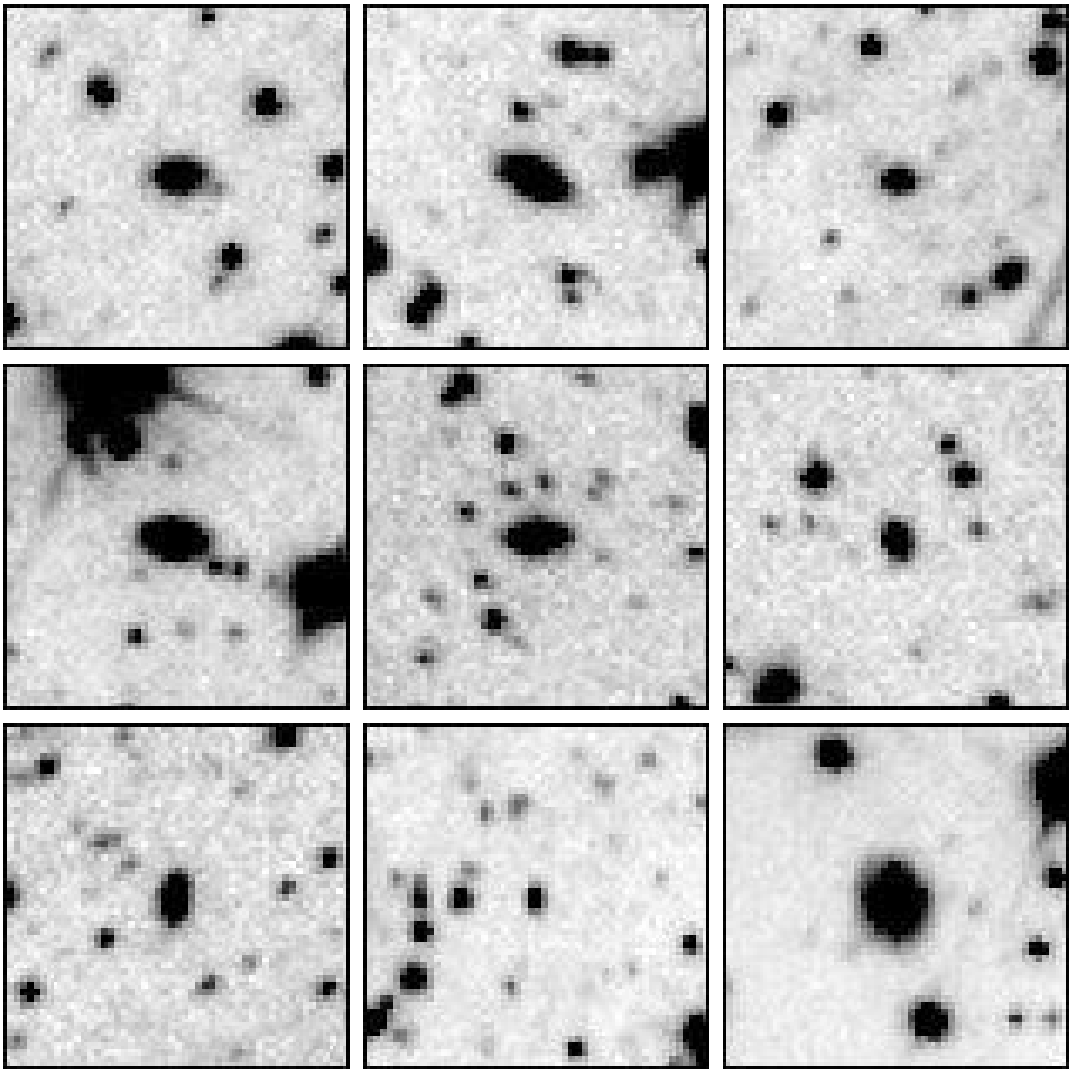

Figure 5.8: Examples of detections in field F2100-45:E at varying levels of face on disk central surface brightness. The top row is for $\mu_{0,i}$ of 20.0–20.5, the middle row for 20.5–21.0, and the bottom row for 21.0–21.5

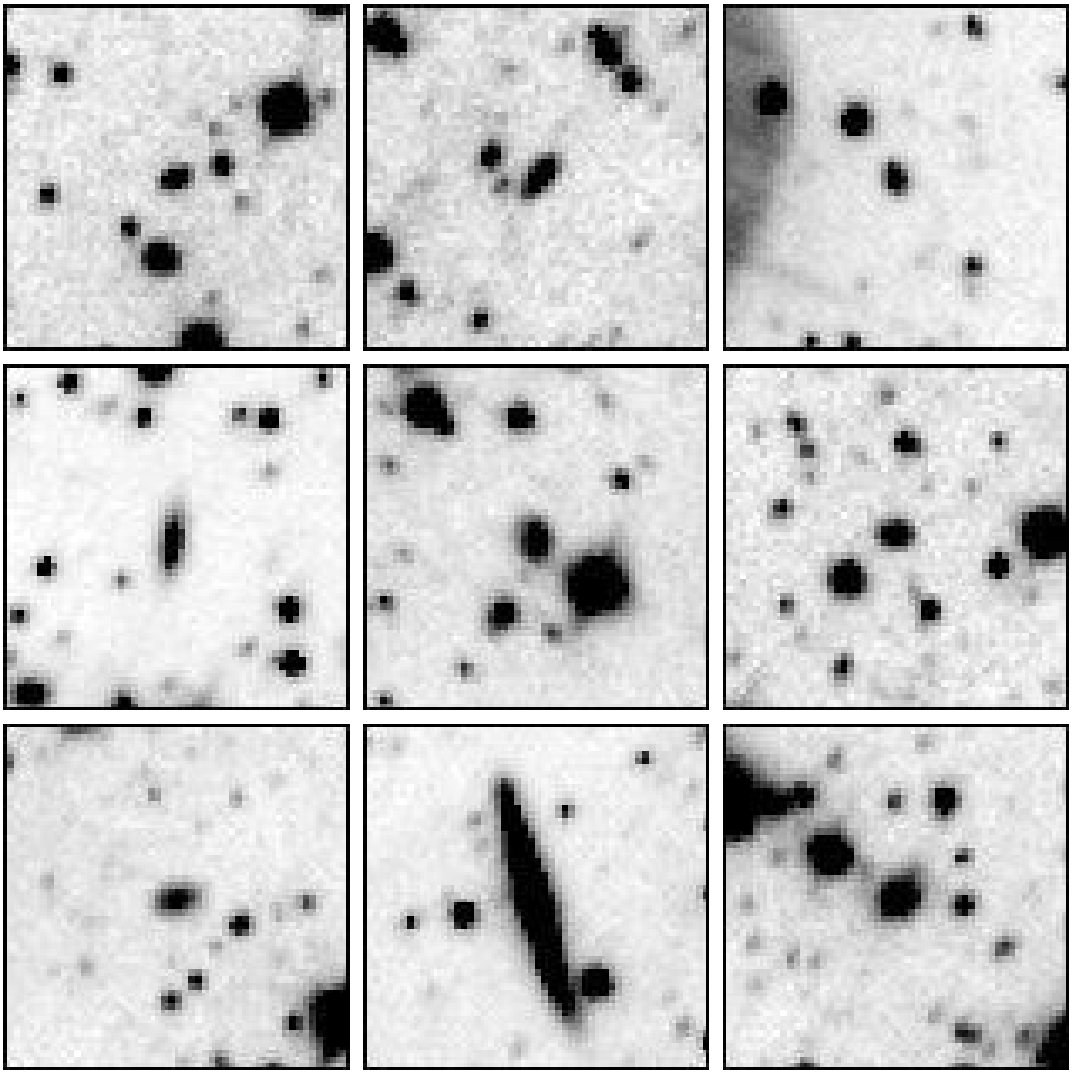

Figure 5.9: Examples of detections in field F2100-45:E at varying levels of face on disk central surface brightness. The top row is for $\mu_{0,i}$ of 21.5–22.0, the middle row for 22.0–22.5, and the bottom row for 22.5–23.0

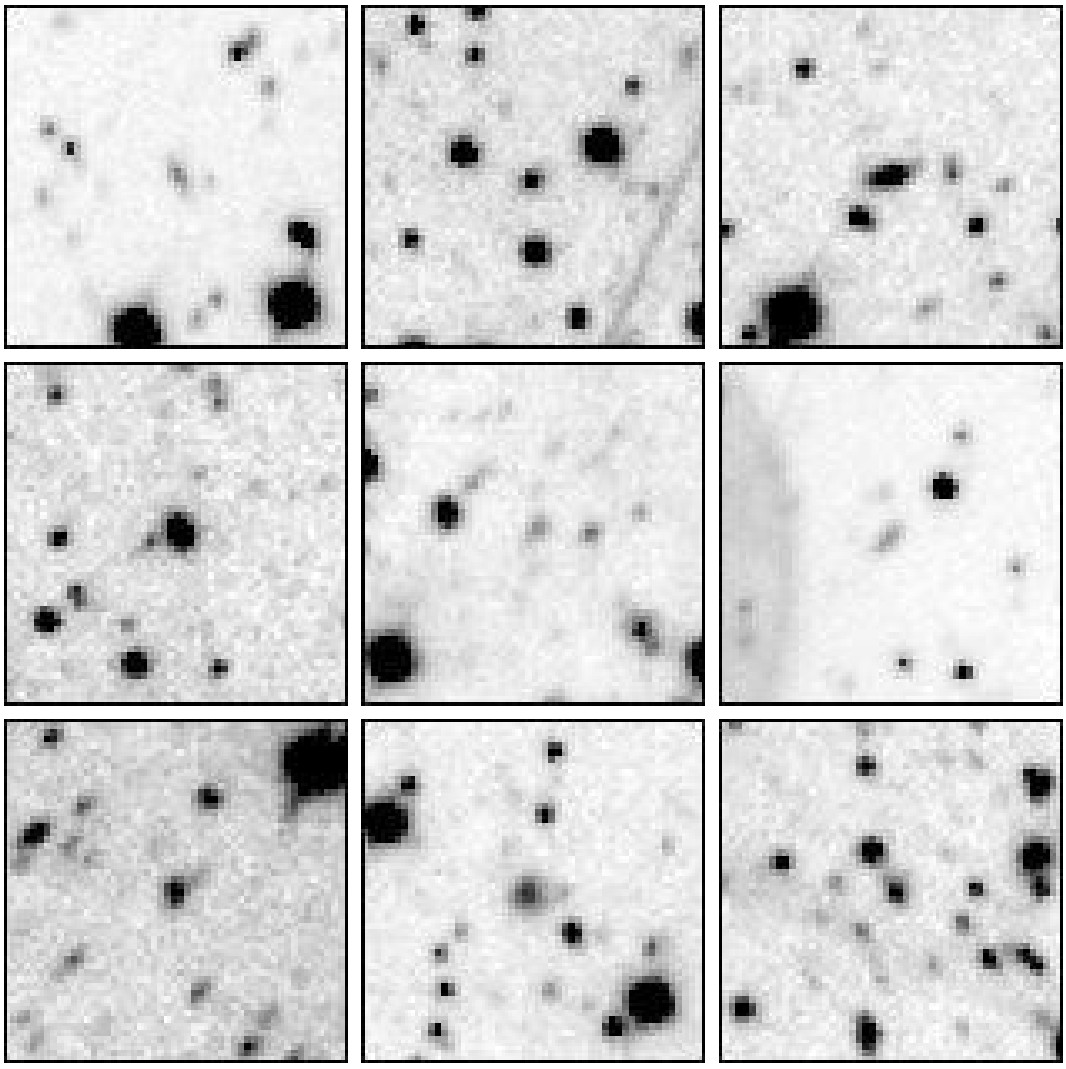

Figure 5.10: Examples of detections in field F2100-45:E at varying levels of face on disk central surface brightness. The top row is for $\mu_{0,i}$ of 23.0–23.5, the middle row for 23.5–24.0, and the bottom row for 24.0–24.5. We also note that these are clearly real objects in spite of their very LSB nature; detection of objects with $\mu_0 \approx 23.5$ R mag arcsec^{-2} was one of the main goals of the survey.

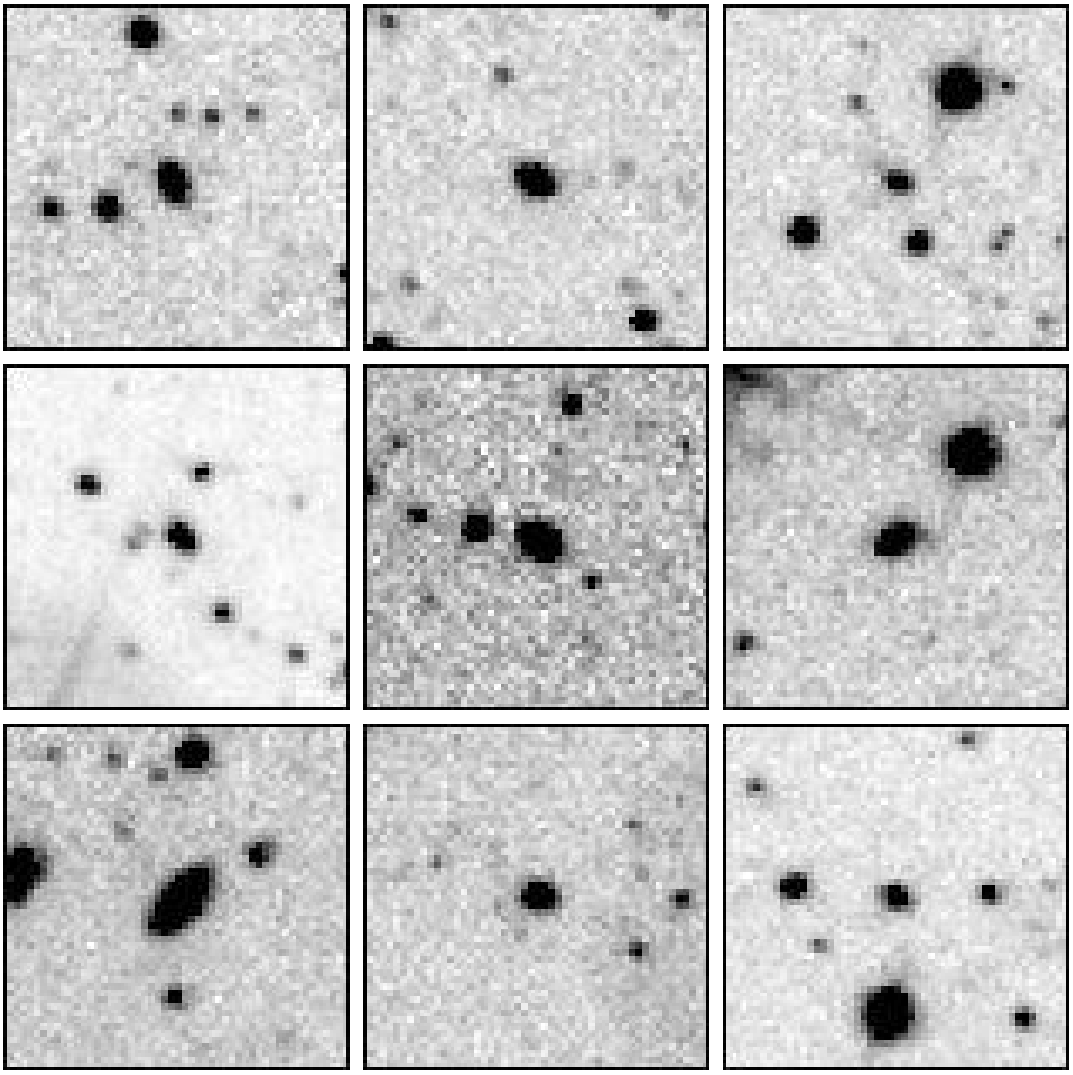

Figure 5.11: Examples of detections in field F0154-39:M at varying levels of face on disk central surface brightness. The top row is for $\mu_{0,i}$ of 20.0–20.5, the middle row for 20.5–21.0, and the bottom row for 21.0–21.5

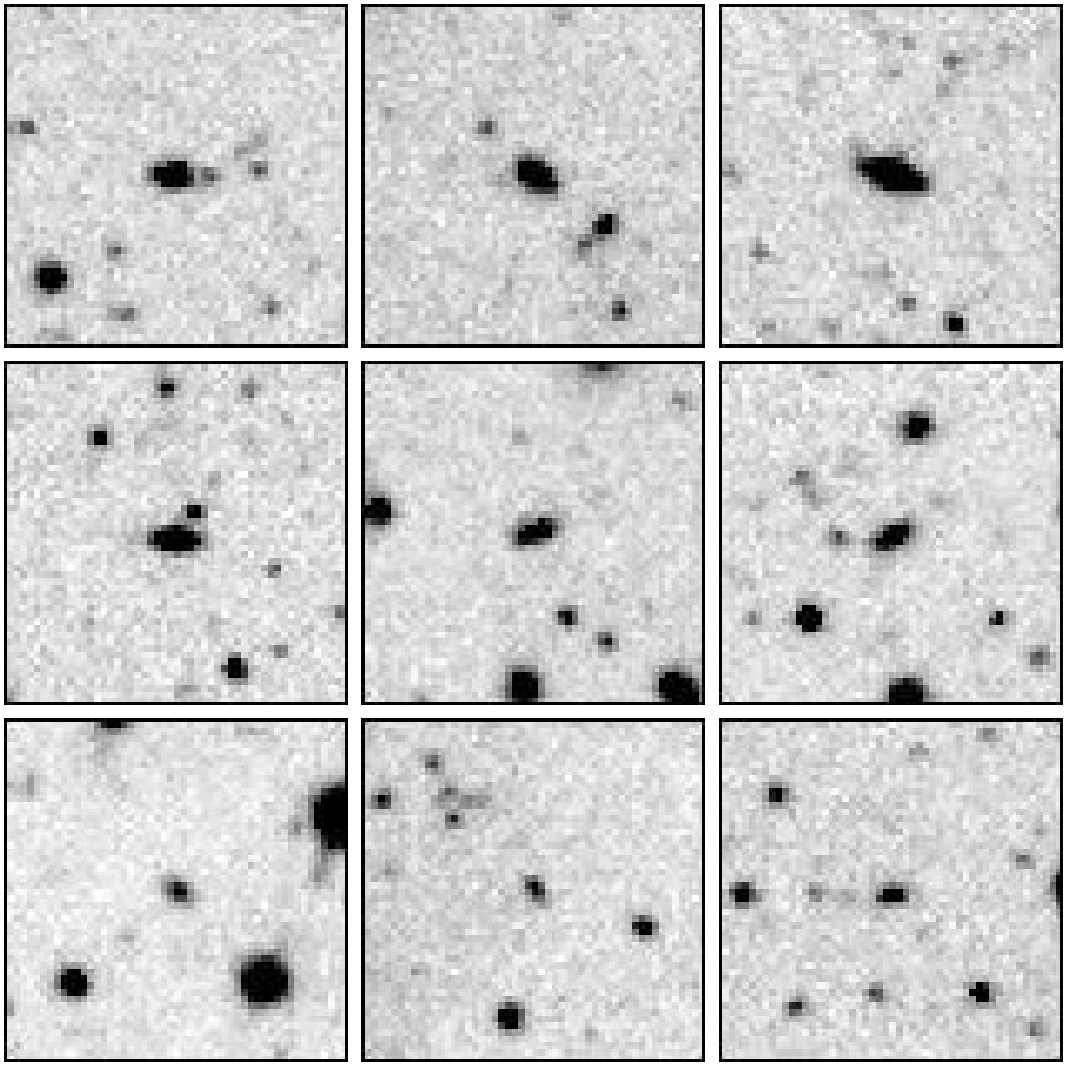

Figure 5.12: Examples of detections in field F0154-39:M at varying levels of face on disk central surface brightness. The top row is for $\mu_{0,i}$ of 21.5–22.0, the middle row for 22.0–22.5, and the bottom row for 22.5–23.0

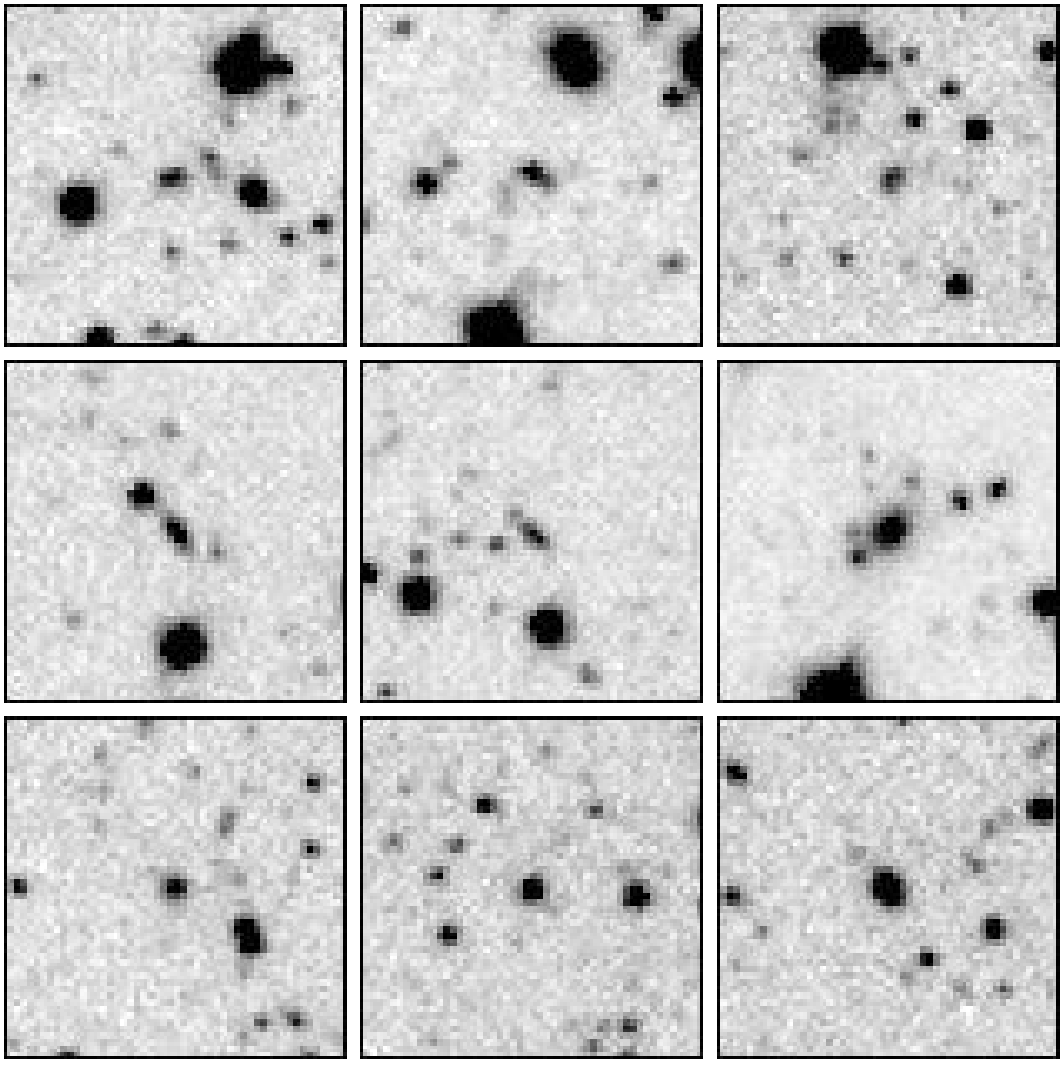

Figure 5.13: Examples of detections in field F0154-39:M at varying levels of face on disk central surface brightness. The top row is for $\mu_{0,i}$ of 23.0–23.5, the middle row for 23.5–24.0, and the bottom row for 24.0–24.5. We also note that these are clearly real objects in spite of their very LSB nature; detection of objects with $\mu_0 \approx 23.5$ R mag arcsec^{-2} was one of the main goals of the survey.

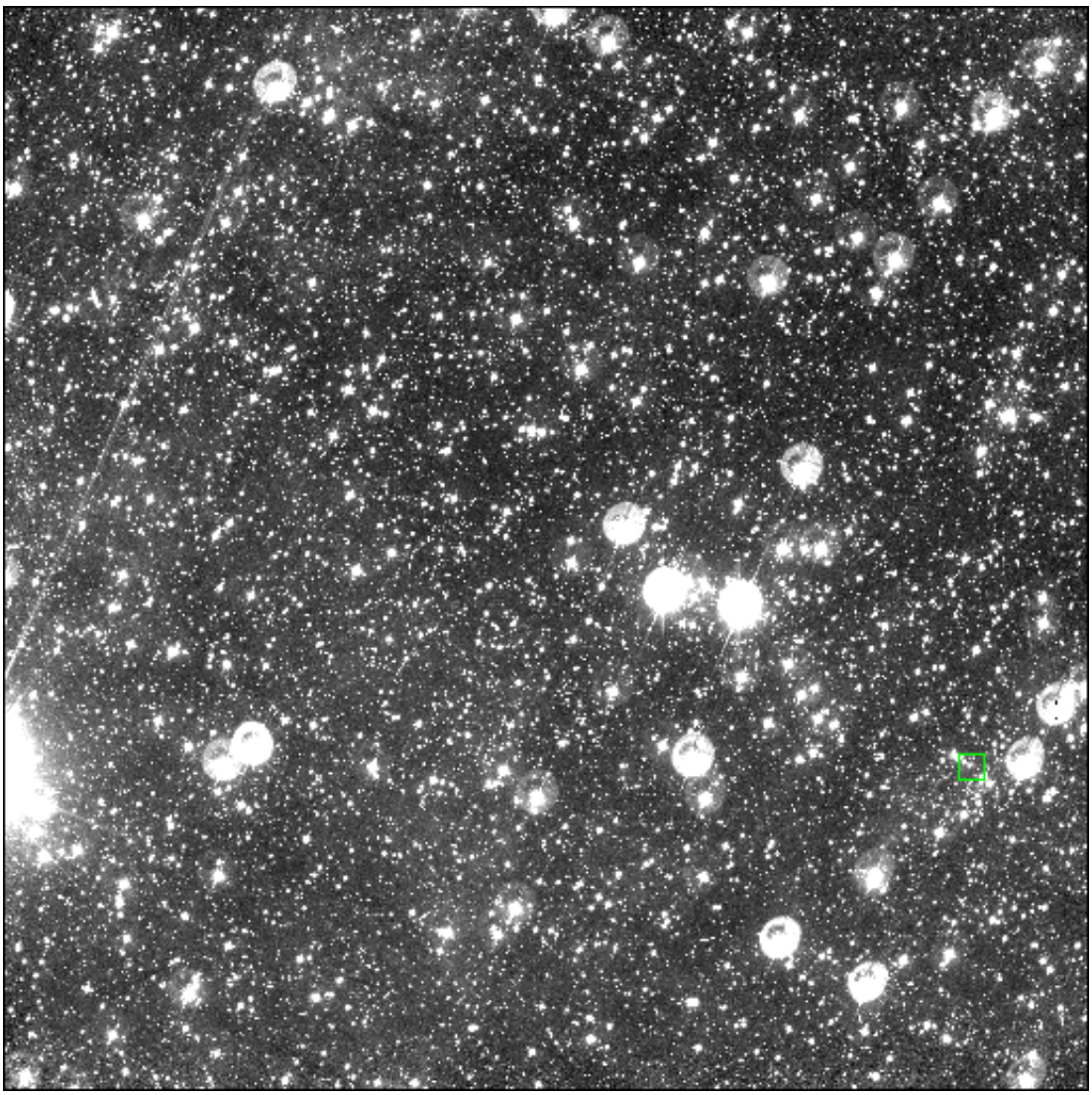

Figure 5.14: Image of field F2100-45:E including a thumbnail sized box.

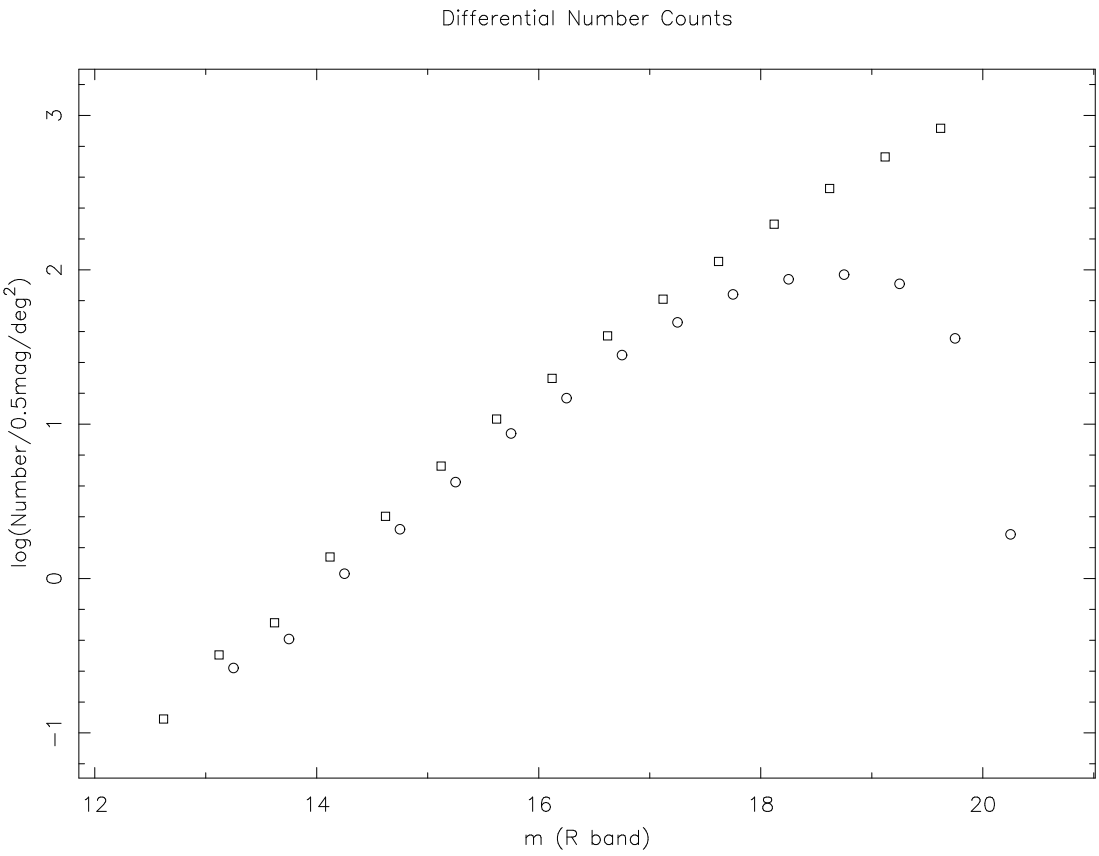

Figure 5.15: Plot of differential number count of objects as a function of R band magnitude. While cosmology affects the shape of the curve, the turn over at faint magnitudes is due to incompleteness. Circles are data points for our survey, squares are SDSS data taken from Table 2 of Yasuda et al. (2001).

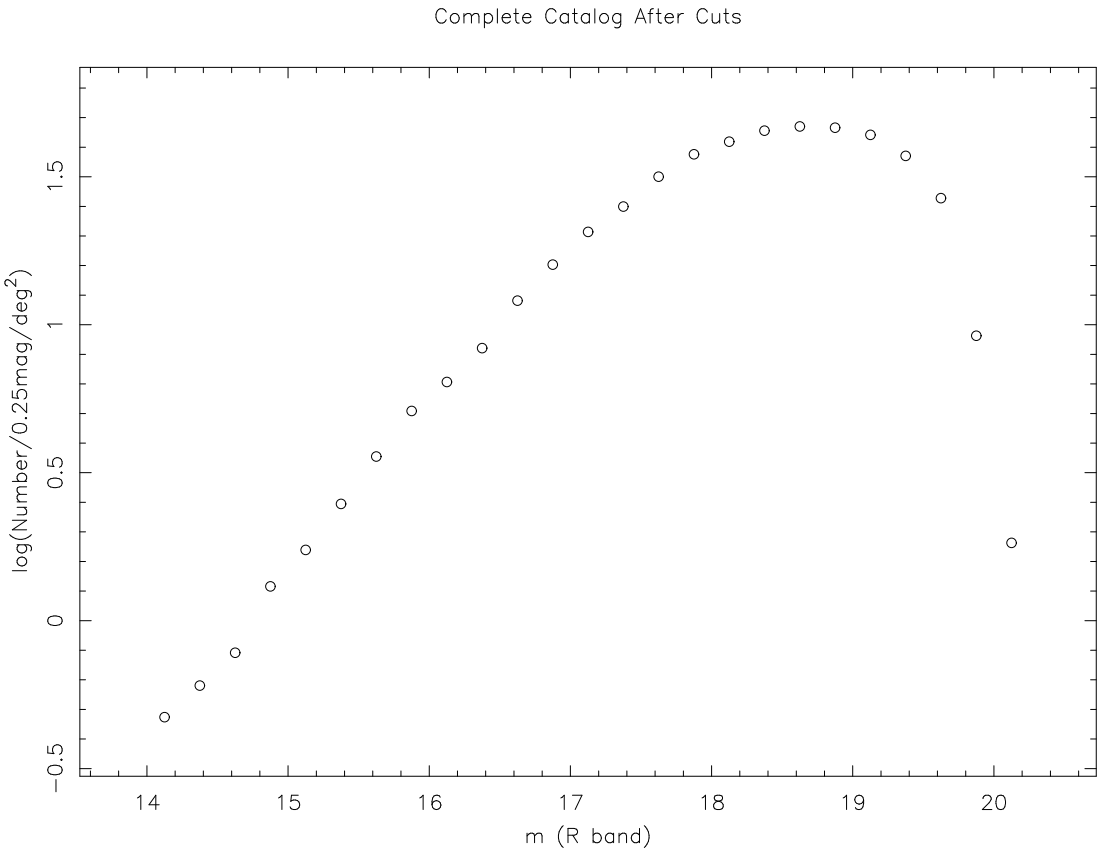

Figure 5.16: Plot of differential number count of objects as a function of R band magnitude for our data alone. A smaller bin size has been used in order to get a more detailed curve.

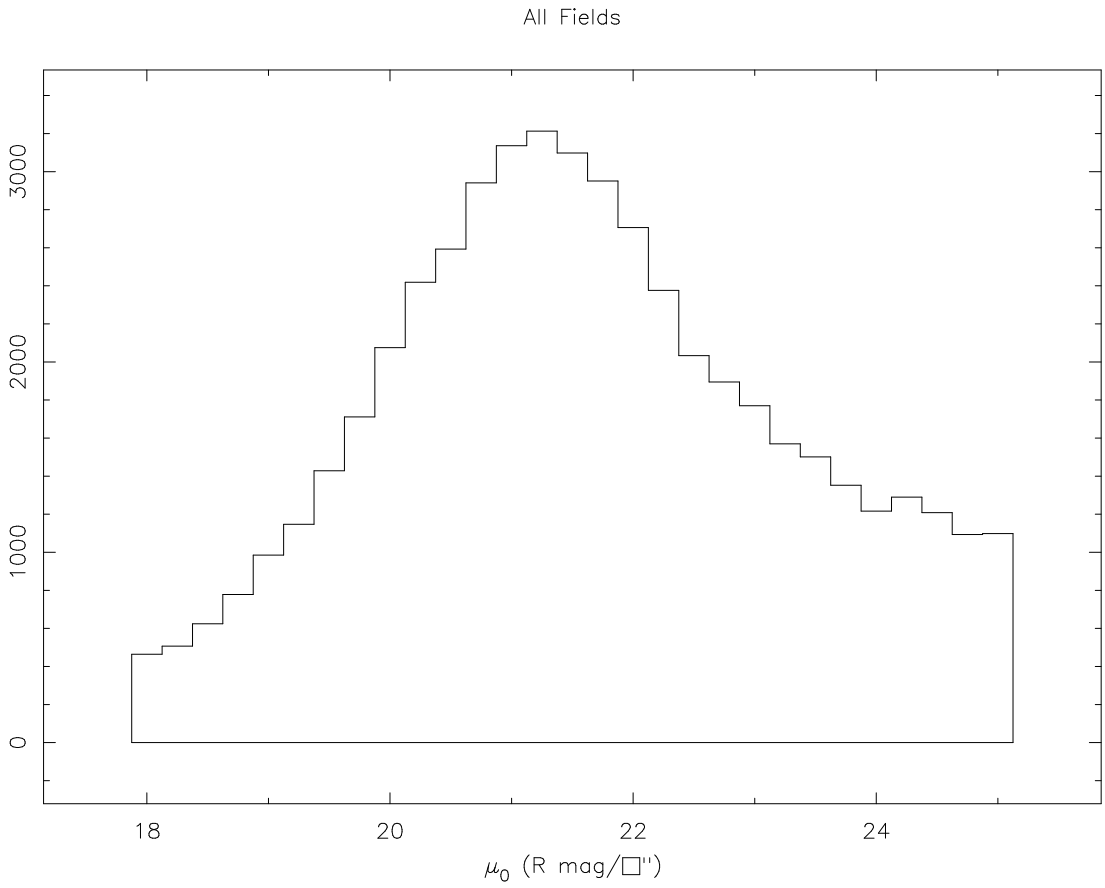

Figure 5.17: Histogram plot showing the distribution of objects with observed disk central surface brightness.

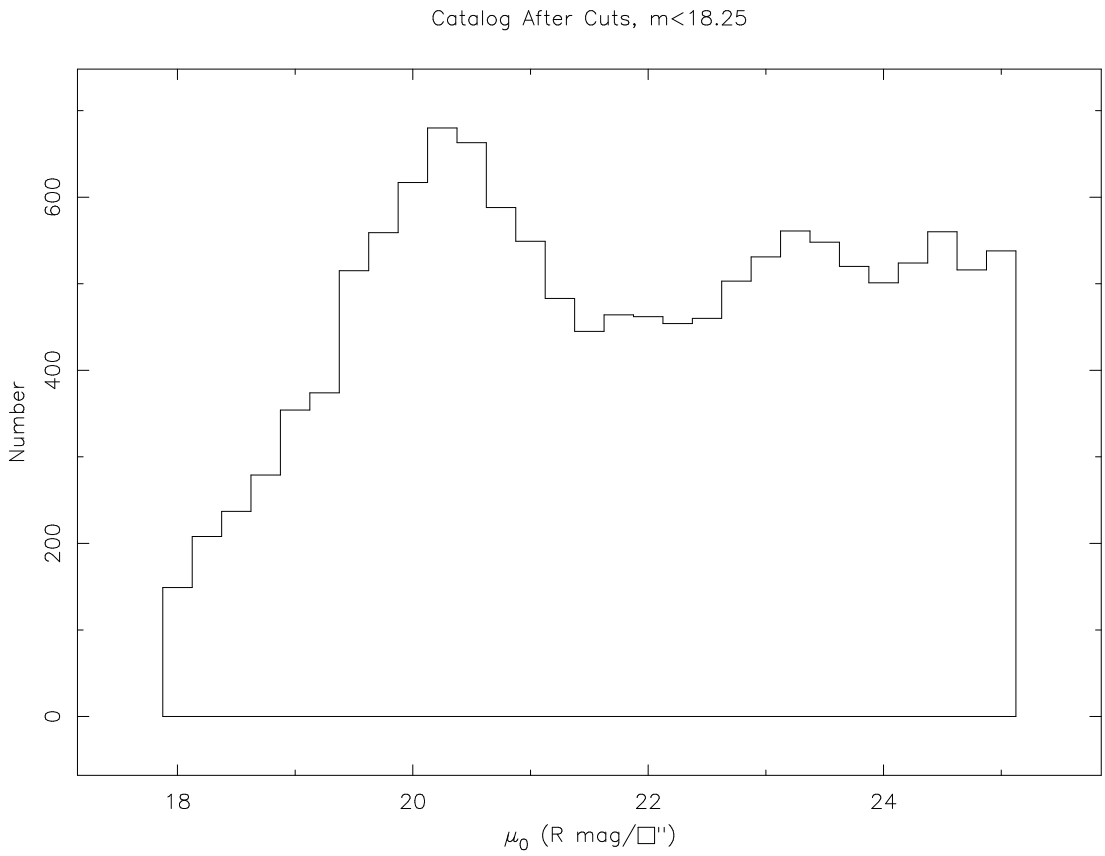

Figure 5.18: Histogram plot showing the distribution of objects with $m < 18.25$ with observed disk central surface brightness.

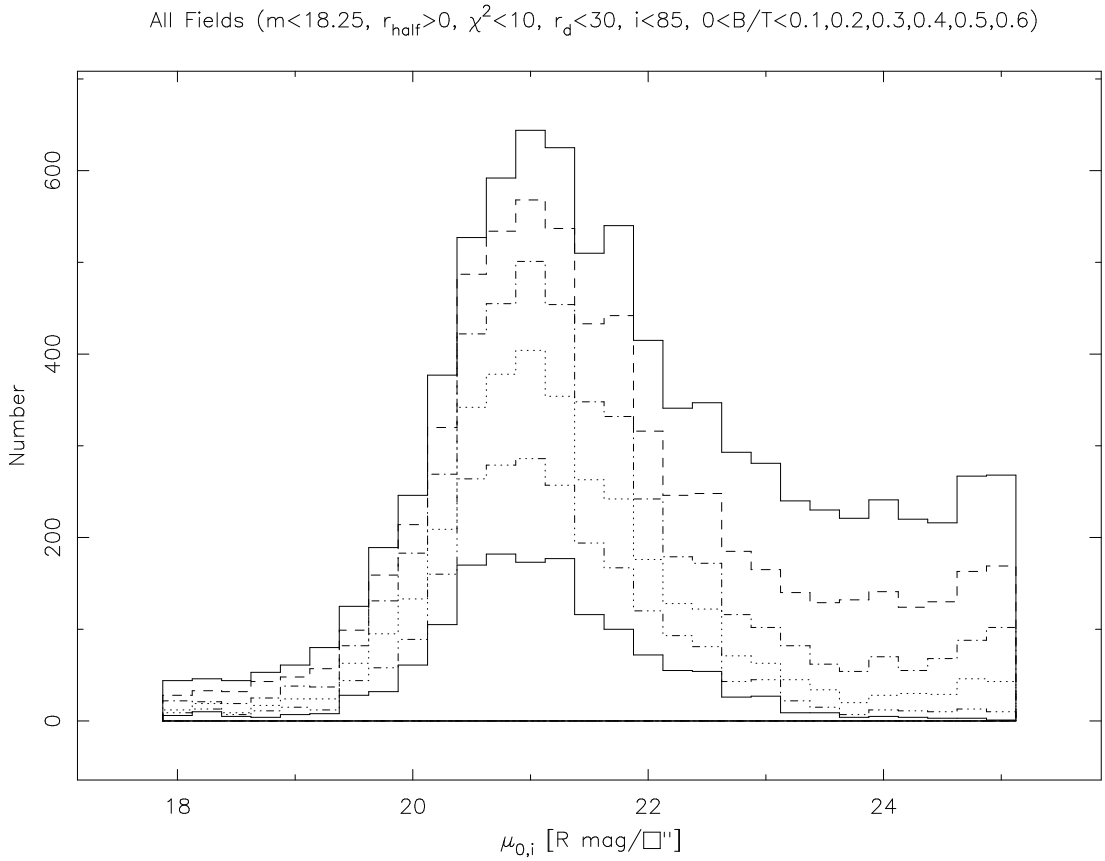

Figure 5.19: Histogram plot showing the effects of different cuts on B/T. The cuts are for $B/T \leq 0.6$, 0.5, 0.4, 0.3, 0.2, 0.1 going down from the top of the plot.

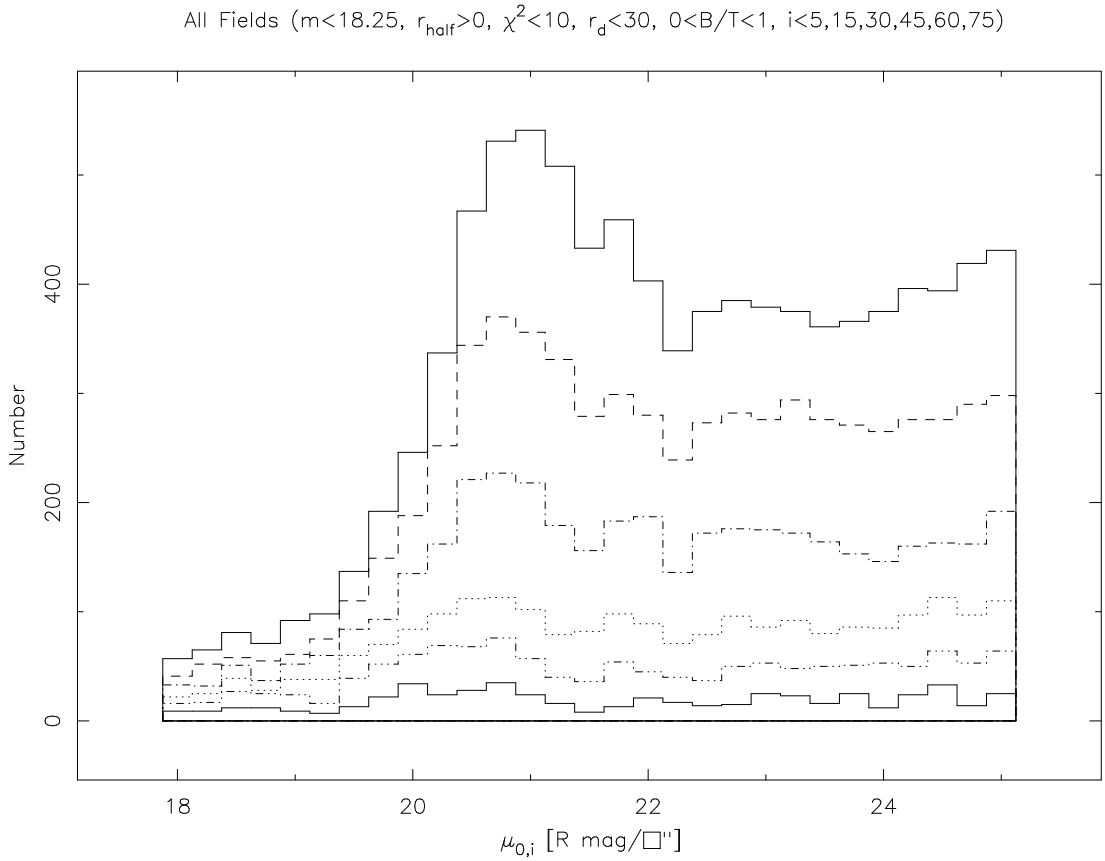

Figure 5.20: Histogram plot showing the effects of different cuts on i. The cuts are for $i < 75$, 60, 45, 30, 15, 5 degrees going down from the top of the plot.

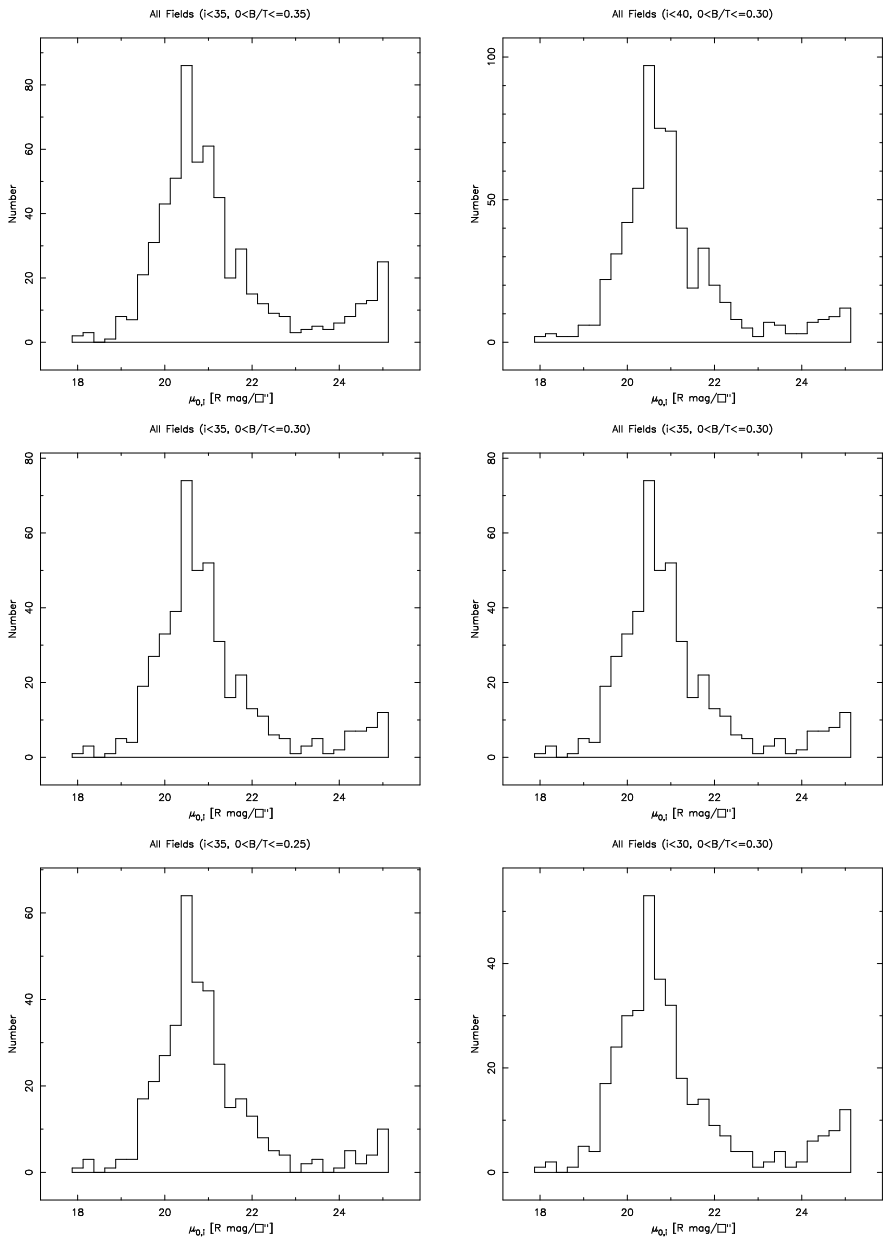

Figure 5.21: Histogram plots demonstrating the effects of changing the cuts on B/T and i. The left column shows a fixed $i < 35°$ cut with $B/T \leq 0.35, 0.30, 0.25$ from top to bottom. The right column shows a fixed $B/T \leq 0.30$ with $i < 40°, 35°, 30°$ from top to bottom. The shape of the distribution is basically the same in all plots, indicating that we have found the level where most of the bad detections have been removed by the cuts.

Chapter 6

The Surface Brightness Distribution

Here we examine the distribution of galaxies with surface brightness and perform the necessary correction to obtain the intrinsic distribution from the one we observe. This was a primary goal of the survey and one of the key points that our survey can contribute to without having additional data and observations such as redshifts to determine distances. As such, we will examine this topic in some detail.

6.1 Observed Distribution

Having performed all of the previous cuts to separate stars from galaxies and remove bad detections from the catalogs, we now have a good selection of objects to study. We begin by plotting a histogram of the number of objects detected with face-on disk central surface brightness in Figure 6.1 and listing the results in Table 6.1. We see that the general shape of the distribution is fairly strongly peaked and this is a well known feature of the observed distribution. In a now classic paper, Freeman (1970) noted the tendency for galaxies in the sample he studied to cluster around a value of $\mu_0 = 21.65 \pm 0.3$ B mag arcsec^{-2}. Our

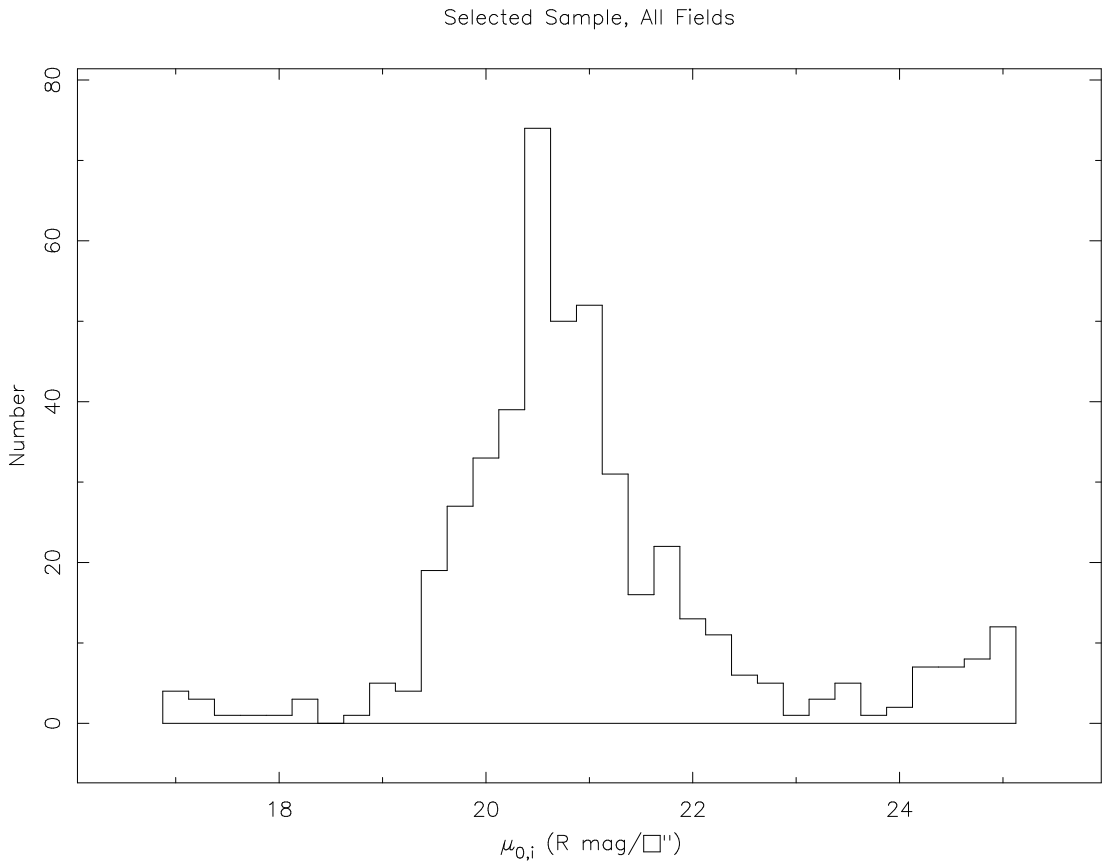

Figure 6.1: Histogram of the number of objects from all fields with $m < 18.25$ in the selected sample for face-on disk central surface brightness $\mu_{0,i}$.

distribution has a maximum around $\mu_{0,i} = 20.5$ R mag arcsec^{-2}. Taking the average B-R color of LSB galaxies to be 0.9 as such work as Padoan et al. (1997) and de Blok et al. (2001) note, this corresponds to $\mu_0 \approx 21.4$ in B. As noted in McGaugh (1996), the original Freeman value was not very well determined and the position of the peak tends to vary somewhat from survey to survey. Our value is in general agreement with the original one, but is a much better measurement because the depth and area of our survey allow us to detect many more objects. The shape of the distribution is partially due to selection effects —

Table 6.1: Observed Surface Brightness Distribution for Selected Sample

$\mu_{0,i}$ Bin Center	Number	$\mu_{0,i}$ Bin Center	Number
17.00	4	21.25	31
17.25	3	21.50	16
17.50	1	21.75	22
17.75	1	22.00	13
18.00	1	22.25	11
18.25	3	22.50	6
18.50	0	22.75	5
18.75	1	23.00	1
19.00	5	23.25	3
19.25	4	23.50	5
19.50	19	23.75	1
19.75	27	24.00	2
20.00	33	24.25	7
20.25	39	24.50	7
20.50	74	24.75	8
20.75	50	25.00	12
21.00	52		

higher surface brightness objects will generally be visible at greater distances, and thus in a larger volume, than lower surface brightness objects. This allows them to dominate over the LSB galaxies which can only be detected in a comparatively small volume and so the number counts will drop off at low surface brightnesses. In the next section we will account for this selection effect and make a correction to obtain the intrinsic distribution from our observed one. The drop off at high surface brightness is real (Allen & Shu 1979). As noted in McGaugh et al. (1995), this is essentially because the brightest objects in the intrinsic distribution will dominate in flux selected catalogs. Galaxies more luminous than that are rare as are ones with brighter surface brightnesses than the peak μ_0. Therefore we do

not expect to detect many very HSB galaxies. Since our distribution drops off at $\mu_{0,i} \approx 18.5$ R mag arcsec^{-2} and brighter than that we find few objects, we will focus our examination on objects with $\mu_{0,i} \geq 18$.

The rise in the number counts at extremely low surface brightness is unusual and warrants further investigation. We do not expect to see this many objects at these levels so we make a visual examination of them. In Figure 6.2, a small sample of objects with $\mu_{0,i} \geq 24.25$ R mag arcsec^{-2} from the deepest field, F2100-45:E, is shown. Most of the extremely LSB objects are similar to the ones pictured here. We find that cases of multiple objects fit as a single one still remain at this level despite our previous cuts to attempt to remove them. Many other objects are so small that it is very difficult to tell whether they should be classified as stars or galaxies even by visual examination so it is very likely that the computer fitting algorithm also had difficulty modeling these objects. Given that the classification of these objects and measurements of their properties is bound to be uncertain, we decide to make one final cut and remove objects with $\mu_{0,i} \geq 24.25$ from our study here. As noted by McGaugh (1996), detecting objects with $\mu_0 \approx \mu_\ell - 2$ is extremely difficult because the volume of space sampled at that level is very small. In Chapter 4 we determined that the limiting surface brightness for our chosen detection parameters is $\mu_\ell = 25.43$ mag arcsec^{-2} meaning that our sensitivity beyond $\mu_0 \approx 23.43$ will become low. We do not make the cut this high though because there is no obvious problem with the detections at this level; it may be difficult to find galaxies at that level, but we only find a small number and the shape of the distribution shows that these numbers are reasonable. Since the problem is with the counts rising beyond about 24.25, that is where we make the cut. This leaves no detections in the $\mu_{0,i} = 24.25$ R mag arcsec^{-2} bin, but the

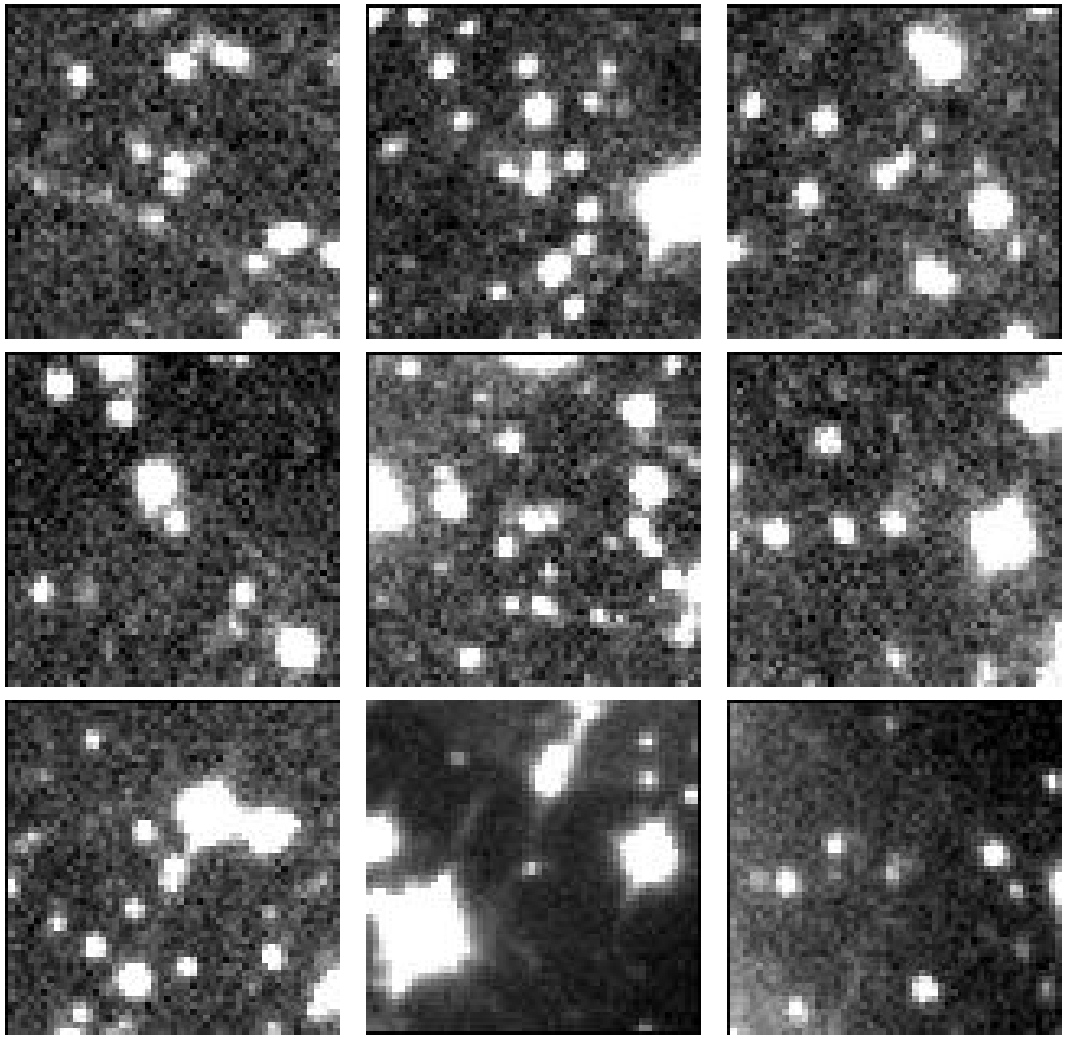

Figure 6.2: Examples of detections with $\mu_{0,i} \geq 24.25$ in field F2100-45:E. Most appear to be artifacts of fitting multiple objects as one or are small enough that it is very difficult to clearly distinguish star from galaxy by eye.

fact that we have detected any galaxies within about 2 mag of our limit indicates that the actual space density of such objects must be large. We show all twelve detections with $23 < \mu_{0,i} < 24.25$ R mag arcsec^{-2} in Figure 6.3, the output best fit model in Figure 6.4, and the residuals after this model is subtracted in Figure 6.5.

Four of these objects lie very close to saturated stars and an examination of their parameters shows that they have large disk scale lengths, $r_d > 15''$. This suggests that the results of the fits are being affected by the nearby star. We also note that among the other objects, two have $\chi^2 > 4$; the middle object of the second row down and the left object of the third row down. These higher χ^2 suggest that the fits here may not be as reliable as the fits to the other objects. When we determine the intrinsic distribution of our sample in the following section, we will include two alternate versions that account for these potential problems — one exluding only the objects near the saturated stars and the other excluding those objects and the two objects with high χ^2 values.

There is a possibility that some of these extremely LSB objects may be distant, cosmologically dimmed galaxies. Without redshifts to measure their distances, we cannot be certain. However, we can make an approximation using previously published magnitude–redshift plots such as the ones by Thompson et al. (1994), Snellen et al. (1996), and Brown et al. (2001). All three present R band plots with essentially the same relation, but it should be noted that they are also all for radio galaxies. Postman et al. (1985) present an R band plot for 561 Abell clusters using "Abell's corrected photo-red magnitudes for the tenth-ranked cluster member". A plot in the R band for field galaxies could not be found; such work was typically done in either the B or K bands. A histogram plot for the magnitude of our detections with $\mu_{0,i} > 24.25$ (Figure 6.6) shows that the majority of them have $m \approx 17$–18 with the peak at about 18 and a greater number of brighter objects than fainter ones. Using the m–z plots from the radio galaxy work as guides, we estimate that $m = 18$ corresponds to a redshift of $z \approx 0.28$, but for the Abell cluster work, $m = 18$ gives $z \approx 0.22$. The surface brightness of objects is dimmed

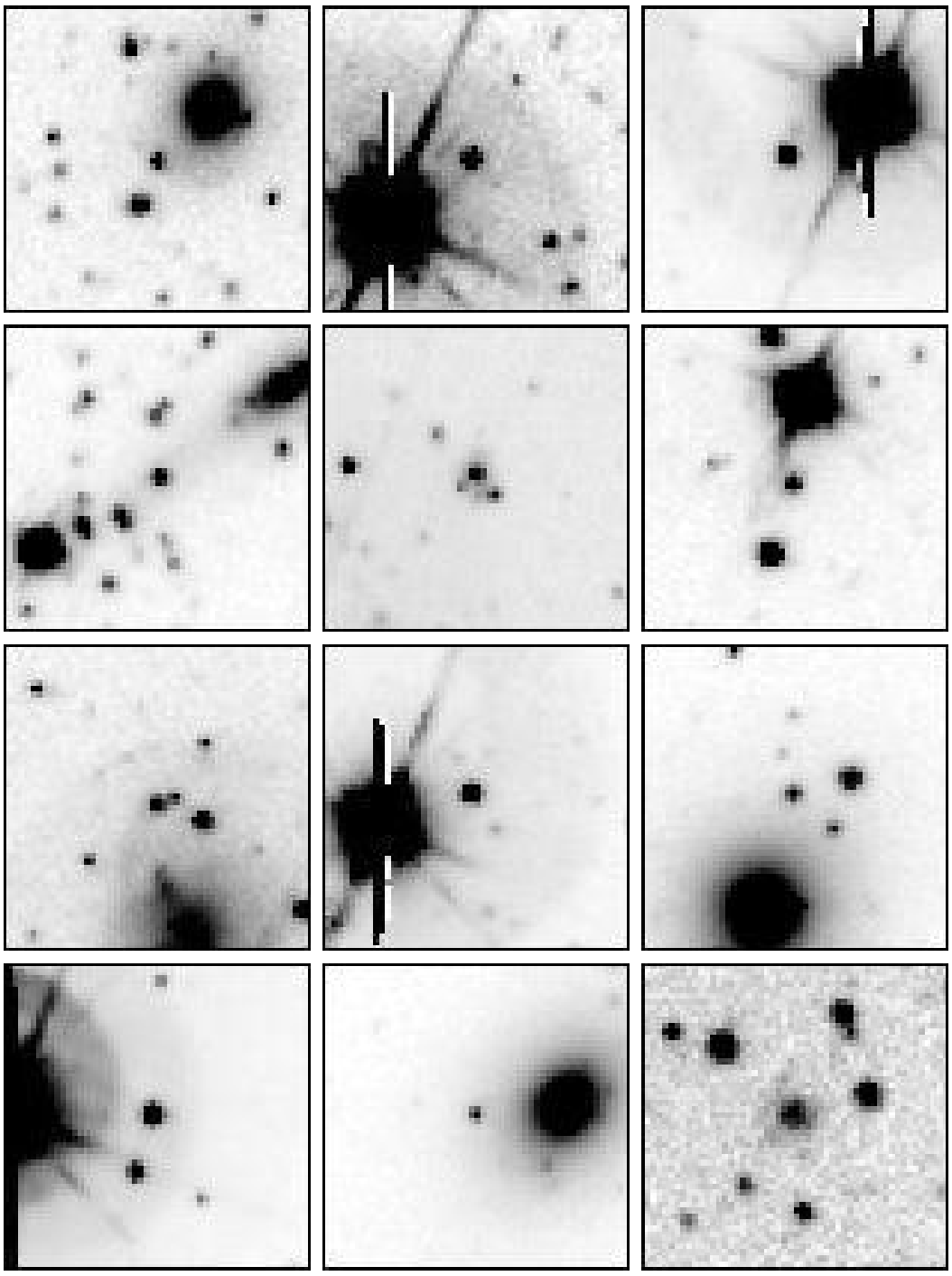

Figure 6.3: The twelve detections with $\mu_{0,i} \geq 23$.

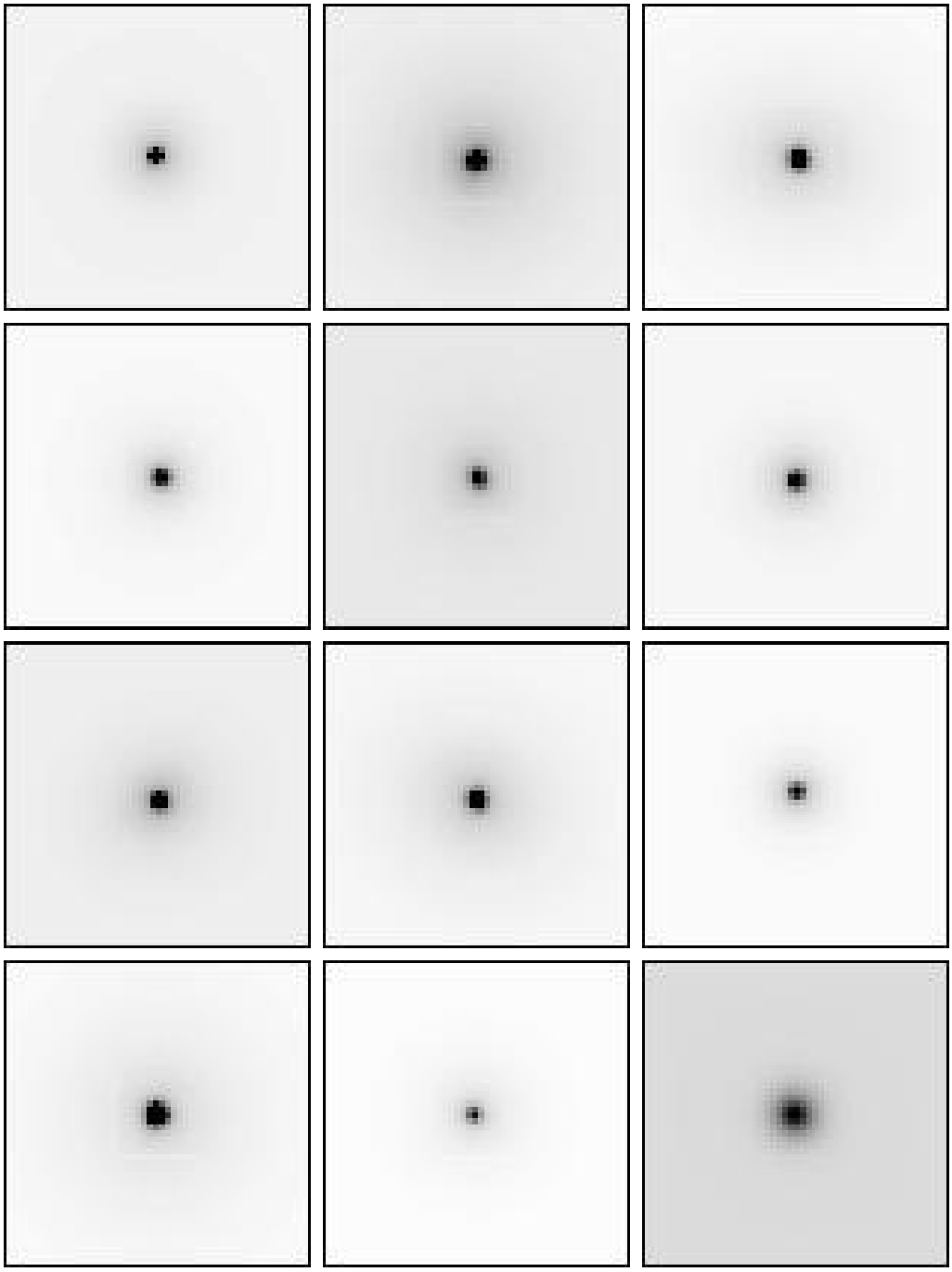

Figure 6.4: Output models for the twelve detections with $\mu_{0,i} \geq 23$.

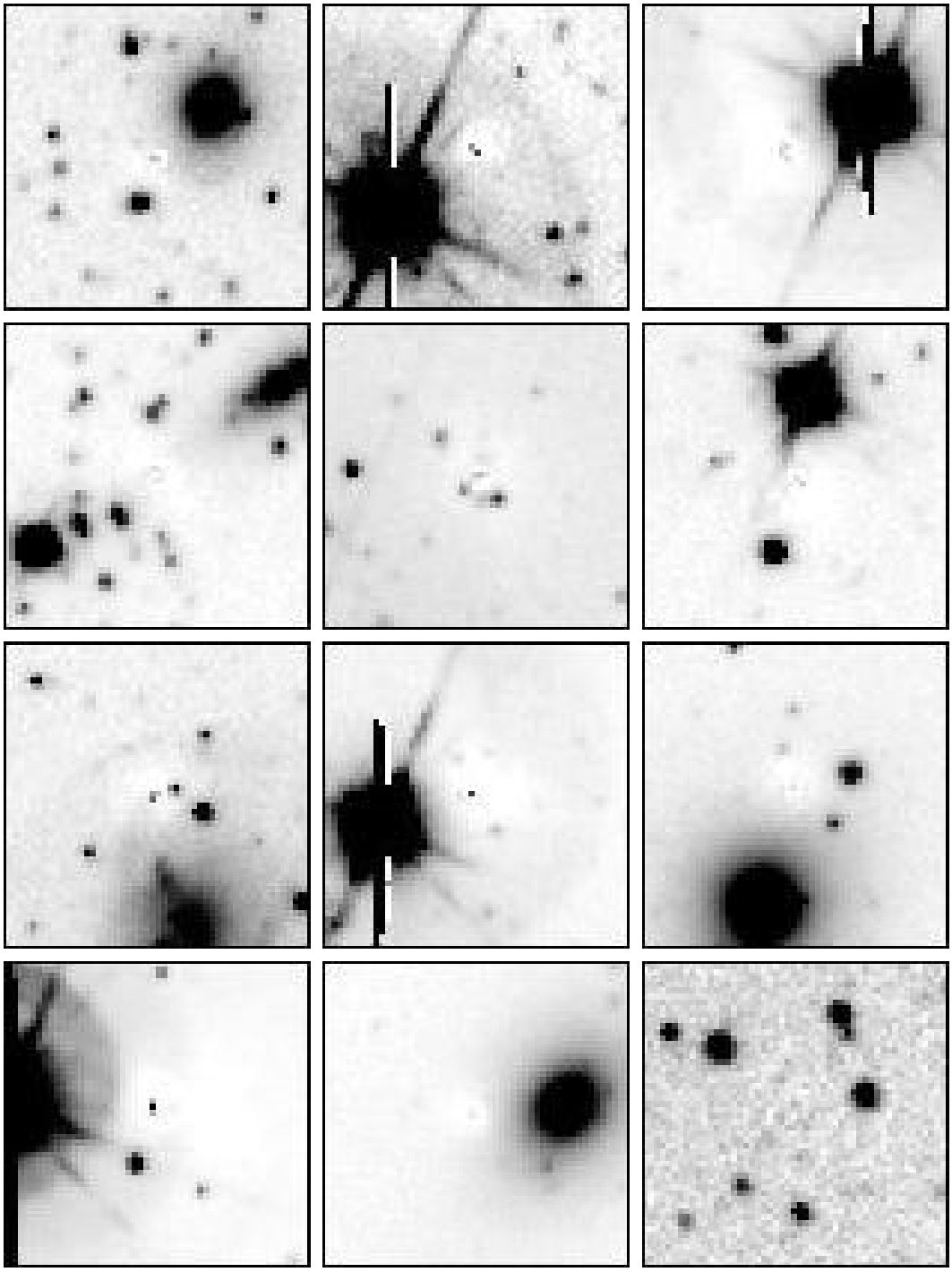

Figure 6.5: Residuals for the twelve detections with $\mu_{0,i} \geq 23$.

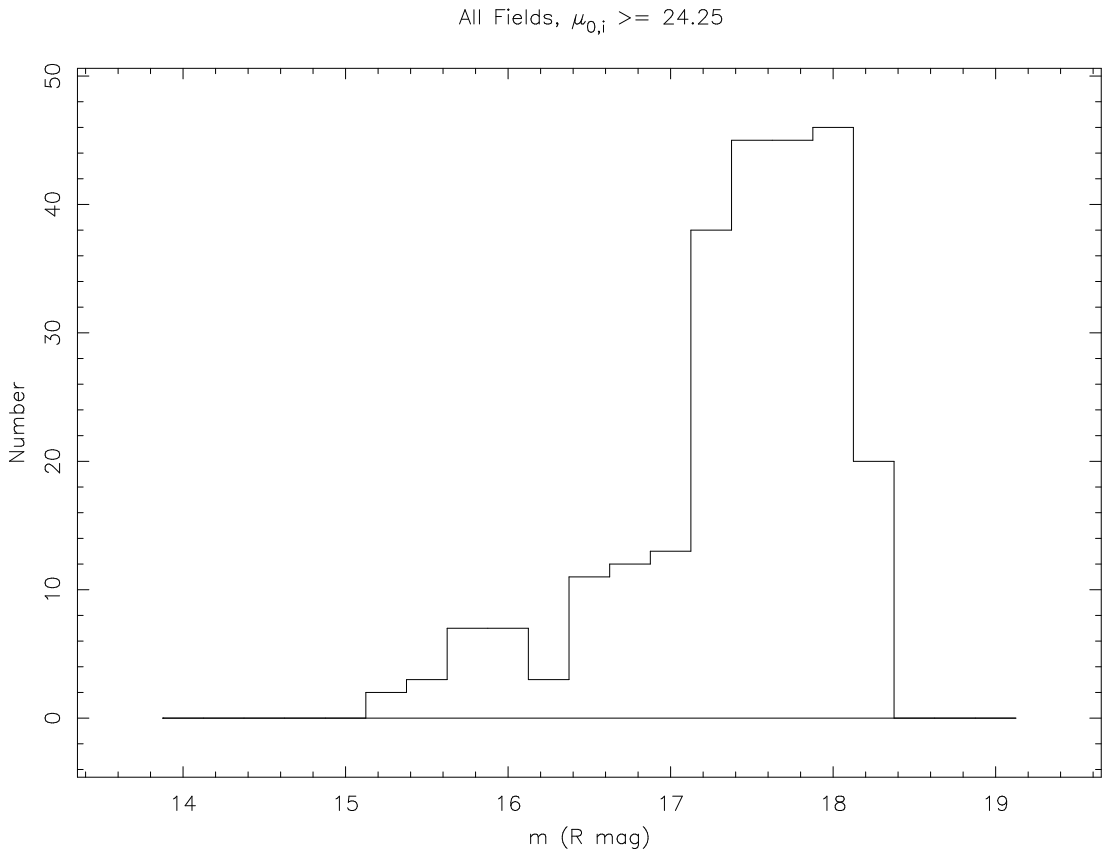

Figure 6.6: Histogram of the number of objects with $m < 18.25$ and $\mu_{0,i} \geq 24.25$.

by a factor of $(1+z)^4$ in an expanding universe, an effect derived by Hubble & Tolman (1935) and noted as one that can be used as a test for the expansion of the universe. In terms of the magnitude scale, this is a factor of $2.5\log((1+z)^4)$ or $10\log(1+z)$ which is about 1.07 for $z = 0.28$ or 0.86 for $z = 0.22$. For our selected sample, the histogram plot in Figure 6.7 shows that the $\mu_{0,i} \leq 24.25$ detections have a peak at $m \approx 18$ indicating that the average redshift is about the same as for the detections with $\mu_{0,i} > 24.25$ with the same average dimming of roughly 1 mag. The fact that this distribution shows the expected rise in number counts while the distribution in Figure 6.6 for the objects with $\mu_{0,i} > 24.25$ does

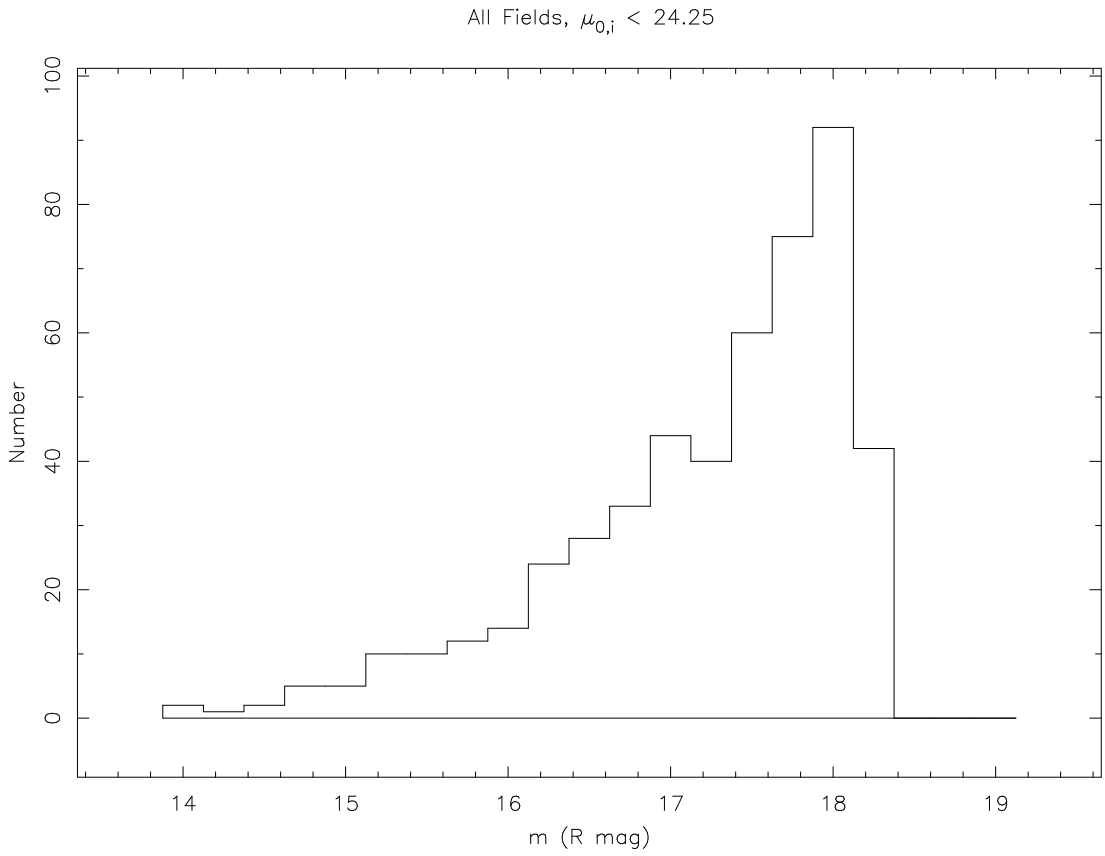

Figure 6.7: Histogram of the number of objects with $m < 18.25$ and $\mu_{0,i} < 24.25$.

not is an indication that these extremely LSB objects are unlikely to be real galaxies. Cosmological dimming may be affecting our results, but it is certainly not the only possible contributing factor as we have already seen that some bad detections are part of this population.

Another method for estimating the redshift to which our sample extends is by assuming values for a typical LSB galaxy and then calculating at what distance it will no longer be included in our sample. We will use a pure exponential disk galaxy with absolute B magnitude $M = -18$ or about $M = -19$ in R and scale length $h = 1$ kpc. When we selected our sample, we excluded objects with

apparent magnitude $m > 18.25$. Using the relation $m = M + 5\log(d) - 5$ with d measured in parsecs, we find that our typical LSB will reach $m = 18.25$ at $d = 282$ Mpc. To convert this to a redshift, we use $z = v/c$ and $v = H_0 d$ to get $z = H_0 d/c$ and assume $H_0 = 75$ km s^{-1} Mpc^{-1}. This results in a redshift of $z = 0.071$. We can also check the size; while we did not place a minimum size cut on our sample, a galaxy with $r_d < 2''$ has a scale length of less than one pixel. Using the simple small angle approximation that $r_d = h/d$ in radians and converting to arcseconds, we find that our typical LSB galaxy will reach $2''$at $d = 103$ Mpc and $1''$at $d = 206$ Mpc. These correspond to redshifts of $z = 0.026$ and $z = 0.052$, respectively. Since we also placed a surface brightness cut on the extremely faint end, we can also check on this value. Using Equation 6 of Simard et al. (1999), that $\mu_0 = M + 5.0\log(r_d) + 38.57$ in the B band for a pure exponential disk, we calculate that our typical LSB has $\mu_0 = 20.57$ mag arcsec^{-2} in B or approximately 19.57 in R. Since the surface brightness is dimmed by a factor of $10\log(1+z)$, we find that $z = 1.87$ would be required to dim the central surface brightness to 24.25. This is well beyond the previous measures which indicate that this is not the limiting factor. In Figure 6.8, we plot $\mu_{0,i}$ vs. r_d for the selected sample. The smaller objects tend to be the brighter ones which demonstrates the difficulty of detecting very small, very low surface brightness objects. This plot also shows that the four lowest surface brightness objects with the largest scale lengths lie off the general trend followed by most of the objects; these are the four objects next to saturated stars mentioned earlier. Our calculations suggest that our survey samples $z < 0.1$ where cosmological dimming is not a dominant effect. At this point we should also note that dimming alone cannot explain our observed distribution. Ferguson & McGaugh (1995) simulated how $(1+z)^4$ dimming would

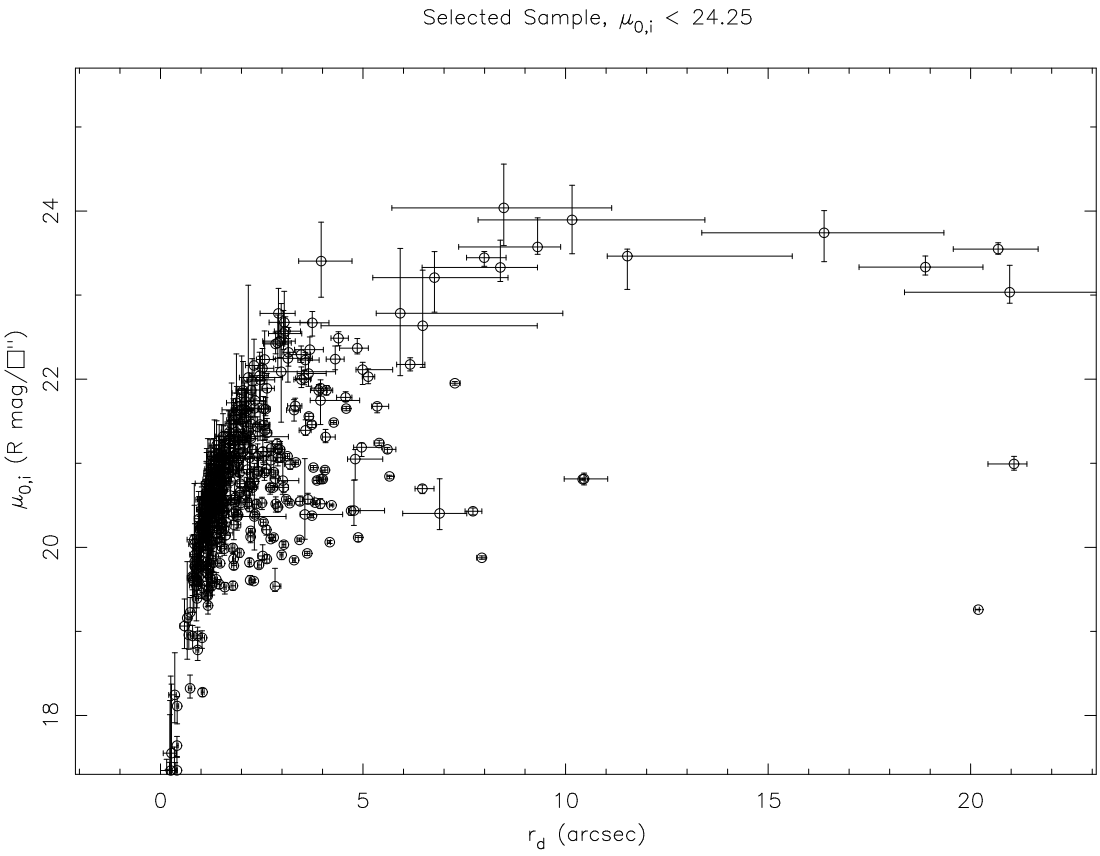

Figure 6.8: Plot of $\mu_{0,i}$ vs. r_d for the selected sample.

affect a sample of pure disks that followed Freeman's law and found that it cannot produce the smooth tail of the observed number–surface brightness distribution, it only affected the scatter. We have detected real LSB galaxies; they cannot all be distant, dimmed HSB galaxies. We have made an estimate of the effect, but until redshifts and thus distances area available for our detections, it is uncertain exactly how strongly cosmological dimming may be affecting our results.

6.2 Selection Effects and the Intrinsic Distribution

The strong peak of the observed surface brightness distribution could be due to selection effects or it could be a feature of the intrinsic distribution. Disney (1976) was one of the first to demonstrate that selection effects could explain the observed distribution. Later work such as that by Disney & Phillipps (1983), Davies (1990), and McGaugh et al. (1995) expanded upon this subject, demonstrating how powerful these selection effects could be. Larger and more luminous galaxies can be detected at a greater distance than smaller and less luminous galaxies. Thus they probe a larger volume of space and so we expect such objects to dominate a flux limited sample. A correction for the volume probed needs to be made to compensate for this selection effect and obtain the intrinsic distribution. One common method for doing this is the V/V_{max} method described by Schmidt (1968) for a magnitude limited catalog. It uses the ratio of the volume corresponding to the observed distance and the volume corresponding to the maximum distance at which the object could lie and still be included in the sample according to its selection limits. This ratio can serve as a weighting factor to correct for incompleteness due to the selection effects. However, this requires knowledge of the distances to the objects in the sample which we do not. Therefore we use another method where we derive the volume probed as a function of the parameters used to describe the galaxies. This has been done in the works noted above and we will follow McGaugh et al. (1995) for deriving the equations that describe the volume sampled by a flux limited survey; this is also done in McGaugh (1996). We can then use this information to convert our observed

distribution into an intrinsic one.

We begin by describing the light profile of a galaxy as an exponential disk:

$$\Sigma(r) = \Sigma_0 \exp\left(-r/\alpha\right) \tag{6.1}$$

which is identical to Equation 4.7 except that r_d has been replaced by α to emphasize that it is an angular scale length. It corresponds to a physical scale length h at a distance d. This can be converted into more familiar magnitude units by taking $-2.5\log$ of both sides and simplifying to get

$$\mu(r) = \mu_0 + 1.086(r/\alpha) \tag{6.2}$$

This implicitly assumes that the objects are face-on. As we have selected our sample to only include disk dominated systems that are relatively face on, these are good approximations to the assumptions made here. The inclination correction to obtain a face-on value is relatively small and as the objects are disk dominated, any bulge component that may be present should not have a strong effect on the results. The total luminosity is obtained by integrating Equation 6.1:

$$L = \int \Sigma(r) r dr d\theta \tag{6.3}$$

from zero to infinity. Since there is no explicit dependence on θ, this just integrates to 2π leaving an integral in r of the form $\int x\exp(ax)dx$ which, when solved, produces

$$L = 2\pi\Sigma_0 h^2 \tag{6.4}$$

where h has been used since we are dealing with the actual physical scale length at this point, not the observed angular size. In the case where only some fraction of the light within $x = r/\alpha$ scale lengths is measured, the integrated luminosity is multiplied by a function $f(x)$ which is obtained by integrating Equation 6.3

from 0 to r and from 0 to infinity, then taking the ratio. After simplifying, we find

$$f(x) = 1 - (1 + x) \exp -x \tag{6.5}$$

In our case, the GIM2D package calculates the total flux by integrating from zero to infinity, as equations in Simard et al. (2002) indicate, so we will not need to use this $f(x)$ factor in our calculations. Normally this will be a relatively small correction, but it is important to include when all the flux is not accounted for, for example when isophotal values are measured. For a flux limited sample, the volume sampled depends on the luminosity visible above the selection limit, typically a limiting isophote. Since $V \propto d^3$ and $L \propto d^2$ from Equation 6.4, $V \propto L^{3/2}$. Then within the limit, $V \propto (\Sigma_0 h^2 f(x_\ell))^{3/2}$ or converting Σ into magnitude units,

$$V \propto h^3 10^{-0.6(\mu_0 - \mu_0^*)} (f(x_\ell))^{3/2} \tag{6.6}$$

which is Equation 10 of McGaugh et al. (1995). The μ_0^* term has been added to provide an arbitrary normalization factor. For simplicity, we will set this to the peak of the observed distribution.

Ideally, we would like to construct a bivariate distribution $\Phi(h, \mu_0)$, but cannot do so without redshifts to determine distances and thus get physical scale lengths. However, we can determine the surface brightness projection, $\phi(\mu_0)$ of this bivariate distribution using

$$\phi(\mu_0) = \frac{N(\mu_0)}{N(\mu_0^*)} \frac{V(h^*, \mu_0^*)}{V(h, \mu_0)} \tag{6.7}$$

where the $*$ indicates a normalization factor; this is Equation 12 of McGaugh et al. (1995). Since we do not have information about physical scale lengths, we make the assumption that the scale length is not correlated with the central

surface brightness; as noted in McGaugh et al. (1995), observational data support this assumption. This simplifies the volume correction to

$$V \propto 10^{-0.6(\mu_0 - \mu_0^*)} \tag{6.8}$$

where μ_0^* is the same normalizing factor as before and $f(x)$ has been dropped since the GIM2D package integrates to infinity to obtain total fluxes. Therefore we can obtain the intrinsic distribution by dividing our observed distribution by the results from Equation 6.8. This has been done in Figure 6.9 where the line for the volume correction has been placed on the histogram of the observed surface brightness distribution in the left hand plot and the division has been performed in order to produce the intrinsic distribution in the right hand plot. The error bars on the points in the intrinsic distribution are simply $\sqrt{N}/N$ from counting statistics errors and in order to get better statistics at very low surface brightnesses where few objects are detected, we use a larger bin size for $\mu_{0,i} \geq 23$ R mag arcsec^{-2}. We used a larger bin size on the very high surface brightness end for the same reason. As noted in the previous section, an examination of the faintest objects shows some potential problems. In Figure 6.10 we show the distribution excluding the four faintest objects that lie near saturated stars and in Figure 6.11 we show the distribution excluding the two additional objects with high χ^2 values. In both cases, the shape of the distribution remains essentially the same as that of the full sample including all of the faintest objects, so we will continue to use the full sample here.

For comparison, we plot our results together with the flux selected sample of Davies (1990) in Figure 6.12. In order to align the Davies B band data with our R band data on this plot, we shifted them by 1.375 magnitudes ((B-R) = 1.375) so that the peaks of both observed distributions were at the same point. Metcalfe

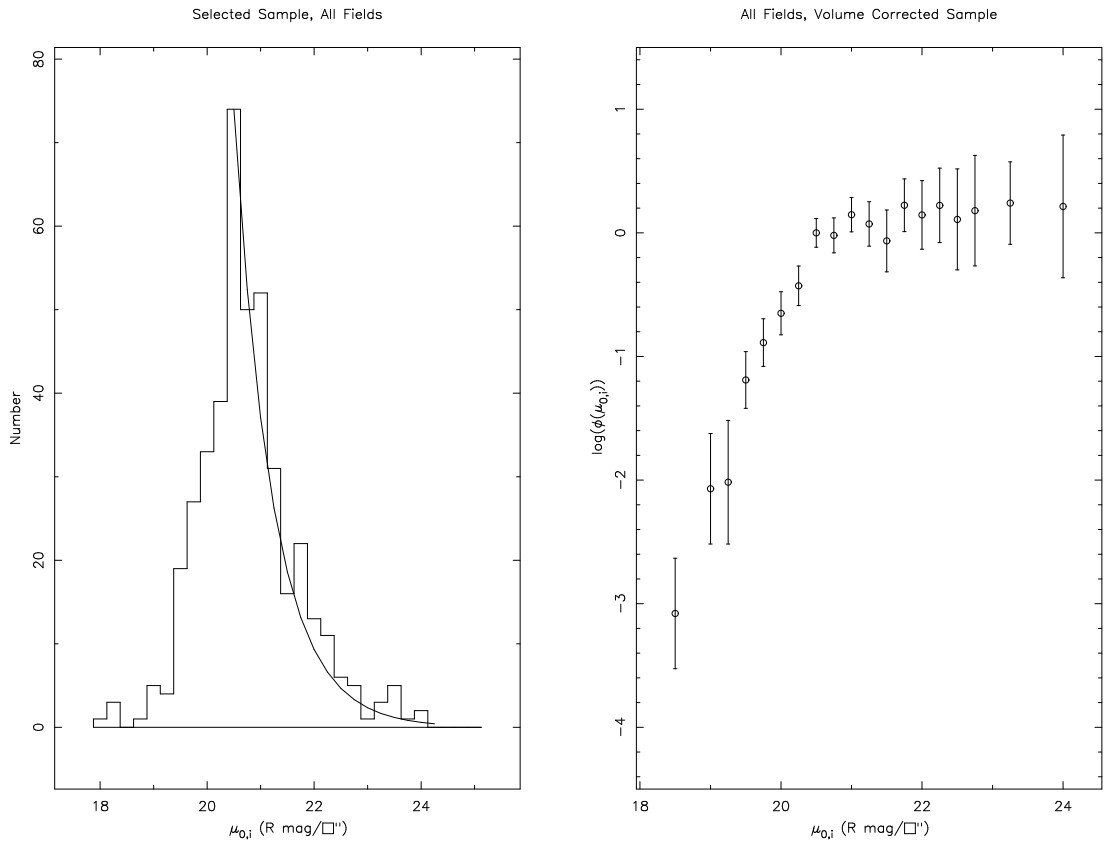

Figure 6.9: Plots of the observed and intrinsic surface brightness distributions for our selected sample. The curve on the observed plot is the volume correction from Equation (6.8). Errors on the volume corrected intrinsic distribution are $\sqrt{N}/N$ counting statistics errors. A bin size of 0.25 was used, but the results were combined near the limits to improve the statistics — a bin size of 1.0 was used for $18 \leq \mu_{0,i} < 19$ and a bin size of 0.75 was used for $23 \leq \mu_{0,i} < 24.25$.

et al. (1991) observed galaxies to m=25 in B and their number counts vs. color histograms tend to peak at approximately (B-R)$_{ccd}$ of 1.2. Using their stated conversion (B-R)$_{ccd}$ = 0.892(B-R) gives (B-R) = 1.35 for (B-R)$_{ccd}$ = 1.2 so our shift is in general agreement with the approximate (B-R) colors of galaxies. We

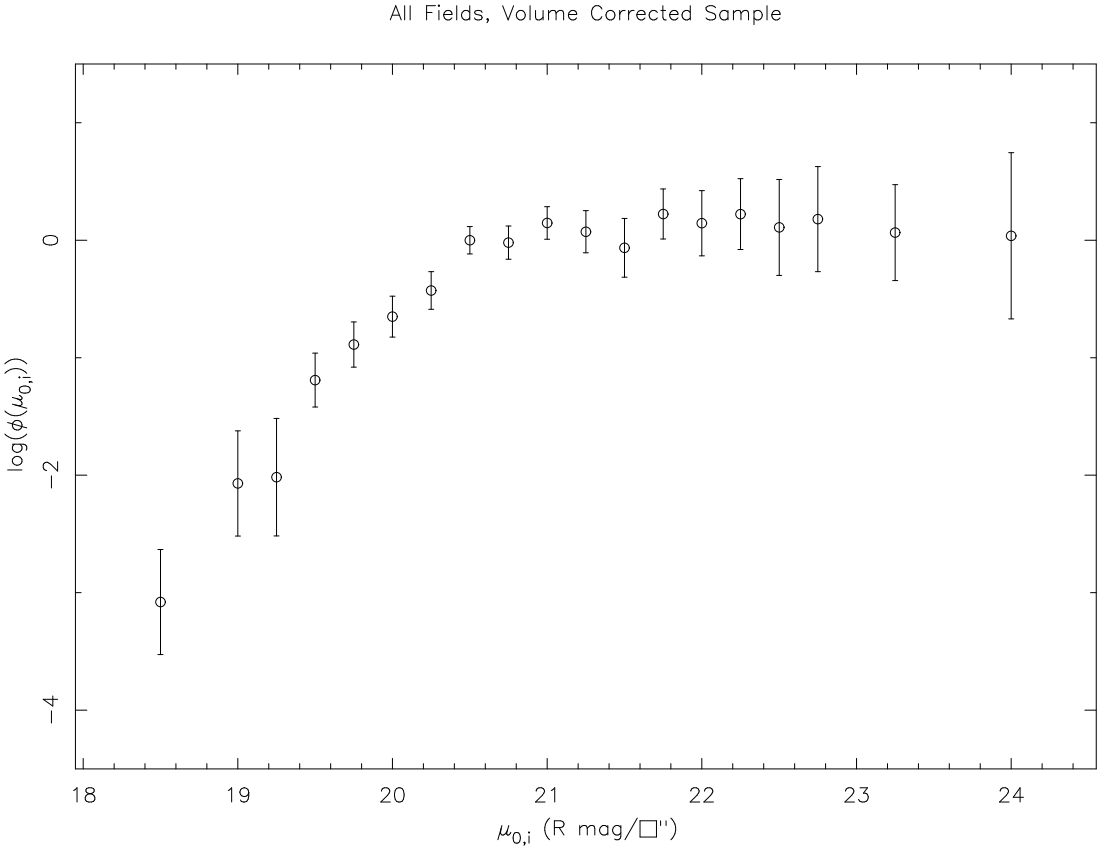

Figure 6.10: Plot of the intrinsic surface brightness distributions for our selected sample excluding the four of the twelve faintest objects that lie near saturated stars. The errors bars are $\sqrt{N}/N$ counting statistics errors. A bin size of 0.25 was used, but the results were combined near the limits to improve the statistics — a bin size of 1.0 was used for $18 \leq \mu_{0,i} < 19$ and a bin size of 0.75 was used for $23 \leq \mu_{0,i} < 24.25$.

see that the intrinsic distribution is roughly flat at very low surface brightness and we generally match the Davies data, though our points are typically somewhat higher relative to μ_0^*. This is in agreement with other work such as that of Phillipps et al. (1987) who also have somewhat higher numbers than Davies

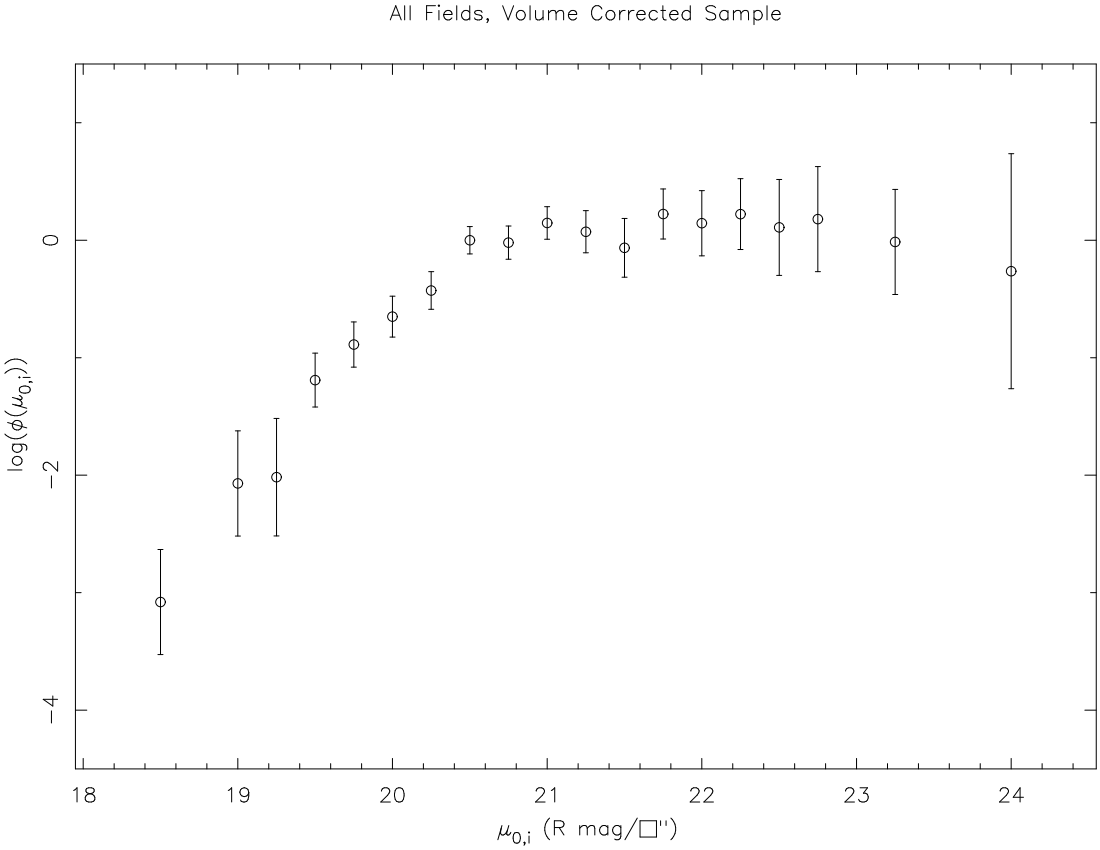

Figure 6.11: Plot of the intrinsic surface brightness distributions for our selected sample excluding the six of the twelve faintest objects that lie near saturated stars or have high χ^2. The error bars are $\sqrt{N}/N$ counting statistics errors. A bin size of 0.25 was used, but the results were combined near the limits to improve the statistics — a bin size of 1.0 was used for $18 \leq \mu_{0,i} < 19$ and a bin size of 0.75 was used for $23 \leq \mu_{0,i} < 24.25$.

(see, e.g., Figure 3 of McGaugh et al. (1995) or Figure 1 of O'Neil (2000)). Most importantly, we note that we have detected galaxies at very low surface brightness levels, down to approximately $\mu_{0,i} = 25$ in B, extending previous results into a region that has not been well explored.

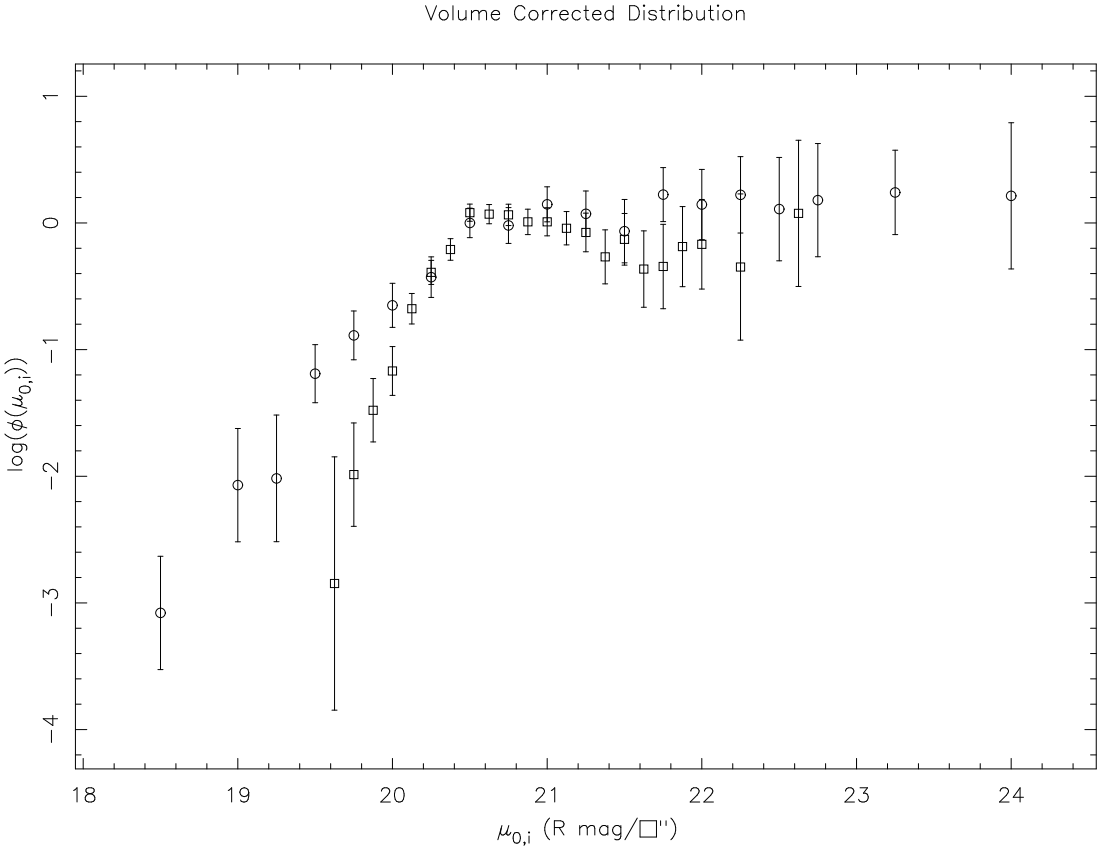

Figure 6.12: Plot of the intrinsic surface brightness distribution for our selected sample (circles) and that of Davies (1990) (squares). The B band data of Davies are aligned with our R band data by shifting them so the peaks of the observed distributions match. The Davies data use a bin size of 0.125, but the two lowest surface brightness points use a bin size of 0.375 to improve the statistics.

We now examine the effects of separating our selected sample into smaller B/T bins. This will allow us to see if mostly disk galaxies show the same distribution as almost pure disk galaxies. To do this, we create three bins: $0 < B/T \leq 0.1$, $0.1 < B/T \leq 0.2$, and $0.2 < B/T \leq 0.3$. In Figure 6.13 we plot the observed distribution for the full sample and each of these three bins with their corresponding

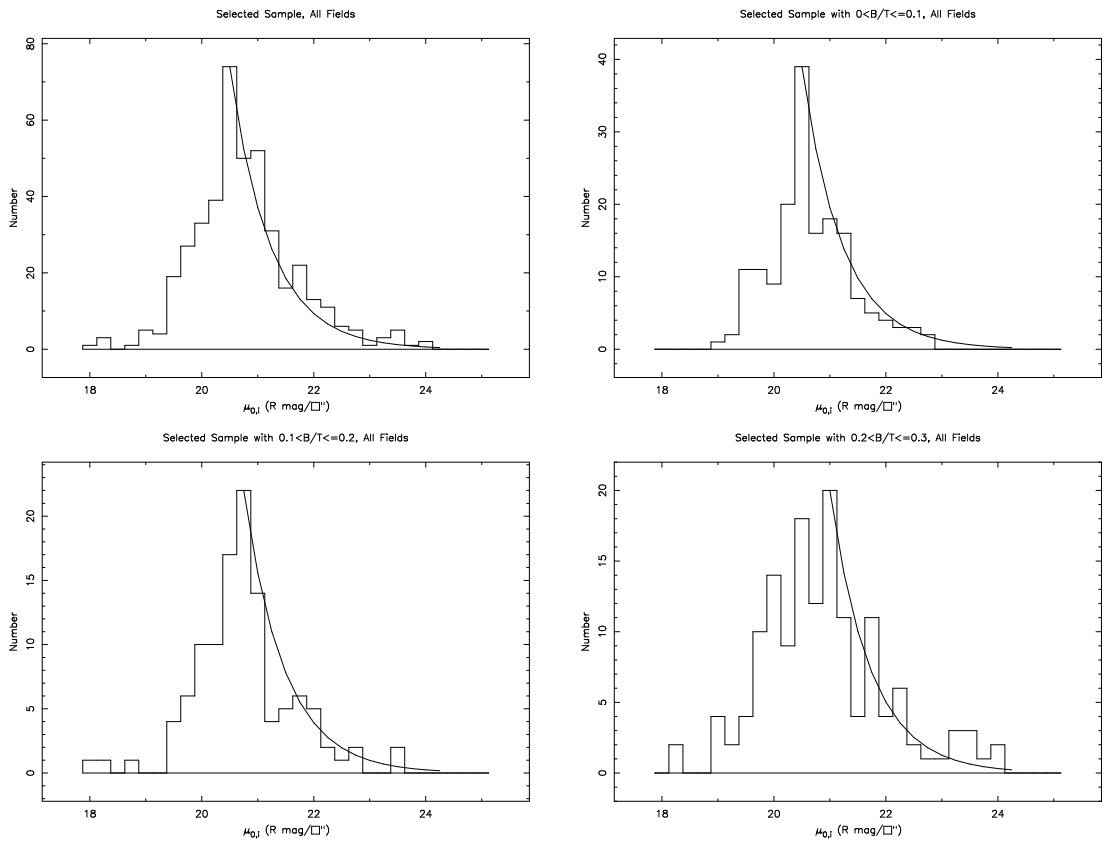

Figure 6.13: Plots of the observed surface brightness distributions for different B/T bins. The full sample, $0 < B/T \leq 0.3$, is shown in the upper left for reference; $0 < B/T \leq 0.1$ is in the upper right, $0.1 < B/T \leq 0.2$ in the lower left, and $0.2 < B/T \leq 0.3$ in the lower right. The curve is the volume correction from Equation (6.8).

volume correction lines. In Figure 6.14 we plot the volume corrected, intrinsic distribution for the full sample and each of these three bins. We use the same bin sizes as before, larger bins being used near the limits in order to improve the statistics, and the scales on all four plots are the same. These plots show that both the observed and intrinsic distributions are roughly the same for all

objects included here; the B/T subsets show essentially the same results as the full sample. The peak position does shift somewhat for the binned data — from 20.5 for $0 < B/T \leq 0.1$ which is also the position for the full sample to 20.75 for $0.1 < B/T \leq 0.2$ to 21.0 for $0.2 < B/T \leq 0.3$, but the volume correction line provides a good match to the observed distributions resulting in roughly flat intrinsic distributions in all cases. We notice that more LSB objects tend to be detected at higher B/T ratios. This is not unexpected given the way we calculated the surface brightnesses of the bulge and disk components. The total flux was divided between the two components according to the B/T ratio — if this is high, there will naturally be less light in the disk component which will tend to result in lower disk central surface brightnesses.

6.3 Discussion of Results

Obtaining the intrinsic surface brightness distribution from our survey allows us to get a better understanding of the true population of LSB galaxies. The most obvious result is that LSB galaxies do exist and in much greater numbers than the Freeman law (Freeman 1970) would predict; this is well known from previous work. For example, McGaugh et al. (1995) collected the information from Phillipps et al. (1987), Davies (1990), and Schombert et al. (1992) to produce the surface brightness distribution corrected for volume sampling effects (their Figure 3). This plot extends to about $\mu_0 = 23.6$ B mag arcsec^{-2} or roughly 22.7 in R. It was extended to about 24.8 in B or roughly 23.9 in R by O'Neil & Bothun (2000) who include data from Sprayberry (1994), de Jong (1996), and O'Neil et al. (2000), but there are only three points on this plot with $\mu_0 \geq 24$ in B (their Figure 2); their faintest bin at $\mu_0 \leq 24.75$ B has only one galaxy in it. As they

note, this is extremely close to their survey limit and the fact that any galaxies at all were detected is significant, but that still leaves this region of parameter space relatively unexplored. A study of the surface brightness distribution for $z \leq 0.1$ was made by O'Neil et al. (2003) which extends to $\mu_0 = 23.75$ in B or about 22.85 in R. Our results, shown above in Figure 6.9, confirm and extend the results of the previous work. We find that the surface brightness distribution is approximately flat for $\mu_0 \gtrsim 21$ R mag arcsec^{-2} (about 21.9 in B) and have extended the distribution out to 24.25, roughly 25.15 in B. We obtain the same results when we bin the data by B/T. The fact that we do not see evidence of a turn down in the intrinsic distribution suggests that there are still many more, even lower surface brightness objects yet to be discovered.

There has been a suggestion (Tully & Verheijen 1997) that the observed surface brightness distribution is bimodal. Their study of the Ursa Major cluster of galaxies shows evidence for a population of HSB galaxies followed by a gap and then a population of LSB galaxies. This gap appears around $\mu_{0,i} = 21$ R mag arcsec^{-2} for the inclination corrected disk central surface brightness. Detections that bright will be very high signal-to-noise detections in our survey since it was designed to reach a very low threshold. This will make any such gap easily visible if one does exist. Our observed distribution (Figure 6.1) has a single peak at about $\mu_{0,i} = 20.5$, quite close to where the proposed gap should lie. These observations do not support the claim of Tully & Verheijen. They suggest that "galaxies avoid a region of parameter space" and this is clearly not seen in our data. Many galaxies exist in this region of the parameter space. We believe that this bimodal effect may be peculiar to this cluster since it has not been seen in field surveys like ours.

While the distribution is consistent with being flat, the points at very low surface brightness are slightly higher than those near the peak of the distribution at higher surface brightness. Performing a simple linear regression on these fainter points gives a slope of approximately 0.07. This is quite consistent with zero slope and a flat distribution. Other studies have resulted in different values for this slope. McGaugh (1996) found a slope of -0.3 for the Davies (1990) data, but also notes that the data of Schombert et al. (1992) which contain many more galaxies at the fainter levels than the Davies sample favor a slope closer to zero. The study of O'Neil et al. (2003) of galaxies with redshifts $z \leq 0.1$ indicate an increase with a slope of 0.08 for the data of Andreon & Cuillandre (2002) or 0.03 when combined with other data sets, but by re-binning and averaging this combined data set, they obtain a slope of -0.1; it decreases. However, Cross et al. (2001) use data from the 2dF Galaxy Redshift Survey to obtain a surface brightness distribution that is a broader version of the original Freeman (1970) distribution. Their results (their Figure 15) show a dramatic drop off in the distribution before $\mu_0 = 24$ in B, a result that would indicate that LSB galaxies are actually very rare. However, they say that they are only complete to $\mu_0 = 23$ and while the function has a steep slope to that point, it has not cut off yet. In addition, they plot the data points of O'Neil & Bothun (2000) which are complete to $\mu_0 = 24$, some of which have relatively small error bars in the region $\mu_0 > 23$, but their function cannot account for these points at much higher number counts. If such a cut off were present at $\mu_0 \lesssim 24$ B mag arcsec^{-2}, it should occur at $\mu_0 \approx 23$ R mag arcsec^{-2} in our data. We do have data beyond this point and while the number counts are are low, they are clearly not consistent with a sharp cutoff in the distribution. Our results are consistent with zero slope and a flat distribution, much like that

of McGaugh et al. (1995) and O'Neil & Bothun (2000), particularly with the addition of points beyond $\mu_0 \approx 24$ in B, but given the large error bars on our faintest points, there is still work to be done.

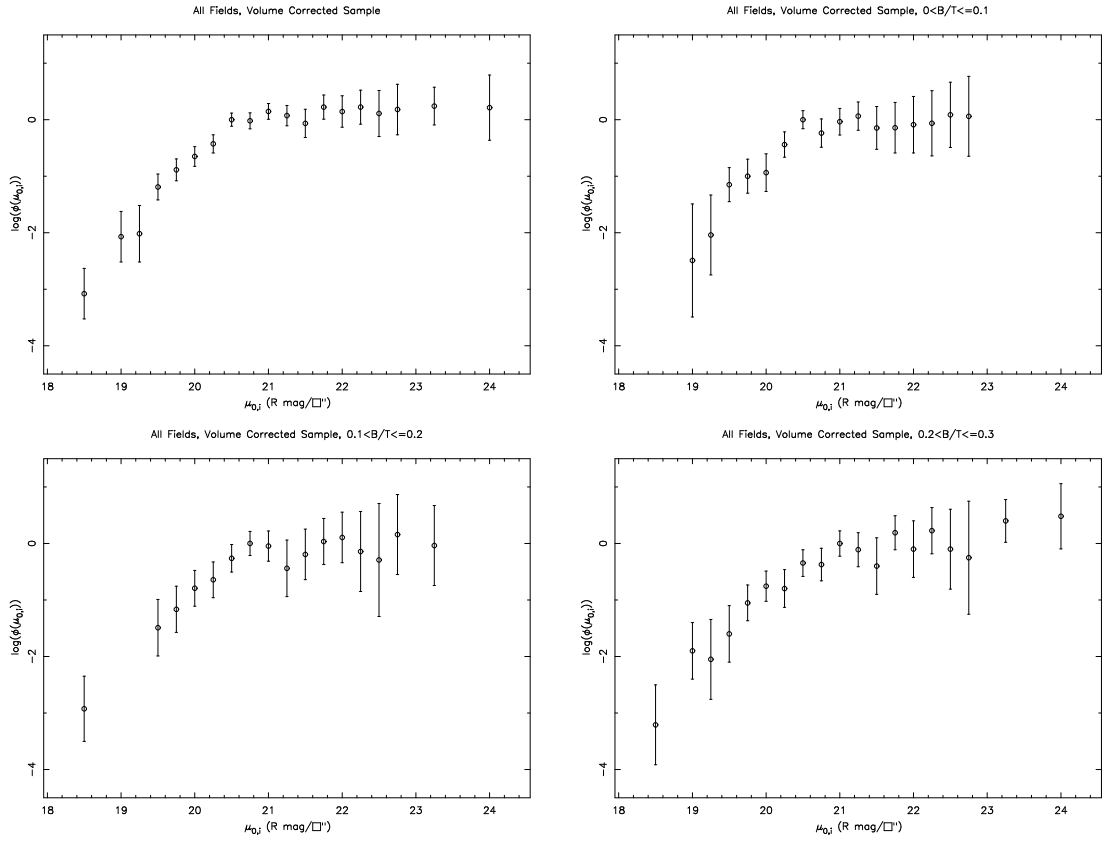

Figure 6.14: Plots of the intrinsic surface brightness distributions for different B/T bins. The full sample, $0 < B/T \leq 0.3$, is shown in the upper left for reference; $0 < B/T \leq 0.1$ is in the upper right, $0.1 < B/T \leq 0.2$ in the lower left, and $0.2 < B/T \leq 0.3$ in the lower right. Errors are $\sqrt{N}/N$ counting statistics errors. A bin size of 0.25 was used, but the results were combined near the limits to improve the statistics — a bin size of 1.0 was used for $18 \leq \mu_{0,i} < 19$ and a bin size of 0.75 was used for $23 \leq \mu_{0,i} < 24.25$.

Chapter 7

Examining Other Results

In this chapter we examine other properties of the detections in our survey. The large number of parameters output by the GIM2D fitting package provides many possible combinations of parameters to examine. Here we select a few of them based on similar studies in previous works. The sample used here will vary depending on the parameters we are studying and each section will mention what sample is being used.

7.1 The Number–Magnitude Relation

We touched upon this briefly in Chapter 5, but only used it to obtain a measure of completeness for our survey so we will discuss it further here. We reproduce Figure 5.15 here as Figure 7.1 which includes all of the data that passed the cuts to remove bad detections, but does not include the magnitude, B/T, or inclination cuts. As we described in Chapter 5, the Gunn r band magnitudes from Yasuda et al. (2001) have been converted to our R band magnitudes using Equation 5.1 taken from Windhorst et al. (1991), the color term being estimated from Figure 2 of Yasuda et al.. One of the first things we notice is that the

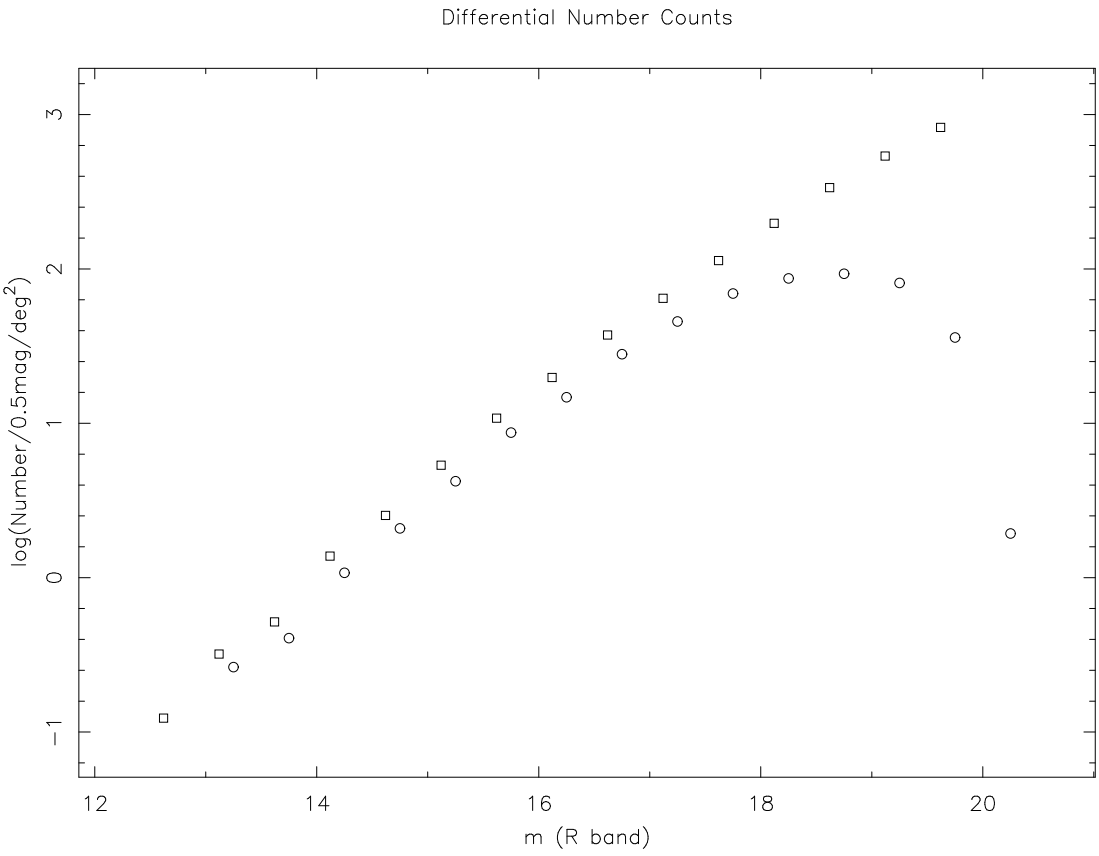

Figure 7.1: Plot of differential number counts of objects per 0.5 mag per square degree as a function of R band magnitude. The circles show our data points and the squares show the data from Table 2 of Yasuda et al. (2001) with their Gunn r magnitudes converted to match our R band magnitudes.

relation appears to be linear, particularly at brighter magnitudes. As noted by both Yoshii & Takahara (1988) and Yasuda et al. (2001), the slope is expected to be 0.6 for a homogeneous distribution in Euclidean space; a derivation of this is available in Binney & Merrifield (1998, §3.6.1). Yasuda et al. show that this expected trend provides a very good match to their data from the Sloan Digital Sky Survey (SDSS) and reproduces the observed number counts at bright

magnitudes. As our counts at bright magnitudes closely parallel those of the SDSS data, our data also show the same Euclidean trend. A variety of other authors have studied this relation; see, for example, Shanks et al. (1984), Tyson (1988), Yoshii & Takahara (1988), Metcalfe et al. (1991), and Yasuda et al. (2001) who all present R band curves for the differential counts. The vertical offset between our data and the SDSS data in Figure 7.1 may, in part, be due to the fact that we have used the total area from which the detections were taken in our calculation. The area covered by stars should be subtracted from the total area since we are unable to survey this area and this would bring our counts up, providing a closer match. If this were the only factor involved, our area would have to be reduced by approximately 30 deg^2 in order to match the SDSS number counts. However, as noted in Chapter 4, we reach our intended limiting surface brightness of $\sim$ 27 R mag arcsec^{-2} at a detection threshold of about 1σ, but the results presented here are for a 3σ threshold and a limit of about 25.4 R mag arcsec^{-2}. Therefore, our number counts could also be increased by analyzing the data at a lower detection threshold and detecting more objects. We also note that there tends to be some variation in number counts from survey to survey; see, for example, Figure 17 of Liske et al. (2003) for a B band plot which includes data from a variety of previous work. Considering these factors, we are in fairly good agreement with this SDSS data.

As mentioned before in Chapter 5, the exact shape of this relation depends on cosmology. The primary factor is the deceleration parameter q_0, but galaxy evolution will also affect the shape of the curve as will the wavelength of the observations, the galaxy type, volume density, and luminosity function (Tyson 1988). These effects can be included in models which can then be compared to

the observations. This has been done by all of the previously mentioned authors as well as Ferguson & McGaugh (1995), Gardner (1998), and Gardner & Satyapal (2000). Currently we do not have data at faint enough magnitudes to make this kind of modeling and comparison worthwhile. At around $m = 18$–19 or so in the R band, the curves for different models hardly separate; see, for example, the plots in Yoshii & Takahara (1988) and Metcalfe et al. (1991). However, our observations may be helpful in these types of studies if pushed to fainter magnitudes. As noted above, we can detect more objects by analyzing the data at a lower detection threshold, one that allows us to get closer to the designed limiting surface brightness. This should provide detections of more fainter objects as well, which would allow us to push into the region where the observations could be useful in distinguishing between different models.

7.2 Disk Inclination and Transparency

An assumption that is often made about disk galaxies is that they are optically thin and essentially transparent. When we ran the GIM2D programs to model our detections, we made this assumption as well. Without any internal extinction, we will receive and measure all of the light from each galaxy regardless of its inclination. This will result in a clear effect on the observed surface brightness: for a fixed luminosity, a more face-on galaxy will have a fainter surface brightness than a more inclined galaxy since the same amount of light has been spread over a larger area. We can calculate the expected trend of surface brightness with inclination and then compare it to the trend seen in our data, allowing us to test the assumption of disk transparency.

In Chapter 6 we derived an expression for the total luminosity (Equation 6.4)

from the one describing the light profile of an exponential disk (Equation 6.1). Converting that expression into magnitude units by taking $-2.5 \log$ of both sides gives

$$m = \mu_0 - 2.5 \log 2\pi r_d^2 \tag{7.1}$$

where we are using the observed scale length r_d rather than the physical scale length h as we did in Chapter 6 because we are dealing only with the observed quantities here. We account for the effect of inclination by realizing that r_d is measured along the major axis; along the minor axis it will be reduced by the axial ratio giving $(b/a)r_d$ where b/a is the ratio of the minor to major axis. This means that in place of r_d^2 we should have $(b/a)r_d^2$. The axial ratio can be factored into a separate term to give

$$m = \mu_0 - 2.5 \log 2\pi r_d^2 + 2.5 \log (b/a) \tag{7.2}$$

where the last factor can also be written as $-2.5 \log (a/b)$. This is how it appears in the work by Han (1992) and Giovanelli et al. (1994). As noted by Giovanelli et al., the axial ratio is related to the inclination by $\cos^2 i = \frac{(b/a)^2 - q^2}{1 - q^2}$ where q describes the intrinsic axial ratio of the disk, assuming it is an oblate spheroid. In general, q is small (Giovanelli et al. use $q = 0.13$ and say the true value is likely to be somewhat lower, around $q = 0.10$) and thus provides only a small correction to the equation. Thus it is normally safe to simplify and take $\cos i = b/a$. This is how we obtained the factor for calculating the inclination corrected surface brightness in Chapter 4, Equation 4.12. From Equation 7.2 we can see that the observed surface brightness for a completely transparent exponential disk is expected to vary as $-2.5 \log (a/b)$.

By converting the inclinations output by the GIM2D package to axial ratios, we can plot the observed disk central surface brightness μ_0 against $\log (a/b)$ and

check how consistent our observations are with the assumption of completely transparent disks. To do this we want to use disk dominated systems, but not restrict the inclination. Therefore, for this plot we use the catalog after cuts and only apply our chosen B/T cut to it. This accepts objects with $B/T < 0.3$ and any inclination. We do not apply the magnitude cut here so that we may examine the trend over the full range of magnitudes in which we detect objects. The results are plotted in Figure 7.2 along with typical 1σ error bars. Average values of μ_0 for 0.1 width bins in $\log(a/b)$ are plotted as filled diamonds as well. We see the general trend expected — detections that are less inclined tend to have fainter surface brightnesses. We notice that there is a more rapid change for $\log(a/b) > 0.9$ which corresponds to inclinations of $i \gtrsim 82.7°$. We saw some problems with high inclination detections in Chapter 5, namely that many $i = 85°$ objects are in fact pairs of objects fit as single objects, so we expect that these results at very high inclination are probably unreliable. Performing a simple linear regression on all points with $\log(a/b) < 0.9$ gives a slope of about -0.45 and for the average binned values in this range, a slope of about -0.47. Including all of the points and using the final average point gives slopes of -0.95 and -0.76, respectively.

Han (1992) performed a study of the surface brightness profiles of the outer parts of spiral galaxies in the I band and found a slope of -1.90. Giovanelli et al. (1994) find almost no noticeable slope in their study of Sc type galaxies in the I band, but in an extension of that work, Giovanelli et al. (1995) find a slope of -0.4 after subtracting off the dependence they found of disk central surface brightness on luminosity. It is apparent in all cases that the observed slope is sufficiently different from -2.5 to indicate that disk galaxies are not completely

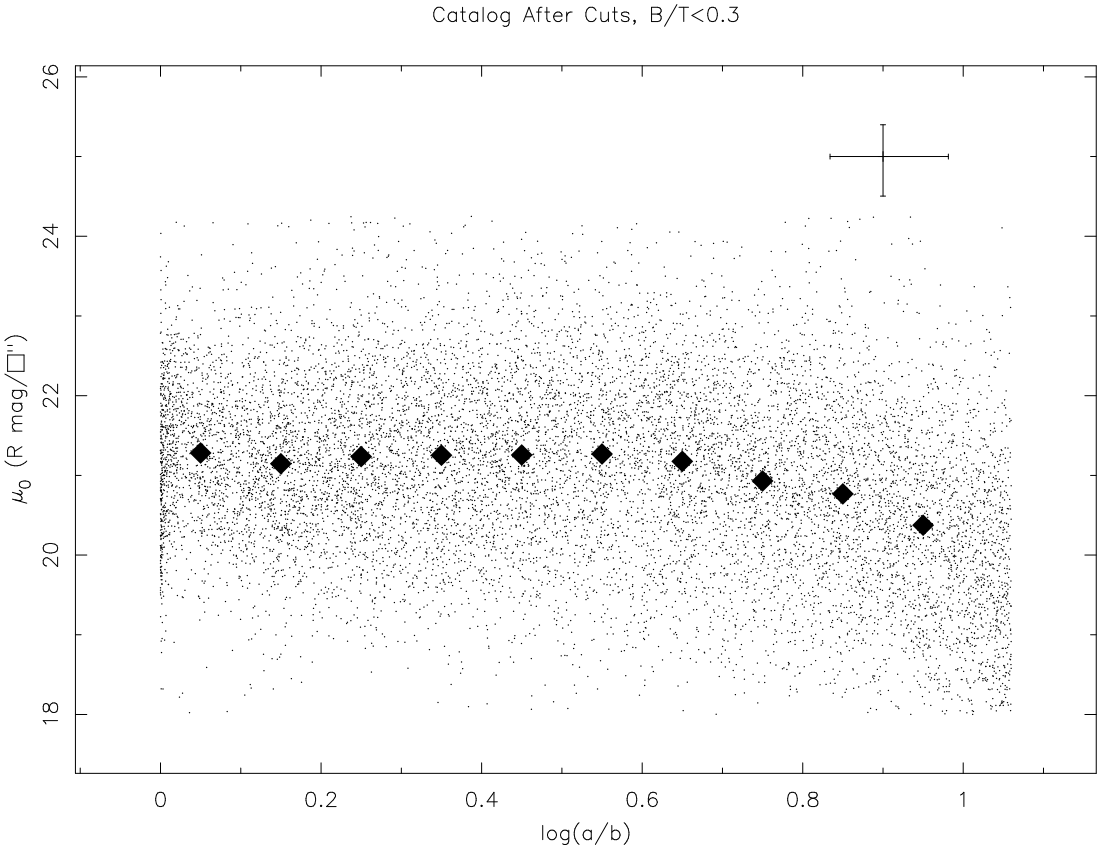

Figure 7.2: Plot of observed disk central surface brightness μ_0 for detections with $B/T < 0.3$ against inclination in terms of the axial ratio, $\cos i = b/a$. The large solid diamonds are average values; e.g, the the point at 0.05 is the average of all points $0 < \log(a/b) \leq 0.1$. The error bars shown are the average 1σ errors.

transparent. This is no surprise as there are observations of galaxies that clearly show the presence of dust lanes. The large variation in the results suggest that this is not a good quantitative test of disk transparency though, a point also mentioned by Giovanelli et al. (1994). However, it does serve as a qualitative confirmation that internal extinction in galaxies should be accounted for as well as possible in order to get the best results. It is possible that our results might be

improved by rerunning the GIM2D model fits with some non-zero value for the internal extinction, but as this value is expected to change from galaxy to galaxy and is not necessarily constant within a given galaxy, there is no guarantee that the overall results would be improved by fitting all of the detections with the same non-zero value.

7.3 Disk vs. Bulge Scale Length

In a study of bulge dominated LSB galaxies, Beijersbergen et al. (1999) found a correlation between the disk and bulge scale lengths at a 99.8% probability which they suggest indicates a coupling in the formation of the bulge and and disk components. A similar study on late type spirals done a few years earlier by Courteau et al. (1996) reached similar conclusions. To examine this with our data, we return to the catalog after performing the cuts to remove bad detections and select our sample with different cuts on B/T and inclination. We accept objects with $B/T > 0.7$ to get bulge dominated systems, this limit being chosen to complement our selection of 0.3 for the limit on disk dominated systems, and apply the same $i < 50^{\circ}$ restriction of Beijersbergen et al.. The inclination cut helps decrease the dependence of the results on internal extinction of the galaxies in the sample. In order to examine this trend over the full range of magnitudes in which we detect objects, the magnitude cut is not applied here. We plot the disk vs. bulge scale lengths for the objects in this sample in Figure 7.3. The plot limits were set to approximately fit the range of the Beijersbergen et al. data and the R band points from their Table 2 have been included in this plot as solid diamonds. In Figure 7.4 we restrict the range of the plot to match that of the Beijersbergen et al. data and include 1σ error bars for our results. We do not see

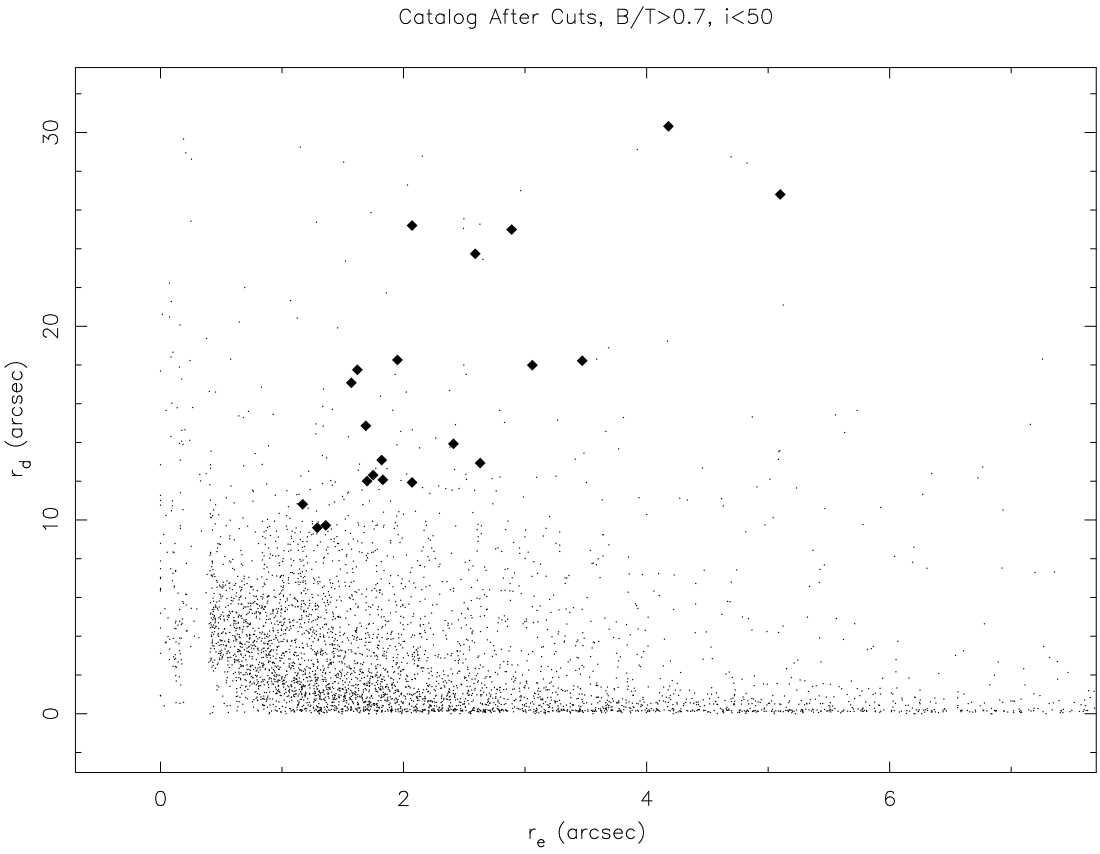

Figure 7.3: Plot of disk scale length vs. bulge scale length. Solid points are the R band data from Table 2 of Beijersbergen et al. (1999).

evidence or continuation of the strong correlation found by Beijersbergen et al. (1999) and the uncertainties in the GIM2D results are large, increasing towards smaller radii. However, it is important to note that our bulge scale length r_e is not defined in the same way as the bulge scale length h_b of Beijersbergen et al. or the r_b of Courteau et al.. We have modeled our bulge components using a de Vaucouleurs $r^{1/4}$ law and the disks using an exponential profile while these other authors have used the exponential profile to model both the bulge and the disk components. As both of these other works explain, not all galaxy bulges are

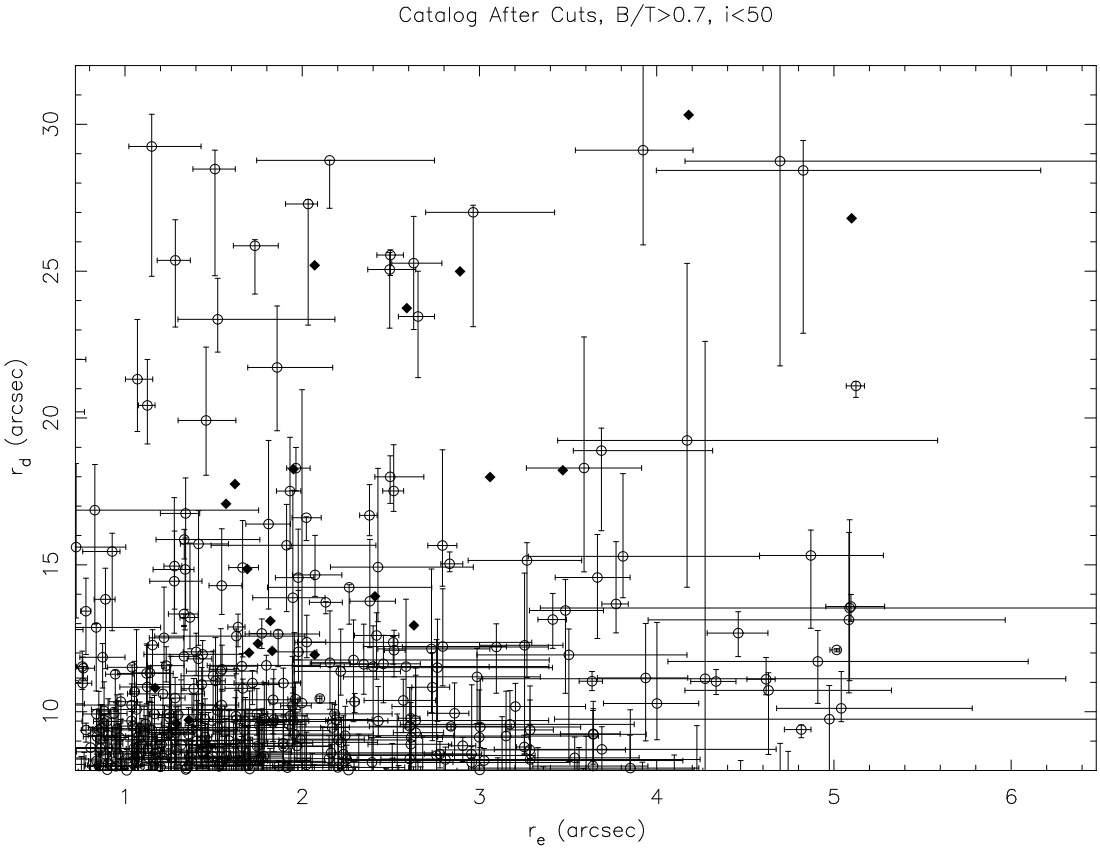

Figure 7.4: Plot of disk scale length vs. bulge scale length, limited range. Solid points are the R band data from Table 2 of Beijersbergen et al. (1999). Also plotted are the 1σ error bars.

well fit by a de Vaucouleurs profile despite it being a long time standard model. It does work well for elliptical and S0 type galaxies, but for early type spirals (around Sa and Sab) an $r^{1/2}$ law fits better and for late type spirals (around Sb, Sc, and later) an exponential bulge profile is generally the best fit. The fact that we have modeled all galaxies with the same $r^{1/4}$ law is very likely to be the reason that the suggested trend is not apparent here. To quote Courteau et al. (1996), "this result would remain unnoticed were one to fit (inappropriately) all the inner

regions with an $r^{1/4}$ law". Future work may be able to perform a better study if it were to separate galaxies by morphological type before fitting and then run GIM2D separately on each group using the most appropriate bulge profile for their type.

Chapter 8

Conclusions

In this final chapter we present a summary of our current results and suggest some possible directions for future work.

8.1 Summary of Results

In this project, we have performed a deep, large area survey designed to detect very low surface brightness galaxies. These observations were described in Chapter 2 along with the data reduction procedure used to process them. Astrometric and photometric calibrations were then performed as described in Chapter 3. The data analysis procedure consisting of detecting objects in the images using the SExtractor program, performing star/galaxy separation on the list of detections, and then fitting the detections that pass this separation with the GIM2D package for IRAF was described in Chapter 4. In Chapter 5 we examined the results of the data analysis procedure and found that detections of objects we were not interested in studying still remained in the catalog of objects. We described the series of cuts we used to remove these bad detections from the catalogs and then selected a sample of relatively face-on, disk dominated systems to study in

greater detail. We studied the surface brightness distribution of this sample of 757 objects in Chapter 6. We found that the observed distribution shows a strong peak at a face-on disk central surface brightness of $\mu_{0,i} = 20.5$ R mag arcsec^{-2} and there were almost 50 objects with $22 \leq \mu_{0,i} < 24.25$ R mag arcsec^{-2}. This corresponds to roughly 23–25.25 in the B band and covers a region of the parameter space that has not been well explored by previous surveys. We took a brief look at the possible effects of cosmological dimming on our sample, but noted that this alone could not explain our observed distribution (Ferguson & McGaugh 1995). We then noted that the sharp decrease in number counts at lower surface brightnesses is due to a selection effect. Larger and more luminous objects can be detected to larger distances and thus within a greater volume than smaller and less luminous objects, causing them to dominate in a flux limited sample. By making a calculation of how the volume probed depends on the properties of the galaxy, we are able to perform a correction for this selection effect and recover the intrinsic surface brightness distribution. This was a primary goal of this survey and we confirmed that the intrinsic distribution is approximately flat at low surface brightnesses in good agreement with most previous work. We have also extended this distribution out to approximately $\mu_{0,i} = 24.25$ R mag arcsec^{-2} providing coverage of an area that most surveys have not been able to explore. The fact that the distribution is approximately flat means that there are roughly equal numbers of LSB galaxies at all surface brightnesses and there are a large number of them; on the order of the same number of galaxies one would find around the Freeman value. Without evidence of a turn down in this distribution, there should be even more very LSB galaxies yet to be discovered. In Chapter 7 we examined some additional properties of the objects in our survey. We dis-

cussed the number–magnitude relation with a comparison to the Sloan Digital Sky Survey data of Yasuda et al. (2001) and noted that at brighter magnitudes we see the trend expected for a uniform distribution of objects in Euclidean space. We performed a test of the assumption that galaxy disks are optically thin and essentially transparent, demonstrating that the relation between surface brightness and inclination does not follow the expected trend for completely transparent disks. Comparing to other results, we see significant variation in the results suggesting that while this may be a good qualitative test, it is not a very good quantitative test. We then examined the relation between the bulge and disk scale lengths for a bulge dominated sample and compared our results with the study of Beijersbergen et al. (1999) who find a strong correlation between these parameters, suggesting a coupling in the formation of the bulge and disk components. We do not see such a trend in our data.

8.2 Potential Future Work

Additional work can be done with the currently available survey data even before making follow-up observations. First, there is one additional observing run which we have not included here because the data were taken with a different CCD than all of the runs here. Since we have already worked out the data reduction and analysis procedure, processing this final run should not be very difficult, but doing so could require some minor modifications to adapt to the parameters of the other CCD. This will obviously provide more galaxies to include in the analysis of results, helping to improve the study we have done here and any future work based on this survey. Also, we have demonstrated that our survey has reached the intended surface brightness limit of approximately $\mu_0 = 27$ R mag arcsec^{-2}, but

at a detection threshold of about 1σ or less. Since we set our threshold to 3σ for this project, an obvious extension is to push the threshold lower so that we can detect and analyze all of the very LSB galaxies currently omitted. While visually inspecting our detections we saw objects on the fields that appeared to be very LSB galaxies, but were undetected with our limits. Modifying these limits should allow for many more LSB galaxies to be detected thereby improving the results we have obtained so far and providing a larger amount of data for future studies. Another option is to place a diameter limit on the survey rather than a magnitude limit. As described in McGaugh et al. (1995), this produces a less biased sample that is more representative of the field galaxy population; a flux limited sample will tend to include very distant and intrinsically luminous galaxies and thus will be dominated by the largest, highest surface brightness galaxies. Since we would like to obtain the fairest sample possible, it would be worth examining the results if a diameter limit is used in place of a magnitude limit.

The settings of the SExtractor detection program and/or GIM2D fitting package might be able to be improved. A noticeable problem was pairs of objects getting fit as one, often resulting in very high inclination fits which were inappropriate. Whether this is due to a problem in the detection or fitting program is not immediately obvious. The fitting program uses the results of the detection program though so one would expect its accuracy to depend on that of the detection program. Perhaps the deblending settings in SExtractor need further adjustment to make sure objects very close together on the image are separated properly. However, care must be taken that the deblending is not set so high that single objects are separated into multiple pieces. Achieving a good balance is a tricky process; we have done the best we could, but perhaps additional experimentation

could result in a better combination of parameters.

More of the GIM2D results can be examined for correlations. We have only looked at a small subset of the results here because GIM2D outputs a large number of parameters and we calculated additional results from them. For example, Simard et al. (2002) notes that the position angles of the bulge and disk components are allowed to be different because a large difference between these values is an indication that the galaxy contains a bar. By studying the relation between these two parameters, it may be possible to separate barred galaxies from unbarred ones in the survey. The R_T and R_A asymmetry indices which roughly measure the total residual flux and asymmetry residual flux in a manner similar to that of Schade et al. (1995) could be used as an indication of galaxy morphology. Simard et al. gives examples of previous work and how they used these parameters to select certain galaxy types for study. They also note that measuring these parameters in multiple bandpasses could show any wavelength dependence the residual structures may have.

Additional observations can provide more information and in fact this survey was designed with the intention of detecting very LSB galaxies that could be used in such follow-up studies. Our primary goal here was to determine the surface brightness distribution, but we did not have distances available to calculate the true space density. Therefore obtaining redshifts for a sample of the LSB galaxies in our survey is an important task. This will enable us to do the volume correction more directly, such as with the V/V_{max} method described by Schmidt (1968), and enable us to determine physical scale lengths from which we can calculate the full bivariate distribution $\Phi(h, \mu_0)$ instead of just its projection $\phi(\mu_0)$ as we have done here. Additional imaging observations can provide data in multiple bandpasses

allowing calculation of galaxy colors which can then be examined for correlations with other parameters. As LSB galaxies tend to have blue colors and there seems to be a lack of extremely red objects (O'Neil 2000), though some have been found (O'Neil et al. 2004), one use of obtaining colors for our survey would be to see if we have detected any extremely red LSB galaxies to add to the known sample. In particular, H I observations can be very useful. LSB galaxies are known to have normal H I contents despite having relatively low star formation rates (Impey & Bothun 1997) making them relatively gas rich. A recent study by O'Neil et al. (2004) has greatly increased the number of massive LSB galaxies known. As they note, some important reasons to study such systems include their contribution to the amount of baryonic as well as dark matter, they serve as tests of models for galaxy evolution since they lie at one extreme of the mass and density distribution of galaxies, and that if LSB galaxies are as common as HSB galaxies, they could be one of the main causes of Lyman α absorption lines seen in the spectra of quasars. With the detection of many LSB galaxies in our survey, this information can be used to help make estimates of how strong of an effect this population could have in explaining the Lyman α absorption issue noted in such work as that of Linder (1998, 2000) and Bowen et al. (2001). Measuring the H I masses allows for studies of the mass to light ratio to be performed. Rotation curves indicate that LSB galaxies tend to be dark matter dominated and nearly all radii making them excellent candidates for testing theories about dark matter. The theories need to match the observations and the more observations, the better the constraints that can be placed on the theories; our survey has provided many more LSB galaxies that can be used in these tests. Also, as noted in McGaugh & de Blok (1998) the mass discrepancy, and thus the implied amount of dark

matter needed to resolve it, increases towards fainter surface brightnesses. The very LSB galaxies found in our survey will therefore be particularly important test cases.

Many paths can be taken from here. Some involve working with the data already on hand in order to improve the survey results, others involve making additional observations to study other relations and properties. In all cases, the large number of LSB galaxies we have detected here will provide important information about this population which has long been overlooked and under-represented in many previous surveys. The potential impact of LSB galaxies in many areas of cosmology and galaxy formation and evolution is great (Bothun et al. 1997; Impey & Bothun 1997) and the more of them we find, the more representative our galaxy samples become, and the better our understanding of these areas will become.

Appendix A

Data Reduction Scripts

The following scripts and programs were used during the data reduction procedure. Unfortunately, they are too long to include here so descriptions of how they work have been provided instead.

A.1 Primary Data Reduction — reduce.cl

This IRAF script performs the majority of the initial data reduction. It is used on each observing run separately with minor modifications as necessary. The basic routine of this script is: set the instrument parameter of the IRAF task CCDRED to the CTIO nfccd values, delete all non-R band images as they will not contain survey data, apply the overscan and trim corrections to all fields with CCDPROC, combine the zero/bias frames with ZEROCOMBINE, apply the zero correction to the dark, flat, and object fields with CCDPROC, combine the dark fields with DARKCOMBINE, determine the average value of each quadrant in the combined dark frame and then make a new image with these mean values in each quadrant using Greg Aldering's mystats script and IMREPLACE, apply the dark correction to the flat and object fields with CCDPROC, combine the twilight flat

fields with FLATCOMBINE, apply the flat correction to the object images using CCDPROC, create sky flats by average combining the unshifted survey fields with IMCOMBINE, normalize the newly created sky flats with NORMALIZE. These sky flats are not applied automatically, though the script can do this, because we wanted to check them to make sure they were acceptable before applying them.

A.2 Shifting and Combining Images

A.2.1 newcoadd_prep.cl

This IRAF script provided by Greg Aldering automates the shifting and combining of object frames. It calculates the required shifts and generates a script as output which is then run, using the calculated shifts, to combine the images. The basic routine of this script is: use DAOFIND to locate objects in a list of images, trim the list to contain a user specified number of unsaturated stars, call the quickmatch5 program to match the image lists, use GEOMAP to obtain a linear transformation between frames, call the match_w_geomap program to match fainter stars using the GEOMAP transformation, use WPHOT to perform photometry on these sources and obtain accurate centers for them, derive the mean (x, y) offset and the mean intensity offset, set image header keywords CLOUDSCL and IMCMBSCL such that the brightest image has these values set to 1 and other fields are > 1, set the image header keyword EFFTIME = EXPTIME/IMCMBSCL, make the reference image the one which is centered the best (or the brightest if there are only two images), write an IRAF script that can be used to run IMCOMBINE to combine the images using the calculated shifts. The keywords added here are meant to help account for data taken under

non-photometric conditions whereby the fluxes of objects are used to determine the relative scaling between images. We do not use these values. Because IMCOMBINE can only accept inter pixel shifts, this script also has an option to use subpixel shifts by block replicating the images before combining them and then block averaging them back after combining. This can be useful, but we determined that it did not have any significant effect on our images and did not use this option.

A.2.2 quickmatch5.c

This C program is used by newcoadd_prep.cl to compare images and generate a list of matching objects on each using a pattern matching method that examines the distance and angle of neighboring objects from each object in the input coordinate lists.

A.2.3 match_w_geomap.c

This C program is used by newcoadd_prep.cl to match a large list of objects from two images using the mapping determined from a shorter list of objects with the IRAF task GEOMAP.

Appendix B

Data Analysis Scripts

The following scripts and programs were used during the data analysis procedure. These files also tend to be long since they have a series of commands to run on every survey field and they repeat the same commands many times, changing the file name and possibly some parameters. Therefore, the full scripts will generally not be included, but examples of how they operate on one field will be provided for illustration.

B.1 Detecting Objects with SExtractor — do_sex

This unix script is simply a series of commands that run SExtractor on each field with the appropriate field dependent parameters specified on the command lines: the catalog name, the effective gain, the zeropoint of the magnitude scale, the seeing FWHM, and the output segmentation image file name. As an example, the first line, here split onto multiple lines for easier reading, is:

```
sex f0020-39a.fits -c lsbg.sex -CATALOG\_NAME f0020-39a.3sig10.cat
-GAIN 42 -MAG\_ZEROPOINT 27.11 -SEEING\_FWHM 1.63
-CHECKIMAGE\_NAME f0020-39a.3sig10.seg.fits
```

B.2 Removing Objects Near Frame Edges — trimedge

This unix script contains a series of awk and sort commands to remove detected objects near the edges of the frames from the catalog lists, excluding them from the fitting process. The pixel coordinates of the center of the image (x_c, y_c) are first determined. Then for each field awk is used to remove the header lines from the detection catalog file (one for each of the SExtractor output parameters included) and output just the list of detections to a new file, this is then sorted on the x coordinate and the results placed in a new file, awk is then called to copy all objects with $x > x_c - 1024$ to one file and again on that file to copy all objects with $x < x_c + 1024$ to another file which is then sorted by the y coordinate. The pair of awk commands is repeated, this time to find all objects with $y > y_c - 1024$ and $y < y_c + 1024$ in the list that already passed the requirement for the x coordinate. The final results are moved over to a new file, the trimmed .gfxt catalog file to be used first for star/galaxy separation and then as input to the GIM2D tasks once the star/galaxy cuts have been applied. As an example, this series of commands for the first field is:

```
awk 'NR > 10 {print $0}' f0020-39a.3sig10.cat > nohead
sort nohead > s1
awk '$1 > 1083-1024 {print $0}' s1 > s1a
awk '$1 < 1083+1024 {print $0}' s1a > s1b
sort -k 2,2 s1b > s2
awk '$2 > 1084-1024 {print $0}' s2 > s2a
awk '$2 < 1084+1024 {print $0}' s2a > s2b
```

```
mv s2b f0020-39a.3trim10.gfxt
```

B.3 Making PSFs — gimpsf.cl and makepsfs.cl

These two simple IRAF scripts are used to generate images of the PSF for each field at the location of each detection in the field. The first, gimpsf.cl, is used to take the filenames of the GIM2D extracted thumbnail images which are named using the (x, y) coordinates of the detection, and manipulate them into a series of SEEPSF commands (the second script) that will create PSFs at the location of each detection. These were written to operate on one field at a time because it was simpler to do so. Thus, gimpsf.cl is very short and can be included here in its entirety:

```
files *_m.fits > c1
files *_m.fits > c2
!gsub "_m.fits" "_p.fits" c1
!gsub "^" "seepsf f0020-39a.psf.1 " c1
!gsub "_m.fits" "" c2
!gsub "gx" "xpsf=" c2
!gsub "y" " ypsf=" c2
!paste c1 c2 > makepsfs.cl
```

The FILES task in IRAF simply lists all files matching the provided pattern and gsub is a simple unix script to perform global replacement of one expression with another in the specified file(s). The unix command paste simply pastes together columns of information. The script takes the first _m.fits file names, changes them to _p.fits and adds the required SEEPSF command to the beginning

of the line, in front of the modified file names. The second _m.fits file names are turned into x and y pixel coordinate positions by substituting the approriate SEEPSF parameter names in place of pieces of the file names. The results are a series of SEEPSF commands to create images of the PSF at each detection's (x, y) location from the PSF model made earlier and these form the makepsfs.cl script. As an example of this script, here is the first line from one of them:

```
seepsf f0020-39a.psf.1 gx1001y850_p.fits xpsf=1001 ypsf=850
```

B.4 Extracting and Calculating Results

As with the previous section, these scripts were written to operate on one field at a time and had to be run separately on each field.

B.4.1 Extracting Fit Parameters — getfit.cl and maketail

These two scripts are used together to extract the final 28 lines of each log file output by GIMFIT2D. These are the lines containing all of the best fit parameter values and asymmetry indices. The IRAF script getfit.cl is run first. As it is very short, it can be included here in its entirety:

```
files gx*.log > z1
files gx*.log > z2
!gsub "gx" "tail -28 gx" z1
!gsub "gx" "> gx" z2
!gsub "log" "tail" z2
!paste z1 z2 > maketail
```

As noted above, the IRAF task FILES is used to list file names, the unix script gsub is used to perform global substitutions in files, and the unix command paste is used to paste together columns. The script takes the first log file names and adds a unix tail command in front of it, then takes the second log file names, adds an output redirection operator in front of it and changes the log extension to tail. The columns are then pasted together to form the maketail script, an example line of which is:

```
tail -28 gx1001y850.log > gx1001y850.tail
```

Once getfit.cl has been run, the maketail script it creates it run to copy all of the parameter values from the model fits into tail files. When this is complete, the original log files are deleted. Since they store information about all iterations of the fitting process, they are very large and would require large amounts of disk space to store. As we are not interested in knowing every step of the fitting procedure, just the final best fits, we delete the log files to save disk space.

B.4.2 Getting Results — getres2.cl

This script does not contain IRAF commands, but was written as an IRAF script because it was simpler to run it from inside IRAF. The basic operation of this script is: use the unix grep command to concatenate all of the parameters as given in the tail files into a single file (we use this rather than say the unix cat command because because grep also includes the file name as part of the output), do some global substitutions to remove the file extension and parameter label from the file name, use the unix split command to separate this one file into separate ones of 28 lines each (the same number of lines we started with for each

file), run awk using the awk program files extract-par.awk and extract-asym.awk to extract parameters from these files into new files, delete all of the split created files (the information is still present in the concatenated file), run gawk using the awk program file newconvert.awk to make some additional calculations using the GIM2D results as described in the text (§4.3) and print them to a new file, then use the integer x and y pixel coordinates from the detection file names with the dx and dy offsets from the GIM2D output to calculate more accurate values for the positions of the detections in both the parameters and asymmetry files. Two files were used to simplify the conversion and calculation process; the asymmetry parameters don't need to be modified at all so it was easier to put them in a separate file from the model fit parameters.

B.4.3 Extracting Model Parameters — extract-par.awk

This is a simple awk program file designed to extract the best fit parameters and their 99% confidence limits from the tail files. These are the first 14 lines of the files. The program file is as follows:

```
NR == 1 {printf "%s\t%f\t%f\t%f\t", $1, $2, $3, $4}
NR == 2 {printf "%f\t%f\t%f\t", $2, $3, $4}
[lines for NR = 3--12 are the same as the previous line]
NR == 13 {printf "%f\t", $2}
NR == 14 {printf "%f\n", $2}
NR == 28 {NR = 0}
```

Column 1 contains the thumbnail image name and this is only needed once. Column 2 contains the best fit value of the parameter and columns 3 and 4 contain

the 99% confidence limits for the parameter. Lines 13 and 14 are the reduced χ^2 of the fit and the half light radius which do not have confidence limits provided. At line 28, the final line for each detection, the record number counter is reset to zero allowing us to use the same record numbers for each detection.

B.4.4 Extracting Asymmetry Parameters — extract-asym.awk

This is a simple awk program file designed to extract the asymmetry parameters from the tail files. These are the last 14 lines if the tail files. The program file is as follows (some single lines have been split into multiple lines for readability):

```
NR == 9 {printf "%s\t%f\t%f\t%f\t", $1, $2, $3, $4}
NR == 10 {printf "%f\t%f\t%f\t", $2, $3, $4}
NR == 15 {printf "%f\t%f\t%f\t%f\t%f\t%f\t%f\t%f\t%f\t%f\t",
$2, $3, $4, $5, $6, $7, $8, $9, $10, $11}
[lines for NR = 16--20 are the same as the previous line]
NR == 21 {printf "%f\t%f\t%f\t%f\t%f\t%f\t%f\t%f\t%f\t",
$2, $3, $4, $5, $6, $7, $8, $9, $10}
[lines for NR = 22--23 are the same as the previous line]
NR == 24 {printf "%f\t", $2}
NR == 25 {printf "%f\t%f\t%f\t", $2, $3, $4}
[lines for NR = 26--27 are the same as the previous line]
NR == 28 {printf "%f\t%f\t%f\n", $2, $3, $4; NR = 0}
```

As before, the thumbnail file name is column 1 which is only needed once so the remaining lines only print out columns 2 and beyond. There are more columns here because most asymmetry parameters are measured at varying multiples of

the half light radius. Columns 9 and 10 are included here because they are dx and dy, the fractional pixel offsets of the center of the detection from the integer pixel values in the thumbnail image name, and they will be required to place (x, y) pixel coordinates in this file the same was as in the file for the model fit parameters above. Also as before, at the last line of each detection's set of results, the record number counter it reset to zero allowing for easy looping.

B.4.5 Conversions and Computing New Parameters — newconvert.awk

Details of the calculations for this stage are described in the text (§4.3). The basic routine of this program file is: set the zeropoint of the magnitude scale (done manually before running), define the exposure time and pixel scale which are constant for us as well as the value of π and the number of radians per degree, radii are then converted from pixels to arcseconds, 99% confidence levels for parameters to be used in calculations are converted to 1σ standard deviations, magnitudes are calculated from fluxes (L_{tot}), surface brightnesses of the bulge and disk components (with and without and inclination correction) are calculated from the total flux (L_{tot}), the bulge to total ratio (B/T), and radii for the bulge (r_e) and disk (r_d), the surface brightness within and at the half light radius (r_{half}) are then calculated using the total flux, bulge and disk radii, and the bulge and disk surface brightnesses calculated previously. Calculated values also had their 1σ standard deviations determined and then converted to 99% confidence limits to match the form of the errors output by the GIM2D task results. At the end, all of the parameters output from GIMFIT2D and calculated here are printed, the getres2.cl IRAF script redirecting this output to new files.

B.4.6 Final Tabulation

A short series of commands is used to take the results from the previous scripts, perform some final calculations, and tabulate the results. The combination of unix and IRAF commands are performed from within IRAF, but were not actually written into a script. Since we named our resulting tables with the same names as the fields, this name changes for each field. These changes could be made to commands issued manually just as easily as a script of commands so we opted to just copy and paste the commands into IRAF after each run of getres2.cl was completed. As an example, here are the commands as run on one of our fields:

```
cp out-par3 ..
cp out-asym3 ..
cd ..
!cut -f 1,2 out-par3 > out-p.xy
!cut -f 3- out-par3 > out-p.rest
!cut -f 1,2 out-asym3 > out-a.xy
!gawk -f asym_3-108.awk out-asym3 > out-a.rest
cctran out-p.xy out-p.rd f0020-39a.udb f0020-39a.umatch
!paste out-p.rd out-p.rest > f0020-39a.par.tab
cctran out-a.xy out-a.rd f0020-39a.udb f0020-39a.umatch
!paste out-a.rd out-a.rest > f0020-39a.asym.tab
del out-p.xy,out-p.rd,out-p.rest,out-par3
del out-a.xy,out-a.rd,out-a.rest,out-asym3
```

Where the awk program file asym_3-108.awk is simply a very long print statement to print out columns 3 through 108. The unix cut command could not be

used with the asymmetry parameters because the program has a limit of 1023 characters per line. This caused it to truncate some lines that were too long for it to handle, removing some parameters from the output, thus necessitating another method of printing the results.

Appendix C

Catalog of Objects in the Selected Sample

Here we provide a catalog of the objects detected in our survey. In order to save space, we have only provided a catalog of the magnitude limited, disk dominated, relatively face on sample we studied. All of the main parameters from the GIM2D model fits are included as are most of the parameters we calculated from them, but the asymmetry parameters GIM2D calculates are not. All four tables begin with the right ascension and declination in J2000.0 coordinates. The other parameters are as follows. Table C.1: R band magnitude (calculated from the total flux output by GIM2D) and its 99% confidence lower and upper bounds, bulge fraction and its 99% confidence lower and upper bounds, semi-major axis effective radius of the bulge (in arcsec) and its 99% confidence lower and upper bounds, bulge ellipticity and its 99% confidence lower and upper bounds. Table C.2: position angle of the bulge (in degrees) and its 99% confidence lower and upper bounds, semi-major axis scale length of the disk (in arcsec) and its 99% confidence lower and upper bounds, inclination of the disk (in degrees) and its 99% confidence lower and upper bounds, position angle of the disk (in degrees) and its 99% confidence lower and upper bounds. Table C.3: reduced χ^2 of the best model fit, half light radius (in arcsec), effective surface brightness of the bulge (in R mag

arcsec^{-2}) and its 99% confidence lower and upper bounds, face on central surface brightness of the disk (in R mag arcsec^{-2}) and its 99% confidence lower and upper bounds, observed central surface brightness of the disk (in R mag arcsec^{-2}) and its 99% confidence lower and upper bounds. Table C.4: surface brightness within the half light radius (in R mag arcsec^{-2}) and its 99% confidence lower and upper bounds, surface brightness at the half light radius (in R mag arcsec^{-2}) and its 99% confidence lower and upper bounds, total flux L_{tot} (in digital units) and its 99% confidence lower and upper bounds, the photometric zeropoint (in R mag) as determined in Chapter 3.

Table C.1: Catalog of Objects Studied

Index	R.A.	Dec.	R mag	−99%	+99%	B/T	−99%	+99%	r_e	−99%	+99%
1	0:10:26.56	-38:28:20.1	18.07	18.04	18.26	0.18	0.11	0.68	0.69	0.00	11.74
2	0:10:27.86	-45:09:10.8	17.68	17.48	17.87	0.27	0.22	0.33	0.10	0.00	0.40
3	0:10:58.04	-38:11:47.0	18.15	18.02	18.23	0.25	0.05	0.53	4.13	2.95	5.17
4	0:11:04.06	-44:49:40.4	17.90	17.80	18.18	0.29	0.24	0.35	0.64	0.00	1.07
5	0:11:06.68	-38:34:15.2	17.54	17.49	17.60	0.28	0.15	0.34	5.65	4.36	7.30
6	0:11:16.38	-44:16:25.1	17.86	17.77	17.92	0.26	0.09	0.48	3.20	2.29	4.53
7	0:11:28.13	-44:08:26.2	18.00	17.94	18.10	0.28	0.00	0.57	1.45	0.00	4.09
8	0:11:35.45	-38:40:07.8	17.45	17.39	17.51	0.19	0.00	0.32	3.43	0.68	4.88
9	0:11:45.81	-44:16:53.4	17.38	17.35	17.41	0.08	0.04	0.13	0.66	0.00	1.78
10	0:11:52.20	-38:08:02.2	15.50	15.49	15.51	0.08	0.06	0.09	2.71	2.00	3.29
11	0:12:05.75	-45:03:37.6	17.81	17.76	17.85	0.11	0.07	0.14	0.15	0.00	0.40
12	0:12:28.87	-38:51:12.0	15.31	15.21	15.33	0.26	0.25	0.71	0.49	0.41	3.80
13	0:12:38.09	-44:17:13.2	18.13	18.08	18.18	0.05	0.00	0.19	4.96	1.68	6.71
14	0:13:14.61	-38:42:04.7	17.33	17.26	17.45	0.22	0.20	0.25	0.58	0.41	0.96
15	0:13:18.68	-39:03:43.3	17.86	17.80	17.92	0.25	0.11	0.42	3.28	2.37	4.71
16	0:13:32.38	-38:26:51.8	17.49	17.46	17.52	0.26	0.21	0.30	1.88	1.27	2.40
17	0:13:39.47	-45:02:50.5	17.86	17.75	17.98	0.22	0.19	0.27	0.07	0.00	0.39
18	0:14:38.15	-44:35:53.5	18.21	18.11	18.28	0.14	0.00	0.53	1.44	0.87	2.21
19	0:15:03.14	-44:22:33.7	16.82	16.79	16.84	0.16	0.11	0.21	0.78	0.42	1.23
20	0:15:14.75	-38:48:05.2	18.03	17.97	18.08	0.01	0.00	0.16	3.81	2.03	5.14
21	0:15:19.05	-38:27:54.6	18.02	17.61	18.28	0.30	0.15	0.47	15.53	10.08	24.40
22	0:15:39.06	-44:15:46.7	17.14	17.10	17.20	0.30	0.25	0.35	0.09	0.00	0.37
23	0:16:23.36	-44:54:35.3	18.24	18.20	18.28	0.02	0.00	0.14	1.58	0.60	6.42
24	0:16:34.89	-44:13:36.1	17.92	17.84	18.01	0.24	0.02	0.41	6.13	4.89	7.85
25	0:18:13.88	-44:23:01.2	17.22	17.19	17.25	0.13	0.01	0.24	1.36	0.42	2.68

Table C.1: (continued)

Index	R.A.	Dec.	R mag	−99%	+99%	B/T	−99%	+99%	r_e	−99%	+99%
26	0:18:24.07	-45:06:05.8	16.60	16.57	16.63	0.14	0.05	0.24	4.31	3.15	6.20
27	0:20:35.11	-44:17:43.6	17.17	17.16	17.48	0.28	0.23	0.36	4.48	3.48	5.75
28	0:21:51.02	-45:08:51.3	18.07	17.92	18.15	0.04	0.00	0.21	22.18	15.95	26.12
29	0:23:01.95	-39:04:49.3	17.66	17.59	17.70	0.08	0.00	0.19	5.02	1.73	8.99
30	0:23:02.15	-38:09:36.4	18.11	17.67	18.23	0.20	0.00	1.00	5.50	3.65	8.69
31	0:23:44.45	-44:19:35.6	18.23	18.22	18.32	0.25	0.21	0.32	0.29	0.00	1.36
32	0:23:47.38	-38:32:24.6	17.08	16.95	17.11	0.06	0.00	0.85	0.99	0.00	1.97
33	0:24:20.80	-45:07:37.1	17.61	17.60	17.64	0.24	0.23	0.25	0.16	0.00	0.40
34	0:24:20.86	-45:15:02.4	16.80	16.77	16.86	0.12	0.11	0.13	0.20	0.00	0.39
35	0:24:28.32	-44:27:41.9	18.11	18.11	18.20	0.25	0.21	0.31	0.14	0.00	0.79
36	0:25:30.63	-44:25:02.4	17.51	17.15	17.62	0.21	0.12	0.29	29.33	15.21	36.31
37	0:25:37.31	-38:32:00.8	17.86	17.78	17.93	0.28	0.12	0.42	4.30	3.14	5.53
38	0:25:49.58	-39:07:37.1	18.02	17.94	18.08	0.11	0.00	0.42	2.08	0.70	3.76
39	0:25:57.58	-45:12:37.2	18.15	18.09	18.25	0.26	0.00	0.42	0.19	0.00	1.39
40	0:27:40.71	-44:56:17.3	16.01	15.94	16.12	0.23	0.19	0.30	0.28	0.00	2.94
41	0:27:55.64	-45:01:15.5	17.74	17.61	17.89	0.17	0.10	0.33	4.10	1.66	9.70
42	0:28:10.01	-44:35:19.5	18.23	18.14	18.28	0.10	0.00	0.38	2.59	1.34	4.67
43	0:28:11.73	-45:09:11.6	17.34	17.34	17.37	0.21	0.20	0.22	0.16	0.00	0.40
44	0:28:17.22	-45:09:22.7	17.75	17.61	17.91	0.11	0.00	0.27	10.91	4.56	18.20
45	0:28:17.72	-44:55:30.1	16.96	16.84	16.98	0.05	0.02	0.36	0.19	0.00	4.40
46	0:28:19.19	-44:40:34.7	18.20	18.20	18.34	0.22	0.19	0.26	0.00	0.00	0.40
47	0:28:19.69	-44:20:39.1	17.65	17.54	17.96	0.22	0.20	0.29	0.17	0.00	0.40
48	0:28:22.15	-39:09:14.9	17.59	17.51	17.63	0.00	0.00	0.16	2.90	1.43	4.24
49	0:28:40.53	-44:53:03.2	18.07	18.02	18.11	0.29	0.17	0.44	1.97	1.31	2.64
50	0:28:50.64	-44:43:17.3	16.28	16.25	16.31	0.02	0.00	0.05	0.31	0.00	2.14

Table C.1: (continued)

Index	R.A.	Dec.	R mag	−99%	+99%	B/T	−99%	+99%	r_e	−99%	+99%
51	0:29:16.44	-44:17:23.7	18.23	18.16	18.30	0.23	0.00	0.40	1.49	0.00	4.33
52	0:41:00.23	-44:29:54.1	16.57	16.45	16.76	0.22	0.18	0.25	3.85	2.97	4.61
53	0:41:22.70	-44:17:09.9	17.15	17.12	17.18	0.06	0.00	0.15	3.04	1.86	5.54
54	0:42:09.38	-44:58:04.6	17.25	17.17	17.28	0.28	0.24	0.35	3.48	2.10	4.67
55	0:42:35.91	-44:56:00.6	17.25	17.20	17.29	0.20	0.16	0.24	24.92	22.71	25.02
56	0:43:40.92	-44:38:07.6	17.60	17.56	17.65	0.16	0.06	0.24	5.23	4.12	6.66
57	0:43:42.30	-44:40:59.1	18.22	18.22	18.32	0.27	0.24	0.31	0.15	0.00	0.40
58	0:45:42.84	-44:31:22.8	18.16	18.11	18.21	0.00	0.00	0.17	2.06	0.00	4.92
59	1:00:47.15	-38:23:15.7	17.02	16.99	17.05	0.27	0.17	0.33	4.16	3.24	5.34
60	1:01:22.91	-38:30:35.8	18.17	18.13	18.21	0.17	0.00	0.27	4.37	3.05	5.53
61	1:01:42.79	-38:41:47.2	17.69	17.61	17.75	0.03	0.00	0.25	2.85	0.87	4.94
62	1:01:42.90	-38:39:50.9	17.75	17.75	17.88	0.21	0.13	0.27	5.93	1.99	7.75
63	1:01:57.85	-38:42:46.1	17.83	17.83	17.98	0.15	0.13	0.17	0.01	0.00	0.44
64	1:02:13.15	-38:42:57.2	17.25	17.22	17.29	0.11	0.00	0.21	0.15	0.00	0.41
65	1:02:13.86	-37:59:51.1	15.99	15.97	16.01	0.12	0.08	0.14	7.12	4.30	9.27
66	1:03:45.16	-38:42:03.5	16.89	16.85	16.92	0.26	0.15	0.30	3.31	2.63	5.14
67	1:04:47.45	-38:24:50.7	17.68	17.64	17.71	0.24	0.15	0.34	4.66	3.56	5.53
68	1:05:11.28	-37:53:11.0	17.62	17.56	17.67	0.23	0.06	0.34	3.69	1.55	5.19
69	1:05:16.21	-38:50:44.0	17.23	17.16	17.39	0.10	0.09	0.13	1.38	0.44	3.02
70	1:05:20.54	-38:45:18.5	18.23	18.16	18.32	0.19	0.02	0.36	2.26	0.10	4.24
71	1:05:41.13	-38:20:04.1	17.60	17.49	17.72	0.26	0.23	0.30	1.59	1.04	2.41
72	1:05:47.72	-44:05:23.8	18.10	18.03	18.15	0.06	0.00	0.38	1.11	0.19	2.03
73	1:05:56.22	-39:23:09.9	17.87	17.87	17.95	0.30	0.25	0.34	1.54	0.74	2.37
74	1:06:47.56	-45:02:45.4	15.53	15.34	15.84	0.26	0.22	0.40	0.14	0.00	0.40
75	1:06:56.09	-38:27:42.8	17.98	17.98	18.02	0.11	0.09	0.14	0.00	0.00	0.64

Table C.1: (continued)

Index	R.A.	Dec.	R mag	−99%	+99%	B/T	−99%	+99%	r_e	−99%	+99%
76	1:07:49.58	-38:31:17.8	17.96	17.92	18.00	0.15	0.00	0.26	2.37	0.53	4.58
77	1:07:53.58	-45:08:49.8	18.07	18.02	18.13	0.05	0.00	0.21	0.38	0.00	2.19
78	1:08:20.42	-38:41:08.5	18.11	18.07	18.15	0.21	0.09	0.28	0.20	0.00	0.40
79	1:08:27.05	-39:21:37.3	17.78	17.73	17.82	0.29	0.23	0.34	4.01	2.88	6.60
80	1:09:20.97	-44:31:46.4	17.82	17.82	17.86	0.21	0.19	0.22	0.19	0.00	0.40
81	1:09:36.92	-44:44:32.0	17.84	17.71	18.04	0.29	0.25	0.38	0.12	0.00	0.40
82	1:10:01.99	-38:21:31.6	18.20	18.16	18.24	0.01	0.00	0.15	1.78	0.64	3.61
83	1:10:17.95	-44:52:35.2	15.12	15.12	15.13	0.24	0.23	0.24	0.93	0.77	1.03
84	1:10:38.30	-39:18:17.5	17.62	17.58	17.69	0.22	0.14	0.33	6.03	2.94	6.88
85	1:11:14.56	-39:20:07.1	18.03	17.94	18.25	0.08	0.00	0.35	8.19	5.60	10.51
86	1:11:16.42	-44:20:04.5	17.94	17.84	17.99	0.10	0.00	0.32	3.14	1.72	4.35
87	1:11:19.38	-44:28:34.5	17.27	17.24	17.29	0.29	0.22	0.35	1.56	1.13	1.97
88	1:11:23.53	-44:09:45.2	18.24	18.10	18.41	0.28	0.19	0.43	1.01	0.00	2.87
89	1:12:52.69	-39:21:37.4	17.21	17.18	17.39	0.23	0.17	0.32	4.79	2.01	6.99
90	1:13:00.84	-38:27:30.3	18.24	18.18	18.30	0.13	0.00	0.30	1.99	0.00	3.81
91	1:14:04.66	-39:17:33.3	16.50	16.48	16.52	0.02	0.00	0.05	14.04	13.14	18.35
92	1:14:09.32	-39:19:24.3	18.08	18.08	18.16	0.25	0.23	0.28	0.03	0.00	0.39
93	1:14:33.46	-38:39:59.3	16.29	16.28	16.30	0.04	0.04	0.05	0.27	0.00	0.40
94	1:15:06.07	-38:30:02.8	16.93	16.91	16.94	0.00	0.00	0.07	1.84	1.23	2.30
95	1:15:10.13	-39:17:16.8	17.04	16.98	17.08	0.23	0.19	0.28	16.62	14.90	16.62
96	1:15:15.91	-38:25:41.4	18.02	17.95	18.06	0.02	0.00	0.26	1.24	0.79	2.59
97	2:00:05.11	-38:36:19.3	15.08	15.06	15.09	0.05	0.05	0.06	0.12	0.00	0.38
98	2:00:29.27	-38:02:53.3	17.93	17.90	17.95	0.03	0.00	0.12	2.43	1.79	3.51
99	2:00:32.39	-38:06:50.4	17.66	17.59	17.69	0.12	0.00	0.32	2.60	1.51	4.17
100	2:00:34.12	-38:02:59.6	18.10	18.06	18.16	0.07	0.00	0.20	0.56	0.00	1.66

Table C.1: (continued)

Index	R.A.	Dec.	R mag	−99%	+99%	B/T	−99%	+99%	r_e	−99%	+99%
101	2:00:34.34	-38:28:16.3	17.38	17.24	17.64	0.26	0.23	0.34	0.10	0.00	0.40
102	2:00:34.48	-38:06:45.1	16.83	16.82	16.85	0.15	0.08	0.27	2.10	1.08	3.47
103	2:01:04.33	-38:49:24.9	17.56	17.38	17.66	0.15	0.13	0.16	0.07	0.00	0.41
104	2:02:14.41	-39:04:46.6	17.72	17.67	18.04	0.28	0.26	0.41	0.19	0.00	0.40
105	2:02:15.75	-39:02:53.0	18.04	17.95	18.10	0.07	0.00	0.34	0.47	0.00	0.96
106	2:02:57.97	-38:31:46.9	17.35	17.30	17.38	0.01	0.00	0.17	2.05	0.90	6.96
107	2:03:24.00	-38:25:37.2	15.35	15.34	15.35	0.03	0.02	0.03	0.25	0.00	0.40
108	2:03:33.03	-38:20:10.6	17.90	17.90	17.93	0.08	0.05	0.13	0.15	0.00	1.62
109	2:03:33.52	-38:35:54.9	17.53	17.50	17.66	0.16	0.09	0.23	12.50	7.10	18.44
110	2:03:34.65	-38:35:45.5	17.80	17.72	17.98	0.11	0.08	0.15	0.87	0.00	2.89
111	2:03:55.66	-39:05:21.5	17.34	17.34	17.41	0.15	0.14	0.16	0.10	0.00	0.39
112	2:04:00.53	-38:03:24.7	16.77	16.75	16.79	0.09	0.00	0.15	2.74	0.94	3.83
113	2:04:19.37	-38:01:11.5	16.06	15.74	16.11	0.10	0.00	0.43	1.92	0.70	3.06
114	2:04:43.42	-39:00:11.2	17.05	17.01	17.20	0.19	0.00	0.22	6.19	2.74	9.54
115	2:08:46.83	-38:47:54.2	15.08	15.07	15.09	0.15	0.13	0.17	1.59	1.16	2.01
116	2:09:10.07	-38:20:49.7	17.17	17.15	17.20	0.23	0.14	0.31	1.67	1.10	2.31
117	2:09:16.44	-39:00:18.5	17.11	17.11	17.14	0.02	0.02	0.04	0.20	0.00	1.30
118	2:09:24.15	-38:03:25.9	18.13	18.06	18.25	0.30	0.25	0.36	3.11	2.23	4.35
119	2:09:28.17	-38:50:35.9	18.08	18.03	18.13	0.11	0.00	0.28	1.73	0.80	3.38
120	2:09:54.59	-39:06:48.7	15.64	15.43	15.73	0.17	0.14	0.18	0.11	0.00	0.39
121	2:10:36.31	-38:47:36.9	16.66	16.36	16.81	0.16	0.13	0.19	0.01	0.00	0.39
122	2:11:11.64	-38:03:03.4	17.35	17.18	17.44	0.27	0.23	0.31	2.02	1.53	2.64
123	2:11:35.87	-38:40:48.9	15.51	15.50	15.51	0.26	0.25	0.27	0.92	0.80	1.05
124	2:11:53.51	-38:57:43.3	17.97	17.90	18.01	0.07	0.00	0.22	6.45	4.16	8.26
125	2:12:57.69	-38:22:43.7	18.11	18.11	18.16	0.23	0.18	0.27	1.19	0.47	2.01

Table C.1: (continued)

Index	R.A.	Dec.	R mag	−99%	+99%	B/T	−99%	+99%	r_e	−99%	+99%
126	2:13:30.48	-38:46:55.8	17.90	17.67	18.11	0.30	0.21	0.39	2.79	1.42	3.99
127	2:13:42.85	-38:10:52.2	17.01	17.00	17.03	0.30	0.28	0.31	0.14	0.00	0.40
128	2:14:05.18	-38:08:18.8	17.02	16.98	17.13	0.29	0.13	0.32	16.46	9.66	16.48
129	2:14:29.57	-38:11:43.1	17.64	17.59	17.87	0.28	0.25	0.32	0.14	0.00	0.39
130	2:20:28.36	-44:49:30.9	17.20	17.20	17.31	0.11	0.10	0.12	0.14	0.00	0.40
131	2:21:20.57	-44:15:33.1	17.74	17.67	17.82	0.20	0.11	0.26	12.17	9.97	12.47
132	2:22:03.69	-44:51:11.4	18.16	18.10	18.21	0.03	0.00	0.13	9.74	8.79	10.40
133	2:24:15.30	-44:17:38.4	17.53	17.31	17.76	0.21	0.12	0.40	2.83	0.00	7.64
134	2:24:16.54	-44:25:38.7	17.66	17.61	17.70	0.02	0.00	0.16	2.76	0.10	3.63
135	2:24:47.47	-44:54:30.4	17.42	17.37	17.45	0.01	0.00	0.13	3.37	1.88	8.00
136	2:25:38.24	-38:32:35.4	17.48	17.48	17.52	0.21	0.19	0.23	0.03	0.00	0.40
137	2:29:19.96	-38:22:13.6	17.38	17.36	17.41	0.27	0.18	0.32	2.94	2.35	3.76
138	2:30:16.16	-39:02:00.6	18.13	18.06	18.19	0.20	0.02	0.37	3.05	0.55	7.43
139	2:40:32.69	-39:13:58.4	17.51	17.44	17.69	0.17	0.14	0.20	0.13	0.00	0.40
140	2:41:32.14	-39:04:35.1	17.92	17.92	17.93	0.24	0.23	0.26	0.06	0.00	0.40
141	2:41:41.48	-38:24:09.1	17.61	17.57	17.65	0.09	0.04	0.14	4.38	3.70	4.80
142	2:42:16.90	-38:52:53.8	16.66	16.64	16.67	0.17	0.15	0.20	0.46	0.41	0.61
143	2:46:15.19	-38:16:28.6	17.73	17.62	17.82	0.13	0.00	0.29	8.15	2.60	9.01
144	2:59:20.76	-44:17:01.1	15.68	15.67	15.96	0.22	0.22	0.30	0.16	0.00	0.39
145	3:00:16.46	-45:03:15.2	16.64	16.63	16.65	0.20	0.15	0.23	1.89	1.34	2.68
146	3:00:20.22	-44:18:27.4	17.62	17.50	17.94	0.30	0.21	0.52	7.06	3.88	18.92
147	3:00:32.88	-44:11:19.2	17.97	17.84	18.04	0.18	0.01	0.40	2.72	2.07	4.15
148	3:00:57.29	-45:08:25.8	17.87	17.78	18.01	0.25	0.21	0.29	0.18	0.00	0.40
149	3:01:04.97	-44:23:18.3	17.26	17.23	17.51	0.27	0.23	0.34	0.69	0.42	0.91
150	3:01:50.90	-44:09:23.6	17.15	17.09	17.19	0.10	0.05	0.23	3.77	2.07	5.92

Table C.1: (continued)

Index	R.A.	Dec.	R mag	−99%	+99%	B/T	−99%	+99%	r_e	−99%	+99%
151	3:02:29.12	-44:37:31.7	17.55	17.54	17.60	0.29	0.25	0.33	2.84	1.96	3.77
152	3:02:38.40	-44:09:34.0	16.42	16.37	16.44	0.02	0.00	0.08	12.33	9.32	20.16
153	3:03:08.41	-38:28:01.4	17.67	17.61	17.76	0.21	0.00	0.41	4.28	0.49	6.71
154	3:05:52.83	-38:31:46.8	16.92	16.68	17.03	0.09	0.05	0.12	15.09	13.28	17.71
155	3:07:08.73	-39:03:18.7	17.10	17.06	17.13	0.20	0.13	0.26	3.27	2.14	5.19
156	10:13:22.89	-3:25:08.8	16.87	16.84	16.91	0.04	0.02	0.05	0.17	0.00	0.41
157	10:13:23.77	-2:45:25.7	17.06	17.03	17.10	0.11	0.06	0.15	14.56	9.87	14.87
158	10:13:29.95	-6:01:30.0	17.24	17.18	17.26	0.24	0.17	0.30	4.02	2.81	7.77
159	10:13:35.61	-6:21:07.7	18.01	17.94	18.07	0.10	0.00	0.30	0.86	0.00	2.93
160	10:13:36.44	-3:01:32.8	17.90	17.84	17.94	0.26	0.18	0.33	6.33	5.68	6.39
161	10:13:57.17	-6:35:18.4	16.82	16.79	16.85	0.08	0.06	0.14	0.97	0.41	2.15
162	10:14:04.19	-3:17:34.5	18.04	17.98	18.09	0.09	0.00	0.26	0.89	0.00	1.51
163	10:14:05.20	-3:22:35.6	17.80	17.75	17.85	0.19	0.00	0.35	3.86	1.99	6.69
164	10:14:14.08	-6:12:28.3	17.33	17.28	17.39	0.24	0.10	0.33	4.28	3.30	6.04
165	10:14:14.62	-3:44:39.5	17.17	17.13	17.20	0.27	0.17	0.36	2.55	1.38	4.19
166	10:14:21.59	-3:25:45.3	17.34	17.34	17.58	0.30	0.29	0.36	0.10	0.00	0.40
167	10:14:37.51	-6:38:03.2	17.15	17.15	17.43	0.28	0.26	0.36	1.20	0.82	1.56
168	10:14:38.06	-2:56:21.5	18.01	17.92	18.06	0.13	0.00	0.42	2.80	1.00	4.40
169	10:15:10.23	-3:13:43.9	17.69	17.69	17.77	0.27	0.24	0.29	0.15	0.00	0.39
170	10:15:13.35	-2:59:15.4	18.17	18.17	18.19	0.18	0.17	0.19	0.15	0.00	0.40
171	10:15:20.32	-6:39:09.1	17.81	17.77	17.88	0.13	0.00	0.27	4.90	2.03	8.28
172	10:15:29.88	-6:13:06.5	16.43	16.40	16.44	0.20	0.17	0.29	2.71	2.28	3.47
173	10:15:31.72	-5:45:07.5	16.72	16.66	16.93	0.24	0.22	0.31	0.13	0.00	0.40
174	10:15:56.65	-3:06:11.8	17.25	17.20	17.30	0.04	0.00	0.15	3.60	0.00	10.03
175	10:16:05.56	-3:27:40.5	16.35	16.32	16.39	0.15	0.09	0.18	7.98	5.59	9.95

Table C.1: (continued)

Index	R.A.	Dec.	R mag	−99%	+99%	B/T	−99%	+99%	r_e	−99%	+99%
176	10:16:06.52	-3:01:05.0	17.91	17.90	18.15	0.16	0.10	0.24	3.89	2.23	5.87
177	10:16:14.55	-3:15:07.7	17.98	17.95	18.09	0.25	0.23	0.29	0.12	0.00	0.40
178	10:16:17.23	-5:47:54.8	18.05	18.03	18.22	0.26	0.23	0.29	0.13	0.00	0.39
179	10:16:40.63	-5:49:20.5	17.70	17.69	17.80	0.22	0.16	0.33	5.51	2.88	9.76
180	10:17:23.10	-6:06:02.5	16.45	16.43	16.47	0.04	0.01	0.07	2.54	0.00	5.02
181	10:17:25.22	-6:48:29.4	17.44	17.29	17.76	0.20	0.15	0.35	0.71	0.00	3.99
182	10:24:11.14	-11:46:12.8	16.91	16.85	16.93	0.05	0.00	0.20	1.84	0.83	2.76
183	10:24:55.58	-11:45:12.8	18.16	18.10	18.22	0.02	0.00	0.14	1.41	0.37	2.25
184	10:25:01.03	-12:35:00.9	16.43	16.30	16.66	0.21	0.16	0.28	0.85	0.41	3.15
185	10:25:08.50	-12:36:22.2	17.16	16.94	17.33	0.28	0.23	0.37	0.75	0.41	1.08
186	10:25:34.59	-11:43:20.6	17.02	17.00	17.05	0.30	0.23	0.35	4.36	3.56	6.79
187	10:26:21.46	-12:06:41.2	17.60	17.48	17.71	0.26	0.15	0.33	34.19	25.09	45.01
188	10:27:09.64	-11:56:05.5	17.32	17.27	17.38	0.24	0.18	0.29	50.42	42.10	51.40
189	10:27:14.66	-12:22:35.6	17.21	17.19	17.24	0.19	0.09	0.27	2.59	1.47	3.63
190	10:27:17.00	-12:25:14.9	17.72	17.67	17.80	0.19	0.00	0.38	2.97	1.90	5.01
191	10:27:19.49	-12:27:43.5	16.69	16.66	16.75	0.13	0.09	0.16	40.56	37.85	40.61
192	10:27:35.63	-11:50:35.0	17.36	17.33	17.40	0.07	0.03	0.19	0.14	0.00	0.87
193	10:27:49.31	-12:19:42.0	16.26	16.25	16.26	0.28	0.26	0.29	0.42	0.41	0.46
194	10:27:55.13	-11:56:41.6	15.62	15.61	15.62	0.13	0.10	0.16	2.51	1.89	3.63
195	10:28:08.42	-12:09:57.8	16.40	16.38	16.41	0.12	0.07	0.17	5.24	4.58	5.96
196	10:28:25.25	-11:36:24.7	16.96	16.95	16.98	0.14	0.10	0.18	0.17	0.00	0.40
197	10:28:27.90	-11:39:17.9	17.45	17.43	17.67	0.18	0.16	0.22	0.00	0.00	0.39
198	10:28:31.02	-12:10:07.2	16.07	16.06	16.09	0.04	0.00	0.08	4.47	3.09	6.79
199	10:32:39.57	-6:23:51.2	16.83	16.78	17.16	0.25	0.23	0.36	0.13	0.00	0.40
200	10:33:41.81	-6:45:34.2	17.24	17.21	17.27	0.24	0.19	0.31	0.90	0.41	1.45

Table C.1: (continued)

Index	R.A.	Dec.	R mag	−99%	+99%	B/T	−99%	+99%	r_e	−99%	+99%
201	10:34:44.34	-6:39:43.1	17.38	17.37	17.73	0.27	0.24	0.33	0.06	0.00	0.39
202	10:35:10.80	-6:33:32.4	17.99	17.95	18.02	0.02	0.00	0.15	3.37	0.60	4.57
203	10:35:11.02	-6:41:53.4	17.72	17.68	17.75	0.03	0.00	0.16	1.94	0.90	4.23
204	10:35:57.53	-5:49:44.5	16.76	16.67	16.79	0.26	0.23	0.32	16.56	12.15	22.41
205	10:36:24.84	-3:48:13.1	16.70	16.67	16.72	0.13	0.08	0.25	1.79	0.82	4.46
206	10:37:09.86	-6:08:37.1	17.41	17.39	17.75	0.25	0.21	0.43	1.36	0.68	2.51
207	10:37:12.38	-6:32:13.7	17.63	17.50	17.79	0.30	0.21	0.45	5.67	2.45	10.63
208	10:37:13.68	-2:52:49.6	17.89	17.83	17.93	0.19	0.04	0.34	3.75	2.92	4.27
209	10:37:40.88	-2:55:24.4	17.85	17.79	17.91	0.15	0.00	0.35	1.29	0.26	2.56
210	10:38:39.13	-6:36:52.9	17.96	17.90	18.02	0.17	0.09	0.24	11.60	8.96	11.82
211	10:39:07.08	-3:28:20.3	16.18	16.17	16.19	0.25	0.22	0.28	2.73	2.30	3.20
212	10:39:19.08	-6:37:33.4	17.69	17.54	17.94	0.24	0.18	0.69	0.72	0.00	7.25
213	10:40:14.34	-6:49:11.1	18.15	17.98	18.22	0.17	0.00	0.60	2.47	0.89	3.79
214	10:40:14.35	-6:49:12.0	18.14	18.05	18.21	0.08	0.00	0.28	4.00	2.87	6.15
215	10:40:21.85	-6:50:15.4	17.47	17.09	17.67	0.25	0.18	0.30	0.04	0.00	0.39
216	10:41:05.88	-6:04:13.1	17.82	17.82	18.03	0.25	0.20	0.31	3.57	1.91	5.55
217	10:42:30.23	-6:30:16.2	14.11	14.07	14.19	0.25	0.23	0.45	0.08	0.00	0.63
218	10:42:32.98	-6:27:45.4	17.80	17.72	17.89	0.24	0.03	0.41	3.75	0.98	9.17
219	10:42:36.87	-2:49:00.2	16.98	16.95	17.00	0.00	0.00	0.06	5.07	4.58	5.59
220	10:42:56.90	-6:52:01.7	15.29	15.22	15.36	0.25	0.20	0.30	53.44	50.42	53.44
221	10:43:28.59	-2:42:25.5	17.12	17.08	17.18	0.16	0.02	0.24	4.50	3.23	5.33
222	10:43:44.80	-3:39:47.3	17.68	17.61	17.71	0.01	0.00	0.23	2.44	1.78	5.32
223	10:43:55.66	-6:21:51.5	17.40	17.28	17.60	0.24	0.21	0.29	0.14	0.00	0.40
224	10:44:06.75	-3:06:06.3	16.83	16.75	17.08	0.28	0.26	0.37	0.47	0.41	1.03
225	10:44:12.05	-2:57:27.3	17.40	17.38	17.44	0.18	0.11	0.25	1.16	0.46	2.01

Table C.1: (continued)

Index	R.A.	Dec.	R mag	−99%	+99%	B/T	−99%	+99%	r_e	−99%	+99%
226	10:44:35.36	-6:50:02.0	16.20	16.16	16.21	0.17	0.11	0.34	0.80	0.00	3.28
227	10:45:00.32	-3:07:51.2	17.57	17.44	17.61	0.20	0.06	0.58	0.10	0.00	0.91
228	10:45:08.38	-6:34:13.8	17.38	17.33	17.43	0.21	0.09	0.31	6.12	5.19	6.62
229	10:45:19.81	-2:58:05.5	17.22	17.19	17.25	0.29	0.26	0.32	0.62	0.41	0.89
230	10:45:37.68	-6:06:58.8	17.35	17.19	17.40	0.06	0.00	0.30	6.51	2.20	12.42
231	10:45:59.98	-3:16:04.8	17.99	17.93	18.05	0.14	0.00	0.25	0.96	0.41	1.94
232	10:46:11.85	-3:32:29.7	18.24	18.18	18.30	0.10	0.00	0.33	2.92	0.93	4.74
233	10:46:46.52	-6:45:11.4	17.76	17.71	17.80	0.00	0.00	0.14	3.39	2.73	6.27
234	10:46:51.01	-6:48:37.5	17.26	17.24	17.28	0.01	0.00	0.09	0.48	0.00	1.41
235	10:46:55.26	-6:01:40.5	18.05	18.05	18.15	0.26	0.20	0.36	3.23	2.26	5.83
236	10:47:49.49	-5:51:18.0	16.31	16.30	16.33	0.22	0.19	0.28	7.12	5.34	7.52
237	10:48:04.60	-6:36:57.1	17.67	17.62	17.70	0.00	0.00	0.12	3.55	2.05	7.83
238	10:49:30.46	-6:08:33.1	17.56	17.56	17.70	0.20	0.17	0.22	0.15	0.00	0.40
239	10:49:57.96	-6:14:39.1	17.51	17.46	17.55	0.28	0.16	0.47	3.45	2.41	4.54
240	10:50:11.70	-6:38:00.9	17.43	17.31	17.51	0.22	0.15	0.31	15.42	8.89	19.77
241	10:50:25.93	-6:07:54.3	18.16	18.05	18.23	0.11	0.00	0.28	5.87	0.43	8.69
242	10:50:56.98	-6:06:21.5	17.77	17.70	17.81	0.26	0.14	0.50	2.47	1.88	2.94
243	10:51:01.59	-6:09:08.4	17.85	17.80	17.93	0.16	0.01	0.34	1.98	0.00	6.10
244	10:51:30.47	-6:06:28.7	17.15	16.95	17.28	0.23	0.18	0.29	4.80	2.65	7.22
245	10:51:32.53	-5:52:17.4	17.58	17.47	17.80	0.29	0.20	0.34	4.60	2.07	5.73
246	10:51:35.10	-6:36:16.2	17.21	17.19	17.28	0.25	0.23	0.26	0.16	0.00	0.40
247	10:52:01.23	-6:19:02.6	17.61	17.56	17.65	0.18	0.04	0.30	5.05	3.75	5.85
248	10:52:30.85	-6:36:20.9	17.75	17.68	17.83	0.24	0.05	0.37	5.30	4.25	8.70
249	10:52:30.85	-6:36:21.1	17.77	17.74	17.81	0.00	0.00	0.14	2.12	0.31	4.47
250	10:52:38.16	-6:57:13.7	17.02	16.94	17.06	0.26	0.24	0.31	7.72	4.30	12.76

Table C.1: (continued)

Index	R.A.	Dec.	R mag	−99%	+99%	B/T	−99%	+99%	r_e	−99%	+99%
251	10:54:05.62	-5:58:42.9	17.49	17.44	17.53	0.20	0.09	0.30	3.85	2.82	4.57
252	10:54:14.38	-6:56:09.0	17.43	17.15	17.61	0.28	0.22	0.38	1.23	0.41	3.09
253	10:54:17.48	-13:07:58.0	17.98	17.93	18.01	0.15	0.04	0.29	2.24	0.44	4.71
254	10:55:08.65	-6:10:44.8	17.96	17.88	18.01	0.09	0.00	0.31	2.61	0.00	4.72
255	10:55:44.99	-12:24:44.6	17.71	17.66	17.75	0.12	0.04	0.19	4.24	2.44	5.86
256	10:55:48.75	-12:51:32.1	17.27	17.24	17.32	0.24	0.14	0.33	6.73	5.61	7.51
257	10:56:10.61	-6:22:09.5	16.97	16.94	17.01	0.21	0.13	0.28	3.24	1.74	4.73
258	10:56:12.65	-6:41:46.3	17.75	17.64	18.10	0.16	0.13	0.22	0.05	0.00	0.39
259	10:56:33.51	-12:33:59.7	17.33	17.27	17.38	0.02	0.00	0.20	6.80	3.48	7.85
260	10:56:38.29	-6:16:04.3	16.43	16.40	16.54	0.28	0.26	0.33	0.08	0.00	0.40
261	10:56:52.81	-12:57:33.1	15.69	15.67	15.69	0.17	0.15	0.27	1.74	1.18	4.18
262	10:56:54.90	-12:54:57.7	16.54	16.53	16.54	0.00	0.00	0.01	4.24	3.47	4.65
263	10:57:03.01	-12:40:13.9	17.01	16.92	17.18	0.27	0.23	0.31	0.64	0.48	0.85
264	10:57:17.52	-13:12:35.1	17.74	17.71	17.77	0.00	0.00	0.10	2.92	2.37	3.43
265	10:57:36.69	-12:26:49.0	16.92	16.90	16.94	0.28	0.24	0.32	5.28	4.56	6.24
266	10:57:44.04	-12:23:06.2	16.82	16.79	16.85	0.14	0.03	0.19	5.75	2.45	8.85
267	10:57:45.01	-6:16:24.6	17.96	17.78	18.09	0.29	0.00	0.49	9.28	4.96	13.39
268	10:57:54.03	-6:49:35.4	15.28	15.25	15.31	0.28	0.16	0.35	8.25	3.39	9.89
269	10:58:04.00	-6:14:36.9	16.59	16.53	16.76	0.28	0.25	0.39	4.72	3.41	6.63
270	10:58:04.04	-6:16:09.4	16.50	16.44	16.75	0.20	0.18	0.26	0.44	0.41	0.63
271	10:58:04.47	-12:42:19.5	17.77	17.70	18.03	0.15	0.11	0.29	0.27	0.00	2.77
272	10:58:07.07	-12:13:28.3	18.06	17.98	18.13	0.01	0.00	0.14	7.13	4.03	9.27
273	10:58:11.65	-5:50:00.0	17.34	17.34	17.42	0.27	0.23	0.33	2.85	2.07	4.03
274	10:59:17.24	-5:47:02.3	16.33	16.32	16.35	0.01	0.01	0.02	0.16	0.00	0.40
275	11:00:05.68	-6:18:37.6	16.36	16.30	16.38	0.22	0.18	0.28	37.94	29.99	41.96

Table C.1: (continued)

Index	R.A.	Dec.	R mag	−99%	+99%	B/T	−99%	+99%	r_e	−99%	+99%
276	11:01:28.43	-12:30:39.8	17.51	17.39	17.59	0.08	0.00	0.27	8.39	5.31	10.08
277	11:02:01.88	-6:57:58.3	13.68	13.65	13.70	0.26	0.25	0.26	2.27	2.17	2.53
278	11:02:21.59	-12:04:24.4	16.46	16.03	16.74	0.25	0.18	0.39	0.01	0.00	0.40
279	11:02:59.66	-12:34:47.7	17.62	17.59	17.65	0.27	0.22	0.33	3.89	3.32	4.48
280	11:03:11.21	-6:30:47.3	16.89	16.68	17.04	0.08	0.00	0.37	11.05	6.14	12.07
281	11:03:13.90	-12:11:44.2	17.94	17.79	18.03	0.08	0.00	0.21	22.19	11.76	27.81
282	11:03:18.93	-6:53:21.2	17.92	17.85	17.96	0.05	0.00	0.15	4.86	2.95	6.57
283	11:03:26.97	-6:34:00.7	16.48	16.47	16.48	0.00	0.00	0.01	5.66	5.27	6.03
284	11:03:49.41	-12:02:11.6	17.88	17.80	18.03	0.22	0.00	0.41	8.28	5.47	9.80
285	11:05:31.44	-6:11:09.3	16.26	16.24	16.29	0.19	0.13	0.25	6.58	5.11	8.26
286	11:05:48.11	-12:41:23.9	15.36	15.35	15.38	0.15	0.10	0.17	5.69	3.72	6.95
287	11:07:52.46	-6:33:41.3	16.46	16.43	16.49	0.24	0.18	0.31	5.04	4.13	6.05
288	11:07:52.47	-6:33:42.0	16.46	16.44	16.48	0.21	0.18	0.25	3.19	2.63	3.93
289	11:08:02.98	-7:01:45.7	17.63	17.57	17.66	0.01	0.00	0.21	1.99	1.03	2.86
290	11:08:15.83	-5:51:21.2	17.02	16.97	17.07	0.27	0.16	0.35	5.00	2.52	7.03
291	11:08:30.25	-6:48:08.8	17.31	17.28	17.34	0.08	0.00	0.19	2.91	2.05	3.60
292	11:08:55.40	-6:11:32.6	15.56	15.55	15.57	0.20	0.17	0.27	1.69	1.20	2.70
293	11:08:55.41	-6:11:31.9	15.58	15.57	15.59	0.23	0.21	0.25	2.46	2.02	2.98
294	11:09:03.91	-6:05:40.0	18.19	18.11	18.24	0.04	0.00	0.18	4.56	2.23	7.92
295	11:09:16.70	-6:40:14.7	17.20	17.09	17.34	0.27	0.22	0.32	2.12	1.19	3.11
296	11:09:16.74	-6:40:16.2	17.07	16.99	17.29	0.25	0.17	0.31	3.04	1.08	4.31
297	11:09:29.59	-6:08:54.5	17.93	17.71	18.27	0.30	0.23	0.41	0.10	0.00	0.93
298	11:09:34.36	-6:19:43.4	18.10	18.04	18.17	0.15	0.00	0.29	2.74	0.86	4.23
299	11:09:47.21	-6:43:47.0	18.25	18.20	18.30	0.02	0.00	0.17	3.78	2.43	4.57
300	11:10:32.63	-6:32:47.8	14.81	14.81	14.81	0.13	0.12	0.14	4.22	3.89	4.93

Table C.1: (continued)

Index	R.A.	Dec.	R mag	−99%	+99%	B/T	−99%	+99%	r_e	−99%	+99%
301	11:10:58.25	-6:06:49.6	17.98	17.98	18.06	0.25	0.19	0.28	0.45	0.00	1.01
302	11:11:30.39	-6:35:42.7	16.00	15.99	16.02	0.15	0.11	0.19	2.85	2.16	4.03
303	11:11:30.39	-6:35:42.8	15.98	15.96	16.01	0.22	0.15	0.27	4.45	2.90	5.61
304	11:12:46.14	-5:49:02.9	18.14	18.00	18.30	0.27	0.10	0.38	17.78	12.35	19.08
305	11:13:26.02	-6:52:30.2	15.92	15.88	15.97	0.25	0.24	0.26	0.42	0.41	0.48
306	11:14:12.99	-6:46:01.6	18.17	18.11	18.39	0.29	0.23	0.37	1.03	0.46	2.02
307	11:14:14.30	-6:37:27.9	18.08	18.04	18.43	0.24	0.21	0.34	0.16	0.00	0.39
308	11:14:19.35	-6:54:49.6	18.06	18.01	18.44	0.22	0.16	1.00	0.54	0.00	17.92
309	11:14:21.24	-6:48:43.3	17.53	17.51	17.73	0.17	0.11	0.22	4.97	1.39	6.53
310	11:14:49.61	-6:21:43.2	17.67	17.57	17.86	0.24	0.16	0.28	0.51	0.23	1.12
311	11:14:58.18	-5:56:56.2	17.78	17.62	17.89	0.25	0.15	0.35	37.97	24.84	50.92
312	11:15:16.55	-6:32:24.7	16.82	16.80	16.84	0.20	0.09	0.29	2.24	0.96	3.23
313	11:15:52.28	-5:50:38.1	17.50	17.44	17.54	0.25	0.11	0.41	3.10	2.24	3.86
314	11:36:40.30	-3:41:01.1	16.06	16.05	16.12	0.25	0.23	0.27	2.62	2.17	3.06
315	11:37:18.01	-3:13:33.9	18.08	18.03	18.13	0.04	0.00	0.16	2.06	0.00	4.77
316	11:37:40.41	-3:13:37.9	17.92	17.88	18.09	0.28	0.22	0.35	1.07	0.48	1.76
317	11:37:55.41	-3:25:29.7	17.25	17.25	17.28	0.25	0.22	0.30	2.65	2.07	3.86
318	11:38:13.93	-3:23:22.1	16.77	16.74	16.79	0.04	0.01	0.11	1.84	0.12	5.99
319	11:39:49.65	-3:06:39.1	17.87	17.87	17.92	0.21	0.19	0.23	0.12	0.00	0.38
320	11:40:02.28	-3:12:37.0	18.16	18.10	18.22	0.23	0.01	0.38	1.65	0.81	4.29
321	11:40:05.83	-3:01:13.3	17.73	17.72	18.03	0.27	0.23	0.32	1.39	0.43	2.20
322	11:40:12.08	-3:37:55.2	17.95	17.88	18.01	0.11	0.00	0.44	1.10	0.00	3.83
323	11:40:26.51	-3:26:59.3	17.34	17.32	17.37	0.03	0.00	0.14	0.69	0.00	2.35
324	11:40:29.52	-2:46:49.4	16.11	15.98	16.17	0.30	0.26	0.33	1.62	1.22	2.42
325	11:40:32.09	-3:45:09.1	18.08	18.03	18.16	0.21	0.00	0.39	3.27	0.30	4.08

Table C.1: (continued)

Index	R.A.	Dec.	R mag	−99%	+99%	B/T	−99%	+99%	r_e	−99%	+99%
326	11:40:43.60	-3:40:18.7	16.90	16.87	16.93	0.09	0.04	0.15	4.74	3.49	9.60
327	11:40:59.25	-2:54:44.9	17.45	17.41	17.48	0.01	0.00	0.12	1.95	0.99	3.39
328	11:42:44.17	-12:29:13.5	18.00	17.93	18.07	0.16	0.00	0.43	1.21	0.00	2.49
329	11:42:50.20	-13:00:15.3	17.74	17.66	17.80	0.10	0.00	0.41	1.26	0.00	4.46
330	11:43:15.61	-12:18:57.9	16.82	16.80	16.85	0.10	0.04	0.17	0.82	0.00	2.24
331	11:43:29.99	-12:55:28.4	17.60	17.47	17.63	0.01	0.00	0.12	44.72	22.86	48.44
332	11:44:11.39	-13:05:29.4	17.97	17.89	18.03	0.12	0.03	0.23	0.98	0.00	2.56
333	11:44:36.38	-12:32:04.7	18.21	18.00	18.36	0.24	0.08	0.34	21.97	14.17	28.01
334	11:44:42.27	-12:21:46.0	18.13	18.03	18.18	0.09	0.00	0.38	1.26	0.39	1.95
335	11:44:49.04	-12:57:14.5	17.71	17.67	17.94	0.28	0.26	0.33	0.04	0.00	0.40
336	11:45:36.95	-12:38:58.2	17.93	17.78	18.02	0.05	0.00	0.30	9.75	5.57	16.85
337	11:45:44.39	-13:04:30.0	16.99	16.96	17.02	0.08	0.04	0.12	4.65	2.69	7.32
338	11:45:54.36	-12:18:28.6	18.09	18.09	18.22	0.28	0.26	0.32	0.08	0.00	0.39
339	11:46:05.93	-12:38:07.9	17.91	17.66	18.16	0.24	0.19	0.30	0.00	0.00	0.40
340	11:46:11.01	-12:04:47.5	17.82	17.77	17.88	0.06	0.00	0.28	3.54	0.00	5.43
341	11:49:56.18	-3:17:42.6	16.79	16.76	16.81	0.25	0.18	0.32	3.84	2.84	5.90
342	11:50:50.00	-3:56:46.6	17.61	17.59	17.74	0.24	0.17	0.28	0.98	0.00	1.64
343	11:50:52.82	-3:12:39.7	16.88	16.86	16.91	0.19	0.13	0.23	0.18	0.00	0.40
344	11:50:55.17	-3:15:15.4	17.55	17.50	17.63	0.24	0.09	0.34	6.18	3.91	9.27
345	11:51:24.32	-3:47:18.3	17.86	17.79	17.95	0.28	0.05	0.42	8.28	4.83	9.98
346	11:51:37.20	-2:57:55.5	16.86	16.82	16.91	0.17	0.09	0.28	6.21	4.26	9.96
347	11:51:38.68	-3:58:22.9	15.86	15.82	15.88	0.15	0.14	0.16	0.09	0.00	0.40
348	11:52:41.24	-3:20:55.7	17.64	17.55	17.70	0.00	0.00	0.22	13.20	7.70	21.51
349	11:52:59.43	-3:24:29.7	17.90	17.86	17.94	0.01	0.00	0.10	7.31	5.68	9.10
350	11:53:21.94	-3:45:59.1	16.34	16.25	16.38	0.17	0.06	0.60	14.57	5.32	14.79

Table C.1: (continued)

Index	R.A.	Dec.	R mag	−99%	+99%	B/T	−99%	+99%	r_e	−99%	+99%
351	11:53:33.34	-3:00:56.3	17.14	17.14	17.18	0.21	0.19	0.24	1.74	1.10	2.44
352	11:53:49.16	-3:43:58.7	17.72	17.63	17.87	0.20	0.15	0.25	3.78	1.87	5.83
353	11:53:50.76	-2:58:15.1	16.24	16.20	16.27	0.19	0.17	0.22	0.47	0.41	0.75
354	12:01:35.92	-11:59:52.0	18.04	17.90	18.15	0.18	0.00	0.34	5.04	2.27	8.17
355	12:01:42.09	-12:36:18.3	17.44	17.41	17.47	0.10	0.07	0.13	0.16	0.00	0.40
356	12:04:37.73	-12:07:34.5	17.57	17.57	17.67	0.22	0.21	0.25	0.12	0.00	0.40
357	12:12:14.93	-12:42:00.3	18.02	17.96	18.11	0.25	0.00	0.45	4.52	1.31	8.45
358	12:12:17.91	-12:01:37.9	18.11	17.79	18.32	0.19	0.00	0.39	43.27	18.37	46.30
359	12:12:34.55	-12:02:13.6	15.85	15.84	15.86	0.03	0.01	0.04	3.70	2.30	5.03
360	12:12:51.34	-11:54:59.6	18.16	17.92	18.30	0.21	0.00	0.51	7.18	3.10	9.27
361	12:13:38.72	-12:06:11.1	17.58	17.55	17.74	0.23	0.21	0.27	0.13	0.00	0.40
362	12:14:07.39	-12:35:10.1	13.29	13.28	13.30	0.08	0.08	0.09	8.62	8.34	9.15
363	12:14:26.02	-11:48:13.9	18.03	17.97	18.10	0.18	0.13	0.44	0.31	0.00	2.00
364	12:14:29.82	-11:59:31.7	16.09	16.08	16.10	0.24	0.20	0.28	2.34	1.71	2.97
365	12:15:46.31	-12:05:11.7	16.70	16.51	16.82	0.22	0.11	0.35	20.83	15.17	31.71
366	12:16:10.12	-12:42:34.7	17.48	17.44	17.52	0.05	0.00	0.23	1.32	0.67	2.56
367	12:23:25.13	-12:59:00.7	18.12	18.04	18.19	0.01	0.00	0.20	4.08	0.67	5.76
368	12:24:09.78	-13:25:24.9	18.08	17.86	18.22	0.27	0.21	0.31	0.08	0.00	0.38
369	12:25:07.22	-13:26:05.2	15.65	15.49	15.86	0.26	0.24	0.33	0.09	0.00	0.40
370	12:25:07.66	-13:03:21.8	15.72	15.63	15.78	0.22	0.19	0.28	1.62	0.43	4.81
371	12:25:09.57	-12:51:03.5	17.74	17.69	17.79	0.14	0.04	0.26	3.53	1.45	7.23
372	12:25:24.07	-12:22:02.6	15.85	15.83	15.86	0.04	0.00	0.08	4.88	4.02	5.44
373	12:25:33.10	-13:15:10.8	17.45	17.33	17.54	0.13	0.00	0.22	1.16	0.00	2.69
374	12:26:07.36	-13:05:20.5	17.64	17.59	17.69	0.09	0.00	0.29	0.41	0.00	1.71
375	12:26:23.58	-13:20:45.5	17.90	17.84	17.96	0.22	0.09	0.47	0.20	0.00	0.84

Table C.1: (continued)

Index	R.A.	Dec.	R mag	−99%	+99%	B/T	−99%	+99%	r_e	−99%	+99%
376	12:26:38.56	-12:42:21.6	17.93	17.87	17.97	0.00	0.00	0.23	2.33	1.77	2.94
377	12:27:15.40	-12:18:35.7	17.55	17.44	17.89	0.26	0.23	0.40	0.10	0.00	0.39
378	12:38:07.97	-12:03:09.5	17.85	17.72	17.95	0.21	0.00	0.45	5.27	3.52	8.12
379	12:38:53.98	-12:09:52.9	17.12	17.10	17.15	0.23	0.18	0.31	11.29	8.25	14.68
380	12:39:30.82	-12:30:46.0	17.41	17.31	17.48	0.18	0.12	0.25	32.08	23.42	34.14
381	12:40:29.65	-11:50:54.9	17.75	17.74	17.87	0.22	0.20	0.24	0.14	0.00	0.40
382	12:40:51.94	-12:07:15.1	17.50	17.47	17.53	0.01	0.00	0.13	4.02	3.05	4.78
383	12:41:25.45	-12:41:01.5	17.51	17.49	17.67	0.21	0.20	0.24	0.08	0.00	0.40
384	12:41:42.13	-11:49:16.4	17.54	17.46	17.59	0.05	0.00	0.20	3.90	2.33	5.50
385	12:42:06.11	-12:11:47.4	16.33	16.32	16.34	0.15	0.13	0.17	0.24	0.00	0.40
386	12:42:08.80	-11:57:57.4	17.98	17.98	18.05	0.25	0.23	0.28	0.13	0.00	0.41
387	12:42:17.84	-12:49:01.6	17.58	17.56	17.81	0.13	0.12	0.17	0.07	0.00	0.39
388	12:42:26.00	-12:13:09.2	18.21	18.09	18.46	0.28	0.20	0.40	1.39	0.42	3.15
389	12:42:43.09	-12:12:34.6	18.01	18.01	18.07	0.28	0.23	0.32	1.18	0.66	1.66
390	12:48:41.09	-12:52:11.2	17.75	17.68	17.79	0.00	0.00	0.25	1.95	0.39	5.37
391	12:48:41.10	-11:49:41.8	18.09	17.92	18.15	0.06	0.00	0.61	1.28	0.00	2.97
392	12:48:44.79	-12:10:45.8	17.39	17.32	17.44	0.29	0.18	0.41	7.34	3.69	8.59
393	12:48:51.07	-11:55:37.6	18.03	17.95	18.08	0.05	0.00	0.28	1.75	0.21	4.91
394	12:48:54.84	-12:09:22.2	16.45	16.45	16.47	0.24	0.22	0.27	0.16	0.00	0.38
395	12:49:34.20	-12:09:09.9	18.06	17.97	18.16	0.23	0.00	0.43	6.31	4.93	9.81
396	12:49:46.12	-12:34:34.0	18.17	18.13	18.22	0.19	0.08	0.27	3.37	1.81	4.26
397	12:50:14.36	-12:51:58.5	17.70	17.60	17.76	0.17	0.10	0.26	6.16	5.52	10.78
398	12:51:50.83	-12:38:46.5	18.06	18.06	18.20	0.17	0.14	0.20	0.11	0.00	0.62
399	12:53:03.84	-12:27:00.9	18.25	18.17	18.32	0.03	0.00	0.27	0.54	0.00	1.37
400	13:07:08.99	-12:32:49.4	17.36	17.30	17.42	0.11	0.05	0.17	20.46	15.72	20.87

Table C.1: (continued)

Index	R.A.	Dec.	R mag	−99%	+99%	B/T	−99%	+99%	r_e	−99%	+99%
401	13:07:12.20	-12:21:52.2	17.93	17.82	17.99	0.23	0.05	0.52	3.53	2.15	5.97
402	13:07:53.47	-12:00:03.8	17.17	17.00	17.33	0.08	0.00	0.28	60.05	43.34	63.50
403	13:08:34.11	-11:53:32.8	16.97	16.91	17.01	0.02	0.00	0.20	2.37	1.42	5.24
404	13:08:36.10	-12:13:31.1	17.84	17.84	17.91	0.25	0.19	0.28	0.74	0.00	1.48
405	13:08:38.90	-11:59:43.9	17.06	17.02	17.08	0.01	0.00	0.07	7.71	6.91	11.82
406	13:08:46.64	-12:22:50.5	17.53	17.49	17.56	0.08	0.00	0.28	1.62	1.03	2.24
407	13:09:08.03	-12:35:52.0	17.58	17.50	17.62	0.11	0.00	0.29	2.52	1.31	4.38
408	13:09:39.96	-12:20:19.4	13.61	13.61	13.62	0.10	0.09	0.10	0.41	0.41	0.42
409	13:10:05.83	-12:22:39.1	15.79	15.79	15.80	0.19	0.18	0.20	11.35	11.29	11.35
410	13:10:30.72	-11:56:46.9	18.25	18.19	18.33	0.11	0.00	0.38	1.61	0.09	3.63
411	13:11:24.79	-11:52:50.5	17.11	17.04	17.16	0.02	0.00	0.18	9.56	6.98	11.05
412	13:49:41.38	-3:05:40.6	17.97	17.79	18.06	0.21	0.00	0.74	0.85	0.41	1.46
413	13:49:44.03	-3:15:04.5	17.74	17.68	17.79	0.24	0.11	0.33	1.40	0.41	2.72
414	13:49:54.03	-2:37:23.4	15.41	15.40	15.42	0.28	0.26	0.32	0.55	0.41	0.85
415	13:50:21.94	-3:12:03.7	16.46	16.41	16.61	0.24	0.22	0.28	0.11	0.00	0.39
416	13:50:27.23	-2:51:52.4	17.10	17.06	17.16	0.08	0.00	0.18	2.72	2.06	4.57
417	13:51:44.72	-2:42:45.1	16.90	16.88	16.93	0.28	0.21	0.37	3.57	2.81	4.44
418	13:52:00.97	-2:59:50.7	16.87	16.83	16.89	0.10	0.05	0.23	0.87	0.00	2.58
419	13:52:08.48	-3:05:00.6	17.45	17.41	17.56	0.14	0.08	0.50	6.99	3.06	7.58
420	13:52:37.59	-3:38:27.5	15.38	15.36	15.38	0.22	0.22	0.23	0.16	0.00	0.40
421	13:52:44.45	-2:55:02.0	16.49	16.44	16.51	0.11	0.10	0.12	0.00	0.00	0.38
422	13:54:42.20	-3:17:51.1	17.08	17.05	17.10	0.00	0.00	0.08	5.92	2.91	9.03
423	13:55:21.62	-3:19:52.4	17.53	17.49	17.57	0.20	0.10	0.31	2.41	1.87	2.67
424	13:55:41.83	-2:35:15.2	17.13	17.12	17.27	0.25	0.22	0.30	2.86	2.19	3.75
425	13:55:50.01	-2:42:35.5	17.66	17.63	17.71	0.09	0.00	0.23	1.14	0.02	2.08

Table C.1: (continued)

Index	R.A.	Dec.	R mag	−99%	+99%	B/T	−99%	+99%	r_e	−99%	+99%
426	13:55:53.40	-3:21:43.7	17.12	16.83	17.45	0.22	0.18	0.37	0.06	0.00	0.40
427	13:56:06.99	-2:58:01.6	18.16	18.11	18.19	0.01	0.00	0.13	1.89	0.47	3.02
428	13:57:08.29	-2:41:31.7	17.55	17.54	17.74	0.27	0.24	0.34	3.22	2.22	4.12
429	13:57:53.99	-3:23:08.3	17.70	17.66	17.75	0.21	0.09	0.37	1.13	0.56	2.11
430	13:58:40.94	-2:53:37.5	17.56	17.50	17.60	0.09	0.00	0.24	2.55	1.60	5.23
431	14:08:21.99	-3:44:41.5	18.19	18.11	18.25	0.14	0.00	0.32	2.93	1.76	4.88
432	14:08:30.71	-3:56:22.8	17.89	17.79	17.97	0.09	0.00	0.35	2.31	0.21	5.08
433	14:08:39.46	-2:49:30.5	18.22	18.10	18.31	0.16	0.00	0.33	6.86	3.27	7.77
434	14:08:51.56	-3:53:12.9	17.96	17.91	18.21	0.19	0.16	0.26	0.12	0.00	0.40
435	14:09:31.34	-3:53:14.3	17.26	17.09	17.42	0.29	0.24	0.37	1.51	0.93	2.25
436	14:10:20.87	-3:02:05.8	17.73	17.68	17.79	0.27	0.11	0.43	1.05	0.15	2.03
437	14:19:00.91	-3:29:20.6	17.39	17.37	17.43	0.23	0.10	0.33	1.31	0.73	1.76
438	14:19:21.01	-3:46:15.2	15.92	15.90	15.93	0.23	0.21	0.25	6.81	6.05	7.89
439	14:19:24.99	-3:07:57.1	18.09	18.03	18.14	0.06	0.01	0.12	0.75	0.00	2.49
440	14:20:33.09	-2:54:42.1	18.17	18.03	18.24	0.07	0.00	0.47	1.97	0.56	4.01
441	14:20:36.10	-3:45:31.9	16.34	16.34	16.35	0.30	0.28	0.32	5.39	4.34	6.30
442	14:20:48.43	-3:15:06.5	18.06	17.95	18.12	0.01	0.00	0.28	2.58	1.10	5.99
443	14:21:06.82	-2:52:38.5	16.79	16.77	16.81	0.28	0.20	0.34	3.33	1.92	3.92
444	14:21:29.32	-2:53:25.1	18.18	18.09	18.42	0.27	0.23	0.34	0.14	0.00	0.40
445	14:21:52.37	-3:07:13.5	16.99	16.95	17.02	0.27	0.24	0.30	34.13	33.25	34.13
446	14:21:57.80	-3:33:42.7	18.03	17.98	18.07	0.01	0.00	0.12	1.91	0.33	6.84
447	14:32:21.37	-6:11:38.0	18.04	17.95	18.11	0.13	0.00	0.27	4.63	2.66	8.19
448	14:34:29.45	-6:32:31.6	18.21	18.21	18.38	0.29	0.25	0.32	0.10	0.00	0.39
449	14:46:43.20	-2:24:59.4	17.61	17.53	17.69	0.08	0.00	0.25	4.13	3.17	5.85
450	14:47:16.96	-2:54:43.6	17.61	17.57	17.64	0.25	0.19	0.33	0.70	0.41	1.25

Table C.1: (continued)

Index	R.A.	Dec.	R mag	−99%	+99%	B/T	−99%	+99%	r_e	−99%	+99%
451	14:47:50.30	-12:32:57.8	15.29	15.02	15.45	0.30	0.24	0.35	0.08	0.00	0.39
452	14:48:19.63	-3:17:40.5	17.81	17.76	18.10	0.23	0.15	0.33	1.59	0.43	3.25
453	14:48:28.88	-3:15:42.6	16.01	16.00	16.02	0.05	0.04	0.06	0.01	0.00	0.25
454	14:48:35.08	-3:18:30.7	17.56	17.50	17.83	0.30	0.25	0.39	1.90	1.37	2.58
455	14:48:54.69	-2:35:28.5	17.75	17.62	17.82	0.07	0.00	0.31	7.32	2.14	12.23
456	14:49:03.63	-3:04:50.5	16.17	16.14	16.40	0.18	0.17	0.22	0.12	0.00	0.40
457	14:49:11.32	-3:05:52.9	17.24	17.11	17.28	0.27	0.23	0.36	16.00	12.51	22.90
458	14:49:11.49	-3:23:43.4	14.83	14.78	14.85	0.18	0.17	0.45	0.41	0.41	3.66
459	14:49:45.11	-2:52:02.6	16.88	16.78	16.94	0.09	0.00	0.30	8.35	6.54	9.24
460	14:49:58.38	-3:01:26.4	16.47	16.45	16.48	0.23	0.21	0.24	0.42	0.41	0.48
461	14:50:31.90	-6:38:24.8	17.09	17.04	17.15	0.07	0.01	0.13	24.68	19.67	25.04
462	14:50:38.86	-2:24:23.6	18.12	18.05	18.18	0.02	0.00	0.18	4.90	2.00	6.48
463	14:50:50.43	-2:27:01.1	17.26	17.22	17.31	0.25	0.19	0.28	31.73	27.36	31.94
464	14:51:18.09	-2:39:33.6	17.19	17.07	17.36	0.28	0.24	0.36	0.85	0.55	1.19
465	14:51:26.25	-5:58:08.7	17.69	17.64	17.74	0.12	0.00	0.25	2.82	0.00	5.88
466	14:52:14.57	-3:34:25.9	17.81	17.72	17.86	0.03	0.00	0.22	2.32	1.86	4.06
467	14:52:29.40	-6:06:32.1	17.59	17.55	17.62	0.20	0.16	0.23	0.19	0.00	0.39
468	14:53:07.04	-6:13:48.6	17.50	17.49	17.72	0.25	0.24	0.31	0.11	0.00	0.40
469	14:53:33.95	-2:54:23.8	15.13	15.12	15.14	0.24	0.23	0.25	0.08	0.00	0.39
470	14:53:37.63	-2:41:32.4	16.87	16.75	16.97	0.11	0.00	0.15	11.56	7.93	14.10
471	14:53:40.36	-6:40:01.1	17.67	17.58	17.92	0.29	0.25	0.44	1.22	0.82	1.93
472	14:53:51.10	-6:26:31.3	17.01	16.86	17.17	0.22	0.03	0.35	21.91	5.74	41.33
473	14:53:54.24	-5:51:46.5	16.20	16.08	16.29	0.17	0.09	0.26	33.89	27.28	44.30
474	14:54:01.81	-6:16:17.2	17.20	17.12	17.25	0.06	0.00	0.20	9.59	4.24	13.10
475	14:54:33.72	-6:47:36.8	16.61	16.57	16.65	0.20	0.14	0.28	5.21	4.14	7.30

Table C.1: (continued)

Index	R.A.	Dec.	R mag	−99%	+99%	B/T	−99%	+99%	r_e	−99%	+99%
476	14:54:36.67	-6:25:10.4	16.49	16.47	16.51	0.02	0.00	0.04	25.33	22.82	26.08
477	14:55:03.87	-6:46:24.6	17.62	17.48	17.70	0.20	0.00	0.29	7.33	3.30	9.70
478	14:59:35.84	-6:34:19.0	17.25	17.24	17.35	0.30	0.29	0.32	0.00	0.00	0.39
479	14:59:48.61	-6:35:44.5	17.49	17.35	17.54	0.09	0.00	0.37	5.36	3.53	9.83
480	15:00:06.45	-6:23:03.5	17.54	17.47	17.58	0.01	0.00	0.11	7.86	2.46	10.83
481	15:00:52.74	-6:25:45.2	17.67	17.60	17.74	0.22	0.14	0.29	15.60	9.11	16.87
482	15:01:25.92	-6:53:24.0	17.43	17.20	17.70	0.28	0.22	0.36	0.72	0.49	1.02
483	15:02:13.46	-6:37:09.3	17.85	17.70	17.97	0.26	0.13	0.36	21.34	12.13	23.05
484	15:02:19.88	-6:05:12.4	16.91	16.89	16.93	0.07	0.04	0.17	0.23	0.00	3.98
485	15:02:38.31	-5:53:46.1	15.78	15.77	15.78	0.01	0.00	0.02	0.20	0.00	0.81
486	15:02:43.98	-6:54:54.7	18.24	18.16	18.34	0.15	0.00	0.27	5.25	2.20	7.75
487	15:03:09.85	-6:58:16.0	18.22	18.22	18.30	0.29	0.10	0.73	7.11	0.83	17.90
488	15:03:49.57	-6:41:44.2	18.16	18.14	18.37	0.24	0.14	1.00	1.48	0.00	18.45
489	15:04:00.46	-6:05:35.8	17.22	17.09	17.23	0.07	0.06	0.20	9.17	9.04	9.60
490	15:06:58.25	-3:19:39.3	18.19	18.14	18.23	0.01	0.00	0.17	0.38	0.00	1.41
491	15:07:43.87	-3:18:35.0	16.79	16.76	16.82	0.20	0.11	0.32	5.44	4.60	6.05
492	15:09:01.09	-2:36:55.9	16.55	16.38	16.65	0.26	0.22	0.27	0.44	0.41	0.53
493	15:09:37.78	-3:07:26.6	17.20	17.19	17.25	0.22	0.18	0.25	0.48	0.41	1.18
494	15:09:49.35	-2:48:45.5	17.53	17.24	17.64	0.16	0.00	0.77	2.46	1.13	9.76
495	15:11:06.45	-2:48:38.7	17.38	17.31	17.47	0.28	0.26	0.30	0.11	0.00	0.40
496	15:12:15.73	-3:08:55.7	17.92	17.87	18.02	0.27	0.06	0.38	1.92	0.53	2.70
497	15:12:28.89	-3:11:45.3	17.47	17.43	17.50	0.02	0.00	0.18	1.44	0.00	5.69
498	15:12:57.84	-3:10:56.5	17.54	17.53	17.61	0.12	0.09	0.15	0.16	0.00	1.13
499	15:13:26.63	-3:19:26.1	16.63	16.61	16.66	0.25	0.22	0.27	0.48	0.41	0.71
500	15:13:46.29	-3:02:18.4	16.19	16.17	16.20	0.07	0.06	0.14	0.15	0.00	1.76

Table C.1: (continued)

Index	R.A.	Dec.	R mag	−99%	+99%	B/T	−99%	+99%	r_e	−99%	+99%
501	15:13:52.26	-2:45:51.1	16.92	16.70	17.04	0.27	0.23	0.30	16.78	13.34	19.06
502	15:14:17.59	-3:09:50.8	16.68	16.47	16.76	0.27	0.21	0.34	0.02	0.00	0.39
503	15:14:39.38	-3:11:12.8	17.68	17.64	17.72	0.23	0.18	0.27	0.25	0.00	0.40
504	15:16:16.35	-3:31:06.0	17.79	17.79	17.88	0.23	0.20	0.25	0.04	0.00	0.39
505	15:16:20.46	-3:27:49.7	15.93	15.93	15.98	0.24	0.23	0.25	0.09	0.00	0.39
506	15:16:20.79	-2:26:54.2	16.46	16.45	16.67	0.25	0.24	0.31	1.42	1.23	1.76
507	15:16:37.77	-2:38:50.6	16.04	16.03	16.05	0.28	0.27	0.28	0.18	0.00	0.39
508	15:17:24.50	-3:08:32.7	16.56	16.55	16.58	0.20	0.18	0.23	1.49	1.02	2.00
509	15:17:24.50	-3:08:33.0	16.40	16.38	16.42	0.17	0.16	0.18	0.11	0.00	0.40
510	15:17:57.71	-2:25:44.8	16.93	16.89	16.98	0.27	0.22	0.30	32.57	29.38	32.57
511	15:18:04.95	-2:35:11.0	16.25	16.24	16.26	0.25	0.23	0.27	0.48	0.41	0.66
512	15:18:19.12	-2:38:54.0	17.53	17.53	17.62	0.15	0.13	0.27	0.14	0.00	2.84
513	15:18:30.69	-2:59:07.2	16.79	16.65	16.90	0.14	0.13	0.19	0.80	0.41	3.32
514	15:19:25.93	-2:51:42.0	16.25	16.20	16.31	0.24	0.20	0.35	7.02	4.26	11.08
515	15:19:26.77	-3:08:37.8	16.23	16.13	16.25	0.19	0.13	0.48	8.16	4.50	11.02
516	15:20:06.54	-2:40:55.4	17.35	17.27	17.54	0.12	0.07	0.19	6.51	4.34	11.16
517	15:20:11.14	-3:06:11.2	17.53	17.49	17.56	0.17	0.07	0.24	2.36	1.62	3.91
518	21:15:54.16	-44:41:31.5	14.62	14.61	14.64	0.21	0.20	0.22	91.34	89.93	91.35
519	21:15:59.03	-44:50:20.9	16.22	16.21	16.23	0.23	0.21	0.24	3.30	3.11	3.60
520	21:15:59.38	-44:31:42.0	17.62	17.45	17.77	0.28	0.25	0.31	0.47	0.41	0.94
521	21:16:10.54	-44:39:33.2	17.35	17.34	17.61	0.20	0.19	0.28	0.09	0.00	0.40
522	21:16:10.68	-44:18:31.9	16.91	16.88	17.07	0.14	0.12	0.18	2.86	1.48	4.04
523	21:16:12.47	-44:18:49.4	18.09	18.09	18.18	0.21	0.19	0.23	0.09	0.00	0.40
524	21:16:14.08	-44:50:13.6	16.92	16.89	16.96	0.11	0.06	0.16	11.22	8.14	13.62
525	21:16:21.81	-44:37:48.9	17.65	17.65	17.78	0.27	0.25	0.30	1.12	0.81	1.48

Table C.1: (continued)

Index	R.A.	Dec.	R mag	−99%	+99%	B/T	−99%	+99%	r_e	−99%	+99%
526	21:16:28.27	-44:56:07.9	18.05	17.95	18.16	0.25	0.14	0.35	15.14	7.02	22.55
527	21:16:31.07	-44:07:29.2	17.58	17.58	17.68	0.19	0.15	0.27	4.33	3.12	8.29
528	21:16:33.39	-44:01:10.1	17.51	17.51	17.53	0.18	0.15	0.22	8.96	7.33	11.72
529	21:16:36.72	-44:00:38.0	16.79	16.69	17.01	0.14	0.13	0.18	0.51	0.41	1.32
530	21:16:37.93	-44:04:42.8	17.76	17.71	17.80	0.18	0.14	0.23	12.59	10.50	14.79
531	21:16:40.85	-44:57:16.0	17.77	17.68	17.84	0.24	0.00	0.58	0.78	0.00	1.45
532	21:17:08.92	-44:48:14.5	17.34	17.31	17.46	0.23	0.21	0.26	0.03	0.00	0.40
533	21:17:09.61	-43:51:43.9	17.64	17.46	17.89	0.18	0.15	0.22	0.04	0.00	0.40
534	21:17:22.53	-44:52:34.8	17.13	17.10	17.31	0.26	0.24	0.30	0.11	0.00	0.40
535	21:17:31.99	-44:22:04.3	18.05	17.97	18.53	0.25	0.22	0.40	0.14	0.00	0.40
536	21:17:48.16	-43:53:59.4	17.22	17.22	17.41	0.29	0.26	0.39	4.39	3.49	5.47
537	21:18:15.78	-44:49:17.0	17.64	17.59	17.73	0.30	0.23	0.34	54.17	43.10	54.31
538	21:18:31.45	-43:55:43.2	17.96	17.92	18.00	0.07	0.00	0.18	0.92	0.00	2.24
539	21:19:32.48	-44:12:52.8	17.86	17.86	17.97	0.18	0.15	0.22	0.14	0.00	0.59
540	21:20:03.00	-44:46:43.1	17.32	17.32	17.37	0.07	0.03	0.12	4.09	1.22	9.07
541	21:20:16.52	-44:02:10.6	18.05	17.90	18.17	0.27	0.18	0.37	33.43	17.44	39.48
542	21:20:35.12	-44:54:58.8	17.34	17.34	17.37	0.24	0.22	0.25	1.15	0.87	1.59
543	21:20:43.19	-44:42:08.9	17.83	17.64	17.85	0.00	0.00	0.15	5.98	4.50	8.58
544	21:20:46.24	-44:23:15.5	16.65	16.64	16.67	0.29	0.26	0.40	0.51	0.41	1.08
545	21:20:48.34	-44:26:21.3	18.19	18.19	18.23	0.18	0.16	0.20	0.18	0.00	0.40
546	21:21:12.90	-44:01:34.1	16.16	15.98	16.30	0.13	0.08	0.23	3.57	0.53	12.47
547	21:21:31.30	-44:14:37.8	18.22	18.22	18.38	0.28	0.19	0.41	3.52	1.33	8.46
548	21:39:22.20	-43:59:07.0	17.39	17.35	17.68	0.24	0.21	0.32	0.08	0.00	0.40
549	21:39:31.36	-38:13:36.1	17.92	17.92	18.12	0.24	0.22	0.29	0.11	0.00	0.39
550	21:39:40.46	-44:03:55.9	16.37	16.36	16.38	0.29	0.25	0.31	4.31	3.60	4.97

Table C.1: (continued)

Index	R.A.	Dec.	R mag	−99%	+99%	B/T	−99%	+99%	r_e	−99%	+99%
551	21:39:46.63	-44:31:55.9	17.66	17.60	17.72	0.27	0.11	0.40	8.51	5.84	10.73
552	21:39:50.99	-44:10:04.2	17.80	17.74	17.85	0.29	0.04	0.51	1.31	0.43	2.55
553	21:39:56.34	-44:57:20.0	17.55	17.50	17.61	0.13	0.00	0.31	2.23	0.00	4.30
554	21:41:07.70	-38:56:58.4	15.16	15.10	15.22	0.21	0.15	0.25	21.42	10.67	23.01
555	21:41:21.06	-38:03:41.6	17.47	17.36	17.54	0.01	0.00	0.26	1.79	0.75	3.56
556	21:41:23.59	-44:23:30.6	16.84	16.66	17.04	0.29	0.25	0.36	0.00	0.00	0.40
557	21:41:34.01	-44:54:20.1	17.61	17.47	17.75	0.27	0.21	0.33	0.57	0.00	1.15
558	21:41:36.91	-38:25:16.6	17.92	17.87	17.99	0.23	0.07	0.40	4.61	3.25	5.56
559	21:41:39.29	-38:50:40.4	15.23	15.22	15.34	0.16	0.16	0.18	0.12	0.00	0.39
560	21:41:53.33	-38:23:31.7	17.44	17.37	17.69	0.19	0.17	0.27	0.09	0.00	0.38
561	21:42:05.03	-38:49:54.4	17.51	17.46	17.58	0.21	0.07	0.35	3.11	1.52	4.28
562	21:42:05.10	-44:45:43.7	17.79	17.79	17.86	0.24	0.21	0.27	0.15	0.00	0.40
563	21:42:07.11	-44:45:36.2	17.47	17.46	17.81	0.27	0.25	0.37	0.12	0.00	0.40
564	21:42:26.40	-44:47:34.9	12.31	12.30	12.32	0.06	0.00	0.13	39.87	14.53	56.88
565	21:42:28.25	-44:39:48.2	15.54	15.50	15.74	0.25	0.18	0.38	1.70	0.00	9.26
566	21:42:44.86	-44:01:02.5	17.91	17.82	17.98	0.27	0.00	0.59	2.46	0.47	5.14
567	21:42:50.05	-44:17:35.9	15.28	15.14	15.51	0.27	0.24	0.34	0.06	0.00	0.38
568	21:42:58.69	-45:01:32.3	17.06	16.94	17.14	0.29	0.14	0.42	28.88	11.93	40.22
569	21:42:59.55	-44:12:16.2	17.35	17.34	17.45	0.30	0.28	0.32	0.05	0.00	0.39
570	21:43:07.58	-38:20:00.7	17.21	17.17	17.24	0.05	0.02	0.10	0.72	0.00	2.32
571	21:43:10.13	-38:37:47.9	13.51	13.47	13.55	0.18	0.17	0.19	1.01	0.83	1.41
572	21:43:33.74	-39:04:00.9	18.08	17.96	18.15	0.06	0.00	0.47	1.68	0.53	2.85
573	21:43:43.52	-38:57:35.6	16.61	16.60	16.84	0.14	0.13	0.18	0.03	0.00	0.39
574	21:44:00.42	-38:27:38.9	15.41	15.39	15.46	0.29	0.27	0.31	0.44	0.41	0.54
575	21:44:13.57	-38:03:31.0	17.74	17.66	17.78	0.04	0.00	0.21	5.56	2.36	8.18

Table C.1: (continued)

Index	R.A.	Dec.	R mag	−99%	+99%	B/T	−99%	+99%	r_e	−99%	+99%
576	21:44:25.51	-44:22:00.2	17.14	17.07	17.25	0.26	0.24	0.29	1.00	0.79	1.22
577	21:44:54.78	-44:11:50.9	17.71	17.60	17.90	0.20	0.15	0.29	1.06	0.35	2.51
578	21:45:08.36	-44:00:40.4	18.05	17.99	18.16	0.29	0.00	0.56	1.66	0.65	2.85
579	21:45:09.12	-44:26:54.0	18.09	18.01	18.18	0.11	0.00	0.21	6.08	5.11	7.86
580	21:46:34.08	-44:12:17.4	17.16	17.13	17.37	0.18	0.17	0.22	0.13	0.00	0.39
581	21:46:56.54	-44:33:07.9	18.01	17.97	18.35	0.30	0.27	0.41	0.12	0.00	0.40
582	21:47:38.40	-44:18:27.2	18.12	18.03	18.21	0.07	0.00	0.25	6.98	5.13	8.87
583	21:47:57.15	-45:07:47.8	15.52	15.49	15.55	0.02	0.00	0.04	1.93	0.00	4.62
584	21:47:58.02	-45:10:39.6	17.88	17.82	17.95	0.29	0.06	0.43	1.81	1.08	2.31
585	21:48:53.28	-45:16:05.6	16.72	16.65	16.82	0.21	0.16	0.40	7.21	1.28	11.50
586	21:50:46.07	-44:25:06.4	14.95	14.93	14.96	0.12	0.11	0.12	0.08	0.00	0.37
587	21:51:29.41	-44:34:29.6	16.96	16.67	17.21	0.27	0.21	0.36	2.28	1.74	2.94
588	21:51:41.97	-45:17:32.0	17.24	17.24	17.27	0.13	0.12	0.14	0.00	0.00	0.40
589	21:53:03.69	-45:07:02.0	15.63	15.60	15.65	0.21	0.19	0.23	42.10	40.96	42.10
590	21:53:12.20	-45:05:25.9	17.13	17.05	17.42	0.27	0.24	0.35	8.66	5.02	12.49
591	21:53:47.00	-44:22:29.4	18.16	17.98	18.27	0.15	0.00	0.47	9.74	8.16	16.96
592	21:54:02.02	-45:06:44.1	16.97	16.72	17.23	0.22	0.14	0.48	1.16	0.00	5.92
593	21:54:06.73	-44:57:42.4	17.78	17.68	17.82	0.03	0.00	0.11	1.52	0.00	3.80
594	21:55:14.53	-44:44:10.5	16.34	16.26	16.44	0.26	0.18	0.31	12.41	6.16	18.14
595	21:56:41.97	-44:46:50.7	16.78	16.75	16.83	0.21	0.13	0.28	6.74	5.31	7.77
596	21:57:23.75	-45:01:49.4	17.45	17.41	17.82	0.28	0.26	0.36	0.01	0.00	0.38
597	21:57:38.33	-44:11:09.7	15.14	15.11	15.15	0.12	0.12	0.29	0.41	0.41	2.75
598	21:59:32.56	-44:23:40.0	15.85	15.47	16.01	0.27	0.21	0.48	0.37	0.17	0.50
599	21:59:57.34	-44:56:10.0	17.37	17.37	17.46	0.17	0.12	0.26	1.34	0.23	4.17
600	22:00:27.36	-38:39:35.4	17.73	17.58	17.87	0.27	0.16	0.36	13.56	3.85	21.22

Table C.1: (continued)

Index	R.A.	Dec.	R mag	−99%	+99%	B/T	−99%	+99%	r_e	−99%	+99%
601	22:00:41.64	-44:17:50.5	18.06	18.00	18.13	0.25	0.00	0.49	1.03	0.20	2.62
602	22:00:54.33	-37:45:25.8	18.10	18.04	18.15	0.07	0.00	0.20	5.32	3.77	6.63
603	22:01:13.14	-37:45:48.7	17.29	17.27	17.33	0.07	0.03	0.10	7.04	4.80	10.45
604	22:01:13.73	-37:46:07.6	17.10	17.02	17.29	0.21	0.16	0.25	1.54	0.64	2.49
605	22:01:16.55	-38:01:11.0	17.52	17.44	17.64	0.24	0.12	0.31	37.26	25.00	39.52
606	22:02:08.22	-44:35:44.7	17.25	17.23	17.30	0.26	0.22	0.33	1.38	0.79	2.04
607	22:02:37.54	-37:44:44.1	15.77	15.49	16.01	0.20	0.16	0.27	0.00	0.00	0.40
608	22:02:56.13	-38:16:01.9	17.62	17.60	17.86	0.24	0.19	0.36	5.66	3.55	10.30
609	22:03:00.53	-37:43:19.2	14.64	14.60	14.67	0.01	0.01	0.02	0.00	0.00	0.38
610	22:03:02.73	-44:52:11.2	17.61	17.58	17.64	0.26	0.18	0.32	0.20	0.00	0.40
611	22:03:05.33	-37:50:35.3	17.14	17.12	17.17	0.01	0.00	0.06	5.23	4.33	6.59
612	22:03:46.99	-38:34:46.1	17.20	16.88	17.26	0.29	0.23	0.33	0.00	0.00	0.39
613	22:03:53.81	-45:05:51.9	17.50	17.47	17.53	0.18	0.14	0.20	0.13	0.00	0.39
614	22:04:19.55	-45:08:37.9	18.04	18.04	18.08	0.26	0.24	0.28	0.19	0.00	0.40
615	22:05:14.44	-44:40:48.9	17.59	17.45	17.84	0.29	0.18	0.66	2.37	0.00	10.52
616	22:05:54.47	-44:28:50.0	17.88	17.84	17.93	0.29	0.17	0.38	0.18	0.00	0.64
617	22:06:02.14	-45:05:40.9	17.96	17.90	18.02	0.22	0.11	0.29	4.76	4.21	7.13
618	22:10:13.61	-38:48:37.4	16.95	16.92	17.00	0.26	0.12	0.32	3.83	3.18	4.46
619	22:10:36.93	-39:24:08.0	16.62	16.55	16.67	0.25	0.23	0.26	0.16	0.00	0.40
620	22:10:45.36	-38:30:50.4	15.91	15.91	15.92	0.09	0.08	0.09	0.29	0.05	0.40
621	22:11:27.63	-38:43:29.4	17.78	17.76	17.95	0.23	0.19	0.29	0.91	0.41	2.01
622	22:11:30.56	-38:43:32.9	18.04	17.98	18.29	0.30	0.18	0.47	7.12	4.10	9.48
623	22:11:39.93	-38:27:24.2	16.60	16.55	16.65	0.30	0.21	0.35	9.46	4.04	10.72
624	22:12:06.31	-38:41:22.4	18.11	18.01	18.18	0.02	0.00	0.23	5.04	1.04	8.16
625	22:12:17.19	-38:51:45.9	16.77	16.77	17.06	0.22	0.20	0.42	2.13	1.54	5.63

Table C.1: (continued)

Index	R.A.	Dec.	R mag	−99%	+99%	B/T	−99%	+99%	r_e	−99%	+99%
626	22:12:50.54	-38:32:24.4	15.85	15.74	15.90	0.25	0.23	0.28	0.42	0.41	1.82
627	22:12:51.38	-39:08:20.7	18.17	18.10	18.22	0.04	0.00	0.18	4.08	2.44	6.39
628	22:13:11.70	-38:28:53.2	17.77	17.53	17.90	0.03	0.00	0.43	6.94	4.40	8.96
629	22:13:37.29	-39:21:32.7	16.73	16.52	16.98	0.27	0.23	0.34	0.19	0.00	0.40
630	22:13:53.69	-38:36:49.8	18.06	18.06	18.10	0.11	0.09	0.13	0.14	0.00	0.42
631	22:14:02.16	-38:31:12.6	18.11	18.11	18.13	0.15	0.11	0.20	1.90	1.16	3.70
632	22:14:15.62	-38:20:41.2	17.83	17.70	17.98	0.27	0.16	0.38	25.54	10.45	33.53
633	22:14:25.10	-39:20:37.9	17.72	17.72	17.74	0.29	0.20	0.36	4.99	1.74	6.88
634	22:14:43.09	-39:21:31.6	17.83	17.76	17.90	0.12	0.00	0.29	0.57	0.29	1.02
635	22:15:02.45	-38:21:14.9	13.97	13.87	13.99	0.20	0.11	0.49	4.77	0.41	13.90
636	22:16:49.78	-44:14:28.9	16.39	16.30	16.46	0.04	0.00	0.13	22.78	14.19	35.68
637	22:16:58.32	-45:05:31.1	18.19	18.09	18.31	0.16	0.00	0.26	4.92	2.77	7.70
638	22:17:12.52	-45:04:08.0	16.55	16.35	16.72	0.25	0.23	0.45	0.27	0.00	1.69
639	22:17:16.89	-37:59:00.3	17.82	17.76	17.86	0.05	0.00	0.27	2.79	0.87	5.35
640	22:17:22.96	-38:25:26.2	17.77	17.70	17.84	0.12	0.00	0.25	7.30	4.33	8.18
641	22:17:24.83	-38:01:06.4	17.58	17.39	17.71	0.23	0.10	0.34	29.84	19.63	39.00
642	22:18:09.26	-38:45:23.6	16.42	16.38	16.51	0.24	0.15	0.28	12.13	7.86	14.67
643	22:18:18.05	-38:25:55.5	17.63	17.59	17.68	0.15	0.03	0.27	1.06	0.00	2.16
644	22:18:37.28	-38:02:13.8	17.86	17.81	17.93	0.16	0.01	0.23	3.71	1.70	4.45
645	22:18:42.02	-38:54:43.1	16.40	16.29	16.60	0.25	0.23	0.30	0.15	0.00	0.40
646	22:18:58.03	-38:48:36.4	17.67	17.67	17.68	0.08	0.07	0.09	0.02	0.00	0.37
647	22:19:13.15	-45:07:15.2	18.02	17.78	18.24	0.28	0.22	0.43	0.18	0.00	2.40
648	22:19:46.69	-38:13:24.3	16.75	16.71	16.77	0.03	0.00	0.11	5.80	2.10	8.00
649	22:19:56.84	-44:02:19.0	16.40	16.39	16.42	0.18	0.15	0.27	1.36	0.80	2.58
650	22:19:59.67	-38:51:21.3	16.36	16.35	16.38	0.17	0.10	0.23	1.72	0.44	2.86

Table C.1: (continued)

Index	R.A.	Dec.	R mag	−99%	+99%	B/T	−99%	+99%	r_e	−99%	+99%
651	22:20:38.32	-37:56:43.5	14.73	14.70	14.78	0.20	0.19	0.21	0.24	0.00	0.40
652	22:20:52.70	-44:59:51.3	15.51	15.50	15.51	0.10	0.09	0.12	5.98	5.20	6.43
653	22:21:15.85	-38:37:36.1	15.88	15.87	15.89	0.04	0.04	0.04	0.18	0.00	0.38
654	22:21:57.85	-43:59:58.1	16.87	16.84	16.90	0.17	0.15	0.22	0.60	0.41	1.29
655	22:22:02.30	-37:51:46.1	18.24	18.24	18.36	0.19	0.12	0.27	5.65	3.40	7.09
656	22:22:02.69	-38:08:08.4	18.10	18.04	18.17	0.17	0.00	0.46	0.92	0.00	2.71
657	22:22:31.38	-44:51:34.5	17.84	17.79	18.10	0.14	0.04	0.19	9.94	3.33	11.15
658	22:22:48.09	-38:15:48.8	16.10	16.09	16.11	0.02	0.01	0.04	0.24	0.00	1.36
659	22:22:55.58	-38:04:39.1	18.14	18.07	18.22	0.01	0.00	0.23	1.51	0.22	4.08
660	22:24:32.32	-38:47:16.9	16.09	15.90	16.19	0.17	0.14	0.19	1.33	0.81	2.28
661	22:25:28.19	-38:51:20.9	18.10	18.03	18.18	0.02	0.00	0.13	1.89	0.00	4.09
662	22:28:36.36	-38:28:25.5	15.71	15.71	15.73	0.13	0.11	0.17	0.62	0.41	1.17
663	22:28:45.43	-38:27:19.9	16.51	16.50	16.52	0.05	0.03	0.06	0.19	0.00	0.40
664	22:29:31.04	-38:24:51.2	18.20	18.08	18.32	0.23	0.00	0.67	0.53	0.00	1.73
665	22:31:15.70	-39:01:34.2	17.88	17.86	18.01	0.28	0.20	0.40	6.29	4.58	10.02
666	22:41:13.53	-38:37:48.3	17.39	17.35	17.42	0.15	0.06	0.24	4.14	2.46	5.54
667	22:41:18.02	-38:18:00.8	17.50	17.47	17.53	0.00	0.00	0.09	5.47	4.38	7.30
668	22:41:27.82	-38:56:04.1	17.76	17.70	17.84	0.19	0.00	0.43	1.92	0.76	3.79
669	22:41:44.10	-38:27:58.0	17.28	17.25	17.59	0.22	0.18	0.31	1.74	0.75	2.41
670	22:41:57.24	-38:58:52.2	17.49	17.49	17.69	0.29	0.25	0.31	0.05	0.00	0.40
671	22:43:00.30	-38:33:06.3	17.99	17.93	18.04	0.26	0.10	0.36	7.14	5.82	8.82
672	22:44:16.18	-38:05:30.2	16.04	15.95	16.11	0.29	0.25	0.37	1.83	1.24	3.29
673	22:44:23.86	-38:11:14.8	17.93	17.85	17.97	0.06	0.00	0.32	0.58	0.00	1.27
674	22:44:32.71	-38:37:28.8	16.50	16.48	16.51	0.27	0.24	0.31	1.47	0.94	1.88
675	22:45:03.31	-38:07:03.2	16.93	16.84	17.16	0.26	0.24	0.35	0.72	0.41	1.15

Table C.1: (continued)

Index	R.A.	Dec.	R mag	−99%	+99%	B/T	−99%	+99%	r_e	−99%	+99%
676	22:45:39.56	-37:56:35.0	17.10	17.05	17.14	0.24	0.13	0.36	6.02	4.95	7.36
677	22:45:48.32	-38:48:44.7	17.02	16.99	17.05	0.01	0.00	0.15	2.78	0.67	3.21
678	22:46:03.95	-38:30:23.2	17.88	17.76	18.05	0.20	0.17	0.22	0.12	0.00	0.40
679	22:46:34.32	-38:44:51.5	18.11	18.10	18.19	0.15	0.09	1.00	0.62	0.00	26.29
680	22:57:20.87	-38:03:40.5	17.72	17.52	17.82	0.27	0.00	0.71	0.65	0.36	1.08
681	22:58:28.47	-38:23:47.1	18.04	17.99	18.09	0.26	0.15	0.34	0.14	0.00	0.40
682	22:58:47.01	-38:11:04.3	16.68	16.67	16.70	0.26	0.21	0.31	1.23	0.86	1.87
683	22:59:05.71	-38:40:19.4	15.69	15.67	15.74	0.21	0.20	0.22	1.06	0.94	1.13
684	22:59:23.68	-38:07:22.9	17.75	17.70	17.83	0.26	0.02	0.43	1.98	1.34	2.99
685	23:00:24.08	-38:46:27.3	18.14	18.10	18.24	0.30	0.24	0.35	1.02	0.47	1.82
686	23:01:55.46	-38:29:21.9	16.25	16.24	16.26	0.18	0.17	0.19	0.19	0.00	0.40
687	23:02:39.56	-38:37:05.6	17.79	17.71	17.86	0.27	0.23	0.31	0.10	0.00	0.40
688	23:08:12.67	-39:14:12.6	17.78	17.73	17.83	0.13	0.00	0.28	2.73	1.13	4.31
689	23:10:04.71	-39:08:17.0	15.77	15.76	15.78	0.08	0.05	0.13	1.68	0.62	3.69
690	23:11:38.70	-38:27:14.6	17.98	17.94	18.05	0.12	0.02	0.18	4.28	1.39	7.69
691	23:12:22.18	-38:19:10.6	17.62	17.58	17.67	0.03	0.00	0.14	2.42	1.45	3.47
692	23:13:33.81	-38:49:20.1	17.39	17.34	17.43	0.02	0.00	0.11	3.36	0.22	8.48
693	23:13:37.74	-39:05:30.4	17.95	17.88	18.02	0.21	0.12	0.38	0.36	0.00	1.36
694	23:21:28.80	-44:52:56.6	14.35	14.29	14.48	0.29	0.17	0.33	40.23	19.37	44.23
695	23:21:55.47	-44:57:52.7	17.40	17.36	17.43	0.27	0.16	0.38	3.07	2.47	3.84
696	23:22:28.52	-44:26:38.7	18.04	17.99	18.07	0.02	0.00	0.12	0.11	0.00	0.45
697	23:23:48.14	-44:52:16.5	18.10	17.83	18.25	0.09	0.00	0.33	7.64	0.00	10.17
698	23:24:33.29	-42:17:25.3	16.81	16.78	16.83	0.14	0.04	0.24	1.72	1.30	2.48
699	23:25:02.16	-41:13:06.7	16.74	16.71	16.76	0.28	0.26	0.30	19.01	17.51	19.12
700	23:25:04.03	-44:09:36.9	15.94	15.93	15.95	0.27	0.25	0.30	9.19	8.01	11.03

Table C.1: (continued)

Index	R.A.	Dec.	R mag	−99%	+99%	B/T	−99%	+99%	r_e	−99%	+99%
701	23:25:05.59	-41:47:56.6	17.86	17.78	17.94	0.22	0.03	0.43	3.24	0.00	6.26
702	23:25:07.59	-41:22:28.2	18.20	18.20	18.28	0.19	0.16	0.24	0.21	0.00	0.43
703	23:25:15.83	-44:42:53.1	16.98	16.88	17.20	0.14	0.10	0.25	9.80	5.28	20.56
704	23:25:17.91	-41:12:03.6	18.18	18.18	18.28	0.27	0.24	0.29	0.17	0.00	0.40
705	23:25:18.53	-44:44:25.0	18.09	18.09	18.15	0.22	0.17	0.26	0.89	0.00	1.65
706	23:25:18.64	-44:43:10.4	18.13	18.13	18.20	0.30	0.23	0.38	6.50	5.29	8.47
707	23:25:22.09	-44:13:00.0	15.94	15.86	16.10	0.19	0.17	0.24	0.58	0.42	1.22
708	23:25:23.46	-41:29:12.7	17.66	17.54	17.76	0.24	0.20	0.26	0.14	0.00	0.39
709	23:25:34.03	-44:46:08.9	17.91	17.91	17.96	0.15	0.11	0.17	0.08	0.00	2.20
710	23:25:40.73	-44:23:09.2	17.89	17.85	17.94	0.20	0.04	0.34	2.65	1.57	3.93
711	23:25:59.53	-41:58:51.3	17.83	17.83	17.88	0.19	0.17	0.20	0.13	0.00	0.40
712	23:26:00.58	-44:39:21.5	17.81	17.62	17.97	0.27	0.00	0.46	10.93	2.95	16.62
713	23:26:33.32	-42:07:30.4	17.88	17.77	18.22	0.30	0.26	0.40	0.20	0.00	0.40
714	23:26:35.44	-41:34:05.8	17.13	17.07	17.19	0.12	0.00	0.28	1.47	0.58	3.31
715	23:27:34.89	-41:30:46.1	18.20	18.20	18.27	0.27	0.17	0.38	9.11	5.85	11.49
716	23:28:23.61	-41:49:46.7	17.28	17.22	17.31	0.00	0.00	0.16	0.78	0.05	2.99
717	23:28:32.56	-41:52:00.6	17.08	16.94	17.19	0.20	0.18	0.23	0.41	0.00	0.83
718	23:28:43.37	-41:19:58.9	10.72	10.72	10.73	0.01	0.01	0.01	0.65	0.49	0.75
719	23:30:13.38	-39:20:26.0	17.80	17.75	18.14	0.25	0.20	0.37	0.95	0.42	1.67
720	23:30:16.72	-38:42:59.6	18.16	18.10	18.21	0.04	0.00	0.17	3.32	2.18	4.25
721	23:31:04.47	-39:14:13.3	17.97	17.90	18.05	0.29	0.08	0.49	1.88	1.15	2.74
722	23:31:14.37	-38:32:56.4	16.83	16.80	16.86	0.19	0.14	0.26	13.58	10.20	17.61
723	23:31:36.68	-39:15:27.2	16.61	16.60	16.63	0.03	0.00	0.06	1.35	0.41	2.20
724	23:32:03.73	-39:33:17.5	14.49	14.48	14.50	0.16	0.13	0.17	10.24	7.13	11.40
725	23:32:19.40	-39:07:17.0	17.86	17.81	17.91	0.06	0.00	0.17	4.23	0.00	6.77

Table C.1: (continued)

Index	R.A.	Dec.	R mag	−99%	+99%	B/T	−99%	+99%	r_e	−99%	+99%
726	23:33:27.04	-38:38:36.9	15.13	15.13	15.14	0.30	0.29	0.31	2.03	1.92	2.23
727	23:33:38.29	-38:47:47.1	17.07	17.04	17.10	0.05	0.00	0.13	3.03	1.60	3.74
728	23:34:12.84	-39:29:40.5	17.76	17.74	17.79	0.00	0.00	0.06	0.59	0.00	2.37
729	23:35:04.87	-39:02:06.7	18.14	18.09	18.19	0.08	0.00	0.28	1.52	0.35	2.50
730	23:35:28.49	-38:57:22.3	17.89	17.84	17.98	0.29	0.03	0.50	4.76	2.54	5.87
731	23:38:03.18	-44:48:28.6	18.11	18.11	18.13	0.23	0.18	0.30	2.30	1.35	4.17
732	23:38:13.63	-38:26:06.4	15.58	15.57	15.58	0.04	0.01	0.07	3.27	1.29	4.54
733	23:38:57.62	-38:27:56.4	16.24	16.22	16.25	0.03	0.02	0.05	0.16	0.00	0.38
734	23:39:48.58	-38:27:11.8	16.68	16.63	16.91	0.17	0.15	0.21	1.86	1.45	2.36
735	23:40:12.45	-38:04:21.4	17.06	17.05	17.08	0.12	0.09	0.14	0.23	0.00	0.40
736	23:41:08.46	-38:03:38.8	18.00	17.96	18.04	0.01	0.00	0.23	1.12	0.39	1.61
737	23:41:43.07	-44:11:41.2	18.11	18.09	18.58	0.24	0.20	1.00	0.21	0.00	4.98
738	23:42:13.92	-44:29:17.7	17.99	17.96	18.14	0.29	0.27	0.33	0.06	0.00	0.39
739	23:42:54.07	-38:35:58.5	14.98	14.98	14.99	0.08	0.07	0.12	0.46	0.41	1.79
740	23:43:30.31	-38:40:35.4	14.69	14.65	14.73	0.21	0.20	0.28	0.33	0.07	0.40
741	23:43:54.47	-37:53:48.3	16.52	16.37	16.59	0.06	0.00	0.50	3.33	0.91	6.26
742	23:43:56.00	-38:42:14.1	17.86	17.86	17.99	0.10	0.00	0.30	8.22	3.12	17.29
743	23:44:47.11	-38:28:05.4	17.29	17.25	17.33	0.00	0.00	0.08	2.00	0.21	4.02
744	23:44:50.18	-38:40:20.3	17.70	17.66	17.85	0.15	0.13	0.18	0.25	0.00	0.40
745	23:45:00.26	-39:12:41.6	17.23	17.21	17.24	0.01	0.00	0.08	2.19	0.90	5.09
746	23:45:14.20	-38:26:01.3	17.24	17.18	17.29	0.25	0.12	0.36	3.19	1.83	4.30
747	23:45:15.29	-38:38:27.3	17.60	17.55	17.68	0.16	0.00	0.28	6.87	5.12	8.27
748	23:45:16.65	-39:04:46.1	17.84	17.78	17.87	0.03	0.00	0.17	2.58	1.71	3.99
749	23:46:39.83	-38:34:30.2	17.94	17.94	18.01	0.25	0.21	0.29	4.64	3.55	5.99
750	23:46:41.47	-38:40:22.8	15.69	15.69	15.70	0.17	0.14	0.18	3.43	3.00	3.81

Table C.1: (continued)

Index	R.A.	Dec.	R mag	-99%	$+99\%$	B/T	-99%	$+99\%$	r_e	-99%	$+99\%$
751	23:46:50.80	-39:15:06.7	16.61	16.47	16.68	0.25	0.22	0.78	0.21	0.00	5.36
752	23:47:51.73	-38:12:14.9	18.09	18.00	18.63	0.29	0.19	0.71	0.67	0.00	2.53
753	23:48:09.28	-38:25:25.0	16.81	16.52	16.99	0.21	0.16	0.26	0.06	0.00	0.39
754	23:48:38.12	-38:52:11.0	17.94	17.88	17.98	0.04	0.00	0.20	1.88	0.00	3.31
755	23:49:59.55	-38:36:06.6	15.63	15.61	15.66	0.07	0.06	0.08	0.45	0.41	0.88
756	23:49:59.88	-39:03:51.6	16.69	16.66	16.73	0.27	0.24	0.30	2.50	1.74	3.27
757	23:50:22.48	-39:15:03.1	17.89	17.84	17.94	0.20	0.14	0.25	0.16	0.00	0.40

Table C.2: Catalog of Objects Studied

Index	e	-99%	$+99\%$	ϕ_b	-99%	$+99\%$	r_d	-99%	$+99\%$	i	-99%	$+99\%$
1	0.02	0.00	0.08	10.10	-22.17	74.29	12.43	10.72	15.15	2.11	0.00	26.04
2	0.06	0.00	0.29	329.46	270.02	360.00	11.61	9.65	13.98	14.34	0.00	37.87
3	0.46	0.29	0.64	76.28	45.32	113.73	1.33	1.16	1.46	26.81	4.19	37.08
4	0.64	0.23	0.70	118.68	17.10	130.03	23.34	15.30	26.22	10.28	0.00	60.17
5	0.50	0.30	0.70	87.52	75.58	100.56	0.95	0.90	1.01	5.64	0.00	18.71
6	0.46	0.21	0.70	163.71	137.51	185.34	2.57	2.37	2.84	7.15	0.00	20.41
7	0.40	0.00	0.70	209.44	114.52	227.54	1.23	1.05	1.38	4.13	0.00	19.64
8	0.08	0.00	0.29	-88.88	-134.45	-23.75	1.21	1.11	1.35	5.95	0.00	22.40
9	0.03	0.00	0.22	-6.09	-63.76	48.49	3.58	3.39	3.92	33.55	29.83	37.65
10	0.62	0.47	0.70	53.19	44.72	60.77	5.40	5.27	5.51	25.88	23.92	28.64
11	0.54	0.29	0.70	218.04	179.97	282.47	2.11	1.94	2.29	2.14	0.00	13.17
12	0.01	0.00	0.04	38.12	22.01	57.44	3.56	3.45	4.50	23.94	18.69	35.13
13	0.61	0.40	0.70	159.11	112.58	226.87	1.52	1.40	1.71	34.02	23.87	45.07
14	0.16	0.00	0.54	195.99	95.61	247.41	24.67	20.67	28.27	6.60	0.00	23.98
15	0.46	0.33	0.70	206.68	187.06	220.52	0.97	0.89	1.03	4.58	0.00	15.93
16	0.70	0.65	0.70	19.30	8.48	27.04	1.67	1.58	1.77	0.80	0.00	8.82
17	0.15	0.00	0.46	-45.64	-273.26	67.89	9.45	8.09	11.02	21.82	5.95	42.93
18	0.64	0.51	0.70	199.32	156.53	266.45	1.14	1.04	1.36	33.78	23.89	51.01
19	0.69	0.59	0.70	-29.59	-47.98	12.61	2.10	1.95	2.19	28.87	11.72	32.91
20	0.30	0.11	0.45	45.45	-17.27	94.33	0.95	0.90	1.00	10.74	0.00	28.02
21	0.60	0.38	0.70	125.12	102.24	175.12	17.38	11.06	22.33	27.92	0.00	78.33
22	0.11	0.00	0.25	-30.42	-91.99	19.65	3.69	3.31	4.02	2.79	0.00	6.88
23	0.26	0.00	0.41	118.16	73.49	144.40	1.83	1.73	1.97	33.94	24.50	41.02
24	0.47	0.19	0.70	-19.83	-41.53	37.39	1.19	1.05	1.35	26.12	5.41	45.79
25	0.31	0.20	0.53	-10.86	-63.82	62.99	1.49	1.42	1.61	2.35	0.00	8.42

Table C.2: (continued)

Index	e	-99%	$+99\%$	ϕ_b	-99%	$+99\%$	r_d	-99%	$+99\%$	i	-99%	$+99\%$
26	0.09	0.00	0.70	55.85	-6.71	136.36	3.95	3.70	4.92	2.52	0.00	53.93
27	0.70	0.65	0.70	170.65	164.61	176.01	18.17	13.15	20.75	1.25	0.00	6.05
28	0.11	0.00	0.33	-355.33	-360.00	-303.93	1.72	1.63	1.83	3.40	0.00	14.02
29	0.30	0.00	0.51	24.13	-265.35	96.86	1.38	1.32	1.44	12.67	0.00	25.89
30	0.30	0.12	0.70	147.33	108.50	159.83	2.17	1.95	3.01	2.92	0.00	30.41
31	0.59	0.00	0.70	107.24	-182.16	145.41	14.22	11.80	17.89	14.32	0.00	28.27
32	0.24	0.06	0.58	102.83	67.11	116.14	1.18	1.14	1.27	1.60	0.00	21.48
33	0.25	0.00	0.39	-136.68	-230.82	-10.45	18.40	16.66	21.31	34.54	3.87	56.89
34	0.06	0.00	0.16	130.43	108.39	163.95	4.86	4.42	5.13	34.63	27.87	39.80
35	0.55	0.32	0.70	353.83	154.40	360.00	14.86	12.16	17.18	12.44	0.00	43.09
36	0.70	0.64	0.70	149.87	141.39	159.07	24.66	20.85	38.71	20.71	0.00	49.93
37	0.24	0.08	0.39	162.54	120.38	197.72	1.03	0.93	1.12	30.32	15.03	40.27
38	0.45	0.28	0.69	82.11	25.57	162.75	1.13	1.05	1.40	24.42	4.29	46.53
39	0.22	0.06	0.34	100.56	71.81	135.84	1.14	0.86	1.46	14.36	0.00	38.22
40	0.68	0.57	0.70	142.39	129.23	152.78	15.92	14.37	17.88	4.39	0.00	12.87
41	0.30	0.04	0.51	157.25	127.30	211.71	14.43	11.50	18.85	8.66	0.00	23.24
42	0.47	0.17	0.62	138.05	89.68	174.67	0.96	0.88	1.02	9.88	0.00	25.61
43	0.34	0.00	0.70	-128.30	-233.20	-61.26	18.94	17.34	20.30	4.01	0.00	23.54
44	0.60	0.15	0.70	197.36	175.71	245.97	12.43	8.93	16.90	30.42	0.00	53.94
45	0.37	0.15	0.44	22.57	-20.20	59.69	2.20	2.08	2.41	28.21	21.25	31.89
46	0.59	0.12	0.70	57.29	-160.81	170.84	10.10	7.83	11.58	26.00	8.23	41.20
47	0.35	0.06	0.70	297.50	164.65	358.65	10.41	6.73	12.31	18.92	0.00	28.02
48	0.14	0.00	0.47	125.96	96.73	174.06	1.55	1.48	1.64	9.72	0.00	23.33
49	0.46	0.24	0.66	19.03	0.78	35.38	0.96	0.84	1.07	16.01	0.00	36.93
50	0.39	0.25	0.62	117.52	50.59	152.51	3.04	2.89	3.16	32.11	29.34	34.93

Table C.2: (continued)

Index	e	-99%	$+99\%$	ϕ_b	-99%	$+99\%$	r_d	-99%	$+99\%$	i	-99%	$+99\%$
51	0.25	0.00	0.47	129.56	56.95	193.79	1.39	1.20	1.61	7.77	0.00	36.57
52	0.70	0.64	0.70	95.96	84.88	102.21	29.65	27.62	29.65	33.90	0.00	61.06
53	0.62	0.31	0.70	76.31	16.23	92.97	1.84	1.74	1.92	24.85	19.26	31.64
54	0.69	0.63	0.70	125.89	119.64	136.16	0.41	0.41	0.44	9.88	0.00	32.17
55	0.07	0.00	0.20	54.82	-70.05	172.92	0.07	0.00	0.39	27.67	0.00	85.00
56	0.67	0.55	0.70	34.42	24.57	44.44	1.36	1.29	1.40	3.53	0.00	15.30
57	0.06	0.00	0.36	88.43	-18.80	185.20	10.32	8.83	12.21	31.04	16.53	50.02
58	0.64	0.49	0.70	-63.16	-112.71	35.79	1.20	1.04	1.30	32.83	9.33	41.56
59	0.23	0.07	0.34	119.18	100.26	137.87	1.17	1.13	1.21	5.38	0.61	13.59
60	0.57	0.33	0.70	205.11	178.77	232.32	1.10	1.03	1.16	4.86	0.00	25.10
61	0.29	0.05	0.47	58.46	5.53	84.17	1.64	1.54	1.71	30.90	22.69	37.76
62	0.70	0.62	0.70	66.11	54.97	79.30	19.32	16.33	22.39	8.80	0.00	36.09
63	0.64	0.25	0.70	-166.12	-360.00	62.60	17.37	15.22	20.76	1.60	0.00	21.35
64	0.41	0.17	0.66	107.43	71.51	154.33	1.18	1.06	1.31	3.40	0.00	9.52
65	0.70	0.67	0.70	88.18	80.33	94.36	2.61	2.53	2.70	15.99	2.08	23.01
66	0.28	0.18	0.38	138.18	121.45	151.76	1.22	1.16	1.26	5.75	0.00	14.00
67	0.55	0.36	0.67	169.05	155.55	179.90	1.07	1.01	1.12	8.51	0.00	19.96
68	0.65	0.54	0.70	128.94	113.61	144.14	2.33	2.11	2.60	33.50	17.67	41.26
69	0.68	0.42	0.70	96.30	71.96	110.98	21.37	17.00	24.08	15.35	0.00	44.14
70	0.14	0.00	0.53	32.83	-66.52	89.75	2.91	2.46	3.33	11.89	0.00	27.68
71	0.68	0.48	0.70	157.36	143.83	168.24	17.28	14.75	20.08	10.58	0.00	46.23
72	0.51	0.22	0.70	174.07	147.45	197.01	1.02	0.94	1.08	3.26	0.00	19.71
73	0.57	0.18	0.70	107.87	89.89	129.74	18.50	16.34	20.00	17.54	0.00	46.30
74	0.60	0.44	0.70	-100.51	-131.46	53.02	20.94	16.73	23.30	2.20	0.00	7.86
75	0.65	0.45	0.70	-73.35	-114.78	48.13	11.37	10.18	11.66	1.03	0.00	9.12

Table C.2: (continued)

Index	e	-99%	$+99\%$	ϕ_b	-99%	$+99\%$	r_d	-99%	$+99\%$	i	-99%	$+99\%$
76	0.57	0.39	0.70	155.76	133.03	177.66	1.26	1.18	1.39	4.05	0.00	13.67
77	0.55	0.43	0.70	84.00	36.41	136.12	1.05	0.95	1.21	26.92	8.05	38.80
78	0.45	0.31	0.58	118.57	72.27	149.79	1.33	1.13	1.46	3.52	0.00	12.37
79	0.66	0.52	0.70	-64.05	-71.73	-56.67	0.13	0.00	0.39	27.49	0.00	46.31
80	0.68	0.57	0.70	207.43	102.98	260.72	12.74	11.85	13.75	2.73	0.00	12.38
81	0.27	0.07	0.52	8.67	-80.97	113.67	11.34	8.86	14.04	19.11	0.00	46.47
82	0.12	0.01	0.26	74.95	-42.51	108.40	1.02	0.95	1.11	33.24	17.94	43.15
83	0.70	0.68	0.70	97.90	93.51	101.30	3.43	3.37	3.47	31.99	29.95	33.09
84	0.03	0.00	0.11	127.78	91.10	145.64	0.73	0.68	0.79	1.83	0.00	9.00
85	0.69	0.61	0.70	353.85	231.29	360.00	1.23	0.91	1.99	8.48	0.00	60.82
86	0.67	0.61	0.70	154.39	129.60	182.86	1.17	1.08	1.25	3.25	0.00	20.90
87	0.70	0.64	0.70	85.51	78.12	92.08	1.88	1.76	2.01	10.83	0.00	19.32
88	0.16	0.00	0.48	188.44	139.33	240.87	14.62	10.38	15.43	31.93	10.45	56.43
89	0.70	0.67	0.70	36.01	28.41	39.50	22.73	18.35	24.75	1.92	0.00	18.07
90	0.54	0.37	0.66	139.55	89.55	166.26	1.08	1.02	1.20	6.93	0.00	20.97
91	0.52	0.41	0.65	133.08	113.87	144.92	0.18	0.00	0.40	4.42	0.00	31.61
92	0.55	0.27	0.70	122.23	7.66	241.35	14.44	12.66	16.65	0.43	0.00	17.17
93	0.53	0.49	0.63	201.65	182.04	212.23	4.28	4.20	4.35	24.36	22.20	26.31
94	0.44	0.34	0.69	75.40	58.37	121.83	1.38	1.35	1.41	33.91	29.70	36.51
95	0.01	0.00	0.30	12.66	-310.69	117.84	0.13	0.01	0.21	27.37	0.00	85.00
96	0.07	0.00	0.27	126.52	100.39	231.48	1.30	1.23	1.37	32.81	24.71	37.75
97	0.01	0.00	0.04	63.31	31.76	80.14	3.62	3.56	3.69	0.09	0.00	1.88
98	0.66	0.30	0.70	160.93	123.80	181.40	0.09	0.00	0.38	11.77	0.00	20.19
99	0.61	0.50	0.70	120.42	80.92	138.40	1.19	1.09	1.26	30.37	20.30	39.88
100	0.37	0.05	0.53	72.40	-17.57	147.63	0.79	0.73	0.89	12.28	0.00	32.26

Table C.2: (continued)

Index	e	-99%	$+99\%$	ϕ_b	-99%	$+99\%$	r_d	-99%	$+99\%$	i	-99%	$+99\%$
101	0.43	0.00	0.70	107.81	0.76	222.54	16.32	11.41	19.84	10.08	0.00	22.56
102	0.02	0.00	0.11	171.82	134.83	227.88	0.73	0.69	0.77	3.50	0.00	11.67
103	0.20	0.00	0.47	-60.62	-88.06	-1.64	13.73	12.22	15.83	20.18	6.80	36.38
104	0.24	0.00	0.46	96.77	-28.91	205.14	16.26	9.92	18.50	10.38	0.00	32.96
105	0.34	0.05	0.70	160.12	123.26	255.91	0.93	0.84	1.11	11.87	0.00	36.52
106	0.63	0.50	0.70	105.48	57.97	117.53	1.41	1.34	1.46	3.29	0.00	10.79
107	0.12	0.04	0.15	343.36	322.69	360.00	4.22	4.17	4.25	31.82	30.83	32.94
108	0.43	0.05	0.70	-330.79	-360.00	-259.67	14.60	12.94	17.77	8.55	0.00	60.34
109	0.69	0.54	0.70	68.93	56.38	82.14	23.88	20.01	24.65	32.04	0.00	55.40
110	0.58	0.21	0.70	47.23	13.21	88.16	17.78	15.43	20.54	27.27	0.00	50.39
111	0.07	0.00	0.32	120.49	48.68	180.61	12.05	10.74	12.68	1.36	0.00	10.40
112	0.59	0.47	0.70	46.95	23.58	59.61	1.03	1.00	1.09	3.73	0.00	9.39
113	0.49	0.28	0.63	182.58	-5.11	201.19	0.41	0.41	0.51	11.73	2.59	27.56
114	0.70	0.17	0.70	-16.17	-63.82	-11.97	0.19	0.00	0.39	11.97	1.10	21.59
115	0.66	0.59	0.70	122.18	117.14	125.00	3.30	3.26	3.33	1.13	0.00	11.41
116	0.65	0.49	0.70	59.83	52.52	67.53	0.79	0.75	0.83	8.82	0.00	19.31
117	0.01	0.00	0.15	145.28	-25.43	262.90	16.73	15.59	20.18	6.79	0.00	47.52
118	0.69	0.61	0.70	110.84	100.98	120.36	14.72	13.13	19.03	29.14	0.00	46.09
119	0.65	0.37	0.70	225.66	160.75	248.25	1.10	0.99	1.17	32.24	16.96	40.16
120	0.69	0.62	0.70	21.01	-28.38	89.62	20.30	18.45	23.55	2.48	0.00	13.16
121	0.06	0.00	0.29	-115.76	-233.24	29.67	22.76	20.05	28.37	7.51	0.00	22.28
122	0.69	0.57	0.70	115.52	105.86	123.08	27.68	21.82	32.19	10.27	0.00	28.14
123	0.70	0.68	0.70	107.11	104.09	109.80	3.96	3.90	4.03	31.13	28.64	33.17
124	0.08	0.00	0.33	15.01	-101.16	43.73	1.16	1.11	1.23	8.19	0.00	21.06
125	0.45	0.20	0.70	-124.31	-199.81	96.88	17.58	14.45	17.88	14.89	0.00	38.82

Table C.2: (continued)

Index	e	-99%	$+99\%$	ϕ_b	-99%	$+99\%$	r_d	-99%	$+99\%$	i	-99%	$+99\%$
126	0.68	0.54	0.70	7.81	-5.10	17.42	16.04	12.42	20.21	15.68	0.00	45.63
127	0.37	0.29	0.46	184.29	117.98	204.05	2.27	2.19	2.35	3.02	0.00	10.00
128	0.70	0.61	0.70	37.58	28.60	79.28	0.07	0.00	0.20	29.43	0.00	40.62
129	0.66	0.45	0.70	351.70	266.79	360.00	15.69	11.24	21.56	7.14	0.00	62.17
130	0.68	0.52	0.70	73.58	32.34	116.47	14.54	13.07	15.29	0.99	0.00	7.25
131	0.14	0.03	0.23	29.13	-10.20	58.94	0.02	0.00	0.13	28.04	15.93	85.00
132	0.13	0.00	0.38	-61.70	-89.70	14.14	0.85	0.78	0.89	9.14	0.00	20.90
133	0.15	0.00	0.48	258.61	62.61	360.00	13.89	9.18	19.58	18.79	0.00	47.74
134	0.28	0.18	0.39	178.44	122.62	208.59	1.78	1.65	1.89	28.73	21.74	34.19
135	0.36	0.24	0.48	105.68	61.22	168.01	1.01	0.98	1.05	4.45	0.00	16.46
136	0.58	0.13	0.70	-76.52	-360.00	88.00	10.90	9.82	13.22	3.04	0.00	48.68
137	0.69	0.44	0.70	56.83	46.52	71.39	2.08	1.98	2.23	31.87	12.28	39.06
138	0.05	0.00	0.22	185.84	99.91	265.76	1.55	1.36	1.86	28.99	0.00	38.66
139	0.30	0.00	0.44	203.61	140.18	326.36	12.60	11.17	14.33	24.63	0.00	47.51
140	0.65	0.40	0.70	354.52	302.08	360.00	13.56	12.12	14.74	1.72	0.00	10.83
141	0.21	0.00	0.32	157.20	97.65	197.49	0.19	0.00	0.40	8.02	0.00	31.10
142	0.69	0.64	0.70	92.80	83.27	100.60	2.90	2.78	2.99	34.57	31.56	38.22
143	0.54	0.15	0.70	94.56	-6.06	191.76	1.50	1.41	1.62	26.12	3.47	36.11
144	0.59	0.43	0.70	-25.73	-57.43	20.48	21.73	18.08	22.46	1.84	0.00	25.70
145	0.69	0.65	0.70	79.31	70.42	85.38	2.15	2.08	2.25	33.65	31.27	37.46
146	0.70	0.67	0.70	79.71	69.67	92.70	26.15	24.61	26.15	0.01	0.00	14.28
147	0.10	0.00	0.25	116.61	-19.50	170.30	1.02	0.91	1.08	28.90	9.04	42.57
148	0.53	0.01	0.70	96.13	18.89	271.52	11.27	9.06	12.58	9.48	0.00	36.66
149	0.68	0.58	0.70	118.46	101.34	130.40	14.54	11.78	16.71	20.50	14.42	29.50
150	0.62	0.20	0.70	117.50	94.97	135.01	3.65	3.37	4.09	23.17	15.08	35.13

Table C.2: (continued)

Index	e	-99%	$+99\%$	ϕ_b	-99%	$+99\%$	r_d	-99%	$+99\%$	i	-99%	$+99\%$
151	0.69	0.60	0.70	30.95	23.98	37.02	21.65	19.97	24.19	16.04	0.00	38.36
152	0.06	0.00	0.38	58.03	-64.77	119.23	0.10	0.00	0.40	1.44	0.00	11.95
153	0.64	0.43	0.70	135.89	56.97	165.43	1.69	1.57	1.98	32.59	21.12	48.54
154	0.70	0.60	0.70	166.92	157.20	173.74	18.60	16.14	22.78	5.99	0.00	22.31
155	0.69	0.62	0.70	195.50	184.41	204.55	2.58	2.44	2.70	17.06	6.37	23.41
156	0.31	0.16	0.70	96.00	41.78	119.38	3.91	3.70	4.12	34.79	31.11	38.11
157	0.66	0.47	0.70	114.37	99.73	127.78	0.04	0.00	0.13	2.84	0.00	13.81
158	0.56	0.48	0.65	100.30	90.64	109.64	1.26	1.15	1.33	16.55	4.16	23.35
159	0.43	0.32	0.61	214.81	105.21	254.47	1.08	1.01	1.24	7.27	0.00	28.57
160	0.70	0.68	0.70	163.44	157.33	167.38	0.03	0.00	0.40	3.32	0.00	11.22
161	0.42	0.00	0.70	179.64	147.25	238.76	3.95	3.73	4.16	25.86	20.24	30.52
162	0.53	0.29	0.70	197.13	131.80	284.39	1.27	1.16	1.52	16.01	3.82	32.31
163	0.61	0.21	0.70	66.83	28.54	91.62	1.33	1.23	1.41	29.18	10.86	43.40
164	0.25	0.00	0.57	27.60	5.82	78.50	2.54	2.42	2.67	29.59	8.13	34.44
165	0.21	0.05	0.38	221.86	200.13	244.11	2.46	2.31	2.70	5.40	0.00	15.40
166	0.39	0.22	0.68	-39.68	-113.99	50.53	12.72	8.49	17.59	24.33	0.50	62.39
167	0.68	0.58	0.70	45.29	34.47	52.59	15.46	10.66	16.29	0.35	0.00	5.50
168	0.56	0.27	0.70	43.80	-1.08	90.30	1.25	1.04	1.36	32.34	13.87	39.54
169	0.49	0.00	0.70	283.08	217.94	360.00	14.41	12.14	16.01	6.68	0.00	43.87
170	0.31	0.00	0.70	-109.35	-156.61	-17.64	13.22	12.00	14.29	4.40	0.00	20.46
171	0.19	0.00	0.44	52.14	8.80	81.82	1.31	1.24	1.39	12.57	0.00	24.97
172	0.69	0.26	0.70	-46.64	-51.01	-41.93	2.80	2.74	2.90	1.83	0.00	6.00
173	0.68	0.58	0.70	236.65	124.28	360.00	25.75	22.26	26.02	27.77	0.00	45.94
174	0.10	0.00	0.28	-37.05	-108.44	-7.35	3.48	3.29	3.70	32.48	27.47	37.44
175	0.20	0.02	0.29	57.84	33.78	90.64	1.59	1.57	1.62	0.78	0.00	5.51

Table C.2: (continued)

Index	e	-99%	$+99\%$	ϕ_b	-99%	$+99\%$	r_d	-99%	$+99\%$	i	-99%	$+99\%$
176	0.61	0.27	0.70	47.20	27.42	80.70	14.42	10.99	16.46	20.19	0.00	60.97
177	0.64	0.26	0.70	52.96	-52.69	139.27	15.68	11.91	16.83	34.56	15.64	52.13
178	0.58	0.21	0.70	-301.31	-360.00	-163.89	13.27	9.50	15.35	3.97	0.00	39.18
179	0.68	0.51	0.70	15.87	-11.03	25.61	17.75	15.65	22.59	28.00	0.00	48.38
180	0.45	0.34	0.66	-18.65	-29.87	-9.54	4.57	4.35	4.73	27.10	23.33	29.72
181	0.68	0.50	0.70	130.37	103.58	158.53	17.34	13.74	21.83	10.07	0.00	41.71
182	0.43	0.30	0.54	242.54	199.32	268.82	1.17	1.13	1.24	26.68	20.28	35.28
183	0.33	0.16	0.70	-24.88	-131.18	54.19	1.95	1.74	2.24	34.30	24.54	42.27
184	0.70	0.65	0.70	161.63	137.96	177.35	23.15	18.15	25.63	15.03	9.28	23.96
185	0.62	0.46	0.70	52.42	41.12	62.47	11.65	9.13	15.89	19.81	10.24	40.52
186	0.46	0.19	0.65	92.96	79.80	109.01	1.63	1.56	1.69	34.95	29.53	40.35
187	0.70	0.59	0.70	136.68	122.86	151.62	0.12	0.00	0.39	7.04	0.00	43.47
188	0.70	0.28	0.70	92.31	68.05	102.40	0.19	0.08	0.25	28.56	12.48	39.10
189	0.65	0.50	0.70	12.09	-4.03	53.67	1.95	1.85	2.12	33.32	28.00	40.61
190	0.65	0.46	0.70	85.58	9.34	98.66	1.46	1.34	1.62	5.84	0.00	14.47
191	0.70	0.62	0.70	85.24	74.13	95.16	0.34	0.13	0.40	4.74	0.00	12.29
192	0.03	0.00	0.10	19.93	-27.86	94.28	1.72	1.59	1.86	7.69	0.00	25.77
193	0.00	0.00	0.02	106.44	75.01	118.79	3.13	3.06	3.19	30.76	29.14	34.07
194	0.28	0.21	0.37	102.20	87.34	116.70	2.63	2.56	2.70	34.23	32.91	36.03
195	0.36	0.26	0.47	203.48	146.34	229.55	2.51	2.43	2.58	27.18	20.75	31.64
196	0.06	0.00	0.22	3.58	-33.14	33.55	1.50	1.41	1.58	4.21	0.00	11.91
197	0.10	0.00	0.44	31.47	-245.46	152.82	15.52	12.44	18.59	6.73	0.00	39.69
198	0.47	0.32	0.68	116.55	76.53	133.39	2.20	2.16	2.24	1.34	0.00	5.15
199	0.27	0.07	0.70	-36.96	-74.47	22.90	22.32	17.48	24.70	5.47	0.00	40.60
200	0.65	0.55	0.70	12.73	-1.80	24.62	2.39	2.27	2.55	16.76	7.82	28.10

Table C.2: (continued)

Index	e	-99%	$+99\%$	ϕ_b	-99%	$+99\%$	r_d	-99%	$+99\%$	i	-99%	$+99\%$
201	0.06	0.00	0.25	219.49	84.12	307.27	18.36	10.49	20.77	5.26	0.00	37.04
202	0.42	0.35	0.50	143.56	120.20	167.75	1.17	1.11	1.24	19.15	6.44	27.74
203	0.50	0.17	0.70	186.51	139.56	226.27	1.54	1.46	1.64	15.15	2.22	25.00
204	0.65	0.32	0.70	125.38	119.01	136.28	0.02	0.00	0.39	7.31	0.00	20.69
205	0.61	0.19	0.70	127.15	110.19	142.08	2.61	2.49	2.71	31.44	26.81	35.65
206	0.70	0.62	0.70	17.67	-0.21	42.82	13.06	9.37	20.25	5.27	0.00	47.10
207	0.56	0.11	0.70	139.53	127.16	162.36	14.86	11.41	16.98	24.36	0.00	40.85
208	0.63	0.49	0.70	59.71	42.61	84.46	1.00	0.95	1.05	6.98	0.00	18.10
209	0.22	0.00	0.38	29.13	-41.41	117.28	1.86	1.66	2.05	30.06	17.70	38.44
210	0.69	0.45	0.70	59.28	44.52	72.38	0.13	0.00	0.40	3.83	0.00	16.58
211	0.55	0.51	0.59	33.75	28.25	38.47	1.95	1.90	1.99	1.20	0.00	6.34
212	0.17	0.08	0.34	13.07	-5.14	44.07	12.55	9.76	15.26	5.68	0.00	13.18
213	0.53	0.20	0.70	149.17	115.88	204.64	1.88	1.63	2.17	32.18	12.36	46.62
214	0.57	0.15	0.70	126.91	101.95	191.67	1.80	1.64	1.98	17.03	0.00	35.75
215	0.57	0.16	0.70	-230.73	-360.00	-82.11	11.48	9.45	14.74	9.71	0.00	23.66
216	0.65	0.37	0.70	74.40	59.75	96.33	18.15	12.16	20.53	27.84	10.22	38.27
217	0.69	0.63	0.70	31.04	6.54	73.75	20.96	18.37	23.26	2.52	0.00	7.47
218	0.41	0.13	0.62	87.06	52.37	136.23	2.45	2.19	2.67	30.29	15.19	42.16
219	0.43	0.31	0.70	-55.18	-72.73	-28.97	1.47	1.42	1.50	1.92	0.00	6.62
220	0.49	0.28	0.57	336.56	329.24	343.60	0.23	0.00	0.40	15.12	0.16	30.77
221	0.16	0.00	0.34	207.68	166.61	240.40	1.31	1.27	1.36	32.53	26.74	37.99
222	0.32	0.25	0.48	26.07	-6.76	117.54	1.18	1.13	1.22	5.44	0.00	10.94
223	0.10	0.00	0.70	144.31	108.10	227.72	11.53	9.96	12.94	7.55	0.00	43.09
224	0.08	0.00	0.38	91.71	59.06	116.04	27.58	19.41	35.39	7.95	0.00	43.40
225	0.61	0.35	0.70	95.58	75.57	113.06	1.92	1.78	2.05	19.88	0.00	29.26

Table C.2: (continued)

Index	e	-99%	$+99\%$	ϕ_b	-99%	$+99\%$	r_d	-99%	$+99\%$	i	-99%	$+99\%$
226	0.68	0.48	0.70	122.74	106.20	132.81	3.02	2.89	3.42	31.86	26.04	44.81
227	0.66	0.57	0.70	-66.42	-92.58	-24.50	1.15	1.02	1.58	1.00	0.00	8.43
228	0.30	0.03	0.52	15.83	-7.04	70.25	1.17	1.05	1.26	2.77	0.00	15.47
229	0.66	0.54	0.70	140.12	131.02	148.87	3.47	3.20	3.70	28.99	23.02	33.80
230	0.11	0.00	0.28	236.73	175.65	360.00	2.56	2.43	2.70	15.24	0.00	25.08
231	0.60	0.32	0.70	99.88	69.89	138.07	1.52	1.36	1.70	15.80	0.00	27.90
232	0.14	0.00	0.58	15.21	-36.57	49.18	1.26	1.18	1.41	15.61	0.00	31.05
233	0.33	0.24	0.45	-52.03	-160.83	-14.40	2.04	1.92	2.15	32.35	25.93	36.78
234	0.15	0.06	0.27	127.14	92.47	196.01	1.14	1.09	1.20	28.05	19.15	32.01
235	0.66	0.34	0.70	30.89	13.45	45.15	14.70	11.88	17.13	3.57	0.00	15.30
236	0.26	0.19	0.34	10.62	2.01	23.08	1.81	1.78	1.85	4.68	0.00	12.23
237	0.38	0.24	0.70	137.65	91.52	157.24	1.39	1.35	1.45	34.67	28.25	38.70
238	0.61	0.14	0.70	221.27	166.78	348.87	12.96	9.65	14.25	0.09	0.00	11.50
239	0.17	0.00	0.48	119.81	71.10	161.09	1.45	1.34	1.62	9.75	0.00	27.88
240	0.46	0.15	0.61	189.67	167.26	220.51	0.02	0.00	0.40	3.32	0.00	26.39
241	0.49	0.17	0.70	58.63	-8.07	94.63	1.44	1.29	1.65	5.69	0.00	26.99
242	0.53	0.14	0.70	47.14	19.00	65.22	0.96	0.82	1.02	13.56	0.00	29.55
243	0.18	0.00	0.70	99.14	-14.69	177.18	2.46	2.14	2.82	32.53	15.27	41.90
244	0.67	0.51	0.70	154.65	148.33	161.71	20.62	15.39	23.56	15.85	0.00	41.88
245	0.70	0.57	0.70	177.77	163.33	188.95	12.97	9.38	15.50	20.29	0.49	31.70
246	0.42	0.00	0.70	-178.51	-228.06	-135.11	20.39	18.92	22.69	11.10	0.00	22.23
247	0.13	0.00	0.26	8.85	-59.54	95.42	1.68	1.60	1.75	28.95	23.06	33.10
248	0.45	0.27	0.59	72.11	40.66	85.40	1.69	1.59	1.81	15.87	0.00	32.80
249	0.31	0.25	0.38	72.23	46.17	89.33	1.84	1.75	1.93	32.99	27.55	39.09
250	0.70	0.69	0.70	8.53	4.51	12.30	0.04	0.00	0.31	28.48	19.31	46.48

Table C.2: (continued)

Index	e	-99%	$+99\%$	ϕ_b	-99%	$+99\%$	r_d	-99%	$+99\%$	i	-99%	$+99\%$
251	0.43	0.16	0.70	124.54	92.29	142.06	2.24	2.09	2.44	21.98	11.99	30.93
252	0.62	0.15	0.70	168.55	154.91	223.79	14.73	11.66	17.16	4.49	0.00	24.72
253	0.69	0.54	0.70	117.49	94.98	140.21	0.03	0.00	0.40	4.65	0.00	26.97
254	0.24	0.04	0.60	212.27	80.20	325.12	1.72	1.60	1.86	33.94	27.03	41.83
255	0.60	0.39	0.70	135.55	115.99	161.60	0.09	0.00	0.40	28.38	5.45	60.13
256	0.61	0.48	0.70	22.65	10.68	29.70	1.54	1.49	1.60	32.69	26.02	36.54
257	0.58	0.43	0.70	93.64	83.58	108.83	1.47	1.40	1.54	2.26	0.00	11.36
258	0.25	0.04	0.47	-111.22	-189.29	-15.35	14.72	10.11	18.03	21.08	0.00	37.20
259	0.05	0.00	0.26	70.26	-28.98	108.84	2.20	2.08	2.54	32.11	23.01	42.04
260	0.45	0.10	0.70	-133.70	-189.06	-95.24	13.59	11.38	14.59	8.76	0.00	45.46
261	0.61	0.42	0.70	7.39	-2.10	18.68	2.52	2.40	2.56	0.44	0.00	3.74
262	0.54	0.49	0.62	53.00	23.33	71.35	0.21	0.00	0.40	1.77	0.00	7.13
263	0.70	0.64	0.70	127.54	120.73	133.34	19.68	17.22	22.71	14.35	1.39	24.74
264	0.03	0.00	0.16	93.58	58.51	128.09	0.93	0.89	0.97	0.69	0.00	5.71
265	0.70	0.65	0.70	33.88	27.86	39.90	4.39	4.21	4.64	31.20	25.23	37.96
266	0.67	0.58	0.70	178.25	162.53	188.17	1.89	1.80	2.00	33.83	29.02	39.40
267	0.51	0.34	0.70	-12.28	-57.53	14.20	2.04	1.89	2.24	22.50	0.00	45.38
268	0.65	0.57	0.70	127.13	107.87	132.68	4.81	4.62	5.49	21.60	1.42	41.10
269	0.70	0.67	0.70	100.94	95.77	106.05	20.60	17.78	21.99	7.80	0.00	43.07
270	0.50	0.29	0.68	120.74	98.42	131.71	9.31	7.36	9.88	3.39	0.00	13.31
271	0.70	0.51	0.70	-35.54	-233.59	19.30	15.49	13.34	19.08	28.34	0.00	43.19
272	0.63	0.38	0.70	117.06	13.66	164.41	1.58	1.36	1.71	31.29	0.00	44.53
273	0.35	0.02	0.51	84.70	60.21	99.56	20.66	18.02	24.70	24.71	5.79	54.86
274	0.04	0.00	0.14	53.78	-14.53	96.37	4.58	4.50	4.67	32.64	30.30	34.97
275	0.69	0.61	0.70	140.72	112.05	150.43	4.99	4.83	5.73	1.88	0.00	37.95

Table C.2: (continued)

Index	e	-99%	$+99\%$	ϕ_b	-99%	$+99\%$	r_d	-99%	$+99\%$	i	-99%	$+99\%$
276	0.53	0.34	0.70	38.38	-46.47	79.20	1.73	1.60	2.07	19.30	0.00	44.38
277	0.70	0.70	0.70	49.34	47.81	49.93	7.71	7.52	7.93	27.38	24.06	28.56
278	0.43	0.19	0.70	161.99	87.79	325.62	14.61	8.88	21.60	9.90	0.00	45.44
279	0.70	0.65	0.70	185.03	173.61	190.26	1.71	1.63	1.80	4.84	0.00	10.52
280	0.68	0.51	0.70	197.11	160.55	246.23	0.06	0.00	0.38	24.25	9.23	55.34
281	0.06	0.00	0.26	243.90	157.31	360.00	0.18	0.00	0.40	17.05	0.00	52.36
282	0.08	0.00	0.41	140.07	60.68	226.06	0.08	0.00	0.40	4.98	0.00	53.25
283	0.67	0.60	0.70	121.25	106.04	138.82	0.25	0.00	0.40	3.28	0.00	7.45
284	0.09	0.00	0.31	328.84	273.64	360.00	0.84	0.74	0.98	1.50	0.00	13.21
285	0.47	0.32	0.56	144.06	129.27	153.30	5.13	4.98	5.29	2.42	0.00	13.95
286	0.70	0.69	0.70	-8.01	-11.36	-5.85	2.99	2.95	3.02	23.79	18.77	25.95
287	0.44	0.11	0.70	44.68	27.95	63.58	2.90	2.79	3.02	25.20	18.77	29.68
288	0.68	0.59	0.70	43.32	34.97	50.03	2.97	2.88	3.08	9.18	1.67	21.04
289	0.10	0.00	0.41	-2.02	-63.89	66.83	1.33	1.26	1.39	4.46	0.00	11.54
290	0.04	0.00	0.21	28.02	-9.14	51.47	1.23	1.16	1.32	11.06	0.00	20.72
291	0.49	0.21	0.70	75.44	53.95	94.43	1.15	1.11	1.18	3.77	0.00	11.99
292	0.63	0.55	0.70	138.78	132.83	143.50	4.01	3.92	4.09	32.64	25.96	34.39
293	0.70	0.68	0.70	144.56	140.52	147.66	3.86	3.78	3.93	30.74	27.49	32.54
294	0.25	0.00	0.39	76.73	52.18	110.69	1.42	1.32	1.55	31.49	22.94	41.60
295	0.27	0.04	0.49	117.32	86.67	139.26	15.56	12.46	18.94	13.30	0.00	35.03
296	0.26	0.00	0.70	314.22	101.62	348.59	16.75	12.70	18.87	4.00	0.00	31.59
297	0.46	0.20	0.70	267.13	115.28	360.00	12.74	8.07	15.80	8.09	0.00	26.54
298	0.66	0.41	0.70	87.27	31.13	100.97	1.20	1.14	1.25	3.24	0.00	12.17
299	0.17	0.08	0.57	127.46	56.28	214.96	1.19	1.07	1.37	8.46	0.00	47.75
300	0.50	0.48	0.51	33.72	30.55	36.29	4.18	4.12	4.20	28.51	27.30	29.23

Table C.2: (continued)

Index	e	-99%	$+99\%$	ϕ_b	-99%	$+99\%$	r_d	-99%	$+99\%$	i	-99%	$+99\%$
301	0.07	0.00	0.33	346.10	254.06	360.00	14.64	12.79	16.58	12.85	0.00	58.26
302	0.63	0.51	0.70	177.43	169.26	183.35	2.90	2.83	2.98	22.44	16.50	25.28
303	0.60	0.52	0.70	179.83	177.31	183.95	2.85	2.77	2.91	1.73	0.00	14.38
304	0.36	0.06	0.70	129.11	81.64	177.50	0.15	0.00	0.40	11.02	0.00	32.63
305	0.50	0.43	0.56	97.40	82.51	106.48	6.16	5.83	6.53	19.25	15.03	22.86
306	0.20	0.00	0.52	218.96	129.94	339.47	16.47	11.68	18.22	15.67	0.00	39.85
307	0.41	0.17	0.56	257.69	180.67	360.00	15.86	10.12	16.39	4.23	0.00	13.57
308	0.10	0.00	0.49	49.04	15.03	170.27	11.29	8.62	11.75	19.78	0.00	35.53
309	0.68	0.55	0.70	113.76	97.33	130.06	22.25	19.05	25.41	9.71	0.00	45.34
310	0.64	0.09	0.70	-5.52	-72.50	20.69	14.19	11.85	15.59	2.06	0.00	20.07
311	0.61	0.26	0.70	182.59	148.05	199.82	0.23	0.00	0.40	28.33	12.81	69.60
312	0.34	0.21	0.42	99.20	76.16	136.85	1.28	1.23	1.34	26.67	9.64	30.95
313	0.55	0.26	0.70	156.02	141.50	177.42	0.98	0.91	1.05	30.75	14.81	38.73
314	0.58	0.51	0.63	102.13	97.41	106.87	26.69	25.09	28.64	34.06	25.83	50.08
315	0.32	0.12	0.70	97.12	37.14	174.87	1.08	1.01	1.14	8.02	0.00	20.80
316	0.65	0.30	0.70	48.95	30.55	64.65	16.72	12.66	18.45	10.24	0.00	32.82
317	0.70	0.65	0.70	28.98	24.31	34.13	18.50	14.00	21.16	11.10	1.57	36.99
318	0.06	0.00	0.25	-33.89	-62.31	12.53	2.95	2.82	3.07	25.83	20.94	29.13
319	0.01	0.00	0.28	81.56	-0.14	167.87	9.86	9.01	11.67	2.76	0.00	17.75
320	0.35	0.12	0.58	228.62	189.46	289.99	1.25	1.09	1.41	23.43	9.81	33.26
321	0.69	0.26	0.70	9.57	-5.14	23.79	15.88	9.86	17.27	6.47	0.00	17.06
322	0.37	0.20	0.56	89.62	52.25	121.67	1.47	1.29	1.80	30.98	15.43	49.40
323	0.13	0.00	0.26	28.54	7.29	53.94	1.53	1.43	1.63	31.93	27.33	36.19
324	0.70	0.68	0.70	21.41	16.17	30.81	23.22	20.31	27.02	2.57	0.00	45.78
325	0.21	0.00	0.36	169.54	120.30	226.01	1.12	1.03	1.45	13.35	0.00	26.07

Table C.2: (continued)

Index	e	-99%	$+99\%$	ϕ_b	-99%	$+99\%$	r_d	-99%	$+99\%$	i	-99%	$+99\%$
326	0.49	0.29	0.70	8.95	-19.64	31.95	2.73	2.63	2.83	27.68	21.64	32.59
327	0.16	0.00	0.39	86.82	57.83	130.68	1.57	1.49	1.67	20.88	9.21	32.57
328	0.64	0.43	0.70	223.72	178.08	305.47	1.30	1.14	1.58	4.11	0.00	18.74
329	0.14	0.00	0.28	77.08	37.23	176.01	0.90	0.82	0.98	14.45	0.00	46.55
330	0.35	0.24	0.45	231.29	201.05	258.02	2.27	2.17	2.37	27.86	21.79	32.60
331	0.08	0.00	0.31	-88.48	-143.83	-4.94	0.22	0.00	0.40	30.57	4.87	44.40
332	0.27	0.14	0.40	251.76	210.26	307.76	2.95	2.52	3.33	11.26	0.00	37.14
333	0.66	0.00	0.70	82.72	36.06	109.26	0.35	0.20	0.39	34.34	9.27	50.29
334	0.50	0.37	0.70	53.08	-37.60	155.59	1.12	0.98	1.41	29.48	4.83	38.06
335	0.03	0.00	0.19	324.92	187.24	360.00	16.12	11.98	17.19	2.58	0.00	15.56
336	0.08	0.00	0.41	6.07	-49.42	33.33	1.81	1.58	2.14	34.39	21.37	49.60
337	0.70	0.64	0.70	141.26	130.15	154.55	0.16	0.00	0.39	3.34	0.00	29.92
338	0.08	0.00	0.58	-10.27	-54.63	127.66	17.41	15.88	17.60	2.50	0.00	21.17
339	0.58	0.22	0.70	-324.62	-360.00	-152.36	14.44	9.81	17.87	18.94	0.00	44.80
340	0.59	0.24	0.70	30.74	-27.44	78.95	1.40	1.32	1.51	8.30	0.00	35.11
341	0.34	0.20	0.45	25.53	14.25	56.04	1.16	1.10	1.25	28.25	22.48	36.46
342	0.23	0.00	0.45	104.35	5.61	234.29	16.05	10.74	18.71	9.73	0.00	50.35
343	0.51	0.36	0.69	153.29	96.64	191.13	1.61	1.48	1.72	14.99	7.66	22.24
344	0.50	0.22	0.70	53.57	34.57	68.40	1.40	1.32	1.57	11.38	0.00	28.36
345	0.64	0.36	0.70	114.04	76.96	136.60	1.70	1.50	1.88	31.32	20.84	40.97
346	0.23	0.01	0.58	130.88	91.91	161.03	4.31	4.09	4.53	12.65	0.00	24.07
347	0.21	0.15	0.29	210.57	147.94	253.04	5.35	5.21	5.63	30.93	27.41	33.79
348	0.46	0.02	0.65	92.42	18.71	141.09	1.93	1.59	2.28	28.23	0.00	47.36
349	0.59	0.43	0.70	146.53	126.12	166.72	1.72	1.61	1.85	31.92	23.41	38.58
350	0.05	0.00	0.21	-311.67	-360.00	-62.31	2.32	1.68	3.10	27.32	0.00	47.70

Table C.2: (continued)

Index	e	-99%	$+99\%$	ϕ_b	-99%	$+99\%$	r_d	-99%	$+99\%$	i	-99%	$+99\%$
351	0.68	0.50	0.70	81.08	67.93	93.79	18.16	16.23	20.73	28.66	16.38	47.10
352	0.68	0.56	0.70	7.75	-12.44	21.86	16.71	13.96	19.63	9.53	0.00	44.52
353	0.36	0.26	0.43	-35.79	-67.30	-5.50	3.20	3.06	3.33	26.53	22.63	30.33
354	0.22	0.02	0.32	130.68	102.86	172.22	1.22	1.11	1.35	4.93	0.00	23.16
355	0.63	0.44	0.70	25.73	-35.06	59.71	2.23	2.09	2.40	15.74	7.29	27.94
356	0.13	0.00	0.41	168.31	50.58	300.02	14.27	11.27	16.02	6.34	0.00	24.66
357	0.33	0.23	0.63	-14.54	-68.03	27.07	1.13	1.01	1.34	11.97	0.00	21.72
358	0.19	0.00	0.60	342.79	272.59	360.00	0.25	0.00	0.40	12.49	0.00	39.65
359	0.69	0.63	0.70	74.30	67.88	92.01	4.06	3.98	4.13	14.94	3.31	20.20
360	0.15	0.00	0.61	122.33	52.19	188.25	3.97	3.41	4.73	9.92	0.00	27.38
361	0.49	0.26	0.70	154.73	62.16	314.88	11.97	10.14	13.69	6.74	0.00	17.60
362	0.70	0.70	0.70	48.42	46.22	51.40	7.93	7.81	8.02	25.21	24.41	26.19
363	0.35	0.17	0.57	185.40	104.66	234.91	3.06	2.68	3.66	23.52	14.76	37.40
364	0.57	0.51	0.63	73.12	67.53	79.81	2.22	2.16	2.29	23.39	18.21	27.93
365	0.00	0.00	0.06	190.91	66.01	305.53	0.09	0.00	0.39	1.53	0.00	7.52
366	0.62	0.46	0.70	195.23	56.14	228.72	1.15	1.06	1.21	34.33	23.09	40.95
367	0.57	0.39	0.70	114.78	76.67	173.26	2.52	2.32	2.80	7.55	0.00	34.41
368	0.02	0.00	0.18	48.18	-50.33	122.45	11.75	8.36	16.38	19.16	0.00	61.54
369	0.04	0.00	0.43	175.92	92.03	215.46	28.30	20.83	38.08	22.52	0.00	55.87
370	0.70	0.46	0.70	87.94	70.83	107.49	29.93	21.27	39.44	28.69	0.00	67.41
371	0.11	0.00	0.28	-63.15	-135.81	-12.09	1.50	1.35	1.64	20.26	0.00	29.89
372	0.20	0.00	0.29	31.24	-51.90	48.55	2.21	2.19	2.24	29.42	26.95	30.88
373	0.06	0.00	0.25	144.84	122.34	188.30	2.21	1.82	3.16	0.38	0.00	4.03
374	0.08	0.00	0.23	103.22	45.75	200.67	1.29	1.16	1.45	31.91	23.99	36.55
375	0.18	0.08	0.40	122.83	51.98	160.38	1.51	1.27	1.71	15.96	6.92	28.49

Table C.2: (continued)

Index	e	-99%	$+99\%$	ϕ_b	-99%	$+99\%$	r_d	-99%	$+99\%$	i	-99%	$+99\%$
376	0.37	0.28	0.70	66.44	47.97	100.48	1.50	1.43	1.60	1.98	0.00	10.65
377	0.57	0.34	0.70	35.43	-151.47	111.42	18.69	11.01	21.73	33.76	15.80	46.82
378	0.32	0.10	0.55	83.46	30.60	119.60	1.28	1.13	1.42	27.57	10.90	38.35
379	0.69	0.63	0.70	110.60	104.51	116.40	1.45	1.40	1.48	32.83	28.90	35.95
380	0.57	0.21	0.70	156.66	123.45	199.53	0.00	0.00	0.00	24.72	0.00	79.21
381	0.44	0.08	0.70	287.91	189.76	360.00	18.42	14.70	19.51	15.21	0.00	52.44
382	0.26	0.16	0.37	49.86	-29.63	86.67	1.61	1.55	1.68	15.00	0.00	27.00
383	0.18	0.00	0.70	330.13	259.73	360.00	19.03	15.75	21.33	24.85	0.00	41.15
384	0.16	0.00	0.28	86.41	63.38	144.07	1.45	1.38	1.54	27.46	19.22	33.22
385	0.65	0.55	0.70	91.51	55.91	122.57	1.81	1.76	1.88	22.61	18.04	25.64
386	0.61	0.22	0.70	310.09	257.01	360.00	10.32	9.01	13.13	7.76	0.00	68.46
387	0.63	0.29	0.70	20.67	-85.08	153.40	10.76	8.98	12.02	3.07	0.00	23.26
388	0.55	0.32	0.70	170.83	145.78	194.27	11.02	9.11	11.21	33.32	3.24	52.18
389	0.69	0.60	0.70	57.79	39.24	72.67	11.76	9.08	13.23	32.63	9.72	54.30
390	0.17	0.08	0.70	62.08	32.82	97.55	1.30	1.24	1.35	1.28	0.00	7.56
391	0.39	0.27	0.70	20.51	-16.76	92.06	0.94	0.85	1.12	6.64	0.00	21.10
392	0.13	0.00	0.49	22.15	-25.33	92.84	1.01	0.91	1.12	28.09	8.82	43.01
393	0.51	0.31	0.62	100.62	40.48	213.40	1.59	1.47	1.76	26.82	15.60	35.83
394	0.67	0.52	0.70	-31.72	-58.38	12.27	1.45	1.39	1.50	0.73	0.00	4.33
395	0.16	0.00	0.54	-45.80	-158.08	19.70	2.31	2.10	2.54	19.58	0.00	31.65
396	0.66	0.43	0.70	53.98	35.57	75.83	0.07	0.00	0.40	12.13	0.00	21.71
397	0.15	0.00	0.56	97.80	56.72	263.22	0.15	0.00	0.40	30.96	16.05	49.31
398	0.61	0.40	0.70	70.89	-13.75	191.05	15.65	11.91	18.33	31.19	0.00	68.27
399	0.27	0.00	0.70	62.05	-25.47	131.83	0.97	0.87	1.12	7.35	0.00	34.46
400	0.70	0.66	0.70	45.50	37.90	52.83	0.18	0.09	0.38	2.55	0.00	18.84

Table C.2: (continued)

Index	e	-99%	$+99\%$	ϕ_b	-99%	$+99\%$	r_d	-99%	$+99\%$	i	-99%	$+99\%$
401	0.31	0.14	0.46	162.23	97.69	191.96	1.45	1.25	1.59	26.31	0.00	40.04
402	0.09	0.00	0.41	25.56	-11.73	179.05	0.11	0.00	0.38	7.72	0.00	63.85
403	0.14	0.00	0.24	186.01	165.19	228.60	2.38	2.28	2.51	33.60	28.35	37.29
404	0.58	0.28	0.70	315.36	293.82	360.00	13.22	11.22	15.49	18.79	0.00	47.31
405	0.62	0.28	0.70	25.81	-54.69	63.16	0.08	0.00	0.38	30.78	0.00	63.24
406	0.08	0.00	0.23	76.66	30.46	108.19	0.90	0.87	0.94	5.19	0.00	14.98
407	0.13	0.00	0.45	-40.86	-108.97	15.36	1.44	1.33	1.54	20.38	0.74	27.90
408	0.29	0.27	0.30	176.62	175.15	178.10	10.42	10.35	10.48	33.35	32.20	34.57
409	0.00	0.00	0.00	24.47	22.03	29.04	0.34	0.29	0.39	15.50	10.06	25.78
410	0.36	0.06	0.70	80.73	2.74	109.17	1.14	1.01	1.26	16.99	0.00	38.78
411	0.44	0.15	0.64	180.69	83.00	273.32	2.53	2.38	2.79	33.68	28.12	38.62
412	0.06	0.00	0.18	-20.96	-58.96	11.34	1.17	1.06	1.94	34.81	23.51	59.17
413	0.64	0.36	0.70	159.66	134.10	186.06	1.42	1.27	1.55	25.38	8.63	32.75
414	0.02	0.00	0.07	-69.46	-96.77	-33.15	3.64	3.50	3.80	10.67	5.42	16.87
415	0.12	0.00	0.54	-145.84	-230.56	-109.56	24.49	21.08	33.08	5.94	0.00	63.15
416	0.66	0.42	0.70	173.08	156.22	198.42	2.40	2.24	2.61	34.54	31.92	38.32
417	0.38	0.16	0.65	123.09	111.62	139.15	1.62	1.55	1.75	20.78	9.47	33.09
418	0.10	0.00	0.23	-100.11	-138.65	4.69	2.30	2.13	2.42	34.40	23.76	38.77
419	0.69	0.60	0.70	80.52	55.17	92.24	0.11	0.00	0.40	18.77	0.00	43.44
420	0.45	0.29	0.53	22.99	5.78	36.95	7.27	7.15	7.40	20.20	17.83	23.33
421	0.68	0.50	0.70	222.71	113.08	334.90	21.51	19.16	26.07	33.50	21.27	59.24
422	0.22	0.00	0.31	72.85	50.64	157.64	1.87	1.82	1.91	4.73	0.00	17.48
423	0.67	0.55	0.70	194.31	182.51	212.64	0.94	0.91	0.96	4.74	0.00	11.85
424	0.09	0.00	0.32	324.63	208.72	360.00	28.22	24.81	29.10	21.32	0.00	43.14
425	0.35	0.21	0.52	82.91	49.64	118.13	1.49	1.39	1.60	34.43	27.30	40.60

Table C.2: (continued)

Index	e	-99%	$+99\%$	ϕ_b	-99%	$+99\%$	r_d	-99%	$+99\%$	i	-99%	$+99\%$
426	0.06	0.00	0.29	140.94	90.00	185.71	8.47	5.71	11.14	2.54	0.00	30.52
427	0.18	0.00	0.57	115.85	59.20	182.76	1.12	1.03	1.20	31.04	18.33	38.50
428	0.70	0.67	0.70	100.32	94.14	105.80	19.52	15.06	23.39	28.80	14.35	63.10
429	0.18	0.01	0.29	117.64	66.01	186.74	1.54	1.41	1.72	14.47	0.00	27.60
430	0.56	0.34	0.70	86.79	56.00	105.48	1.52	1.43	1.67	31.83	24.71	37.09
431	0.15	0.00	0.65	244.52	184.69	354.92	1.14	1.07	1.29	4.02	0.00	32.30
432	0.37	0.12	0.60	165.47	124.87	235.67	1.16	1.02	1.29	10.27	0.00	47.43
433	0.41	0.00	0.66	111.66	74.84	163.69	1.02	0.89	1.16	18.02	0.00	39.69
434	0.38	0.22	0.60	-54.45	-135.82	6.57	13.27	10.18	15.89	15.24	0.00	48.78
435	0.40	0.00	0.63	-90.08	-118.71	-53.32	16.80	14.29	21.52	6.47	0.00	26.58
436	0.65	0.34	0.70	47.85	17.13	82.81	1.46	1.27	1.74	6.61	0.00	19.04
437	0.66	0.56	0.70	212.81	194.05	226.08	1.43	1.34	1.53	33.55	22.85	40.47
438	0.53	0.46	0.59	107.74	99.23	118.78	1.04	1.01	1.08	18.75	11.68	31.27
439	0.23	0.00	0.37	58.10	21.03	101.73	2.84	2.55	3.07	29.01	18.36	36.29
440	0.10	0.00	0.32	2.23	-69.49	108.64	1.76	1.60	1.98	4.00	0.00	15.37
441	0.70	0.69	0.70	153.62	151.49	155.82	22.71	20.93	25.47	3.76	0.00	16.12
442	0.04	0.00	0.19	101.61	50.95	158.75	2.07	1.87	2.31	22.66	0.00	36.58
443	0.39	0.26	0.51	94.36	84.26	104.30	0.92	0.88	0.98	15.90	8.96	27.40
444	0.68	0.41	0.70	-351.77	-360.00	-184.85	17.72	14.62	17.85	19.21	0.00	63.07
445	0.70	0.68	0.70	5.88	0.75	9.99	0.36	0.26	0.41	1.17	0.00	6.82
446	0.39	0.13	0.47	220.32	166.72	317.92	1.27	1.22	1.33	10.35	0.00	18.63
447	0.09	0.00	0.47	70.22	13.46	105.03	1.43	1.33	1.50	29.07	19.42	38.70
448	0.61	0.37	0.70	312.69	74.88	360.00	10.61	8.01	11.45	3.52	0.00	13.49
449	0.12	0.00	0.29	209.39	169.55	245.35	2.18	2.05	2.35	33.55	26.27	40.45
450	0.26	0.12	0.42	-54.74	-113.47	-2.24	1.91	1.73	2.14	33.21	23.87	40.24

Table C.2: (continued)

Index	e	-99%	$+99\%$	ϕ_b	-99%	$+99\%$	r_d	-99%	$+99\%$	i	-99%	$+99\%$
451	0.01	0.00	0.08	277.61	204.10	312.15	16.38	13.36	19.34	0.70	0.00	8.90
452	0.54	0.28	0.70	64.56	25.38	108.46	11.83	9.28	15.63	6.97	0.00	31.34
453	0.70	0.66	0.70	221.95	154.40	249.84	3.78	3.70	3.87	31.31	29.47	33.45
454	0.59	0.42	0.70	39.34	27.28	49.71	22.08	16.64	23.10	32.28	0.00	51.23
455	0.25	0.00	0.34	19.69	-30.72	100.47	3.16	3.02	3.34	34.52	30.15	40.46
456	0.17	0.00	0.48	240.86	212.50	300.44	15.47	11.68	17.37	30.67	9.19	45.13
457	0.67	0.43	0.70	277.72	267.36	285.74	0.08	0.00	0.39	18.95	5.73	32.02
458	0.06	0.00	0.20	162.64	136.82	205.51	4.78	4.65	5.53	28.19	1.53	30.11
459	0.05	0.00	0.17	74.40	9.75	102.48	1.91	1.84	1.99	12.05	0.00	20.86
460	0.66	0.62	0.70	-8.47	-15.39	2.16	3.66	3.57	3.77	26.10	21.54	28.74
461	0.04	0.00	0.22	174.80	55.21	281.04	0.09	0.00	0.29	20.46	0.00	54.88
462	0.63	0.42	0.70	312.15	234.45	360.00	1.50	1.38	1.61	7.71	0.00	26.91
463	0.70	0.64	0.70	117.50	109.14	123.84	0.09	0.00	0.33	0.76	0.00	17.12
464	0.64	0.47	0.70	18.30	2.92	28.65	19.24	17.14	21.43	25.21	0.00	53.35
465	0.15	0.00	0.41	-14.92	-130.80	20.44	1.58	1.48	1.75	2.97	0.00	16.08
466	0.50	0.21	0.70	69.50	44.94	110.77	1.36	1.29	1.49	2.33	0.00	25.92
467	0.29	0.10	0.52	-112.62	-153.97	-61.29	2.32	2.11	2.50	17.29	0.26	30.93
468	0.28	0.00	0.48	242.41	169.86	288.82	15.26	12.18	17.17	4.35	0.00	21.38
469	0.55	0.28	0.62	57.87	45.21	67.87	5.60	5.53	5.81	33.52	31.60	36.15
470	0.19	0.04	0.31	277.64	246.68	360.00	0.13	0.00	0.40	6.79	0.00	16.88
471	0.39	0.20	0.58	-215.11	-246.22	-188.01	13.63	12.27	13.63	3.56	0.00	35.59
472	0.70	0.32	0.70	154.83	125.94	204.01	0.01	0.00	0.04	3.97	0.00	19.88
473	0.02	0.00	0.14	69.19	33.73	148.34	0.12	0.00	0.40	2.27	0.00	27.59
474	0.33	0.06	0.57	36.90	-90.90	120.44	2.63	2.53	2.75	28.95	22.03	34.25
475	0.12	0.00	0.25	4.73	-19.77	33.54	2.73	2.61	2.87	26.66	17.84	31.66

Table C.2: (continued)

Index	e	-99%	$+99\%$	ϕ_b	-99%	$+99\%$	r_d	-99%	$+99\%$	i	-99%	$+99\%$
476	0.69	0.61	0.70	31.31	12.93	44.10	0.12	0.00	0.39	24.76	0.00	44.79
477	0.70	0.58	0.70	120.62	97.68	136.01	0.05	0.00	0.39	2.75	0.00	22.37
478	0.04	0.00	0.38	350.00	249.34	360.00	18.90	14.95	19.69	1.74	0.00	13.48
479	0.61	0.46	0.70	79.94	56.76	108.59	2.04	1.92	2.24	31.34	20.47	48.11
480	0.34	0.00	0.52	131.30	70.09	179.36	1.92	1.85	2.04	4.06	0.00	26.07
481	0.51	0.25	0.70	104.15	74.82	120.80	0.04	0.00	0.40	32.54	8.15	49.00
482	0.42	0.17	0.67	194.94	161.82	214.90	15.92	11.17	19.82	33.53	22.72	45.01
483	0.12	0.00	0.31	35.91	-83.97	123.56	0.15	0.00	0.40	27.77	0.00	78.59
484	0.29	0.16	0.43	84.72	55.04	118.08	2.42	2.20	2.52	33.22	28.14	36.76
485	0.26	0.20	0.30	164.31	149.88	177.69	2.30	2.26	2.33	26.36	24.53	27.63
486	0.63	0.25	0.70	81.90	66.12	128.62	0.07	0.00	0.40	8.62	0.00	85.00
487	0.27	0.00	0.62	344.24	269.05	360.00	11.47	9.43	12.49	20.85	0.00	50.83
488	0.27	0.00	0.52	50.36	26.46	76.84	10.33	4.26	10.76	5.21	0.00	37.13
489	0.69	0.66	0.70	62.66	51.65	86.12	0.41	0.41	0.41	12.93	0.00	18.76
490	0.06	0.00	0.18	169.56	141.12	220.10	1.38	1.27	1.53	30.38	23.32	37.14
491	0.34	0.22	0.51	25.68	7.05	46.11	2.12	2.06	2.19	29.54	25.95	33.16
492	0.35	0.16	0.42	217.24	187.75	237.85	12.11	10.82	13.93	4.74	0.00	18.76
493	0.68	0.56	0.70	5.64	-9.78	23.06	23.90	20.93	27.93	1.08	0.00	12.25
494	0.69	0.52	0.70	78.03	65.52	134.59	2.98	2.52	4.32	0.87	0.00	11.64
495	0.11	0.00	0.34	245.74	146.80	360.00	9.42	7.91	11.26	22.16	14.92	38.37
496	0.63	0.52	0.70	175.80	132.59	195.10	1.89	1.52	2.26	24.26	5.48	39.37
497	0.33	0.19	0.56	-26.21	-50.50	22.51	1.54	1.48	1.67	26.80	19.20	35.94
498	0.06	0.00	0.49	-124.61	-360.00	14.68	15.15	12.57	20.32	18.27	0.00	60.93
499	0.51	0.21	0.62	179.82	164.33	188.18	2.88	2.76	2.98	25.55	20.58	28.60
500	0.20	0.00	0.29	99.27	66.87	124.93	4.07	3.99	4.31	0.51	0.00	4.25

Table C.2: (continued)

Index	e	-99%	$+99\%$	ϕ_b	-99%	$+99\%$	r_d	-99%	$+99\%$	i	-99%	$+99\%$
501	0.70	0.67	0.70	7.51	2.71	12.05	29.12	25.19	30.17	14.13	0.00	39.74
502	0.01	0.00	0.19	-138.02	-290.20	46.61	14.55	10.29	17.24	5.10	0.00	20.42
503	0.12	0.00	0.36	152.73	52.06	183.25	2.03	1.82	2.24	33.23	25.01	38.96
504	0.04	0.00	0.31	-243.95	-360.00	82.30	13.51	11.84	18.98	34.86	6.83	64.39
505	0.69	0.60	0.70	240.76	152.19	272.67	23.28	22.65	23.94	14.66	7.15	17.53
506	0.39	0.28	0.51	303.21	291.83	313.37	26.38	21.69	26.38	0.37	0.00	9.64
507	0.39	0.22	0.47	82.84	55.56	102.02	3.34	3.27	3.40	0.11	0.00	1.59
508	0.69	0.63	0.70	206.61	199.32	215.20	4.10	3.95	4.25	30.20	25.22	33.85
509	0.11	0.00	0.21	176.68	160.45	196.62	3.74	3.62	3.83	1.65	0.00	5.67
510	0.70	0.65	0.70	10.12	3.35	16.84	0.34	0.12	0.40	29.20	4.06	49.61
511	0.27	0.21	0.44	10.88	0.94	26.13	2.71	2.61	2.89	17.16	9.79	25.89
512	0.43	0.13	0.70	302.99	169.09	360.00	15.46	14.04	19.65	27.03	0.00	38.12
513	0.06	0.00	0.42	106.39	-18.31	192.14	18.71	16.38	22.30	9.58	0.00	37.23
514	0.70	0.64	0.70	175.76	169.09	185.53	0.21	0.00	0.40	23.51	0.00	62.28
515	0.54	0.02	0.70	45.85	21.69	62.22	0.12	0.00	0.40	0.92	0.00	6.32
516	0.30	0.05	0.51	111.69	59.78	186.27	15.91	11.75	17.82	23.58	11.63	37.73
517	0.58	0.12	0.70	214.25	195.98	232.71	1.18	1.10	1.26	2.51	0.00	12.22
518	0.36	0.33	0.37	114.20	105.15	122.64	0.18	0.08	0.20	34.06	29.25	39.46
519	0.70	0.68	0.70	51.05	48.86	52.88	2.77	2.73	2.82	0.94	0.00	4.17
520	0.07	0.00	0.27	27.30	-29.80	93.88	13.25	11.42	15.19	6.00	0.00	28.84
521	0.06	0.00	0.29	215.25	136.88	324.79	19.84	16.09	21.55	4.96	0.00	28.64
522	0.70	0.59	0.70	132.08	119.46	142.05	29.34	26.44	33.01	23.21	0.00	45.40
523	0.39	0.15	0.70	336.88	183.95	360.00	14.34	11.91	15.47	17.93	0.00	41.82
524	0.08	0.00	0.15	164.19	150.00	177.20	1.98	1.94	2.01	29.91	27.36	31.85
525	0.69	0.64	0.70	-11.73	-20.30	-1.78	19.65	15.96	20.52	5.31	0.00	26.21

Table C.2: (continued)

Index	e	-99%	$+99\%$	ϕ_b	-99%	$+99\%$	r_d	-99%	$+99\%$	i	-99%	$+99\%$
526	0.70	0.58	0.70	65.91	53.25	79.22	0.14	0.07	0.20	0.94	0.00	9.26
527	0.70	0.63	0.70	145.76	137.92	153.81	20.81	18.13	22.65	3.28	0.00	21.82
528	0.70	0.65	0.70	84.82	75.63	91.60	17.04	16.06	17.86	1.96	0.00	9.52
529	0.21	0.00	0.32	248.24	114.90	360.00	20.77	16.67	24.79	3.25	0.00	35.00
530	0.70	0.65	0.70	-127.39	-133.60	-120.02	0.17	0.00	0.40	0.93	0.00	6.64
531	0.04	0.00	0.22	310.69	268.22	360.00	0.83	0.76	0.91	12.17	0.00	21.06
532	0.45	0.00	0.70	-8.27	-281.65	260.97	23.70	22.41	23.70	25.62	0.00	54.29
533	0.45	0.00	0.59	232.56	89.47	360.00	14.85	11.51	18.17	23.47	1.01	41.88
534	0.18	0.00	0.32	17.77	-74.97	74.94	22.31	17.82	25.82	18.36	0.00	40.11
535	0.38	0.21	0.54	74.85	-35.86	107.90	13.39	6.58	18.13	1.61	0.00	22.68
536	0.70	0.64	0.70	43.82	37.88	48.25	18.03	16.88	18.03	0.54	0.00	30.81
537	0.70	0.64	0.70	61.70	53.43	70.00	0.13	0.02	0.22	0.35	0.00	15.25
538	0.27	0.06	0.47	225.74	183.39	252.74	0.88	0.83	0.92	3.08	0.00	15.84
539	0.50	0.00	0.68	180.22	124.93	272.42	12.49	10.54	13.72	1.29	0.00	16.72
540	0.41	0.00	0.70	29.46	14.00	54.14	16.34	15.12	17.68	8.84	0.00	39.04
541	0.46	0.25	0.70	16.35	-14.75	55.22	0.27	0.07	0.40	17.15	0.00	42.71
542	0.70	0.67	0.70	15.67	10.23	21.28	24.22	22.17	25.99	30.17	8.16	47.04
543	0.62	0.53	0.70	51.56	21.54	89.36	0.00	0.00	0.37	3.76	0.00	76.91
544	0.01	0.00	0.03	60.78	25.30	78.89	2.23	2.15	2.32	15.83	10.26	20.64
545	0.65	0.54	0.70	220.64	164.19	286.82	10.07	9.31	10.86	1.07	0.00	9.30
546	0.70	0.63	0.70	229.27	220.18	243.99	24.54	20.70	28.00	4.37	0.00	18.07
547	0.70	0.58	0.70	41.27	27.12	52.21	14.13	12.50	16.57	12.11	0.00	50.89
548	0.48	0.08	0.70	192.07	142.03	360.00	21.12	14.44	22.76	8.20	0.00	57.65
549	0.27	0.10	0.48	-154.05	-319.58	-16.01	15.16	11.02	16.86	3.77	0.00	19.52
550	0.70	0.69	0.70	104.73	101.92	107.64	1.79	1.74	1.84	1.51	0.00	5.16

Table C.2: (continued)

Index	e	-99%	$+99\%$	ϕ_b	-99%	$+99\%$	r_d	-99%	$+99\%$	i	-99%	$+99\%$
551	0.30	0.00	0.59	190.78	138.11	259.98	2.12	1.99	2.26	5.49	0.00	16.04
552	0.26	0.02	0.52	91.23	16.06	138.86	1.23	1.12	1.52	9.66	0.00	25.32
553	0.24	0.00	0.54	111.16	-46.57	184.65	1.92	1.72	2.11	25.99	14.12	35.07
554	0.00	0.00	0.02	85.75	-8.45	168.51	0.02	0.00	0.35	0.48	0.00	19.22
555	0.56	0.37	0.65	-31.78	-65.97	14.87	1.38	1.23	1.79	14.32	0.00	41.96
556	0.63	0.10	0.70	306.10	205.19	360.00	19.71	15.83	22.62	0.77	0.00	9.56
557	0.63	0.42	0.70	213.94	57.18	251.88	12.50	10.16	17.14	29.57	19.88	41.21
558	0.14	0.00	0.47	145.85	112.38	190.09	0.59	0.48	0.68	9.97	0.00	22.63
559	0.67	0.56	0.70	-106.91	-129.38	-24.25	23.65	22.10	24.24	5.60	0.00	16.87
560	0.06	0.00	0.19	304.96	206.94	360.00	15.36	11.77	17.29	14.76	0.00	49.58
561	0.15	0.00	0.50	40.54	-7.68	138.68	3.15	2.79	3.75	30.90	19.29	41.29
562	0.08	0.00	0.22	69.62	9.70	155.36	10.94	9.42	11.79	5.08	0.00	20.57
563	0.15	0.00	0.32	215.50	120.62	360.00	15.20	8.45	18.08	20.51	0.00	47.37
564	0.70	0.35	0.70	31.15	25.92	47.81	21.07	20.43	21.39	32.45	28.17	36.42
565	0.70	0.66	0.70	157.30	146.92	215.40	19.77	13.49	24.84	3.49	0.00	29.14
566	0.30	0.00	0.70	304.57	240.14	360.00	1.13	0.97	1.33	33.10	15.96	49.65
567	0.45	0.19	0.69	276.09	234.21	360.00	27.39	21.28	29.64	0.87	0.00	4.28
568	0.70	0.67	0.70	141.33	135.87	147.85	28.50	26.09	35.39	1.93	0.00	14.17
569	0.42	0.00	0.70	349.50	277.65	360.00	20.02	18.33	20.02	34.77	0.00	52.45
570	0.49	0.17	0.69	167.51	119.16	212.82	3.55	3.34	3.72	28.95	19.28	33.73
571	0.14	0.05	0.23	140.51	106.11	149.45	10.46	9.97	11.04	0.50	0.00	8.16
572	0.40	0.19	0.60	191.35	138.73	229.52	0.79	0.66	0.91	21.20	8.89	57.44
573	0.67	0.38	0.70	-59.46	-158.66	-11.18	13.34	10.96	14.57	5.67	0.00	31.97
574	0.70	0.67	0.70	3.06	-14.44	15.82	29.37	26.88	31.48	27.88	15.77	34.64
575	0.27	0.16	0.39	220.71	172.92	242.08	1.24	1.18	1.29	0.29	0.00	10.97

Table C.2: (continued)

Index	e	-99%	$+99\%$	ϕ_b	-99%	$+99\%$	r_d	-99%	$+99\%$	i	-99%	$+99\%$
576	0.20	0.00	0.35	51.58	10.32	80.74	24.05	21.78	24.77	12.03	0.00	46.96
577	0.31	0.00	0.70	140.33	94.80	157.74	12.95	10.77	14.70	10.05	0.00	33.63
578	0.61	0.15	0.70	168.49	135.78	187.49	0.84	0.70	0.98	11.25	0.00	47.56
579	0.06	0.00	0.55	77.78	36.86	105.31	0.07	0.00	0.40	33.94	2.33	60.65
580	0.67	0.41	0.70	-73.69	-176.94	66.30	21.92	15.85	26.22	9.00	0.00	48.54
581	0.63	0.38	0.70	-30.76	-150.62	138.47	13.28	7.61	16.69	21.80	0.00	56.53
582	0.58	0.11	0.70	-101.25	-139.39	31.34	1.88	1.67	2.10	24.00	0.99	41.14
583	0.02	0.00	0.31	92.44	28.88	131.48	3.94	3.75	4.10	0.19	0.00	3.99
584	0.60	0.36	0.70	14.24	-7.54	35.27	0.98	0.91	1.07	12.97	0.00	36.11
585	0.70	0.69	0.70	129.47	126.69	137.66	0.03	0.00	0.37	31.10	19.01	54.96
586	0.42	0.33	0.49	0.65	-10.00	32.40	5.65	5.59	5.75	0.34	0.00	2.02
587	0.69	0.52	0.70	47.77	39.82	56.21	15.17	11.25	19.79	4.97	0.00	27.16
588	0.15	0.00	0.48	-115.50	-351.58	-33.38	14.53	12.78	16.29	24.76	0.00	43.36
589	0.47	0.38	0.56	85.43	77.18	92.17	0.00	0.00	0.04	8.05	1.39	18.07
590	0.70	0.64	0.70	177.79	169.84	183.03	20.13	14.98	22.50	13.93	0.00	48.07
591	0.36	0.20	0.52	204.85	139.93	245.02	2.00	1.77	2.35	32.28	16.05	44.08
592	0.70	0.65	0.70	125.42	99.32	146.05	16.98	13.98	19.45	1.82	0.00	15.60
593	0.26	0.00	0.70	168.74	122.38	205.27	3.75	3.45	4.16	5.91	0.00	22.01
594	0.43	0.08	0.54	179.78	167.65	216.24	0.14	0.00	0.40	24.76	16.36	32.47
595	0.09	0.00	0.26	-5.19	-51.19	38.98	3.30	3.11	3.45	27.01	18.45	32.60
596	0.69	0.49	0.70	53.85	-17.09	199.32	14.64	9.54	17.89	20.44	0.00	43.76
597	0.00	0.00	0.02	19.24	1.52	26.37	2.83	2.78	2.97	20.44	18.76	22.94
598	0.70	0.66	0.70	-59.42	-87.11	-8.48	17.03	12.50	24.62	0.52	0.00	7.89
599	0.04	0.00	0.20	-86.20	-199.14	6.57	21.57	17.02	25.55	5.70	0.00	51.27
600	0.50	0.21	0.68	-86.53	-128.29	-62.98	0.03	0.00	0.05	23.86	0.00	50.35

Table C.2: (continued)

Index	e	-99%	$+99\%$	ϕ_b	-99%	$+99\%$	r_d	-99%	$+99\%$	i	-99%	$+99\%$
601	0.49	0.26	0.70	149.25	102.50	179.06	1.20	1.01	1.39	34.31	14.58	46.77
602	0.60	0.27	0.70	40.42	-24.24	78.06	1.17	1.10	1.24	7.60	0.00	21.00
603	0.70	0.57	0.70	22.39	7.42	34.21	0.14	0.00	0.40	13.63	0.00	31.45
604	0.16	0.00	0.32	270.82	127.70	308.32	12.12	9.39	13.58	11.65	0.00	31.55
605	0.63	0.46	0.70	112.66	93.60	126.09	0.08	0.00	0.17	33.74	0.00	54.83
606	0.62	0.50	0.70	97.72	81.98	106.75	2.59	2.39	2.71	5.41	0.00	14.26
607	0.68	0.56	0.70	263.12	144.75	360.00	22.38	18.52	32.11	9.70	0.00	51.32
608	0.69	0.58	0.70	155.98	145.25	163.17	20.55	14.41	22.03	22.48	0.00	45.88
609	0.02	0.00	0.23	97.97	86.57	103.21	6.46	6.29	6.75	4.30	0.00	17.20
610	0.53	0.37	0.64	91.49	62.59	116.33	1.48	1.32	1.67	24.66	14.01	30.59
611	0.24	0.14	0.34	267.70	216.51	310.10	1.13	1.10	1.17	32.13	27.85	36.17
612	0.22	0.00	0.70	314.15	261.48	360.00	25.09	21.43	28.19	18.64	3.42	33.02
613	0.29	0.08	0.70	218.89	204.02	252.27	1.96	1.84	2.09	1.84	0.00	8.32
614	0.06	0.00	0.34	-18.27	-360.00	60.44	9.94	8.97	11.17	6.57	0.00	27.60
615	0.69	0.65	0.70	160.77	152.77	170.33	14.97	9.95	17.73	24.61	18.28	32.24
616	0.46	0.17	0.70	192.83	128.09	241.80	1.34	1.07	1.55	32.56	21.38	41.04
617	0.68	0.00	0.70	199.93	169.91	209.96	0.24	0.00	0.40	10.04	0.00	29.90
618	0.33	0.00	0.64	81.11	67.68	118.31	2.14	2.00	2.33	32.37	23.51	36.65
619	0.06	0.00	0.33	4.32	-15.52	20.24	7.99	7.56	8.53	9.59	0.00	19.06
620	0.21	0.12	0.35	148.26	131.72	167.60	3.19	3.13	3.25	17.92	14.72	20.41
621	0.35	0.18	0.70	58.29	16.90	151.34	12.96	9.12	15.54	30.13	17.16	43.28
622	0.62	0.31	0.70	123.03	101.63	141.11	18.40	10.74	22.58	8.86	0.00	54.24
623	0.19	0.00	0.28	224.25	172.37	301.80	1.81	1.74	1.98	6.12	0.00	16.82
624	0.16	0.00	0.34	102.58	54.81	184.27	3.04	2.67	3.49	32.67	0.00	42.17
625	0.70	0.68	0.70	70.58	65.04	77.31	28.97	28.28	28.97	1.16	0.00	16.44

Table C.2: (continued)

Index	e	-99%	$+99\%$	ϕ_b	-99%	$+99\%$	r_d	-99%	$+99\%$	i	-99%	$+99\%$
626	0.48	0.30	0.62	-41.58	-48.79	-33.78	11.52	11.03	15.60	24.12	1.71	49.44
627	0.29	0.00	0.45	35.53	-1.74	87.15	1.12	1.01	1.20	28.09	6.24	36.23
628	0.36	0.02	0.53	-61.87	-122.87	19.02	0.89	0.72	1.16	17.69	0.00	28.89
629	0.05	0.00	0.15	65.47	24.97	140.11	12.22	9.31	14.42	1.61	0.00	21.24
630	0.01	0.00	0.15	80.45	18.41	360.00	14.14	11.72	16.73	23.50	0.00	45.62
631	0.69	0.57	0.70	36.41	-9.88	52.70	11.87	10.33	13.00	0.65	0.00	8.75
632	0.70	0.60	0.70	144.31	132.89	154.26	0.01	0.00	0.15	31.55	0.00	57.35
633	0.65	0.46	0.70	28.24	17.40	44.53	15.53	13.67	16.68	2.15	0.00	15.04
634	0.41	0.16	0.67	93.34	52.87	166.63	1.24	1.11	1.46	6.90	0.00	18.09
635	0.69	0.39	0.70	183.47	177.73	191.70	6.89	5.98	7.56	31.11	11.11	39.86
636	0.41	0.15	0.70	19.82	-12.94	52.97	28.76	24.03	33.11	33.98	16.09	50.64
637	0.04	0.00	0.29	107.08	-83.27	246.51	0.09	0.00	0.40	24.18	6.08	63.49
638	0.69	0.61	0.70	49.84	17.48	70.85	10.16	7.84	13.44	27.23	21.99	44.01
639	0.64	0.39	0.70	54.36	7.05	113.51	0.99	0.92	1.06	3.12	0.00	16.28
640	0.54	0.40	0.70	-126.84	-159.19	18.75	1.11	1.04	1.17	5.15	0.00	16.68
641	0.14	0.00	0.41	119.58	16.92	244.89	0.12	0.00	0.40	15.07	0.00	26.38
642	0.69	0.00	0.70	-91.96	-103.22	-47.39	0.10	0.00	0.40	4.62	0.00	18.47
643	0.43	0.00	0.70	4.08	-63.30	54.84	1.81	1.58	2.10	25.95	5.14	38.19
644	0.46	0.23	0.66	84.87	36.23	101.05	0.41	0.41	0.45	23.05	18.70	30.48
645	0.67	0.43	0.70	150.03	79.77	206.78	8.39	6.46	9.31	2.52	0.00	8.33
646	0.07	0.00	0.30	-360.00	-360.00	-247.97	12.29	11.68	12.91	1.92	0.00	9.19
647	0.16	0.00	0.50	141.50	97.64	171.89	14.06	9.36	17.72	15.45	0.00	55.85
648	0.13	0.07	0.29	142.79	111.35	173.73	2.19	2.13	2.27	30.35	27.40	32.73
649	0.14	0.00	0.43	-6.35	-23.92	59.09	3.58	3.42	3.72	29.72	25.82	34.55
650	0.26	0.09	0.48	-3.60	-16.52	54.76	2.84	2.71	2.92	3.87	0.00	12.16

Table C.2: (continued)

Index	e	-99%	$+99\%$	ϕ_b	-99%	$+99\%$	r_d	-99%	$+99\%$	i	-99%	$+99\%$
651	0.00	0.00	0.09	-1.49	-16.10	9.87	20.68	19.57	21.67	34.60	31.63	38.35
652	0.70	0.68	0.70	195.67	191.64	199.07	3.82	3.77	3.86	34.62	33.39	35.75
653	0.60	0.43	0.70	85.97	49.81	118.27	2.72	2.69	2.76	2.88	0.00	9.59
654	0.07	0.00	0.26	117.48	60.48	160.21	3.33	3.14	3.49	16.79	5.71	24.15
655	0.70	0.50	0.70	35.42	14.33	51.66	16.21	14.29	18.22	2.02	0.00	24.99
656	0.14	0.05	0.28	189.12	148.39	250.17	1.31	1.14	1.59	31.02	23.17	42.24
657	0.64	0.37	0.70	66.03	44.55	79.86	14.87	12.75	17.96	19.61	0.00	59.01
658	0.17	0.05	0.33	194.50	170.37	207.59	3.10	3.05	3.15	24.08	22.15	26.07
659	0.38	0.13	0.52	126.92	54.42	245.25	1.26	1.14	1.40	13.59	0.00	33.02
660	0.40	0.20	0.70	2.61	-27.80	126.69	23.03	20.09	27.75	1.18	0.00	12.94
661	0.31	0.12	0.49	112.30	57.77	293.55	3.08	2.81	3.46	24.88	13.49	33.76
662	0.03	0.00	0.14	87.20	61.85	107.69	2.43	2.39	2.49	3.94	0.00	6.98
663	0.57	0.49	0.70	137.11	117.05	165.49	2.33	2.28	2.39	25.19	22.58	27.90
664	0.15	0.00	0.44	71.93	9.17	217.89	0.84	0.66	1.02	4.90	0.00	17.01
665	0.63	0.30	0.70	124.62	106.76	148.38	16.38	14.63	16.67	19.10	0.00	47.00
666	0.60	0.37	0.70	67.66	54.08	82.07	1.51	1.45	1.57	2.70	0.00	14.49
667	0.56	0.36	0.70	78.65	38.60	135.20	1.14	1.10	1.17	4.44	0.00	23.10
668	0.26	0.05	0.50	207.70	163.51	257.77	1.19	1.09	1.33	5.20	0.00	20.01
669	0.67	0.51	0.70	53.55	41.71	63.98	17.21	12.12	21.69	9.65	0.00	63.68
670	0.65	0.46	0.70	-3.25	-356.43	165.97	21.22	14.66	22.00	8.35	0.00	52.80
671	0.54	0.35	0.70	177.86	158.05	196.02	1.13	1.03	1.20	4.18	0.00	16.60
672	0.59	0.40	0.70	18.81	1.34	32.72	25.92	20.10	31.26	0.00	0.00	11.12
673	0.07	0.00	0.50	243.99	180.74	299.30	0.90	0.84	1.05	5.09	0.00	15.25
674	0.64	0.57	0.70	181.85	173.31	192.44	2.57	2.49	2.72	26.40	21.50	31.49
675	0.69	0.63	0.70	45.74	34.58	58.92	14.58	12.20	17.55	4.36	0.00	11.48

Table C.2: (continued)

Index	e	-99%	$+99\%$	ϕ_b	-99%	$+99\%$	r_d	-99%	$+99\%$	i	-99%	$+99\%$
676	0.21	0.05	0.33	76.66	46.20	106.56	1.51	1.45	1.58	4.12	0.00	14.40
677	0.36	0.25	0.69	92.23	64.53	117.30	1.27	1.21	1.32	20.07	0.00	27.08
678	0.21	0.00	0.46	61.76	-248.89	156.88	8.60	6.88	10.19	16.02	0.00	49.81
679	0.18	0.00	0.60	37.00	-34.91	74.36	11.00	5.42	13.28	5.85	0.00	66.83
680	0.37	0.01	0.70	116.49	80.33	139.09	0.66	0.60	0.77	5.93	0.00	23.42
681	0.22	0.00	0.42	192.11	145.82	220.34	1.37	1.20	1.62	16.52	0.00	34.44
682	0.61	0.49	0.70	93.00	83.03	105.75	1.57	1.48	1.64	3.41	0.00	17.75
683	0.25	0.18	0.33	-26.25	-34.80	-21.72	27.12	25.53	27.97	10.65	4.32	15.52
684	0.07	0.00	0.18	254.27	169.65	360.00	0.81	0.73	0.89	26.29	0.80	37.60
685	0.60	0.47	0.70	78.72	52.77	103.68	12.63	11.63	12.63	5.19	0.00	22.27
686	0.48	0.40	0.65	14.46	2.74	33.52	2.23	2.18	2.27	2.82	0.00	5.64
687	0.30	0.00	0.60	21.45	-67.29	107.67	2.24	1.86	2.64	3.53	0.00	14.87
688	0.52	0.33	0.70	84.89	31.98	105.45	1.42	1.34	1.52	3.06	0.00	14.74
689	0.59	0.41	0.70	15.06	-26.62	51.68	3.44	3.34	3.51	25.72	19.77	29.40
690	0.70	0.65	0.70	97.13	85.11	108.33	0.01	0.00	0.39	1.27	0.00	11.44
691	0.46	0.24	0.58	136.19	71.50	170.12	2.07	1.92	2.21	31.70	25.53	37.79
692	0.39	0.14	0.70	63.44	-9.62	105.20	1.51	1.41	1.59	26.25	0.28	35.16
693	0.58	0.33	0.70	122.59	36.83	162.60	2.26	2.01	2.56	30.23	21.13	40.30
694	0.00	0.00	0.26	150.73	103.16	249.53	0.03	0.00	0.37	0.42	0.00	5.52
695	0.35	0.21	0.59	57.85	42.23	75.54	0.70	0.65	0.74	5.59	0.00	14.00
696	0.64	0.25	0.70	165.38	93.74	193.38	1.21	1.14	1.35	18.02	4.19	29.57
697	0.03	0.00	0.13	-38.30	-283.78	17.87	1.19	0.87	1.97	27.35	0.00	67.04
698	0.36	0.17	0.51	170.28	144.58	212.21	0.92	0.87	0.94	4.46	0.00	13.46
699	0.70	0.69	0.70	28.92	24.61	31.84	0.37	0.26	0.40	21.71	8.88	34.41
700	0.43	0.16	0.49	15.64	6.27	19.78	1.79	1.74	1.85	6.42	0.00	16.71

Table C.2: (continued)

Index	e	-99%	$+99\%$	ϕ_b	-99%	$+99\%$	r_d	-99%	$+99\%$	i	-99%	$+99\%$
701	0.24	0.00	0.70	148.40	40.21	274.35	2.90	2.55	3.23	25.49	14.22	41.01
702	0.08	0.00	0.63	4.69	-39.35	149.48	17.98	14.51	19.63	19.61	0.00	43.73
703	0.70	0.65	0.70	133.15	121.96	139.62	21.46	16.72	25.21	11.82	0.00	33.28
704	0.06	0.00	0.46	74.47	-29.90	201.73	11.85	8.47	13.61	2.94	0.00	24.21
705	0.58	0.26	0.70	334.19	304.69	360.00	12.41	10.86	14.55	12.21	0.00	24.32
706	0.70	0.61	0.70	131.90	114.96	143.92	15.30	12.51	16.97	3.27	0.00	18.21
707	0.69	0.44	0.70	148.42	109.99	160.40	28.89	23.22	32.61	0.60	0.00	16.39
708	0.61	0.46	0.70	-22.50	-57.44	107.04	10.95	9.13	12.65	15.46	0.00	44.50
709	0.07	0.00	0.70	-207.87	-360.00	80.71	13.48	11.83	15.18	4.27	0.00	23.20
710	0.69	0.27	0.70	184.24	157.19	197.56	2.01	1.76	2.14	2.75	0.00	12.67
711	0.05	0.00	0.27	-37.54	-120.87	93.33	12.42	11.08	13.65	8.82	0.00	27.87
712	0.02	0.00	0.44	83.03	-22.48	138.22	1.68	1.46	2.02	1.62	0.00	31.26
713	0.24	0.00	0.70	-16.19	-57.52	153.58	9.80	6.39	12.48	8.78	0.00	40.61
714	0.03	0.00	0.16	146.90	114.53	176.40	1.29	1.17	1.51	28.35	19.92	51.32
715	0.70	0.63	0.70	81.09	68.26	91.02	10.91	8.99	12.68	0.00	0.00	12.95
716	0.27	0.19	0.42	112.04	85.20	142.72	1.83	1.76	1.90	31.19	23.10	35.36
717	0.68	0.57	0.70	231.36	209.24	270.13	11.06	9.43	13.56	1.69	0.00	8.14
718	0.20	0.15	0.31	6.49	5.79	6.81	20.19	20.11	20.21	10.11	9.78	10.30
719	0.66	0.52	0.70	55.79	40.09	76.26	13.98	7.77	17.82	9.69	0.00	64.25
720	0.13	0.00	0.30	119.85	31.31	155.95	1.16	1.09	1.23	7.21	0.00	16.56
721	0.12	0.00	0.45	52.91	-22.51	91.83	1.13	1.04	1.27	6.59	0.00	30.21
722	0.02	0.00	0.13	-91.20	-237.24	6.32	2.55	2.46	2.71	31.79	27.96	35.63
723	0.28	0.22	0.37	-16.89	-38.91	5.67	2.37	2.27	2.42	32.28	30.18	34.02
724	0.70	0.70	0.70	11.16	9.53	13.84	4.88	4.81	4.97	0.17	0.00	1.40
725	0.56	0.38	0.65	-31.78	-62.47	-12.43	1.60	1.53	1.69	4.50	0.00	14.85

Table C.2: (continued)

Index	e	-99%	$+99\%$	ϕ_b	-99%	$+99\%$	r_d	-99%	$+99\%$	i	-99%	$+99\%$
726	0.70	0.69	0.70	16.54	15.17	17.81	3.74	3.69	3.78	33.69	31.91	34.60
727	0.57	0.35	0.70	-23.18	-54.29	21.85	1.81	1.75	1.91	30.47	23.12	34.83
728	0.24	0.16	0.49	144.10	83.33	248.31	2.02	1.95	2.11	11.51	2.76	19.22
729	0.06	0.00	0.60	-61.51	-169.90	3.61	1.56	1.44	1.73	30.15	24.20	37.85
730	0.51	0.36	0.65	146.16	112.75	175.56	0.85	0.72	1.01	29.30	16.08	43.16
731	0.66	0.41	0.70	169.06	148.34	189.40	12.13	10.22	12.97	3.35	0.00	19.60
732	0.39	0.16	0.70	113.45	97.76	123.19	3.04	3.00	3.09	21.88	16.42	24.52
733	0.30	0.18	0.38	48.08	29.11	105.39	2.54	2.47	2.60	31.34	29.17	33.03
734	0.24	0.04	0.36	199.33	158.90	229.43	25.21	22.66	25.71	6.23	0.00	48.11
735	0.32	0.08	0.48	123.34	106.70	143.89	1.96	1.86	2.05	33.13	27.97	36.06
736	0.25	0.00	0.52	11.62	-156.89	109.08	1.11	1.05	1.22	8.35	0.00	41.71
737	0.59	0.17	0.70	210.10	138.94	261.47	10.76	5.03	12.41	0.41	0.00	25.85
738	0.60	0.30	0.70	319.07	258.77	360.00	15.93	14.27	16.11	21.09	0.00	57.73
739	0.02	0.00	0.08	66.75	15.33	150.37	4.70	4.64	4.93	12.06	3.54	16.50
740	0.51	0.30	0.70	328.51	216.36	348.63	18.88	17.24	20.30	30.72	22.14	44.10
741	0.28	0.00	0.45	-100.66	-263.45	-3.53	6.47	3.96	9.30	32.69	0.00	68.36
742	0.60	0.12	0.70	38.78	-45.82	127.06	13.81	10.34	22.29	29.50	0.00	73.85
743	0.23	0.00	0.31	-8.82	-165.40	42.22	1.97	1.89	2.10	22.96	15.36	29.98
744	0.27	0.00	0.61	109.74	59.46	260.41	11.27	8.40	14.37	23.60	6.05	64.87
745	0.13	0.00	0.50	79.82	59.64	110.02	1.57	1.52	1.63	29.27	23.16	33.25
746	0.37	0.22	0.60	107.81	82.78	130.15	1.39	1.30	1.50	4.98	0.00	14.48
747	0.10	0.00	0.40	147.82	94.94	200.50	2.63	2.51	2.81	26.50	19.53	33.15
748	0.22	0.00	0.32	92.48	7.73	125.93	1.52	1.45	1.62	29.00	22.97	35.68
749	0.70	0.65	0.70	177.18	165.49	187.63	20.33	18.10	20.53	4.22	0.00	20.97
750	0.70	0.68	0.70	-11.89	-16.35	-8.63	2.80	2.73	2.84	34.85	33.05	36.54

Table C.2: (continued)

Index	e	-99%	$+99\%$	ϕ_b	-99%	$+99\%$	r_d	-99%	$+99\%$	i	-99%	$+99\%$
751	0.02	0.00	0.13	-197.92	-256.51	7.06	5.92	5.32	9.93	0.71	0.00	6.82
752	0.24	0.02	0.51	124.99	88.82	193.19	10.65	6.98	10.85	10.99	0.00	26.59
753	0.03	0.00	0.17	185.20	141.90	235.17	6.76	5.24	8.58	3.47	0.00	16.63
754	0.41	0.27	0.65	173.79	104.77	259.36	1.24	1.18	1.32	8.67	0.00	21.63
755	0.49	0.30	0.61	188.32	167.55	205.67	4.97	4.77	5.46	17.82	0.80	35.39
756	0.70	0.66	0.70	65.85	59.10	69.90	13.78	12.63	14.99	18.94	7.05	35.06
757	0.12	0.00	0.29	-197.98	-331.98	-91.31	2.10	1.85	2.30	25.60	13.42	36.77

Table C.3: Catalog of Objects Studied

Index	ϕ_d	-99%	$+99\%$	χ^2	r_{half}	μ_e	-99%	$+99\%$	$\mu_{0,i}$	-99%	$+99\%$
1	186.37	85.31	312.72	1.05	16.91	22.52	5.24	25.81	25.75	25.50	26.45
2	-2.95	-116.35	65.75	1.12	13.26	17.41	14.01	18.52	25.34	25.04	25.62
3	68.06	9.73	139.19	1.14	2.43	26.13	25.19	27.38	21.08	20.74	21.52
4	145.18	7.28	194.11	1.26	25.23	21.66	20.91	22.79	27.11	26.93	27.59
5	109.38	73.01	132.75	1.33	1.93	26.07	25.47	26.43	19.78	19.56	19.90
6	70.73	14.48	120.16	1.17	4.12	25.25	24.39	26.22	22.23	21.94	22.57
7	123.04	88.24	152.91	1.01	1.95	23.57	21.34	25.11	20.81	20.35	21.28
8	57.66	27.36	83.92	0.85	2.15	25.32	24.16	26.48	20.08	19.79	20.29
9	43.49	32.69	52.17	1.08	5.60	22.64	20.72	23.99	22.23	22.11	22.32
10	-21.82	-27.30	-15.66	1.54	8.66	23.86	23.53	24.21	21.24	21.21	21.27
11	136.72	94.29	200.34	1.11	3.14	19.42	17.49	20.54	21.55	21.44	21.65
12	-49.73	-59.24	-38.84	1.71	4.30	18.59	11.33	20.46	20.39	20.10	21.05
13	125.69	87.65	143.65	1.04	2.60	28.35	27.20	31.87	21.09	20.94	21.28
14	146.13	118.14	176.73	1.17	31.11	21.18	20.47	21.54	26.56	26.38	26.77
15	150.03	127.13	173.57	1.06	1.80	25.34	24.57	26.15	20.10	19.88	20.37
16	-38.34	-75.01	0.58	1.40	2.64	23.69	23.32	24.07	20.93	20.82	21.02
17	325.87	137.13	360.00	1.55	11.84	17.21	12.62	18.31	25.01	24.79	25.21
18	176.12	116.21	197.45	1.03	1.89	24.50	23.28	27.49	20.66	20.37	21.17
19	202.02	182.20	218.21	1.62	3.10	21.62	20.90	22.21	20.62	20.53	20.72
20	158.29	123.38	199.95	0.90	1.60	29.21	28.06	44.21	19.93	19.85	20.11
21	-12.35	-99.81	133.77	1.07	25.98	28.68	27.77	29.47	26.60	26.04	27.14
22	62.83	35.26	113.64	1.25	3.97	16.60	13.22	17.70	22.35	22.22	22.50
23	164.47	149.52	181.21	1.21	3.06	27.14	23.68	35.81	21.57	21.47	21.72
24	1.22	-30.73	47.31	1.26	2.31	26.78	25.75	27.59	20.59	20.24	20.89
25	59.02	34.88	79.27	1.18	2.39	23.53	22.09	24.73	20.23	20.06	20.38

Table C.3: (continued)

Index	ϕ_d	-99%	$+99\%$	χ^2	r_{half}	μ_e	-99%	$+99\%$	$\mu_{0,i}$	-99%	$+99\%$
26	101.28	24.30	128.73	1.96	6.41	25.26	24.44	26.05	21.75	21.46	21.89
27	142.47	64.31	190.12	2.01	22.55	25.20	24.85	25.70	25.82	25.65	26.26
28	322.86	287.47	357.43	1.25	2.98	31.68	30.57	36.33	21.30	21.13	21.51
29	154.33	103.51	189.40	1.18	2.39	27.25	25.87	28.80	20.44	20.31	20.58
30	65.03	46.66	87.16	2.39	3.81	26.97	25.65	31.46	22.02	21.36	23.12
31	196.19	135.13	360.00	1.33	16.85	20.41	16.44	21.52	26.31	26.02	26.53
32	16.86	-1.43	24.57	3.17	1.95	23.59	22.07	39.26	19.50	19.34	20.42
33	164.81	109.43	202.02	1.42	22.41	18.50	16.82	19.58	26.22	26.05	26.33
34	125.03	117.99	132.48	2.11	7.14	19.04	18.03	20.12	22.37	22.30	22.48
35	74.30	-27.86	208.02	0.88	17.66	18.74	13.83	19.85	26.28	26.11	26.51
36	357.34	256.17	360.00	1.20	39.71	29.94	29.31	30.64	26.71	25.99	26.95
37	276.46	240.59	310.27	1.19	2.01	25.77	25.06	26.38	20.28	20.00	20.53
38	183.24	94.98	303.92	1.07	1.91	25.34	23.95	28.29	20.41	20.11	20.80
39	48.39	-26.28	73.59	1.01	1.40	19.40	12.60	20.66	20.76	20.26	21.13
40	338.14	82.70	360.00	2.75	19.81	18.24	8.08	19.38	24.29	24.14	24.48
41	231.27	171.83	356.41	1.35	20.77	26.12	24.58	27.34	25.74	25.37	26.07
42	176.41	138.67	208.47	1.08	1.66	26.18	24.79	29.27	20.25	20.09	20.60
43	65.76	0.37	131.21	1.77	24.28	18.43	16.84	19.50	25.98	25.90	26.08
44	136.88	106.53	168.18	1.05	20.06	28.73	27.42	30.45	25.35	24.91	25.74
45	37.56	19.01	51.74	1.40	3.53	19.94	-4.27	26.66	20.72	20.56	21.08
46	152.03	102.70	201.34	0.91	0.81	-999.00	-999.00	-999.00	25.49	25.32	25.77
47	84.73	0.20	148.81	1.07	13.08	18.83	17.37	19.99	25.01	24.78	25.50
48	281.76	209.99	330.78	1.35	2.60	29.44	28.24	78.40	20.53	20.43	20.72
49	34.75	-24.65	60.64	1.19	1.66	24.26	23.68	24.90	20.34	20.11	20.60
50	150.32	145.17	155.92	2.78	5.03	21.42	14.89	23.37	20.71	20.66	20.78

Table C.3: (continued)

Index	ϕ_d	-99%	$+99\%$	χ^2	r_{half}	μ_e	-99%	$+99\%$	$\mu_{0,i}$	-99%	$+99\%$
51	69.08	23.91	107.50	1.09	2.19	24.10	21.78	25.45	21.21	20.85	21.50
52	42.04	-72.80	64.30	1.48	38.45	24.55	24.24	24.90	26.20	26.06	26.40
53	32.69	8.08	54.33	1.14	3.08	26.04	24.64	27.83	20.54	20.45	20.66
54	117.34	106.22	142.16	3.53	0.85	24.74	24.33	25.25	17.64	17.51	17.75
55	157.17	131.59	211.85	2.23	0.14	29.37	29.16	29.61	13.72	8.92	14.79
56	169.57	132.99	213.01	1.19	2.43	26.59	25.86	27.20	20.45	20.31	20.57
57	88.50	-3.86	138.34	0.93	11.72	18.89	17.08	19.98	25.62	25.42	25.82
58	18.32	-16.27	45.74	1.02	2.01	30.36	28.51	174.20	20.55	20.45	20.78
59	113.30	96.32	125.16	1.21	2.21	24.92	24.41	25.27	19.69	19.54	19.80
60	161.70	123.16	186.87	1.16	2.01	26.65	25.53	27.32	20.58	20.34	20.73
61	64.87	50.38	88.38	0.95	2.76	27.10	25.76	34.69	20.79	20.69	21.05
62	160.80	83.03	263.74	1.10	26.89	26.72	26.18	27.51	26.42	26.22	26.65
63	75.52	-173.08	204.55	1.03	34.27	12.25	-62.25	13.34	26.20	25.99	26.40
64	138.47	124.43	152.56	1.13	1.78	18.98	16.90	20.43	19.73	19.55	19.90
65	34.54	-16.67	72.36	1.81	4.52	25.95	25.45	26.43	20.21	20.14	20.26
66	137.37	111.78	154.02	1.22	2.21	24.35	23.59	24.64	19.64	19.47	19.73
67	173.82	155.93	189.75	1.29	2.03	25.97	25.53	26.51	20.11	19.98	20.28
68	85.28	60.29	110.91	1.13	3.89	25.43	24.50	26.22	21.74	21.46	21.93
69	-338.30	-360.00	-235.80	1.31	32.08	23.76	22.47	24.56	25.99	25.84	26.26
70	4.11	-153.86	82.30	1.02	4.48	25.18	23.82	26.58	22.78	22.50	23.08
71	-299.48	-360.00	-239.25	1.22	20.54	23.45	22.87	23.88	26.11	25.90	26.32
72	104.06	79.84	127.15	1.21	1.70	24.82	23.42	30.97	20.21	20.10	20.59
73	-284.80	-360.00	-66.43	1.16	20.32	23.52	22.92	24.11	26.58	26.47	26.75
74	-156.86	-182.25	-34.78	2.32	24.28	16.17	14.24	17.43	24.46	24.23	24.89
75	-329.02	-360.00	-60.61	1.39	0.81	-999.00	-999.00	-999.00	25.39	25.35	25.51

Table C.3: (continued)

Index	ϕ_d	-99%	$+99\%$	χ^2	r_{half}	μ_e	-99%	$+99\%$	$\mu_{0,i}$	-99%	$+99\%$
76	173.48	142.14	201.91	1.26	2.15	25.26	23.79	26.40	20.64	20.41	20.81
77	31.56	-18.57	87.18	0.94	1.70	22.57	17.43	25.97	20.24	20.06	20.46
78	100.18	77.39	116.43	1.25	1.74	19.65	18.38	20.77	20.98	20.78	21.17
79	-23.40	-65.68	25.43	1.45	0.30	25.52	24.79	25.87	15.67	13.46	16.74
80	-15.12	-48.82	28.79	1.46	16.49	19.27	18.04	20.35	25.59	25.50	25.68
81	146.34	84.35	268.89	1.10	12.27	17.92	15.36	19.06	25.48	25.19	25.82
82	-31.99	-68.35	12.05	1.27	1.72	28.17	26.63	48.54	20.26	20.16	20.43
83	20.14	17.81	23.11	1.78	4.56	19.92	19.79	20.10	20.09	20.07	20.11
84	99.86	85.57	109.54	1.13	1.46	26.53	26.09	27.27	19.23	19.07	19.40
85	148.36	27.78	181.06	2.05	2.17	28.75	27.62	32.47	20.57	19.90	21.04
86	224.03	123.03	260.38	1.31	2.01	26.36	25.19	28.99	20.38	20.21	20.67
87	187.65	172.58	214.20	1.30	2.78	22.96	22.58	23.32	21.01	20.88	21.12
88	187.32	147.54	226.63	0.98	16.57	23.04	21.03	24.27	26.42	26.22	26.84
89	-18.18	-50.89	15.45	2.22	29.83	25.60	25.03	26.37	26.27	26.14	26.57
90	210.29	181.27	235.43	0.92	1.83	25.37	23.90	27.22	20.55	20.34	20.78
91	335.91	303.87	354.97	4.23	0.30	29.81	28.80	31.34	14.82	13.53	15.89
92	-282.34	-360.00	89.27	1.22	17.08	15.10	0.50	16.19	26.19	26.02	26.35
93	204.63	197.61	211.16	1.75	6.87	20.22	19.67	21.30	21.48	21.46	21.51
94	86.54	80.59	93.10	1.43	2.31	27.97	26.85	53.64	19.62	19.59	19.70
95	333.98	236.13	360.00	1.81	0.28	28.12	27.94	28.39	14.87	14.17	15.90
96	117.65	100.54	140.49	1.05	2.17	26.28	24.68	41.53	20.61	20.51	20.88
97	165.15	153.22	178.10	3.86	5.78	17.16	14.99	18.24	19.93	19.90	19.95
98	257.82	183.19	302.60	1.26	0.14	26.97	25.79	29.81	14.65	11.03	15.73
99	125.13	100.94	145.78	1.05	2.03	25.43	24.17	27.33	20.17	19.99	20.44
100	306.58	263.19	338.62	1.11	1.28	23.14	20.78	25.49	19.66	19.49	19.84

Table C.3: (continued)

Index	ϕ_d	-99%	$+99\%$	χ^2	r_{half}	μ_e	-99%	$+99\%$	$\mu_{0,i}$	-99%	$+99\%$
101	109.86	9.00	164.20	1.22	18.92	17.33	14.30	18.47	25.77	25.50	26.20
102	169.03	155.78	185.56	1.54	1.28	23.85	22.97	24.80	18.32	18.21	18.48
103	237.50	183.84	298.12	1.28	19.47	17.33	12.43	18.42	25.41	25.17	25.57
104	26.06	-34.30	108.74	1.99	18.09	18.92	17.75	20.15	26.12	25.97	26.69
105	246.08	181.84	273.95	0.95	1.50	22.67	21.10	26.96	19.97	19.74	20.31
106	134.35	91.76	157.95	1.32	2.37	27.31	24.52	45.03	20.11	20.04	20.29
107	155.80	153.79	157.27	2.30	6.92	19.64	19.00	20.72	20.50	20.49	20.51
108	-137.10	-192.23	-24.47	1.56	22.53	19.90	9.37	21.16	25.81	25.58	25.95
109	288.52	194.30	332.82	1.19	36.24	28.42	27.75	29.10	26.60	26.51	26.83
110	-59.53	-103.51	48.93	1.14	26.45	23.27	20.75	24.42	26.18	25.99	26.41
111	-42.45	-172.04	45.56	1.62	17.01	17.73	14.49	18.81	24.92	24.86	25.05
112	125.01	112.31	137.85	1.30	1.76	24.98	23.81	26.04	18.92	18.80	19.01
113	-293.95	-360.00	-276.21	8.62	0.73	23.33	22.03	26.77	16.23	15.79	16.62
114	-86.28	-127.48	-24.23	2.37	0.41	26.18	24.95	26.82	15.71	14.56	16.79
115	166.74	124.55	190.08	1.93	4.99	21.50	21.19	21.81	19.85	19.82	19.87
116	59.03	39.95	70.60	1.44	1.38	23.27	22.66	23.78	18.95	18.80	19.07
117	-326.45	-360.00	-189.96	1.34	27.46	21.00	14.92	22.23	25.25	25.03	25.33
118	54.11	10.97	81.74	1.01	17.44	25.30	24.83	25.70	26.34	26.02	26.54
119	193.60	160.03	225.35	1.07	1.83	25.03	23.54	26.75	20.41	20.25	20.64
120	60.68	15.02	106.75	1.86	27.84	16.25	13.68	17.33	24.37	24.10	24.51
121	55.51	30.91	226.94	1.20	45.77	12.49	-19.96	13.58	25.64	25.24	25.83
122	269.94	101.65	340.37	1.53	32.00	23.69	23.28	24.02	26.89	26.65	27.15
123	141.59	137.21	145.21	1.96	5.03	20.18	20.02	20.32	20.81	20.79	20.83
124	110.47	80.01	132.80	1.18	2.03	28.30	27.18	30.67	20.37	20.25	20.56
125	-6.19	-122.75	88.46	1.15	22.06	23.49	22.72	24.18	26.61	26.54	26.82

Table C.3: (continued)

Index	ϕ_d	-99%	$+99\%$	χ^2	r_{half}	μ_e	-99%	$+99\%$	$\mu_{0,i}$	-99%	$+99\%$
126	53.27	-20.47	141.81	1.24	18.62	24.84	24.24	25.51	26.30	25.92	26.66
127	199.18	171.44	217.41	1.23	2.45	17.47	15.51	18.54	21.17	21.11	21.21
128	-184.01	-234.06	-48.40	2.63	0.18	27.84	27.24	28.31	13.68	11.85	14.76
129	-119.21	-211.54	43.33	1.29	17.54	18.11	16.14	19.22	25.96	25.56	26.35
130	148.52	102.64	221.99	1.29	21.76	18.80	16.85	19.89	25.13	25.07	25.28
131	124.92	73.28	215.63	1.25	0.06	28.32	27.84	28.71	11.82	6.93	12.90
132	81.22	54.23	105.89	1.62	1.46	30.40	29.31	34.56	19.83	19.74	19.98
133	-189.08	-253.73	-83.45	1.00	18.60	24.86	22.96	26.32	25.50	24.99	26.00
134	180.12	160.17	195.38	1.25	2.98	27.80	26.66	37.95	20.92	20.83	21.10
135	177.72	158.84	200.49	1.15	1.70	28.30	26.47	39.40	19.46	19.39	19.60
136	-341.33	-360.00	-226.34	1.25	23.46	14.70	-0.16	15.77	24.93	24.70	25.04
137	26.03	14.73	42.54	1.13	3.41	24.55	24.08	24.87	21.30	21.15	21.41
138	42.66	16.27	140.15	1.09	2.64	25.68	23.84	26.95	21.32	20.98	21.59
139	88.20	-130.51	144.57	1.11	17.22	18.44	16.31	19.54	25.21	25.04	25.43
140	-208.44	-360.00	110.38	3.03	16.39	16.58	9.87	17.65	25.88	25.79	26.00
141	-174.22	-261.81	-131.53	1.49	0.34	26.82	26.18	27.44	16.13	14.98	17.20
142	104.62	98.17	108.88	1.16	4.06	20.27	19.90	20.46	21.17	21.12	21.23
143	42.25	1.97	91.43	0.99	2.74	27.85	26.75	29.29	20.76	20.55	20.99
144	205.37	132.47	243.95	3.34	27.34	16.77	15.25	17.93	24.64	24.60	24.98
145	111.29	103.23	122.76	1.21	3.37	23.18	22.68	23.56	20.53	20.46	20.60
146	350.36	287.45	360.00	1.67	31.98	26.58	24.75	27.58	27.09	26.91	27.56
147	196.35	160.81	257.18	1.17	1.80	25.40	24.21	26.75	20.23	19.96	20.55
148	127.50	39.38	222.96	1.02	13.43	19.04	17.73	20.13	25.44	25.28	25.70
149	243.18	191.47	284.91	1.52	16.77	21.28	20.91	21.86	25.40	25.23	25.74
150	32.31	4.55	53.99	1.52	5.98	25.93	25.10	27.49	22.07	21.92	22.25

Table C.3: (continued)

Index	ϕ_d	-99%	$+99\%$	χ^2	r_{half}	μ_e	-99%	$+99\%$	$\mu_{0,i}$	-99%	$+99\%$
151	-264.94	-360.00	-185.28	1.23	24.78	24.55	24.17	24.93	26.59	26.45	26.71
152	-95.60	-149.24	-36.29	4.06	0.16	29.50	28.27	32.73	13.34	9.92	14.41
153	67.45	49.09	98.50	1.05	2.98	25.92	24.67	27.34	21.06	20.72	21.36
154	122.35	46.63	192.60	1.67	30.18	28.82	28.29	29.26	25.37	25.02	25.55
155	173.05	127.33	201.17	0.99	4.20	24.82	24.08	25.33	21.39	21.28	21.50
156	136.64	129.89	145.91	0.97	6.35	19.99	18.36	21.16	21.87	21.80	21.94
157	-251.42	-360.00	-41.44	1.56	0.08	28.70	28.22	29.25	12.08	9.40	13.16
158	94.31	75.41	108.90	1.18	2.31	25.19	24.14	25.62	20.03	19.90	20.16
159	150.92	113.21	257.77	0.91	1.74	23.60	20.81	26.04	20.28	20.07	20.53
160	-33.28	-53.95	36.51	1.57	0.08	26.76	26.41	27.08	12.67	-0.27	13.74
161	170.89	158.62	184.98	1.20	6.17	22.83	21.48	23.83	21.89	21.82	21.99
162	259.06	212.05	296.13	1.06	2.05	23.73	22.40	25.96	20.66	20.42	20.90
163	50.13	30.26	83.78	1.03	2.37	25.90	24.56	26.91	20.65	20.37	20.88
164	23.43	4.38	91.16	1.30	4.28	25.42	24.65	25.88	21.65	21.44	21.79
165	150.68	110.11	195.82	1.24	3.81	24.00	23.20	24.60	21.46	21.27	21.61
166	62.65	18.45	120.46	1.52	13.53	17.14	14.16	18.26	25.25	24.84	25.69
167	37.28	-19.11	179.11	1.55	17.54	22.32	21.98	22.87	25.45	25.38	25.90
168	45.52	-8.94	108.51	1.11	2.15	25.85	24.60	28.37	20.64	20.43	21.05
169	153.33	72.66	213.02	1.13	16.55	18.36	16.57	19.43	25.81	25.69	26.01
170	-346.57	-360.00	-144.51	2.10	17.87	19.27	17.43	20.34	25.99	25.90	26.09
171	26.47	-18.09	59.06	1.10	2.33	26.85	25.53	28.14	20.55	20.37	20.74
172	30.44	17.49	40.14	1.86	4.40	23.74	23.40	24.28	20.90	20.83	21.02
173	58.29	-32.34	176.82	1.58	31.23	17.15	14.82	18.29	26.06	26.00	26.34
174	2.84	-8.42	11.24	1.08	5.80	27.03	24.84	30.75	22.00	21.90	22.15
175	89.72	80.04	98.19	1.91	2.90	26.34	25.84	26.74	19.53	19.45	19.58

Table C.3: (continued)

Index	ϕ_d	-99%	$+99\%$	χ^2	r_{half}	μ_e	-99%	$+99\%$	$\mu_{0,i}$	-99%	$+99\%$
176	120.24	70.98	284.26	1.04	20.81	26.20	25.52	26.94	25.89	25.72	26.26
177	114.03	61.82	147.67	1.20	18.54	18.26	15.76	19.35	26.27	26.18	26.56
178	190.89	88.47	252.45	0.86	15.43	18.55	16.48	19.64	25.99	25.82	26.34
179	-18.91	-81.70	25.50	1.20	24.25	26.43	25.56	27.17	26.22	25.91	26.44
180	3.92	-5.62	10.11	2.61	7.52	25.41	24.09	26.75	21.78	21.73	21.85
181	7.54	-63.15	119.44	0.86	22.73	21.83	16.85	23.21	25.87	25.55	26.31
182	169.26	146.53	186.80	1.22	1.97	24.77	23.56	27.75	19.31	19.21	19.48
183	75.04	47.36	95.89	0.92	3.24	26.60	25.34	33.79	21.63	21.46	21.82
184	1.45	-60.14	99.74	3.60	29.97	21.18	18.28	21.90	25.50	25.31	25.84
185	202.87	162.67	258.24	1.03	13.26	21.32	20.77	21.96	24.84	24.38	25.16
186	25.64	12.04	44.01	1.22	2.98	24.92	24.28	25.19	20.47	20.35	20.56
187	288.57	173.48	360.00	1.08	0.28	30.14	29.56	30.60	15.29	12.84	16.38
188	265.46	93.36	360.00	1.80	0.43	30.77	30.47	31.05	16.03	15.69	16.69
189	22.61	7.60	41.88	1.17	3.18	24.49	23.78	25.16	20.89	20.72	21.01
190	1.27	-15.32	24.73	0.78	2.51	25.26	23.95	26.35	20.77	20.48	21.04
191	249.73	138.63	360.00	2.00	0.65	30.32	29.95	30.61	16.48	16.26	17.14
192	88.83	36.41	115.78	0.92	2.68	19.23	13.35	21.26	20.62	20.51	20.78
193	76.09	71.44	83.11	1.61	3.69	19.15	19.04	19.21	21.08	21.06	21.12
194	58.42	55.51	61.02	1.45	4.24	23.23	22.69	23.62	19.86	19.81	19.91
195	127.06	115.52	137.41	1.18	4.28	25.67	25.14	26.11	20.53	20.45	20.60
196	-44.59	-66.16	-20.86	1.28	2.15	18.55	17.01	19.65	20.01	19.93	20.09
197	-74.43	-360.00	34.14	0.90	0.81	-999.00	-999.00	-999.00	25.62	25.40	25.92
198	33.96	20.50	48.34	0.89	3.71	26.29	25.07	27.51	19.82	19.77	19.87
199	-59.42	-170.33	59.68	2.97	26.63	17.36	15.22	18.58	25.88	25.75	26.31
200	-4.22	-86.36	32.21	1.44	3.24	21.92	21.23	22.58	21.43	21.32	21.55

Table C.3: (continued)

Index	ϕ_d	-99%	$+99\%$	χ^2	r_{half}	μ_e	-99%	$+99\%$	$\mu_{0,i}$	-99%	$+99\%$
201	313.96	76.91	360.00	2.24	20.89	15.92	9.44	17.08	26.04	25.89	26.63
202	140.49	34.02	188.90	1.23	1.99	28.23	27.08	34.88	20.35	20.28	20.51
203	108.94	73.26	172.87	1.25	2.58	26.44	24.77	31.85	20.68	20.59	20.84
204	29.36	-14.82	71.41	2.22	0.06	27.72	27.30	28.10	10.71	-8.20	11.78
205	76.40	66.60	83.80	1.15	4.12	23.61	21.98	24.81	20.93	20.85	21.09
206	255.96	124.99	360.00	1.56	16.00	22.98	22.06	24.00	25.29	24.70	25.82
207	190.77	135.42	360.00	1.07	19.08	26.10	25.10	26.93	25.88	25.63	26.25
208	149.75	128.60	165.61	1.08	1.83	25.95	25.09	26.84	20.11	19.89	20.31
209	57.76	19.64	80.88	0.94	2.90	23.88	22.37	25.60	21.37	21.15	21.65
210	150.02	20.48	228.47	1.79	0.26	28.60	28.10	29.09	15.67	13.35	16.75
211	-46.28	-59.45	-33.89	1.73	3.18	23.25	23.02	23.46	19.93	19.88	19.98
212	-213.50	-336.63	-44.14	1.36	15.47	21.95	12.26	24.32	25.47	25.19	26.21
213	124.22	83.62	160.77	0.97	3.08	25.41	24.17	28.18	21.72	21.39	22.30
214	134.08	35.81	183.58	0.94	3.06	27.23	26.00	29.72	21.51	21.34	21.77
215	-308.13	-360.00	-152.56	0.73	13.55	15.60	7.29	16.71	25.08	24.59	25.37
216	260.40	196.22	322.00	1.27	22.79	25.46	24.82	26.05	26.43	26.26	26.85
217	239.51	217.53	245.23	5.15	24.72	13.39	5.59	14.75	23.03	22.90	23.35
218	36.31	4.44	74.28	1.29	4.06	25.61	23.79	26.72	22.04	21.71	22.32
219	31.78	14.47	49.14	1.39	2.47	32.27	31.18	169.22	19.81	19.78	19.89
220	31.90	-27.67	70.24	7.68	0.55	28.81	28.56	29.04	14.46	13.68	15.53
221	106.01	96.18	117.56	1.18	2.35	25.79	24.81	26.47	19.89	19.71	20.02
222	15.17	-0.92	29.21	1.00	1.99	28.18	26.51	56.11	20.04	19.96	20.29
223	66.94	-23.45	149.25	1.54	14.05	18.14	16.25	19.26	25.00	24.82	25.26
224	151.13	56.81	179.59	1.78	30.48	19.97	18.69	20.40	26.39	26.08	26.82
225	45.62	10.81	92.36	1.00	2.90	22.96	22.07	23.72	21.03	20.92	21.16

Table C.3: (continued)

Index	ϕ_d	-99%	$+99\%$	χ^2	r_{half}	μ_e	-99%	$+99\%$	$\mu_{0,i}$	-99%	$+99\%$
226	49.15	33.04	61.50	2.24	4.34	21.03	17.67	22.59	20.79	20.63	21.03
227	30.57	19.22	40.44	1.83	1.52	17.72	9.04	20.05	20.12	19.66	20.65
228	19.50	-16.46	55.88	2.03	2.23	26.37	25.72	26.89	19.97	19.77	20.15
229	94.04	76.46	108.34	1.10	4.06	20.90	20.42	21.29	22.29	22.20	22.40
230	116.49	59.02	181.49	1.15	4.36	27.81	26.34	31.92	21.46	21.27	21.74
231	-21.22	-71.34	24.82	0.96	2.37	23.44	21.91	24.52	21.06	20.84	21.25
232	40.27	15.31	69.53	0.96	2.15	26.45	25.17	29.00	20.85	20.66	21.14
233	7.54	-6.98	23.17	1.17	3.43	30.13	28.71	80.50	21.30	21.22	21.47
234	188.34	161.66	223.08	1.11	1.91	24.64	22.33	39.45	19.54	19.48	19.64
235	350.82	223.00	360.00	1.09	18.37	25.43	24.53	25.95	26.21	26.01	26.48
236	83.92	19.41	99.53	1.70	3.37	25.61	25.43	26.02	19.86	19.81	19.95
237	160.90	149.91	170.97	1.40	2.33	30.13	28.44	72.39	20.39	20.32	20.52
238	146.04	103.00	200.88	1.58	16.93	18.53	16.66	19.61	25.36	25.24	25.67
239	222.75	173.78	295.15	0.85	2.58	24.96	24.37	25.75	20.67	20.43	20.96
240	79.33	38.83	163.77	1.52	0.06	28.39	27.89	29.02	11.45	-6.46	12.53
241	92.23	16.44	168.22	0.99	2.54	27.83	26.63	29.92	21.06	20.83	21.32
242	62.44	33.75	82.59	1.41	1.72	24.60	24.06	25.64	19.99	19.79	20.37
243	14.62	-28.96	37.31	0.94	3.87	24.72	22.27	26.33	21.99	21.74	22.27
244	216.43	163.84	270.16	1.52	27.18	25.54	24.91	26.11	26.00	25.74	26.32
245	173.35	132.36	292.90	1.15	16.73	25.64	25.20	26.31	25.51	25.23	25.89
246	-55.12	-92.86	-25.23	1.84	24.52	18.15	16.57	19.22	26.06	25.93	26.17
247	37.85	12.01	50.38	1.19	3.00	26.39	25.55	27.18	20.95	20.76	21.12
248	-72.24	-115.70	-8.43	1.20	3.10	26.32	25.20	26.97	21.19	20.89	21.40
249	87.36	70.95	98.95	1.18	3.08	28.67	27.06	63.35	21.09	21.03	21.26
250	-123.50	-227.19	-43.66	3.61	0.10	26.30	25.58	26.80	12.40	5.38	13.47

Table C.3: (continued)

Index	ϕ_d	-99%	$+99\%$	χ^2	r_{half}	μ_e	-99%	$+99\%$	$\mu_{0,i}$	-99%	$+99\%$
251	150.42	111.16	175.77	1.28	3.77	25.57	24.97	26.21	21.47	21.29	21.63
252	40.88	-10.32	133.44	1.41	16.59	22.64	20.98	23.46	25.62	25.29	25.95
253	287.54	205.00	360.00	1.53	0.06	25.20	23.77	26.57	12.61	-0.16	13.70
254	96.06	80.26	110.74	1.11	2.88	26.06	24.67	28.92	21.23	21.07	21.50
255	73.70	-38.58	161.97	1.52	0.18	26.51	25.69	27.25	14.68	11.14	15.75
256	77.27	60.00	102.48	1.20	2.94	26.37	25.92	26.85	20.51	20.36	20.66
257	28.28	4.30	52.54	1.19	2.56	24.59	23.95	25.17	20.06	19.93	20.17
258	-1.42	-43.18	40.20	1.10	20.60	16.85	10.27	18.05	25.77	25.50	26.26
259	158.95	144.85	172.11	1.12	3.73	29.06	27.96	38.01	21.07	20.89	21.28
260	-305.34	-360.00	-270.68	5.28	15.23	15.71	11.42	16.81	24.45	24.36	24.67
261	117.54	100.95	128.84	2.49	3.89	22.19	20.68	22.88	19.90	19.85	20.03
262	72.08	24.05	88.11	6.91	0.34	29.79	28.84	33.47	15.14	14.14	16.21
263	142.57	108.66	161.79	1.37	22.65	20.88	20.49	21.24	25.82	25.62	26.04
264	114.38	99.77	123.95	1.16	1.56	30.00	28.89	73.19	19.59	19.54	19.71
265	4.09	-8.67	19.25	1.62	6.96	25.30	25.05	25.51	22.49	22.40	22.56
266	159.49	147.90	167.72	1.13	3.33	26.13	25.10	26.86	20.36	20.20	20.45
267	-167.71	-296.52	0.16	1.05	4.02	27.53	26.34	28.45	21.87	21.38	22.21
268	-28.34	-37.39	2.99	1.75	8.09	24.62	24.09	25.31	21.05	20.80	21.16
269	18.51	-29.59	127.40	1.86	25.27	24.73	24.27	25.27	25.51	25.41	25.79
270	248.28	217.42	294.08	1.73	12.27	19.88	19.41	20.31	23.57	23.49	23.92
271	-12.66	-103.33	14.71	1.24	21.96	20.39	10.44	21.90	25.89	25.63	26.24
272	69.78	-51.47	111.32	0.77	2.66	30.73	29.59	45.14	21.05	20.93	21.27
273	30.10	-5.34	105.78	1.28	24.40	24.41	23.93	24.78	26.26	26.04	26.44
274	173.49	169.63	178.15	1.60	7.61	20.37	18.62	21.53	21.65	21.62	21.68
275	30.21	-18.60	52.97	2.33	9.90	29.28	29.06	29.63	22.11	21.94	22.20

Table C.3: (continued)

Index	ϕ_d	-99%	$+99\%$	χ^2	r_{half}	μ_e	-99%	$+99\%$	$\mu_{0,i}$	-99%	$+99\%$
276	186.09	141.77	231.40	1.51	3.02	28.24	27.13	30.74	20.79	20.53	21.04
277	29.26	22.38	32.10	2.26	10.06	20.33	20.20	20.39	20.43	20.39	20.47
278	309.00	144.48	360.00	1.49	33.64	11.54	-25.97	12.79	24.60	23.92	25.14
279	89.40	65.62	115.52	1.85	3.02	25.37	25.11	25.65	21.13	21.03	21.23
280	348.18	264.87	360.00	6.10	0.12	28.22	27.11	32.03	13.01	7.71	14.14
281	151.99	86.44	200.97	1.09	0.32	30.83	29.70	32.70	16.28	14.91	17.36
282	-74.69	-175.29	50.15	1.63	0.14	28.06	26.91	30.54	14.59	10.52	15.67
283	248.38	231.40	269.64	5.43	0.43	30.17	29.09	32.52	15.49	14.86	16.56
284	170.79	158.10	208.85	1.39	1.70	27.51	26.40	28.52	19.78	19.41	20.10
285	188.29	123.74	246.74	1.52	8.36	25.57	25.15	26.01	22.03	21.95	22.12
286	81.43	65.83	85.71	4.18	5.07	24.60	24.20	24.99	19.91	19.85	19.94
287	86.62	56.07	113.94	1.23	4.89	24.92	24.58	25.28	21.06	20.97	21.17
288	105.02	52.97	161.18	1.10	4.73	24.08	23.79	24.36	21.07	21.01	21.14
289	-2.95	-22.79	13.68	1.34	2.23	27.73	26.54	54.00	20.25	20.18	20.48
290	0.66	-22.67	28.85	1.11	2.35	25.34	24.71	25.97	19.80	19.61	19.95
291	166.62	154.60	178.58	1.02	1.97	25.82	24.70	27.46	19.69	19.60	19.83
292	137.52	132.77	140.68	1.49	5.78	21.84	21.18	22.34	20.81	20.76	20.91
293	132.66	124.11	138.26	1.43	5.68	22.51	22.27	22.73	20.79	20.76	20.83
294	76.52	48.93	92.86	1.08	2.41	28.50	27.15	32.98	20.99	20.85	21.18
295	-287.35	-360.00	-163.11	1.45	18.41	23.63	23.07	24.16	25.50	25.23	25.77
296	12.45	-35.56	98.75	1.55	21.19	24.40	23.83	25.17	25.50	25.30	25.85
297	51.95	-26.57	112.37	1.05	13.63	17.60	8.49	18.80	25.84	25.48	26.39
298	-6.87	-34.99	16.82	1.09	2.07	25.71	24.48	26.91	20.67	20.46	20.86
299	9.20	-21.92	98.74	0.98	2.01	28.79	27.68	37.39	20.64	20.46	20.85
300	-19.04	-21.93	-16.31	1.94	6.75	23.52	23.32	23.64	20.06	20.05	20.08

Table C.3: (continued)

Index	ϕ_d	-99%	$+99\%$	χ^2	r_{half}	μ_e	-99%	$+99\%$	$\mu_{0,i}$	-99%	$+99\%$
301	-244.12	-360.00	-22.71	1.05	17.32	21.13	19.77	22.21	26.12	25.95	26.28
302	169.38	154.69	179.58	1.32	4.66	23.75	23.23	24.16	20.48	20.42	20.54
303	128.01	109.01	191.58	1.56	4.75	24.27	23.84	24.73	20.52	20.42	20.60
304	251.88	114.25	360.00	1.19	0.37	29.20	28.52	29.78	16.38	14.61	17.48
305	134.83	116.96	149.83	2.82	7.44	18.96	18.80	19.06	22.17	22.10	22.26
306	147.92	45.83	237.58	0.85	18.23	22.98	21.93	23.69	26.62	26.46	27.02
307	331.66	216.28	360.00	1.19	19.14	18.99	17.40	20.19	26.38	26.31	26.92
308	45.54	-109.28	123.54	0.99	14.20	21.73	-12.74	25.67	25.59	25.48	26.77
309	170.04	104.42	253.04	1.43	31.60	26.33	25.83	27.19	26.46	26.29	26.73
310	-274.50	-360.00	-127.66	1.44	17.24	21.13	19.78	21.78	25.73	25.55	25.99
311	182.60	36.45	265.34	1.27	0.53	30.59	30.02	31.21	16.92	16.11	18.01
312	150.68	124.46	208.10	1.19	2.15	23.73	22.99	24.53	19.58	19.43	19.71
313	182.06	129.09	240.67	1.22	1.80	24.84	24.15	25.57	19.77	19.54	20.01
314	104.23	92.91	114.69	1.43	32.61	23.07	22.87	23.29	25.50	25.41	25.59
315	191.81	152.57	217.74	0.82	1.83	26.50	24.73	29.91	20.30	20.21	20.47
316	45.48	-126.70	132.37	0.97	18.70	22.82	22.08	23.47	26.39	26.24	26.72
317	336.94	234.49	360.00	1.63	22.71	24.24	23.73	24.56	25.90	25.74	26.17
318	63.72	53.06	73.48	1.25	4.87	24.96	22.41	27.12	21.16	21.10	21.26
319	-202.56	-360.00	12.71	1.70	12.70	18.39	16.12	19.46	25.09	24.89	25.20
320	171.79	142.30	212.33	1.02	2.03	24.22	22.22	25.13	20.93	20.59	21.19
321	-204.92	-360.00	-93.49	1.25	18.43	23.26	22.61	24.08	26.07	25.96	26.58
322	37.23	-1.23	87.15	0.97	2.35	23.99	21.12	27.56	20.90	20.62	21.33
323	7.62	-5.31	24.52	0.91	2.51	23.63	20.83	27.30	20.29	20.20	20.43
324	56.89	4.29	71.32	2.64	25.05	21.85	21.28	22.14	25.32	25.09	25.48
325	231.69	179.90	269.73	1.00	2.01	25.76	24.64	27.12	20.58	20.16	20.86

Table C.3: (continued)

Index	ϕ_d	-99%	$+99\%$	χ^2	r_{half}	μ_e	-99%	$+99\%$	$\mu_{0,i}$	-99%	$+99\%$
326	46.34	32.37	62.92	1.17	4.60	26.33	25.07	27.14	21.18	21.10	21.26
327	43.23	-3.72	100.27	0.94	2.64	27.63	26.28	44.71	20.43	20.35	20.57
328	128.23	74.09	166.58	1.50	2.07	23.80	22.23	25.94	20.76	20.44	21.13
329	122.94	76.78	224.27	0.96	1.50	24.12	21.21	27.60	19.62	19.44	20.01
330	193.92	177.94	201.85	1.00	3.53	22.29	20.33	23.62	20.71	20.62	20.81
331	-45.04	-206.31	26.24	2.20	0.39	33.98	32.88	43.35	16.37	15.50	17.44
332	229.64	92.89	297.84	1.15	4.48	23.59	21.65	25.05	22.45	22.26	22.67
333	-208.55	-360.00	-8.05	1.10	0.79	29.85	29.02	30.47	18.25	17.91	18.75
334	35.28	-17.08	91.18	1.08	1.85	24.58	23.34	27.98	20.47	20.16	20.85
335	125.42	71.20	297.71	1.42	17.99	15.59	6.49	16.70	26.09	26.01	26.47
336	42.30	14.08	71.74	1.53	3.12	29.51	28.16	34.94	21.27	21.03	21.60
337	130.59	99.34	160.45	1.93	0.30	26.40	25.57	27.01	15.14	13.63	16.21
338	227.49	86.75	302.12	1.28	19.37	17.37	13.18	18.46	26.64	26.61	26.82
339	-218.05	-360.00	-111.90	1.03	0.81	-999.00	-999.00	-999.00	26.00	25.63	26.43
340	39.76	-85.61	115.23	1.06	2.37	27.04	25.82	31.26	20.61	20.48	20.87
341	-14.63	-32.11	6.48	1.17	2.15	24.62	23.97	25.05	19.42	19.29	19.54
342	124.72	-14.84	181.82	1.05	19.65	22.51	21.73	23.60	25.92	25.72	26.31
343	253.21	159.84	329.31	1.12	2.17	18.33	16.96	19.43	20.14	20.04	20.24
344	103.09	62.13	140.27	1.00	2.66	26.45	25.57	27.05	20.57	20.31	20.75
345	85.78	64.06	137.50	1.04	3.39	27.20	26.27	27.88	21.37	20.99	21.62
346	210.08	127.92	244.09	0.95	7.14	26.12	25.30	26.86	22.24	22.11	22.39
347	109.94	100.61	116.11	1.21	7.56	16.13	12.54	17.20	21.68	21.60	21.71
348	32.63	-86.66	96.30	2.62	3.24	33.75	32.47	201.80	21.06	20.84	21.37
349	151.28	132.49	167.33	1.02	2.90	30.89	29.77	44.20	21.08	20.99	21.21
350	40.89	3.79	65.16	8.33	4.36	27.45	26.74	30.18	20.37	19.97	21.00

Table C.3: (continued)

Index	ϕ_d	-99%	$+99\%$	χ^2	r_{half}	μ_e	-99%	$+99\%$	$\mu_{0,i}$	-99%	$+99\%$
351	-35.46	-227.96	37.54	1.25	23.46	23.41	22.96	23.83	25.69	25.54	25.82
352	35.71	-4.45	169.80	1.10	22.94	25.76	25.11	26.39	26.07	25.85	26.31
353	6.89	-4.39	16.50	1.30	4.34	19.79	19.17	20.00	20.99	20.93	21.06
354	193.53	148.81	211.25	1.28	2.23	26.82	25.54	28.00	20.69	20.39	20.95
355	185.16	110.40	216.13	0.94	3.39	19.34	17.65	20.46	21.29	21.19	21.38
356	-64.86	-232.21	90.57	1.05	17.93	17.96	15.41	19.05	25.61	25.48	25.86
357	18.56	-76.97	70.80	1.14	2.15	26.19	24.75	27.34	20.59	20.17	20.92
358	157.66	71.64	218.08	1.33	0.53	31.48	30.35	32.79	17.35	16.59	18.47
359	45.66	21.72	97.83	2.12	6.75	26.05	25.28	26.95	20.92	20.89	20.95
360	120.08	49.81	254.35	0.92	6.73	27.52	26.37	29.20	23.40	22.98	23.87
361	261.37	136.99	360.00	0.95	14.87	18.19	16.01	19.29	25.25	25.09	25.48
362	35.33	32.48	38.20	7.71	13.06	24.05	23.97	24.12	19.88	19.86	19.90
363	130.47	95.27	151.57	1.00	4.14	20.73	14.93	22.57	22.68	22.44	23.05
364	150.38	140.22	160.24	1.61	3.49	22.86	22.51	23.18	20.13	20.06	20.18
365	-354.55	-360.00	-331.14	1.76	0.20	28.32	27.51	29.01	13.80	10.37	14.89
366	31.54	-2.89	49.18	1.10	1.91	24.81	23.32	29.27	19.83	19.74	20.06
367	68.28	4.70	144.49	0.98	4.22	29.41	28.24	47.32	22.13	21.98	22.36
368	44.49	-43.14	94.09	1.29	13.49	17.42	13.43	18.52	25.76	25.28	26.11
369	137.91	97.65	152.81	1.64	32.79	15.19	11.38	16.32	25.23	24.83	25.60
370	22.05	-110.44	60.37	5.67	37.74	21.78	19.67	22.63	25.36	25.01	25.69
371	58.54	-55.46	96.03	0.97	2.60	26.00	24.62	27.09	20.79	20.62	20.98
372	44.20	39.37	49.51	1.51	3.73	26.25	25.16	27.60	19.61	19.56	19.66
373	173.13	157.19	188.22	4.36	3.43	23.40	21.62	24.72	21.32	20.82	21.56
374	163.29	142.97	178.25	0.96	2.01	21.68	18.14	24.22	20.29	20.11	20.56
375	32.57	-13.94	88.13	0.94	1.97	19.48	16.06	21.10	21.07	20.83	21.46

Table C.3: (continued)

Index	ϕ_d	-99%	$+99\%$	χ^2	r_{half}	μ_e	-99%	$+99\%$	$\mu_{0,i}$	-99%	$+99\%$
376	5.41	-9.13	18.30	1.52	2.51	29.06	27.94	86.06	20.81	20.72	21.07
377	-23.43	-162.61	98.55	1.36	21.84	17.41	14.27	18.67	26.23	26.02	26.82
378	124.87	87.39	156.64	0.99	2.37	26.56	25.32	27.89	20.63	20.30	21.00
379	128.06	118.04	150.21	1.60	2.90	27.36	26.95	27.81	20.21	20.13	20.33
380	-216.12	-360.00	44.69	1.17	0.02	30.17	29.77	30.68	5.00	1.94	6.07
381	-21.23	-146.11	120.86	1.05	23.28	18.54	16.56	19.62	26.34	26.27	26.59
382	71.89	32.54	111.36	1.24	2.72	28.48	27.37	36.88	20.55	20.50	20.69
383	341.79	175.59	360.00	1.54	24.23	17.19	13.16	18.28	26.17	26.03	26.41
384	111.30	77.62	136.40	1.09	2.47	27.10	25.93	30.29	20.40	20.28	20.59
385	136.40	122.58	146.92	1.08	2.60	18.67	17.91	19.75	19.78	19.73	19.83
386	26.39	-39.02	131.25	1.05	12.17	18.39	16.07	19.47	25.36	25.06	25.52
387	156.10	101.76	220.47	1.18	15.51	17.48	12.89	18.61	24.89	24.76	25.19
388	302.80	241.91	360.00	0.86	12.90	23.71	22.31	24.64	25.76	25.60	26.13
389	-25.04	-74.11	-2.21	1.31	13.45	23.13	22.64	23.63	25.72	25.56	25.98
390	1.34	-13.00	13.78	1.22	2.17	28.34	26.17	81.72	20.31	20.24	20.59
391	-12.78	-67.84	19.58	1.10	1.56	25.15	23.37	36.09	20.01	19.74	20.66
392	-43.84	-168.07	6.03	1.02	2.13	26.44	25.96	27.13	19.78	19.56	20.00
393	26.10	-16.91	59.16	1.02	2.64	25.82	23.60	30.61	21.10	20.95	21.38
394	6.01	-3.66	13.37	1.73	1.80	17.34	15.75	18.41	19.56	19.51	19.62
395	-119.98	-276.88	-12.27	1.00	4.14	27.03	25.79	27.98	22.16	21.80	22.48
396	285.01	229.72	329.99	1.69	0.14	26.00	25.33	26.69	14.52	9.21	15.60
397	82.16	-89.68	155.56	1.78	0.30	26.94	26.02	27.49	15.73	13.85	16.81
398	32.53	-39.42	128.03	1.06	21.56	18.62	13.69	19.72	26.22	26.04	26.52
399	188.62	104.36	224.91	0.78	1.60	23.96	22.00	31.46	20.22	20.04	20.51
400	-358.13	-360.00	-337.99	1.63	0.34	29.72	29.16	30.38	15.76	14.57	16.29

Table C.3: (continued)

Index	ϕ_d	-99%	$+99\%$	χ^2	r_{half}	μ_e	-99%	$+99\%$	$\mu_{0,i}$	-99%	$+99\%$
401	179.13	132.68	231.20	1.02	2.56	25.65	24.52	27.08	21.02	20.72	21.46
402	116.54	72.81	179.46	2.86	0.20	32.26	31.16	35.30	14.48	11.92	15.59
403	173.71	166.90	179.51	1.47	3.97	26.35	24.65	34.73	20.87	20.78	21.07
404	98.28	-147.19	209.05	1.06	15.72	22.07	20.98	23.16	25.76	25.56	25.94
405	82.81	-22.63	156.88	2.33	0.12	29.93	28.71	36.54	13.49	9.24	14.57
406	2.30	-13.83	28.14	1.16	1.52	24.71	23.55	27.47	19.39	19.28	19.63
407	30.31	-5.41	63.51	1.12	2.43	25.39	24.04	27.31	20.50	20.33	20.74
408	145.27	143.57	147.48	3.04	15.78	17.59	17.54	17.62	20.81	20.80	20.82
409	-329.61	-360.00	-262.90	7.86	0.69	26.26	26.20	26.29	15.67	15.49	15.82
410	166.84	72.16	271.72	0.99	1.89	25.08	23.35	27.93	20.65	20.46	21.00
411	130.04	117.82	143.20	1.91	4.28	29.69	28.59	38.46	21.14	21.01	21.33
412	37.36	12.14	65.33	1.08	1.78	22.70	21.35	25.52	20.56	19.77	21.29
413	42.44	-1.06	65.88	1.22	2.21	23.40	22.23	24.26	20.80	20.58	20.98
414	37.25	-3.15	64.35	1.30	4.28	18.90	18.32	19.22	20.57	20.51	20.64
415	-50.08	-115.44	-2.37	2.19	29.95	16.64	13.98	17.74	25.69	25.31	25.91
416	126.34	114.54	141.13	1.43	3.95	25.44	24.13	26.86	21.08	20.95	21.23
417	208.25	176.60	226.92	1.43	2.84	24.43	24.04	24.83	20.30	20.16	20.44
418	42.20	34.57	54.49	1.88	3.59	22.47	20.29	24.23	20.78	20.69	20.96
419	-217.00	-303.61	29.06	1.89	0.22	27.23	26.80	30.25	14.83	12.04	16.01
420	23.42	13.52	31.30	1.95	9.11	16.44	14.87	17.51	21.95	21.93	21.97
421	91.52	77.45	113.31	3.91	0.81	-999.00	-999.00	-999.00	25.28	25.04	25.40
422	99.81	77.36	130.06	1.65	3.14	31.00	29.78	71.72	20.43	20.39	20.52
423	109.10	88.41	125.91	1.15	1.66	24.56	23.98	25.19	19.64	19.49	19.80
424	52.00	21.07	89.98	1.32	34.05	24.29	23.94	24.65	26.70	26.64	26.90
425	89.77	76.64	105.02	0.88	2.41	24.01	22.62	26.12	20.62	20.48	20.81

Table C.3: (continued)

Index	ϕ_d	-99%	$+99\%$	χ^2	r_{half}	μ_e	-99%	$+99\%$	$\mu_{0,i}$	-99%	$+99\%$
426	144.75	13.51	196.34	1.54	10.61	16.04	10.02	17.37	24.04	23.59	24.56
427	106.52	58.93	130.50	1.01	1.89	28.31	27.05	48.03	20.41	20.33	20.58
428	188.80	160.55	214.15	1.23	23.40	24.88	24.55	25.35	26.35	26.13	26.67
429	184.32	140.06	233.85	0.98	2.33	23.03	21.89	24.00	20.90	20.69	21.14
430	38.22	17.24	63.41	0.99	2.56	25.58	24.01	27.40	20.57	20.41	20.76
431	206.35	137.66	239.08	0.86	1.99	26.06	24.76	27.59	20.63	20.40	20.88
432	158.61	60.33	211.71	0.91	1.97	25.67	23.98	28.83	20.32	20.12	20.66
433	152.64	104.07	222.67	0.94	1.91	27.76	26.65	28.98	20.45	20.17	20.72
434	11.20	-39.24	46.72	1.19	17.60	18.53	15.99	19.69	25.80	25.58	26.16
435	182.37	127.33	267.52	1.54	18.86	22.89	22.31	23.42	25.75	25.40	26.01
436	-26.61	-73.40	6.53	1.17	2.15	22.67	21.48	23.79	20.89	20.58	21.17
437	169.29	146.59	187.03	1.11	2.21	22.97	22.26	23.64	20.45	20.26	20.61
438	70.81	-7.40	91.39	1.51	2.05	25.08	24.88	25.22	18.28	18.22	18.32
439	85.49	69.64	104.73	0.96	4.52	23.87	21.26	25.39	22.42	22.30	22.56
440	42.56	14.93	71.33	0.84	2.90	25.88	24.33	31.96	21.47	21.26	21.96
441	-19.97	-73.07	46.91	1.23	27.13	24.69	24.50	24.92	25.50	25.37	25.59
442	13.71	-103.50	37.67	0.93	3.47	29.11	27.33	80.27	21.64	21.48	21.96
443	87.64	67.04	101.28	1.10	1.74	24.16	23.81	24.67	18.95	18.81	19.05
444	103.27	12.39	282.19	1.26	20.26	18.69	16.61	19.83	26.76	26.64	27.08
445	-349.93	-360.00	-131.53	4.02	0.87	29.46	29.33	29.57	17.13	17.00	17.44
446	166.29	137.45	205.84	1.07	2.13	28.51	25.54	51.23	20.56	20.49	20.70
447	7.76	-21.65	37.38	1.13	2.51	26.96	25.59	28.21	20.96	20.77	21.16
448	306.96	83.08	360.00	1.30	11.50	17.96	14.87	19.05	25.71	25.60	26.02
449	124.62	112.68	139.91	1.12	3.69	26.79	25.61	29.08	21.39	21.24	21.61
450	-1.62	-20.53	12.30	1.09	2.58	21.73	20.86	22.30	21.33	21.17	21.49

Table C.3: (continued)

Index	ϕ_d	-99%	$+99\%$	χ^2	r_{half}	μ_e	-99%	$+99\%$	$\mu_{0,i}$	-99%	$+99\%$
451	89.08	20.15	118.89	1.74	17.52	14.64	10.78	15.73	23.74	23.40	24.00
452	-14.57	-129.94	68.95	0.82	15.05	23.80	22.62	24.76	25.45	25.09	25.86
453	58.78	55.70	62.10	4.47	6.65	12.22	-18.85	13.30	20.95	20.92	20.97
454	42.97	-11.70	101.01	1.23	24.32	23.67	23.25	24.20	26.65	26.55	27.06
455	80.62	69.87	92.71	1.10	5.37	28.40	27.09	32.43	22.32	22.15	22.62
456	54.92	-15.84	65.44	2.61	20.87	16.77	14.17	17.90	24.33	24.20	24.68
457	287.61	180.52	360.00	2.58	0.18	28.07	27.56	28.48	13.99	9.53	15.07
458	221.36	175.59	235.00	2.60	6.47	18.14	9.73	19.75	20.44	20.26	20.80
459	14.38	-13.87	43.75	1.26	3.35	27.54	26.45	30.24	20.39	20.23	20.65
460	32.19	24.10	39.88	1.34	4.66	19.61	19.44	19.69	21.56	21.52	21.59
461	258.32	115.10	360.00	2.51	0.16	30.32	29.35	31.20	13.97	11.61	15.05
462	151.36	85.93	254.46	1.10	2.54	29.01	27.87	35.91	21.02	20.91	21.22
463	157.58	124.36	180.88	1.40	0.20	29.66	29.42	29.87	14.34	11.51	15.41
464	-47.81	-86.58	-13.40	1.61	21.62	21.61	21.14	22.13	25.96	25.78	26.20
465	27.92	-26.69	68.16	1.16	2.66	25.61	24.02	27.20	20.82	20.62	21.00
466	-3.12	-29.11	19.76	1.61	2.29	26.85	25.50	33.93	20.51	20.37	20.74
467	-6.61	-79.45	36.70	1.17	3.04	19.05	17.84	20.14	21.65	21.55	21.76
468	102.30	-101.66	174.35	1.59	18.21	17.51	14.55	18.63	25.72	25.58	26.04
469	80.17	73.75	85.90	3.81	6.85	14.47	9.99	15.54	21.17	21.12	21.19
470	227.44	166.68	290.78	3.48	0.24	28.00	26.88	28.60	14.52	12.24	15.60
471	-31.34	-95.31	44.07	1.06	15.09	22.82	22.17	23.52	25.71	25.60	26.07
472	338.63	282.25	360.00	1.88	0.02	28.76	27.41	29.81	8.12	2.37	9.22
473	178.95	139.37	235.18	3.31	0.24	29.19	28.57	29.83	13.77	11.24	14.85
474	132.36	116.31	147.89	1.05	4.52	28.48	27.33	30.88	21.36	21.25	21.53
475	1.18	-9.69	16.12	1.00	4.64	25.31	24.76	25.79	21.04	20.92	21.16

Table C.3: (continued)

Index	ϕ_d	-99%	$+99\%$	χ^2	r_{half}	μ_e	-99%	$+99\%$	$\mu_{0,i}$	-99%	$+99\%$
476	-109.41	-159.28	-38.30	4.45	0.20	31.22	30.20	32.44	13.92	11.53	14.99
477	177.74	59.22	248.18	1.70	0.10	27.07	25.92	27.84	13.35	5.93	14.43
478	-31.74	-129.76	45.78	1.59	47.25	7.37	-338.91	8.45	26.01	25.96	26.26
479	23.56	-5.56	48.10	1.02	3.51	27.10	25.69	30.36	21.13	20.93	21.48
480	321.84	202.66	341.63	1.17	3.22	30.82	29.66	47.12	20.96	20.86	21.08
481	259.22	42.70	360.00	1.26	0.08	28.66	28.24	29.22	12.83	2.57	13.91
482	178.82	148.16	217.25	1.31	17.89	21.49	20.93	22.02	25.79	25.43	26.23
483	187.73	-40.78	358.93	1.15	0.34	29.34	28.77	29.97	16.02	14.20	17.11
484	115.12	106.23	126.40	1.17	3.77	19.96	2.45	21.76	20.91	20.85	21.06
485	168.32	163.16	173.39	1.75	3.83	20.35	17.00	21.61	19.60	19.58	19.62
486	167.51	65.04	232.39	1.25	0.14	27.26	26.05	28.28	14.70	9.77	15.79
487	-232.91	-360.00	-121.93	1.05	16.10	27.21	25.43	29.09	25.88	25.58	26.58
488	-17.63	-72.72	34.75	1.09	13.06	23.97	11.72	27.63	25.52	25.38	26.79
489	41.28	35.43	59.64	2.95	0.73	28.26	27.99	30.20	17.35	17.21	17.50
490	174.39	146.52	194.38	1.39	2.31	24.52	21.44	43.06	20.89	20.77	21.10
491	57.04	41.95	80.56	1.03	3.75	25.61	25.10	26.28	20.67	20.53	20.83
492	228.71	172.11	274.61	1.33	14.30	19.66	19.36	19.81	24.28	24.04	24.43
493	-269.23	-342.26	-85.24	2.17	30.34	20.64	19.05	20.86	26.35	26.17	26.50
494	157.11	113.83	179.97	5.07	4.68	24.83	21.46	28.87	22.09	21.49	22.90
495	107.80	37.34	179.71	1.39	10.61	17.31	14.36	18.39	24.59	24.37	24.79
496	96.69	64.12	126.38	1.07	2.92	24.13	23.16	25.02	21.63	21.25	21.91
497	57.16	32.09	75.03	1.02	2.58	25.97	22.62	35.16	20.43	20.33	20.61
498	16.04	-71.36	62.19	1.29	22.31	19.26	12.79	20.38	25.57	25.21	25.77
499	125.36	109.86	141.43	1.22	3.63	19.97	19.46	20.17	21.23	21.17	21.29
500	-10.73	-21.15	3.01	2.01	6.37	18.32	6.58	19.92	21.31	21.24	21.40

Table C.3: (continued)

Index	ϕ_d	-99%	$+99\%$	χ^2	r_{half}	μ_e	-99%	$+99\%$	$\mu_{0,i}$	-99%	$+99\%$
501	-204.75	-360.00	-102.84	1.37	40.93	27.84	27.53	28.11	26.59	26.35	26.77
502	294.62	151.61	321.71	2.62	34.80	12.85	-8.41	13.96	24.84	24.53	25.18
503	174.01	161.44	188.57	1.08	2.60	19.63	18.90	20.72	21.50	21.36	21.63
504	50.90	-39.93	187.27	1.42	16.69	15.97	7.50	17.04	25.73	25.29	25.89
505	353.63	228.83	360.00	2.76	28.37	15.73	12.37	16.80	25.05	25.02	25.12
506	-235.70	-360.00	35.57	1.97	31.37	22.10	21.83	22.46	25.88	25.86	26.18
507	110.85	102.95	117.69	4.89	3.75	17.03	15.72	18.10	21.01	20.99	21.04
508	142.45	130.00	153.75	1.15	5.80	22.54	22.14	22.91	21.87	21.81	21.93
509	116.66	98.58	133.16	1.19	5.11	16.97	14.31	18.05	21.46	21.43	21.50
510	-72.32	-146.02	-15.50	1.68	0.81	29.32	29.13	29.50	16.94	16.73	17.62
511	84.52	70.42	117.91	1.11	3.43	19.56	19.13	19.75	20.71	20.63	20.76
512	194.30	146.25	243.97	1.77	21.74	18.67	-2.11	20.04	25.65	25.36	25.86
513	333.23	138.97	360.00	2.01	26.77	21.82	18.44	22.49	25.31	25.06	25.49
514	175.22	120.01	230.64	5.12	0.47	25.43	24.79	26.08	15.14	14.16	16.22
515	48.06	-148.56	148.30	5.74	0.26	25.99	25.49	27.72	13.91	11.50	15.05
516	-19.22	-112.42	165.14	1.18	24.50	27.12	26.22	27.90	25.49	25.32	25.84
517	122.62	104.20	140.11	1.21	2.01	24.72	23.77	25.31	20.09	19.93	20.21
518	147.37	141.84	159.57	6.91	0.39	29.49	29.44	29.54	13.14	13.03	13.75
519	133.57	116.51	151.22	2.08	4.44	23.81	23.69	23.90	20.71	20.68	20.74
520	143.33	104.72	216.93	1.55	14.89	20.75	19.64	21.00	25.58	25.34	25.80
521	234.67	170.18	360.00	0.77	25.72	17.17	13.35	18.34	26.08	25.99	26.43
522	-328.69	-360.00	-107.53	1.39	42.10	24.69	24.21	25.30	26.41	26.27	26.60
523	134.26	85.38	214.03	1.25	18.41	17.84	13.99	18.92	26.12	26.03	26.33
524	191.71	186.61	197.83	2.10	3.55	27.97	27.39	28.58	20.53	20.45	20.61
525	107.47	36.64	250.65	1.32	22.77	22.73	22.38	23.08	26.45	26.40	26.69

Table C.3: (continued)

Index	ϕ_d	-99%	$+99\%$	χ^2	r_{half}	μ_e	-99%	$+99\%$	$\mu_{0,i}$	-99%	$+99\%$
526	154.01	88.17	200.38	1.49	0.32	28.83	28.13	29.56	16.13	15.70	16.71
527	327.54	177.98	360.00	1.10	28.86	25.98	24.98	26.54	26.39	26.29	26.59
528	178.05	156.20	218.56	2.18	25.41	27.51	27.15	27.82	25.88	25.82	25.96
529	-100.60	-208.91	-30.64	1.49	29.61	20.84	19.15	21.27	25.54	25.31	25.85
530	328.83	292.62	360.00	3.95	0.34	28.50	28.18	28.82	16.13	14.66	17.20
531	135.18	112.89	150.65	1.08	1.28	22.17	20.74	24.02	19.66	19.28	20.15
532	359.51	311.60	360.00	1.18	52.48	14.84	2.53	15.93	26.49	26.46	26.64
533	22.38	-40.11	57.39	1.07	30.50	16.11	7.54	17.24	25.71	25.41	26.06
534	198.00	95.77	314.08	1.41	26.14	17.28	14.58	18.39	26.20	26.02	26.48
535	265.02	198.66	360.00	2.06	16.10	18.69	16.70	20.04	25.99	25.60	26.74
536	12.71	-43.41	50.18	1.29	21.86	25.16	24.88	25.64	25.87	25.83	26.13
537	349.68	260.41	360.00	1.97	0.34	31.02	30.76	31.30	15.66	14.94	16.58
538	139.27	124.93	155.83	1.20	1.46	24.13	22.24	26.33	19.74	19.64	19.89
539	72.97	8.60	131.52	1.47	16.97	18.91	15.54	20.02	25.55	25.44	25.76
540	33.45	-148.21	67.08	2.60	25.80	26.63	25.18	27.73	25.46	25.36	25.58
541	-148.15	-229.18	-20.06	1.56	0.65	30.48	30.03	31.13	17.55	17.01	18.37
542	-354.07	-360.00	-174.79	2.03	29.71	22.59	22.18	22.87	26.55	26.47	26.65
543	335.04	91.62	360.00	4.51	0.02	30.93	29.73	65.09	7.00	-138.73	8.09
544	80.18	65.58	99.62	1.13	2.70	19.92	18.70	20.40	20.76	20.69	20.93
545	171.50	112.23	265.02	1.17	13.59	19.67	18.28	20.74	25.42	25.33	25.51
546	-243.21	-360.00	92.20	2.66	36.12	24.54	21.84	25.80	25.25	25.01	25.51
547	114.82	36.23	231.10	1.28	17.42	25.71	24.17	26.55	26.32	26.10	26.61
548	-83.85	-169.45	141.71	1.57	25.84	16.89	12.63	18.06	26.30	26.21	26.76
549	-11.04	-145.81	86.89	0.91	18.37	18.09	15.37	19.20	26.12	26.00	26.48
550	11.10	1.79	20.84	2.44	3.18	24.29	24.07	24.49	19.99	19.93	20.04

Table C.3: (continued)

Index	ϕ_d	-99%	$+99\%$	χ^2	r_{half}	μ_e	-99%	$+99\%$	$\mu_{0,i}$	-99%	$+99\%$
551	44.02	9.73	90.43	1.15	4.06	27.14	26.43	27.78	21.63	21.37	21.84
552	185.01	102.76	227.80	0.98	1.91	23.11	21.73	24.20	20.62	20.16	20.97
553	173.91	142.18	198.49	0.99	3.14	24.87	23.40	26.69	21.12	20.92	21.38
554	21.86	-32.77	78.52	9.18	0.04	26.89	26.57	27.47	8.72	-10.90	9.79
555	161.46	64.81	336.16	3.19	2.31	27.17	25.65	54.98	20.17	19.84	20.47
556	32.85	-110.38	93.33	1.12	0.81	-999.00	-999.00	-999.00	25.69	25.44	25.99
557	-5.26	-63.02	58.04	1.36	14.18	21.20	20.08	22.30	25.44	25.01	25.70
558	172.77	142.98	210.31	0.87	1.18	26.24	25.47	27.12	19.06	18.80	19.39
559	74.23	57.72	87.66	1.45	32.75	16.04	13.74	17.12	24.29	24.26	24.42
560	28.67	-74.11	144.99	1.39	20.26	17.42	14.01	18.61	25.61	25.45	25.97
561	192.84	173.51	215.24	0.82	4.95	25.08	24.26	26.00	22.25	21.97	22.48
562	155.99	39.28	248.72	0.84	13.36	18.63	16.85	19.71	25.28	25.19	25.44
563	240.63	42.48	321.02	1.19	17.40	17.73	15.30	18.93	25.72	25.51	26.32
564	47.38	39.72	54.96	6.85	35.53	26.73	25.55	28.17	20.99	20.92	21.08
565	203.79	137.86	338.13	5.16	23.95	21.59	16.80	22.82	24.33	24.03	24.77
566	302.53	238.10	340.51	0.83	1.99	24.68	23.08	26.24	20.51	20.06	21.02
567	174.08	116.37	207.10	2.02	31.23	14.11	8.77	15.24	24.81	24.64	25.15
568	67.41	9.66	152.72	2.05	43.64	29.08	28.36	29.87	26.71	26.34	26.94
569	163.54	129.87	265.64	1.33	21.27	15.64	8.77	16.72	26.24	26.21	26.38
570	192.68	180.95	206.62	1.17	5.72	23.25	20.80	24.94	22.01	21.93	22.10
571	183.59	137.48	206.00	2.13	14.30	18.81	18.38	19.03	20.81	20.74	20.88
572	120.93	-64.38	182.37	1.12	1.34	25.70	24.38	33.52	19.63	19.43	20.14
573	-252.11	-360.00	-138.30	1.11	19.12	14.86	3.83	15.99	24.40	24.30	24.70
574	-10.23	-22.60	14.94	3.32	31.68	18.37	18.12	18.50	25.13	25.04	25.23
575	119.60	97.78	143.89	1.50	2.13	28.34	27.14	32.85	20.25	20.15	20.45

Table C.3: (continued)

Index	ϕ_d	-99%	$+99\%$	χ^2	r_{half}	μ_e	-99%	$+99\%$	$\mu_{0,i}$	-99%	$+99\%$
576	44.03	-21.33	74.46	1.78	28.23	21.99	21.72	22.26	26.37	26.28	26.52
577	312.64	166.92	360.00	1.04	16.97	22.96	21.47	23.83	25.51	25.31	25.80
578	208.45	146.91	259.43	0.99	1.46	23.89	22.55	25.10	20.04	19.56	20.50
579	132.67	66.41	222.17	1.53	0.12	27.79	26.66	28.82	14.30	8.86	15.38
580	62.76	9.61	115.78	1.14	29.39	17.93	15.72	19.04	26.08	25.87	26.44
581	322.07	168.53	358.49	1.50	14.24	18.16	15.75	19.36	26.00	25.72	26.60
582	-34.90	-64.27	59.30	1.22	3.24	28.60	27.47	31.39	21.57	21.40	21.83
583	81.18	64.72	103.78	2.66	6.53	24.47	22.62	25.74	20.52	20.46	20.58
584	103.58	68.63	150.39	1.06	1.68	23.89	22.97	24.56	20.21	19.83	20.44
585	-59.01	-133.92	7.34	3.15	0.08	26.08	25.38	27.38	11.54	0.47	12.64
586	64.85	50.98	74.26	2.14	8.38	15.14	11.05	16.21	20.84	20.81	20.86
587	-20.36	-128.75	98.79	1.41	18.21	23.56	23.08	24.08	25.20	24.76	25.60
588	13.04	-81.56	62.91	1.40	0.81	-999.00	-999.00	-999.00	25.20	25.07	25.33
589	243.77	163.76	282.11	5.63	0.02	28.83	28.72	28.96	5.70	-4.24	6.77
590	25.83	-360.00	179.26	1.81	27.09	26.62	26.12	27.23	25.99	25.83	26.41
591	149.40	127.53	192.46	1.34	3.65	28.56	27.21	30.92	21.84	21.52	22.28
592	48.19	28.69	67.32	3.07	21.64	22.33	17.93	24.03	25.38	25.07	25.86
593	83.83	4.26	168.95	0.97	6.17	25.91	23.97	29.13	22.67	22.51	22.81
594	172.37	99.82	248.32	8.23	0.34	26.67	26.07	27.27	14.47	12.56	15.54
595	5.61	-8.44	18.61	1.36	5.68	25.99	25.54	26.42	21.63	21.50	21.76
596	130.68	69.94	199.50	1.17	35.59	12.59	-20.84	13.75	25.63	25.39	26.17
597	-24.27	-29.48	-16.52	2.93	4.18	18.87	12.76	20.37	19.54	19.48	19.75
598	190.57	88.81	360.00	2.86	19.35	18.52	17.93	19.55	24.35	23.72	24.80
599	112.22	82.38	140.28	1.46	29.71	23.33	21.06	24.40	26.24	26.03	26.51
600	28.42	-75.73	156.04	0.96	0.08	28.21	27.44	29.07	12.73	12.05	13.82

Table C.3: (continued)

Index	ϕ_d	-99%	$+99\%$	χ^2	r_{half}	μ_e	-99%	$+99\%$	$\mu_{0,i}$	-99%	$+99\%$
601	156.28	123.74	228.14	1.07	1.83	23.02	21.06	24.38	20.75	20.35	21.14
602	100.45	62.00	146.07	1.05	2.05	27.94	26.82	29.79	20.52	20.40	20.69
603	-96.14	-157.23	111.29	2.60	0.24	27.85	27.00	28.56	15.07	13.06	16.15
604	155.02	113.90	198.09	1.65	15.90	23.12	22.41	23.81	24.77	24.60	25.08
605	270.07	199.20	315.42	1.31	0.18	30.31	29.75	30.81	14.20	12.87	15.28
606	148.61	114.30	178.19	1.05	3.65	22.80	22.26	23.34	21.64	21.56	21.78
607	155.53	120.51	189.96	2.31	0.81	-999.00	-999.00	-999.00	24.77	24.22	25.08
608	86.93	29.73	131.10	1.54	27.05	26.31	25.41	27.01	26.49	26.38	26.92
609	26.22	-23.13	70.15	1.81	0.81	-999.00	-999.00	-999.00	20.70	20.64	20.74
610	133.41	98.77	173.40	1.09	1.80	18.94	17.78	20.04	20.78	20.60	20.93
611	106.24	85.92	123.14	1.37	1.91	28.69	27.57	32.29	19.43	19.38	19.49
612	215.04	142.42	296.61	2.06	0.81	-999.00	-999.00	-999.00	26.57	26.21	26.74
613	137.98	115.08	154.27	1.54	2.66	18.26	15.97	19.34	21.17	21.08	21.25
614	112.57	35.94	360.00	1.35	11.48	19.27	18.07	20.34	25.36	25.22	25.47
615	346.20	167.71	360.00	1.82	17.30	24.19	20.49	25.93	25.84	25.53	26.54
616	153.28	121.53	182.49	1.04	1.56	18.87	16.07	20.01	20.88	20.64	21.15
617	120.65	-137.91	360.00	1.45	0.51	26.36	25.61	26.72	17.10	16.33	18.18
618	117.71	95.64	147.75	1.03	3.63	24.72	24.13	25.03	20.92	20.71	21.05
619	-330.48	-360.00	-288.85	2.03	9.51	17.56	16.00	18.63	23.45	23.34	23.52
620	126.89	112.25	139.66	1.51	4.91	19.24	18.81	20.14	20.53	20.50	20.55
621	236.14	162.24	278.37	0.78	16.04	22.54	21.23	23.20	25.63	25.41	25.99
622	85.20	5.81	218.22	0.84	23.69	27.01	26.44	27.81	26.75	26.43	27.32
623	174.51	148.68	202.64	1.15	3.67	26.19	25.83	26.83	20.27	20.09	20.37
624	108.59	75.79	130.28	1.29	5.09	29.14	27.87	39.33	22.54	22.35	22.82
625	353.77	213.58	360.00	2.52	36.79	23.44	21.68	24.50	26.35	26.32	26.75

Table C.3: (continued)

Index	ϕ_d	-99%	$+99\%$	χ^2	r_{half}	μ_e	-99%	$+99\%$	$\mu_{0,i}$	-99%	$+99\%$
626	347.44	322.63	360.00	6.45	13.71	18.84	15.25	19.00	23.46	23.07	23.55
627	0.52	-64.16	37.42	1.05	1.91	28.04	26.80	31.49	20.45	20.33	20.64
628	352.93	146.46	360.00	2.34	1.52	29.07	27.92	42.00	19.54	19.13	20.05
629	70.30	41.38	126.54	1.98	13.89	17.96	16.76	19.09	24.50	24.22	24.87
630	250.54	153.57	360.00	1.32	21.01	19.59	17.52	20.68	25.94	25.74	26.13
631	-176.65	-360.00	43.98	1.56	17.08	24.96	23.90	25.54	25.65	25.54	25.81
632	97.31	11.95	288.86	1.40	0.02	29.67	29.09	30.44	10.66	-1.43	11.75
633	-31.19	-81.60	49.95	1.54	19.67	25.95	25.42	26.70	26.04	25.88	26.21
634	0.92	-23.70	32.64	0.89	1.93	22.36	20.99	24.09	20.43	20.18	20.68
635	100.66	91.33	120.19	4.41	10.42	22.47	20.36	24.27	20.40	20.21	20.82
636	35.91	-15.68	210.29	1.24	47.48	29.99	28.74	32.20	25.73	25.54	25.94
637	-5.97	-123.54	72.73	1.20	0.18	27.00	25.75	27.79	15.16	11.48	16.25
638	60.43	38.57	82.27	4.17	12.09	18.61	13.01	19.99	23.89	23.49	24.31
639	122.37	98.84	144.41	1.03	1.68	26.77	25.31	32.12	19.85	19.75	20.12
640	187.23	168.66	217.93	1.06	2.01	27.82	26.73	29.21	20.13	19.96	20.33
641	104.21	-122.11	169.07	1.29	0.26	29.95	29.23	30.61	15.28	12.79	16.37
642	114.37	74.54	211.78	5.59	0.22	26.77	26.29	27.19	13.75	10.56	14.83
643	94.86	38.65	154.44	0.87	2.78	23.19	21.77	24.57	21.09	20.85	21.30
644	1.98	-15.86	18.29	1.84	0.77	26.11	25.10	26.87	18.11	17.90	18.23
645	-20.34	-81.91	10.56	1.95	9.98	17.11	15.23	18.22	23.33	23.16	23.65
646	64.12	-163.04	179.52	2.78	22.47	14.87	-7.64	15.95	25.21	25.15	25.26
647	-29.57	-81.35	25.07	1.38	15.66	19.03	5.58	20.27	26.12	25.74	26.59
648	81.81	73.99	90.83	1.24	3.71	27.82	26.66	31.13	20.48	20.42	20.58
649	80.54	70.50	87.46	1.18	5.19	22.29	21.31	22.97	21.39	21.33	21.52
650	79.72	49.21	96.93	1.07	4.34	22.89	22.06	23.80	20.82	20.72	20.92

Table C.3: (continued)

Index	ϕ_d	-99%	$+99\%$	χ^2	r_{half}	μ_e	-99%	$+99\%$	$\mu_{0,i}$	-99%	$+99\%$
651	95.67	88.93	100.72	2.46	27.07	16.81	16.10	17.88	23.55	23.49	23.62
652	130.38	127.81	132.39	2.51	6.39	25.26	25.09	25.46	20.53	20.51	20.55
653	201.05	185.94	212.34	1.73	4.40	19.04	17.83	20.12	20.10	20.08	20.11
654	116.72	63.08	152.70	1.33	4.66	21.05	19.79	21.51	21.68	21.61	21.77
655	308.66	208.84	360.00	1.14	23.06	27.17	26.66	27.77	26.52	26.36	26.72
656	123.13	87.56	142.81	0.92	2.03	23.21	20.87	25.27	20.89	20.56	21.29
657	44.78	-35.72	75.11	1.13	23.28	28.37	27.56	29.23	25.86	25.60	26.17
658	156.45	149.63	163.23	1.79	5.13	20.72	15.77	22.22	20.57	20.55	20.60
659	-52.37	-142.97	-4.36	0.88	2.11	27.48	25.36	52.99	20.65	20.52	20.93
660	35.47	4.48	99.79	3.43	31.47	22.00	21.19	22.44	25.10	24.81	25.27
661	37.47	8.22	61.11	0.93	5.11	26.93	25.27	32.03	22.57	22.42	22.74
662	118.22	104.56	129.12	1.84	3.63	20.28	19.32	20.76	19.79	19.75	19.84
663	163.30	153.43	171.45	1.39	3.75	19.63	18.39	20.75	20.39	20.36	20.42
664	3.45	-25.54	34.44	1.00	1.24	21.80	19.11	24.13	20.09	19.67	20.76
665	191.34	113.57	288.46	1.05	21.56	26.65	25.94	27.23	26.30	26.17	26.55
666	61.52	40.55	88.46	1.36	2.64	25.90	25.14	26.65	20.46	20.33	20.58
667	193.56	166.48	219.18	1.03	1.91	31.30	30.15	77.78	19.78	19.73	19.89
668	117.89	93.51	149.64	1.00	1.99	24.34	22.83	25.80	20.36	20.06	20.70
669	36.26	-12.49	118.66	0.94	22.13	23.52	23.06	24.36	25.72	25.43	26.18
670	9.19	-51.47	93.80	1.26	23.22	15.83	8.79	16.92	26.49	26.42	26.88
671	101.64	73.11	119.76	1.11	2.27	27.10	26.39	27.55	20.57	20.32	20.75
672	-102.59	-275.09	-26.59	2.32	28.35	22.07	21.20	22.52	25.48	25.23	25.76
673	104.12	79.54	130.00	1.00	1.46	23.25	21.56	28.47	19.74	19.54	20.06
674	186.98	165.85	200.39	1.36	3.61	22.12	21.78	22.52	20.89	20.80	20.95
675	92.20	25.28	145.15	1.75	17.06	21.07	20.41	21.72	25.07	24.83	25.39

Table C.3: (continued)

Index	ϕ_d	-99%	$+99\%$	χ^2	r_{half}	μ_e	-99%	$+99\%$	$\mu_{0,i}$	-99%	$+99\%$
676	124.20	101.67	148.51	1.44	2.84	25.94	25.37	26.50	20.28	20.11	20.46
677	73.20	30.83	98.30	1.27	2.13	27.54	26.45	41.17	19.54	19.48	19.70
678	109.70	63.28	168.43	1.13	11.24	18.34	15.74	19.44	24.79	24.55	25.06
679	-64.91	-127.03	-5.47	1.01	15.47	22.50	-21.74	28.58	25.49	25.26	26.71
680	189.20	158.41	210.06	0.92	1.01	21.56	20.24	23.37	19.16	18.67	19.83
681	87.79	23.55	144.45	0.95	1.64	18.69	16.68	19.81	21.03	20.78	21.22
682	26.27	-3.30	58.05	1.00	2.35	22.00	21.42	22.40	19.98	19.90	20.09
683	92.48	85.21	112.99	1.81	34.96	20.90	20.81	21.03	25.11	25.07	25.19
684	75.33	-6.83	163.64	0.99	1.44	24.08	22.92	24.88	19.60	19.23	19.89
685	144.69	67.76	275.31	1.59	13.89	22.90	22.04	23.52	26.02	25.93	26.18
686	42.01	27.25	48.57	2.64	3.04	17.95	16.83	19.02	20.20	20.17	20.22
687	111.27	68.80	145.50	1.04	2.58	17.63	14.47	18.71	21.87	21.65	22.07
688	3.35	-21.58	16.63	1.28	2.41	25.56	24.31	26.91	20.70	20.51	20.90
689	-21.50	-31.04	-3.37	1.57	5.50	22.99	21.64	23.90	20.55	20.50	20.61
690	344.65	191.92	360.00	1.34	0.02	26.87	25.64	27.78	9.46	-46.25	10.54
691	167.38	149.28	184.21	1.01	3.45	26.82	25.64	31.46	21.22	21.13	21.38
692	53.14	11.74	139.22	0.99	2.54	27.79	25.83	33.53	20.30	20.22	20.43
693	-251.40	-278.47	-218.43	1.05	2.98	20.76	17.72	22.12	21.98	21.78	22.24
694	68.00	36.71	88.65	9.53	0.08	27.11	26.67	27.70	9.26	-1.82	10.34
695	89.94	77.62	100.81	1.10	1.36	24.66	24.16	25.17	18.96	18.79	19.14
696	88.00	41.15	124.25	0.98	1.99	20.66	16.99	25.43	20.47	20.33	20.60
697	51.29	-18.77	76.70	2.91	2.11	28.55	27.38	31.75	20.57	19.80	21.00
698	79.72	67.41	94.95	1.10	1.56	23.53	22.65	24.36	18.78	18.65	18.92
699	162.96	139.29	191.92	2.06	0.89	27.89	27.81	28.00	16.93	16.83	17.24
700	10.04	-10.74	22.67	1.97	3.55	25.57	25.34	25.76	19.54	19.49	19.60

Table C.3: (continued)

Index	ϕ_d	-99%	$+99\%$	χ^2	r_{half}	μ_e	-99%	$+99\%$	$\mu_{0,i}$	-99%	$+99\%$
701	107.28	66.75	155.54	0.94	4.62	25.47	24.11	27.00	22.43	22.14	22.76
702	-159.60	-360.00	30.95	1.11	23.99	19.99	18.85	21.11	26.70	26.59	26.93
703	136.07	-120.91	204.03	1.50	32.65	27.45	26.23	28.44	25.80	25.58	26.15
704	5.03	-46.14	133.90	0.92	13.53	19.17	17.73	20.25	25.89	25.72	26.21
705	-354.54	-360.00	-287.48	1.20	15.82	22.87	21.91	23.96	25.82	25.62	25.98
706	276.46	29.97	360.00	1.09	20.00	26.89	26.49	27.25	26.43	26.28	26.67
707	265.84	203.48	305.74	2.18	38.37	19.94	18.74	20.38	25.47	25.30	25.74
708	-11.31	-56.56	39.71	1.12	13.38	18.29	16.28	19.37	25.15	24.94	25.35
709	-320.51	-360.00	148.28	1.18	19.02	17.78	-11.89	18.86	25.73	25.58	25.87
710	112.83	95.82	137.53	1.37	3.27	25.13	24.10	26.01	21.64	21.40	21.88
711	356.48	236.59	360.00	1.38	16.63	18.66	16.47	19.73	25.52	25.41	25.65
712	59.25	-23.81	91.05	1.24	3.43	27.82	26.58	28.92	21.27	20.78	21.62
713	64.40	-59.38	118.05	1.35	10.44	19.05	17.93	20.24	25.21	24.90	25.75
714	193.18	172.21	226.15	1.27	2.11	23.67	21.94	25.25	19.81	19.57	20.04
715	253.37	125.79	360.00	1.13	16.31	27.79	27.28	28.37	25.73	25.50	25.99
716	130.44	115.18	143.48	1.10	3.06	29.16	25.93	739.45	20.59	20.51	20.77
717	125.36	3.74	182.29	1.76	14.54	20.31	19.22	21.40	24.54	24.25	24.73
718	14.91	14.39	15.02	9.87	33.52	17.95	17.77	18.22	19.26	19.26	19.26
719	11.75	-48.44	87.04	1.14	16.91	22.59	21.75	23.47	25.83	25.52	26.44
720	166.64	139.07	192.38	1.00	1.97	27.58	26.45	30.81	20.52	20.42	20.69
721	-21.85	-64.83	57.37	1.21	1.91	24.07	23.12	24.92	20.61	20.25	20.93
722	124.31	116.14	132.08	2.81	4.79	27.70	27.28	28.19	21.08	20.98	21.19
723	-6.01	-11.34	-2.54	1.21	3.89	24.34	23.06	25.61	20.51	20.47	20.57
724	93.31	78.02	107.30	3.49	8.38	24.89	24.61	25.22	20.12	20.07	20.14
725	60.68	30.57	83.32	1.27	2.72	27.50	26.24	29.96	20.94	20.84	21.09

Table C.3: (continued)

Index	ϕ_d	-99%	$+99\%$	χ^2	r_{half}	μ_e	-99%	$+99\%$	$\mu_{0,i}$	-99%	$+99\%$
726	-10.90	-14.00	-7.39	1.44	5.09	21.37	21.25	21.44	20.38	20.35	20.40
727	1.43	-7.88	19.67	1.03	3.04	26.09	24.98	27.87	20.41	20.32	20.51
728	72.50	49.11	96.97	1.04	3.39	28.04	24.62	139.12	21.28	21.23	21.36
729	21.03	-4.77	43.14	1.25	2.56	25.22	23.94	28.15	21.19	21.03	21.45
730	114.81	88.26	141.24	1.09	1.74	26.01	25.01	26.93	19.91	19.47	20.28
731	-305.61	-360.00	-103.48	1.36	15.82	24.91	24.01	25.47	25.80	25.71	26.00
732	139.74	130.14	154.68	1.49	5.07	25.09	24.31	26.14	20.03	20.00	20.07
733	18.75	13.36	26.50	1.38	4.12	19.27	17.73	20.40	20.30	20.26	20.33
734	102.22	61.41	197.29	1.26	34.50	23.31	22.99	23.72	25.90	25.83	26.16
735	141.47	133.25	149.66	1.37	2.90	19.60	18.78	20.69	20.66	20.59	20.72
736	261.98	206.93	354.58	0.94	1.87	26.67	25.49	51.11	20.24	20.13	20.49
737	352.34	243.94	360.00	1.55	13.04	19.66	-4.52	23.26	25.56	25.39	26.88
738	315.05	217.63	360.00	0.98	17.26	16.55	10.45	17.63	26.37	26.32	26.57
739	239.34	210.03	272.80	3.29	7.26	19.39	16.27	19.92	20.44	20.38	20.48
740	-66.32	-101.59	26.44	3.27	24.03	17.37	17.14	18.28	23.33	23.24	23.46
741	-150.78	-225.66	47.26	1.39	10.51	25.65	24.21	34.23	22.63	22.14	23.30
742	66.33	36.62	138.43	0.88	21.94	28.33	26.73	30.59	25.67	25.00	26.05
743	-3.46	-30.57	32.04	1.02	3.31	28.50	26.97	55.53	20.76	20.68	20.86
744	120.07	69.58	149.99	1.04	15.88	20.09	19.40	21.19	25.13	24.83	25.45
745	101.99	89.96	122.82	1.22	2.64	27.17	25.38	33.85	20.21	20.17	20.30
746	51.39	25.51	76.40	1.34	2.43	24.67	23.99	25.36	20.25	20.04	20.44
747	159.33	134.25	179.65	1.01	4.58	27.13	26.02	27.95	21.89	21.66	22.07
748	92.28	72.60	123.99	0.94	2.56	27.26	26.02	33.30	20.77	20.68	20.94
749	352.91	278.47	360.00	1.63	25.98	26.16	25.80	26.47	26.79	26.73	26.94
750	16.41	12.45	19.11	1.37	4.56	23.71	23.52	23.88	20.12	20.08	20.15

Table C.3: (continued)

Index	ϕ_d	-99%	$+99\%$	χ^2	r_{half}	μ_e	-99%	$+99\%$	$\mu_{0,i}$	-99%	$+99\%$
751	6.17	-115.76	142.94	2.96	7.06	18.15	-7.73	20.67	22.78	22.04	23.56
752	62.01	5.17	254.84	0.97	11.72	21.94	18.94	23.92	25.59	25.42	26.51
753	68.38	-31.71	119.87	2.45	8.70	15.87	10.29	16.99	23.21	22.80	23.52
754	93.80	58.61	121.25	1.05	2.09	26.27	24.91	31.17	20.45	20.35	20.65
755	113.69	74.24	134.91	2.34	7.75	20.12	19.08	20.28	21.19	21.08	21.24
756	225.94	172.97	279.04	1.73	16.81	23.50	23.15	23.85	24.72	24.61	24.83
757	1.77	-36.25	43.57	1.03	2.76	19.06	17.41	20.16	21.73	21.59	21.89

Table C.4: Catalog of Objects Studied

Index	μ_0	-99%	$+99\%$	$\mu_{r<r_{half}}$	-99%	$+99\%$	$\mu_{r_{half}}$	-99%	$+99\%$
1	25.74	25.49	26.45	19.45	19.43	19.65	27.22	26.83	27.93
2	25.31	24.98	25.59	18.54	18.34	18.73	26.58	26.25	26.88
3	20.96	20.60	21.44	15.33	15.20	15.41	22.91	22.58	23.34
4	27.10	26.85	27.57	20.16	20.06	20.44	28.28	28.09	28.79
5	19.77	19.55	19.90	14.22	14.17	14.27	21.84	21.62	21.97
6	22.23	21.93	22.57	16.18	16.09	16.24	23.79	23.49	24.12
7	20.80	20.35	21.28	14.70	14.63	14.79	22.32	21.66	22.84
8	20.07	19.78	20.28	14.36	14.30	14.42	21.90	21.59	22.14
9	22.03	21.90	22.13	16.37	16.34	16.40	23.91	23.76	24.02
10	21.13	21.09	21.16	15.43	15.42	15.45	22.95	22.91	22.99
11	21.55	21.43	21.65	15.54	15.50	15.58	23.16	23.03	23.28
12	20.29	19.98	20.96	13.72	13.63	13.74	21.63	20.67	22.26
13	20.89	20.68	21.12	15.45	15.40	15.50	22.92	22.73	23.14
14	26.55	26.37	26.77	20.04	19.97	20.16	27.92	27.72	28.17
15	20.10	19.87	20.36	14.39	14.33	14.45	21.97	21.74	22.24
16	20.93	20.82	21.02	14.84	14.81	14.87	22.45	22.33	22.57
17	24.93	24.66	25.16	18.48	18.36	18.59	26.37	26.13	26.59
18	20.46	20.10	20.99	14.84	14.74	14.91	22.36	22.03	22.90
19	20.48	20.38	20.68	14.53	14.50	14.54	22.15	22.03	22.27
20	19.91	19.81	20.10	14.30	14.24	14.35	21.75	21.66	21.95
21	26.47	25.71	27.07	20.34	19.93	20.60	28.00	27.46	28.53
22	22.35	22.22	22.50	15.39	15.34	15.45	23.52	23.38	23.68
23	21.36	21.23	21.56	15.92	15.88	15.96	23.37	23.25	23.55
24	20.48	20.08	20.83	14.98	14.91	15.08	22.58	22.22	22.87
25	20.23	20.06	20.38	14.36	14.33	14.39	21.89	21.68	22.07

Table C.4: (continued)

Index	μ_0	-99%	$+99\%$	$\mu_{r<r_{half}}$	-99%	$+99\%$	$\mu_{r_{half}}$	-99%	$+99\%$
26	21.75	21.46	21.89	15.88	15.85	15.91	23.42	23.08	23.57
27	25.82	25.65	26.26	19.19	19.17	19.49	27.03	26.85	27.46
28	21.29	21.13	21.51	15.69	15.54	15.77	23.16	22.99	23.39
29	20.41	20.27	20.57	14.80	14.73	14.85	22.29	22.14	22.44
30	22.02	21.36	23.12	16.26	15.82	16.38	23.81	23.12	24.90
31	26.27	25.98	26.51	19.61	19.60	19.70	27.59	27.26	27.84
32	19.50	19.33	20.42	13.78	13.65	13.80	21.26	21.08	22.25
33	26.01	25.68	26.43	19.61	19.61	19.64	27.55	27.35	27.67
34	22.16	22.06	22.30	16.32	16.29	16.38	23.96	23.88	24.10
35	26.26	26.04	26.49	19.60	19.59	19.68	27.57	27.37	27.83
36	26.64	25.89	26.92	20.75	20.39	20.87	28.32	27.55	28.58
37	20.12	19.82	20.42	14.62	14.54	14.69	22.23	21.95	22.48
38	20.31	19.95	20.73	14.67	14.58	14.73	22.17	21.81	22.59
39	20.73	20.22	21.10	14.13	14.07	14.23	22.01	20.90	22.41
40	24.29	24.13	24.48	17.74	17.67	17.85	25.64	25.47	25.84
41	25.73	25.36	26.06	19.58	19.45	19.73	27.23	26.79	27.59
42	20.23	20.07	20.59	14.58	14.50	14.63	22.07	21.89	22.45
43	25.98	25.89	26.07	19.51	19.51	19.55	27.37	27.28	27.48
44	25.19	24.68	25.70	19.51	19.37	19.67	27.03	26.52	27.48
45	20.58	20.42	20.95	14.94	14.82	14.96	22.46	22.24	22.82
46	25.37	25.16	25.70	12.99	12.99	13.13	25.57	25.41	25.86
47	24.95	24.71	25.46	18.48	18.37	18.79	26.37	26.11	26.92
48	20.52	20.41	20.70	14.91	14.83	14.95	22.35	22.24	22.56
49	20.30	20.04	20.57	14.42	14.37	14.46	22.02	21.78	22.29
50	20.53	20.47	20.61	15.04	15.00	15.06	22.51	22.44	22.59

Table C.4: (continued)

Index	μ_0	-99%	$+99\%$	$\mu_{r<r_{half}}$	-99%	$+99\%$	$\mu_{r_{half}}$	-99%	$+99\%$
51	21.20	20.83	21.50	15.18	15.11	15.25	22.77	22.22	23.13
52	25.99	25.62	26.47	19.75	19.62	19.93	27.56	27.42	27.76
53	20.43	20.32	20.57	14.84	14.81	14.87	22.32	22.21	22.46
54	17.63	17.48	17.74	12.15	12.07	12.18	19.80	19.65	19.91
55	13.59	8.76	14.70	8.26	8.21	8.30	15.91	9.10	17.43
56	20.45	20.31	20.57	14.78	14.74	14.82	22.31	22.17	22.44
57	25.46	25.16	25.71	18.81	18.81	18.91	26.86	26.63	27.07
58	20.36	20.21	20.73	14.92	14.88	14.97	22.36	22.24	22.64
59	19.69	19.53	19.80	13.99	13.96	14.02	21.58	21.42	21.69
60	20.57	20.33	20.72	14.93	14.89	14.97	22.47	22.22	22.62
61	20.63	20.50	20.90	15.14	15.07	15.20	22.60	22.50	22.90
62	26.41	26.19	26.64	20.14	20.14	20.27	27.84	27.62	28.10
63	26.20	25.99	26.40	20.76	20.76	20.91	28.34	28.05	28.58
64	19.73	19.55	19.90	13.76	13.72	13.79	21.36	21.16	21.55
65	20.17	20.09	20.26	14.51	14.50	14.53	22.02	21.94	22.09
66	19.64	19.46	19.73	13.86	13.82	13.89	21.44	21.24	21.54
67	20.10	19.96	20.27	14.46	14.42	14.50	22.04	21.90	22.21
68	21.55	21.25	21.82	15.82	15.76	15.87	23.39	23.10	23.62
69	25.95	25.74	26.24	20.01	19.94	20.17	27.62	27.43	27.94
70	22.76	22.47	23.06	16.74	16.67	16.83	24.33	23.99	24.68
71	26.09	25.84	26.30	19.41	19.30	19.53	27.36	27.13	27.58
72	20.21	20.09	20.59	14.51	14.44	14.55	21.98	21.85	22.40
73	26.53	26.32	26.73	19.66	19.66	19.74	27.72	27.59	27.90
74	24.46	24.23	24.89	17.70	17.51	18.02	25.72	25.47	26.17
75	25.39	25.35	25.51	12.78	12.78	12.82	25.47	25.43	25.59

Table C.4: (continued)

Index	μ_0	-99%	$+99\%$	$\mu_{r<r_{half}}$	-99%	$+99\%$	$\mu_{r_{half}}$	-99%	$+99\%$
76	20.64	20.41	20.80	14.87	14.83	14.91	22.39	22.12	22.59
77	20.12	19.90	20.40	14.48	14.42	14.54	21.98	21.71	22.22
78	20.98	20.78	21.17	14.56	14.53	14.61	22.35	22.12	22.58
79	15.54	13.32	16.65	10.44	10.39	10.48	18.22	14.93	19.81
80	25.59	25.50	25.68	19.15	19.15	19.19	26.99	26.89	27.09
81	25.42	25.08	25.78	18.53	18.40	18.73	26.65	26.33	27.01
82	20.06	19.91	20.32	14.63	14.59	14.67	22.08	21.96	22.28
83	19.91	19.89	19.94	13.67	13.66	13.67	21.43	21.40	21.46
84	19.23	19.07	19.40	13.69	13.65	13.76	21.30	21.13	21.48
85	20.56	19.87	21.03	14.96	14.87	15.18	22.45	21.59	22.98
86	20.38	20.21	20.67	14.70	14.60	14.76	22.19	22.01	22.51
87	20.99	20.85	21.11	14.74	14.71	14.76	22.40	22.25	22.53
88	26.24	25.89	26.73	19.59	19.45	19.75	27.62	27.39	28.07
89	26.27	26.14	26.57	19.83	19.80	20.02	27.61	27.46	27.93
90	20.54	20.33	20.77	14.79	14.74	14.85	22.30	22.06	22.57
91	14.82	13.52	15.89	9.17	9.14	9.18	16.64	14.95	18.03
92	26.19	26.02	26.35	19.49	19.49	19.57	27.47	27.28	27.65
93	21.38	21.36	21.41	15.72	15.71	15.73	23.23	23.20	23.26
94	19.42	19.37	19.51	14.00	13.98	14.01	21.44	21.41	21.53
95	14.74	13.84	15.81	9.55	9.49	9.60	17.26	16.22	18.77
96	20.42	20.31	20.71	14.95	14.88	14.99	22.41	22.30	22.72
97	19.93	19.90	19.95	14.14	14.12	14.15	21.66	21.63	21.69
98	14.63	11.00	15.71	8.94	8.91	8.96	16.42	11.76	17.81
99	20.01	19.80	20.30	14.44	14.38	14.47	21.95	21.75	22.24
100	19.63	19.45	19.82	13.88	13.84	13.94	21.38	21.16	21.59

Table C.4: (continued)

Index	μ_0	-99%	$+99\%$	$\mu_{r<r_{half}}$	-99%	$+99\%$	$\mu_{r_{half}}$	-99%	$+99\%$
101	25.75	25.48	26.18	19.01	18.87	19.27	27.03	26.72	27.50
102	18.32	18.21	18.48	12.61	12.60	12.63	20.13	19.99	20.31
103	25.34	25.08	25.53	19.25	19.08	19.35	26.95	26.69	27.13
104	26.11	25.93	26.68	19.25	19.21	19.58	27.33	27.16	27.95
105	19.95	19.70	20.29	14.17	14.08	14.23	21.68	21.40	22.04
106	20.10	20.04	20.29	14.47	14.42	14.51	21.92	21.85	22.14
107	20.32	20.31	20.34	14.79	14.79	14.80	22.28	22.27	22.29
108	25.80	25.52	25.94	19.91	19.91	19.94	27.49	27.19	27.65
109	26.42	26.13	26.87	20.58	20.54	20.70	28.16	28.05	28.42
110	26.05	25.75	26.40	20.16	20.08	20.34	27.79	27.56	28.05
111	24.92	24.86	25.05	18.74	18.74	18.82	26.45	26.38	26.61
112	18.92	18.80	19.01	13.25	13.24	13.27	20.74	20.60	20.84
113	16.21	15.76	16.60	10.63	10.30	10.68	18.13	17.64	18.53
114	15.69	14.54	16.77	10.34	10.30	10.49	17.97	16.36	19.49
115	19.85	19.82	19.87	13.82	13.81	13.83	21.41	21.37	21.45
116	18.93	18.78	19.06	13.12	13.10	13.15	20.68	20.52	20.82
117	25.25	25.01	25.33	19.55	19.55	19.58	27.04	26.75	27.13
118	26.20	25.82	26.56	19.58	19.52	19.70	27.49	27.15	27.69
119	20.23	20.04	20.53	14.64	14.59	14.68	22.14	21.95	22.41
120	24.37	24.10	24.51	18.11	17.90	18.20	25.86	25.57	26.01
121	25.63	25.22	25.83	20.21	19.92	20.36	27.82	27.34	28.06
122	26.88	26.62	27.13	20.12	19.96	20.22	28.12	27.86	28.40
123	20.64	20.61	20.68	14.26	14.25	14.27	22.08	22.04	22.11
124	20.36	20.23	20.55	14.75	14.68	14.79	22.23	22.10	22.43
125	26.57	26.44	26.79	20.08	20.08	20.13	27.96	27.88	28.19

Table C.4: (continued)

Index	μ_0	-99%	$+99\%$	$\mu_{r<r_{half}}$	-99%	$+99\%$	$\mu_{r_{half}}$	-99%	$+99\%$
126	26.26	25.84	26.63	19.49	19.27	19.71	27.44	27.06	27.80
127	21.16	21.11	21.21	14.21	14.19	14.22	22.31	22.17	22.39
128	13.53	11.69	14.66	8.58	8.54	8.68	16.42	13.49	18.14
129	25.96	25.53	26.34	19.10	19.05	19.33	27.18	26.71	27.60
130	25.13	25.07	25.28	19.14	19.14	19.25	26.75	26.68	26.93
131	11.69	6.76	12.77	6.91	6.84	6.99	14.65	6.63	16.41
132	19.82	19.72	19.97	14.23	14.17	14.28	21.69	21.59	21.86
133	25.44	24.90	25.96	19.13	18.91	19.36	26.88	26.29	27.42
134	20.78	20.67	20.97	15.28	15.23	15.32	22.73	22.63	22.93
135	19.46	19.39	19.60	13.83	13.77	13.85	21.28	21.20	21.43
136	24.92	24.69	25.04	19.58	19.58	19.62	27.26	26.93	27.42
137	21.13	20.95	21.38	15.29	15.27	15.32	22.89	22.72	23.00
138	21.17	20.82	21.58	15.49	15.41	15.54	23.04	22.60	23.35
139	25.11	24.85	25.42	18.94	18.87	19.12	26.69	26.50	26.93
140	25.88	25.79	26.00	19.25	19.25	19.25	27.19	27.08	27.33
141	16.12	14.97	17.19	10.54	10.51	10.58	18.06	16.54	19.48
142	20.96	20.89	21.03	14.95	14.93	14.96	22.65	22.59	22.71
143	20.65	20.41	20.95	15.16	15.06	15.25	22.68	22.46	22.92
144	24.64	24.60	24.98	18.12	18.10	18.39	26.00	25.96	26.36
145	20.34	20.25	20.41	14.52	14.51	14.53	22.10	21.99	22.19
146	27.09	26.91	27.56	20.39	20.28	20.71	28.25	27.79	28.69
147	20.08	19.78	20.47	14.50	14.37	14.57	22.04	21.76	22.37
148	25.43	25.24	25.69	18.76	18.66	18.90	26.73	26.55	27.02
149	25.33	25.15	25.68	18.63	18.60	18.88	26.64	26.45	27.00
150	21.98	21.80	22.17	16.28	16.22	16.32	23.79	23.60	23.99

Table C.4: (continued)

Index	μ_0	-99%	$+99\%$	$\mu_{r<r_{half}}$	-99%	$+99\%$	$\mu_{r_{half}}$	-99%	$+99\%$
151	26.55	26.37	26.70	19.77	19.76	19.82	27.75	27.60	27.88
152	13.34	9.92	14.41	7.72	7.67	7.74	15.18	10.69	16.59
153	20.88	20.48	21.21	15.29	15.23	15.38	22.85	22.47	23.18
154	25.36	25.02	25.54	19.57	19.33	19.67	27.08	26.70	27.28
155	21.34	21.22	21.47	15.46	15.43	15.49	23.02	22.87	23.15
156	21.65	21.57	21.74	16.13	16.10	16.17	23.63	23.55	23.71
157	12.08	9.40	13.16	6.86	6.82	6.90	14.40	10.48	15.96
158	19.99	19.85	20.13	14.31	14.24	14.33	21.88	21.67	22.03
159	20.27	20.05	20.53	14.47	14.40	14.53	21.98	21.67	22.27
160	12.66	-0.27	13.74	7.69	7.63	7.74	15.51	-5.74	17.28
161	21.78	21.70	21.89	16.02	15.99	16.05	23.56	23.47	23.67
162	20.62	20.36	20.86	14.84	14.78	14.89	22.36	22.07	22.62
163	20.50	20.19	20.80	14.92	14.88	14.97	22.47	22.17	22.72
164	21.50	21.28	21.77	15.73	15.69	15.79	23.31	23.08	23.46
165	21.46	21.27	21.61	15.32	15.29	15.36	22.95	22.70	23.13
166	25.15	24.62	25.63	18.25	18.24	18.48	26.40	25.94	26.88
167	25.45	25.38	25.90	18.62	18.62	18.90	26.65	26.57	27.12
168	20.46	20.23	20.92	14.92	14.83	14.97	22.43	22.20	22.87
169	25.81	25.66	26.00	19.03	19.03	19.11	27.06	26.92	27.28
170	25.99	25.90	26.09	19.68	19.68	19.70	27.46	27.35	27.58
171	20.53	20.33	20.72	14.90	14.85	14.96	22.41	22.21	22.62
172	20.89	20.83	21.02	14.89	14.86	14.90	22.47	22.39	22.60
173	25.93	25.74	26.32	19.44	19.38	19.65	27.38	27.32	27.67
174	21.81	21.70	21.97	16.32	16.27	16.36	23.78	23.66	23.96
175	19.53	19.45	19.58	13.91	13.88	13.95	21.44	21.36	21.50

Table C.4: (continued)

Index	μ_0	-99%	$+99\%$	$\mu_{r<r_{half}}$	-99%	$+99\%$	$\mu_{r_{half}}$	-99%	$+99\%$
176	25.83	25.49	26.21	19.75	19.74	19.98	27.40	27.20	27.79
177	26.06	25.81	26.44	19.57	19.54	19.68	27.55	27.45	27.88
178	25.99	25.81	26.34	19.24	19.22	19.41	27.25	27.06	27.65
179	26.08	25.71	26.44	19.88	19.86	19.97	27.59	27.24	27.83
180	21.66	21.60	21.73	16.08	16.06	16.10	23.55	23.49	23.64
181	25.86	25.52	26.29	19.47	19.32	19.79	27.29	26.92	27.75
182	19.19	19.06	19.37	13.62	13.57	13.65	21.10	20.98	21.29
183	21.42	21.23	21.65	15.96	15.91	16.03	23.42	23.21	23.65
184	25.46	25.27	25.80	19.06	18.93	19.29	26.90	26.70	27.27
185	24.77	24.30	25.10	18.02	17.80	18.20	26.05	25.55	26.39
186	20.25	20.11	20.37	14.64	14.62	14.67	22.25	22.07	22.35
187	15.28	12.83	16.37	10.12	10.00	10.23	17.88	14.08	19.55
188	15.89	15.53	16.57	10.72	10.66	10.77	18.44	17.95	19.42
189	20.69	20.50	20.83	14.98	14.96	15.00	22.53	22.35	22.68
190	20.76	20.47	21.04	14.97	14.92	15.05	22.51	22.20	22.79
191	16.47	16.25	17.14	11.00	10.97	11.06	18.57	18.27	19.49
192	20.61	20.49	20.77	14.75	14.71	14.79	22.30	22.17	22.48
193	20.92	20.87	20.96	14.34	14.33	14.35	22.28	22.25	22.32
194	19.65	19.60	19.71	14.00	14.00	14.01	21.53	21.46	21.59
195	20.40	20.31	20.49	14.80	14.79	14.82	22.31	22.22	22.38
196	20.01	19.92	20.09	13.87	13.86	13.89	21.54	21.44	21.65
197	25.61	25.38	25.92	12.24	12.22	12.46	25.67	25.46	25.98
198	19.82	19.77	19.87	14.17	14.16	14.18	21.63	21.58	21.69
199	25.87	25.73	26.31	19.20	19.15	19.53	27.17	27.03	27.63
200	21.39	21.26	21.51	15.04	15.01	15.08	22.77	22.60	22.93

Table C.4: (continued)

Index	μ_0	-99%	$+99\%$	$\mu_{r<r_{half}}$	-99%	$+99\%$	$\mu_{r_{half}}$	-99%	$+99\%$
201	26.03	25.87	26.62	19.23	19.22	19.58	27.27	27.10	27.92
202	20.29	20.20	20.47	14.73	14.69	14.76	22.18	22.09	22.36
203	20.64	20.54	20.81	15.02	14.99	15.05	22.48	22.37	22.67
204	10.70	-8.21	11.77	5.93	5.84	5.96	13.84	-19.31	15.71
205	20.76	20.67	20.93	15.02	14.99	15.04	22.57	22.39	22.75
206	25.29	24.69	25.81	18.68	18.65	19.02	26.58	25.91	27.12
207	25.77	25.49	26.20	19.29	19.15	19.44	27.08	26.74	27.47
208	20.10	19.88	20.31	14.44	14.38	14.48	21.99	21.77	22.20
209	21.21	20.97	21.53	15.41	15.35	15.47	22.97	22.71	23.29
210	15.67	13.34	16.74	10.31	10.26	10.37	17.92	14.59	19.46
211	19.93	19.88	19.98	13.94	13.93	13.95	21.53	21.47	21.59
212	25.47	25.18	26.20	18.89	18.74	19.13	26.80	26.37	27.54
213	21.54	21.16	22.17	15.84	15.67	15.92	23.39	23.04	23.99
214	21.46	21.26	21.74	15.82	15.73	15.89	23.31	23.11	23.59
215	25.07	24.57	25.35	18.38	18.00	18.58	26.36	25.84	26.67
216	26.29	26.10	26.75	19.85	19.85	20.07	27.69	27.50	28.14
217	23.03	22.90	23.35	16.33	16.28	16.40	24.31	24.17	24.64
218	21.88	21.53	22.21	16.09	16.01	16.17	23.67	23.23	23.99
219	19.81	19.78	19.89	14.19	14.17	14.22	21.64	21.60	21.72
220	14.42	13.64	15.50	9.23	9.16	9.30	16.98	15.80	18.63
221	19.71	19.51	19.86	14.23	14.18	14.28	21.75	21.56	21.89
222	20.04	19.96	20.29	14.42	14.35	14.45	21.87	21.78	22.15
223	24.99	24.79	25.25	18.39	18.27	18.59	26.32	26.13	26.60
224	26.38	26.05	26.81	19.50	19.42	19.75	27.59	27.24	28.05
225	20.97	20.83	21.15	14.96	14.94	15.00	22.56	22.39	22.72

Table C.4: (continued)

Index	μ_0	-99%	$+99\%$	$\mu_{r<r_{half}}$	-99%	$+99\%$	$\mu_{r_{half}}$	-99%	$+99\%$
226	20.62	20.39	20.86	14.63	14.59	14.65	22.29	21.91	22.55
227	20.12	19.66	20.65	13.73	13.60	13.77	21.53	20.90	22.07
228	19.97	19.77	20.15	14.37	14.32	14.42	21.94	21.73	22.13
229	22.15	22.04	22.27	15.50	15.48	15.54	23.44	23.31	23.56
230	21.42	21.23	21.71	15.80	15.64	15.85	23.27	23.08	23.58
231	21.02	20.79	21.23	15.12	15.06	15.18	22.67	22.41	22.89
232	20.81	20.60	21.11	15.15	15.09	15.21	22.65	22.43	22.96
233	21.12	21.02	21.30	15.68	15.63	15.72	23.13	23.03	23.32
234	19.41	19.33	19.54	13.91	13.89	13.93	21.36	21.28	21.47
235	26.21	26.01	26.48	19.62	19.62	19.72	27.46	27.20	27.73
236	19.86	19.80	19.95	14.20	14.18	14.21	21.76	21.70	21.86
237	20.17	20.09	20.33	14.76	14.71	14.79	22.21	22.13	22.36
238	25.36	25.24	25.67	18.95	18.95	19.09	26.78	26.64	27.13
239	20.65	20.41	20.95	14.81	14.76	14.85	22.41	22.17	22.70
240	11.45	-6.46	12.53	6.60	6.48	6.68	14.41	-15.81	16.22
241	21.06	20.82	21.31	15.43	15.32	15.50	22.93	22.66	23.21
242	19.96	19.75	20.35	14.20	14.13	14.24	21.78	21.58	22.16
243	21.81	21.53	22.16	16.04	15.99	16.12	23.60	23.20	23.93
244	25.96	25.66	26.29	19.57	19.36	19.70	27.34	27.07	27.68
245	25.44	25.15	25.84	18.95	18.83	19.17	26.73	26.46	27.13
246	26.04	25.91	26.15	19.40	19.39	19.48	27.36	27.22	27.48
247	20.80	20.61	20.98	15.24	15.20	15.29	22.78	22.59	22.96
248	21.14	20.84	21.38	15.46	15.39	15.54	23.03	22.72	23.24
249	20.90	20.80	21.08	15.46	15.43	15.50	22.91	22.83	23.10
250	12.26	5.23	13.34	7.30	7.22	7.34	15.09	3.95	16.79

Table C.4: (continued)

Index	μ_0	-99%	$+99\%$	$\mu_{r<r_{half}}$	-99%	$+99\%$	$\mu_{r_{half}}$	-99%	$+99\%$
251	21.39	21.20	21.56	15.62	15.58	15.66	23.17	22.98	23.34
252	25.62	25.28	25.95	18.77	18.50	18.96	26.80	26.44	27.14
253	12.61	-0.17	13.70	7.14	7.10	7.18	14.72	-3.02	16.22
254	21.03	20.84	21.31	15.50	15.42	15.55	23.00	22.81	23.30
255	14.54	10.99	15.64	9.27	9.22	9.30	16.82	11.89	18.31
256	20.32	20.17	20.49	14.86	14.83	14.91	22.44	22.30	22.59
257	20.06	19.93	20.17	14.26	14.22	14.29	21.81	21.66	21.95
258	25.69	25.40	26.21	19.57	19.46	19.92	27.29	26.97	27.83
259	20.88	20.67	21.12	15.44	15.38	15.49	22.89	22.67	23.13
260	24.44	24.30	24.66	17.59	17.56	17.71	25.66	25.57	25.91
261	19.90	19.85	20.03	13.89	13.87	13.89	21.47	21.25	21.61
262	15.14	14.14	16.21	9.47	9.47	9.48	16.93	15.64	18.31
263	25.78	25.58	26.02	19.04	18.95	19.21	27.06	26.85	27.30
264	19.59	19.54	19.71	13.95	13.93	13.99	21.40	21.34	21.54
265	22.32	22.20	22.42	16.38	16.36	16.40	24.00	23.90	24.08
266	20.16	19.99	20.27	14.68	14.65	14.71	22.19	22.02	22.30
267	21.78	21.27	22.17	16.22	16.05	16.35	23.84	23.38	24.17
268	20.97	20.68	21.16	15.07	15.03	15.09	22.67	22.42	22.86
269	25.50	25.36	25.78	18.85	18.80	19.02	26.71	26.58	26.98
270	23.57	23.48	23.92	17.19	17.13	17.44	25.00	24.90	25.37
271	25.75	25.45	26.21	19.73	19.66	19.99	27.43	27.12	27.79
272	20.88	20.69	21.31	15.43	15.35	15.50	22.88	22.73	23.14
273	26.16	25.82	26.40	19.53	19.52	19.60	27.47	27.22	27.65
274	21.46	21.43	21.50	15.99	15.97	16.00	23.45	23.42	23.48
275	22.11	21.94	22.20	16.58	16.53	16.61	24.17	23.96	24.27

Table C.4: (continued)

Index	μ_0	-99%	$+99\%$	$\mu_{r<r_{half}}$	-99%	$+99\%$	$\mu_{r_{half}}$	-99%	$+99\%$
276	20.73	20.42	21.00	15.16	15.04	15.24	22.65	22.34	22.91
277	20.30	20.26	20.35	13.94	13.91	13.96	21.71	21.67	21.75
278	24.58	23.89	25.12	19.34	18.92	19.63	27.10	26.20	27.82
279	21.13	21.03	21.23	15.27	15.24	15.30	22.86	22.76	22.97
280	12.91	7.60	14.05	7.57	7.35	7.71	15.07	7.77	16.60
281	16.23	14.84	17.32	10.75	10.59	10.84	18.26	16.41	19.72
282	14.58	10.52	15.66	8.93	8.86	8.97	16.42	11.11	17.83
283	15.49	14.86	16.56	9.87	9.87	9.88	17.32	16.49	18.72
284	19.78	19.41	20.10	14.29	14.20	14.43	21.89	21.51	22.23
285	22.03	21.94	22.12	16.12	16.10	16.14	23.67	23.58	23.77
286	19.81	19.75	19.87	14.13	14.12	14.15	21.66	21.59	21.71
287	20.96	20.85	21.08	15.16	15.13	15.18	22.73	22.63	22.84
288	21.06	20.98	21.13	15.08	15.06	15.10	22.66	22.58	22.73
289	20.25	20.17	20.47	14.62	14.56	14.65	22.07	21.98	22.32
290	19.78	19.59	19.93	14.12	14.08	14.18	21.72	21.52	21.89
291	19.69	19.59	19.83	14.02	13.99	14.05	21.51	21.40	21.66
292	20.62	20.57	20.75	14.62	14.61	14.63	22.27	22.16	22.38
293	20.63	20.59	20.68	14.60	14.59	14.61	22.24	22.18	22.29
294	20.81	20.63	21.03	15.35	15.27	15.41	22.82	22.66	23.02
295	25.47	25.18	25.74	18.77	18.66	18.91	26.71	26.42	26.99
296	25.49	25.29	25.84	18.95	18.87	19.17	26.79	26.58	27.16
297	25.83	25.46	26.38	18.85	18.63	19.19	27.00	26.61	27.59
298	20.67	20.46	20.86	14.93	14.87	14.99	22.45	22.22	22.66
299	20.62	20.42	20.84	15.01	14.96	15.06	22.46	22.24	22.70
300	19.92	19.90	19.94	14.20	14.20	14.21	21.73	21.71	21.76

Table C.4: (continued)

Index	μ_0	-99%	$+99\%$	$\mu_{r<r_{half}}$	-99%	$+99\%$	$\mu_{r_{half}}$	-99%	$+99\%$
301	26.09	25.83	26.27	19.42	19.42	19.50	27.40	27.21	27.58
302	20.39	20.33	20.47	14.59	14.58	14.61	22.13	22.05	22.21
303	20.52	20.42	20.60	14.61	14.59	14.64	22.18	22.07	22.28
304	16.36	14.59	17.46	11.20	11.06	11.36	18.98	16.26	20.65
305	22.11	22.03	22.20	15.53	15.49	15.58	23.46	23.38	23.55
306	26.58	26.37	26.99	19.72	19.67	19.94	27.79	27.61	28.22
307	26.38	26.31	26.92	19.74	19.69	20.09	27.69	27.62	28.28
308	25.52	25.37	26.71	19.07	19.02	19.45	26.95	26.32	28.13
309	26.45	26.24	26.71	20.28	20.25	20.48	27.95	27.76	28.23
310	25.73	25.54	25.99	19.10	19.00	19.29	27.04	26.85	27.32
311	16.78	15.87	17.88	11.64	11.48	11.74	19.37	18.17	20.99
312	19.46	19.31	19.67	13.73	13.71	13.74	21.28	21.11	21.44
313	19.61	19.36	19.91	14.03	13.97	14.07	21.61	21.38	21.85
314	25.29	25.07	25.44	18.88	18.86	18.94	26.79	26.69	26.88
315	20.29	20.19	20.46	14.64	14.59	14.69	22.10	21.99	22.29
316	26.37	26.21	26.70	19.52	19.48	19.70	27.58	27.41	27.93
317	25.88	25.69	26.15	19.28	19.28	19.31	27.16	26.98	27.46
318	21.05	20.98	21.15	15.45	15.43	15.48	22.93	22.83	23.04
319	25.09	24.89	25.19	18.64	18.64	18.69	26.49	26.25	26.61
320	20.84	20.49	21.12	14.94	14.89	15.01	22.53	22.05	22.81
321	26.07	25.95	26.57	19.31	19.29	19.60	27.29	27.16	27.83
322	20.74	20.38	21.20	15.06	14.99	15.12	22.58	22.18	23.05
323	20.11	20.01	20.26	14.59	14.57	14.62	22.07	21.95	22.22
324	25.32	25.09	25.48	18.35	18.22	18.42	26.46	26.21	26.62
325	20.55	20.12	20.84	14.85	14.79	14.93	22.40	21.93	22.71

Table C.4: (continued)

Index	μ_0	-99%	$+99\%$	$\mu_{r<r_{half}}$	-99%	$+99\%$	$\mu_{r_{half}}$	-99%	$+99\%$
326	21.05	20.95	21.15	15.47	15.43	15.49	22.96	22.84	23.05
327	20.36	20.24	20.52	14.80	14.76	14.83	22.25	22.15	22.41
328	20.75	20.44	21.13	14.83	14.76	14.90	22.38	22.01	22.80
329	19.59	19.35	19.98	13.87	13.79	13.93	21.37	21.08	21.80
330	20.58	20.48	20.70	14.81	14.79	14.83	22.36	22.21	22.49
331	16.20	15.32	17.32	10.78	10.64	10.81	18.23	17.09	19.65
332	22.43	22.21	22.65	16.47	16.40	16.54	24.05	23.80	24.31
333	18.04	17.65	18.63	12.94	12.74	13.09	20.65	20.31	21.36
334	20.32	19.99	20.78	14.70	14.61	14.76	22.20	21.83	22.62
335	26.09	26.00	26.46	19.23	19.19	19.46	27.31	27.21	27.71
336	21.06	20.75	21.44	15.65	15.50	15.74	23.12	22.83	23.48
337	15.14	13.63	16.21	9.65	9.63	9.69	17.16	15.11	18.61
338	26.64	26.60	26.82	19.77	19.77	19.91	27.85	27.81	28.04
339	25.94	25.53	26.39	12.70	12.45	12.96	26.06	25.69	26.49
340	20.60	20.45	20.86	14.95	14.89	15.01	22.42	22.27	22.71
341	19.28	19.13	19.42	13.70	13.67	13.72	21.28	21.11	21.41
342	25.91	25.67	26.29	19.32	19.30	19.45	27.24	27.01	27.67
343	20.10	19.99	20.21	13.81	13.79	13.84	21.58	21.45	21.70
344	20.55	20.28	20.73	14.92	14.87	15.00	22.51	22.23	22.69
345	21.20	20.80	21.48	15.76	15.69	15.85	23.37	23.01	23.64
346	22.21	22.08	22.38	16.38	16.33	16.43	23.92	23.76	24.09
347	21.51	21.43	21.56	15.51	15.46	15.53	23.21	23.13	23.25
348	20.92	20.63	21.34	15.44	15.35	15.51	22.88	22.61	23.24
349	20.90	20.78	21.07	15.46	15.42	15.50	22.91	22.79	23.06
350	20.24	19.79	20.92	14.78	14.70	14.83	22.33	21.84	23.00

Table C.4: (continued)

Index	μ_0	-99%	$+99\%$	$\mu_{r<r_{half}}$	-99%	$+99\%$	$\mu_{r_{half}}$	-99%	$+99\%$
351	25.55	25.30	25.73	19.24	19.24	19.28	27.06	26.88	27.21
352	26.06	25.81	26.30	19.77	19.68	19.92	27.49	27.24	27.75
353	20.87	20.80	20.94	14.67	14.64	14.71	22.42	22.34	22.49
354	20.68	20.39	20.95	15.03	14.89	15.14	22.57	22.27	22.85
355	21.25	21.13	21.35	15.34	15.30	15.37	22.94	22.82	23.03
356	25.60	25.47	25.86	19.09	19.09	19.19	26.97	26.82	27.26
357	20.57	20.15	20.89	14.93	14.87	15.02	22.51	22.06	22.85
358	17.32	16.56	18.44	11.96	11.65	12.18	19.60	18.60	21.18
359	20.88	20.84	20.95	15.25	15.24	15.26	22.71	22.68	22.75
360	23.39	22.95	23.85	17.55	17.31	17.69	25.11	24.67	25.58
361	25.24	25.08	25.48	18.69	18.66	18.85	26.60	26.41	26.85
362	19.77	19.75	19.79	14.12	14.10	14.13	21.61	21.59	21.64
363	22.58	22.32	22.96	16.36	16.30	16.43	24.12	23.75	24.50
364	20.03	19.95	20.11	14.05	14.04	14.06	21.65	21.56	21.74
365	13.80	10.37	14.89	8.49	8.29	8.61	16.18	11.11	17.79
366	19.62	19.50	19.89	14.13	14.09	14.16	21.60	21.50	21.86
367	22.12	21.96	22.36	16.49	16.41	16.57	23.94	23.77	24.21
368	25.70	25.15	26.07	18.98	18.76	19.12	27.01	26.47	27.40
369	25.14	24.66	25.56	18.47	18.32	18.69	26.49	26.03	26.89
370	25.22	24.69	25.66	18.85	18.76	18.91	26.72	26.31	27.10
371	20.72	20.54	20.96	15.06	15.01	15.11	22.58	22.36	22.79
372	19.46	19.41	19.52	13.95	13.94	13.97	21.42	21.37	21.48
373	21.32	20.82	21.56	15.37	15.25	15.47	22.93	22.34	23.22
374	20.12	19.93	20.40	14.40	14.36	14.45	21.95	21.68	22.23
375	21.03	20.78	21.42	14.62	14.56	14.68	22.43	22.05	22.83

Table C.4: (continued)

Index	μ_0	-99%	$+99\%$	$\mu_{r<r_{half}}$	-99%	$+99\%$	$\mu_{r_{half}}$	-99%	$+99\%$
376	20.81	20.72	21.07	15.18	15.12	15.22	22.63	22.52	22.92
377	26.03	25.76	26.66	19.50	19.38	19.83	27.50	27.27	28.14
378	20.50	20.15	20.90	14.97	14.85	15.07	22.53	22.19	22.90
379	20.02	19.93	20.15	14.68	14.66	14.71	22.29	22.20	22.41
380	4.89	1.80	5.99	4.19	4.09	4.26	22.57	11.63	26.42
381	26.30	26.10	26.56	19.83	19.83	19.95	27.71	27.63	28.00
382	20.52	20.43	20.67	14.92	14.89	14.95	22.37	22.31	22.53
383	26.06	25.86	26.39	19.68	19.66	19.84	27.55	27.39	27.82
384	20.27	20.14	20.48	14.76	14.67	14.80	22.23	22.09	22.43
385	19.70	19.64	19.75	13.65	13.64	13.66	21.32	21.25	21.38
386	25.35	25.02	25.51	18.65	18.65	18.73	26.64	26.30	26.82
387	24.89	24.76	25.19	18.78	18.76	19.01	26.45	26.30	26.78
388	25.57	25.28	26.09	19.01	18.89	19.26	26.96	26.73	27.33
389	25.53	25.23	25.91	18.90	18.90	18.97	26.90	26.73	27.18
390	20.31	20.24	20.59	14.68	14.61	14.72	22.13	22.04	22.44
391	20.00	19.73	20.66	14.30	14.14	14.37	21.78	21.46	22.50
392	19.65	19.38	19.94	14.28	14.21	14.33	21.93	21.70	22.17
393	20.98	20.80	21.27	15.39	15.31	15.43	22.86	22.68	23.18
394	19.56	19.51	19.62	12.98	12.98	13.00	20.87	20.73	20.97
395	22.10	21.73	22.44	16.39	16.30	16.49	23.96	23.59	24.27
396	14.50	9.19	15.57	9.18	9.14	9.22	16.81	9.18	18.35
397	15.56	13.67	16.65	10.37	10.26	10.42	17.97	15.31	19.50
398	26.05	25.59	26.52	19.97	19.97	20.11	27.72	27.49	28.06
399	20.21	20.02	20.51	14.52	14.44	14.59	21.99	21.77	22.32
400	15.76	14.57	16.29	10.30	10.24	10.36	17.84	16.19	18.57

Table C.4: (continued)

Index	μ_0	-99%	$+99\%$	$\mu_{r<r_{half}}$	-99%	$+99\%$	$\mu_{r_{half}}$	-99%	$+99\%$
401	20.90	20.58	21.41	15.22	15.10	15.27	22.78	22.47	23.23
402	14.47	11.91	15.58	8.95	8.78	9.11	16.46	13.00	17.94
403	20.67	20.57	20.88	15.21	15.15	15.25	22.67	22.57	22.90
404	25.70	25.43	25.92	19.07	19.07	19.14	27.04	26.80	27.24
405	13.33	9.06	14.46	7.74	7.69	7.75	15.21	9.78	16.58
406	19.39	19.27	19.63	13.69	13.65	13.72	21.17	21.05	21.44
407	20.43	20.25	20.71	14.76	14.68	14.80	22.26	22.07	22.53
408	20.61	20.60	20.63	14.85	14.84	14.86	22.45	22.44	22.47
409	15.63	15.44	15.78	10.23	10.23	10.24	17.85	17.61	18.06
410	20.60	20.37	20.97	14.87	14.81	14.95	22.38	22.14	22.77
411	20.94	20.79	21.14	15.52	15.44	15.56	22.97	22.81	23.18
412	20.34	19.50	21.09	14.47	14.29	14.56	22.08	21.22	22.81
413	20.69	20.46	20.92	14.71	14.65	14.76	22.31	22.01	22.56
414	20.55	20.49	20.63	13.82	13.81	13.83	21.75	21.65	21.84
415	25.69	25.29	25.90	19.09	19.04	19.24	27.02	26.58	27.26
416	20.87	20.73	21.02	15.34	15.30	15.39	22.83	22.66	22.99
417	20.23	20.06	20.39	14.42	14.39	14.44	22.01	21.86	22.15
418	20.57	20.46	20.80	14.89	14.85	14.91	22.44	22.27	22.63
419	14.77	11.98	15.95	9.44	9.40	9.55	17.01	13.08	18.59
420	21.88	21.85	21.91	15.42	15.41	15.43	23.31	23.29	23.33
421	25.08	24.68	25.27	11.28	11.24	11.31	25.32	25.08	25.44
422	20.43	20.38	20.52	14.81	14.78	14.83	22.26	22.21	22.36
423	19.64	19.48	19.80	13.89	13.85	13.92	21.44	21.28	21.60
424	26.62	26.45	26.88	20.04	20.03	20.18	27.96	27.90	28.17
425	20.41	20.25	20.62	14.82	14.79	14.87	22.33	22.17	22.55

Table C.4: (continued)

Index	μ_0	-99%	$+99\%$	$\mu_{r<r_{half}}$	-99%	$+99\%$	$\mu_{r_{half}}$	-99%	$+99\%$
426	24.04	23.59	24.56	17.50	17.21	17.83	25.40	24.90	25.96
427	20.24	20.12	20.47	14.78	14.74	14.82	22.23	22.13	22.43
428	26.21	25.79	26.56	19.65	19.63	19.83	27.55	27.32	27.88
429	20.87	20.64	21.11	14.79	14.74	14.83	22.40	22.12	22.66
430	20.39	20.22	20.60	14.84	14.79	14.89	22.34	22.14	22.55
431	20.63	20.39	20.88	14.93	14.85	14.99	22.44	22.17	22.71
432	20.30	20.07	20.65	14.61	14.51	14.68	22.10	21.87	22.48
433	20.39	20.08	20.69	14.87	14.75	14.96	22.41	22.11	22.70
434	25.76	25.48	26.13	19.43	19.39	19.68	27.24	26.98	27.64
435	25.74	25.39	26.00	18.88	18.72	19.05	26.91	26.54	27.18
436	20.88	20.57	21.16	14.64	14.59	14.70	22.30	21.91	22.65
437	20.25	20.04	20.46	14.37	14.34	14.40	21.97	21.76	22.16
438	18.22	18.12	18.28	12.73	12.71	12.74	20.32	20.25	20.37
439	22.27	22.13	22.45	16.61	16.55	16.66	24.13	23.98	24.30
440	21.47	21.26	21.95	15.73	15.59	15.80	23.22	22.98	23.75
441	25.50	25.36	25.59	18.75	18.75	18.77	26.64	26.50	26.75
442	21.55	21.36	21.92	16.00	15.90	16.07	23.45	23.26	23.82
443	18.91	18.75	19.01	13.24	13.22	13.27	20.84	20.70	20.97
444	26.70	26.38	27.04	19.96	19.87	20.20	28.00	27.89	28.34
445	17.13	17.00	17.44	11.94	11.90	11.97	19.72	19.52	20.19
446	20.54	20.46	20.68	14.92	14.87	14.96	22.37	22.29	22.53
447	20.81	20.59	21.04	15.29	15.20	15.36	22.80	22.59	23.01
448	25.70	25.60	26.02	18.76	18.76	18.93	26.88	26.77	27.23
449	21.19	21.02	21.43	15.69	15.62	15.77	23.18	23.01	23.42
450	21.13	20.95	21.33	14.91	14.87	14.95	22.65	22.41	22.83

Table C.4: (continued)

Index	μ_0	-99%	$+99\%$	$\mu_{r<r_{half}}$	-99%	$+99\%$	$\mu_{r_{half}}$	-99%	$+99\%$
451	23.74	23.40	24.00	16.76	16.49	16.91	24.90	24.54	25.19
452	25.45	25.08	25.85	18.94	18.89	19.24	26.78	26.36	27.20
453	20.78	20.74	20.81	15.38	15.37	15.38	22.86	22.83	22.89
454	26.47	26.22	27.03	19.74	19.68	20.01	27.80	27.69	28.21
455	22.11	21.93	22.41	16.65	16.52	16.72	24.13	23.95	24.45
456	24.17	23.96	24.59	18.02	17.98	18.24	25.80	25.63	26.19
457	13.93	9.47	15.01	8.80	8.67	8.84	16.59	9.65	18.26
458	20.30	20.12	20.75	14.13	14.08	14.16	21.89	21.53	22.25
459	20.36	20.20	20.63	14.75	14.65	14.81	22.24	22.09	22.52
460	21.44	21.39	21.50	15.06	15.04	15.07	22.90	22.85	22.94
461	13.90	11.52	14.99	8.39	8.34	8.45	15.90	12.74	17.33
462	21.01	20.89	21.21	15.38	15.32	15.45	22.84	22.72	23.06
463	14.34	11.51	15.41	9.04	9.00	9.10	16.78	12.53	18.39
464	25.85	25.54	26.18	19.11	18.99	19.28	27.17	26.97	27.41
465	20.82	20.62	21.00	15.06	15.01	15.11	22.57	22.32	22.79
466	20.51	20.37	20.74	14.86	14.77	14.91	22.32	22.15	22.57
467	21.60	21.47	21.75	15.25	15.22	15.29	23.06	22.94	23.19
468	25.72	25.58	26.04	19.05	19.04	19.27	27.02	26.86	27.36
469	20.97	20.91	21.00	14.56	14.54	14.57	22.49	22.44	22.52
470	14.52	12.23	15.59	9.05	8.93	9.15	16.59	13.45	18.06
471	25.71	25.59	26.07	18.81	18.72	19.07	26.86	26.74	27.21
472	8.12	2.36	9.21	3.79	3.65	3.95	11.86	0.41	14.01
473	13.77	11.24	14.85	8.38	8.26	8.47	15.99	12.37	17.52
474	21.22	21.09	21.40	15.72	15.65	15.78	23.20	23.08	23.38
475	20.91	20.79	21.06	15.20	15.16	15.23	22.75	22.62	22.88

Table C.4: (continued)

Index	μ_0	-99%	$+99\%$	$\mu_{r<r_{half}}$	-99%	$+99\%$	$\mu_{r_{half}}$	-99%	$+99\%$
476	13.82	11.42	14.91	8.28	8.26	8.29	15.74	12.63	17.14
477	13.34	5.93	14.43	7.90	7.75	7.97	15.55	5.02	17.08
478	26.01	25.96	26.26	20.87	20.86	20.97	28.72	28.65	29.10
479	20.96	20.68	21.33	15.46	15.32	15.52	22.95	22.72	23.31
480	20.95	20.86	21.08	15.33	15.26	15.37	22.78	22.67	22.91
481	12.65	2.38	13.77	7.46	7.39	7.53	15.16	0.15	16.73
482	25.59	25.20	26.05	18.94	18.71	19.21	27.00	26.61	27.46
483	15.89	14.00	17.01	10.78	10.63	10.90	18.55	15.78	20.19
484	20.71	20.64	20.87	15.04	15.02	15.06	22.59	22.40	22.76
485	19.48	19.46	19.51	13.94	13.94	13.95	21.40	21.38	21.43
486	14.69	9.75	15.78	9.25	9.17	9.35	16.84	9.95	18.34
487	25.81	25.44	26.53	19.50	19.50	19.58	27.20	26.68	27.90
488	25.52	25.37	26.79	18.99	18.97	19.20	26.83	25.53	28.11
489	17.32	17.18	17.48	11.79	11.65	11.80	19.29	19.15	19.44
490	20.73	20.59	20.95	15.25	15.21	15.29	22.71	22.55	22.93
491	20.52	20.38	20.69	14.91	14.88	14.94	22.46	22.33	22.63
492	24.28	24.04	24.43	17.58	17.40	17.67	25.56	25.30	25.72
493	26.35	26.17	26.50	19.86	19.85	19.91	27.73	27.51	27.90
494	22.09	21.49	22.90	16.13	15.85	16.24	23.69	22.91	24.53
495	24.51	24.26	24.72	17.75	17.69	17.85	25.82	25.57	26.04
496	21.53	21.12	21.86	15.49	15.45	15.59	23.12	22.72	23.45
497	20.30	20.17	20.50	14.78	14.73	14.80	22.23	22.10	22.44
498	25.52	25.06	25.75	19.53	19.52	19.60	27.17	26.72	27.41
499	21.12	21.05	21.19	14.68	14.66	14.71	22.52	22.43	22.59
500	21.31	21.24	21.40	15.46	15.43	15.47	23.01	22.92	23.10

Table C.4: (continued)

Index	μ_0	-99%	$+99\%$	$\mu_{r<r_{half}}$	-99%	$+99\%$	$\mu_{r_{half}}$	-99%	$+99\%$
501	26.55	26.29	26.75	20.23	20.01	20.35	27.92	27.72	28.11
502	24.83	24.53	25.17	19.63	19.42	19.72	27.43	27.05	27.94
503	21.30	21.15	21.47	15.00	14.96	15.04	22.84	22.68	23.01
504	25.51	24.93	25.92	19.15	19.15	19.24	27.07	26.56	27.25
505	25.02	24.98	25.09	18.44	18.44	18.49	26.38	26.34	26.44
506	25.88	25.86	26.18	19.19	19.18	19.40	27.15	27.13	27.47
507	21.01	20.99	21.04	14.16	14.15	14.17	22.21	22.15	22.26
508	21.71	21.64	21.79	15.63	15.61	15.65	23.30	23.22	23.38
509	21.46	21.42	21.50	15.19	15.17	15.21	22.94	22.90	22.99
510	16.79	16.49	17.53	11.73	11.69	11.77	19.49	19.19	20.54
511	20.66	20.57	20.73	14.17	14.16	14.18	22.00	21.90	22.06
512	25.53	25.21	25.86	19.46	19.46	19.56	27.18	26.82	27.39
513	25.30	25.03	25.48	19.18	19.04	19.28	26.86	26.58	27.07
514	15.05	14.01	16.15	9.84	9.79	9.90	17.53	16.11	19.10
515	13.91	11.50	15.05	8.58	8.49	8.60	16.22	12.73	17.81
516	25.39	25.19	25.76	19.54	19.46	19.73	27.11	26.91	27.50
517	20.09	19.93	20.21	14.29	14.25	14.32	21.82	21.64	21.96
518	12.94	12.81	13.54	7.80	7.79	7.81	15.48	15.31	16.36
519	20.71	20.68	20.74	14.70	14.70	14.71	22.29	22.26	22.32
520	25.58	25.33	25.79	18.73	18.56	18.88	26.79	26.54	27.02
521	26.08	25.98	26.42	19.65	19.64	19.91	27.49	27.38	27.86
522	26.32	26.09	26.59	20.28	20.25	20.44	27.95	27.78	28.16
523	26.07	25.90	26.30	19.66	19.66	19.75	27.51	27.41	27.75
524	20.37	20.29	20.46	14.92	14.88	14.95	22.42	22.35	22.51
525	26.45	26.38	26.69	19.69	19.69	19.82	27.69	27.63	27.96

Table C.4: (continued)

Index	μ_0	-99%	$+99\%$	$\mu_{r<r_{half}}$	-99%	$+99\%$	$\mu_{r_{half}}$	-99%	$+99\%$
526	16.13	15.70	16.71	10.85	10.76	10.97	18.58	17.97	19.42
527	26.39	26.28	26.59	20.13	20.13	20.23	27.84	27.69	28.05
528	25.88	25.81	25.96	19.78	19.78	19.80	27.39	27.31	27.49
529	25.54	25.31	25.85	19.40	19.30	19.62	27.09	26.81	27.43
530	16.13	14.66	17.20	10.70	10.65	10.74	18.32	16.25	19.83
531	19.63	19.25	20.13	13.55	13.46	13.62	21.16	20.75	21.70
532	26.38	26.11	26.65	21.19	21.16	21.31	28.89	28.86	29.05
533	25.61	25.28	26.02	20.31	20.13	20.56	27.94	27.55	28.37
534	26.14	25.92	26.44	19.47	19.43	19.64	27.47	27.27	27.78
535	25.99	25.60	26.74	19.33	19.26	19.81	27.29	26.84	28.12
536	25.87	25.83	26.13	19.17	19.16	19.36	27.04	26.97	27.28
537	15.66	14.94	16.58	10.58	10.52	10.67	18.45	17.28	19.92
538	19.74	19.64	19.89	14.03	13.99	14.07	21.51	21.37	21.68
539	25.55	25.43	25.76	19.26	19.26	19.37	27.02	26.89	27.26
540	25.45	25.32	25.57	19.63	19.63	19.68	27.16	27.03	27.29
541	17.50	16.94	18.33	12.36	12.21	12.48	20.14	19.34	21.39
542	26.39	26.19	26.65	19.95	19.95	19.98	27.87	27.78	27.98
543	7.00	-138.74	8.08	4.62	4.42	4.63	15.11	-547.79	19.24
544	20.71	20.64	20.89	14.06	14.05	14.07	21.93	21.67	22.11
545	25.42	25.33	25.51	19.10	19.10	19.14	26.88	26.78	26.99
546	25.25	25.01	25.50	19.19	19.02	19.34	26.83	26.55	27.11
547	26.30	26.02	26.59	19.67	19.67	19.83	27.52	27.13	27.82
548	26.29	26.13	26.75	19.70	19.66	19.98	27.63	27.52	28.13
549	26.12	25.99	26.48	19.49	19.48	19.69	27.44	27.29	27.84
550	19.99	19.93	20.04	14.14	14.12	14.15	21.73	21.66	21.79

Table C.4: (continued)

Index	μ_0	-99%	$+99\%$	$\mu_{r<r_{half}}$	-99%	$+99\%$	$\mu_{r_{half}}$	-99%	$+99\%$
551	21.62	21.37	21.84	15.95	15.89	16.01	23.54	23.30	23.76
552	20.60	20.14	20.96	14.45	14.39	14.50	22.08	21.56	22.46
553	21.00	20.78	21.28	15.28	15.23	15.34	22.81	22.56	23.11
554	8.72	-10.90	9.79	3.44	3.39	3.51	11.13	-18.17	12.73
555	20.14	19.78	20.45	14.54	14.43	14.60	21.99	21.56	22.33
556	25.69	25.44	25.99	11.63	11.45	11.83	25.73	25.48	26.04
557	25.29	24.84	25.57	18.62	18.47	18.76	26.66	26.17	26.94
558	19.05	18.78	19.37	13.52	13.47	13.59	21.12	20.83	21.48
559	24.29	24.25	24.41	18.06	18.04	18.16	25.80	25.76	25.93
560	25.57	25.33	25.94	19.23	19.15	19.47	27.04	26.85	27.44
561	22.08	21.78	22.35	16.23	16.18	16.30	23.82	23.51	24.08
562	25.27	25.18	25.44	18.67	18.67	18.74	26.60	26.50	26.79
563	25.65	25.37	26.26	18.92	18.91	19.26	26.96	26.72	27.62
564	20.81	20.72	20.91	15.31	15.30	15.32	22.79	22.70	22.89
565	24.33	24.03	24.76	17.69	17.64	17.88	25.61	25.16	26.08
566	20.32	19.83	20.87	14.65	14.56	14.72	22.23	21.73	22.75
567	24.81	24.64	25.15	18.00	17.87	18.23	26.04	25.87	26.42
568	26.71	26.34	26.94	20.51	20.39	20.59	28.15	27.77	28.43
569	26.03	25.79	26.51	19.24	19.23	19.34	27.40	27.37	27.54
570	21.86	21.77	22.00	16.25	16.20	16.27	23.75	23.66	23.86
571	20.81	20.74	20.88	14.53	14.50	14.58	22.28	22.20	22.35
572	19.56	19.22	20.08	13.96	13.85	14.03	21.44	21.19	22.00
573	24.39	24.28	24.69	18.27	18.26	18.50	25.95	25.83	26.28
574	24.99	24.88	25.15	18.17	18.14	18.21	26.30	26.20	26.41
575	20.25	20.15	20.45	14.63	14.55	14.67	22.09	21.99	22.31

Table C.4: (continued)

Index	μ_0	-99%	$+99\%$	$\mu_{r<r_{half}}$	-99%	$+99\%$	$\mu_{r_{half}}$	-99%	$+99\%$
576	26.35	26.18	26.51	19.65	19.57	19.75	27.64	27.54	27.80
577	25.49	25.28	25.78	19.10	18.99	19.30	26.91	26.69	27.22
578	20.02	19.52	20.48	14.12	14.06	14.23	21.72	21.23	22.19
579	14.10	8.64	15.25	8.76	8.68	8.85	16.30	8.92	17.77
580	26.07	25.82	26.43	19.75	19.72	19.96	27.54	27.28	27.95
581	25.92	25.53	26.54	19.02	18.98	19.37	27.16	26.85	27.81
582	21.48	21.25	21.80	15.93	15.84	16.01	23.41	23.21	23.70
583	20.52	20.46	20.58	14.84	14.81	14.87	22.30	22.24	22.38
584	20.18	19.79	20.41	14.26	14.20	14.33	21.86	21.50	22.10
585	11.37	0.30	12.48	6.52	6.45	6.61	14.24	-3.40	15.97
586	20.84	20.81	20.86	14.82	14.80	14.82	22.45	22.42	22.47
587	25.20	24.75	25.60	18.51	18.22	18.76	26.42	25.97	26.82
588	25.09	24.89	25.35	12.03	12.03	12.06	25.26	25.13	25.39
589	5.69	-4.25	6.76	2.41	2.38	2.44	11.71	-17.52	14.85
590	25.96	25.73	26.38	19.54	19.46	19.84	27.28	27.09	27.69
591	21.65	21.31	22.14	16.22	16.04	16.33	23.74	23.39	24.19
592	25.38	25.07	25.86	18.89	18.65	19.16	26.75	26.39	27.24
593	22.67	22.50	22.80	16.97	16.87	17.02	24.45	24.26	24.60
594	14.36	12.45	15.44	9.28	9.19	9.37	17.04	14.11	18.69
595	21.51	21.37	21.66	15.80	15.77	15.85	23.36	23.23	23.49
596	25.56	25.27	26.12	20.45	20.41	20.82	28.27	27.90	28.98
597	19.47	19.40	19.68	13.50	13.47	13.51	21.12	20.88	21.33
598	24.35	23.72	24.80	17.53	17.15	17.70	25.58	24.90	26.06
599	26.23	26.01	26.50	19.99	19.98	20.07	27.73	27.48	28.04
600	12.63	11.92	13.74	7.53	7.37	7.66	15.31	14.29	16.98

Table C.4: (continued)

Index	μ_0	-99%	$+99\%$	$\mu_{r<r_{half}}$	-99%	$+99\%$	$\mu_{r_{half}}$	-99%	$+99\%$
601	20.54	20.11	21.01	14.61	14.56	14.68	22.23	21.70	22.66
602	20.51	20.39	20.68	14.90	14.85	14.96	22.39	22.25	22.57
603	15.04	13.02	16.12	9.47	9.45	9.51	16.98	14.30	18.40
604	24.75	24.56	25.06	18.35	18.28	18.54	26.15	25.97	26.49
605	14.00	12.65	15.16	9.07	8.99	9.20	16.83	14.76	18.51
606	21.64	21.56	21.78	15.31	15.29	15.36	23.00	22.86	23.17
607	24.75	24.19	25.06	10.57	10.29	10.80	24.81	24.26	25.12
608	26.40	26.19	26.87	20.03	20.01	20.27	27.80	27.61	28.24
609	20.69	20.63	20.74	9.43	9.40	9.46	20.83	20.78	20.88
610	20.68	20.49	20.85	14.14	14.11	14.17	22.04	21.81	22.24
611	19.24	19.18	19.33	13.79	13.77	13.82	21.25	21.20	21.32
612	26.51	26.14	26.71	12.00	11.68	12.05	26.61	26.24	26.78
613	21.17	21.08	21.25	14.87	14.84	14.90	22.64	22.52	22.72
614	25.35	25.21	25.47	18.59	18.59	18.63	26.61	26.45	26.74
615	25.73	25.42	26.44	19.03	18.88	19.28	26.98	26.27	27.69
616	20.69	20.43	20.99	14.10	14.06	14.15	22.06	21.59	22.38
617	17.08	16.31	18.16	11.73	11.67	11.79	19.38	18.31	20.88
618	20.74	20.52	20.90	14.99	14.97	15.05	22.58	22.36	22.71
619	23.43	23.32	23.51	16.76	16.69	16.80	24.74	24.62	24.82
620	20.47	20.44	20.50	14.62	14.61	14.62	22.19	22.16	22.22
621	25.47	25.21	25.86	19.05	19.04	19.22	26.95	26.69	27.36
622	26.74	26.39	27.31	20.16	20.10	20.41	27.95	27.64	28.51
623	20.26	20.08	20.37	14.67	14.62	14.72	22.30	22.12	22.45
624	22.36	22.13	22.84	16.89	16.80	16.96	24.35	24.12	24.67
625	26.34	26.32	26.74	19.85	19.84	20.13	27.70	27.63	28.10

Table C.4: (continued)

Index	μ_0	-99%	$+99\%$	$\mu_{r<r_{half}}$	-99%	$+99\%$	$\mu_{r_{half}}$	-99%	$+99\%$
626	23.36	22.91	23.57	16.78	16.67	16.83	24.75	24.29	24.84
627	20.32	20.17	20.61	14.82	14.75	14.87	22.29	22.15	22.50
628	19.49	19.07	20.01	13.93	13.69	14.06	21.40	20.89	21.94
629	24.50	24.21	24.87	17.69	17.49	17.94	25.74	25.43	26.14
630	25.84	25.58	26.11	19.92	19.92	19.96	27.55	27.31	27.78
631	25.65	25.54	25.81	19.52	19.52	19.54	27.18	27.04	27.36
632	10.48	-1.61	11.63	4.62	4.48	4.77	12.42	-3.15	13.81
633	26.04	25.88	26.21	19.44	19.44	19.46	27.25	27.07	27.48
634	20.42	20.17	20.67	14.50	14.43	14.58	22.06	21.77	22.33
635	20.23	20.02	20.71	14.31	14.21	14.33	21.91	21.51	22.36
636	25.52	25.24	25.83	20.02	19.93	20.09	27.49	27.27	27.75
637	15.06	11.37	16.16	9.75	9.65	9.87	17.34	12.17	18.86
638	23.77	23.33	24.18	17.21	17.01	17.38	25.18	24.73	25.62
639	19.85	19.74	20.12	14.20	14.14	14.24	21.67	21.54	21.97
640	20.13	19.96	20.32	14.53	14.46	14.60	22.04	21.87	22.25
641	15.24	12.75	16.34	9.94	9.74	10.07	17.64	13.98	19.23
642	13.75	10.55	14.82	8.41	8.37	8.50	16.13	11.42	17.71
643	20.97	20.71	21.26	15.09	15.05	15.15	22.67	22.38	22.93
644	18.02	17.80	18.14	12.54	12.50	12.61	20.09	19.87	20.21
645	23.33	23.16	23.65	16.64	16.53	16.84	24.62	24.44	24.98
646	25.21	25.15	25.26	19.67	19.67	19.68	27.19	27.12	27.26
647	26.08	25.64	26.56	19.24	19.00	19.46	27.33	26.92	27.84
648	20.32	20.26	20.43	14.85	14.81	14.87	22.31	22.24	22.42
649	21.24	21.16	21.37	15.23	15.22	15.25	22.87	22.73	23.01
650	20.81	20.72	20.92	14.80	14.79	14.82	22.38	22.25	22.53

Table C.4: (continued)

Index	μ_0	-99%	$+99\%$	$\mu_{r<r_{half}}$	-99%	$+99\%$	$\mu_{r_{half}}$	-99%	$+99\%$
651	23.34	23.26	23.42	17.14	17.11	17.19	24.97	24.90	25.05
652	20.32	20.29	20.35	14.78	14.78	14.79	22.28	22.26	22.31
653	20.10	20.08	20.11	14.35	14.34	14.36	21.85	21.83	21.87
654	21.63	21.55	21.75	15.47	15.44	15.50	23.16	23.04	23.26
655	26.52	26.35	26.72	20.31	20.31	20.42	27.97	27.79	28.18
656	20.72	20.37	21.14	14.88	14.83	14.95	22.46	22.00	22.90
657	25.79	25.42	26.13	19.92	19.87	20.19	27.48	27.18	27.80
658	20.47	20.45	20.51	14.90	14.88	14.91	22.37	22.34	22.40
659	20.62	20.46	20.91	15.01	14.94	15.08	22.46	22.30	22.77
660	25.10	24.81	25.27	18.82	18.64	18.92	26.58	26.25	26.77
661	22.46	22.29	22.66	16.90	16.82	16.97	24.36	24.17	24.55
662	19.79	19.75	19.84	13.76	13.75	13.77	21.37	21.29	21.43
663	20.28	20.24	20.32	14.63	14.62	14.64	22.14	22.10	22.17
664	20.09	19.66	20.76	13.91	13.79	14.03	21.55	20.90	22.24
665	26.24	26.01	26.52	19.79	19.78	19.93	27.56	27.37	27.81
666	20.46	20.32	20.58	14.74	14.70	14.77	22.26	22.12	22.40
667	19.78	19.72	19.88	14.15	14.12	14.18	21.60	21.54	21.71
668	20.36	20.06	20.69	14.50	14.44	14.58	22.05	21.70	22.40
669	25.70	25.37	26.17	19.25	19.22	19.56	27.08	26.75	27.58
670	26.48	26.34	26.87	19.57	19.57	19.77	27.68	27.61	28.11
671	20.57	20.32	20.74	15.02	14.96	15.07	22.63	22.39	22.82
672	25.48	25.23	25.76	18.55	18.46	18.62	26.63	26.36	26.93
673	19.74	19.53	20.05	14.00	13.92	14.04	21.49	21.23	21.83
674	20.77	20.66	20.84	14.53	14.51	14.54	22.23	22.11	22.34
675	25.07	24.83	25.39	18.34	18.24	18.57	26.33	26.06	26.66

Table C.4: (continued)

Index	μ_0	-99%	$+99\%$	$\mu_{r<r_{half}}$	-99%	$+99\%$	$\mu_{r_{half}}$	-99%	$+99\%$
676	20.28	20.11	20.46	14.61	14.57	14.65	22.19	22.02	22.36
677	19.48	19.40	19.69	13.91	13.87	13.93	21.36	21.29	21.54
678	24.74	24.45	25.03	18.38	18.26	18.55	26.21	25.94	26.51
679	25.49	25.22	26.70	19.30	19.30	19.39	27.01	26.42	28.28
680	19.15	18.66	19.82	12.99	12.80	13.10	20.62	20.13	21.27
681	20.99	20.71	21.20	14.37	14.31	14.41	22.29	21.97	22.51
682	19.98	19.90	20.09	13.79	13.77	13.80	21.43	21.28	21.55
683	25.09	25.04	25.17	18.66	18.63	18.71	26.50	26.46	26.59
684	19.49	19.10	19.86	13.79	13.74	13.87	21.37	20.99	21.65
685	26.02	25.92	26.18	19.10	19.06	19.21	27.17	27.05	27.33
686	20.20	20.17	20.22	13.91	13.90	13.92	21.66	21.62	21.71
687	21.87	21.65	22.07	15.09	15.02	15.16	23.11	22.85	23.33
688	20.70	20.51	20.90	14.94	14.89	14.99	22.46	22.25	22.68
689	20.43	20.38	20.52	14.72	14.71	14.73	22.24	22.15	22.32
690	9.46	-46.25	10.54	4.77	4.72	4.83	12.43	-81.93	14.25
691	21.04	20.93	21.22	15.55	15.52	15.60	23.01	22.90	23.20
692	20.18	20.07	20.45	14.66	14.60	14.70	22.11	22.02	22.26
693	21.82	21.59	22.10	15.57	15.50	15.64	23.35	22.99	23.64
694	9.26	-1.82	10.34	4.14	4.08	4.27	11.98	-5.77	13.70
695	18.95	18.78	19.14	13.31	13.27	13.34	20.91	20.74	21.10
696	20.41	20.26	20.57	14.78	14.73	14.81	22.25	22.08	22.39
697	20.44	19.58	20.94	14.97	14.70	15.12	22.46	21.50	22.96
698	18.78	18.65	18.91	13.02	12.99	13.04	20.54	20.40	20.69
699	16.85	16.71	17.17	11.74	11.72	11.76	19.53	19.37	19.99
700	19.54	19.48	19.59	13.94	13.93	13.95	21.55	21.49	21.61

Table C.4: (continued)

Index	μ_0	-99%	$+99\%$	$\mu_{r<r_{half}}$	-99%	$+99\%$	$\mu_{r_{half}}$	-99%	$+99\%$
701	22.32	21.99	22.67	16.44	16.36	16.51	24.02	23.67	24.40
702	26.63	26.44	26.90	20.35	20.35	20.43	28.15	28.02	28.42
703	25.77	25.54	26.13	19.79	19.70	20.02	27.38	27.10	27.76
704	25.89	25.72	26.21	19.09	19.09	19.19	27.13	26.94	27.49
705	25.80	25.59	25.96	19.33	19.33	19.40	27.19	26.96	27.37
706	26.43	26.27	26.67	19.88	19.88	19.95	27.65	27.48	27.89
707	25.47	25.30	25.74	19.10	19.03	19.27	26.91	26.72	27.22
708	25.11	24.85	25.33	18.54	18.42	18.64	26.47	26.24	26.71
709	25.73	25.58	25.87	19.55	19.55	19.60	27.26	27.09	27.43
710	21.64	21.40	21.88	15.71	15.66	15.76	23.27	23.01	23.53
711	25.50	25.38	25.64	19.18	19.18	19.23	26.97	26.84	27.12
712	21.27	20.78	21.62	15.73	15.54	15.89	23.35	22.86	23.72
713	25.20	24.87	25.73	18.22	18.12	18.56	26.37	26.02	26.94
714	19.67	19.34	19.91	14.00	13.94	14.06	21.51	21.21	21.76
715	25.73	25.50	25.99	19.51	19.51	19.58	27.16	26.91	27.43
716	20.42	20.33	20.62	14.96	14.90	14.98	22.40	22.32	22.60
717	24.54	24.25	24.73	18.14	18.00	18.25	25.96	25.64	26.18
718	19.24	19.24	19.25	13.60	13.60	13.60	21.06	21.06	21.07
719	25.81	25.46	26.43	19.19	19.14	19.53	27.12	26.77	27.79
720	20.51	20.41	20.68	14.87	14.82	14.93	22.34	22.23	22.52
721	20.60	20.24	20.92	14.62	14.55	14.70	22.23	21.86	22.54
722	20.91	20.80	21.02	15.48	15.44	15.50	23.03	22.92	23.14
723	20.33	20.28	20.40	14.81	14.80	14.83	22.28	22.23	22.36
724	20.12	20.07	20.14	14.35	14.35	14.36	21.88	21.82	21.92
725	20.94	20.83	21.09	15.28	15.23	15.33	22.76	22.64	22.92

Table C.4: (continued)

Index	μ_0	-99%	$+99\%$	$\mu_{r<r_{half}}$	-99%	$+99\%$	$\mu_{r_{half}}$	-99%	$+99\%$
726	20.18	20.15	20.21	13.91	13.91	13.92	21.64	21.60	21.67
727	20.25	20.15	20.38	14.74	14.71	14.77	22.21	22.10	22.32
728	21.26	21.20	21.35	15.66	15.63	15.68	23.10	23.04	23.19
729	21.04	20.85	21.30	15.43	15.38	15.48	22.92	22.73	23.21
730	19.76	19.30	20.16	14.35	14.29	14.44	21.98	21.53	22.35
731	25.80	25.70	26.00	19.35	19.35	19.37	27.14	26.99	27.36
732	19.95	19.91	20.01	14.35	14.34	14.36	21.82	21.78	21.86
733	20.13	20.08	20.17	14.56	14.54	14.57	22.06	22.01	22.10
734	25.89	25.78	26.15	19.62	19.57	19.85	27.37	27.31	27.64
735	20.46	20.39	20.55	14.62	14.61	14.64	22.25	22.17	22.33
736	20.23	20.08	20.48	14.60	14.56	14.65	22.06	21.92	22.34
737	25.56	25.39	26.88	18.93	18.91	19.40	26.88	26.67	28.23
738	26.30	26.02	26.54	19.43	19.40	19.57	27.55	27.50	27.75
739	20.41	20.35	20.47	14.54	14.53	14.54	22.10	22.03	22.15
740	23.17	22.99	23.33	16.85	16.80	16.88	24.71	24.61	24.86
741	22.45	21.79	23.22	16.88	16.73	16.95	24.37	23.76	25.12
742	25.52	24.70	26.02	19.82	19.82	19.94	27.34	26.53	27.77
743	20.67	20.57	20.78	15.13	15.09	15.17	22.58	22.48	22.69
744	25.04	24.58	25.38	18.95	18.92	19.10	26.66	26.30	27.03
745	20.07	20.00	20.18	14.58	14.56	14.60	22.03	21.97	22.13
746	20.25	20.03	20.43	14.42	14.36	14.47	21.99	21.77	22.19
747	21.77	21.53	21.96	16.16	16.10	16.23	23.69	23.44	23.87
748	20.63	20.51	20.81	15.12	15.07	15.16	22.58	22.47	22.77
749	26.79	26.72	26.94	20.26	20.26	20.33	28.07	27.99	28.23
750	19.90	19.86	19.94	14.24	14.23	14.24	21.78	21.74	21.82

Table C.4: (continued)

Index	μ_0	-99%	$+99\%$	$\mu_{r<r_{half}}$	-99%	$+99\%$	$\mu_{r_{half}}$	-99%	$+99\%$
751	22.78	22.04	23.56	16.11	15.97	16.17	24.07	23.16	24.84
752	25.57	25.39	26.49	18.68	18.60	19.23	26.76	26.51	27.68
753	23.21	22.79	23.52	16.75	16.46	16.93	24.60	24.15	24.95
754	20.44	20.33	20.64	14.79	14.73	14.83	22.25	22.14	22.48
755	21.14	20.98	21.25	15.33	15.31	15.35	22.88	22.74	22.94
756	24.66	24.51	24.80	18.07	18.03	18.11	25.95	25.82	26.07
757	21.62	21.45	21.81	15.34	15.30	15.39	23.15	22.98	23.32

Appendix D

Images of Survey Fields

Here we provide images of all of the fields used in this work. These are the final, fully reduced and combined images. They are presented in the same order as Table 2.1 and Table 3.1 — numerically by observing run. As in the latter table, we have omitted the two fields listed in the former table that were unusable and have not included the two fields that were observed more times on other observing runs. Images are oriented with north down and east left except for the last observing run (the last 20 images) which have north up and east right.

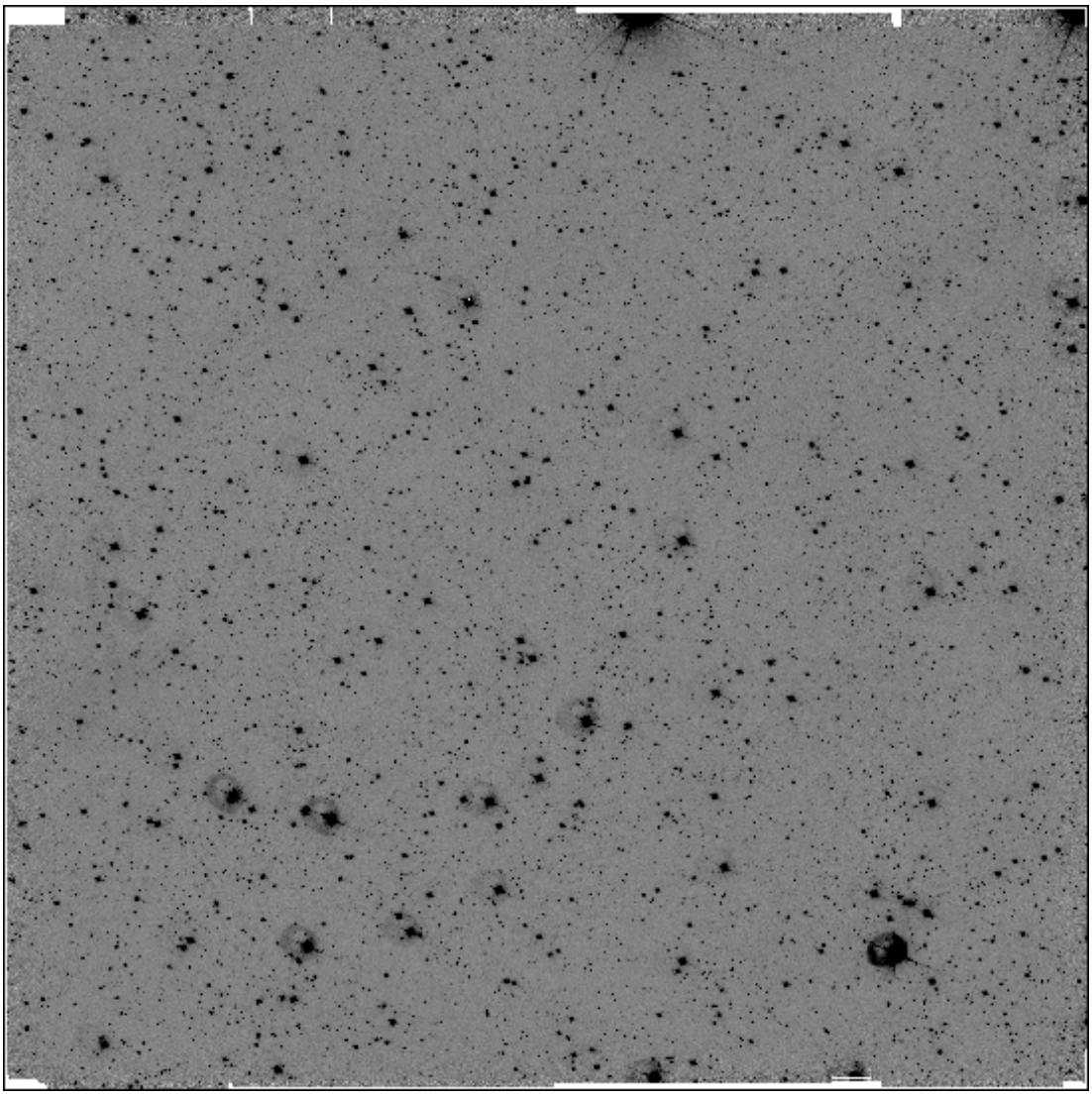

Figure D.1: LCRS Field 0020-39a

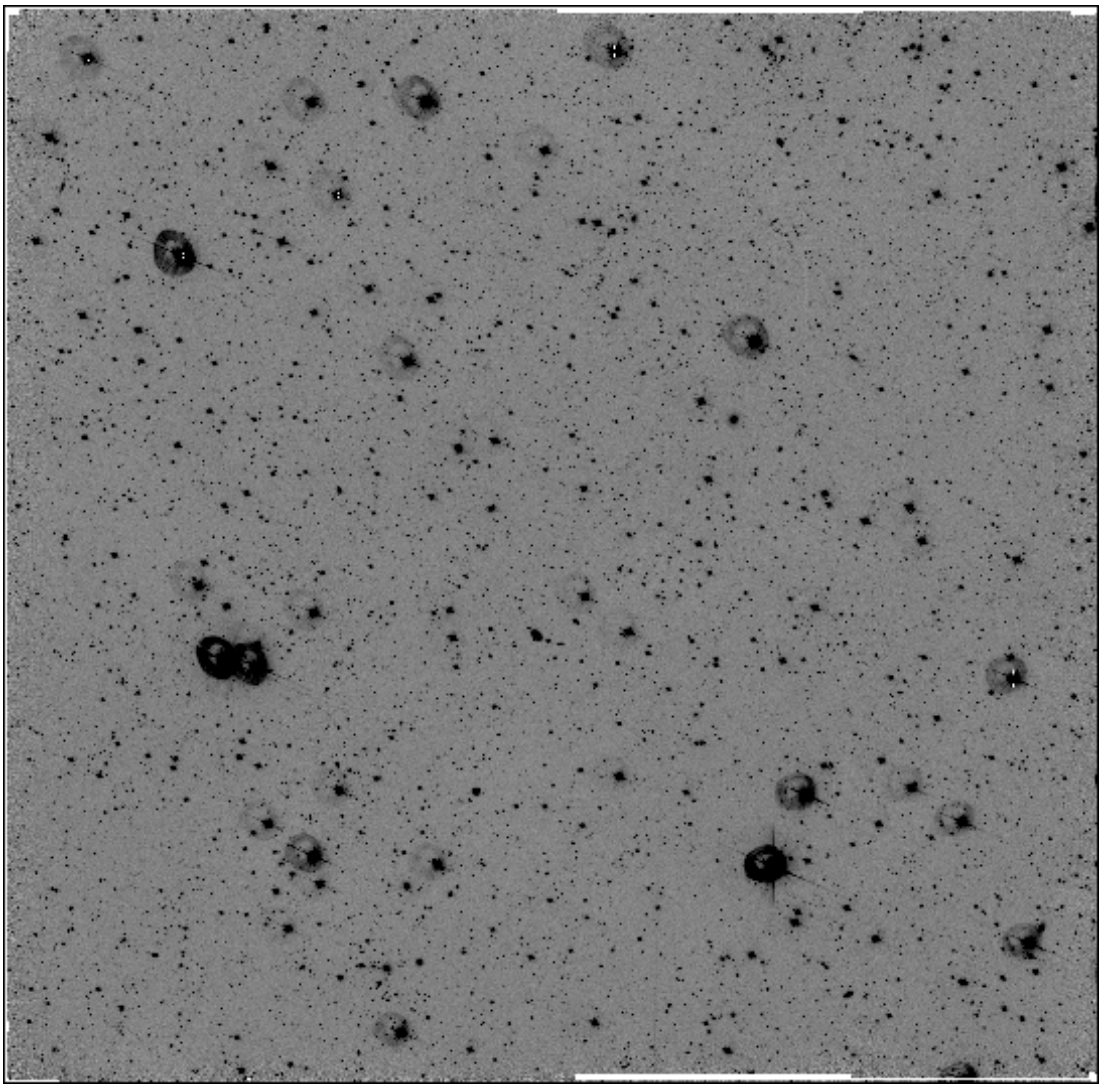

Figure D.2: LCRS Field 0020-45a

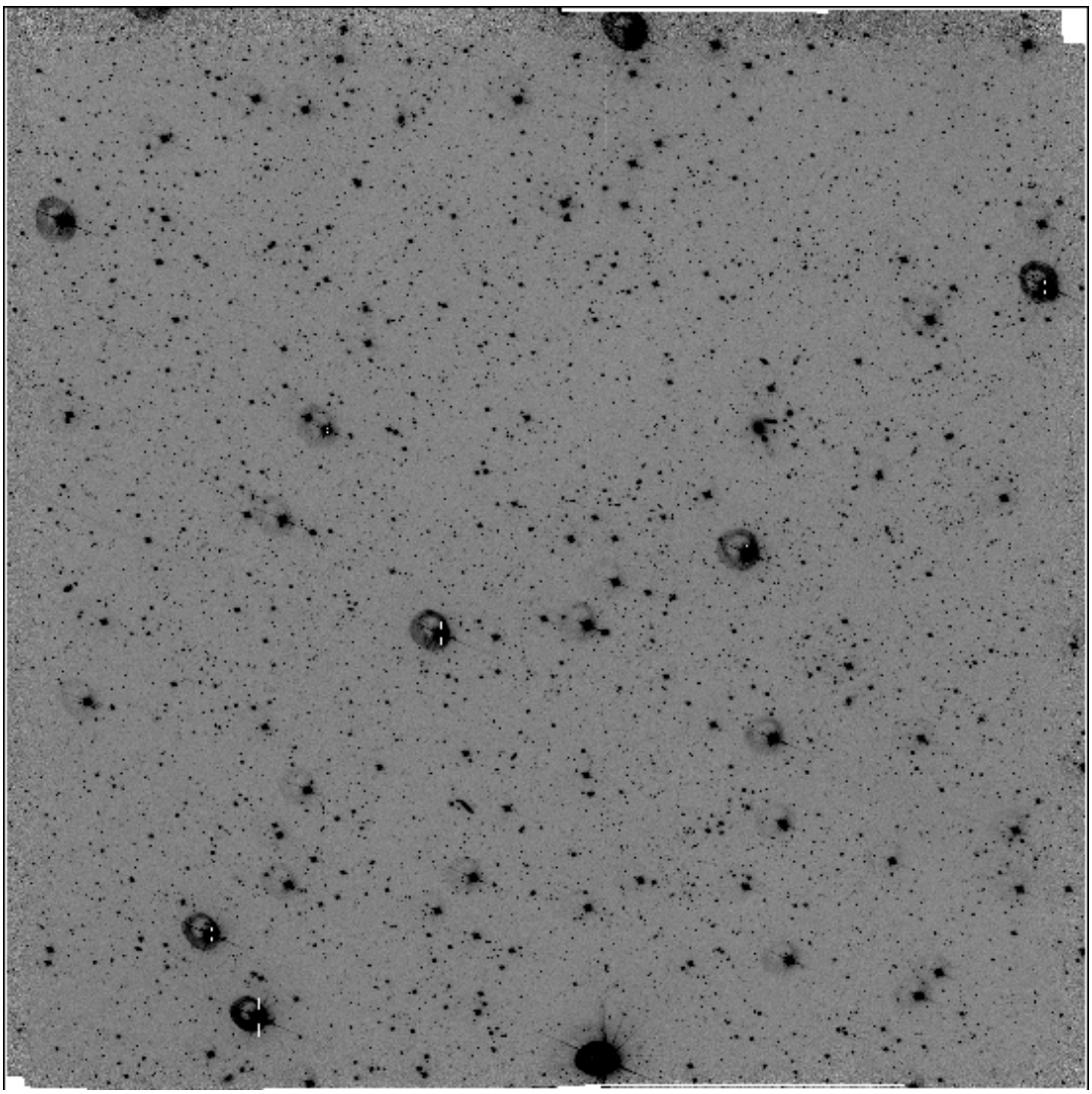

Figure D.3: LCRS Field 0100-39a

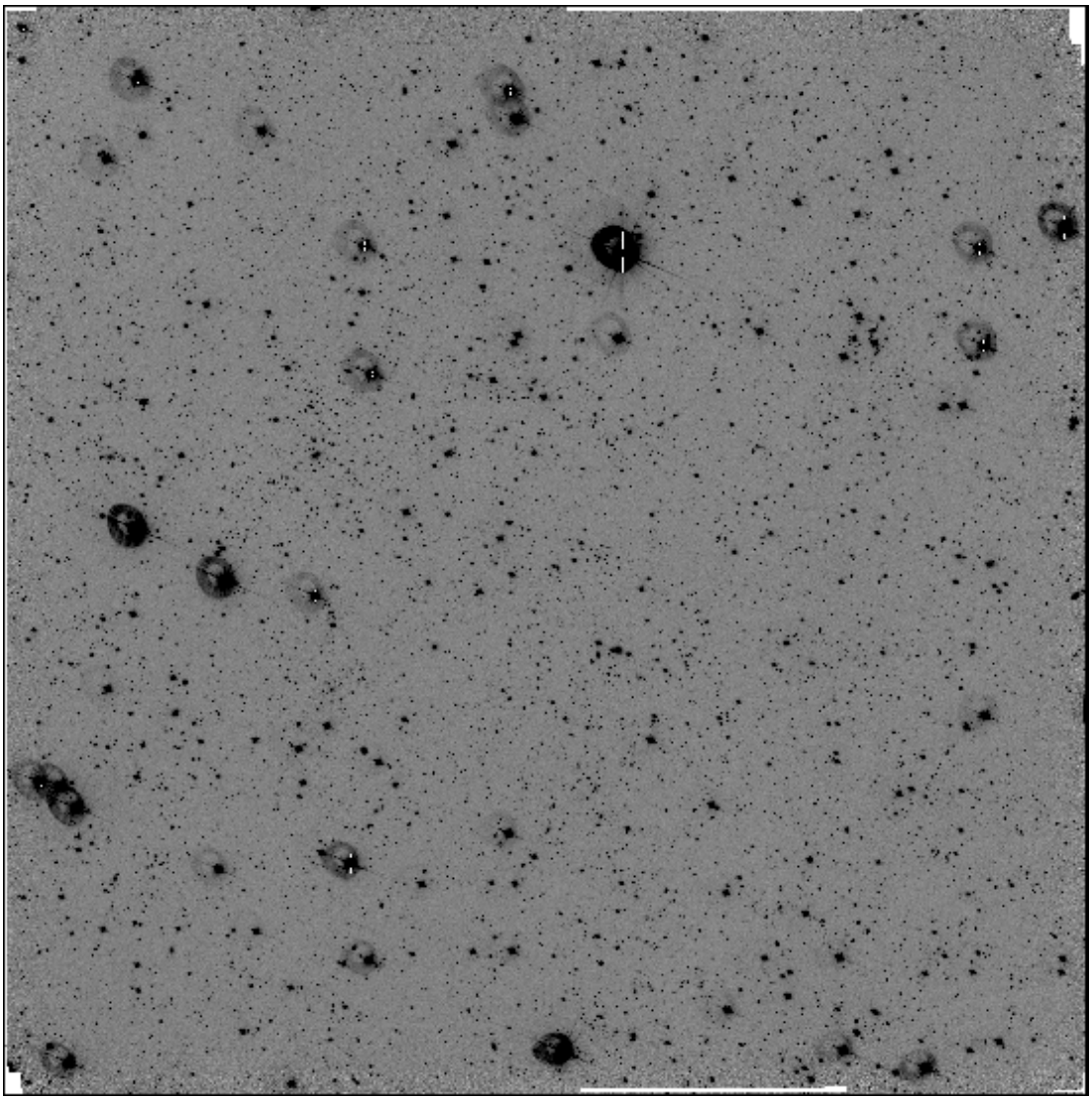

Figure D.4: LCRS Field 0100-39b

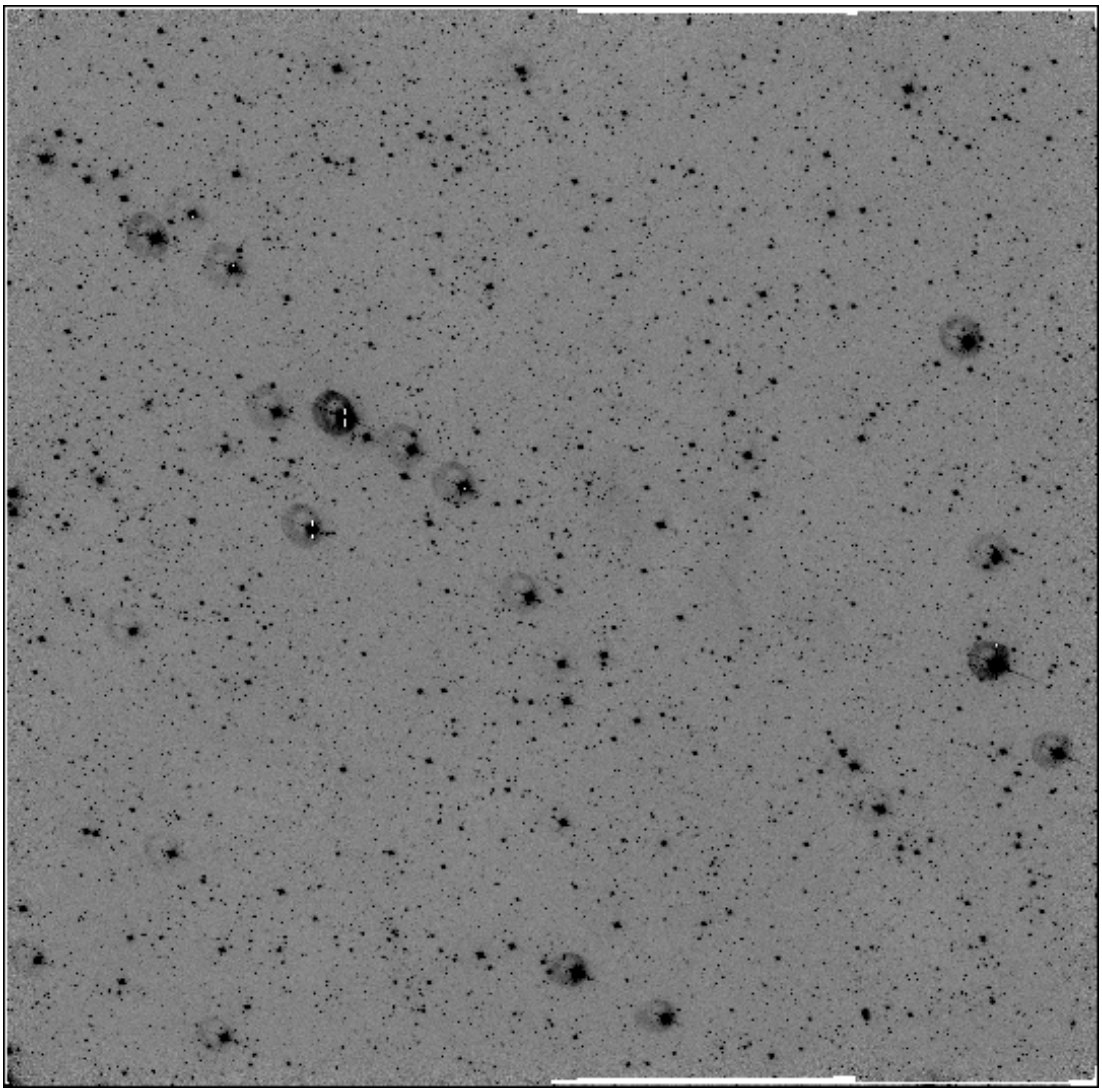

Figure D.5: LCRS Field 0220-39a

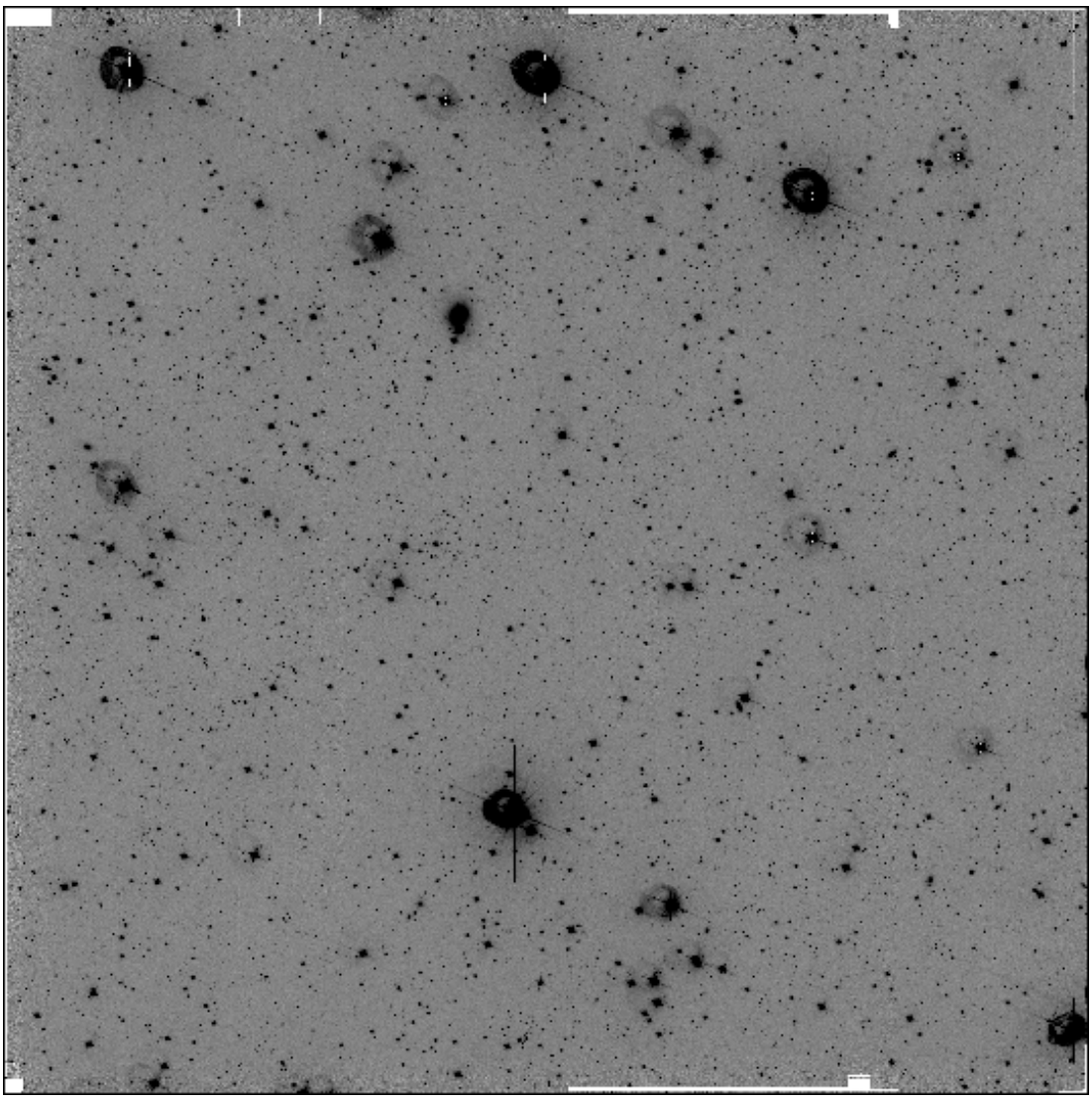

Figure D.6: LCRS Field 0300-39a

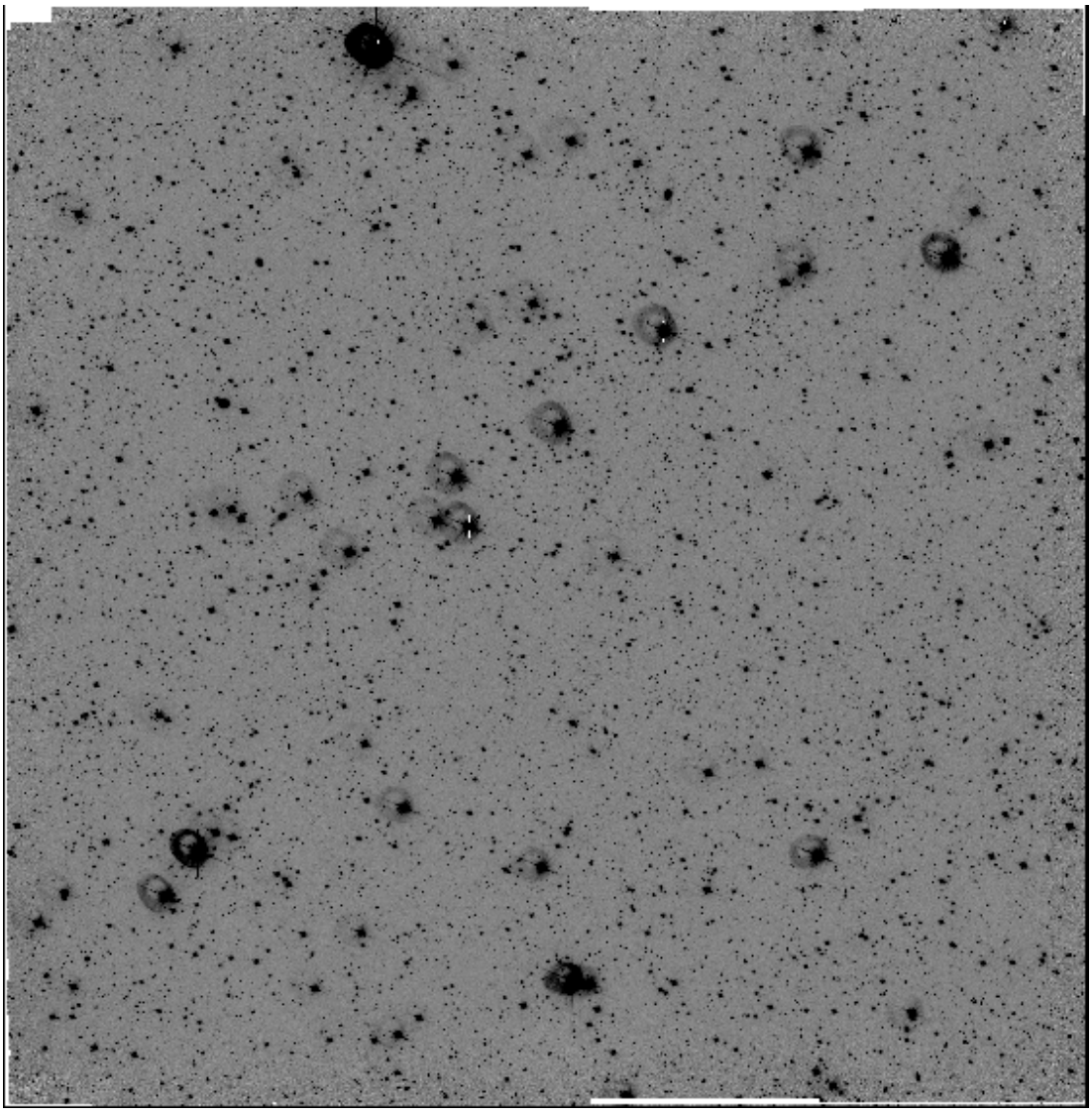

Figure D.7: LCRS Field 2140-45a

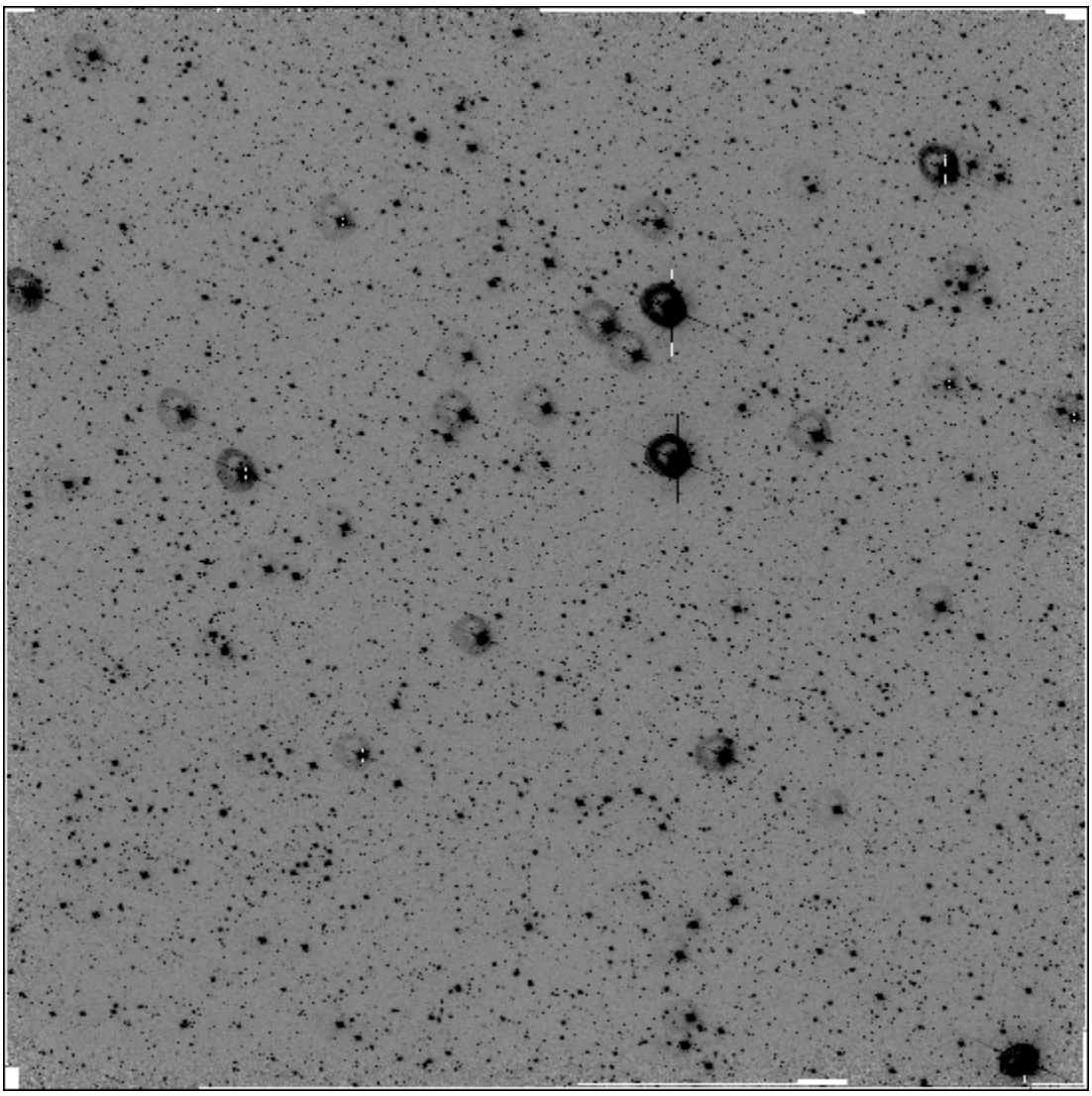

Figure D.8: LCRS Field 2140-45b

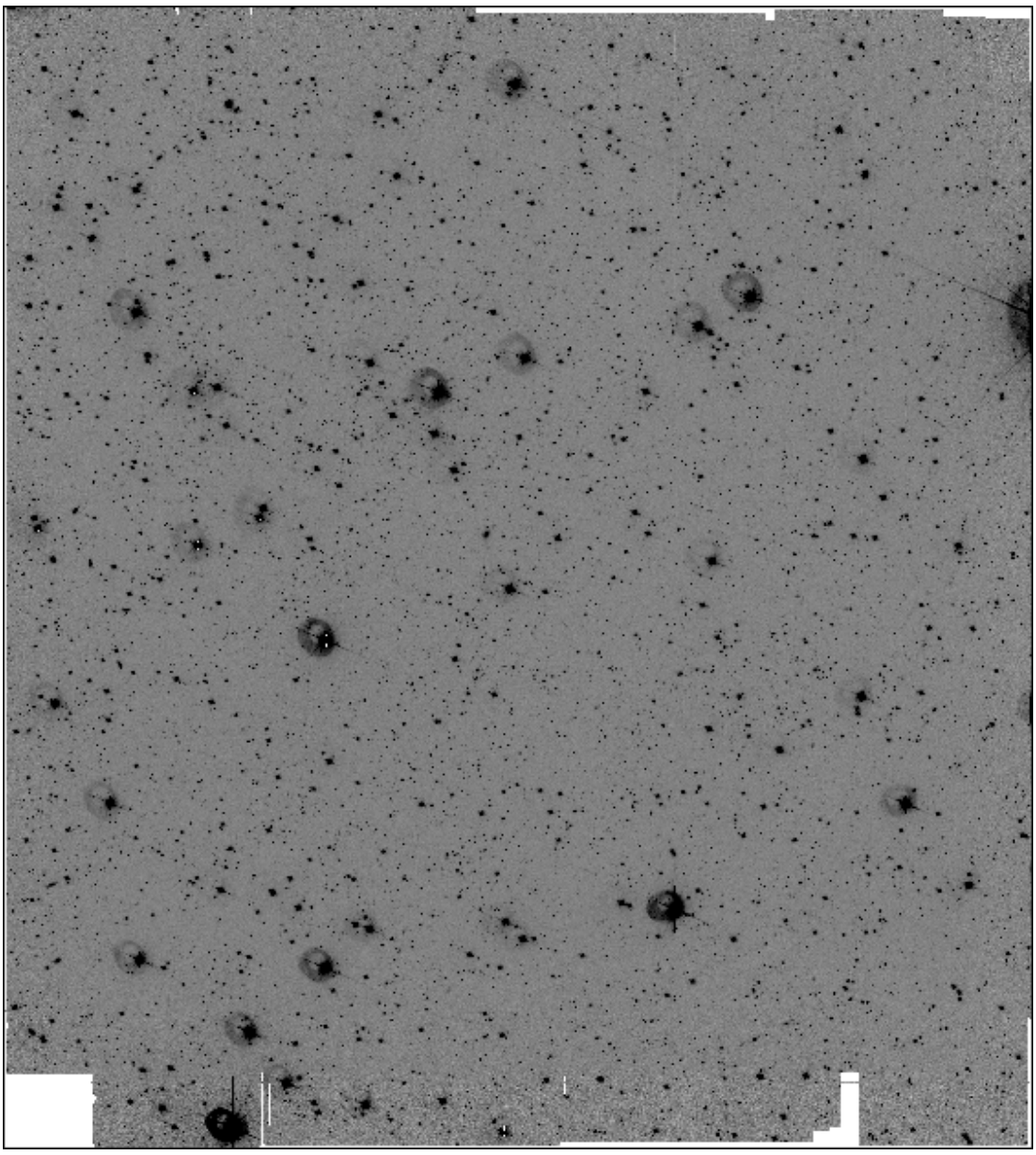

Figure D.9: LCRS Field 2220-39a

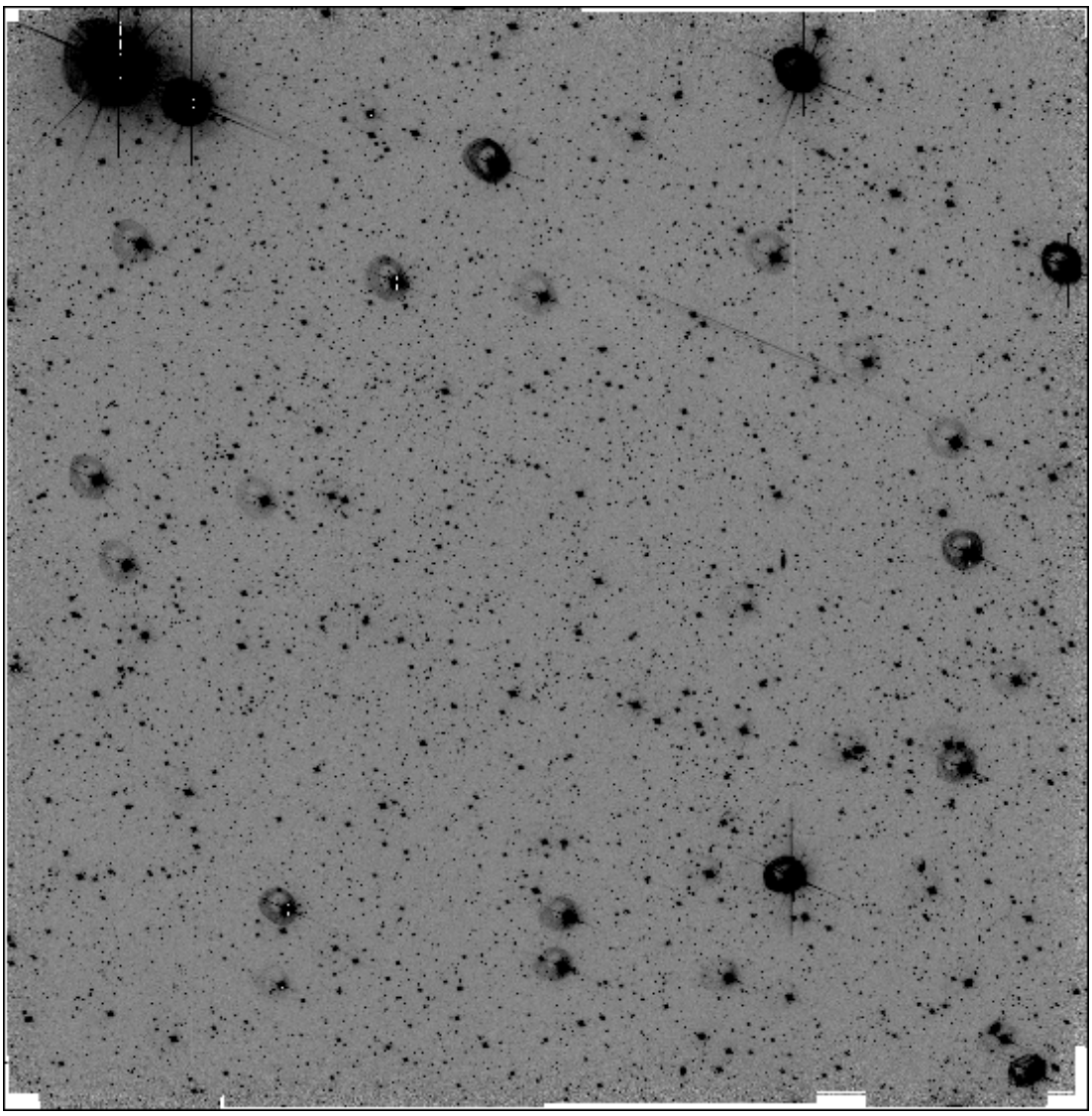

Figure D.10: LCRS Field 2220-39b

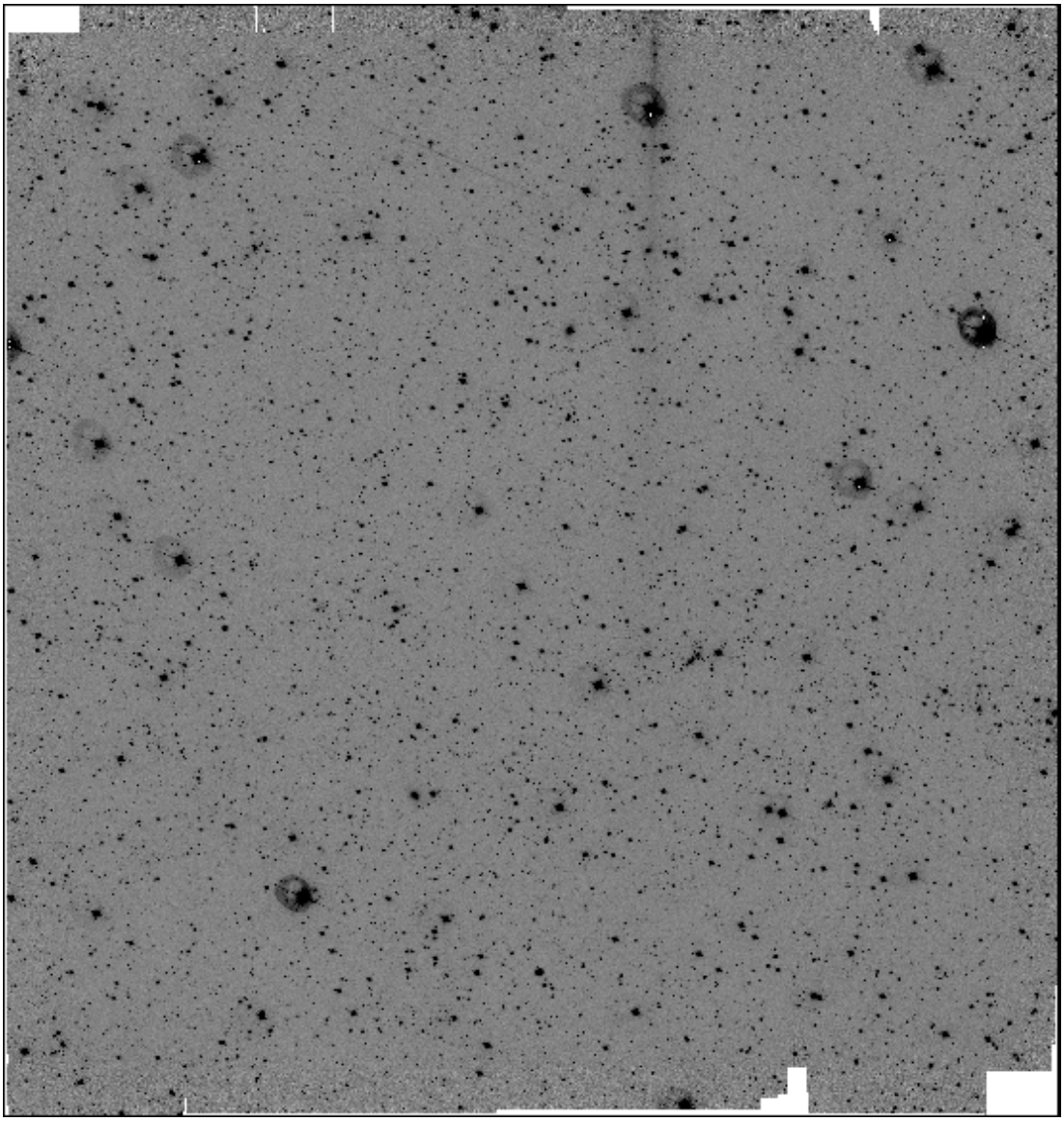

Figure D.11: LCRS Field 2300-39a

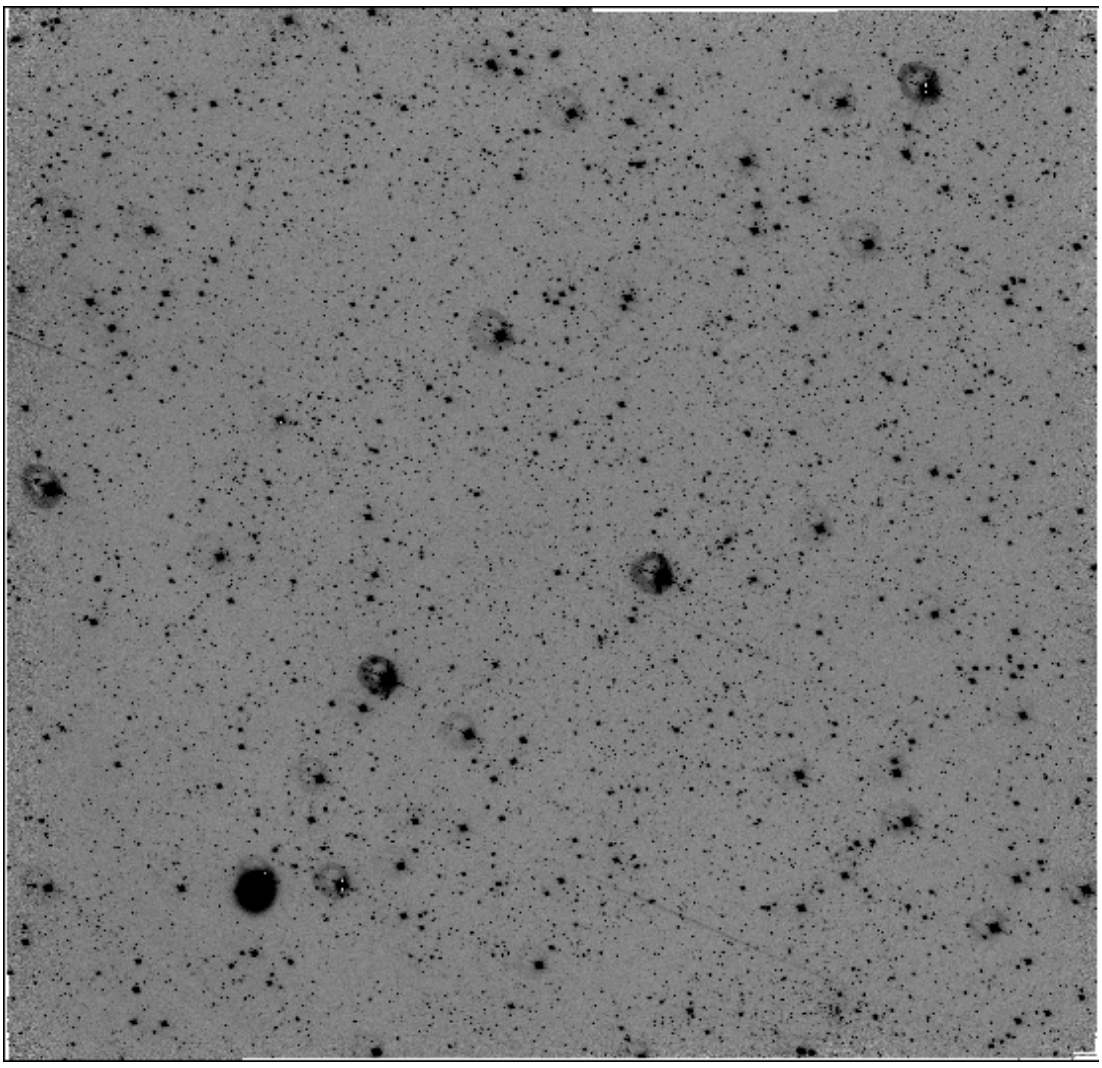

Figure D.12: LCRS Field 2320-42a

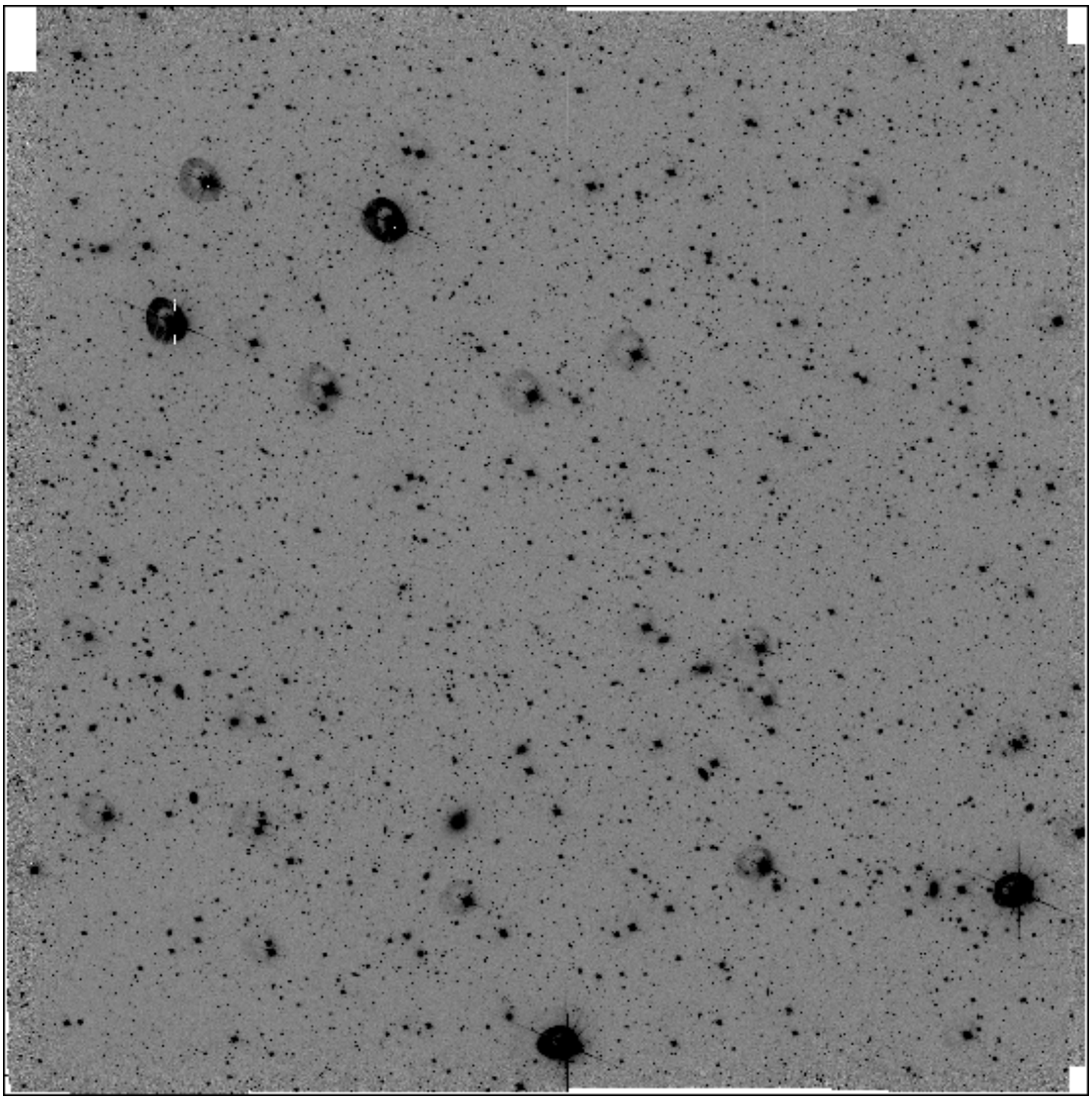

Figure D.13: LCRS Field 2340-39a

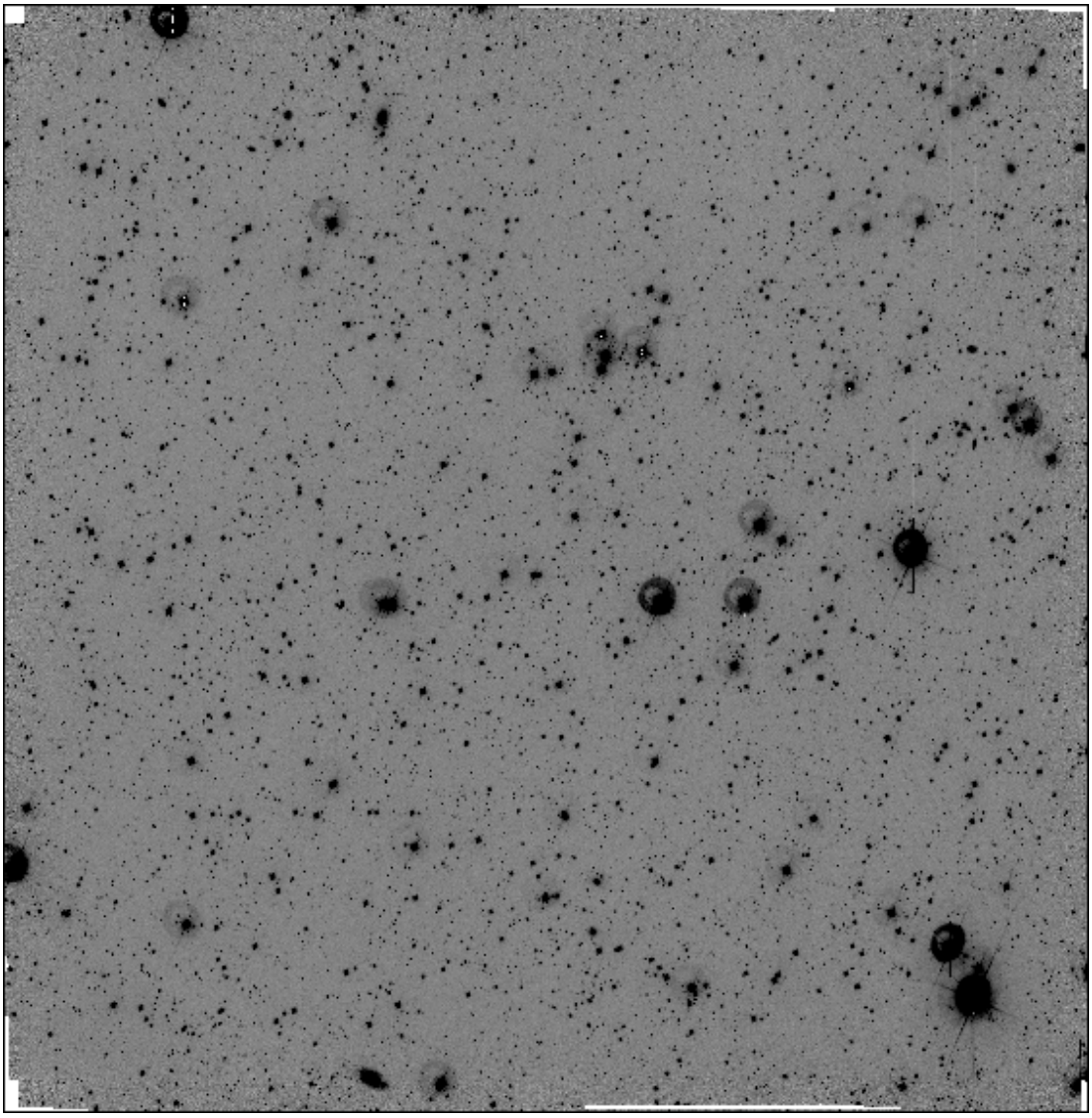

Figure D.14: LCRS Field 1003-03:E

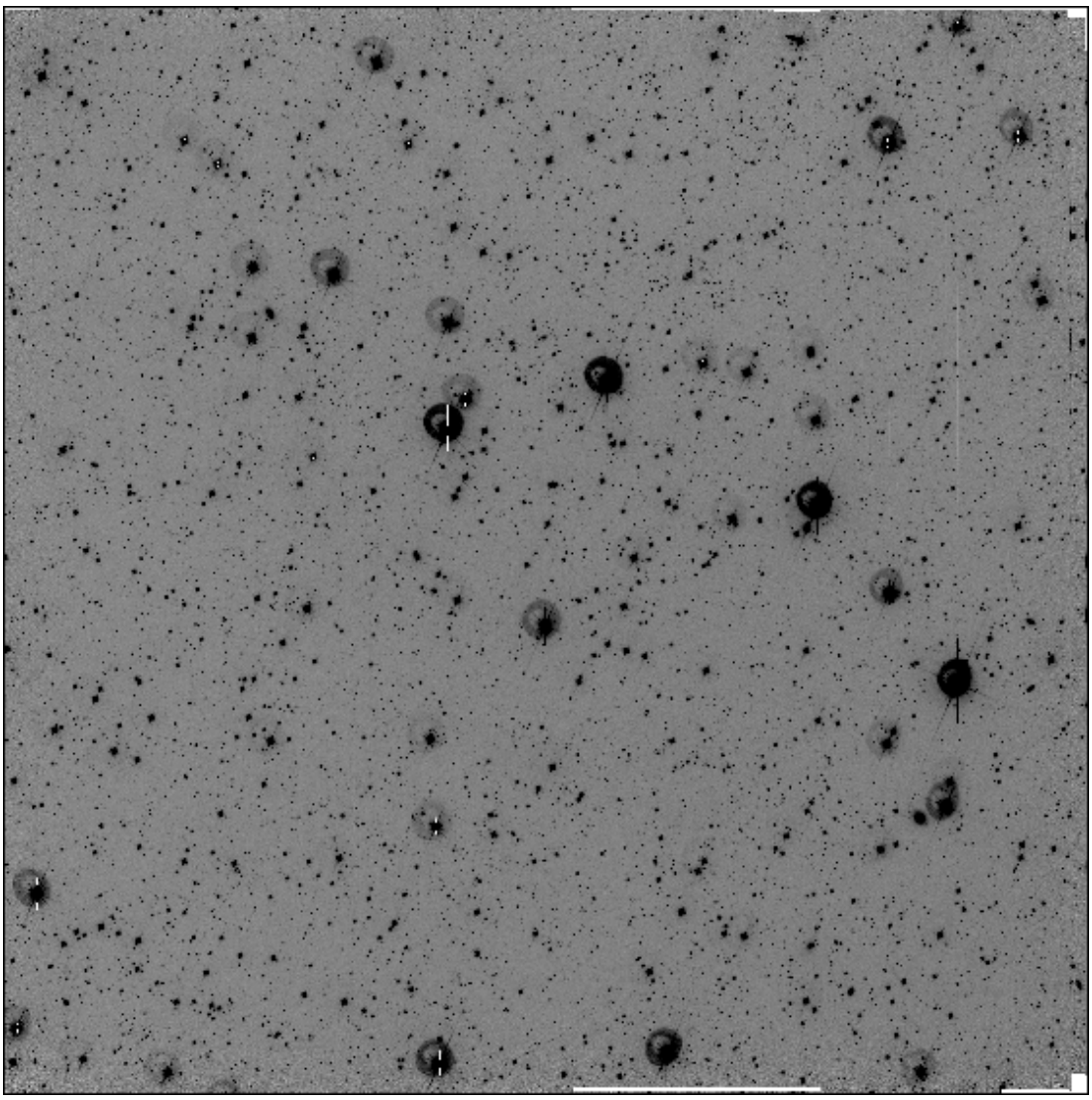

Figure D.15: LCRS Field 1003-06:E

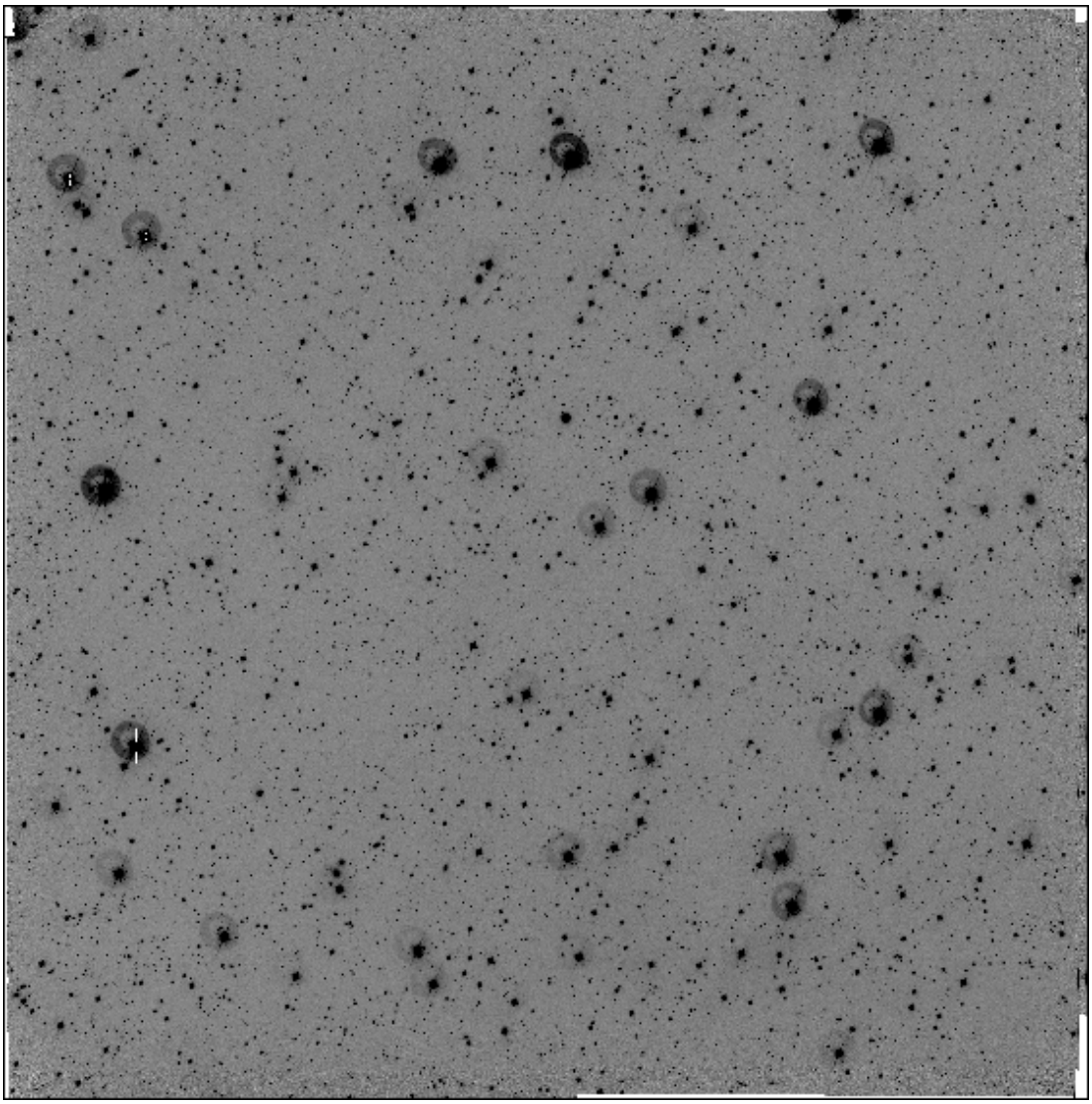

Figure D.16: LCRS Field 1027-03:E

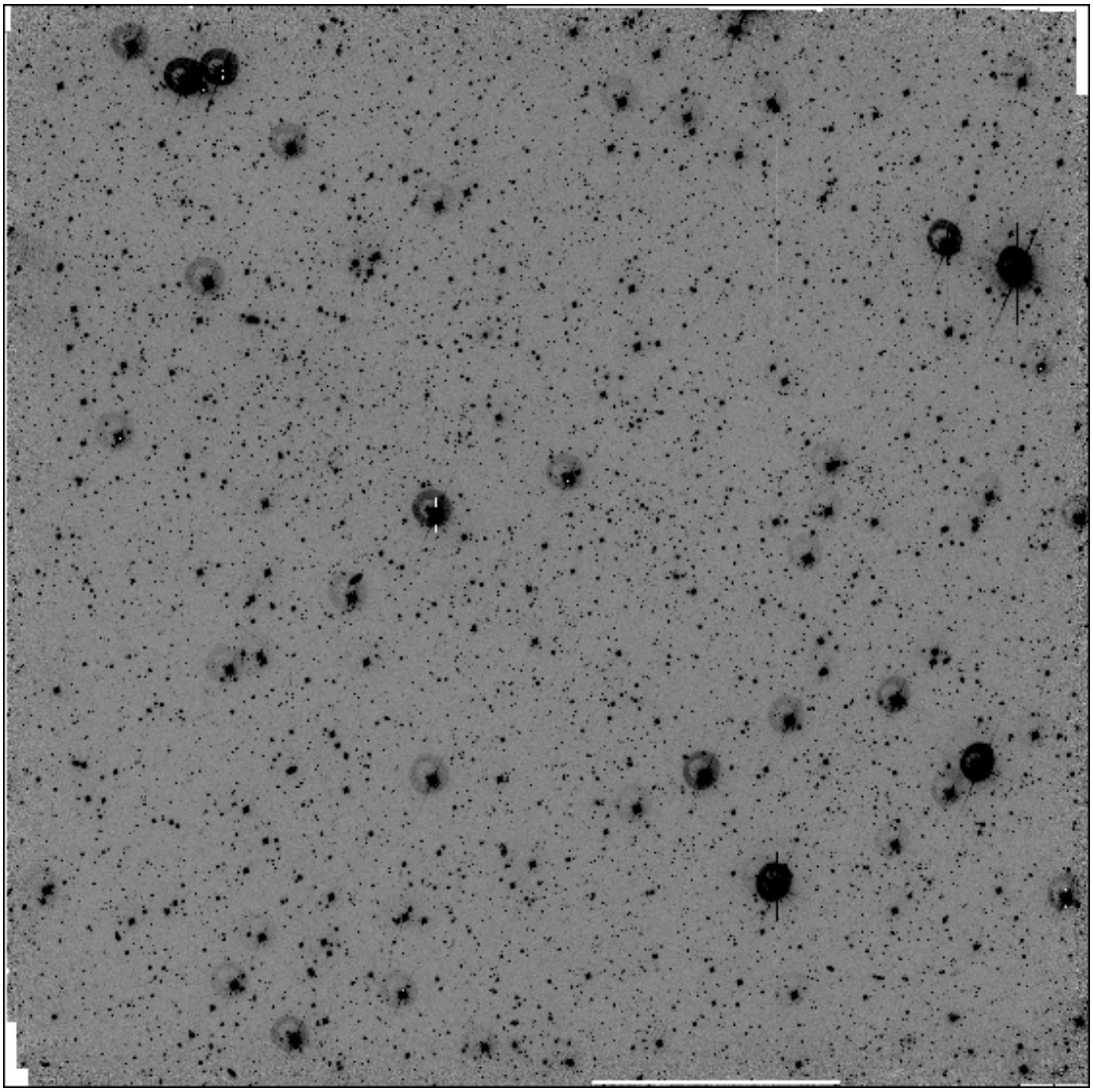

Figure D.17: LCRS Field 1051-12:W

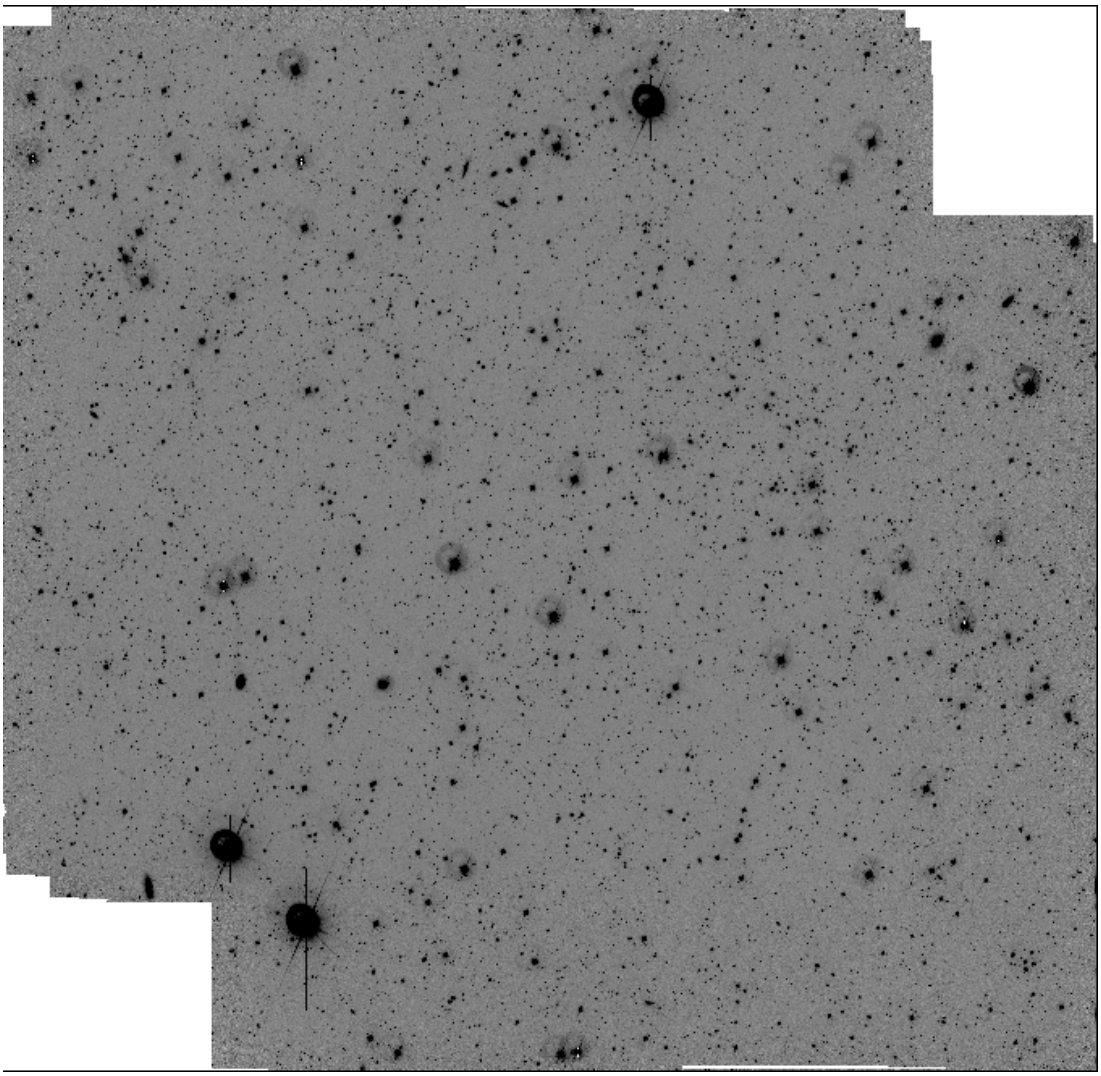

Figure D.18: LCRS Field 1139-03:E

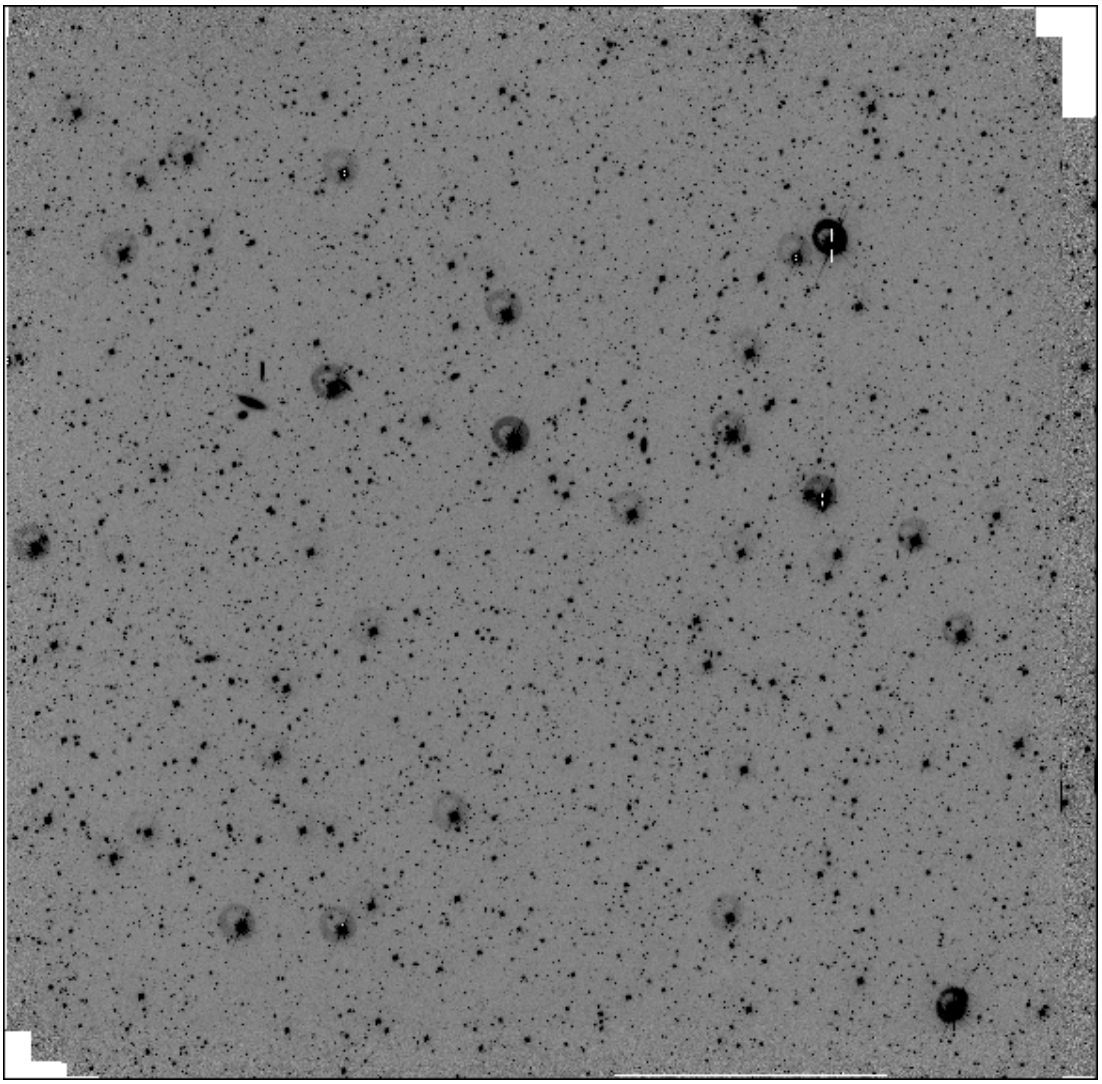

Figure D.19: LCRS Field 1139-12:W

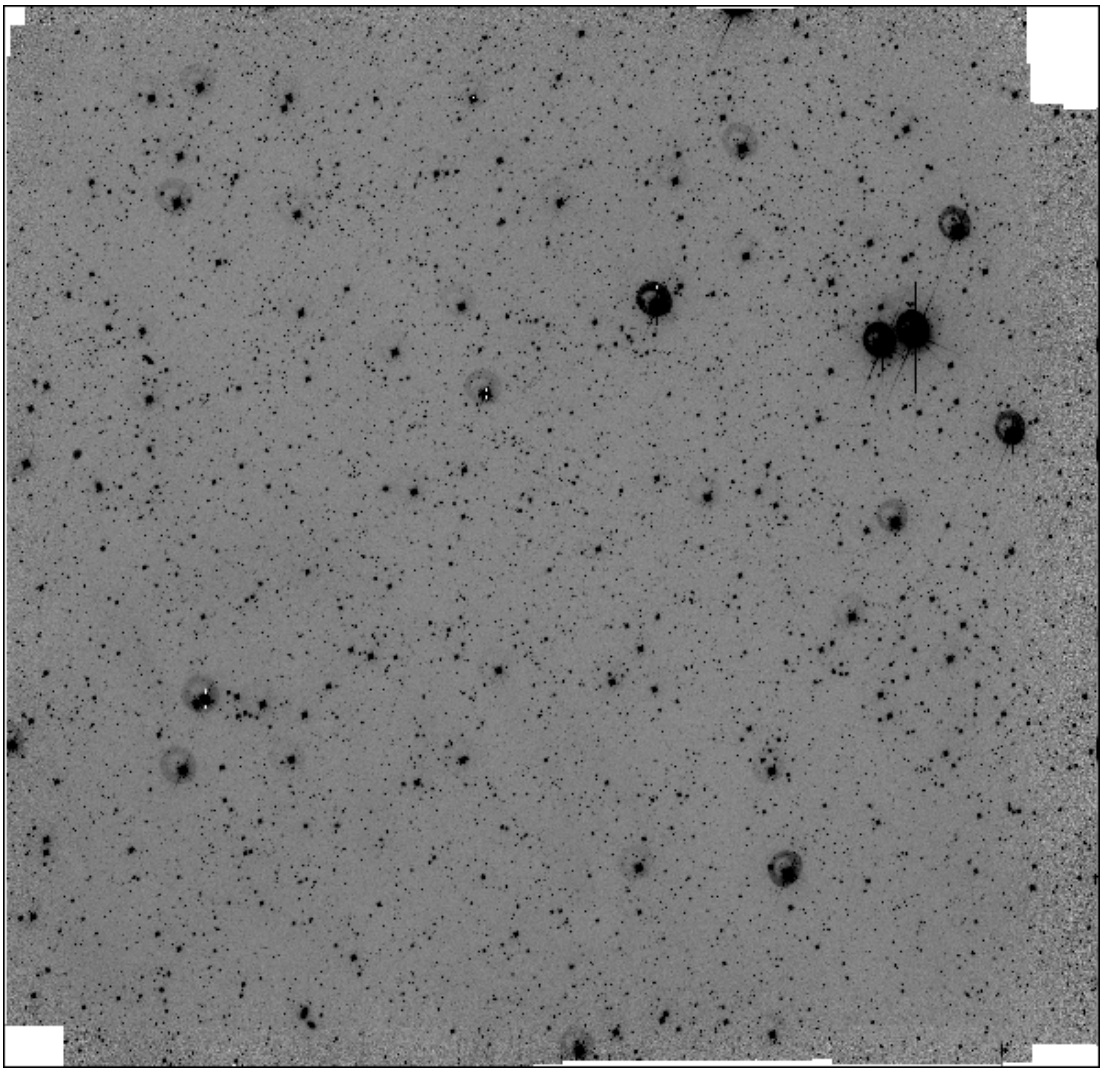

Figure D.20: LCRS Field 1151-12:E

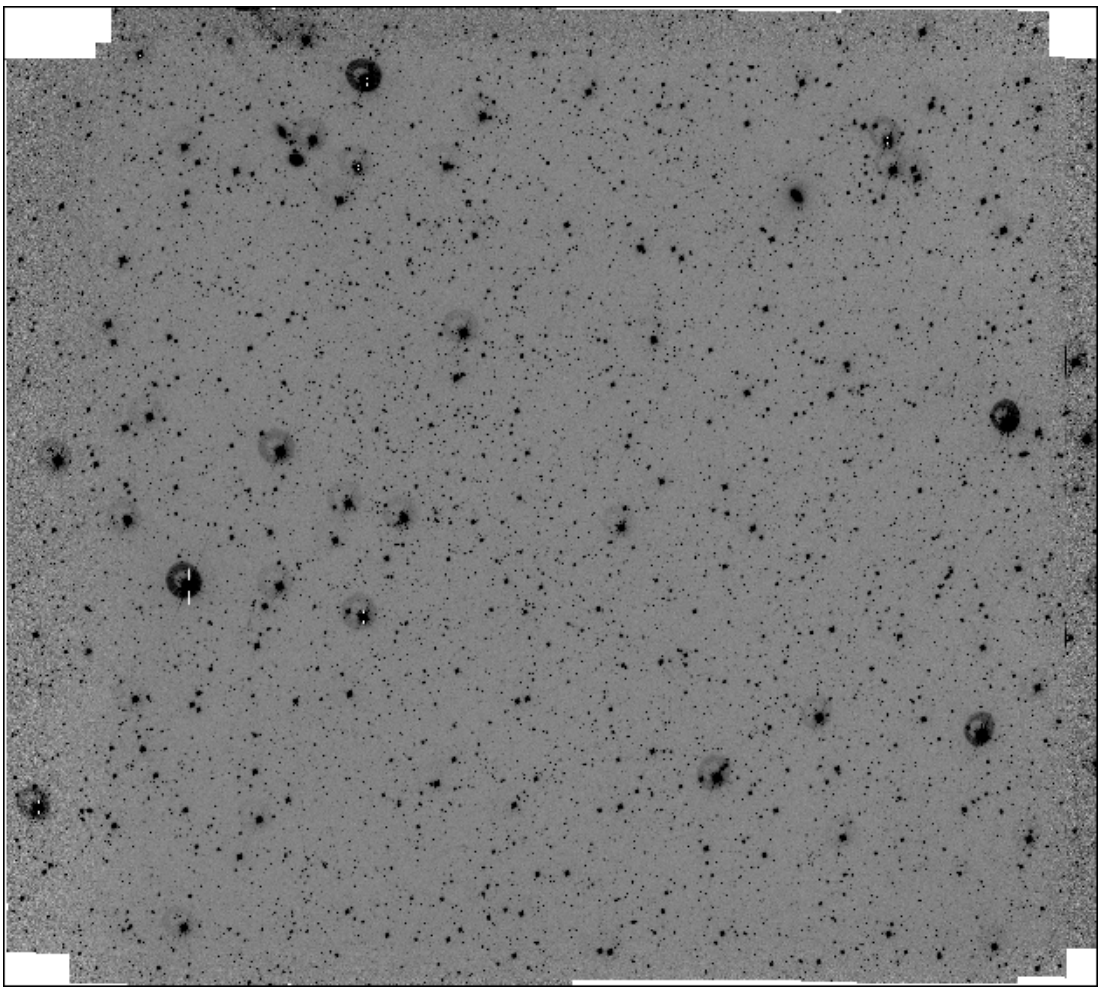

Figure D.21: LCRS Field 1215-12:E

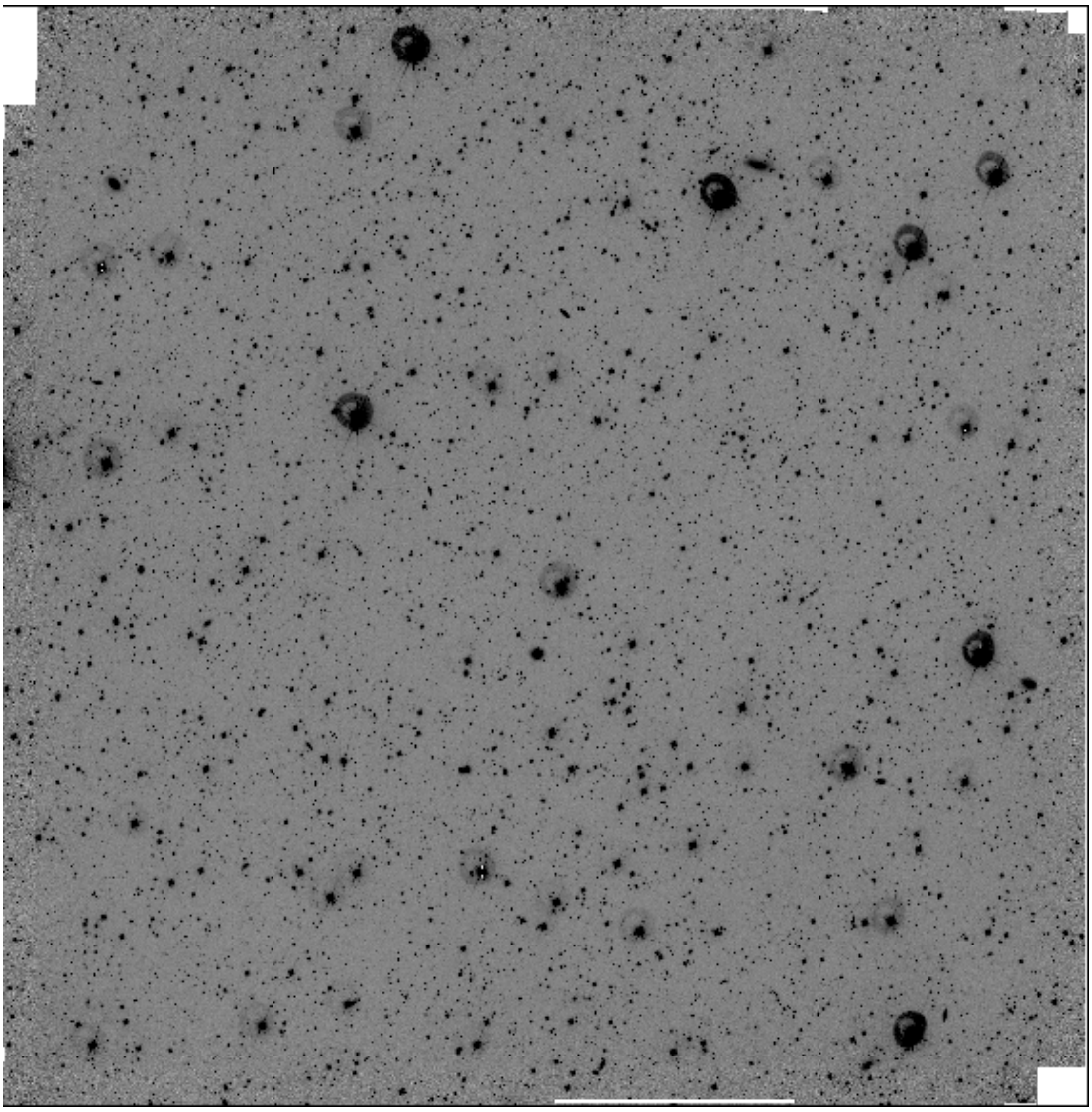

Figure D.22: LCRS Field 1239-12:E

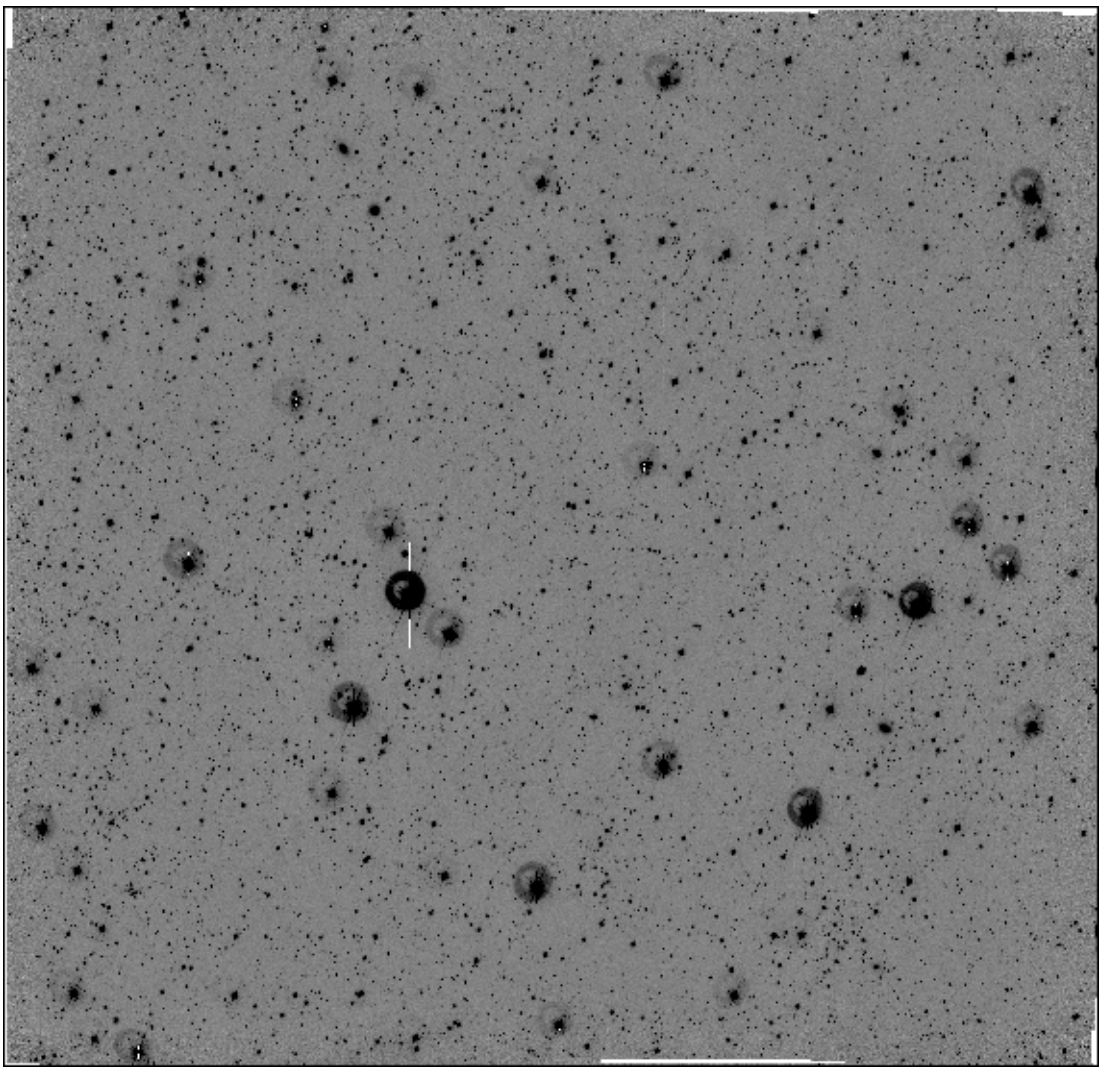

Figure D.23: LCRS Field 1403-03:W

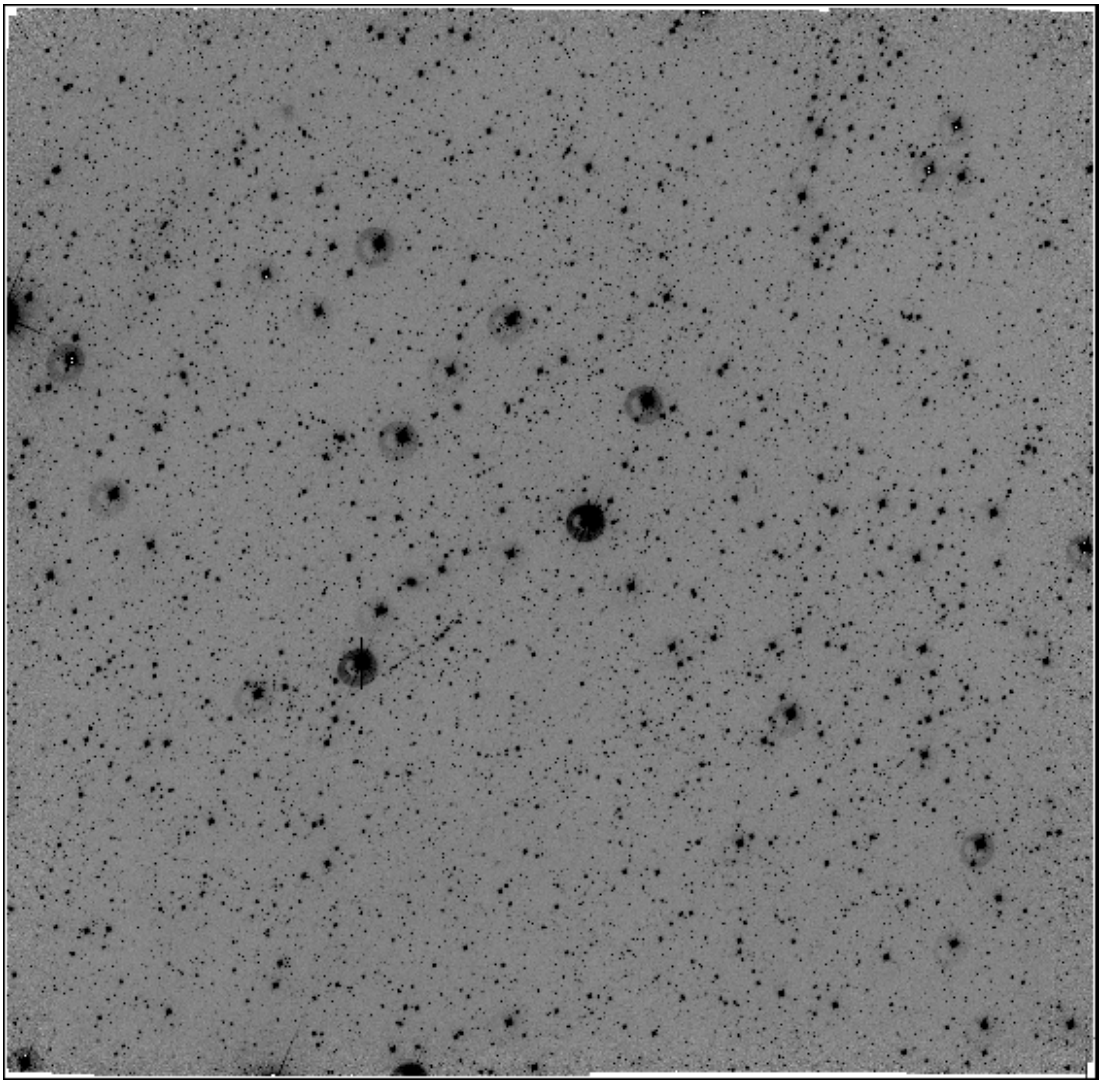

Figure D.24: LCRS Field 1015-12:E

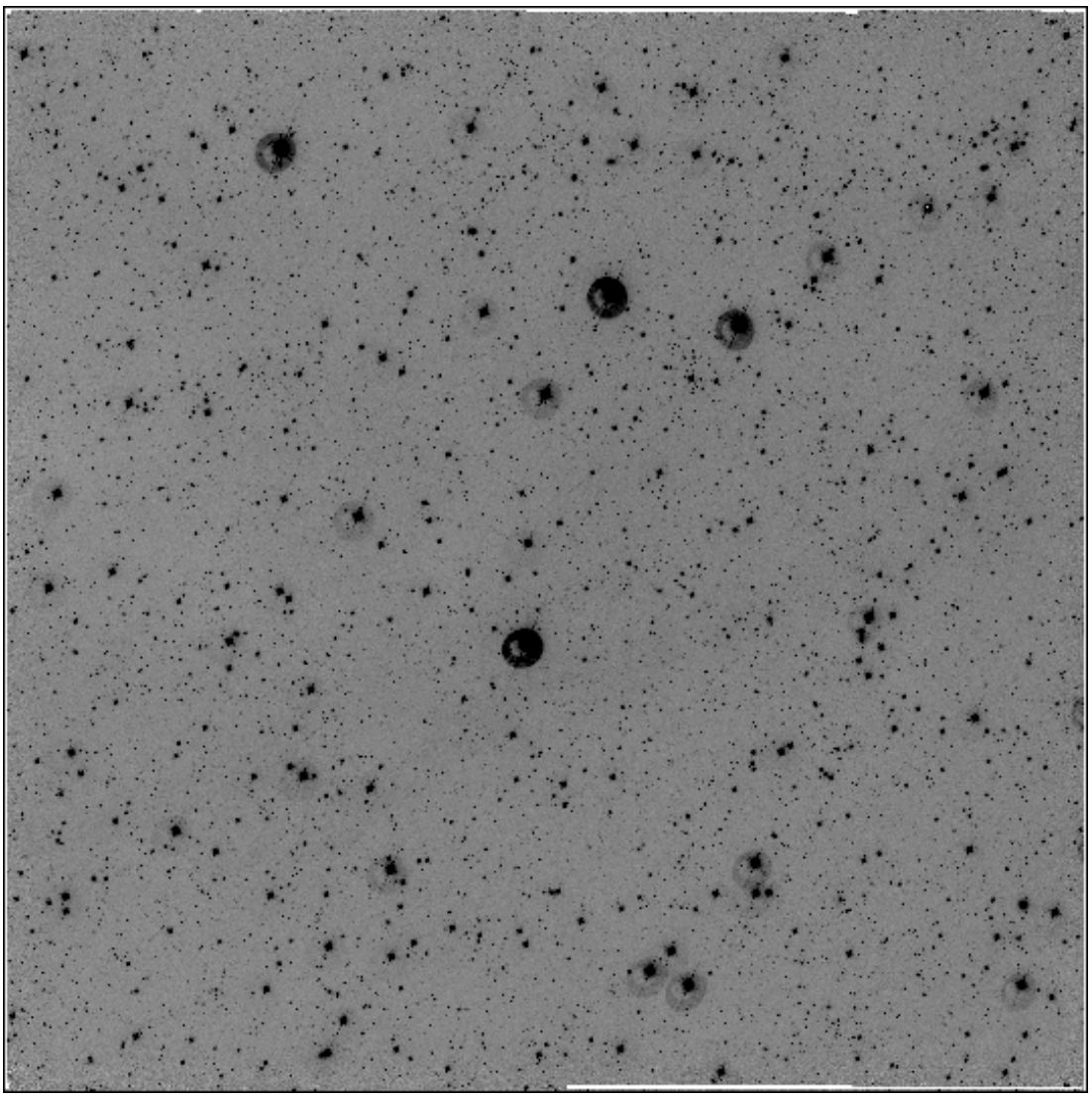

Figure D.25: LCRS Field 1039-03:W

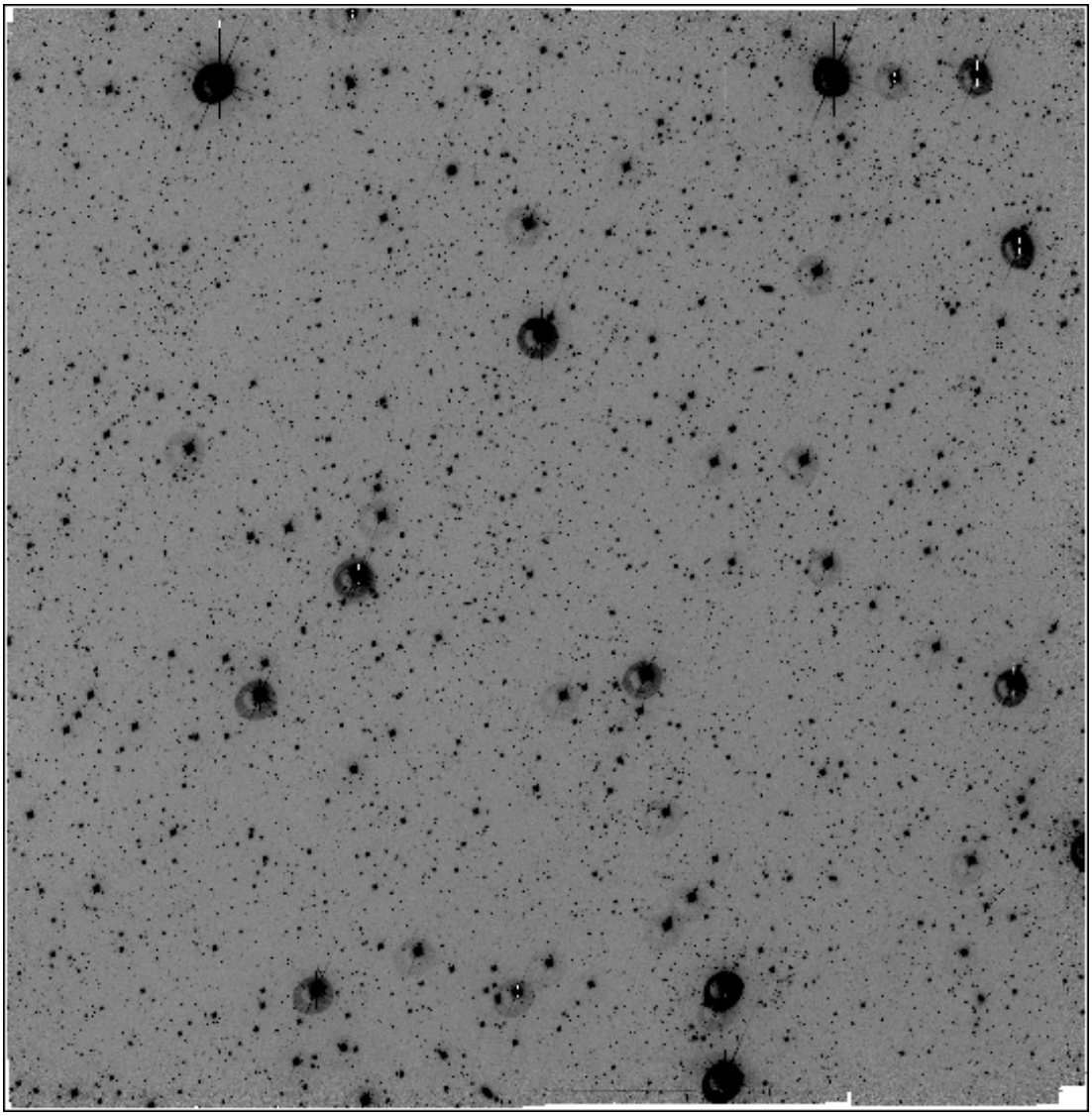

Figure D.26: LCRS Field 1051-12:E

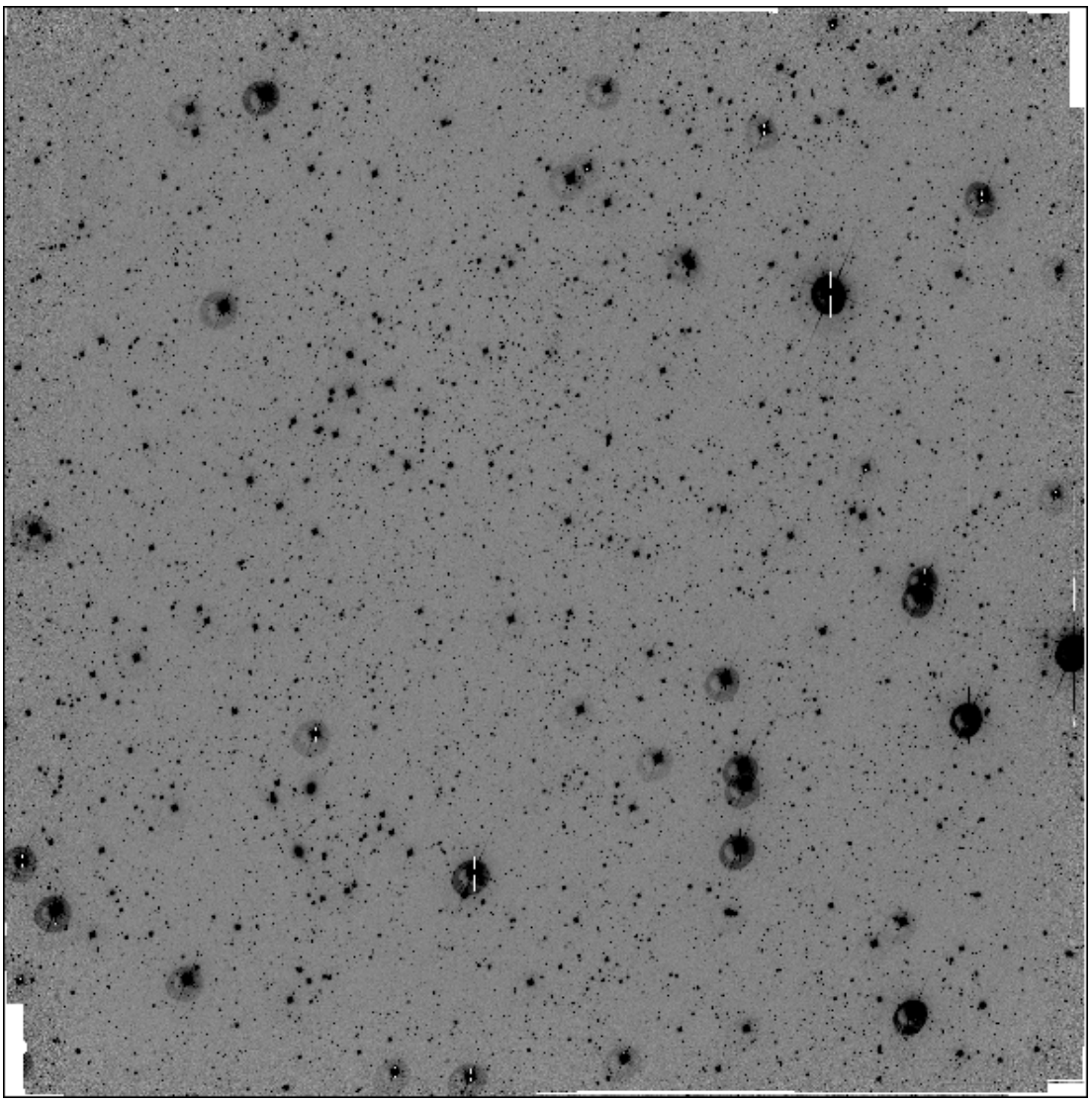

Figure D.27: LCRS Field 1127-03:E

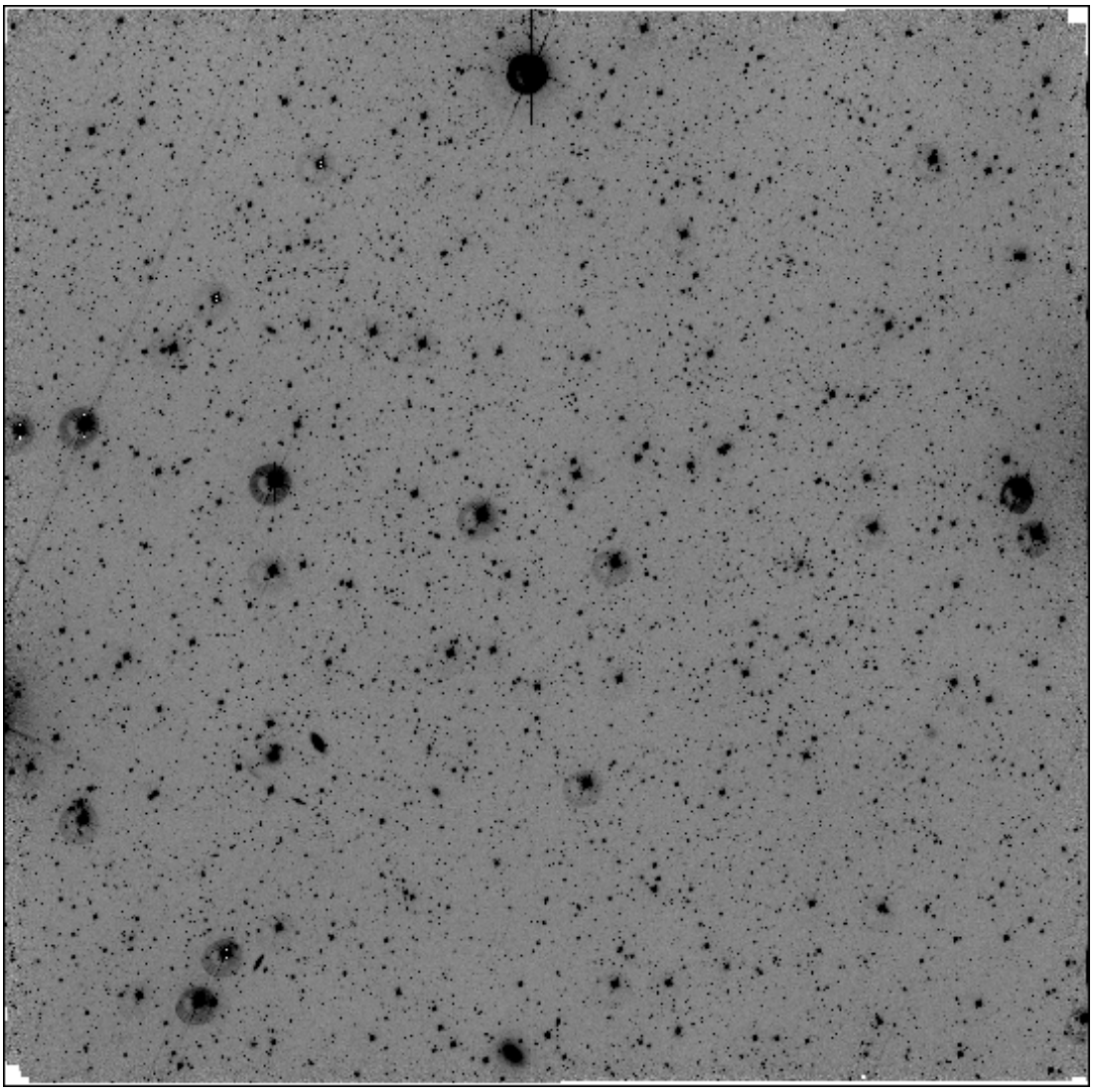

Figure D.28: LCRS Field 1227-12:E

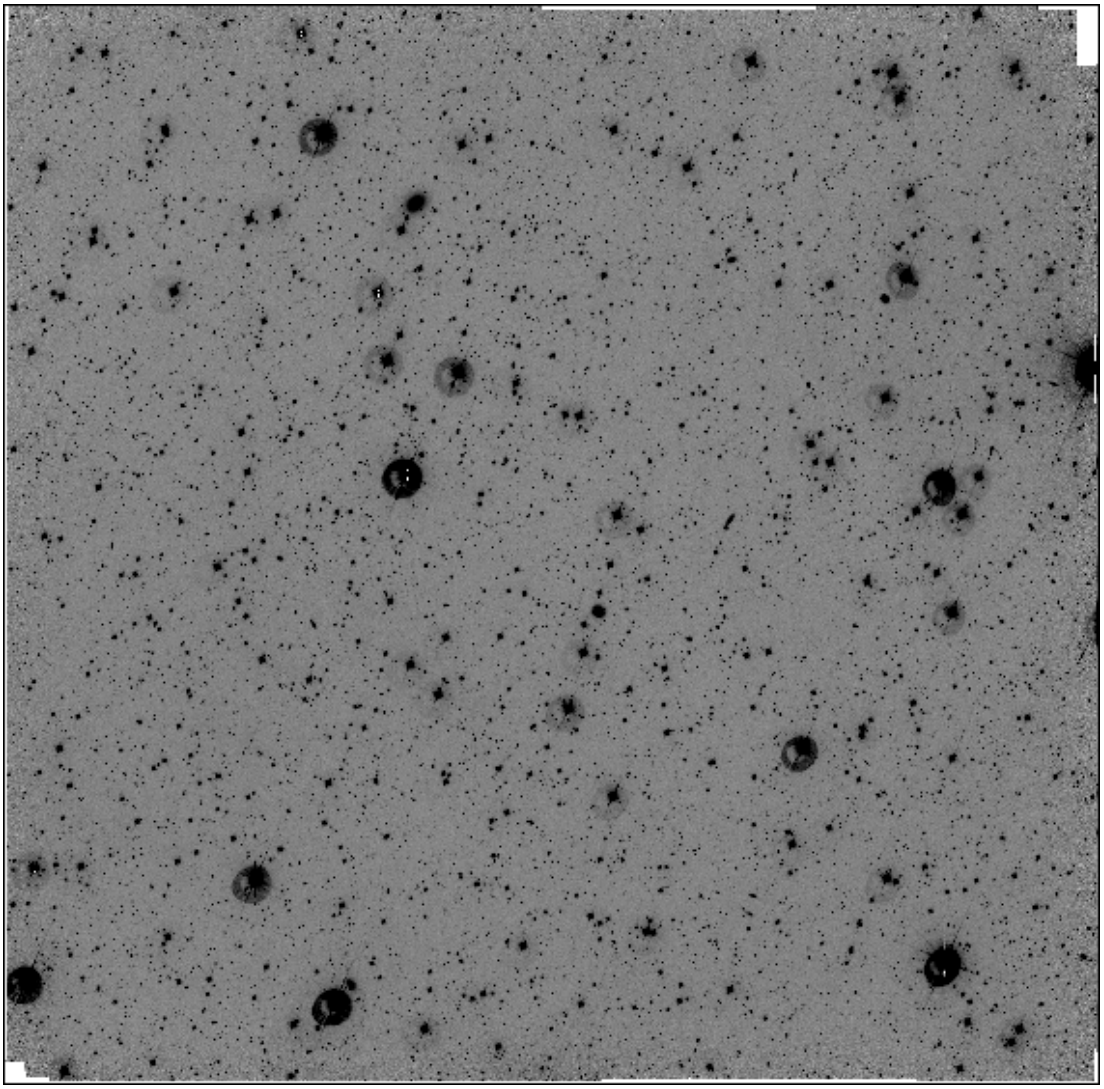

Figure D.29: LCRS Field 1303-12:W

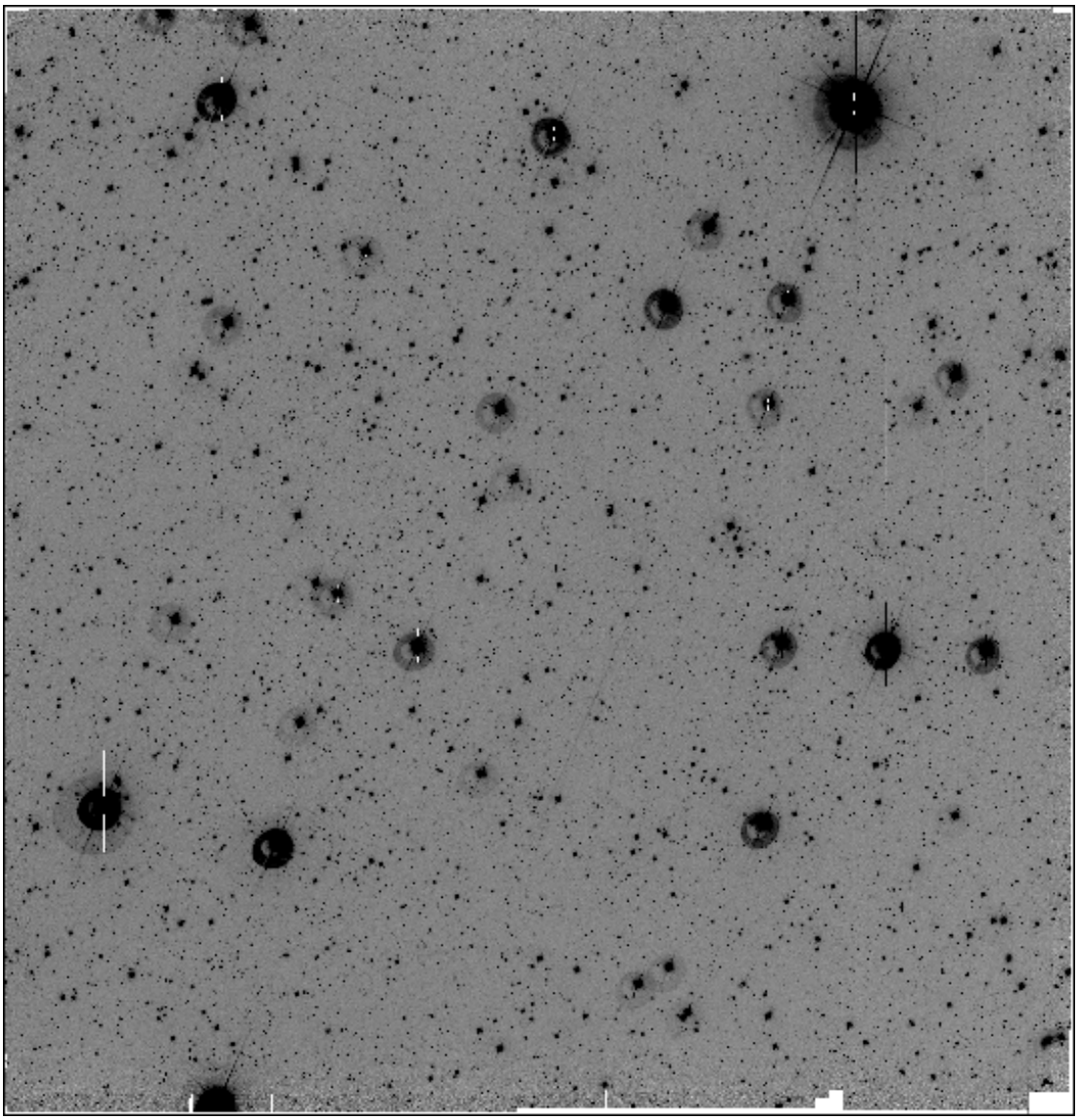

Figure D.30: LCRS Field 1339-03:E

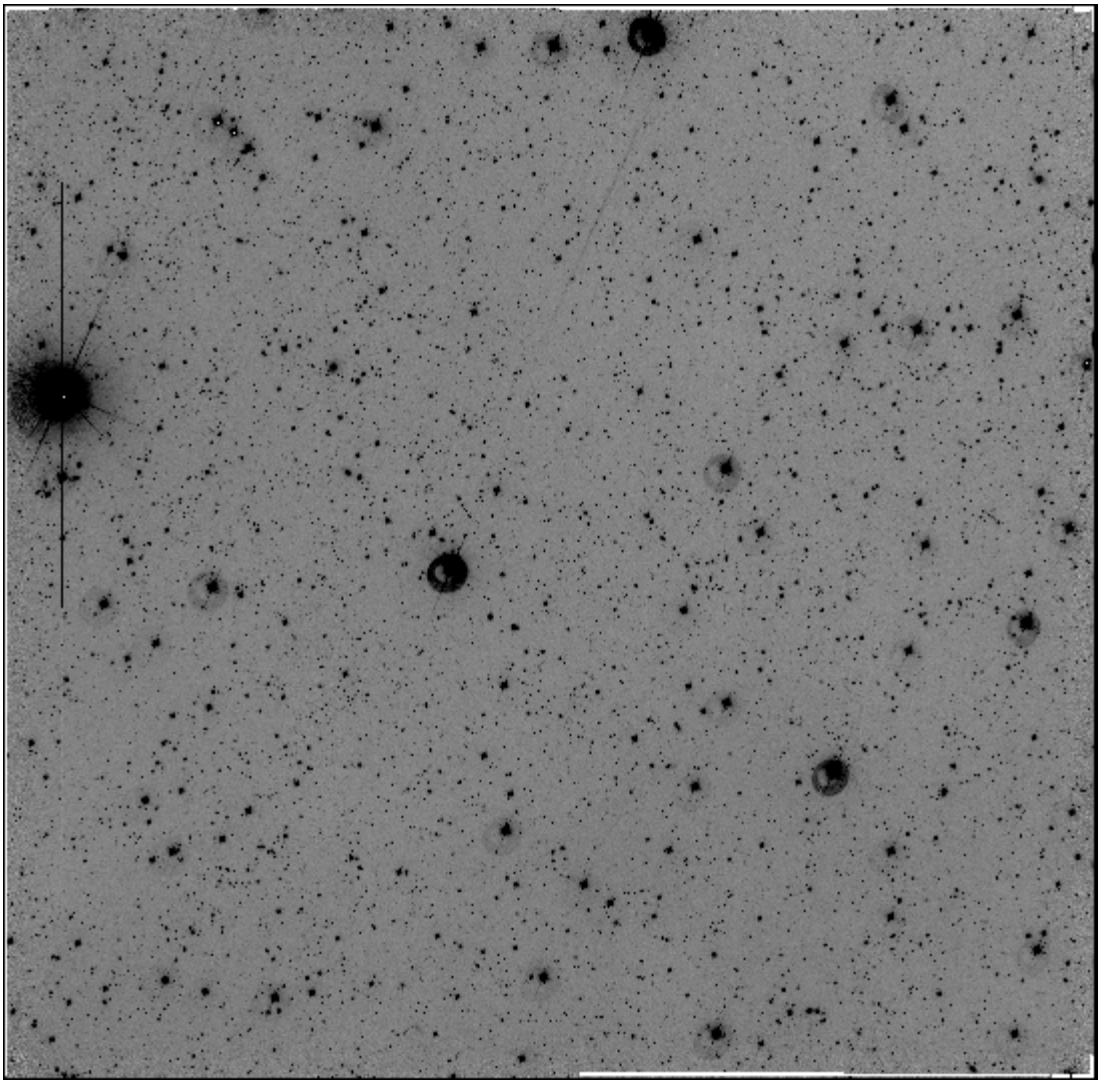

Figure D.31: LCRS Field 1351-03:W

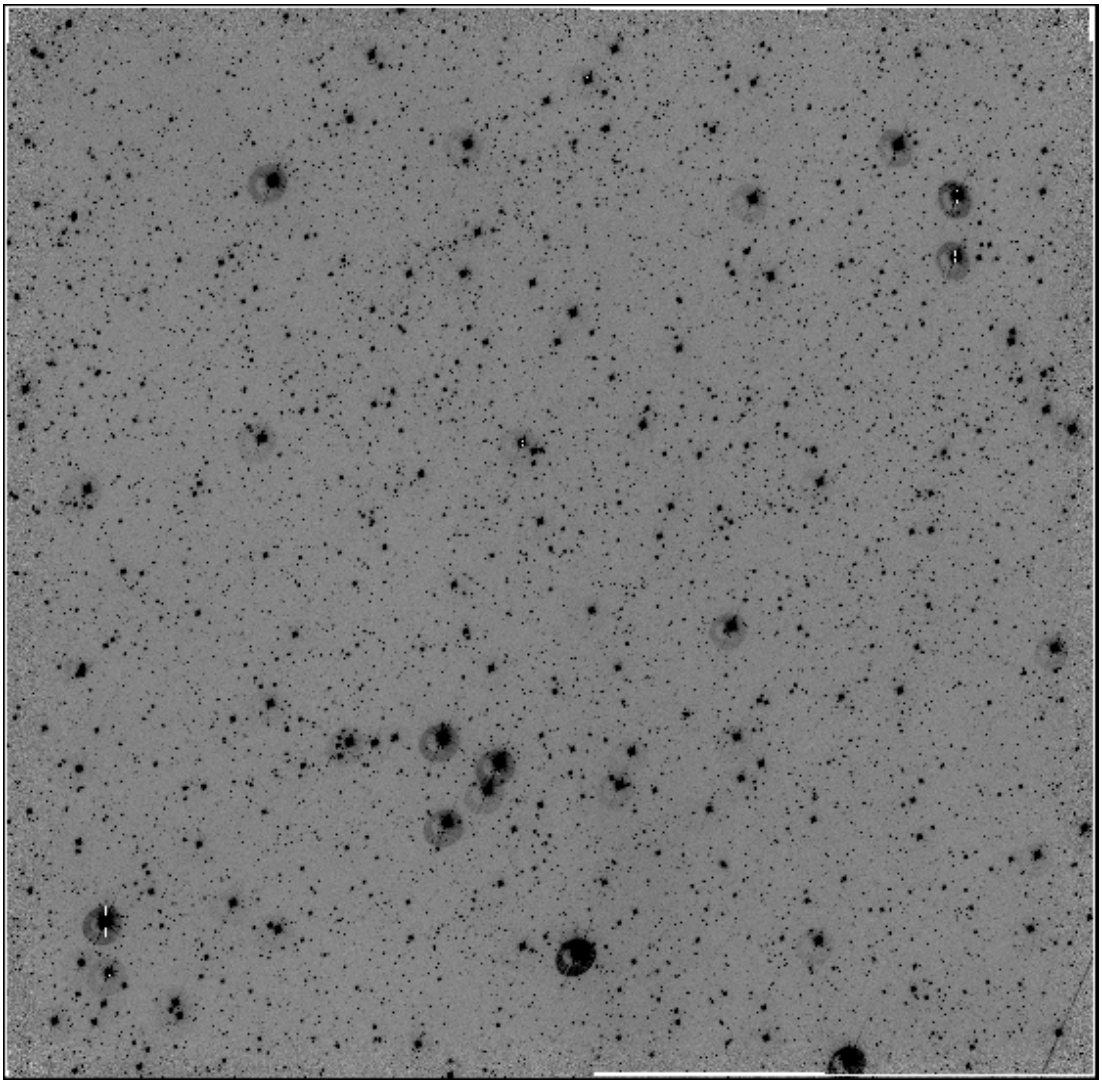

Figure D.32: LCRS Field 1415-03:W

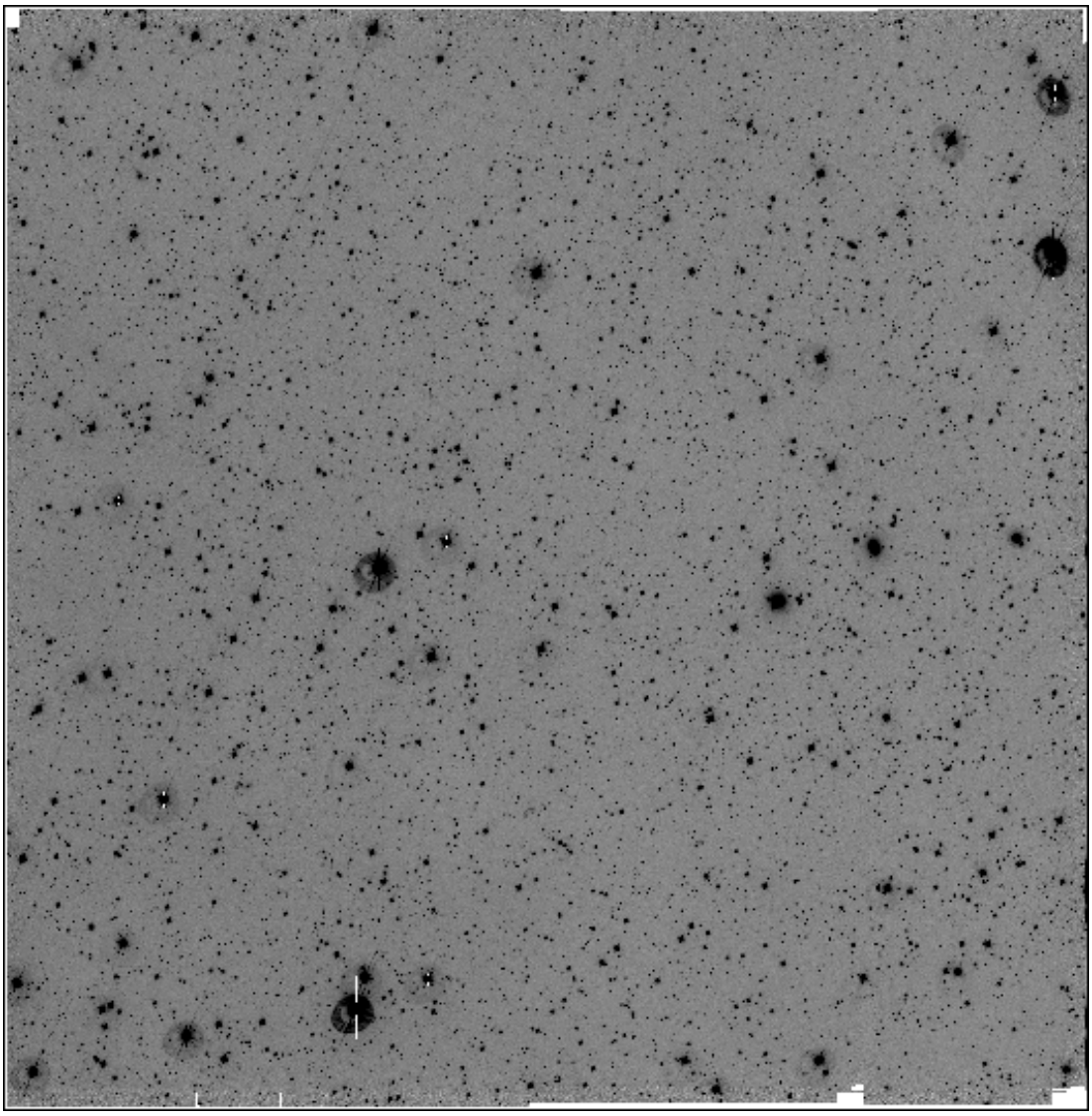

Figure D.33: LCRS Field 1439-12:W

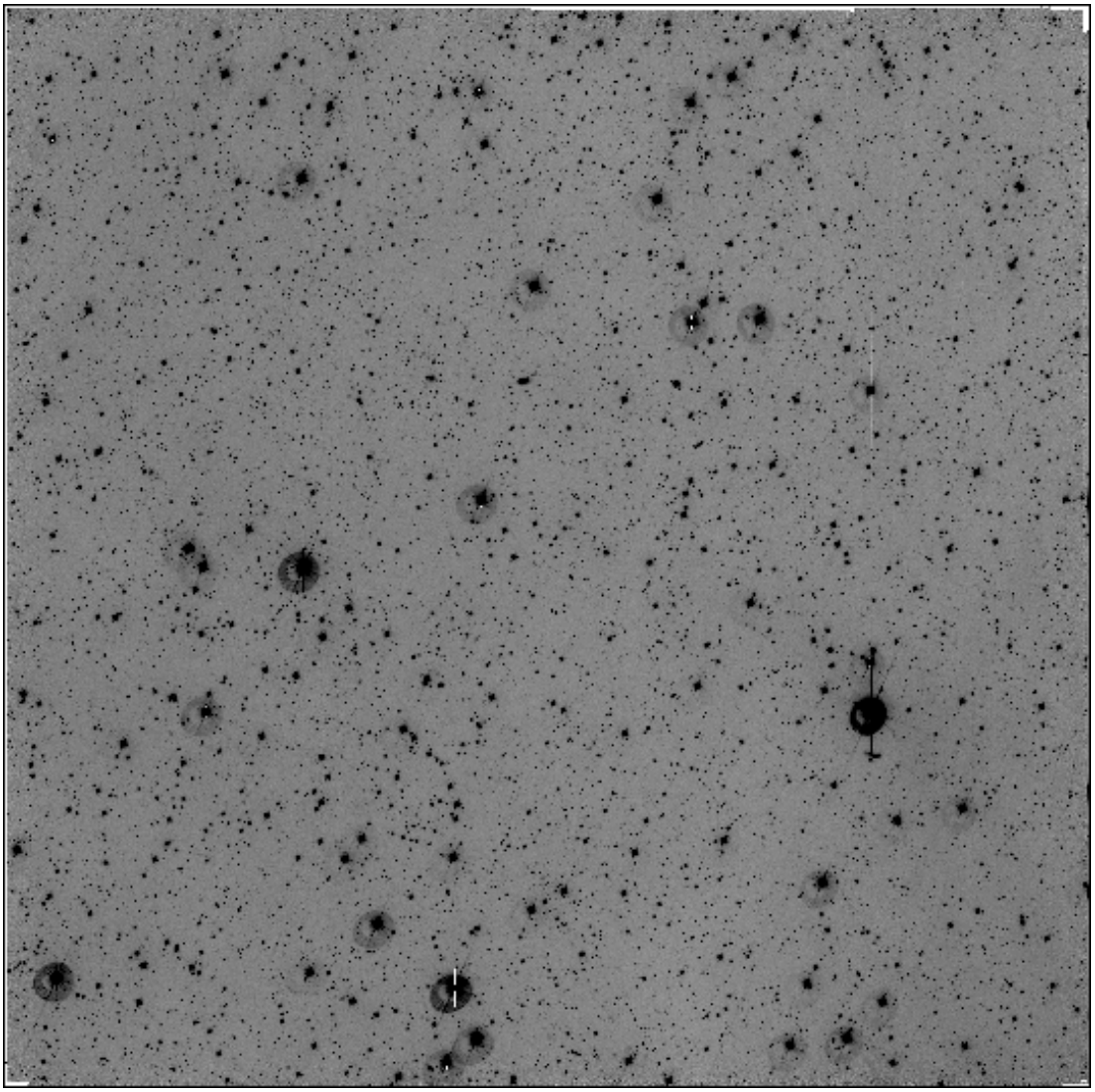

Figure D.34: LCRS Field 1516-03:H

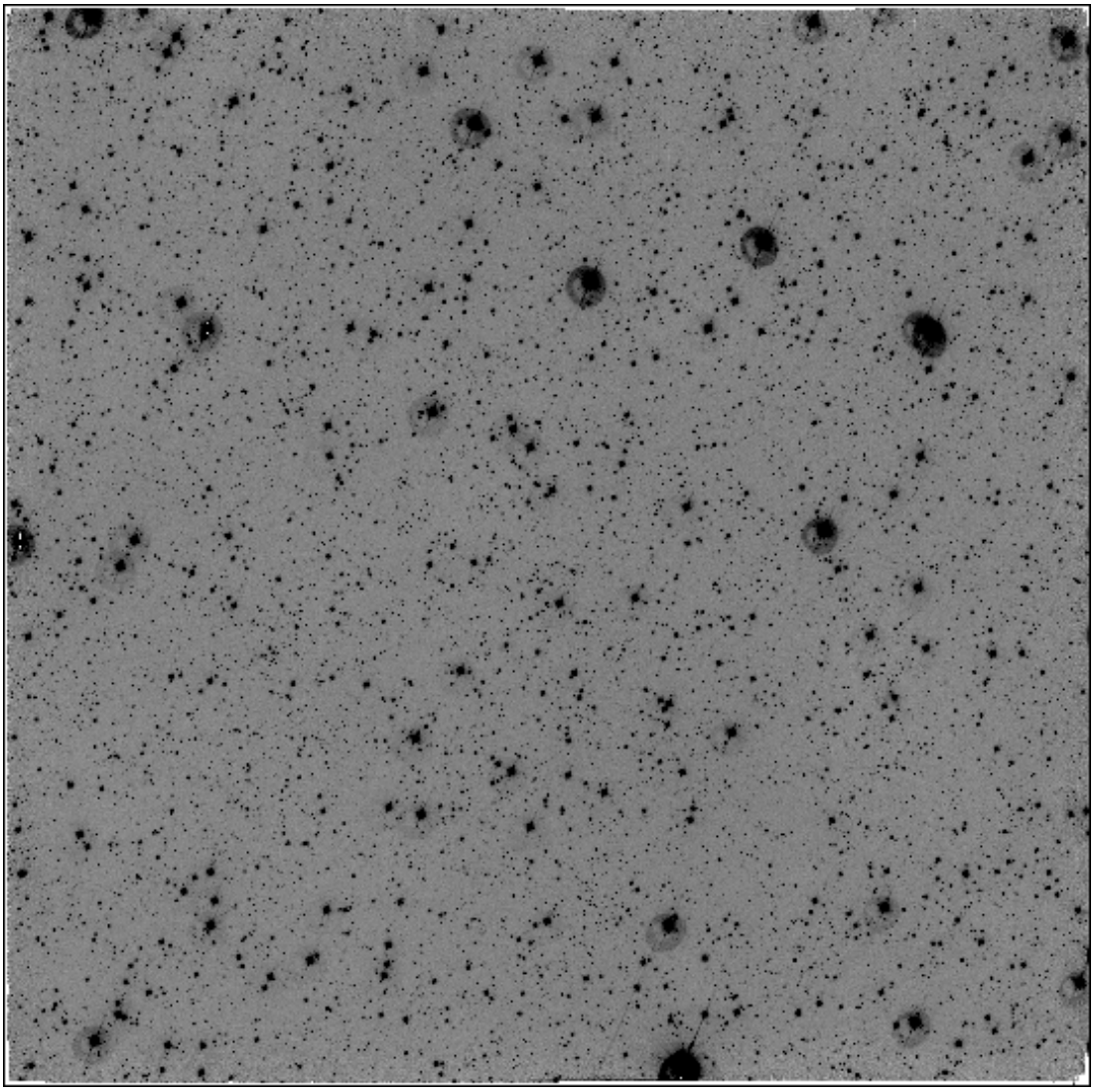

Figure D.35: LCRS Field 2155-45:W

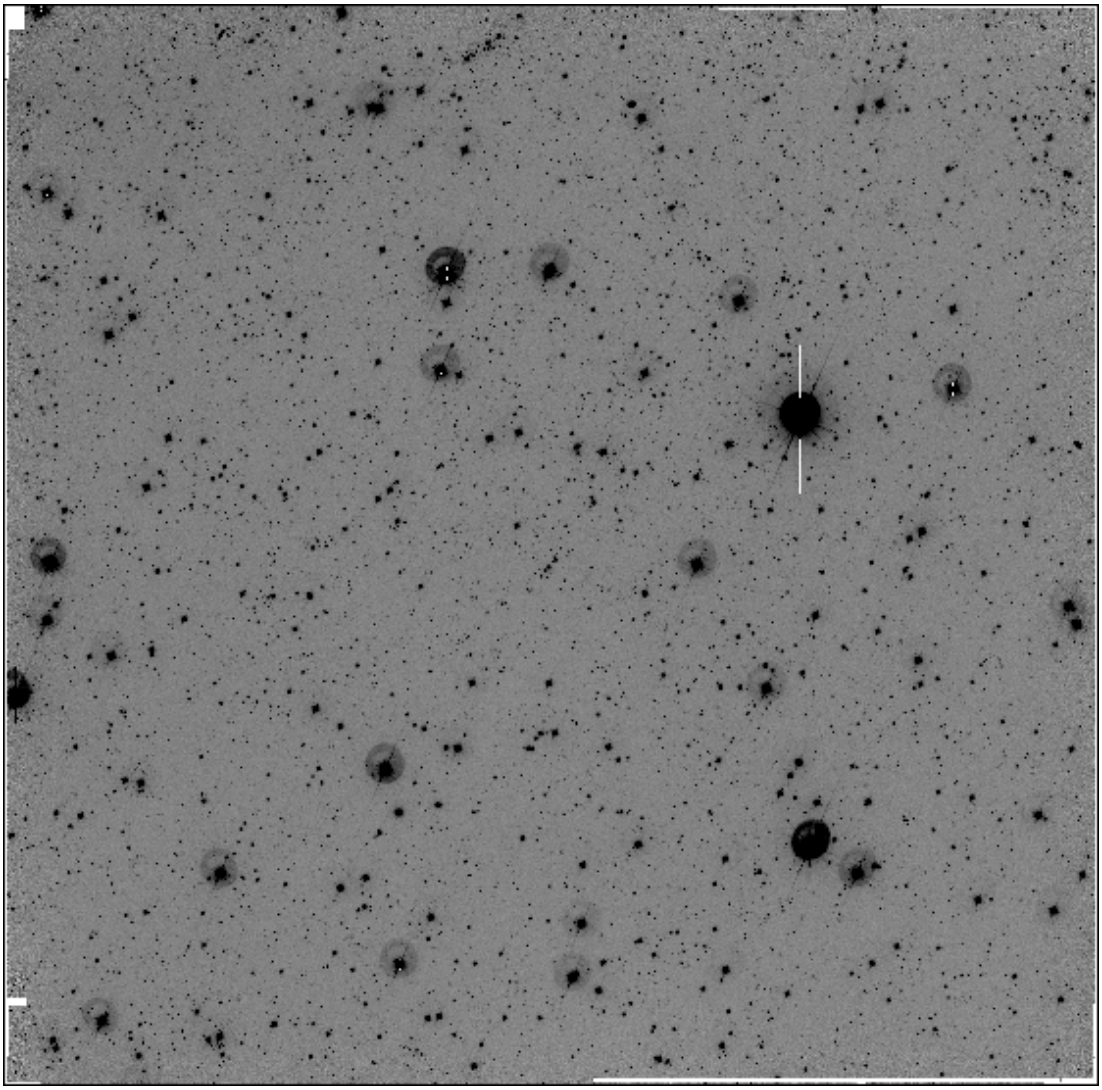

Figure D.36: LCRS Field 0035-45:W

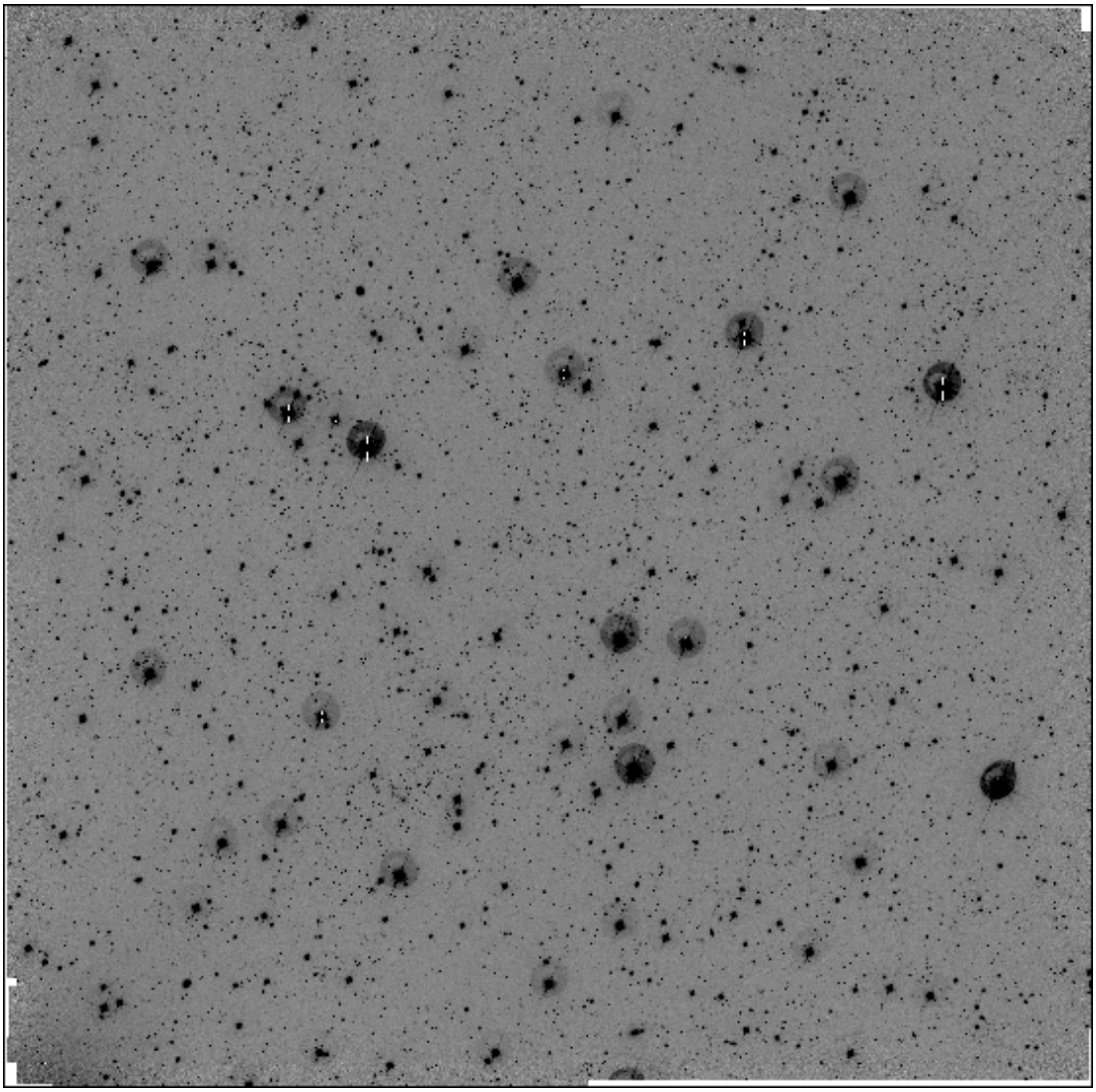

Figure D.37: LCRS Field 0100-45:W

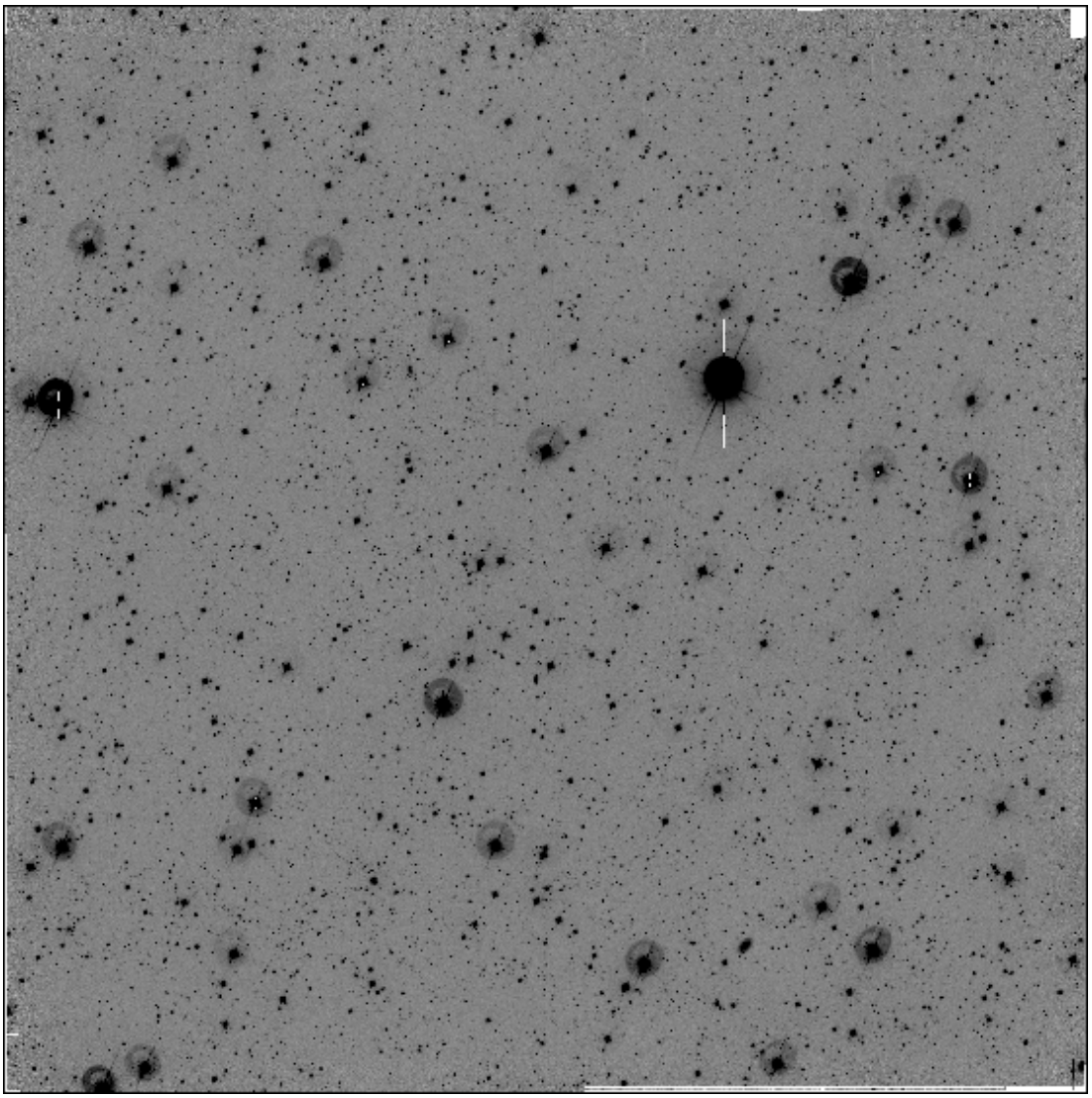

Figure D.38: LCRS Field 0154-39:M

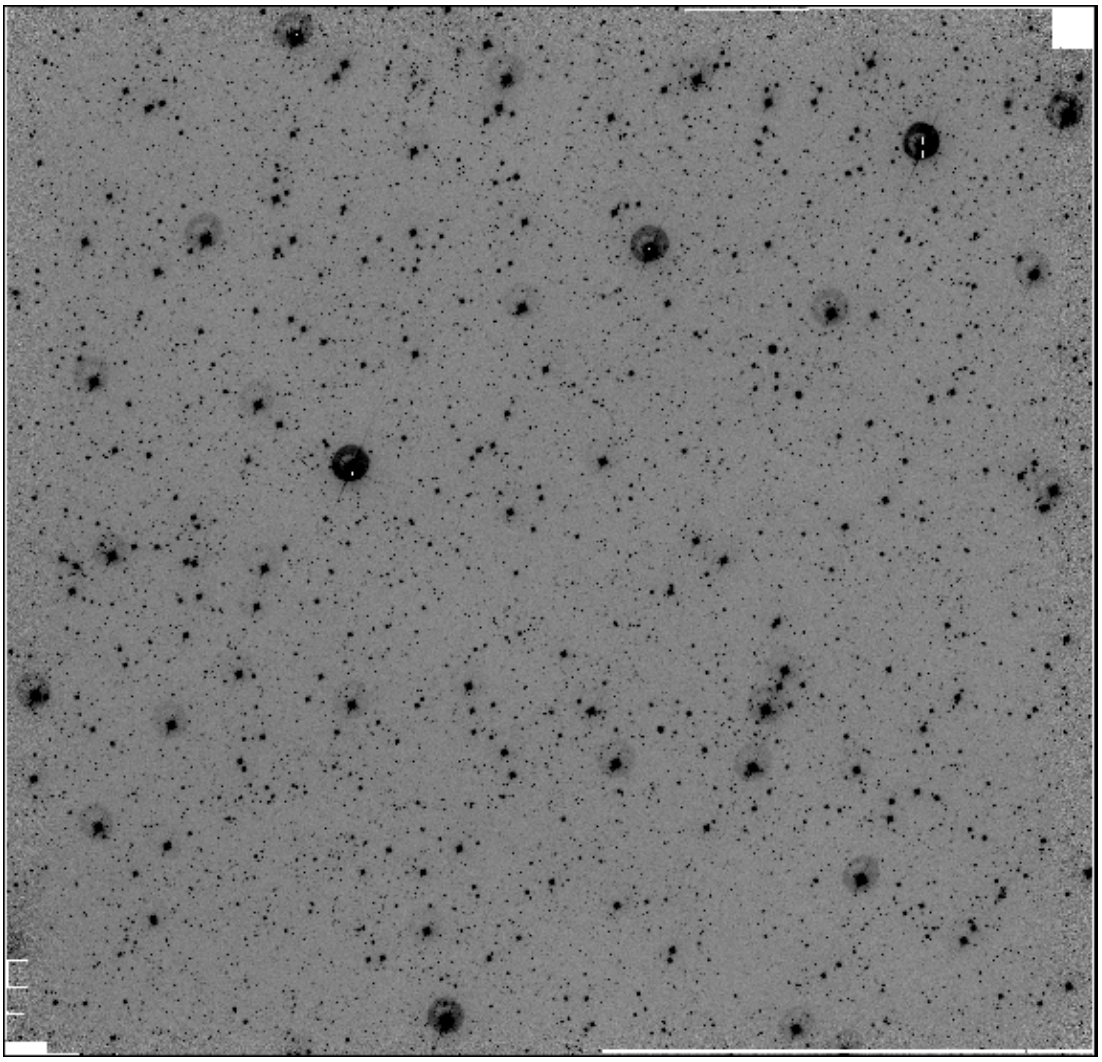

Figure D.39: LCRS Field 0154-39:W

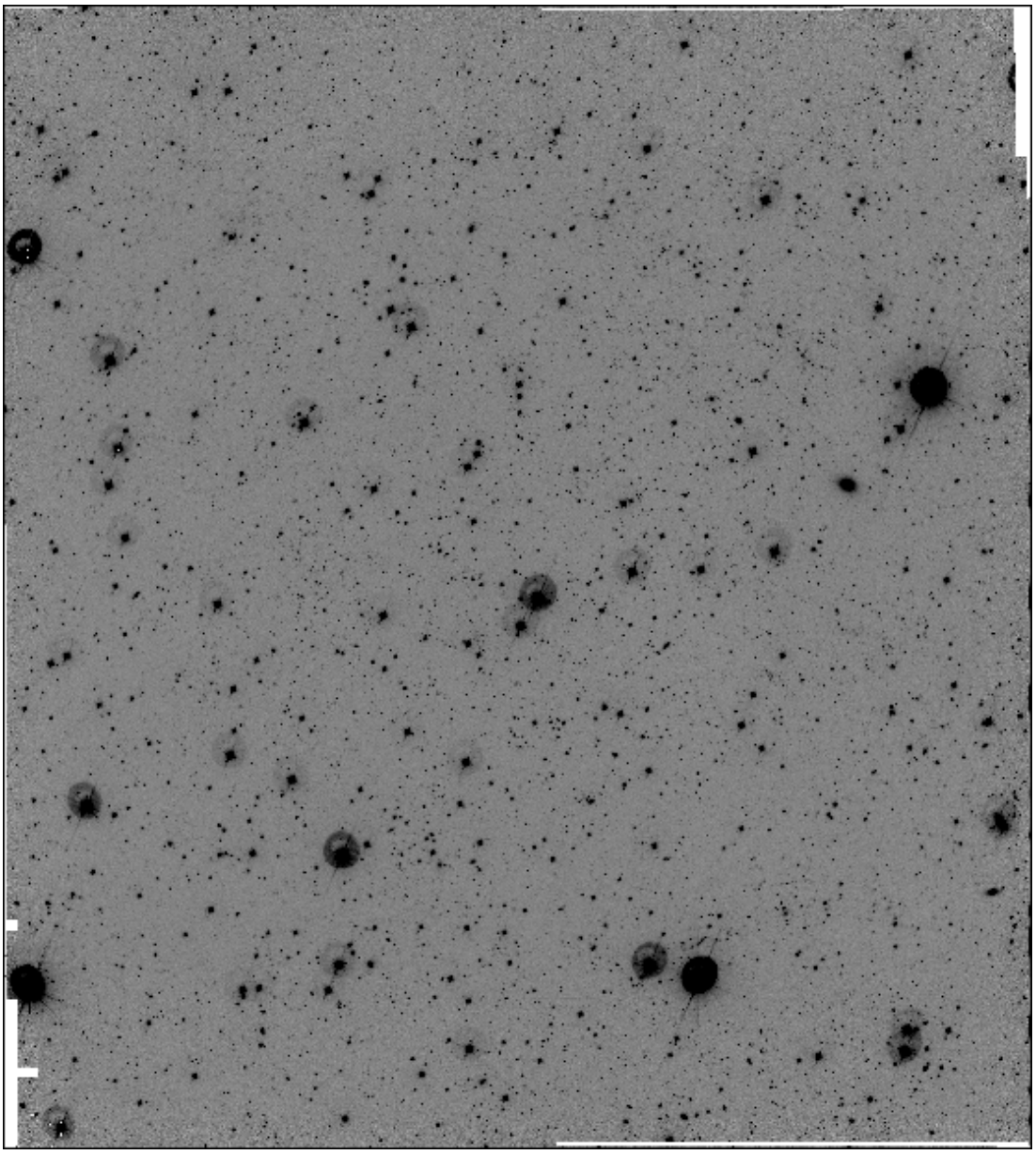

Figure D.40: LCRS Field 0155-45:E

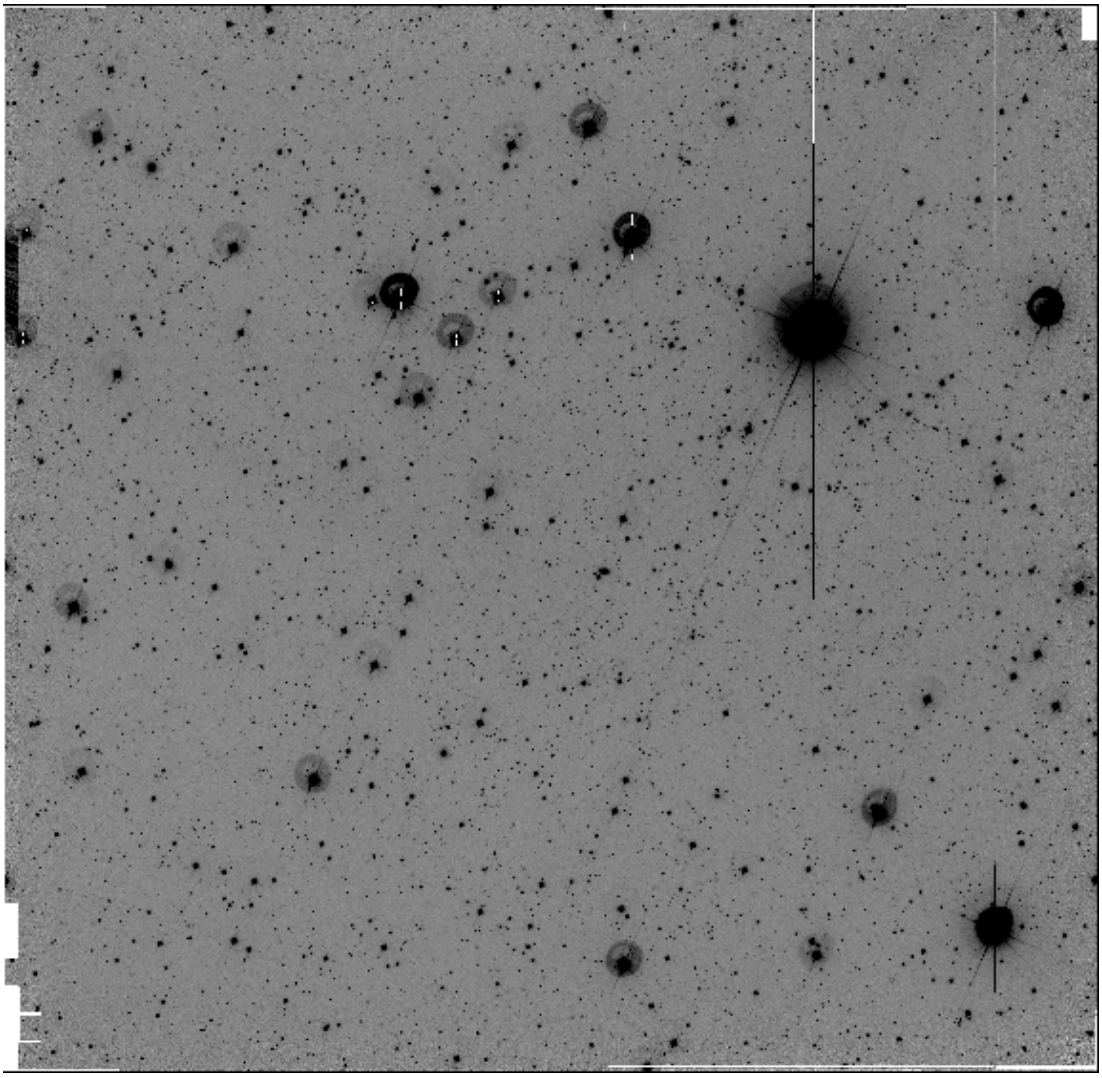

Figure D.41: LCRS Field 0234-39:W

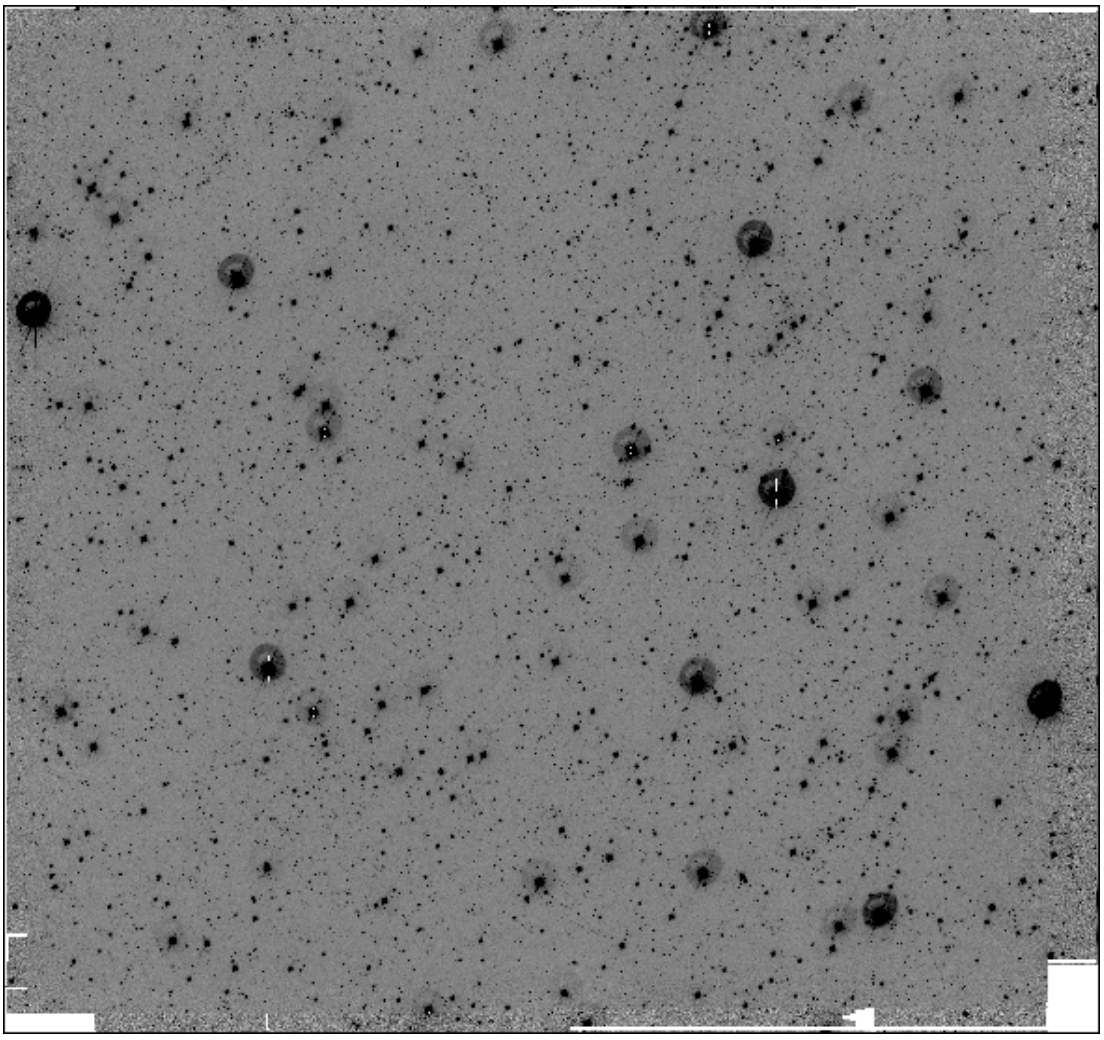

Figure D.42: LCRS Field 0235-45:E

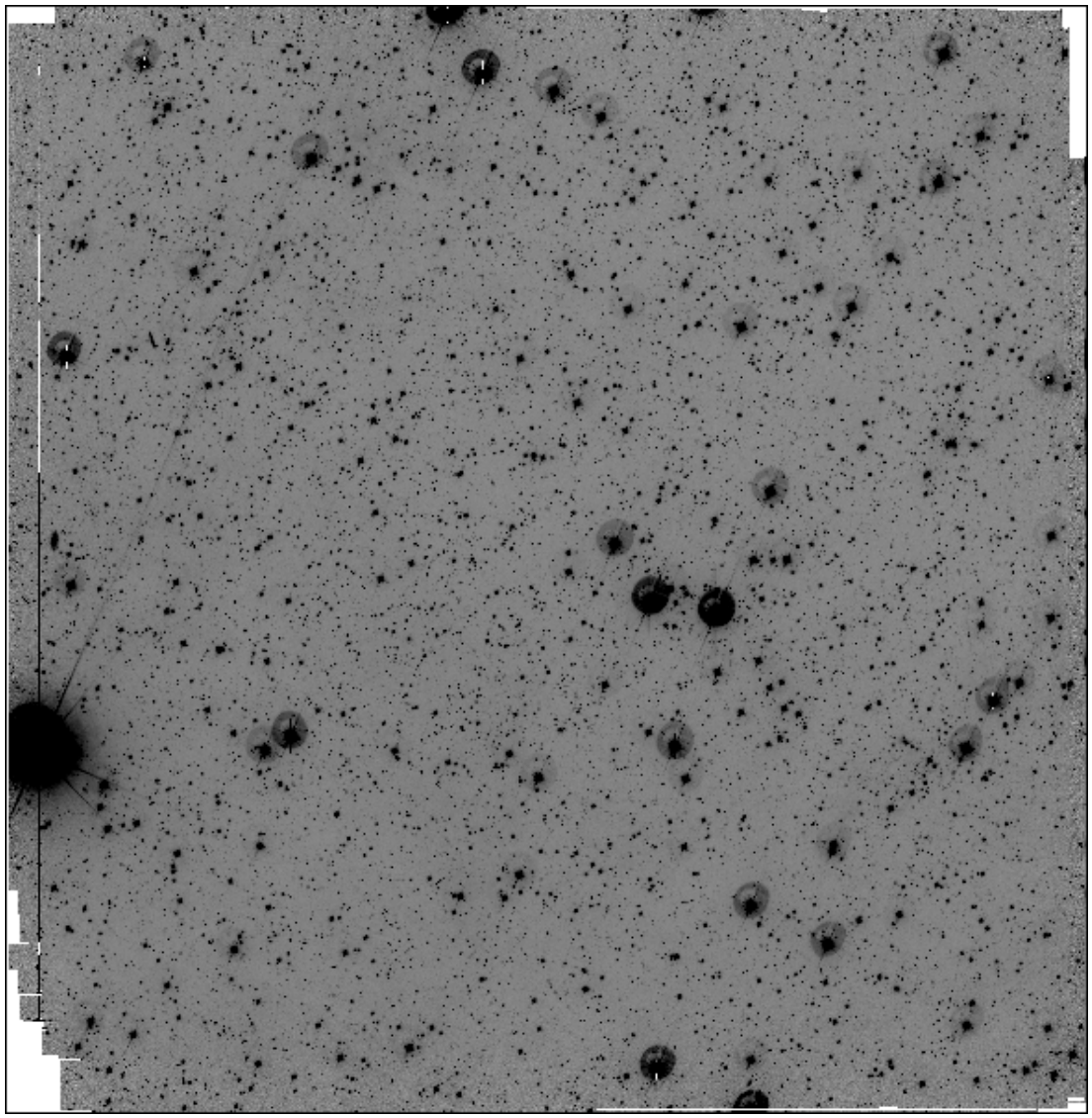

Figure D.43: LCRS Field 2100-45:E

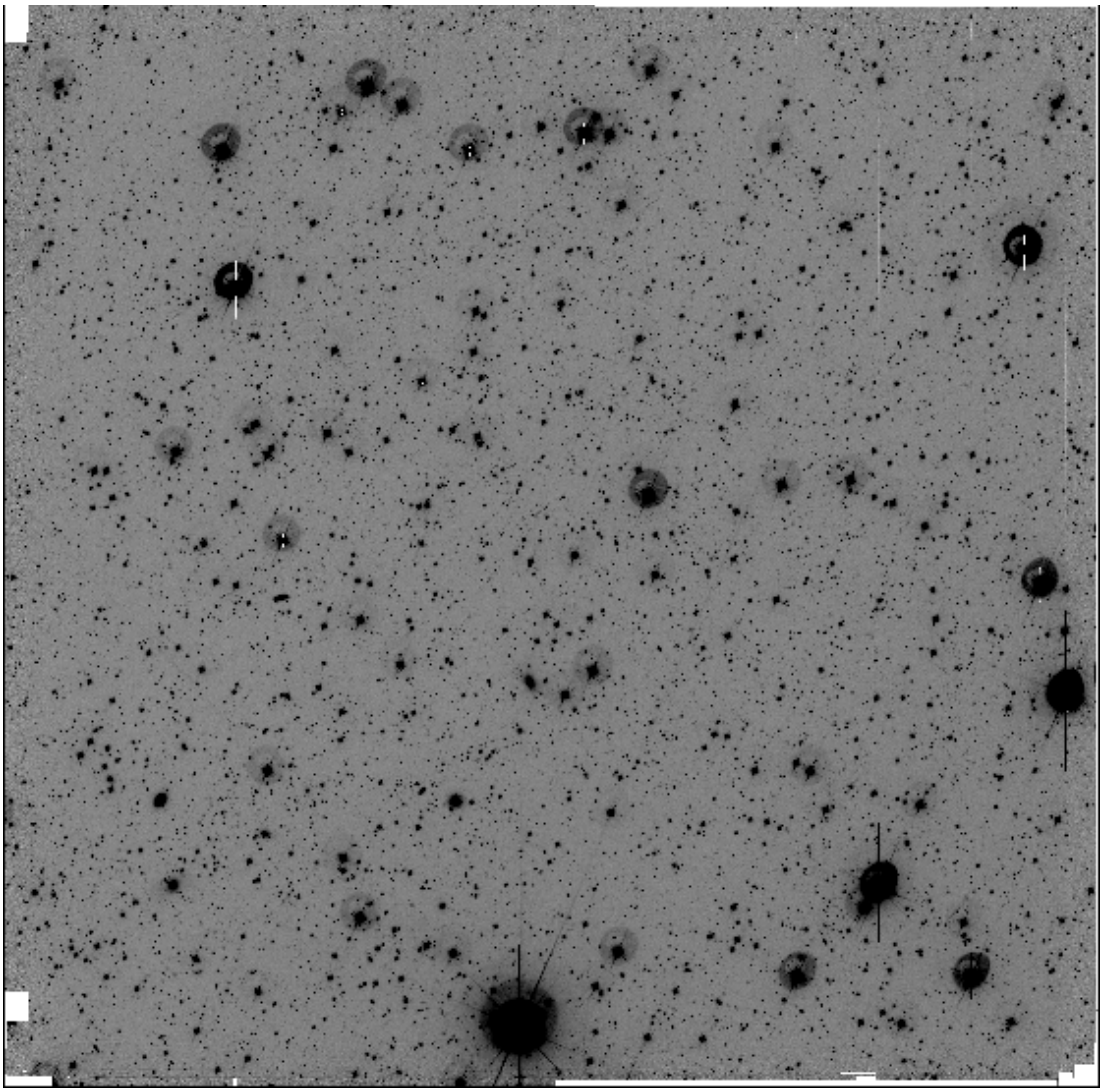

Figure D.44: LCRS Field 2114-39:E

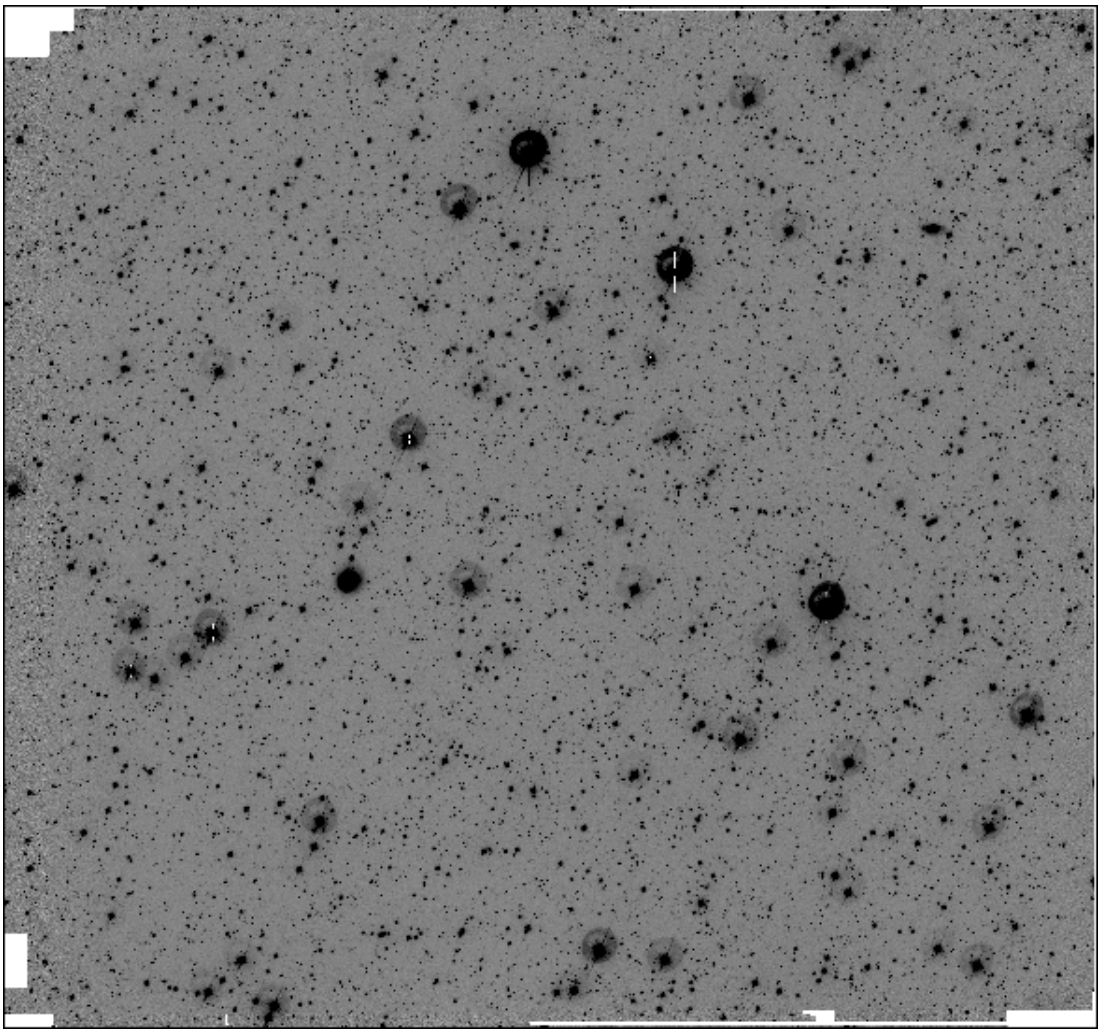

Figure D.45: LCRS Field 2115-45:E

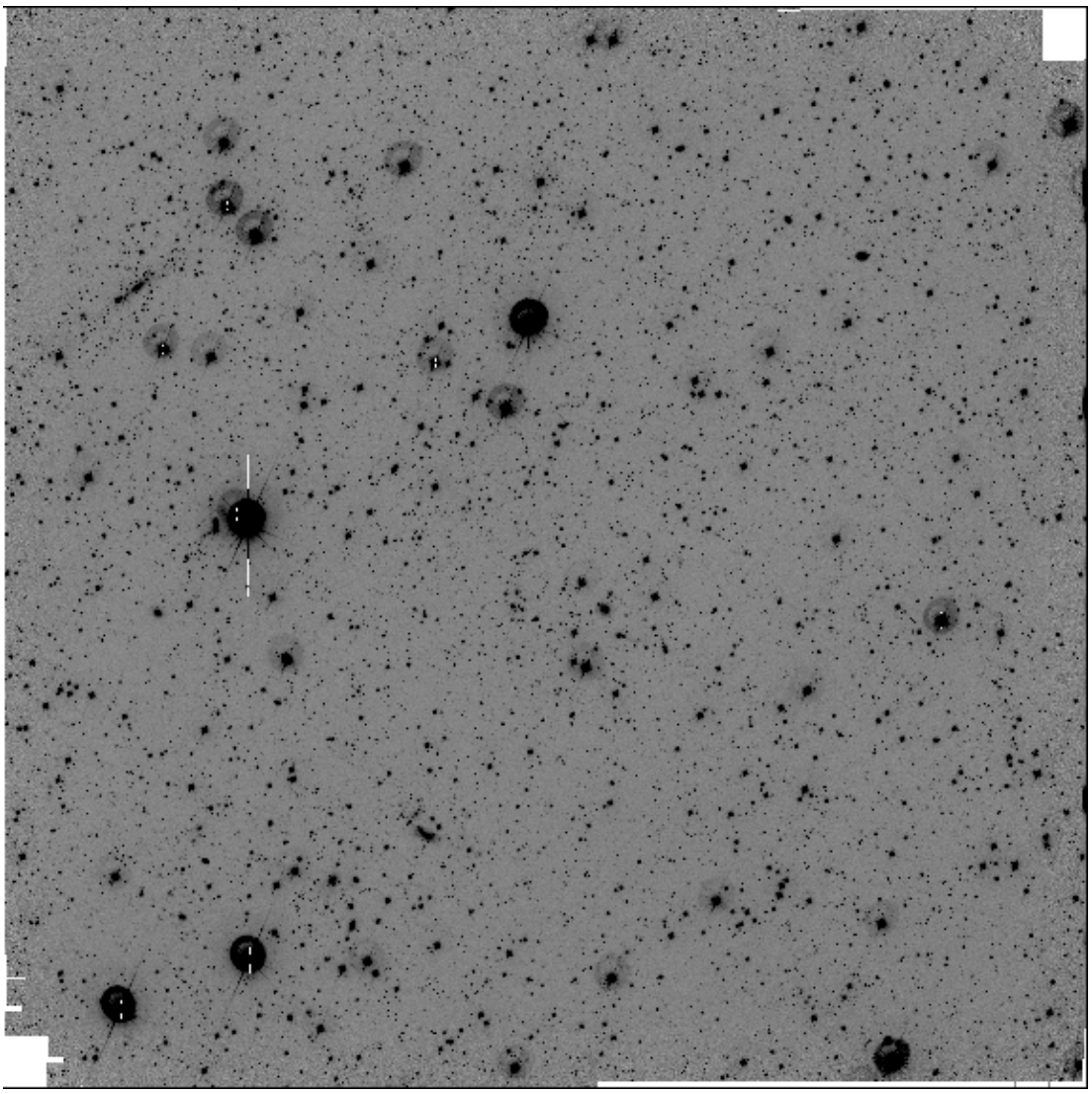

Figure D.46: LCRS Field 2154-39:E

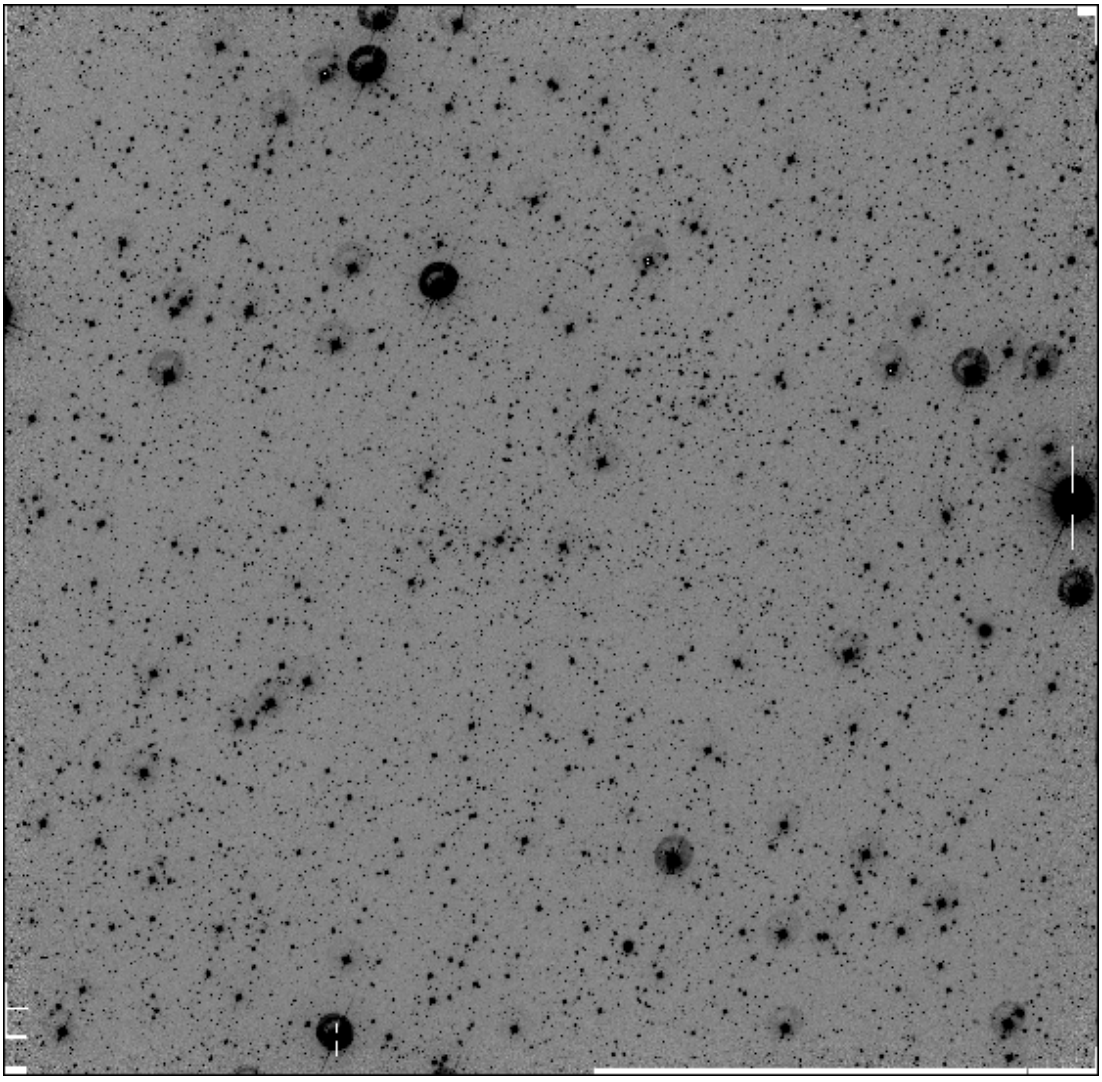

Figure D.47: LCRS Field 2154-39:M

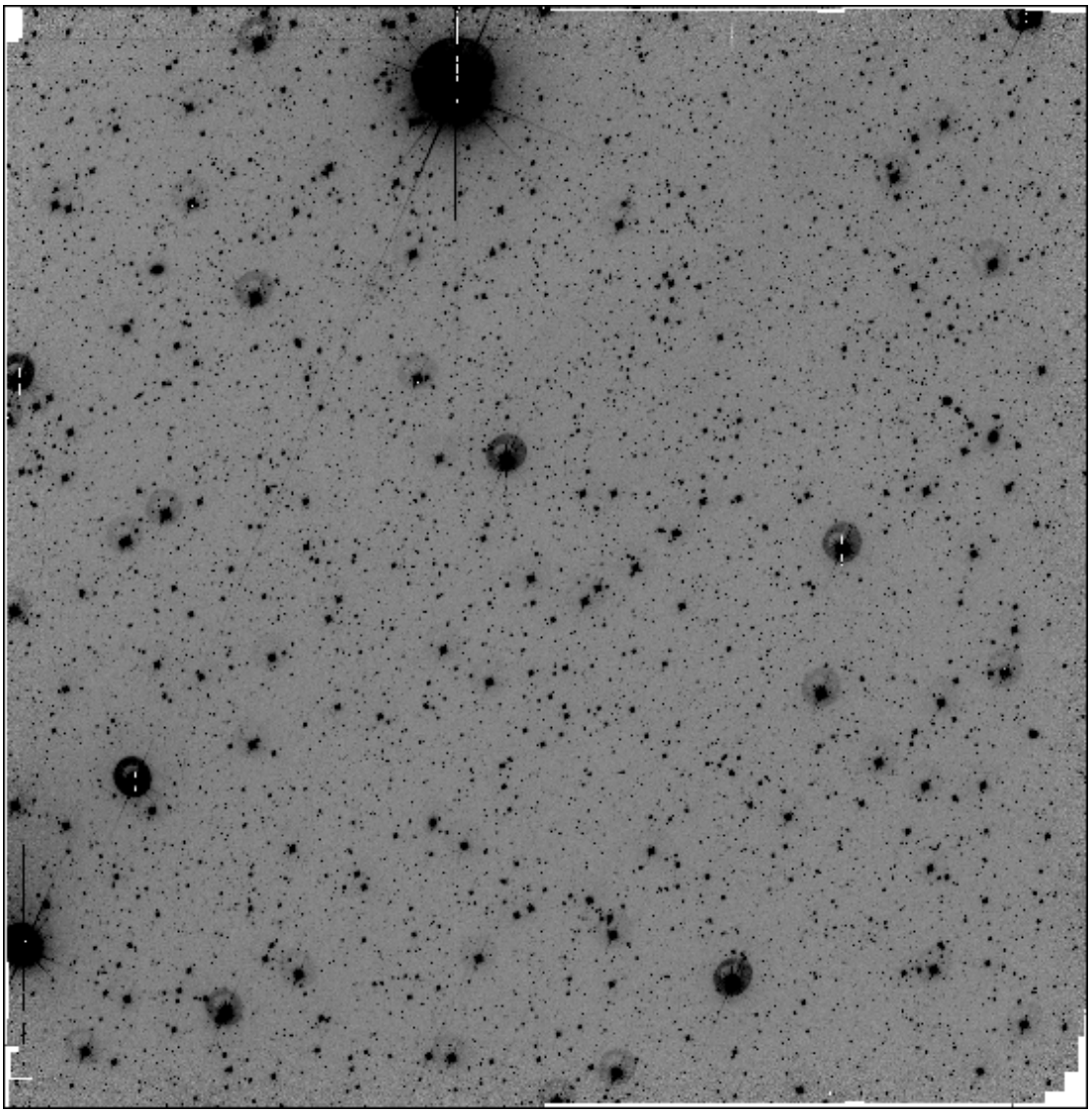

Figure D.48: LCRS Field 2154-39:W

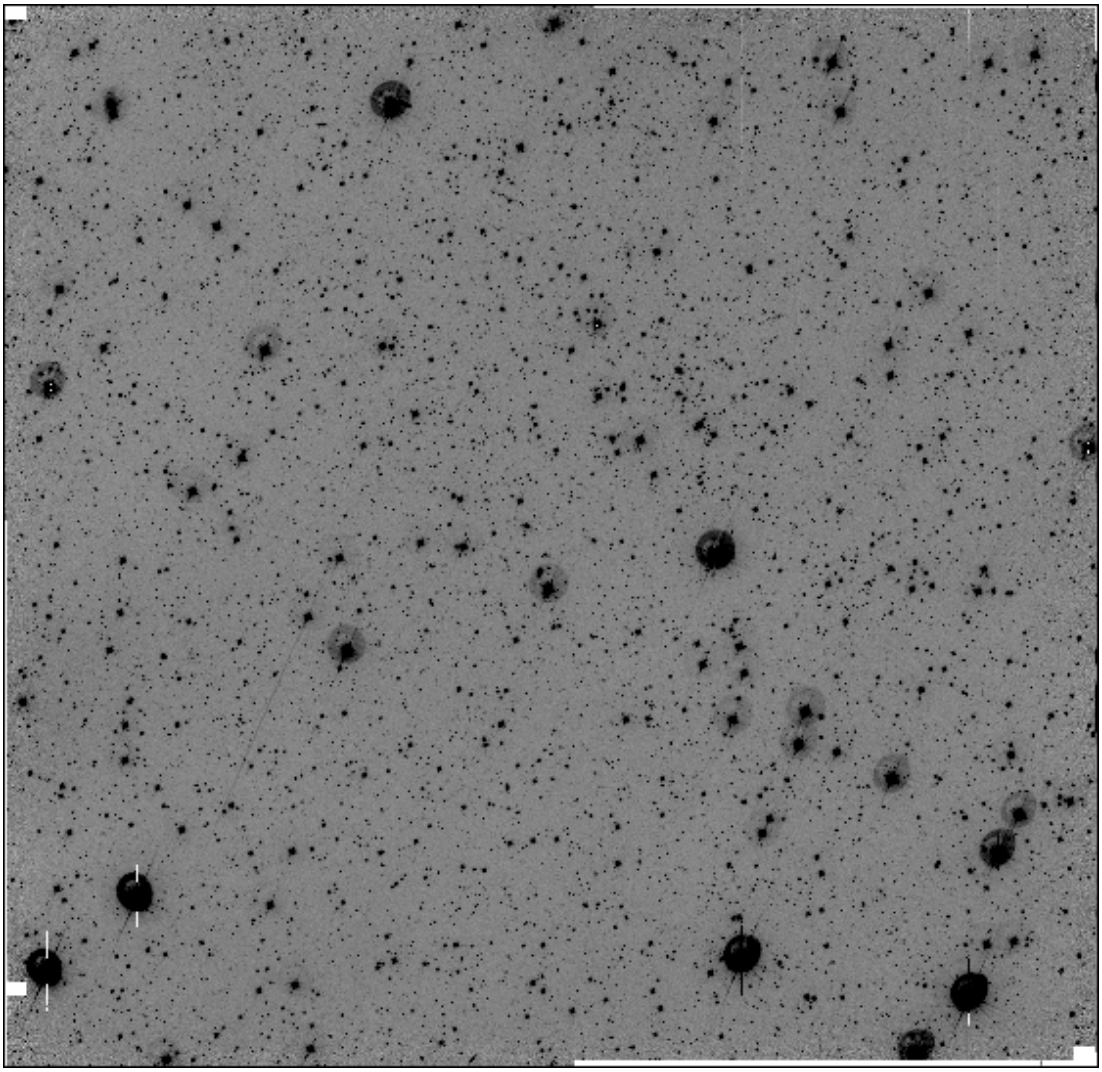

Figure D.49: LCRS Field 2155-45:E

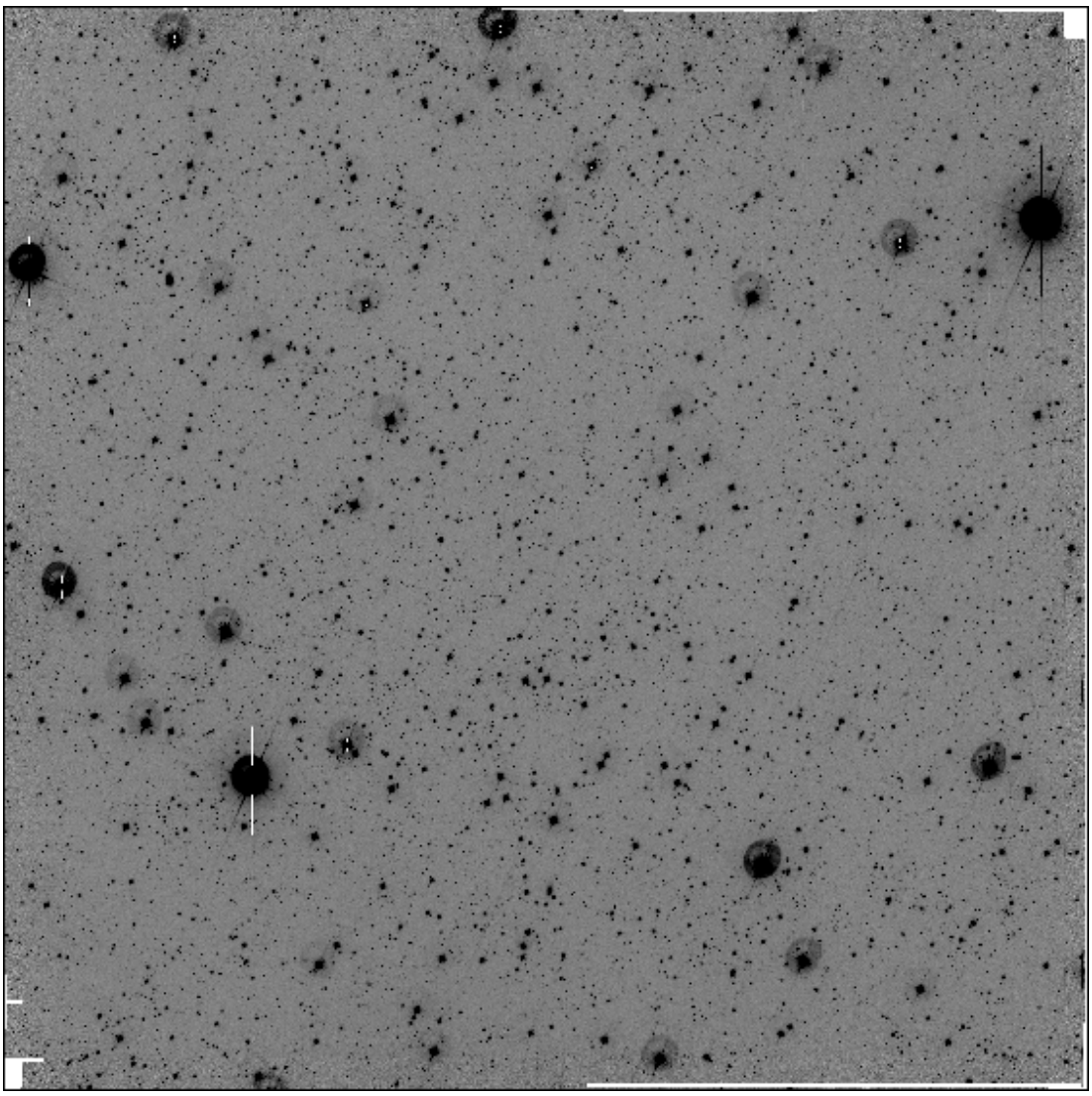

Figure D.50: LCRS Field 2234-39:E

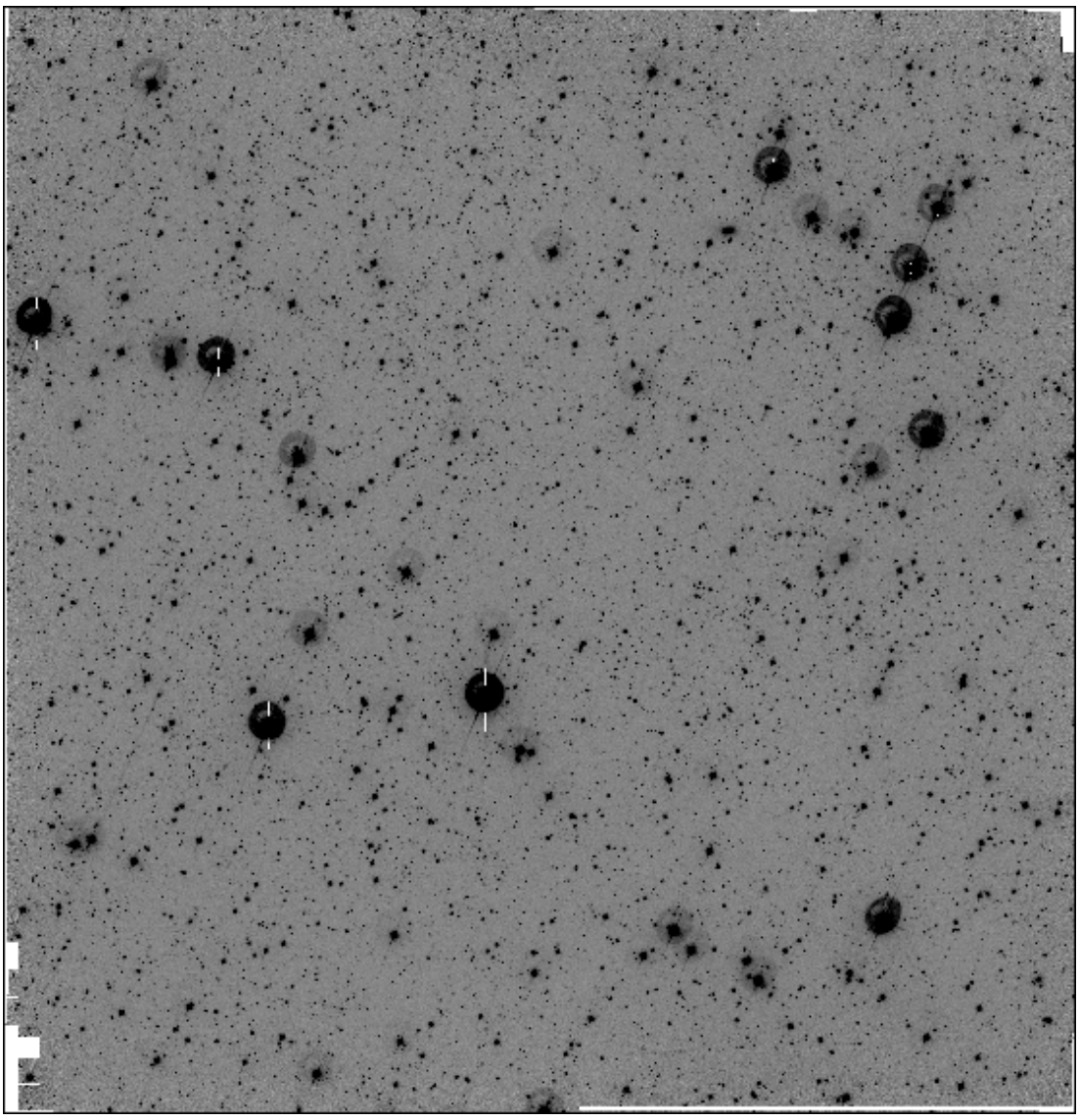

Figure D.51: LCRS Field 2234-39:W

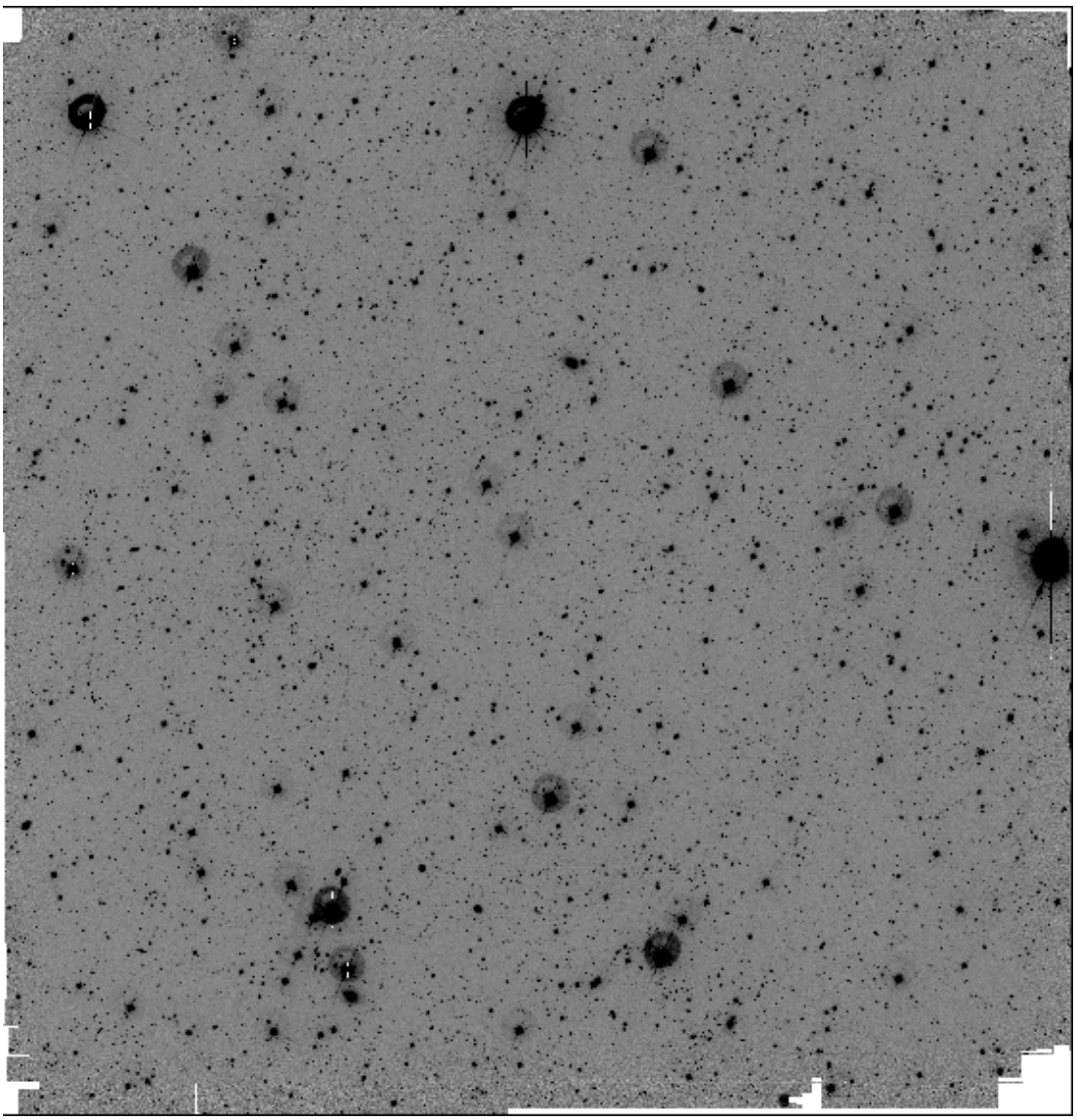

Figure D.52: LCRS Field 2314-39:E

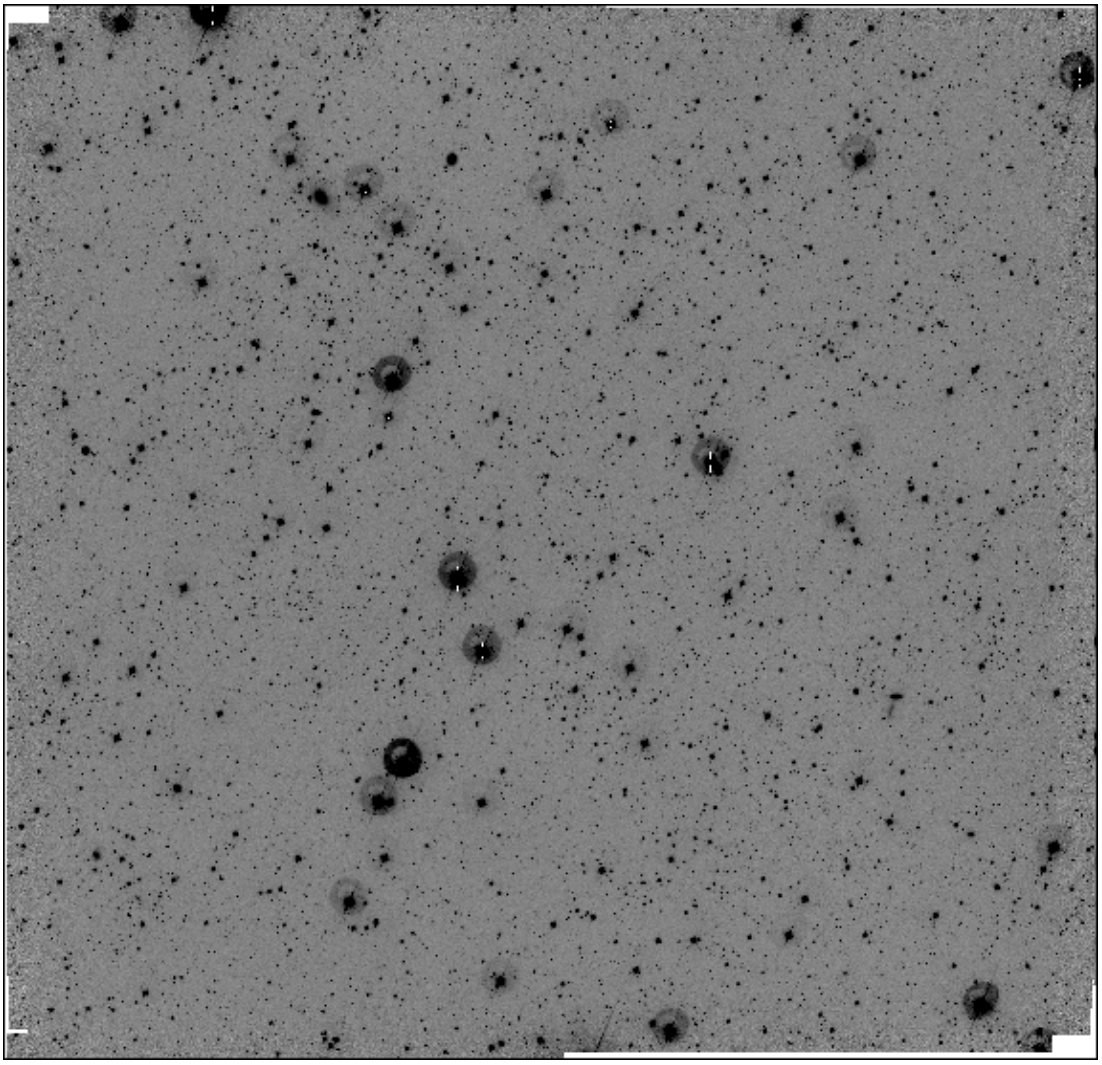

Figure D.53: LCRS Field 2314-39:M

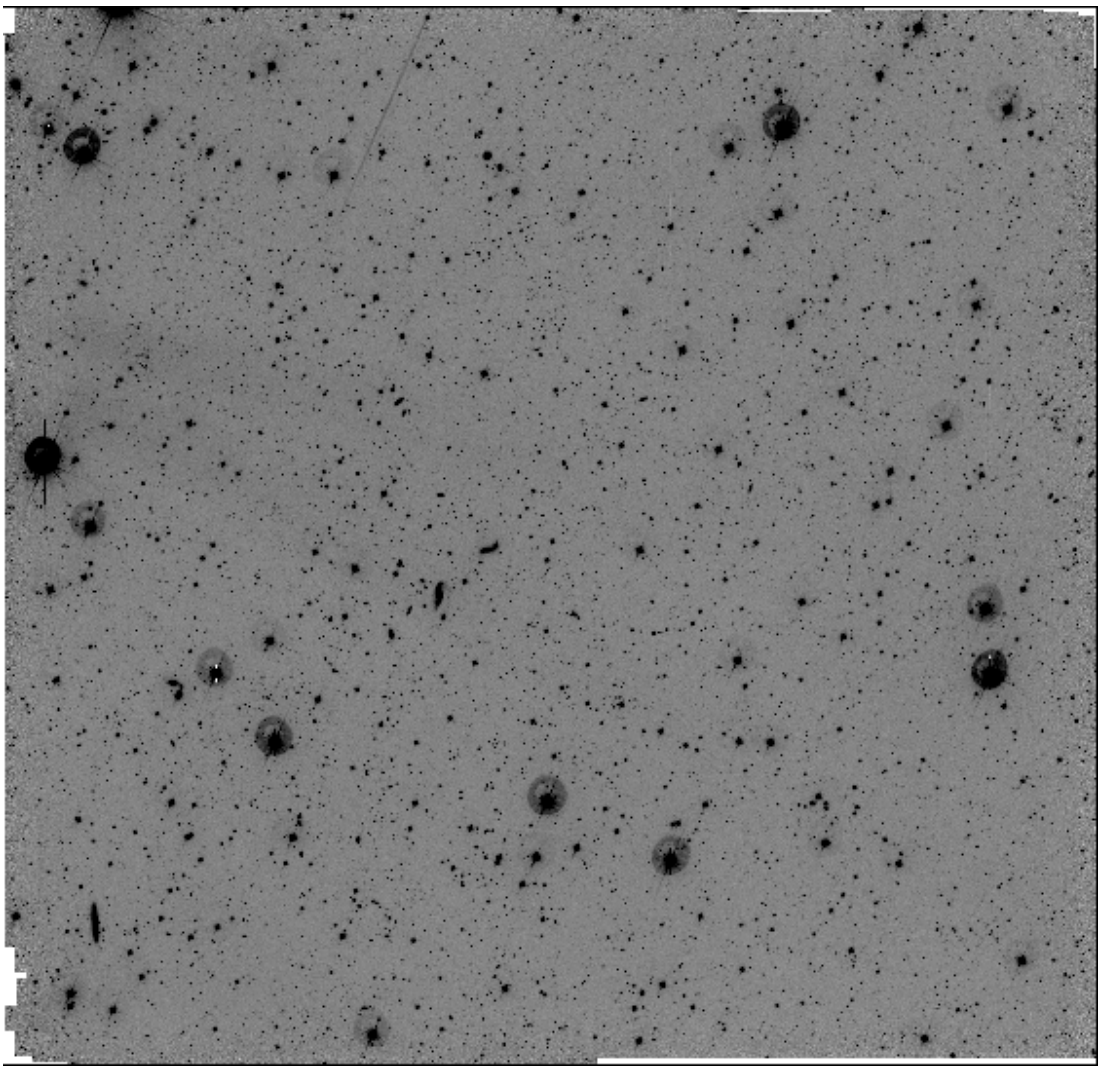

Figure D.54: LCRS Field 2315-45:E

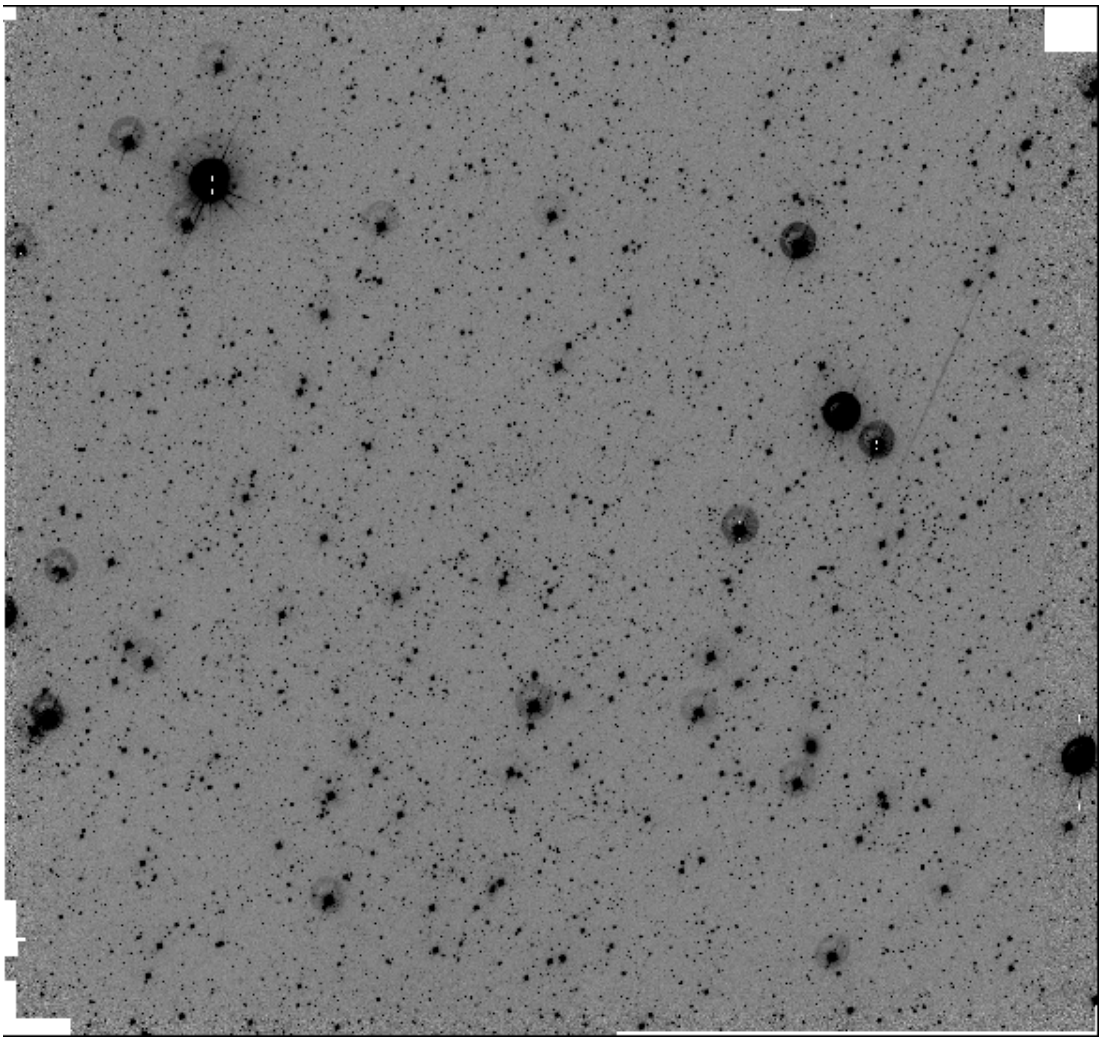

Figure D.55: LCRS Field 2315-45:W

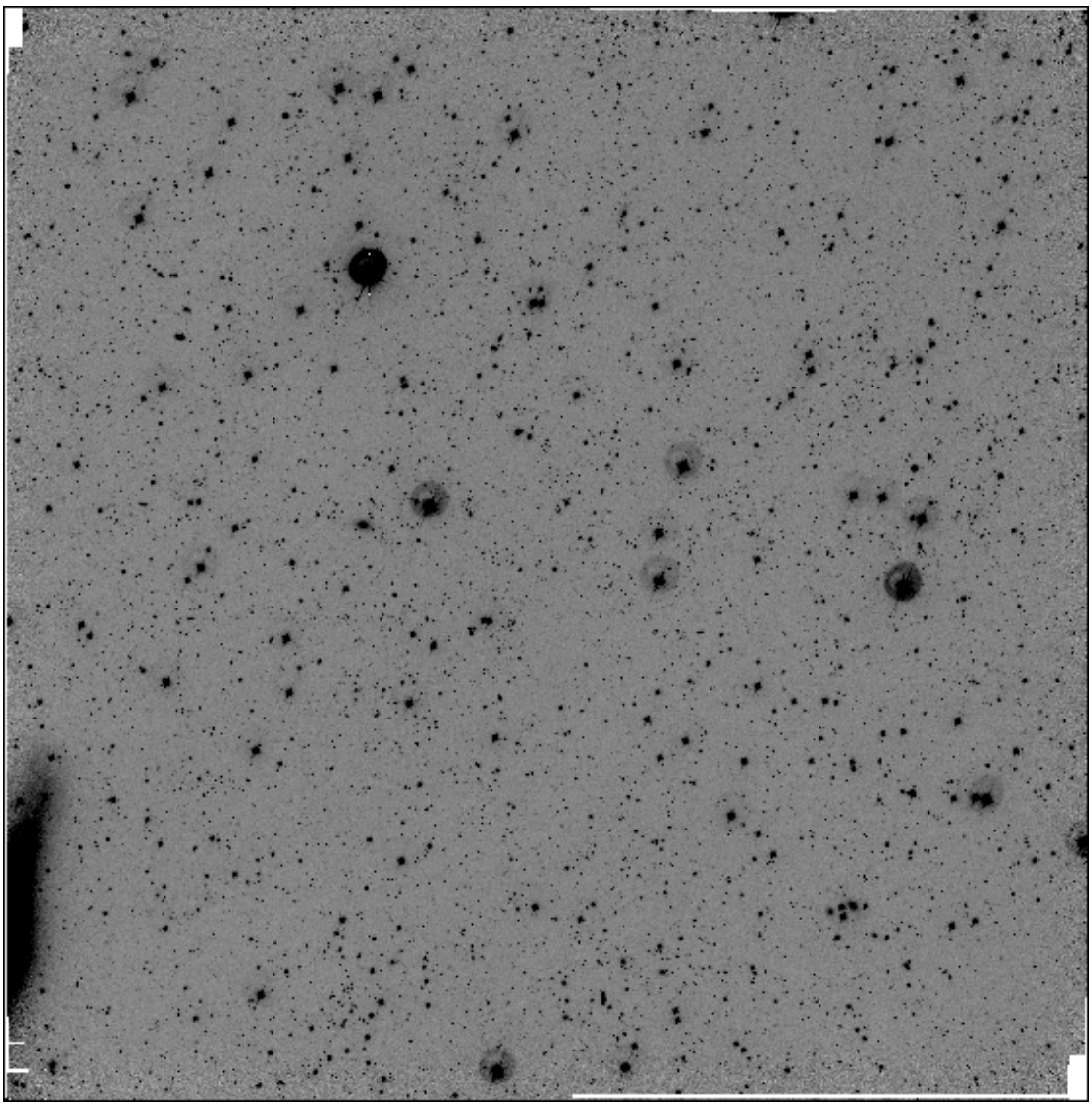

Figure D.56: LCRS Field 2354-39:M

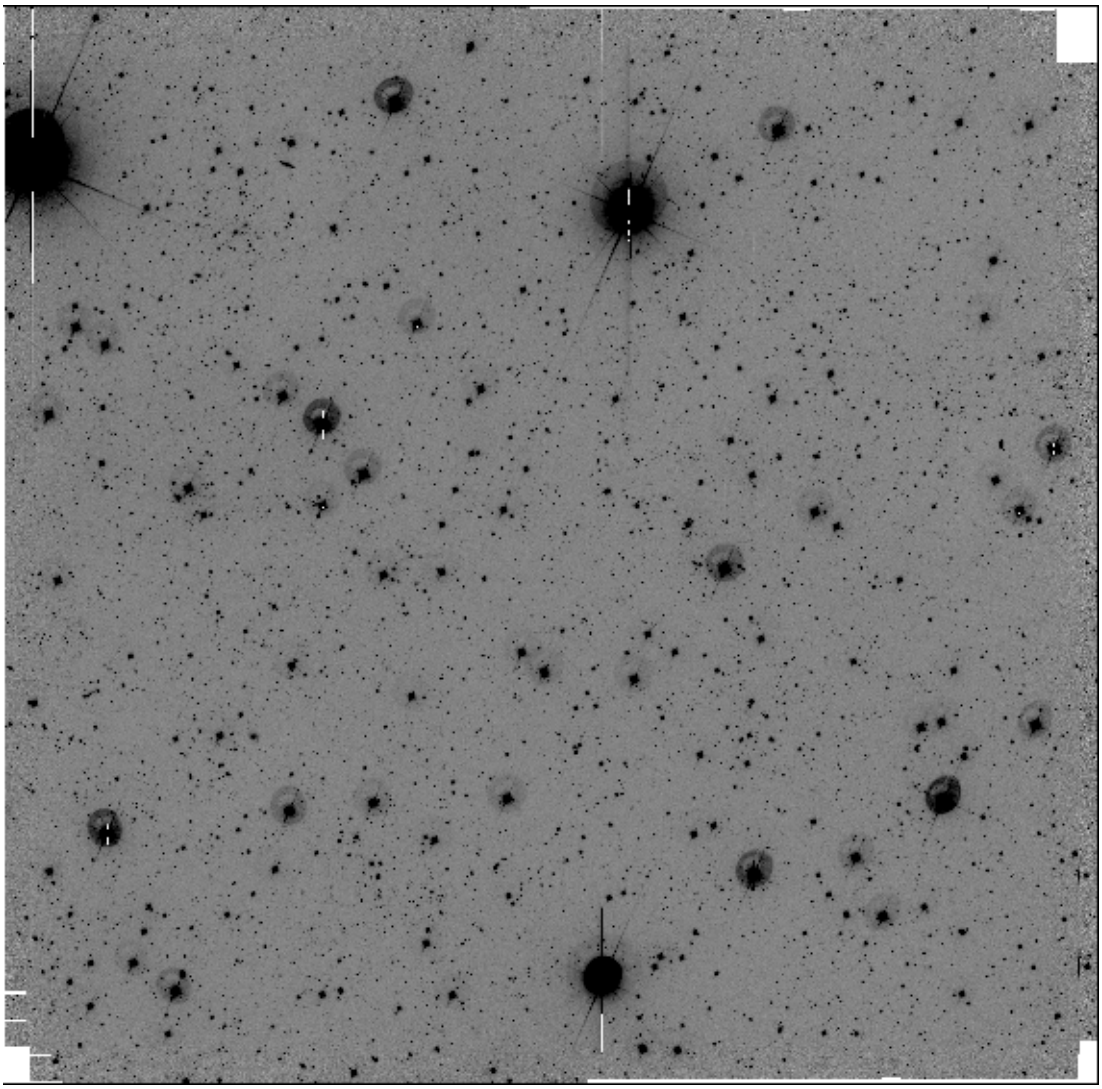

Figure D.57: LCRS Field 2354-39:W

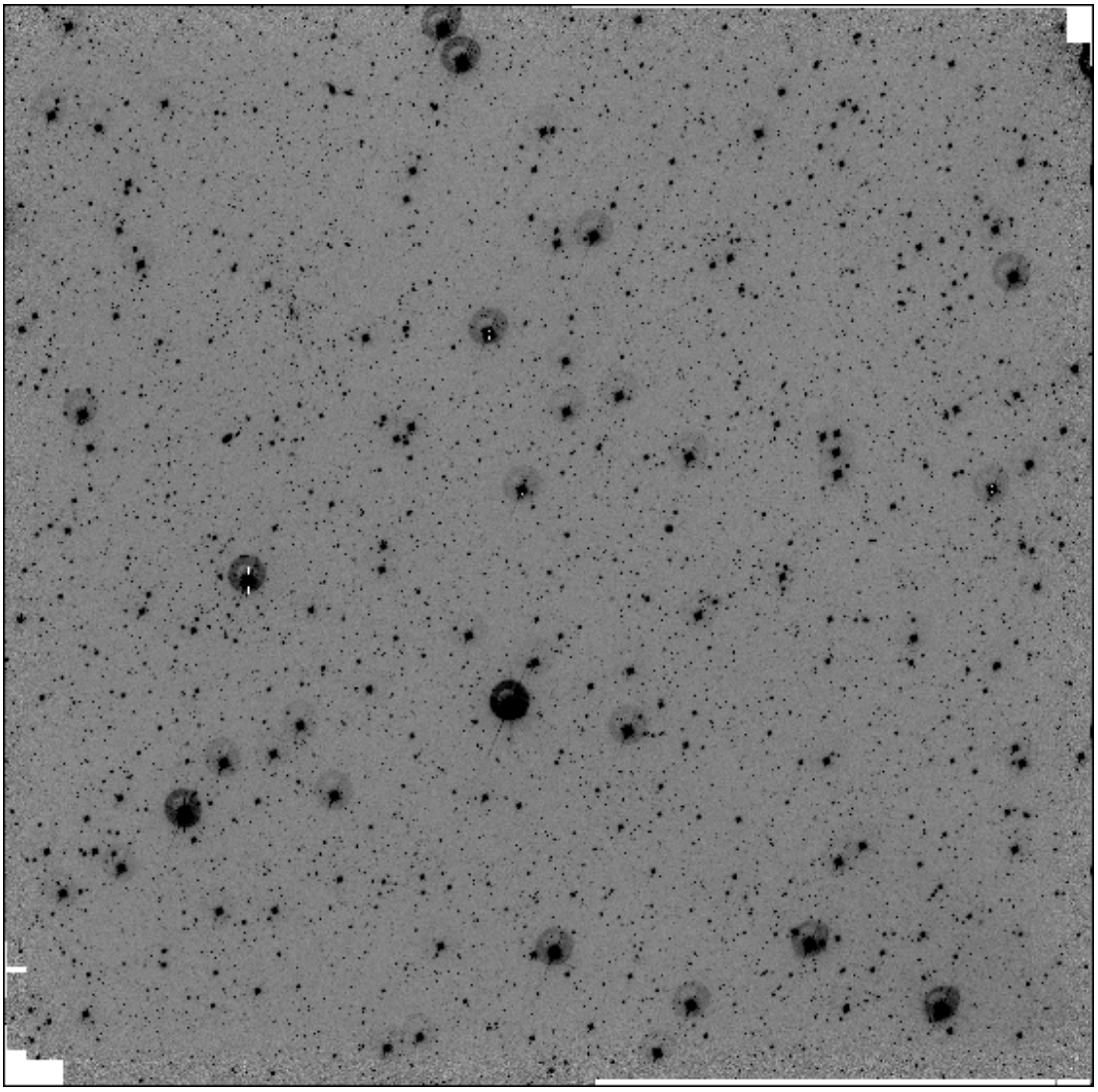

Figure D.58: LCRS Field 2355-45:E

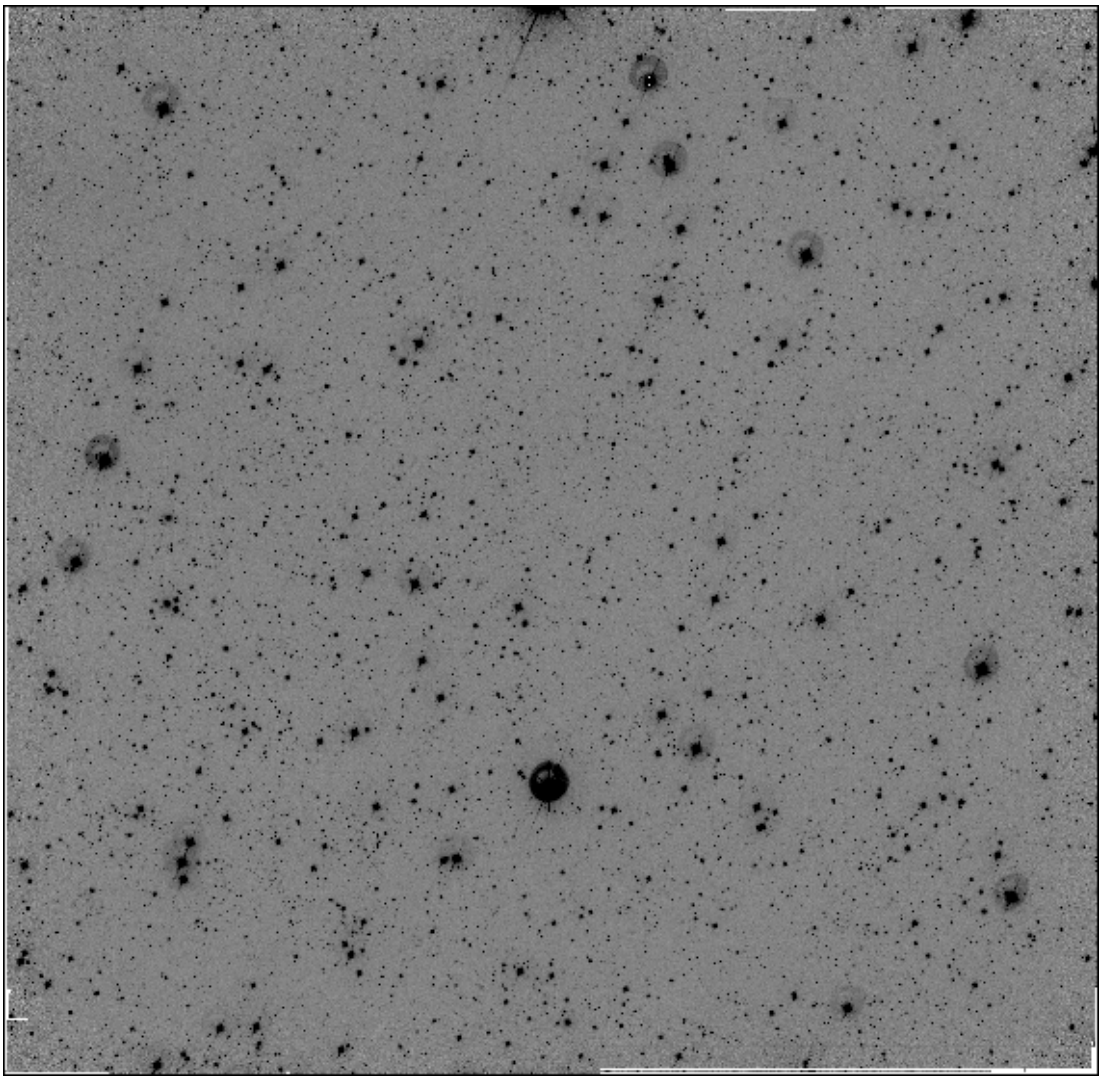

Figure D.59: LCRS Field 2355-45:M

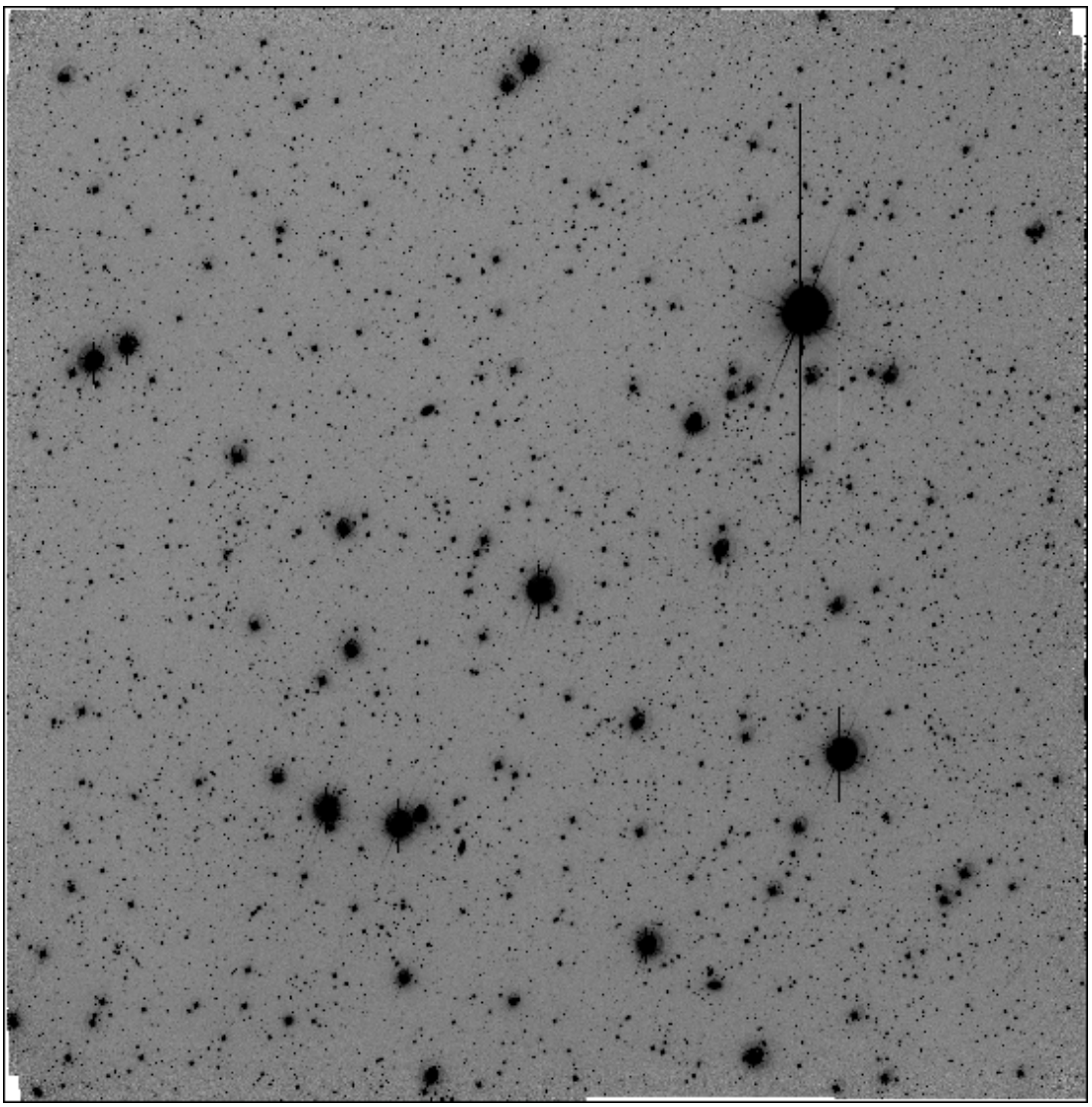

Figure D.60: LCRS Field 1032-06:S

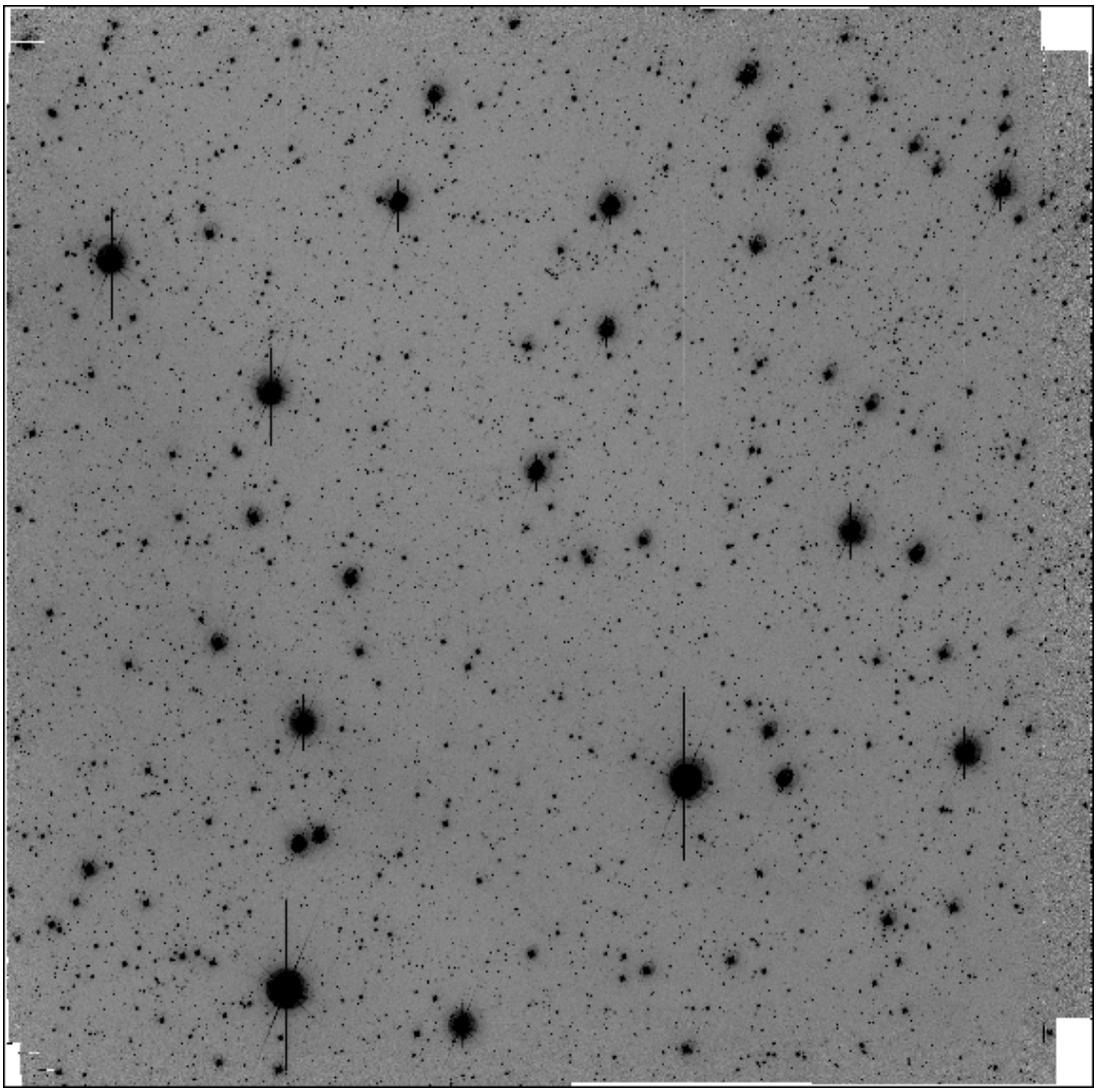

Figure D.61: LCRS Field 1036-06:S

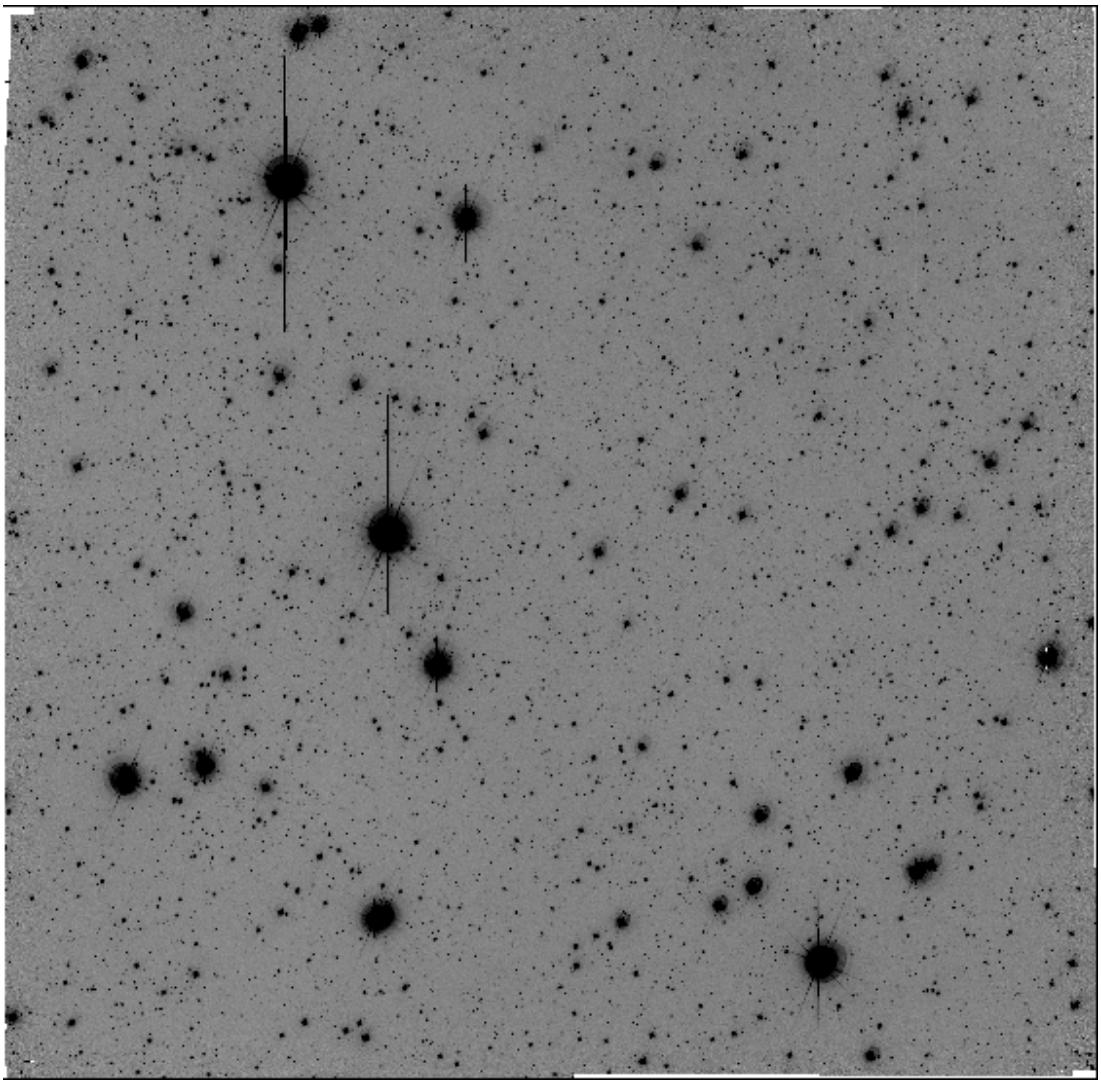

Figure D.62: LCRS Field 1040-06:S

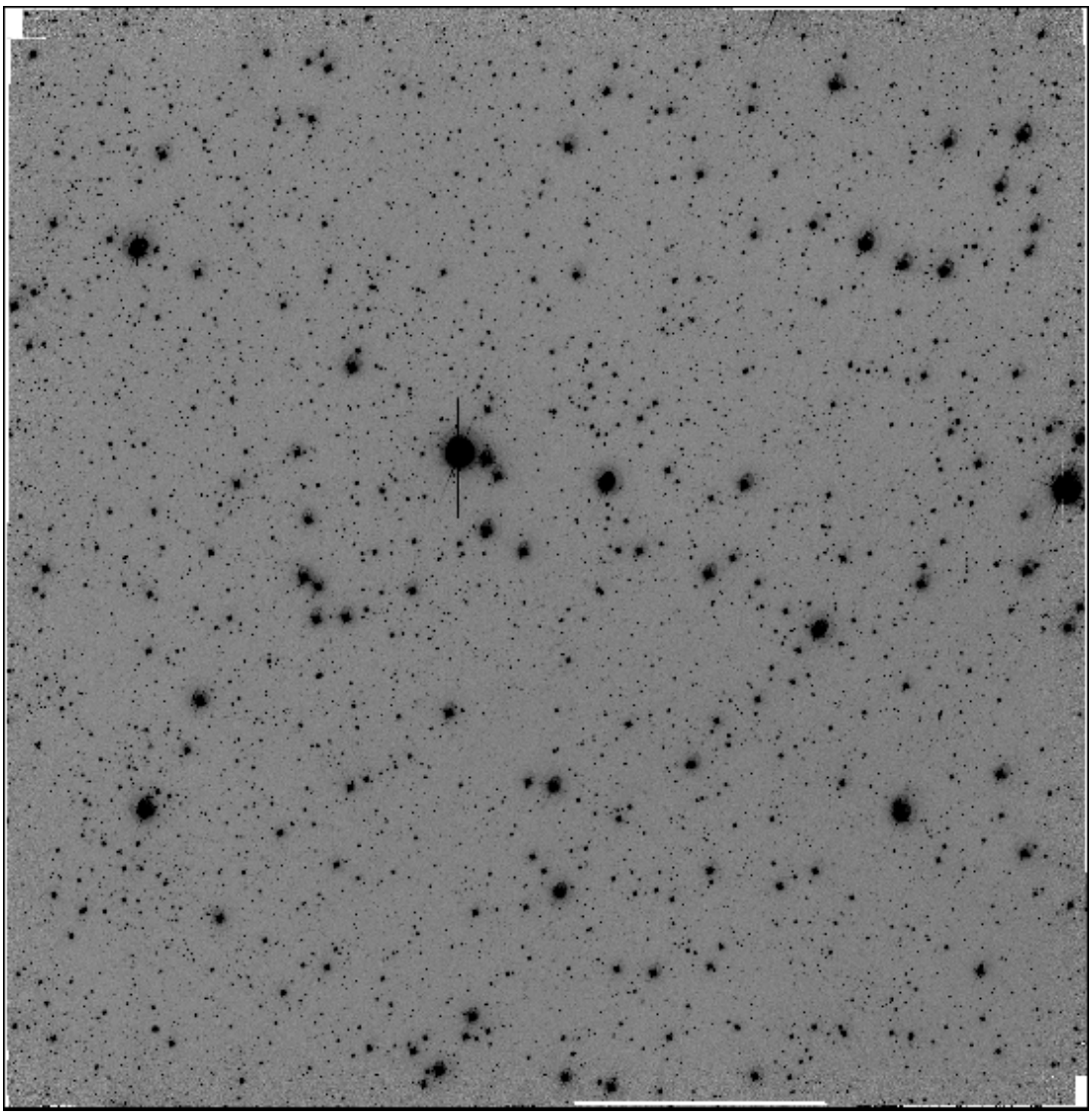

Figure D.63: LCRS Field 1044-06:S

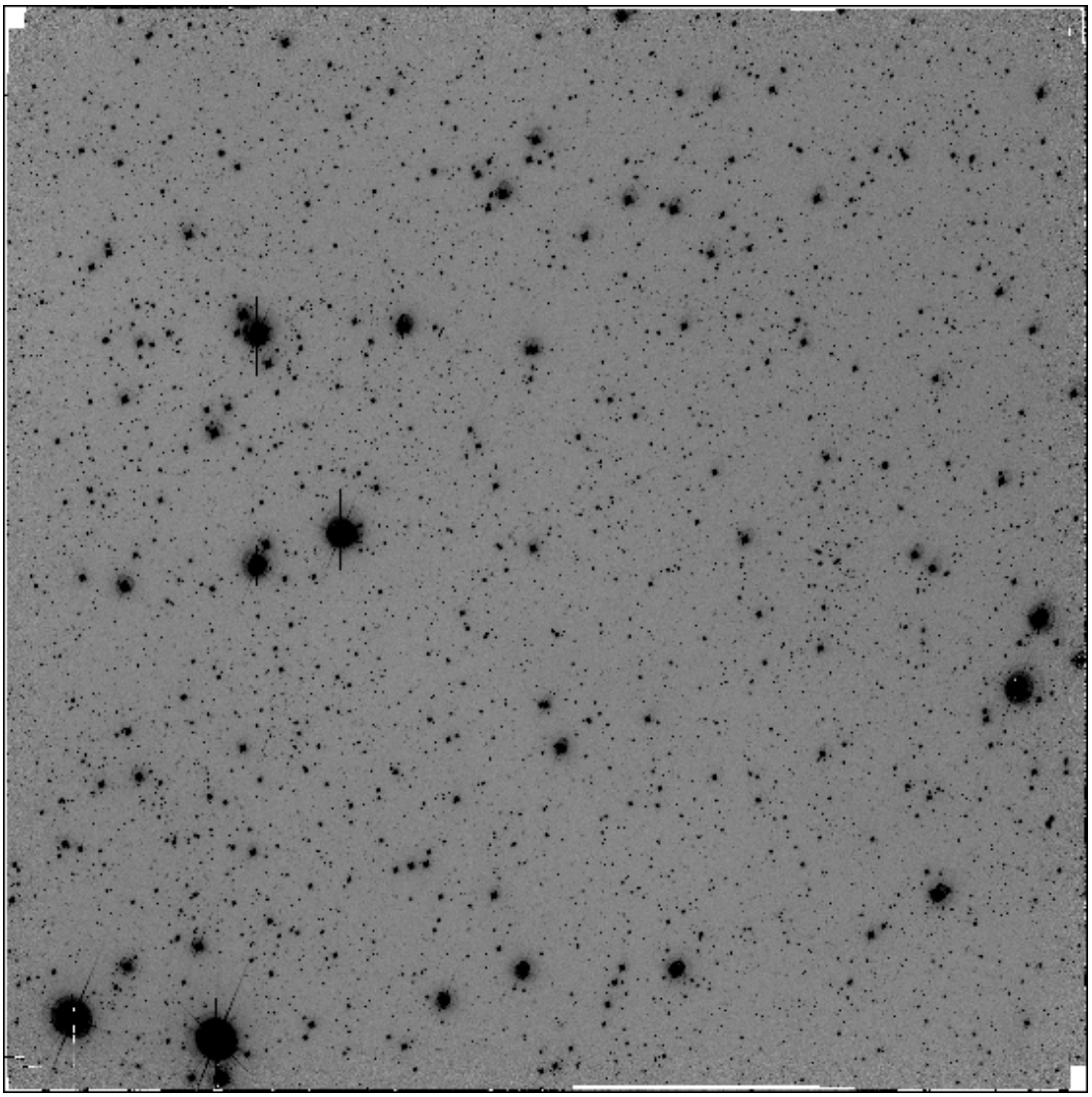

Figure D.64: LCRS Field 1048-06:S

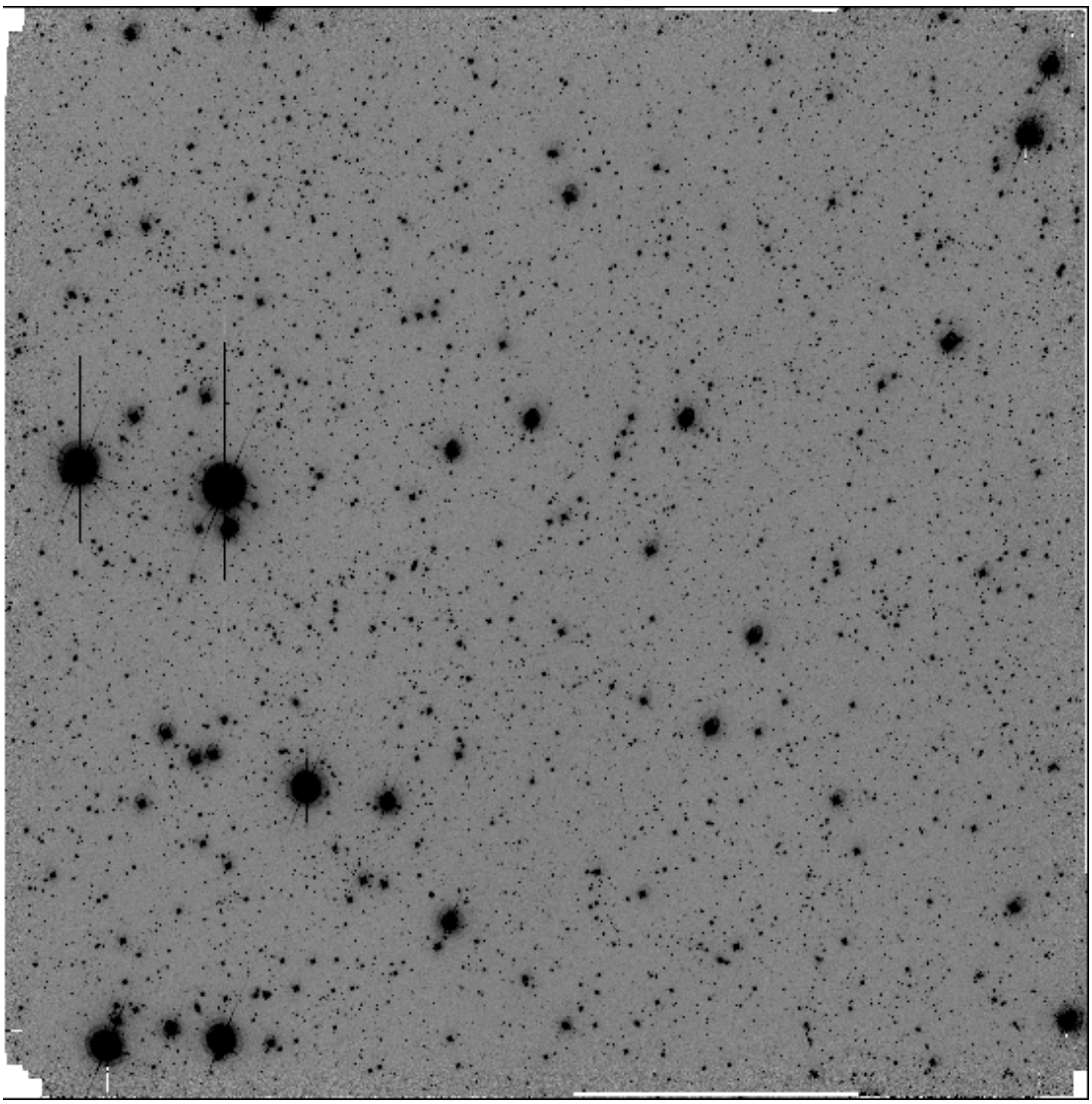

Figure D.65: LCRS Field 1052-06:S

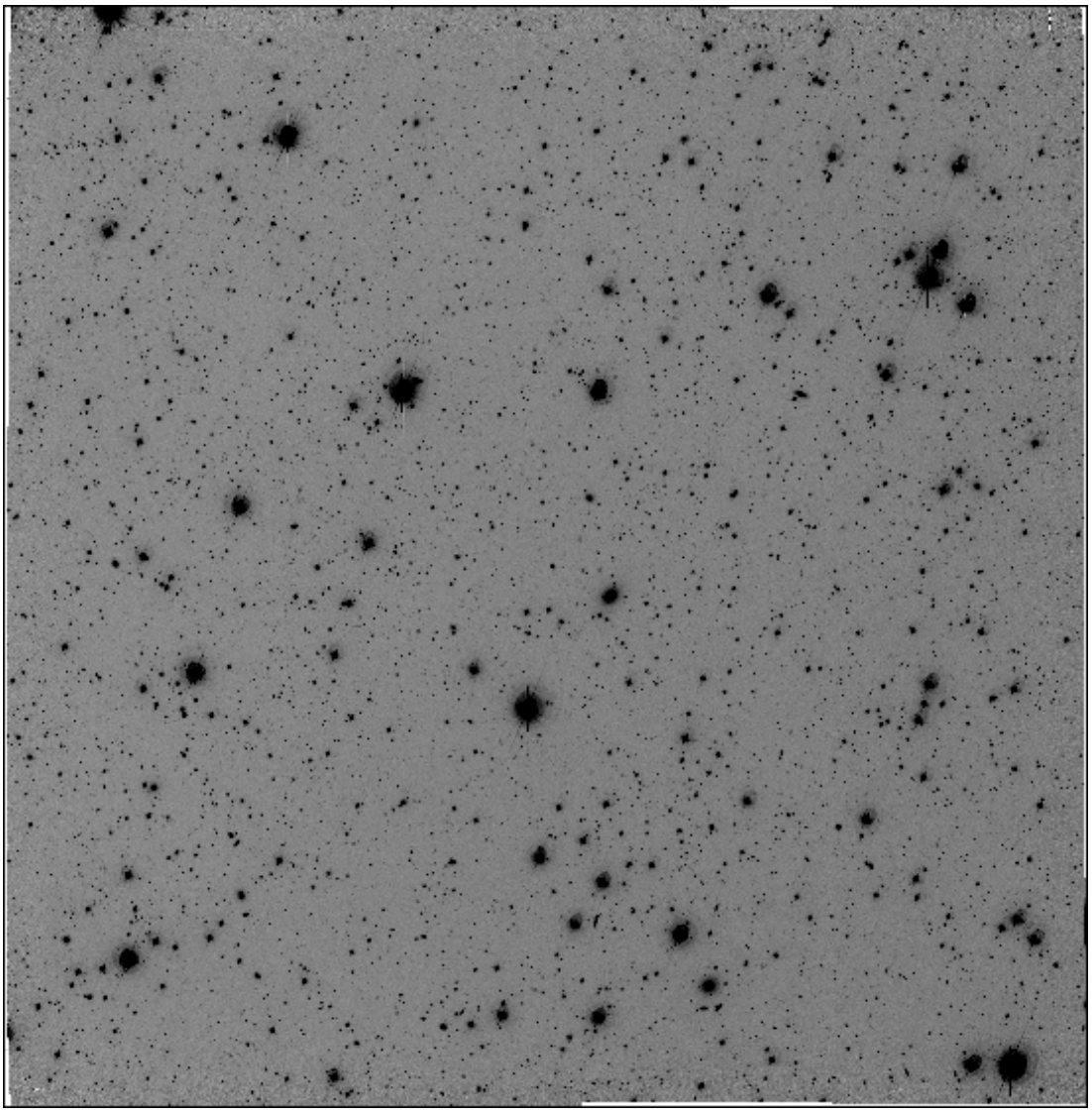

Figure D.66: LCRS Field 1056-06:S

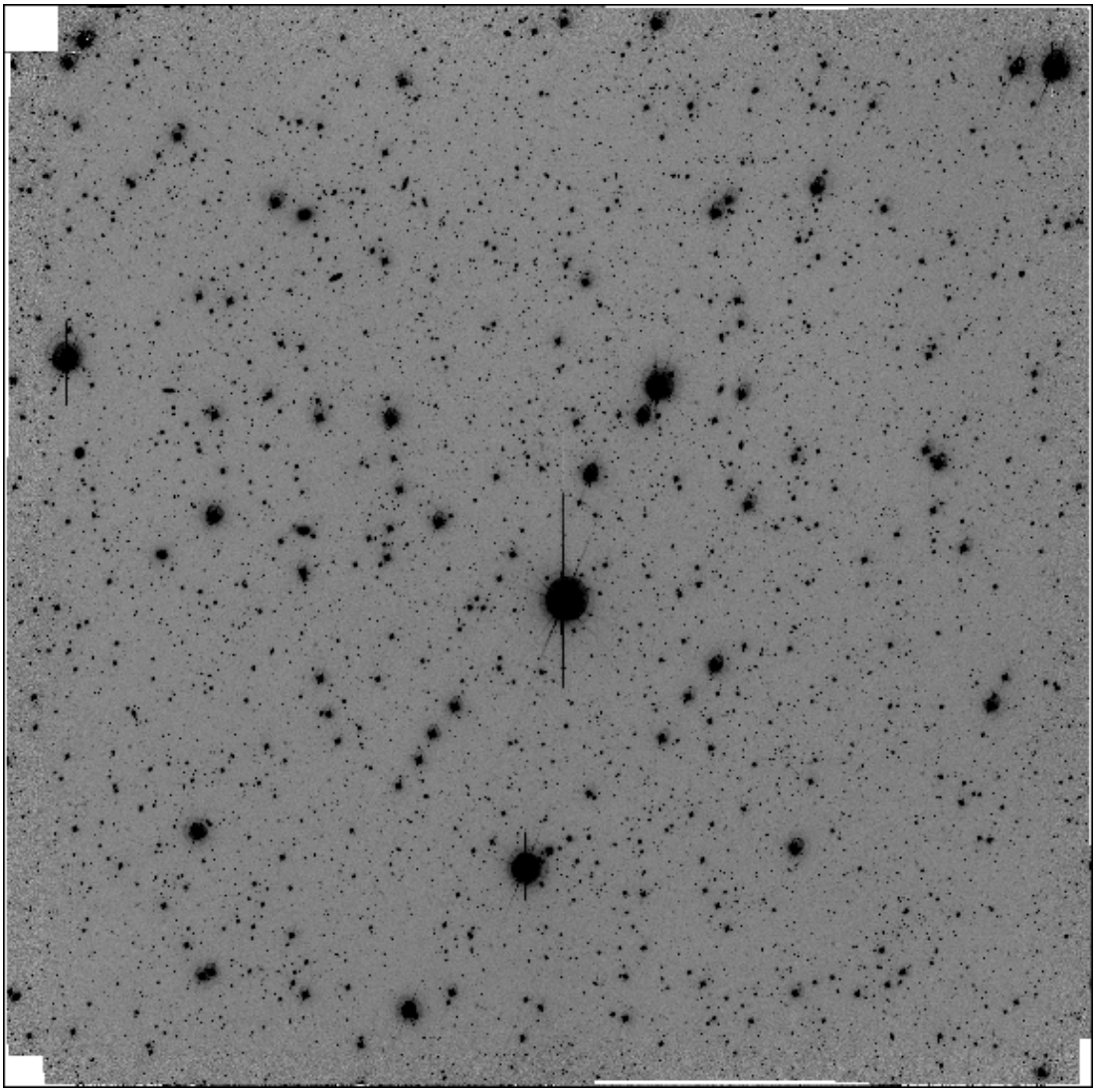

Figure D.67: LCRS Field 1100-06:S

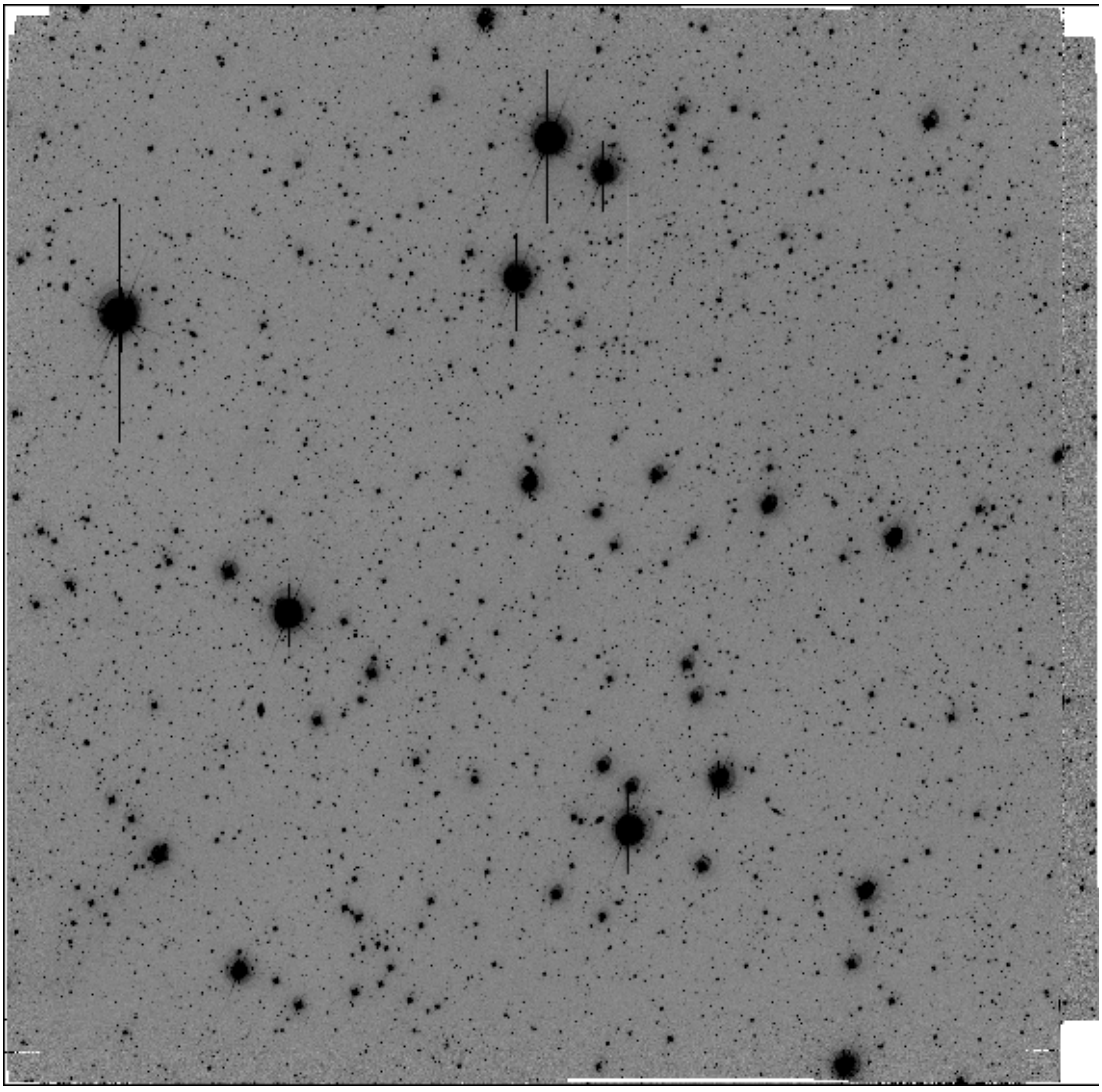

Figure D.68: LCRS Field 1104-06:S

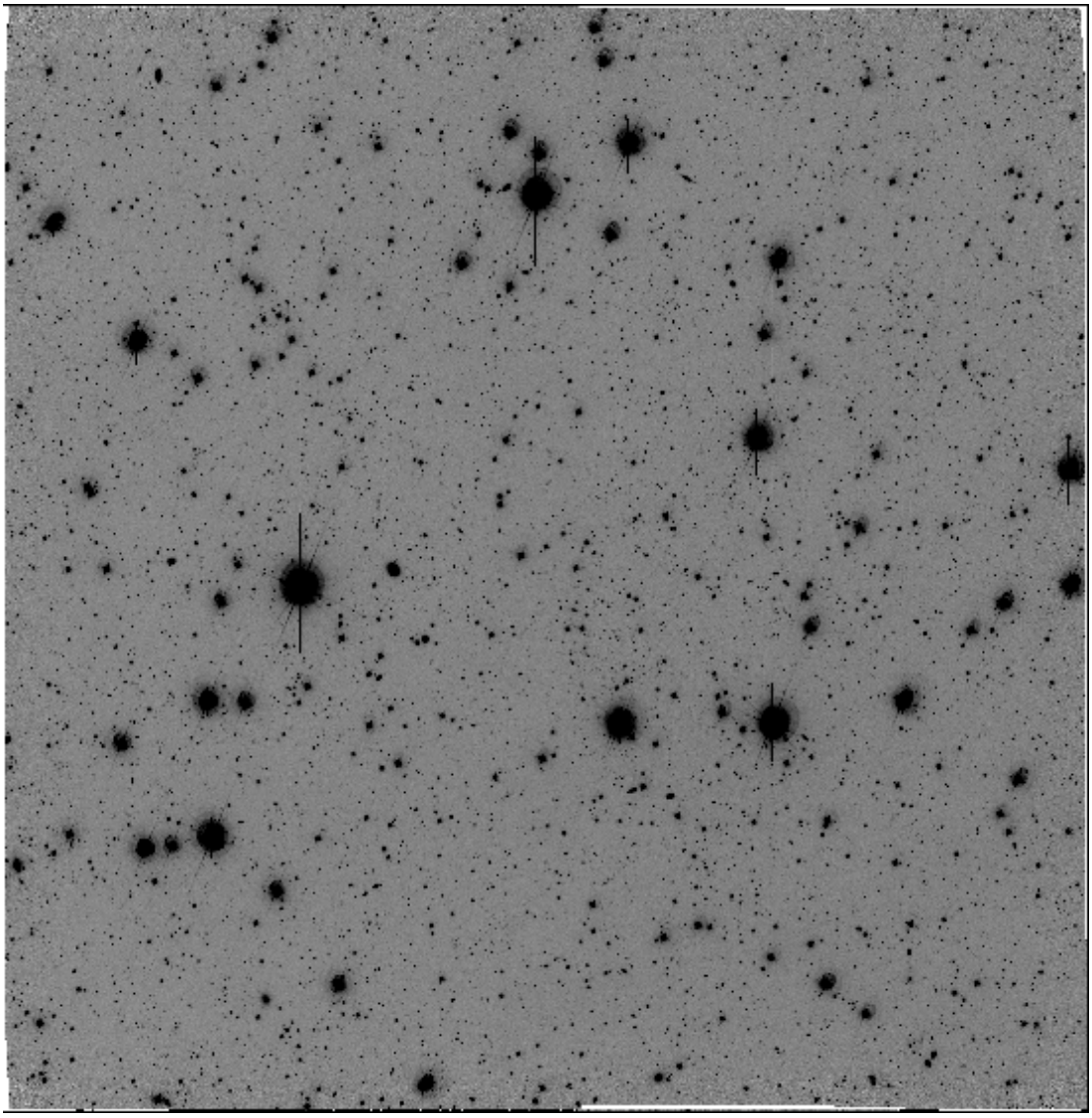

Figure D.69: LCRS Field 1108-06:S

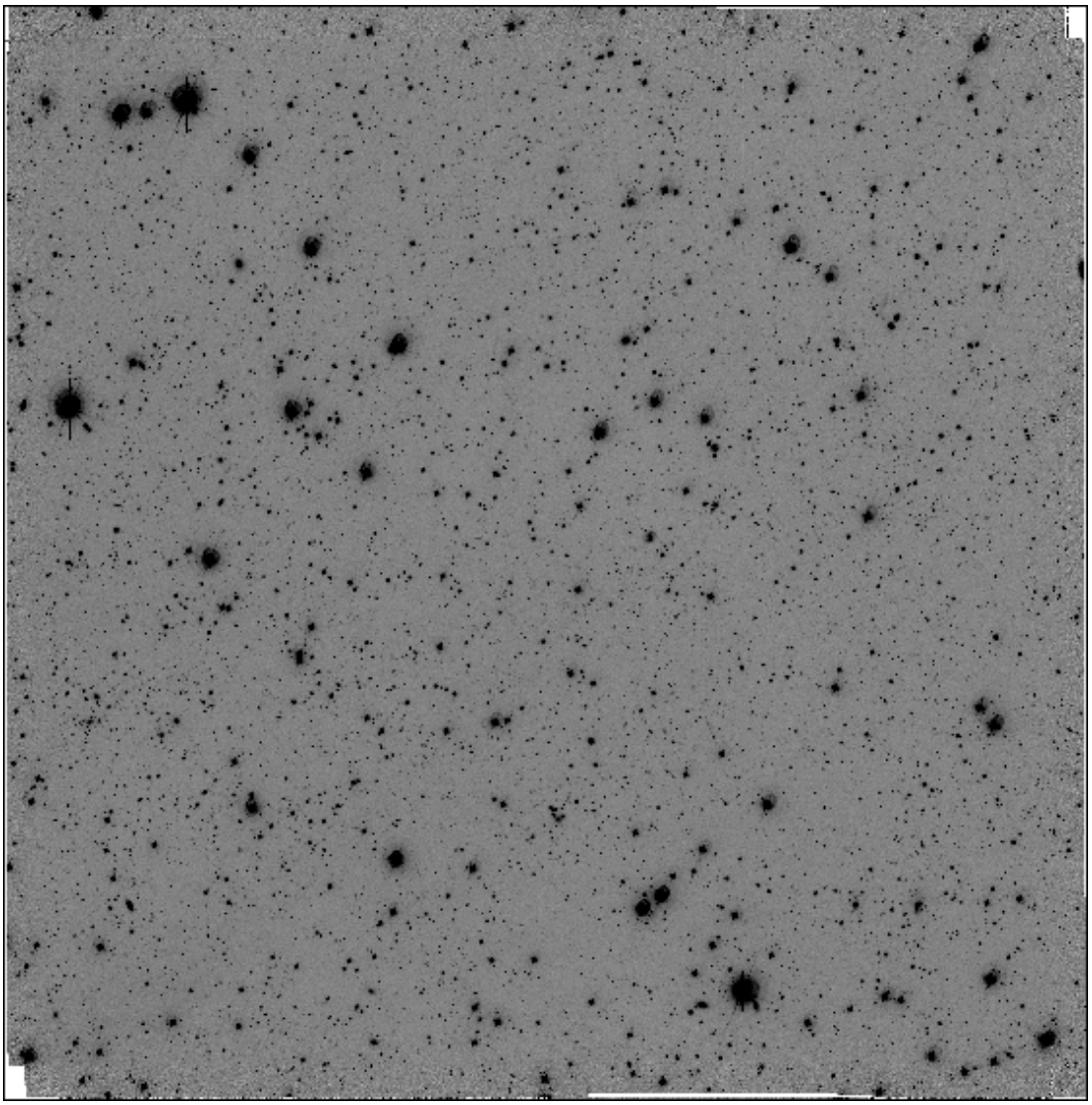

Figure D.70: LCRS Field 1112-06:S

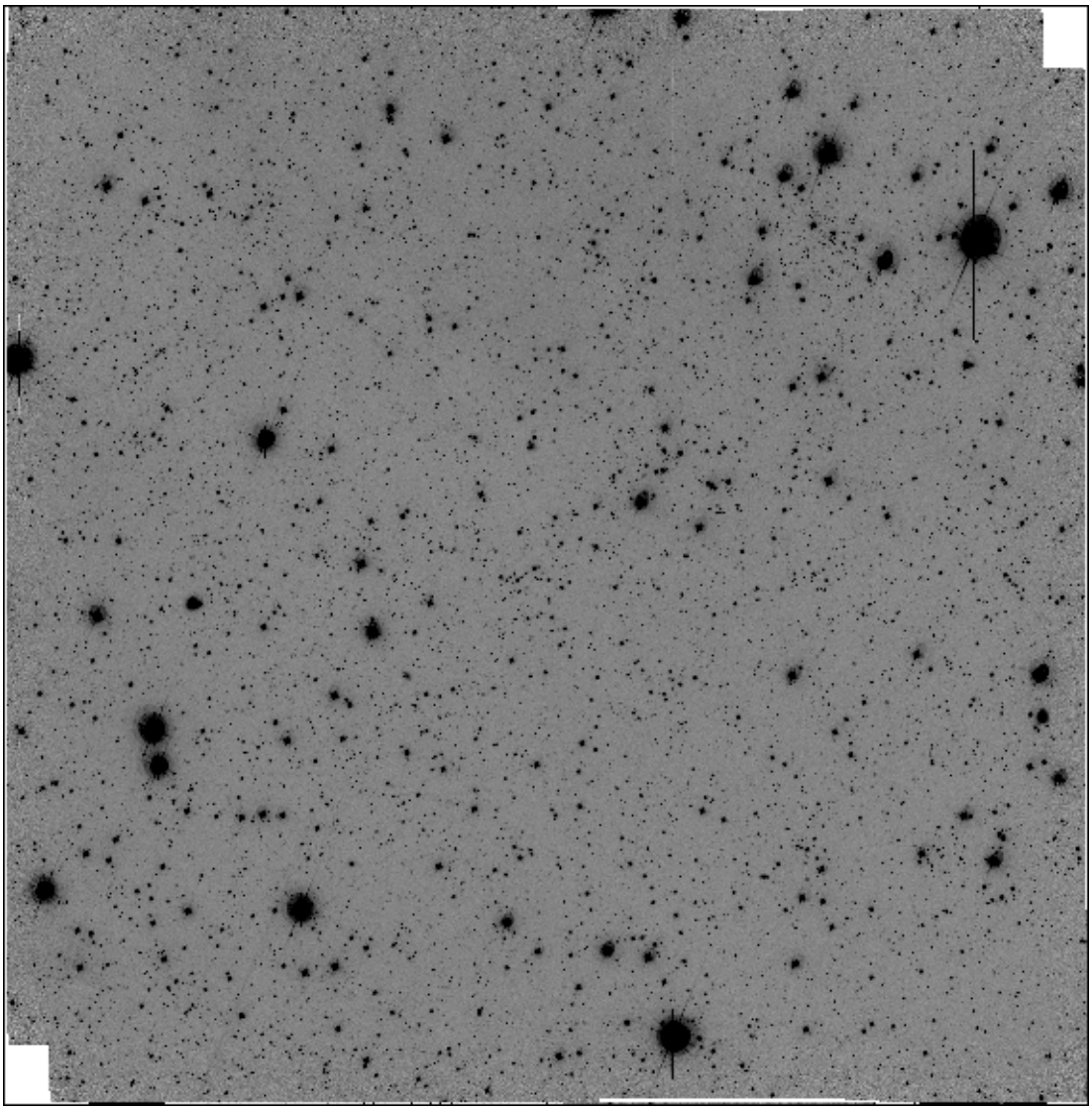

Figure D.71: LCRS Field 1203-12:E

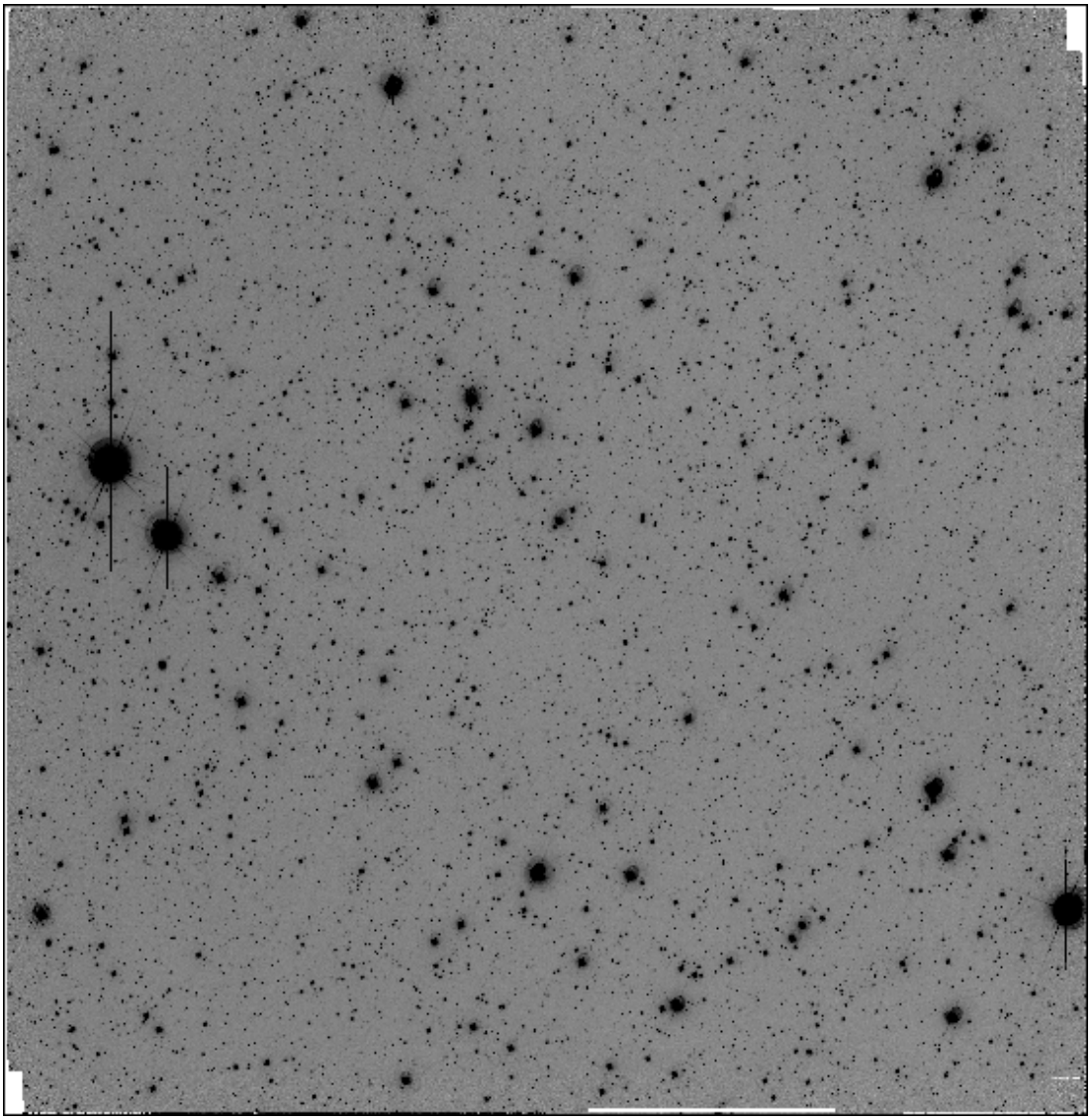

Figure D.72: LCRS Field 1427-06:W

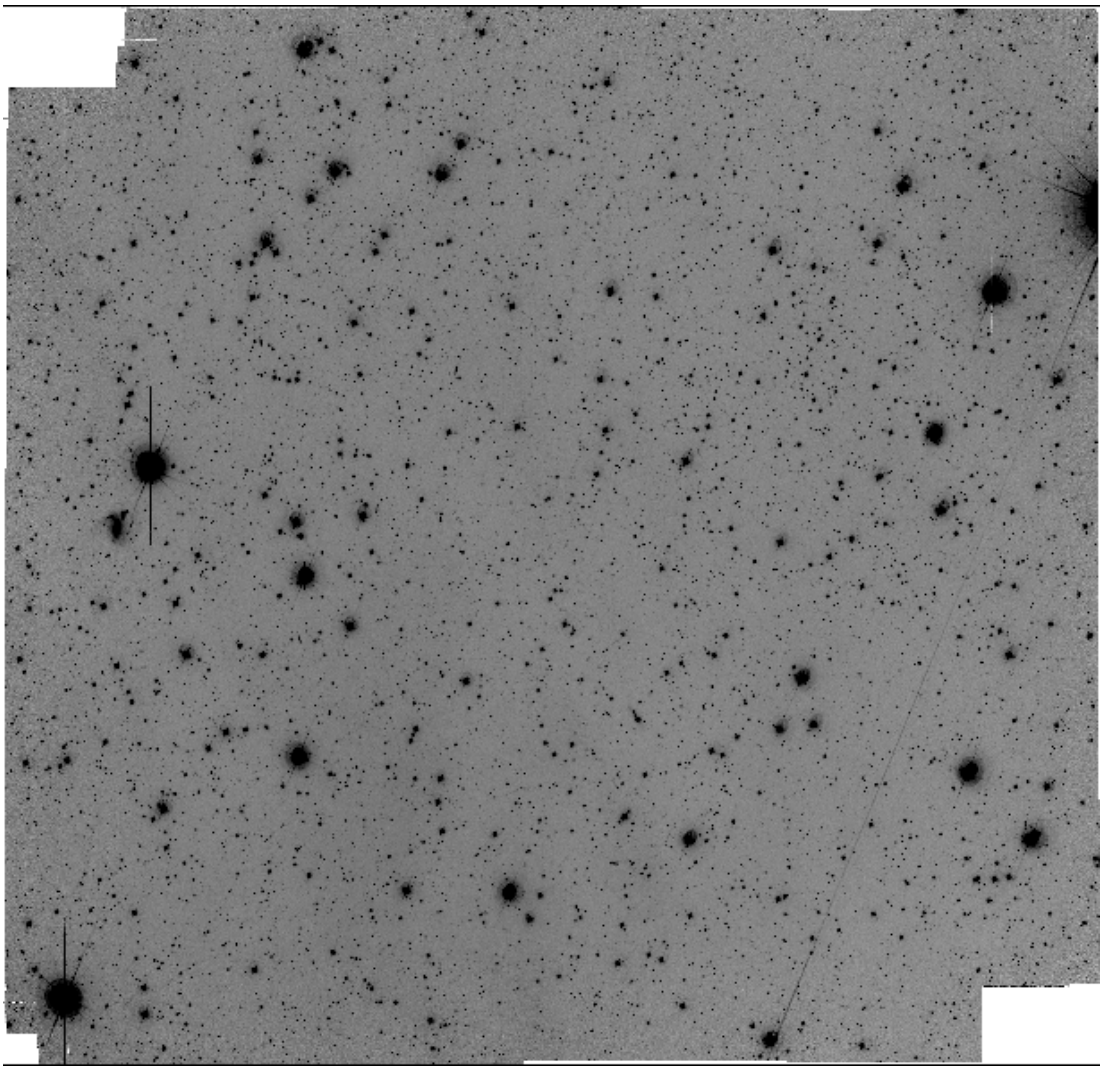

Figure D.73: LCRS Field 1439-03:E

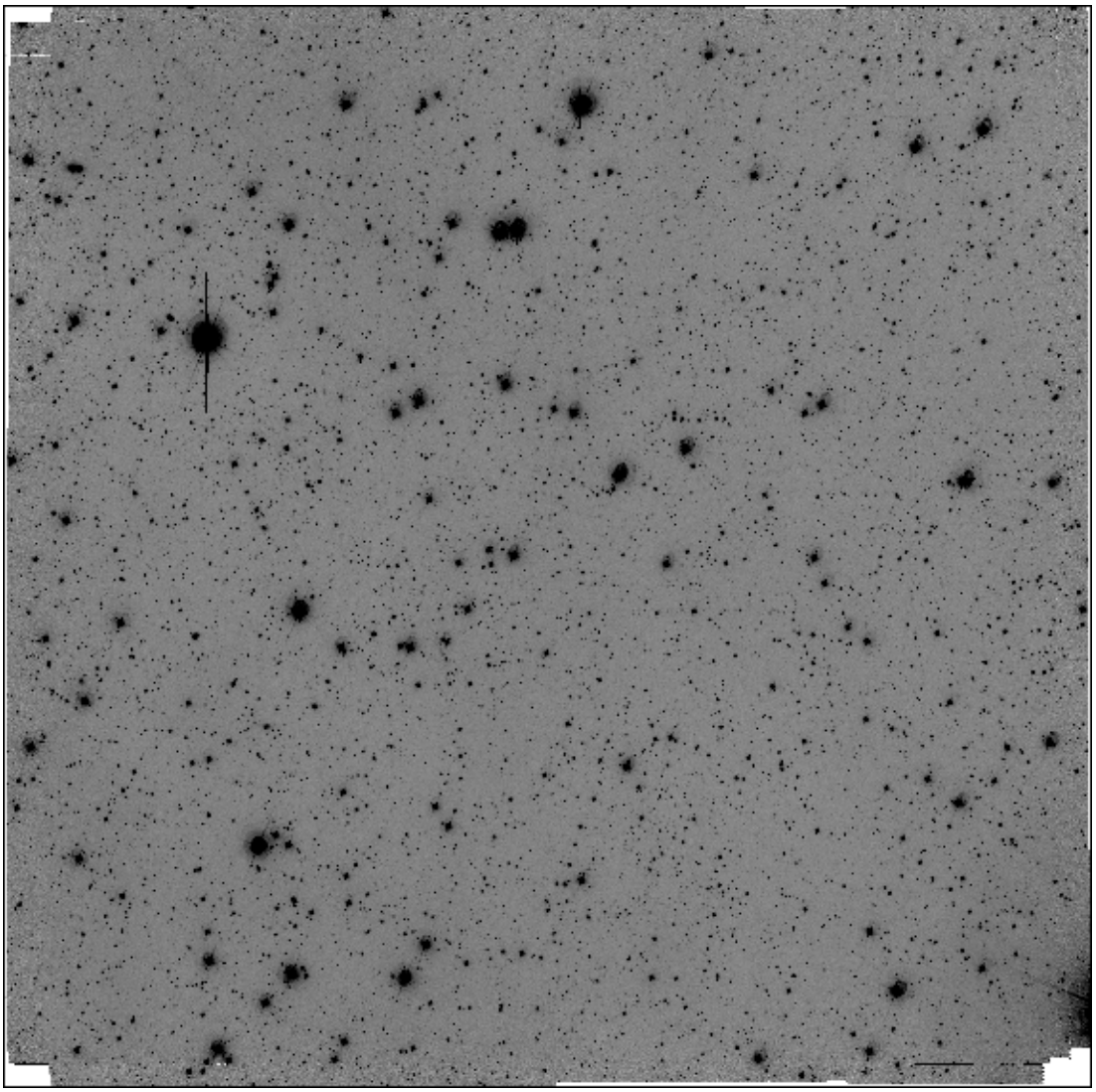

Figure D.74: LCRS Field 1439-03:M

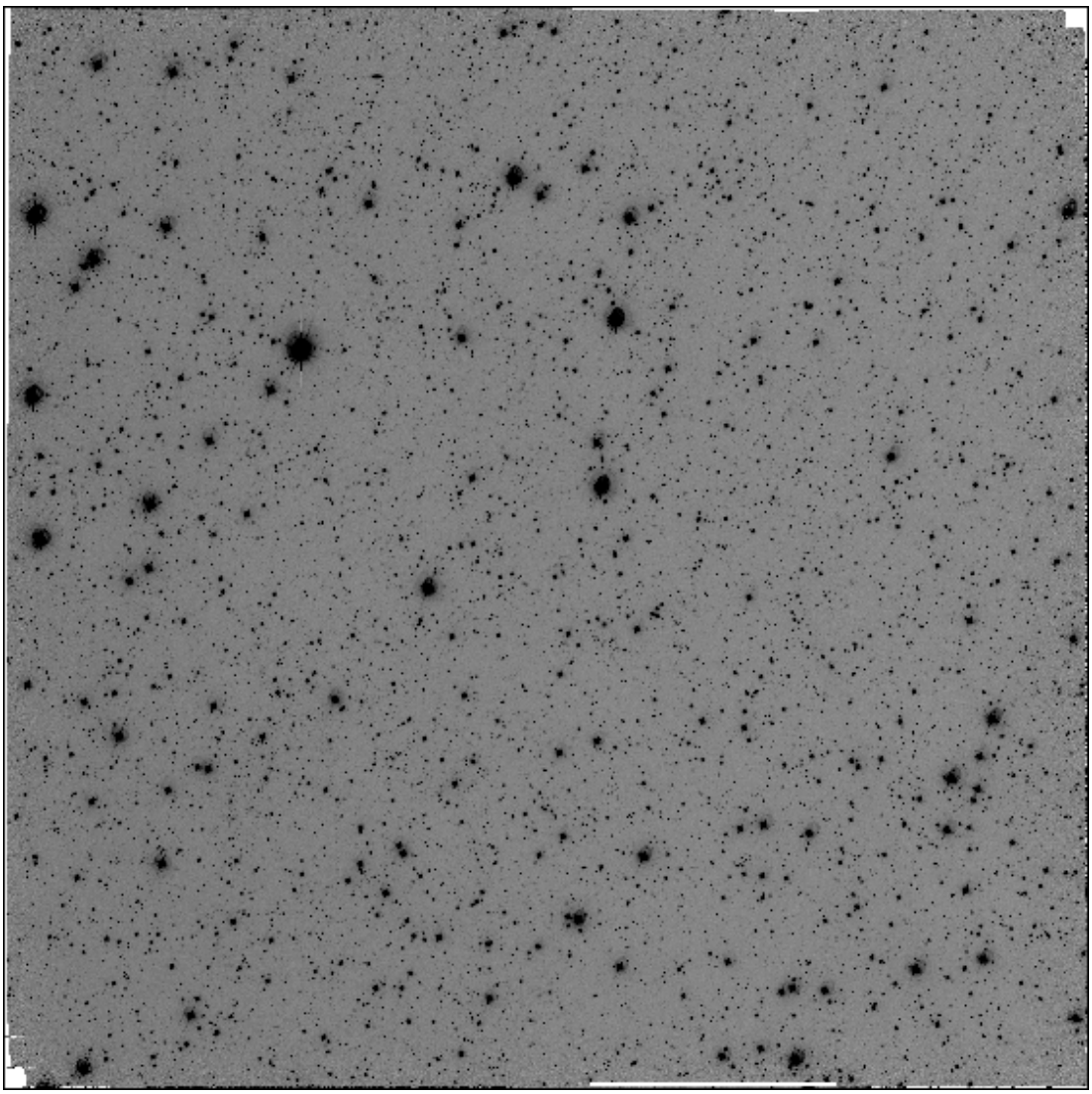

Figure D.75: LCRS Field 1439-06:H

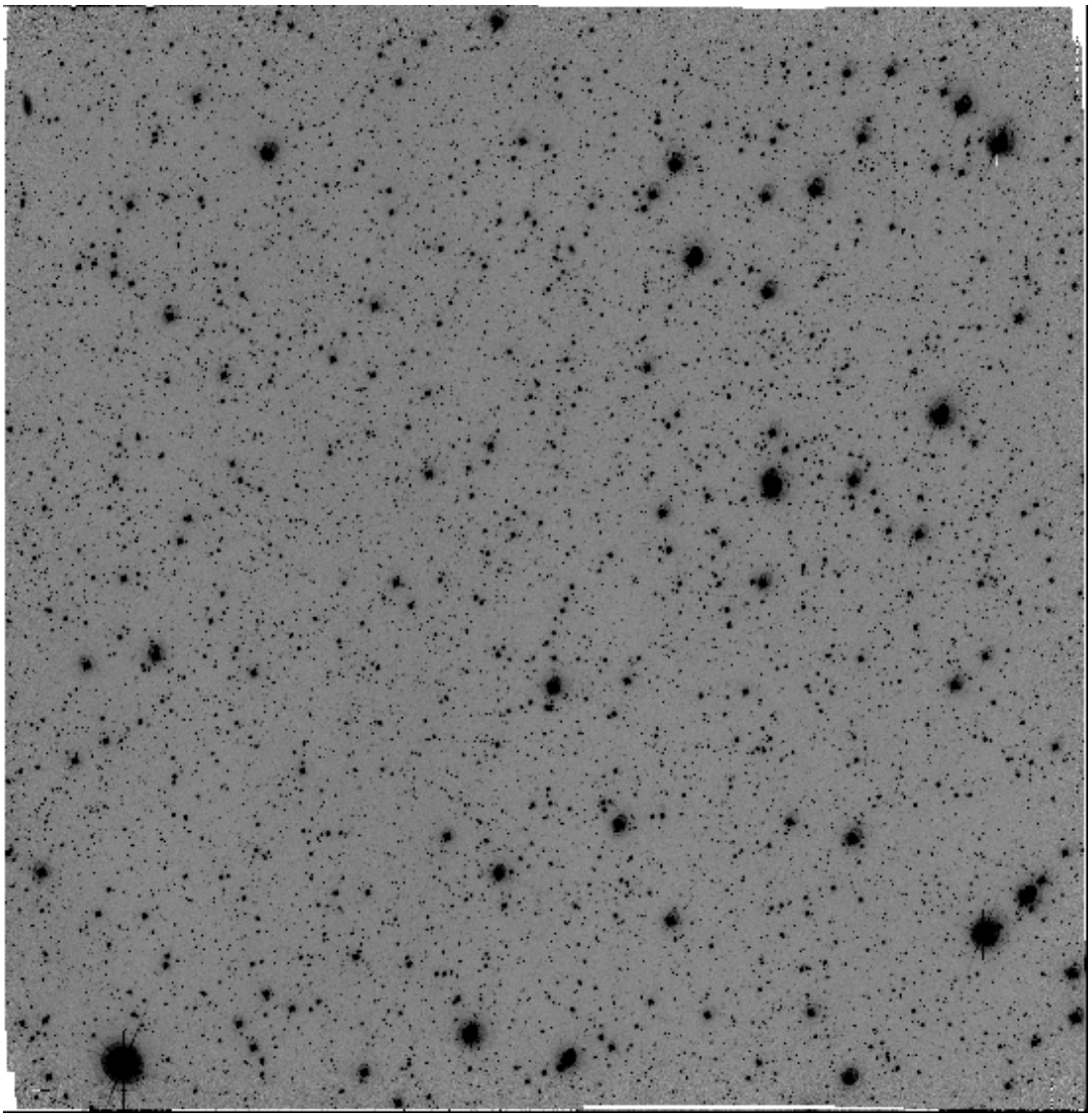

Figure D.76: LCRS Field 1451-06:H

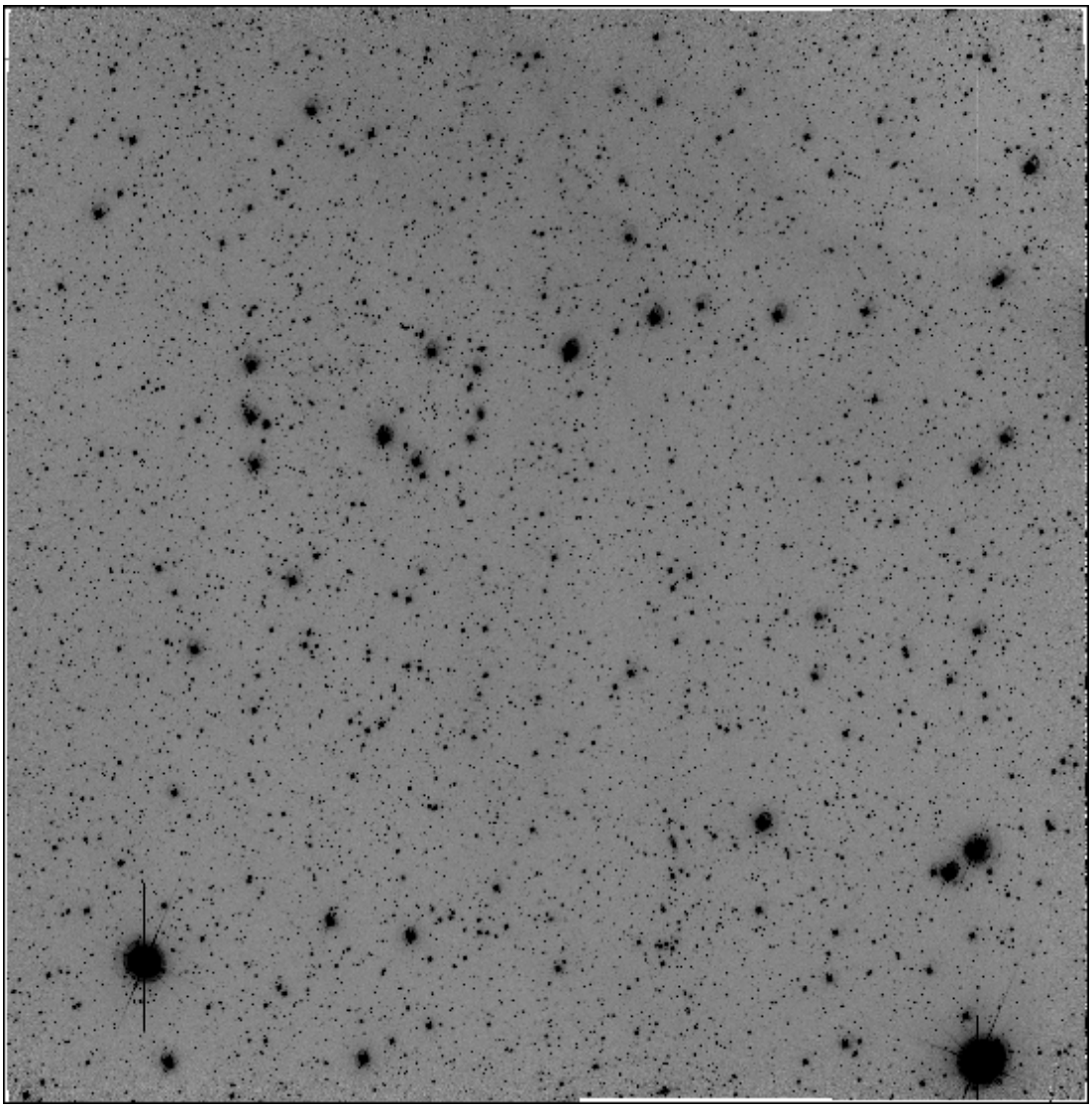

Figure D.77: LCRS Field 1503-03:M

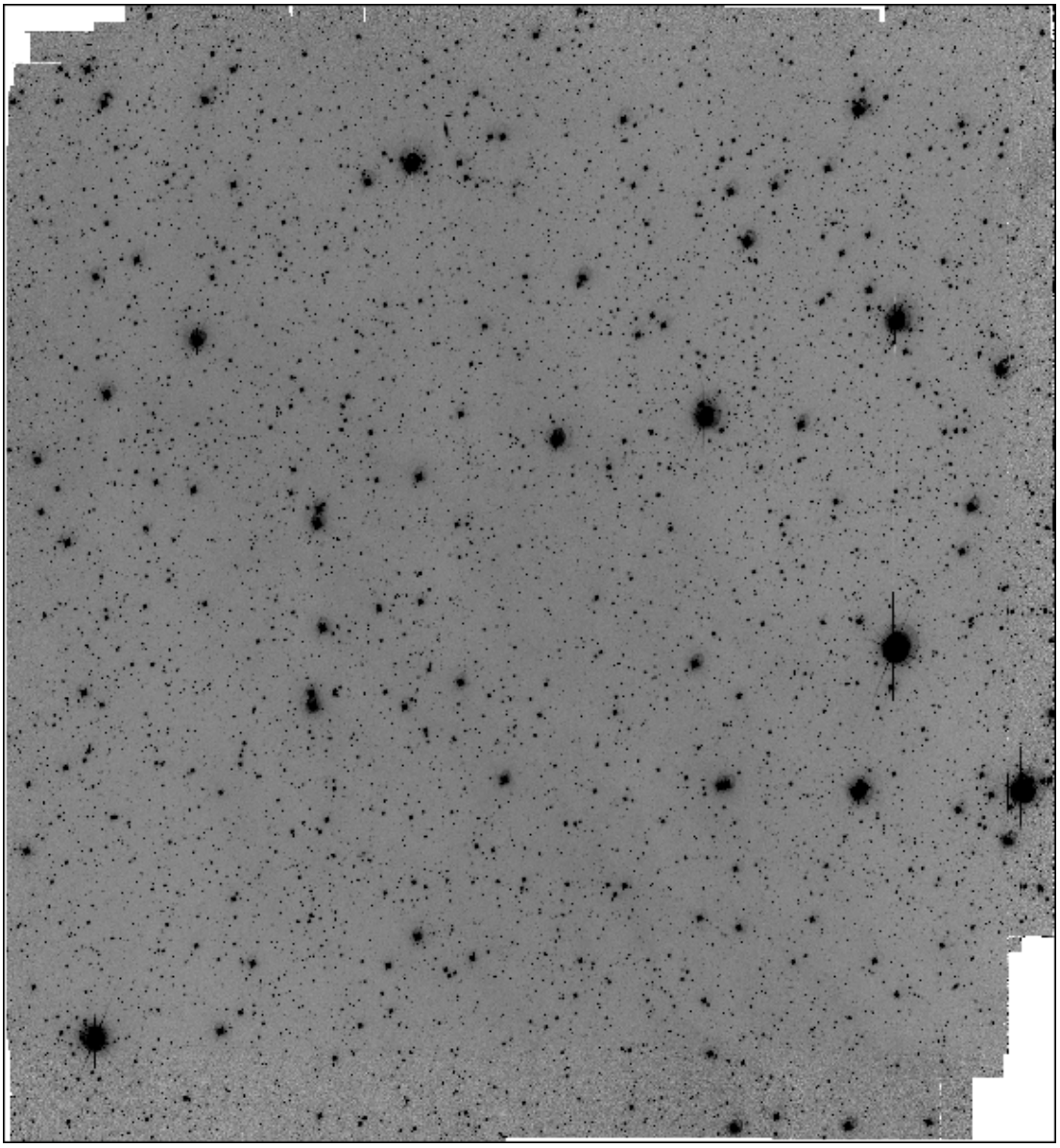

Figure D.78: LCRS Field 1503-03:W

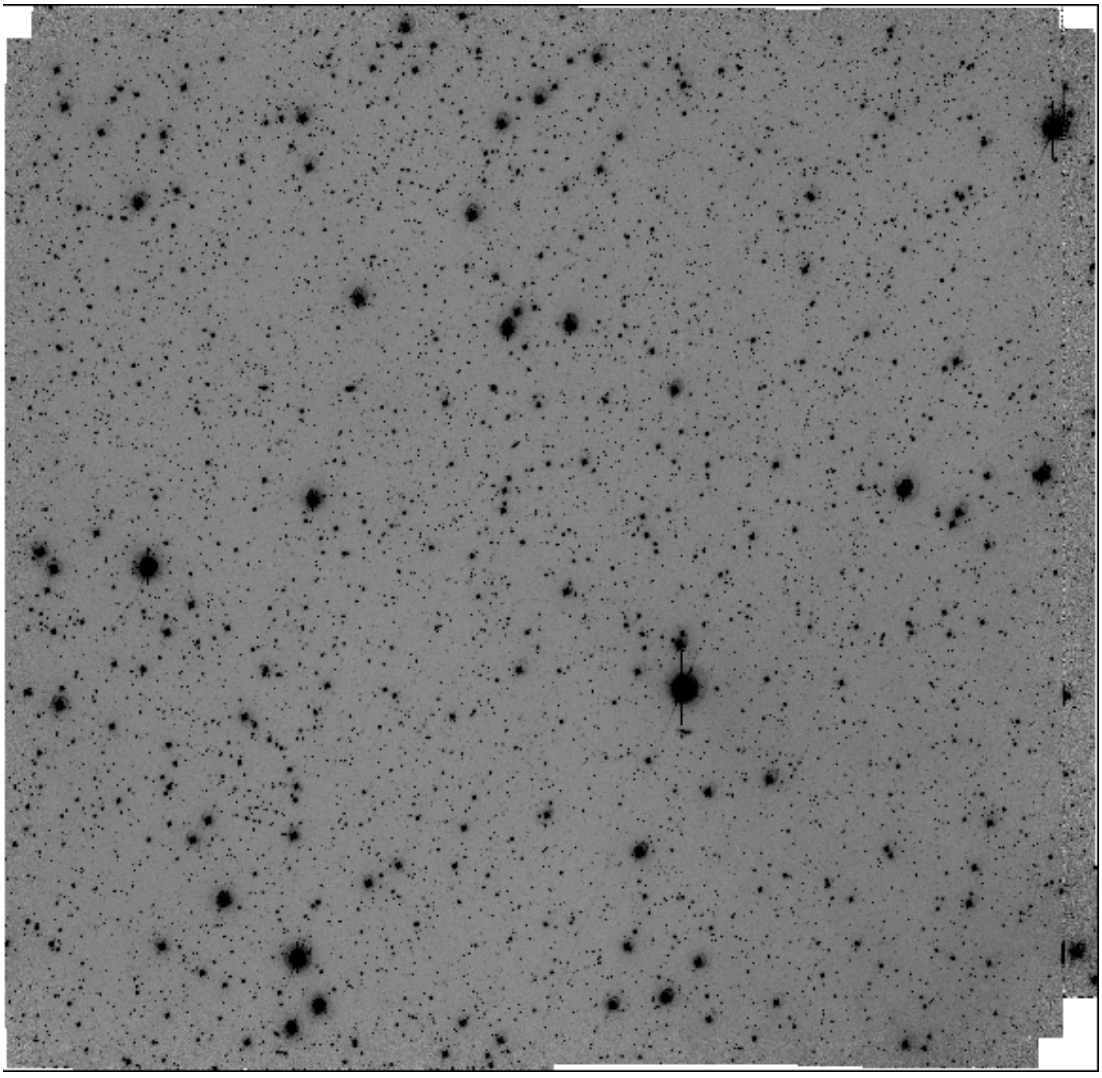

Figure D.79: LCRS Field 1515-03:W

BIBLIOGRAPHY

Abraham, R. G., Tanvir, N. R., Santiago, B. X., Ellis, R. S., Glazebrook, K., & van den Bergh, S. 1996, MNRAS, 279, L47

Abraham, R. G., Valdes, F., Yee, H. K. C., & van den Bergh, S. 1994, ApJ, 432, 75

Allen, R. J., & Shu, F. H. 1979, ApJ, 227, 67

Andreon, S., & Cuillandre, J.-C. 2002, ApJ, 569, 144

Arp, H. 1965, ApJ, 142, 402

Baldwin, J. A., & Stone, R. P. S. 1984, MNRAS, 206, 241

Beijersbergen, M., de Blok, W. J. G., & van der Hulst, J. M. 1999, A&A, 351, 903

Bertin, E. 2003, SExtractor v2.3 User's manual

Bertin, E., & Arnouts, S. 1996, A&AS, 117, 393

Binney, J., & Merrifield, M. 1998, Galactic astronomy (Galactic astronomy / James Binney and Michael Merrifield. Princeton, NJ : Princeton University Press, 1998. (Princeton series in astrophysics) QB857 .B522 1998 ($35.00))

Bothun, G., Impey, C., & McGaugh, S. 1997, PASP, 109, 745

Bothun, G. D., Impey, C. D., Malin, D. F., & Mould, J. R. 1987, AJ, 94, 23

Bowen, D. V., Tripp, T. M., & Jenkins, E. B. 2001, AJ, 121, 1456

Brown, M. J. I., Webster, R. L., & Boyle, B. J. 2001, AJ, 121, 2381

Courteau, S., de Jong, R. S., & Broeils, A. H. 1996, ApJ, 457, L73+

Cross, N. et al. 2001, MNRAS, 324, 825

Dalcanton, J. J., Spergel, D. N., Gunn, J. E., Schmidt, M., & Schneider, D. P. 1997, AJ, 114, 635

Davies, J. I. 1990, MNRAS, 244, 8

Davis, L. E. 1994, A Reference Guide to the IRAF/DAOPHOT Package

de Blok, W. J. G., & McGaugh, S. S. 1997, MNRAS, 290, 533

de Blok, W. J. G., McGaugh, S. S., & Rubin, V. C. 2001, AJ, 122, 2396

de Jong, R. S. 1996, A&A, 313, 45

de Vaucouleurs, G. 1948, Annales d'Astrophysique, 11, 247

Disney, M., & Phillipps, S. 1983, MNRAS, 205, 1253

Disney, M. J. 1976, Nature, 263, 573

Ferguson, H. C., & McGaugh, S. S. 1995, ApJ, 440, 470

Fish, R. A. 1964, ApJ, 139, 284

Freeman, K. C. 1970, ApJ, 160, 811

Freeman, K. C. 1999, in ASP Conf. Ser. 170: The Low Surface Brightness Universe, 3–92

Gardner, J. P. 1998, PASP, 110, 291

Gardner, J. P., & Satyapal, S. 2000, AJ, 119, 2589

Giovanelli, R., Haynes, M. P., Salzer, J. J., Wegner, G., da Costa, L. N., & Freudling, W. 1994, AJ, 107, 2036

—. 1995, AJ, 110, 1059

Graham, J. A. 1982, PASP, 94, 244

Green, R. M. 1985, Spherical astronomy (Cambridge and New York, Cambridge University Press, 1985, 533 p.)

Han, M. 1992, ApJ, 391, 617

Holwerda, B. W. 2003, Source Extractor for Dummies

Hook, R. N., & Fruchter, A. S. 2000, in ASP Conf. Ser. 216: Astronomical Data Analysis Software and Systems IX, 521–+

Hubble, E., & Tolman, R. C. 1935, ApJ, 82, 302

Impey, C., & Bothun, G. 1997, ARA&A, 35, 267

Impey, C. D., Sprayberry, D., Irwin, M. J., & Bothun, G. D. 1996, ApJS, 105, 209

Kron, R. G. 1980, ApJS, 43, 305

Landolt, A. U. 1992, AJ, 104, 340

Linder, S. M. 1998, ApJ, 495, 637

—. 2000, ApJ, 529, 644

Liske, J., Lemon, D. J., Driver, S. P., Cross, N. J. G., & Couch, W. J. 2003, MNRAS, 344, 307

Massey, P. 1997, A User's Guide to CCD Reductions with IRAF

McGaugh, S. S. 1996, MNRAS, 280, 337

McGaugh, S. S., Bothun, G. D., & Schombert, J. M. 1995, AJ, 110, 573

McGaugh, S. S., & de Blok, W. J. G. 1998, ApJ, 499, 41

McGlynn, T., Scollick, K., & White, N. 1997, in IAU Symposium, 465–466

McGlynn, T., Scollick, K., & White, N. 1998, in IAU Symp. 179: New Horizons from Multi-Wavelength Sky Surveys, 465–+

Metcalfe, N., Shanks, T., Fong, R., & Jones, L. R. 1991, MNRAS, 249, 498

Metropolis, N., Rosenbluth, A. W., Rosenbluth, M. N., Teller, A. H., & Teller, E. 1953, J. Chem. Phys., 21, 1087

Morshidi-Esslinger, Z., Davies, J. I., & Smith, R. M. 1999, MNRAS, 304, 297

O'Neil, K. 2000, in ASP Conf. Ser. 215: Cosmic Evolution and Galaxy Formation: Structure, Interactions, and Feedback, 178–+

O'Neil, K., Andreon, S., & Cuillandre, J.-C. 2003, A&A, 399, L35

O'Neil, K., & Bothun, G. 2000, ApJ, 529, 811

O'Neil, K., Bothun, G., van Driel, W., & Ragaigne, D. M. 2004, ArXiv Astrophysics e-prints

O'Neil, K., Bothun, G. D., & Cornell, M. E. 1997, AJ, 113, 1212

O'Neil, K., Bothun, G. D., & Schombert, J. 2000, AJ, 119, 136

Padoan, P., Jimenez, R., & Antonuccio-Delogu, V. 1997, ApJ, 481, L27+

Phillipps, S., Disney, M. J., Kibblewhite, E. J., & Cawson, M. G. M. 1987, MNRAS, 229, 505

Postman, M., Huchra, J. P., Geller, M. J., & Henry, J. P. 1985, AJ, 90, 1400

Schade, D., Lilly, S. J., Crampton, D., Hammer, F., Le Fevre, O., & Tresse, L. 1995, ApJ, 451, L1+

Schmidt, M. 1968, ApJ, 151, 393

Schombert, J. M., Bothun, G. D., Schneider, S. E., & McGaugh, S. S. 1992, AJ, 103, 1107

Schwartzenberg, J. M., Phillipps, S., Smith, R. M., Couch, W. J., & Boyle, B. J. 1995, MNRAS, 275, 121

Sersic, J. L. 1968, Atlas de galaxias australes (Cordoba, Argentina: Observatorio Astronomico, 1968)

Shanks, T., Stevenson, P. R. F., Fong, R., & MacGillivray, H. T. 1984, MNRAS, 206, 767

Shectman, S. A., Landy, S. D., Oemler, A., Tucker, D. L., Lin, H., Kirshner, R. P., & Schechter, P. L. 1996, ApJ, 470, 172

Simard, L. et al. 1999, ApJ, 519, 563

—. 2002, ApJS, 142, 1

Smart, W. M. 1931, Text-book on spherical astronomy (Cambridge [Eng.] The University press, 1931.)

Smith, C. 1993, The Arcon-IRAF Interface: A Preliminary User's Guide for Direct Imaging

—. 1998, The Curtis Schmidt User's Manual; Part 1: The Telescope and Instruments

Snellen, I. A. G., Bremer, M. N., Schilizzi, R. T., Miley, G. K., & van Ojik, R. 1996, MNRAS, 279, 1294

Sprayberry, D. 1994, PhD thesis, The University of Arizona

Stone, R. P. S., & Baldwin, J. A. 1983, MNRAS, 204, 347

Thompson, D., Djorgovski, S., Vigotti, M., & Grueff, G. 1994, AJ, 108, 828

Tomaney, A. B., & Crotts, A. P. S. 1996, AJ, 112, 2872

Tran, K. 2000, GIM2D V2.2.0 Cookbook

Tully, R. B., & Fisher, J. R. 1977, A&A, 54, 661

Tully, R. B., & Verheijen, M. A. W. 1997, ApJ, 484, 145

Tyson, J. A. 1988, AJ, 96, 1

Vettolani, G. et al. 1997, A&A, 325, 954

Walker, A. 1995, NOAO Newsletter, 42

Windhorst, R. A. et al. 1991, ApJ, 380, 362

Yasuda, N. et al. 2001, AJ, 122, 1104

Yoshii, Y., & Takahara, F. 1988, ApJ, 326, 1

Zwaan, M. A., van der Hulst, J. M., de Blok, W. J. G., & McGaugh, S. S. 1995, MNRAS, 273, L35

Zwicky, F. 1957, Morphological astronomy (Berlin: Springer, 1957)